NATIONAL ADVISORY COMMITTEE FOR AERONAUTICS

WARTIME REPORT

ORIGINALLY ISSUED
January 1944 as
Advance Confidential Report 4A11

COLLECTION OF BALANCED-AILERON TEST DATA

By F. M. Rogallo

Langley Memorial Aeronautical Laboratory
Langley Field, Va.

NACA

WASHINGTON

NATIONAL ADVISORY COMMITTEE FOR AERONAUTICS

ADVANCE CONFIDENTIAL REPORT

COLLECTION OF BALANCED-AILERON TEST DATA

By F. M. Rogallo

SUMMARY

Test data of balanced ailerons have been collected from NACA and British sources. These data, which are presented in the form of charts, are grouped as A - ailerons with Frise balances, B - ailerons with blunt-nose balances, C - ailerons with internal balances, D - ailerons with contour modifications, and E - ailerons with tabs. Results of flight tests and of wind-tunnel tests in both two- and three-dimensional flow are presented but no correlation nor résumé of the data has been included. Résumés are being published separately as completed.

INTRODUCTION

The demand for high rates of roll at high speed in combat aircraft and the general increase in the size and speed of airplanes of all types have made it necessary to provide very close aileron balance.

Provision of close balance at large aileron deflections at high speed frequently results in overbalance at small aileron deflections or at low speeds. In some installations, moreover, an undesirable shaking of the controls has occurred under some conditions of flight.

Many experimental investigations of ailerons have been made but all the results obtained have not been available to the manufacturers and, in general, the results have not been correlated nor summarized. A large amount of test data has been collected herein for convenient reference. These data are being analyzed, correlated, and summarized by the NACA; the results of these studies are being published separately as completed. (See references 1 and 2.)

Test results of balanced control surfaces of larger chord than are generally used for ailerons are not included in the present collection but are collected in reference 3.

CLASSIFICATION OF DATA

The present collection of data is divided into five sections as follows:

A - ailerons with Frise balances

B - ailerons with blunt-nose balances

C - ailerons with internal balances

D - ailerons with contour modifications

E - ailerons with tabs

The parameters and symbols used in the presentation of data are:

C_L lift coefficient

C_D drag coefficient

c_l section lift coefficient

c_{d_o} section profile-drag coefficient

C_h hinge-moment coefficient

c_h section hinge-moment coefficient

$C_{l'}$ rolling-moment coefficient about axis in plane of symmetry of complete model or airplane, referred to wind axes

$C_{n'}$ yawing-moment coefficient about axis in plane of symmetry of complete airplane or model, referred to wind axes

C_m pitching-moment coefficient

c_m section pitching-moment coefficient about quarter-chord point of airfoil

pb/2V helix angle of airplane in roll

p rolling velocity; also, static pressure

p_o free-stream static pressure

α angle of attack

α_o section angle of attack

ψ angle of yaw

δ deflection angle

A aspect ratio

λ ratio of tip chord to root chord

b wing span; also used with subscripts to denote components of wing

y_i distance from plane of symmetry to inboard end of aileron

y_o distance from plane of symmetry to outboard end of aileron

c wing chord; also used with subscripts to denote components of wing

$\bar{c}$ mean wing chord; also used with subscripts to denote components of wing

t_a aileron semithickness at hinge

Δt increase of aileron trailing-edge thickness

R_b radius of juncture between bevel and control surface

ϕ trailing-edge angle, included between sides which form trailing edge

q local dynamic pressure

q_o free-stream dynamic pressure

Δp pressure across balance

P pressure coefficient $\left(\frac{p - p_o}{q_o}\right)$

V free-stream velocity

V_i indicated velocity

R Reynolds number

M Mach number

F_s stick force

Subscripts:

a aileron

b balance; also, bevel

f flap

s stick

t tab

Results of flight tests and of wind-tunnel tests in both two- and three-dimensional flow are presented. Some of the data have been replotted and are given in a form different from that in the original source. Supplementary information on the models and on the test conditions is given in table I. This table also gives published references and serves as an index to the results presented because the model or airplane designation is given in the first column of the table and

in the upper right-hand corner of each page of model drawings or test results. Some of the data have been corrected for tunnel-boundary effects. When such corrections have been estimated but not applied to the data, the estimated correction factors are given in table I.

AILERONS WITH FRISE BALANCES

The results of tests and the test conditions for models and airplanes having ailerons with Frise balances are given in table IA and in figures A1 to A86. The section characteristics of three models equipped with Frise ailerons are presented in figures A1 to A13. In general, the ailerons tested did not seem very satisfactory in the negative deflection range; that is, sharp breaks occurred in the hinge-moment and effectiveness curves at relatively low negative deflections. This characteristic seems to be caused by separation of flow at the protruding nose. Figure A4 shows that such separation may be delayed considerably by increasing the radius of the nose. A similar improvement was obtained for the aileron of model A-VIII by raising the nose but maintaining the same nose radius (fig. A39). The ailerons of model A-III buffeted very badly over a large part of the negative deflection range (reference 6) and only a few test points could be obtained in this region (fig. A13). The results of tests of various partial-span wing models and complete airplane models are presented in figures A14 to A49. Flight test results are given in figures A50 to A86. The improvement obtained by increasing the nose radius is again evident from figure A22. Figure A24 shows that a high pressure peak can be expected at the nose portion which protrudes below the lower surface even though the nose radius is relatively large. The buffeting tendency of Frise ailerons was again evident in the tests of model A-VI (reference 7). The deflections at which oscillation occurred are indicated in figures A27 to A34. The characteristics of the ailerons of this series of tests were improved by bulging the lower surface or by attaching a slat to the aileron nose. The same modifications were found to reduce aileron buffeting in the flight tests of airplane A-XII. In connection with this series of tests, it was pointed out that bulging the lower surface may be unsatisfactory in some installations because it increases the downfloating tendency of the aileron. The

buffeting tendency of the ailerons of airplane A-XV was almost eliminated by slightly reducing the maximum negative deflections. Practically no loss in effectiveness accompanied this alteration.

AILERONS WITH BLUNT-NOSE BALANCES

Data pertaining to the tests of models having ailerons with blunt-nose balances are given in table IB and in figures B1 to B43. Section characteristics for two models equipped with blunt-nose ailerons are presented in figures B1 to B14. The blunt-nose ailerons on an NACA 23012 airfoil seemed to be more satisfactory than similar ailerons on an NACA 66(215)-216, $a = 1.0$ airfoil; that is, the values of $\left(\partial c_h/\partial \delta_a\right)_\alpha$ and $\left(\partial c_h/\partial \alpha\right)_{\delta_a}$ were close to zero and the unstalled deflection range was greater for the NACA 23012 airfoil. Increasing the nose radii resulted in a slight loss in $\left(\partial \Delta c_l/\partial \delta_a\right)_\alpha$ and a slight negative increase in $\left(\partial c_h/\partial \delta_a\right)_\alpha$ for small deflections but, because the ailerons with small nose radii tended to stall at lower deflections, the maximum values of Δc_l were usually greater and the corresponding hinge moments were usually lower for the ailerons with larger nose radii. These characteristics may also be noted from the results of tests of blunt-nose ailerons on conventional and low-drag wing models of finite span as given in figures B15 to B32. The peak pressures that occurred over the noses of ailerons of this type were relatively high, as may be seen from figure B17. That the effectiveness of ailerons with blunt-nose balances was greater than the effectiveness of plain unbalanced ailerons is indicated by figure B19. The results of tests of a blunt-nose aileron on a complete airplane model are given in figures B33 to B43. The effects of controlling the boundary-layer thickness by fixing the point of transition and the effects of moving the hinge axis rearward to obtain a higher degree of balance may be obtained from these results.

AILERONS WITH INTERNAL BALANCES

Data pertaining to ailerons with internal balances are given in table IC and in figures C1 to C89. Section characteristics are shown in figures C1 to C33; data for finite-span models in figures C34 to C77; and flight data in figures C78 to C89. Many of these data have been analyzed and summarized in reference 2 in which a discussion is given of the balance required. The effects of changing the vent location, the surface contour at the vents, or the amount of leakage across the seal are also discussed and it is shown that these modifications may sometimes be utilized for adjustment of the hinge-moment characteristics. The importance of leakage cannot be overemphasized. The reduction of aileron rolling-moment effectiveness due to leakage may be inconsequential but a leakage area of only two-tenths of the vent area may reduce the effectiveness of the internal balance by 30 percent, as shown in figure 7 of reference 2. The effects of varying the length of the fabric seal and of varying the shape of the balance chamber near the seal may sometimes be important but these effects cannot be determined from the data now available. An investigation of these variables, however, is now under way.

AILERONS WITH CONTOUR MODIFICATIONS

The material presented in table ID and in figures D1 to D60 includes data on several contour modifications that reduce hinge moments - such as bevels, bulges, and increased profile thickness - and also data on several contour modifications that increase hinge moments - such as trailing-edge strips, increased aileron chord and span, and decreased profile thickness. Section characteristics are shown in figures D1 to D17; data for finite-span models in figures D18 to D54; and flight data in figures D55 to D60. A preliminary correlation has been made of the effect of bevels at small deflections of sealed control surfaces (reference 1). The correlation was made on the basis of the included angle between the upper and the lower surfaces at the trailing edge and included most of the data for sealed ailerons presented in figures D2 to D39.

The improvement in effectiveness and the more nearly linear hinge-moment curves obtainable by sealing the aileron gap when a bevel is used are shown in figures D22 to D24, D34, and D39.

The data on bulged or thickened aileron profiles shown in figures D46 to D48 were obtained on an unsealed Frise aileron. The effect of the changed profile was correlated in references 25 to 27 with the maximum amount of the change in profile thickness and its position along the aileron chord as parameters. The effect of a hollow or a thickened profile on a plain sealed aileron is shown in figures D2 to D7. An unsymmetrical bulge or bevel (figs. D30, D35, and D47) or a reflexed trailing edge (fig. D17) may be used to give an upfloating or a downfloating tendency; this effect may be desirable if the aileron has a differential linkage.

The aileron-contour modifications previously mentioned provide balance by utilizing the difference in the boundary-layer thickness over the upper and the lower surfaces of the rear portion of the airfoil in such a way that the lift over this portion is altered. The aileron effectiveness as indicated by the static rolling moments will thus be reduced when a bevel or bulge is used. As is pointed out in reference 1, the loss in rolling power of an aileron will be less than the loss in static rolling moment indicates, however, because the damping in roll is also reduced by the bevel or bulge.

The results of flight tests of several unsealed-aileron arrangements on a fighter airplane are given in figures D56 to D60. The effects of using large trailing-edge angles and of fixing transition are shown.

The modifications shown in figures D16 and D49 to D54 are intended to increase the ratio of the hinge-moment parameters $\left(\partial C_h/\partial\alpha\right)_{\delta_a}$ and $\left(\partial C_h/\partial\delta_a\right)_{\alpha}$. Analysis shows that increasing the positive value of the ratio $\dfrac{\left(\partial C_h/\partial\alpha\right)_{\delta_a}}{\left(\partial C_h/\partial\delta_a\right)_{\alpha}}$ will tend to lighten stick forces during rolling.

AILERONS WITH TABS

The results of tests and the test conditions for models and airplanes having ailerons with tabs are given in table IE and in figures E1 to E53. Section characteristics of tabs on two low-drag airfoils are presented in figures E1 to E7. Characteristics of ailerons with tabs on a number of semispan and full-span models are presented in figures E8 to E46. A fairly large range of wing sections, tab chords, tab spans, aileron chords, and aileron balances is covered.

A fair amount of data for tabs on ailerons with thickened and beveled trailing edges is included. Tabs on such ailerons, unfortunately, are most effective in producing aileron hinge moment when deflected in the same direction as the aileron. Figure E30 shows a decrease in tab effectiveness $\partial C_h/\partial \delta_t$ with increase in trailing-edge angle.

Data from flight tests of an aileron equipped with a spring tab (fig. E47) are shown in figure E48. Because the spring unit was preloaded, the tab did not deflect until the stick force exceeded approximately $9\frac{1}{2}$ pounds. Both aileron and tab were mass-balanced. Severe flutter was experienced when play developed in the tab linkage. This phenomenon is not peculiar to spring tab but may occur with any tab linkage having backlash.

Characteristics of an airplane having ailerons with beveled trailing edges are shown in figures E49 to E53. For the balancing-tab tests (fig. E52), the stick travel was inadvertently set at ±8 inches instead of ±9 inches. As a result, figures E52 and E53 are not directly comparable. Information presented in figure E50 for balancing tabs in operation has been corrected to a stick travel of ±9 inches.

Langley Memorial Aeronautical Laboratory,
National Advisory Committee for Aeronautics,
Langley Field, Va.

REFERENCES

1. Purser, Paul E., and Gillis, Clarence L.: Preliminary Correlation of the Effects of Beveled Trailing Edges on the Hinge-Moment Characteristics of Control Surfaces. NACA C.B. No. 3E14, May 1943.

2. Rogallo, F. M., and Lowry, John G.: Résumé of Data for Internally Balanced Ailerons. NACA R.B., March 1943.

3. Sears, Richard I.: Wind-Tunnel Data on the Aerodynamic Characteristics of Airplane Control Surfaces. NACA A.C.R. No. 3L08, Dec. 1943.

4. Jacobs, Eastman N., Abbott, Ira H., and Davidson, Milton: Supplement (loose-leaf) to NACA Advance Confidential Report, Preliminary Low-Drag-Airfoil and Flap Data from Tests at Large Reynolds Numbers and Low Turbulence. NACA, March 1942, p. 21a.

5. Letko, W., and Kemp, W. B.: Wind-Tunnel Tests of Ailerons at Various Speeds. III - Ailerons of 0.20 Airfoil Chord and True Contour with 0.35-Aileron-Chord Frise Balance on the NACA 23012 Airfoil. NACA A.C.R. No. 3I14, 1943.

6. Holtzclaw, Ralph W., and Erickson, Myles D.: Wind-Tunnel Investigation of Flap, Aileron, and Exterior Bomb Installations on a 24-Inch Constant-Chord North American XB-28 Wing Model. NACA A.R.R., July 1942.

7. Rogallo, F. M., and Purser, Paul E.: Wind-Tunnel Investigation of 20-Percent-Chord Plain and Frise Ailerons on an NACA 23012 Airfoil. NACA A.R.R., Dec. 1941.

8. Davies, H., and Brown, E. C.: Note on the Effect of Nose Shape on the Characteristics of Frise Ailerons. Rep. No. B.A. 1621, R.A.E., Aug. 1940.

9. Kleckner, Harold F.: Flight Measurements of the Aileron Characteristics of a Grumman F4F-3 Airplane. NACA A.C.R., Sept. 1942.

10. Phillips, William H., and Vensel, Joseph R.: Measurements of the Flying Qualities of a Supermarine Spitfire VA Airplane. NACA A.C.R., Sept. 1942.

11. Letko, W., Hollingworth, T. A., and Anderson, R. A.: Wind-Tunnel Tests of Ailerons at Various Speeds. IV - Ailerons of 0.20 Airfoil Chord and True Contour with 0.35 Aileron-Chord Extreme Blunt-Nose Balance on the NACA 23012 Airfoil. NACA A.C.R. No. 3H28, 1943.

12. Letko, W., Denaci, H. G., and Freed, C.: Wind-Tunnel Tests of Ailerons at Various Speeds. I - Ailerons of 0.20 Airfoil Chord and True Contour with 0.35 Aileron-Chord Extreme Blunt Nose Balance on the NACA 66,2-216 Airfoil. NACA A.C.R. No. 3F11, 1943.

13. Purser, Paul E., and Toll, Thomas A.: Wind-Tunnel Investigation of the Characteristics of Blunt-Nose Ailerons on a Tapered Wing. NACA A.R.R., Feb. 1943.

14. Denaci, H. G., and Bird, J. D.: Wind-Tunnel Tests of Ailerons at Various Speeds. II - Ailerons of 0.20 Airfoil Chord and True Contour with 0.60 Aileron-Chord Sealed Internal Balance on the NACA 66, 2-216 Airfoil. NACA A.C.R., No.3F18, June 1943.

15. Rogallo, F. M., and Lowry, John G.: Wind-Tunnel Investigation of a Plain Aileron and a Balanced Aileron on a Tapered Wing with Full-Span Duplex Flaps. NACA A.R.R., July 1942.

16. Rogallo, F. M., and Lowry, John G.: Wind-Tunnel Development of Ailerons for the Curtiss XP-60 Airplane. NACA A.C.R., Sept. 1942.

17. Harris, Thomas A., and Purser, Paul E.: Wind-Tunnel Investigation of Plain Ailerons for a Wing with a Full-Span Flap Consisting of an Inboard Fowler and an Outboard Retractable Split Flap. NACA A.C.R., March 1941.

18. Irving, H. B., Batson, A. S., and Warsap, J. H.: Notes and Exploratory Experiments on the Aerodynamic Balancing of Controls. 4284, S. & C. 1093, N.P.L., Nov. 27, 1939.

19. Rogallo, F. M., Lowry, John G., and Fischel, Jack: Wind-Tunnel Investigation of a Full-Span Retractable Flap in Combination with Full-Span Plain and Internally Balanced Ailerons on a Tapered Wing. NACA A.R.R. No. 3H23, 1943.

20. Williams, W. C., and Kleckner, H. F.: A Flight Investigation of Internally Balanced Sealed Ailerons. NACA A.R.R., Dec. 1941.

21. Gilruth, R. R.: Flight Tests of Internally Balanced, Sealed Ailerons on the Curtiss XP-60 Airplane. NACA C.B., July 1942.

22. Rogallo, F. M., and Purser, Paul E.: Wind-Tunnel Investigation of a Plain Aileron with Various Trailing-Edge Modifications on a Tapered Wing. II - Ailerons with Thickened and Beveled Trailing Edges. NACA A.R.R., Oct. 1942.

23. Purser, Paul E., and McKee, John W.: Wind-Tunnel Investigation of a Plain Aileron with Thickened and Beveled Trailing Edges on a Tapered Low-Drag Wing. NACA A.C.R., Jan. 1943.

24. Rogallo, F. M., and Crandall, Stewart M.: Wind-Tunnel Investigation of Trimming Tabs on a Thickened and Beveled Aileron on a Tapered Low-Drag Wing. NACA A.C.R., March 1943.

25. Batson, A. S., Burge, C. N., and Skelton, W. C.: Experiments on the Effect of Curvature of Surface and Thickness of Trailing Edge on Aileron Hinge Moments (Part III). 6188, S. & C. 1426, N.P.L., Oct. 20, 1942.

26. Batson, A. S., Burge, C. H., and Greening, J. R.: The Effect of Curvature of Surface and Thickness of Trailing Edge on Aileron Hinge Moments. 5310, S. & C. 1257, N.P.L., Sept. 9, 1941.

27. Batson, A. S., Burge, C. H., and Skelton, W. C.: Experiments on the Effect of Curvature of Surface and Thickness of Trailing Edge on Aileron Hinge Moments (Part II). 5490, S. & C. 1290, N.P.L., Dec. 2, 1941.

28. Bryant, L. W., Burge, C. H., Sweeting, N. E., and Greening, J. R.: Experiments on the Balancing of Ailerons by Geared Tabs and Trailing Edge Strips. 5044, S. & C. 1195a, N.P.L., April 5, 1941.

29. Batson, A. S., and Warsap, J. H.: Effect on Hinge Moment of Fitting Strips near Aileron Trailing Edge and of Increasing Aileron Chord, with an Appendix on Pressures over Surface of Control Fitted with Strips. 4613, S. & C. 1147, Ae 1683, N.P.L., July 2, 1940.

30. Batson, A. S., and Warsap, J. H.: Effect on Hinge Moment of Extending Aileron to Wing Tip. 4737, S. & C. 1172, N.P.L., Oct. 4, 1940.

31. Harris, Thomas A.: Reduction of Hinge Moments of Airplane Control Surfaces by Tabs. Rep. No. 528, NACA, 1935.

32. Rogallo, F. M., and Purser, Paul E.: Wind-Tunnel Investigation of a Plain Aileron with Various Trailing-Edge Modifications on a Tapered Wing. III - Ailerons with Simple and Spring-Linked Balancing Tabs. NACA A.R.R., Jan. 1943.

33. Halliday, A. S., Cox, D. K., and Skelton, W. C.: Wind Tunnel Tests on the Folland E.28/40 Aileron. 5463, S. & C. 1288, N.P.L., Nov. 18, 1941.

34. Morgan, M. B., Morris, D. E., and Bethwaite, C. F.: Flight Tests of Spring Tab Ailerons on a Spitfire. Rep. No. Aero 1771, R.A.E., Aug. 1942.

TABLE I.- SUPPLEMENTARY INFORMATION REGARDING TESTS OF MODELS AND AIRPLANES HAVING BALANCED AILERONS - Continued

C - AILERONS WITH INTERNAL BALANCES

Model or airplane		Typical aileron section	Airfoil section		A	λ	Aileron location		c_a/c	Type of test	Corrections estimated but not applied	Air-flow characteristics	Published reference
Designation (1)	Plan form of surface		Root	Tip			$\frac{y_1}{b/2}$	$\frac{y_o}{b/2}$					
C-I	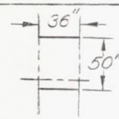	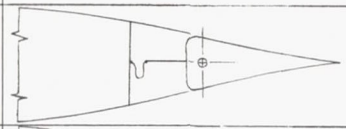	NACA 66(2x15)-216, a = 0.6		∞	---------	-----	-----	0.1642 and 0.1539	Two dimensional	None	$R = 4.2 \times 10^6$ to 5.3×10^6 M = 0.14 to 0.18	
C-II	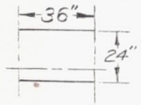	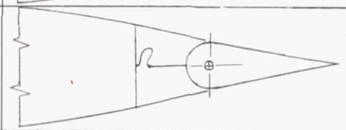	NACA 66(2x15)-116, a = 0.6		∞	---------	-----	-----	0.167	Two dimensional	None	$R = 6 \times 10^6$ M = 0.14	
C-III	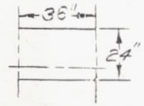	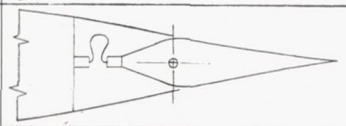	NACA low drag (See fig. C10.)		∞	---------	-----	-----	0.20	Two dimensional	None	$R = 2.5 \times 10^6$ M = 0.17	
C-IV	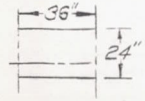	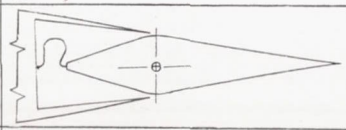	NACA low drag (See fig. C13.)		∞	---------	-----	-----	0.232	Two dimensional	None	$R = 6 \times 10^6$ M = 0.14	
C-V	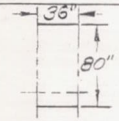	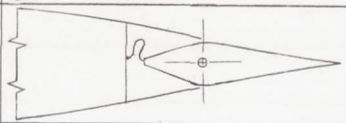	NACA 66(215)-216, a = 0.6		∞	---------	-----	-----	0.1725	Two dimensional	None	$R = 9.6 \times 10^6$ M = 0.20	
C-VI	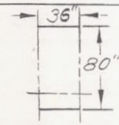	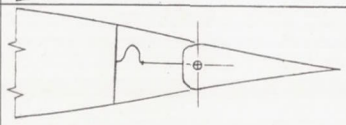	NACA low drag (See fig. C17.)		∞	---------	-----	-----	0.173	Two dimensional	None	$R = 7.5 \times 10^6$ M = 0.16	
C-VII	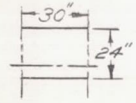	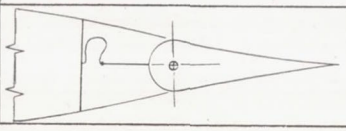	NACA 66(215)-216, a = 1.0		∞	---------	-----	-----	0.20	Two dimensional	None	$R = 2.8 \times 10^6$ to 5.95×10^6 M = 0.20 to 0.42	14

[1]All designations that have the same superscript (a,b,c,..., or p) denote models or airplanes having the same wing plan form and the same airfoil section.

TABLE I.- SUPPLEMENTARY INFORMATION REGARDING TESTS OF MODELS AND AIRPLANES HAVING BALANCED AILERONS - Continued

C - AILERONS WITH INTERNAL BALANCES - Continued

Model or airplane		Typical aileron section	Airfoil section		A	λ	Aileron location		c_a/c	Type of test	Corrections estimated but not applied	Air-flow characteristics	Published reference
Designation (1)	Plan form of surface		Root	Tip			$\frac{y_1}{b/2}$	$\frac{y_o}{b/2}$					
C-VIII[a]	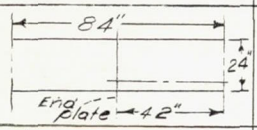	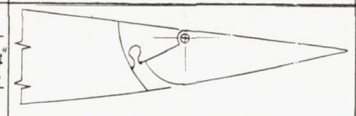	NACA conventional (approx. 14 percent thick)		∞	---------	-----	-----	0.20	Two dimensional	None	$R = 1.91 \times 10^6$ $M = 0.13$	6
C-IX[j]	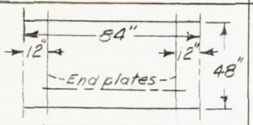	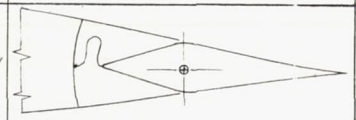	NACA 66(215)-216, a = 0.6		∞	---------	-----	-----	0.20	Two dimensional	None	$R = 6.7 \times 10^5$ to 9.5×10^6 $M = 0.24$ to 0.33	
C-X[g]	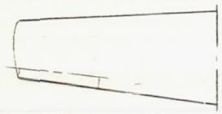	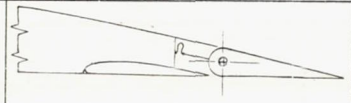	NACA 23015.5 (approx.)	NACA 23008.25 (approx.)	5.6	0.60	0.579	0.984	0.155	Semispan wing model	None	$R = 2.05 \times 10^6$ $M = 0.11$	15
C-XI[k]	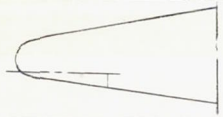	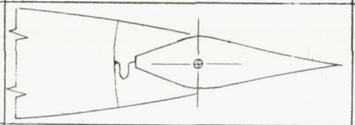	NACA 66,2-118, a = 1.0	NACA 66(2x15)-116, a = 1.0	6.2	0.33	0.496	0.906 and 0.977	0.175 0.162 and 0.149	Semispan wing model	$C_l'_c = 0.90C_l$ $C_{n'_c} = C_{n'} - 0.031C_l'C_L$	$R = 1.9 \times 10^6$ $M = 0.11$	16
C-XII[d]	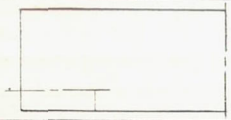	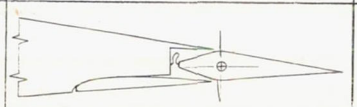	NACA 23012		4.0	1.00	0.63	1.000	0.15	Semispan wing model	$C_l'_c = 0.86C_l$ $C_{n'_c} = C_{n'} - 0.045C_l'C_L$	$R = 1.44 \times 10^6$ $M = 0.05$	17
C-XIII[e]	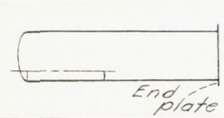	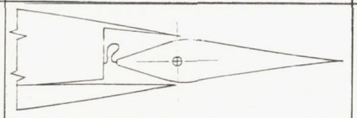	Davis (16 percent thick)		8.1	1.00	0.565	0.976	0.15	Semispan wing model	End-plate effects uncertain	$R = 2.25 \times 10^6$ $M = 0.16$	
C-XIV[b]	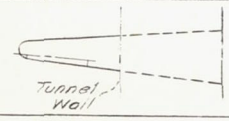	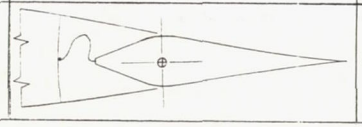	NACA 65(223)-222, a = 1.0	NACA 65(216)-415, a = 0.5	12.0	0.32	0.641	0.945	0.23	Quarter-span wing model	None	$R = 1.99 \times 10^6$ $M = 0.11$	

[1]All designations that have the same superscript (a,b,c,..., or p) denote models or airplanes having the same wing plan form and the same airfoil section.

TABLE I.- SUPPLEMENTARY INFORMATION REGARDING TESTS OF MODELS AND AIRPLANES HAVING BALANCED AILERONS - Continued

C - AILERONS WITH INTERNAL BALANCES - Concluded

NATIONAL ADVISORY COMMITTEE FOR AERONAUTICS

Model or airplane		Typical aileron section	Airfoil section		A	λ	Aileron location		c_a/c	Type of test	Corrections estimated but not applied	Air-flow characteristics	Published reference
Designation (1)	Plan form of surface		Root	Tip			$\frac{y_i}{b/2}$	$\frac{y_o}{b/2}$					
C-XV[c]	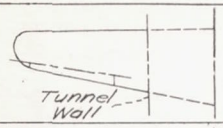	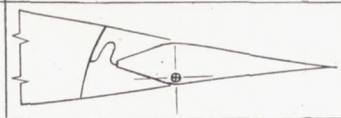	NACA low drag (See fig. C56.)		7.3	0.42	0.509	0.980	0.200	Third-span wing model	None	$R = 2.35 \times 10^6$ $M = 0.11$	
C-XVI	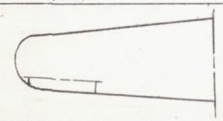	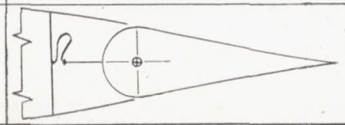	NACA 66(215)-1(16.5), a = 1.0	NACA 67(115)-213, a = 0.7	5.4	0.60	0.54	0.953	0.25 (approx.)	Complete model	None	$R = 0.99 \times 10^6$ $M = 0.11$	
C-XVII[m]	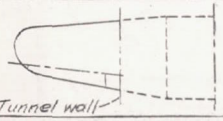	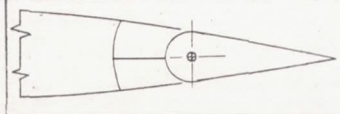	Clark YH modified (19 percent thick)	Clark YH (12.2 percent thick)	6.2	0.49	0.54	0.93	0.18	Quarter-span wing model	Whether corrections were applied not known	$R = 1.1 \times 10^6$ $M = 0.05$	18
C-XVIII[g]	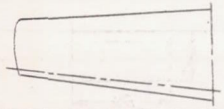	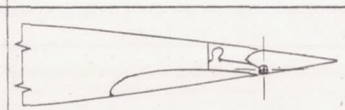	NACA 23015.5 (approx.)	NACA 23008.25 (approx.)	5.6	0.60	0	0.984	0.08	Semispan wing model	None	$R = 2.05 \times 10^6$ $M = 0.11$	19
C-XIX	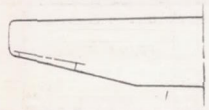	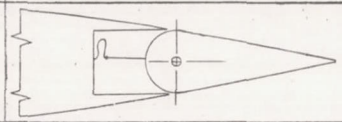	NACA 23017	NACA 23010	6.0	0.55 (tip)	0.585	0.940	0.20	Complete model	None	$R = 0.74 \times 10^6$ $M = 0.092$	
C-XX	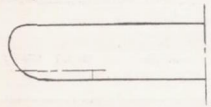	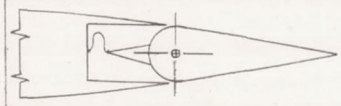	NACA 23012		7.2	1.00	0.56	0.94	0.20	Flight	None	----------	20
C-XXI[k]	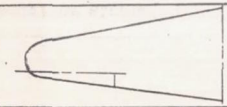	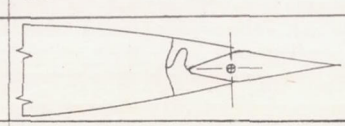	NACA 66,2-118, a = 1.0	NACA 66(2x15)-116, a = 1.0	6.2	0.33	0.485	0.992	0.14 (approx.)	Flight	None	----------	21

[1] All designations that have the same superscript (a,b,c,..., or p) denote models or airplanes having the same wing plan form and the same airfoil section.

TABLE I.- SUPPLEMENTARY INFORMATION REGARDING TESTS OF MODELS AND AIRPLANES HAVING BALANCED AILERONS - Continued

D - AILERONS WITH CONTOUR MODIFICATIONS

NATIONAL ADVISORY
COMMITTEE FOR AERONAUTICS

Model or airplane		Typical aileron section	Airfoil section		A	λ	Aileron location		c_a/c	Type of test	Corrections estimated but not applied	Air-flow characteristics	Published reference
Designation (1)	Plan form of surface		Root	Tip			$\frac{y_i}{b/2}$	$\frac{y_o}{b/2}$					
D-I[j]	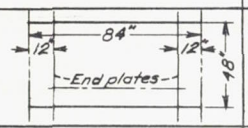	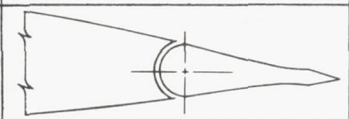	NACA 66(215)-216, a = 0.6		∞	---------	-----	-----	0.20 and 0.15	Two dimensional	None	$R = 3.8 \times 10^6$ to 9.5×10^6 M = 0.14 to 0.34	
D-II	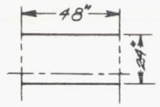	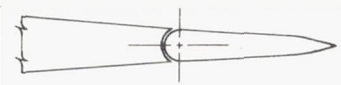	NACA 0009		∞	---------	-----	-----	0.20	Two dimensional	Correction applied only to lift	$R = 1.43 \times 10^6$ M = 0.10	
D-III[a]	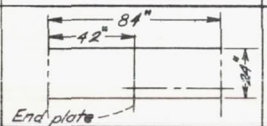	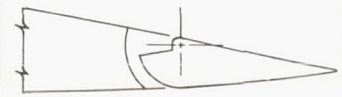	NACA conventional section (approx. 14 percent thick)		∞	---------	-----	-----	0.20	Two dimensional	Undetermined	$R = 1.91 \times 10^6$ M = 0.13	6
D-IV[g]	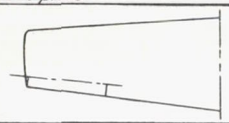	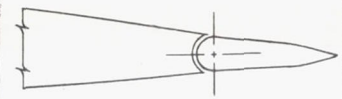	NACA 23015.5 (approx.)	NACA 23008.25 (approx.)	5.6	0.60	0.579	0.984	0.155	Semispan wing model	None	$R = 1.54 \times 10^6$ M = 0.08	22
D-V[c]	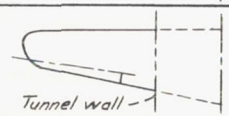	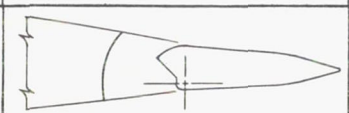	NACA low drag (See fig. D27.)		7.3	0.42	0.509	0.980	0.20	Third-span wing model	None	$R = 2.35 \times 10^6$ M = 0.11	23
D-VI[c]	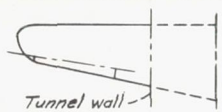	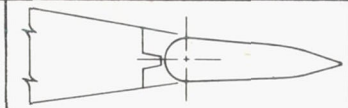	NACA low drag (See fig. D38.)		7.3	0.42	0.509	0.933	0.20	Third-span wing model	None	$R = 2.35 \times 10^6$ M = 0.11	24
D-VII[f]	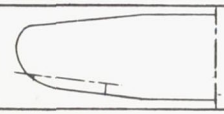		NACA 23018	NACA 23009	5.3	0.67	0.565	0.931	0.20	Full-scale complete model	Correction applied to angle of attack	$R = 6.0 \times 10^6$ M = 0.10	

[1]All designations that have the same superscript (a,b,c,..., or p) denote models or airplanes having the same wing plan form and the same airfoil section.

TABLE I.- SUPPLEMENTARY INFORMATION REGARDING TESTS OF MODELS AND AIRPLANES HAVING BALANCED AILERONS - Continued

D - AILERONS WITH CONTOUR MODIFICATIONS - Concluded

NATIONAL ADVISORY
COMMITTEE FOR AERONAUTICS

Model or airplane		Typical aileron section	Airfoil section		A	λ	Aileron location		c_a/c	Type of test	Corrections estimated but not applied	Air-flow characteristics	Published reference
Designation (1)	Plan form of surface		Root	Tip			$\frac{y_1}{b/2}$	$\frac{y_o}{b/2}$					
D-VIII[h]	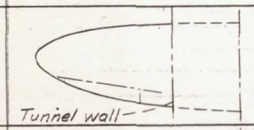	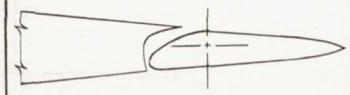	NACA 2213	NACA 2205	5.7	Elliptical wing	0.500	0.868	0.17	Third-span wing model	Whether corrections were applied not known	$R = 1.5 \times 10^6$ $M = 0.05$	25 26 27
D-IX[h]	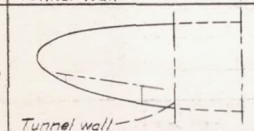	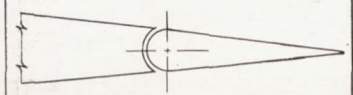	NACA 2213	NACA 2205	5.7	Elliptical wing	0.500	0.868	0.222	Third-span wing model	Whether corrections were applied not known	$R = 1.5 \times 10^6$ $M = 0.05$	28
D-X[m]	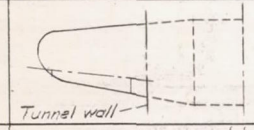	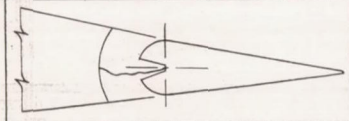	Clark YH modified (19 percent thick)	Clark YH (12.2 percent thick)	6.2	0.49	0.54	0.93 to 1.00	0.18 to 0.26	Quarter-span wing model	Whether corrections were applied not known	$R = 1.2 \times 10^6$ $M = 0.05$	29 30
D-XI[n]	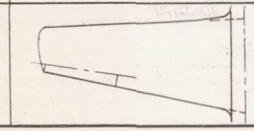	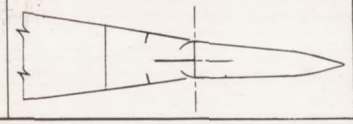	NACA compromise low drag		5.8	0.45	0.61	0.965	0.187	Flight	None	R = full scale $M_{max} = 0.69$	

[1] All designations that have the same superscript (a,b,c,..., or p) denote models of airplanes having the same wing plan form and the same airfoil section.

TABLE I.- SUPPLEMENTARY INFORMATION REGARDING TESTS OF MODELS AND AIRPLANES HAVING BALANCED AILERONS - Continued

E - AILERONS WITH TABS

NATIONAL ADVISORY
COMMITTEE FOR AERONAUTICS

Model or airplane		Typical aileron section	Airfoil section		A	λ	Aileron location		c_a/c	Type of test	Corrections estimated but not applied	Air-flow characteristics	Published reference
Designation (1)	Plan form of surface		Root	Tip			$\frac{y_1}{b/2}$	$\frac{y_o}{b/2}$					
E-I[j]	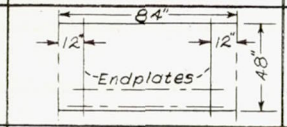	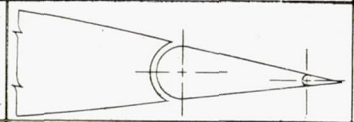	NACA 66(215)-216, a = 0.6		∞	---------	-----	-----	0.20	Two dimensional	None	$R = 6.7 \times 10^6$ to 9.0×10^6 M = 0.24 to 0.34	
E-II	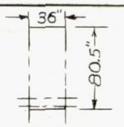	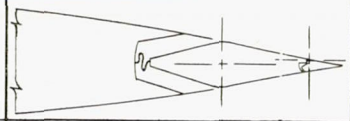	NACA 66,2-118, a = 1.0 (approx.)		∞	---------	-----	-----	0.1475	Two dimensional	None	$R = 9.6 \times 10^6$ M = 0.202	
E-III[p]	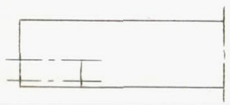	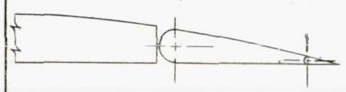	Clark Y		6.0	1.00	0.70	1.00	0.40	Full-span wing model	None	$R = 0.6 \times 10^6$ M = 0.11	31
E-IV[p]	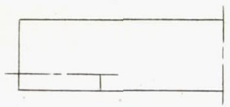		Clark Y		6.0	1.00	0.60	1.00	0.25	Full-span wing model	None	$R = 0.6 \times 10^6$ M = 0.11	31
E-V[g]	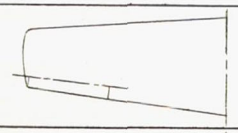	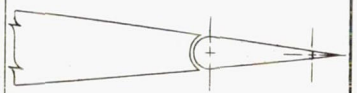	NACA 23015.5	NACA 23008.25	5.6	0.60	0.579	0.984	0.155	Semispan wing model	None	$R = 1.5 \times 10^6$ M = 0.08	32
E-VI[k]	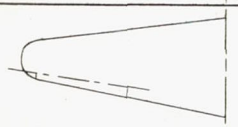	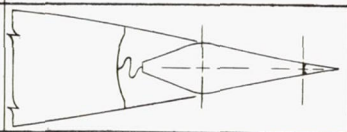	NACA 66,2-118, a = 1.0	NACA 66(2x15)-116, a = 1.0	6.2	0.33	0.490 0.490	0.894 0.940	0.149 0.162	Semispan wing model	$C_l'_c = 0.90C_l$ $C_{n'_c} = C_{n'} - 0.031C_l'C_L$	$R = 1.9 \times 10^6$ M = 0.11	16
E-VII[c]	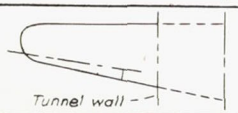	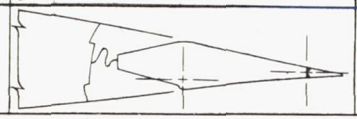	NACA low drag (See fig. E23.)		7.3	0.42	0.509	0.980	0.20	Third-span wing model	None	$R = 2.4 \times 10^6$ M = 0.11	

[1]All designations that have the same superscript (a,b,c,..., or p) denote models or airplanes having the same wing plan form and the same airfoil section.

TABLE I.- SUPPLEMENTARY INFORMATION REGARDING TESTS OF MODELS AND AIRPLANES HAVING BALANCED AILERONS - Concluded

E - AILERONS WITH TABS - Concluded

Model or airplane: Designation (1)	Plan form of surface	Typical aileron section	Airfoil section: Root	Airfoil section: Tip	A	λ	Aileron location: $y_1/(b/2)$	Aileron location: $y_o/(b/2)$	c_a/c	Type of test	Corrections estimated but not applied	Air-flow characteristics	Published reference
E-VIII[c]	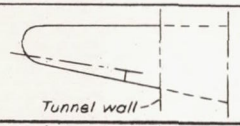	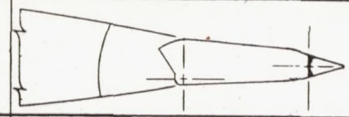	NACA low drag (See fig. E28.)		7.3	0.42	0.509	0.980	0.20	Third-span wing model	None	$R = 2.4 \times 10^6$ $M = 0.11$	23
E-IX[c]	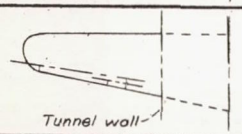	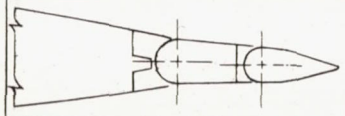	NACA low drag (See fig. E33.)		7.3	0.42	0.509	0.935	0.20	Third-span wing model	None	$R = 2.4 \times 10^6$ $M = 0.11$	24
E-X	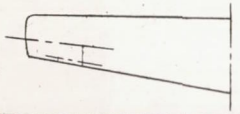	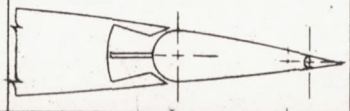	----------	----------	7.0 (approx.)	0.54 (approx.)	0.72	0.99 (approx.)	0.40	Semispan wing model	No corrections applied	$R \approx 0.6 \times 10^6$ $M = 0.06$	33
E-XI[h]	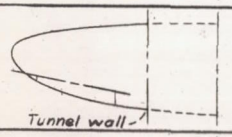	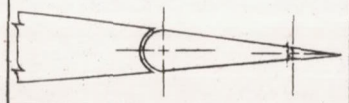	NACA 2213	NACA 2205	5.7	Elliptical wing	0.50	0.868	0.222 (approx.)	Third-span wing model	Probably no corrections applied	$R = 1.3 \times 10^6$ $M = 0.06$	28
E-XII[h]	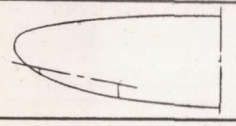	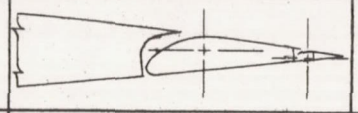	NACA 2213	NACA 2205	5.7	Elliptical wing	0.5	0.868	0.17 (approx.)	Flight	None	----------	34
E-XIII[n]	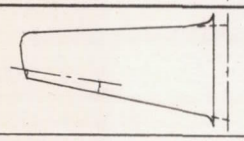	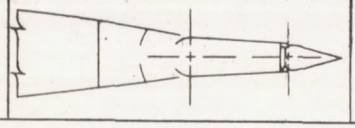	NACA compromise low drag		5.8	0.45	0.61	0.965	0.187	Flight	None	----------	

[1]All designations that have the same superscript (a,b,c,..., or p) denote models or airplanes having the same wing plan form and the same airfoil section.

TABLE I.- SUPPLEMENTARY INFORMATION REGARDING TESTS OF MODELS AND AIRPLANES HAVING BALANCED AILERONS

[Designations of low-drag airfoils, regardless of the form in which they appear in the other references, are changed throughout to the form described on p.21a of reference 4]

A - AILERONS WITH FRISE BALANCES

NATIONAL ADVISORY COMMITTEE FOR AERONAUTICS

Model or airplane: Designation (1)	Model or airplane: Plan form of surface	Typical aileron section	Airfoil section: Root	Airfoil section: Tip	A	λ	Aileron location: $\frac{y_1}{b/2}$	Aileron location: $\frac{y_o}{b/2}$	c_a/c	Type of test	Corrections estimated but not applied	Air-flow characteristics	Published reference
A-I	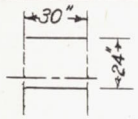		NACA 23012		∞	----	-----	-----	0.20	Two dimensional	$\Delta c_{l_c} = 1.035 \Delta c_l$	$R = 2.8 \times 10^6$ to 6.8×10^6 $M = 0.20$ to 0.48	5
A-II	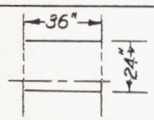	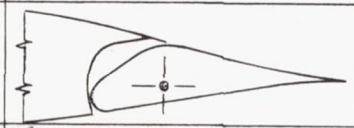	NACA low drag (See fig. A8.)		∞	----	-----	-----	0.224	Two dimensional	None	$R = 6.0 \times 10^6$ $M = 0.14$	
A-III[a]	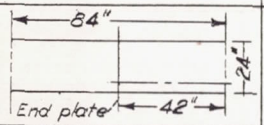	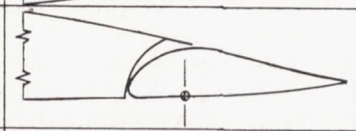	NACA conventional (approx. 14 percent thick)		∞	----	-----	-----	0.20	Two dimensional	End-plate effects uncertain	$R = 1.91 \times 10^6$ $M = 0.13$	6
A-IV[b]	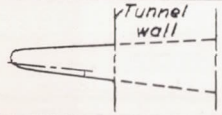	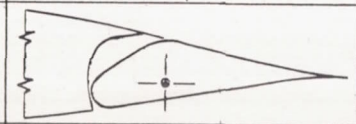	NACA 65(223)-222, a = 1.0	NACA 65(216)-415, a = 0.5	12.0	0.32	0.641	0.945	0.23	Quarter-span wing model	None	$R = 1.99 \times 10^6$ $M = 0.11$	
A-V[c]	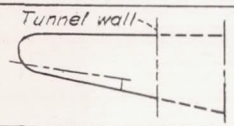	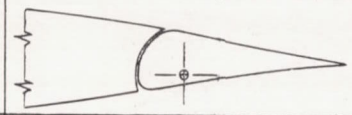	NACA low drag (See fig. A18.)		7.3	0.42	0.509	0.980	0.20	Third-span wing model	None	$R = 2.35 \times 10^6$ $M = 0.11$	
A-VI[d]	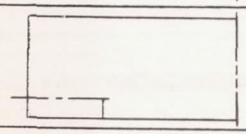	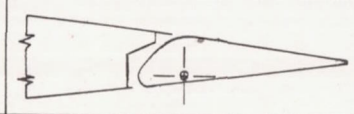	NACA 23012		4.0	1.00	0.63	1.000	0.20	Semispan wing model	$C_l'_c = 0.86 C_l'$ $C_{n'_c} = C_{n'} - 0.045 C_l' C_L$	$R = 1.44 \times 10^6$ and 2.88×10^6 $M = 0.05$ and 0.11	7
A-VII[e]	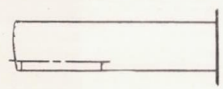	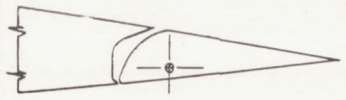	Davis (16 percent thick)		8.1	1.00	0.565	0.976	0.21	Semispan wing model	End-plate effects uncertain	$R = 2.25 \times 10^6$ $M = 0.16$	

[1] All designations that have the same superscript (a,b,c,..., or p) denote models or airplanes having the same wing plan form and the same airfoil section.

TABLE I.- SUPPLEMENTARY INFORMATION REGARDING TESTS OF MODELS AND AIRPLANES HAVING BALANCED AILERONS - Continued

A - AILERONS WITH FRISE BALANCES - Continued

NATIONAL ADVISORY COMMITTEE FOR AERONAUTICS

Model or airplane		Typical aileron section	Airfoil section		A	λ	Aileron location		c_a/c	Type of test	Corrections estimated but not applied	Air-flow characteristics	Published reference
Designation (1)	Plan form of surface		Root	Tip			$\frac{y_1}{b/2}$	$\frac{y_o}{b/2}$					
A-VIII	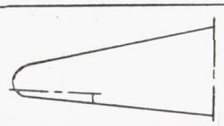	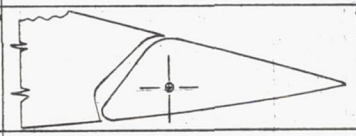	Unknown	NACA 4415	6.8 (approx.)	0.30 (approx.)	0.594	0.978	0.22	Complete model	Whether corrections were applied not known	Unknown	8
A-IX	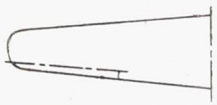	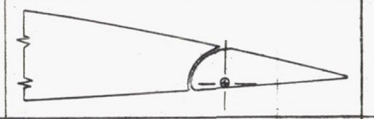	NACA 2418	NACA 4409	8	0.5	0.459	0.931	0.15	Complete model	None	$R = 0.75 \times 10^6$ $M = 0.11$	
A-X	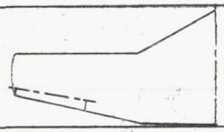	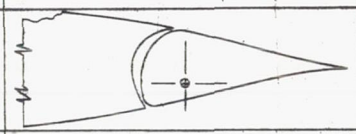	NACA 67(115)-1(14.5)		6.2	0.46 (tip)	0.651	1.00	0.20	Complete model	None	$R = 6.38 \times 10^6$ $M = 0.13$	
A-XI[f]	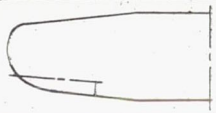	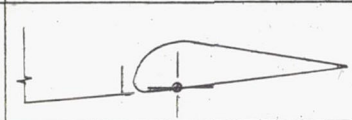	NACA 23018	NACA 23009	5.3	0.67	0.565	0.931	0.20 (approx.)	Complete model	None	$R = 2.74 \times 10^6$	
A-XII[f]			NACA 23018	NACA 23009	5.3	0.67	0.66	0.95	0.20 (approx.)	Flight	None	----------	
A-XIII	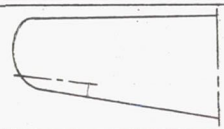	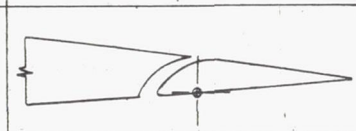	Conventional		4.93	0.66	0.64	0.96	0.19 (approx.)	Flight	None	----------	
A-XIV[g]	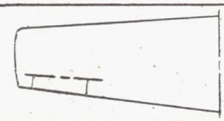	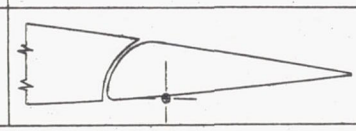	NACA 23015.5 (approx.)	NACA 23008.25 (approx.)	5.6	0.60	0.655	0.925	0.228	Flight	None	----------	9

[1]All designations that have the same superscript (a,b,c,..., or p) denote models or airplanes having the same wing plan form and the same airfoil section.

TABLE I.- SUPPLEMENTARY INFORMATION REGARDING TESTS OF MODELS AND AIRPLANES HAVING BALANCED AILERONS - Continued

NATIONAL ADVISORY COMMITTEE FOR AERONAUTICS

A - AILERONS WITH FRISE BALANCES - Concluded

Model or airplane		Typical aileron section	Airfoil section		A	λ	Aileron location		c_a/c	Type of test	Corrections estimated but not applied	Air-flow characteristics	Published reference
Designation (1)	Plan form of surface		Root	Tip			$\frac{y_1}{b/2}$	$\frac{y_o}{b/2}$					
A-XV	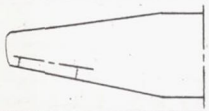	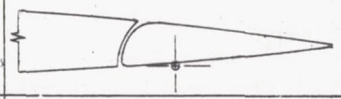	NACA 23015	NACA 23009	6.0	0.38	0.681	0.957	0.198	Flight	None	----------	
A-XVI	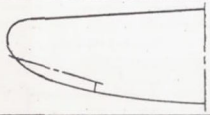		----------	----------	5.5	---------	0.54	0.94	0.17 (approx.)	Flight	None	----------	
A-XVII	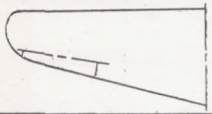		NACA 2215	NACA 2209	5.9	0.40	0.569	0.933	0.20 (approx.)	Flight	None	----------	
A-XVIII[h]	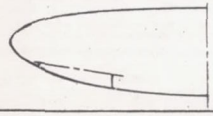	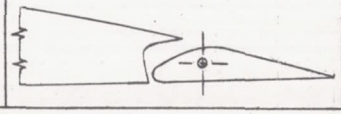	NACA 2213	NACA 2205	5.6	Elliptical wing	0.500	0.868	0.17 (approx.)	Flight	None	----------	10

[1]All designations that have the same superscript (a,b,c,..., or p) denote models or airplanes having the same wing plan form and the same airfoil section.

TABLE I.- SUPPLEMENTARY INFORMATION REGARDING TESTS OF MODELS AND AIRPLANES HAVING BALANCED AILERONS - Continued

B - AILERONS WITH BLUNT-NOSE BALANCES

Model or airplane		Typical aileron section	Airfoil section		A	λ	Aileron location		c_a/c	Type of test	Corrections estimated but not applied	Air-flow characteristics	Published reference
Designation (1)	Plan form of surface		Root	Tip			$\frac{y_1}{b/2}$	$\frac{y_o}{b/2}$					
B-I	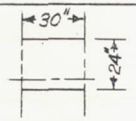	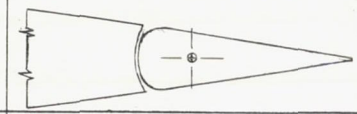	NACA 23012		∞	---------	-----	-----	0.20	Two dimensional	$\Delta c_{l_c} = 1.035\Delta c_l$	$R = 2.8 \times 10^6$ to 6.8×10^6 $M = 0.20$ to 0.48	11
B-II	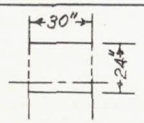	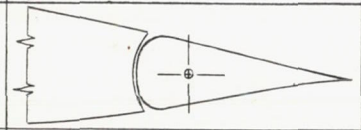	NACA 66(215)-216, a = 1.0		∞	---------	-----	-----	0.20	Two dimensional	$\Delta c_{l_c} = 1.039\Delta c_l$	$R = 2.8 \times 10^6$ to 6.8×10^6 $M = 0.20$ to 0.48	12
B-III[g]	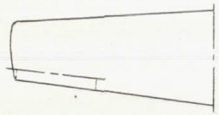	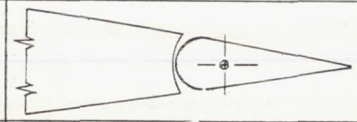	NACA 23015.5 (approx.)	NACA 23008.25 (approx.)	5.6	0.60	0.579	0.984	0.155	Semispan wing model	None	$R = 1.54 \times 10^6$ $M = 0.08$	13
B-IV[b]	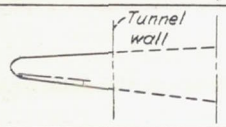	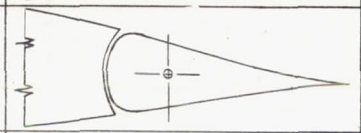	NACA 65(223)-222, a = 1.0	NACA 65(216)-415, a = 0.5	12.0	0.32	0.641	0.945	0.23	Quarter-span wing model	None	$R = 1.99 \times 10^6$ $M = 0.11$	
B-V	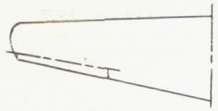	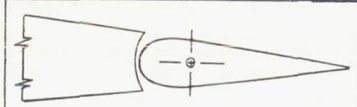	NACA 23015	NACA 4412	7.2	0.42	0.500	0.960	0.195 and 0.206	Complete model	$C_l'_c = 0.97C_l'$ $C_n'_c = C_n' - 0.02C_l'C_L$	$R = 0.8 \times 10^6$ $M = 0.11$	

[1] All designations that have the same superscript (a,b,c,..., or p) denote models or airplanes having the same wing plan form and the same airfoil section.

NATIONAL ADVISORY
COMMITTEE FOR AERONAUTICS

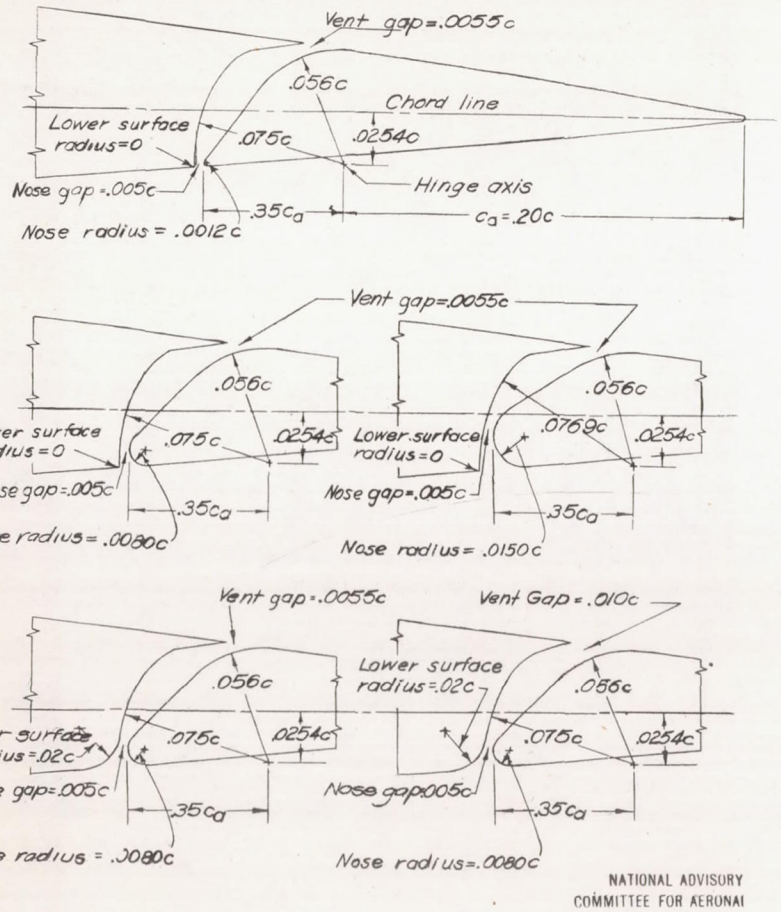

Figure A1.- The various Frise ailerons tested on an NACA 23012 airfoil section in two-dimensional flow. NACA stability tunnel.

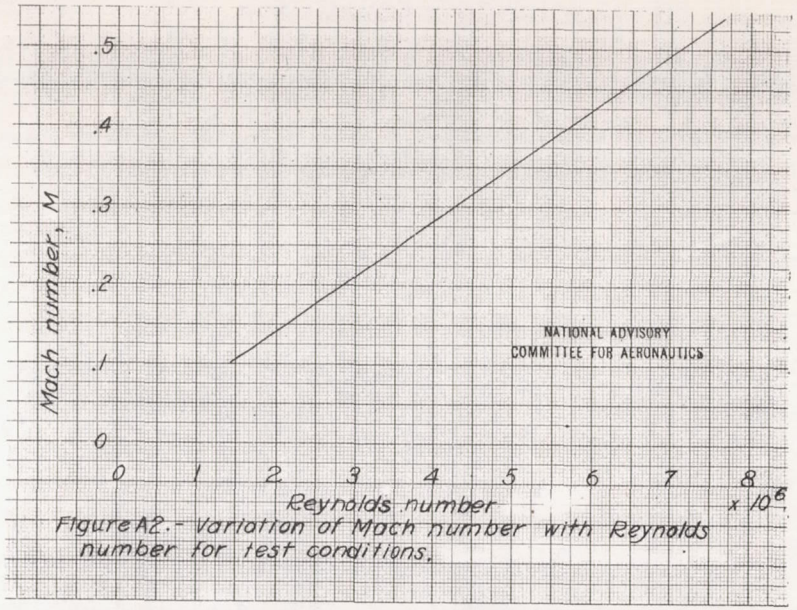

Figure A2.- Variation of Mach number with Reynolds number for test conditions.

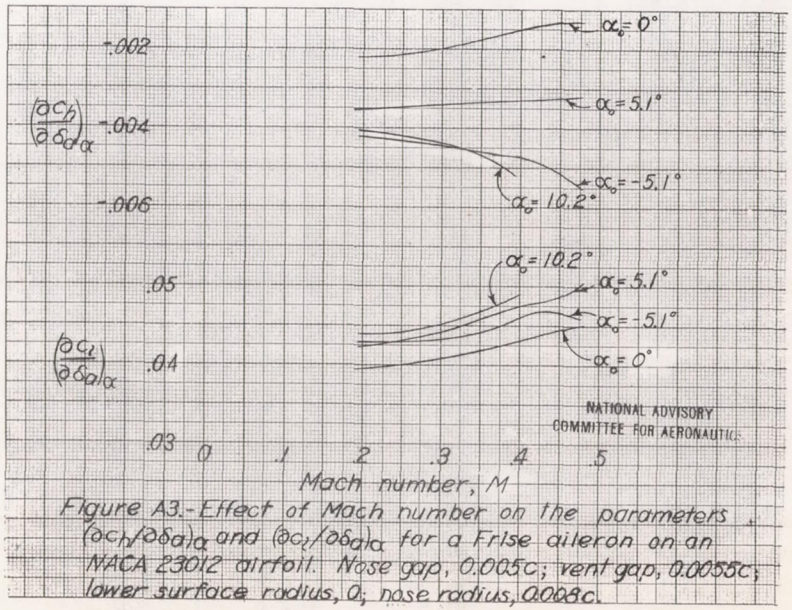

Figure A3.- Effect of Mach number on the parameters $(\partial c_h/\partial \delta_a)_\alpha$ and $(\partial c_l/\partial \delta_a)_\alpha$ for a Frise aileron on an NACA 23012 airfoil. Nose gap, 0.005c; vent gap, 0.0055c; lower surface radius, 0; nose radius, 0.008c.

Model A-1

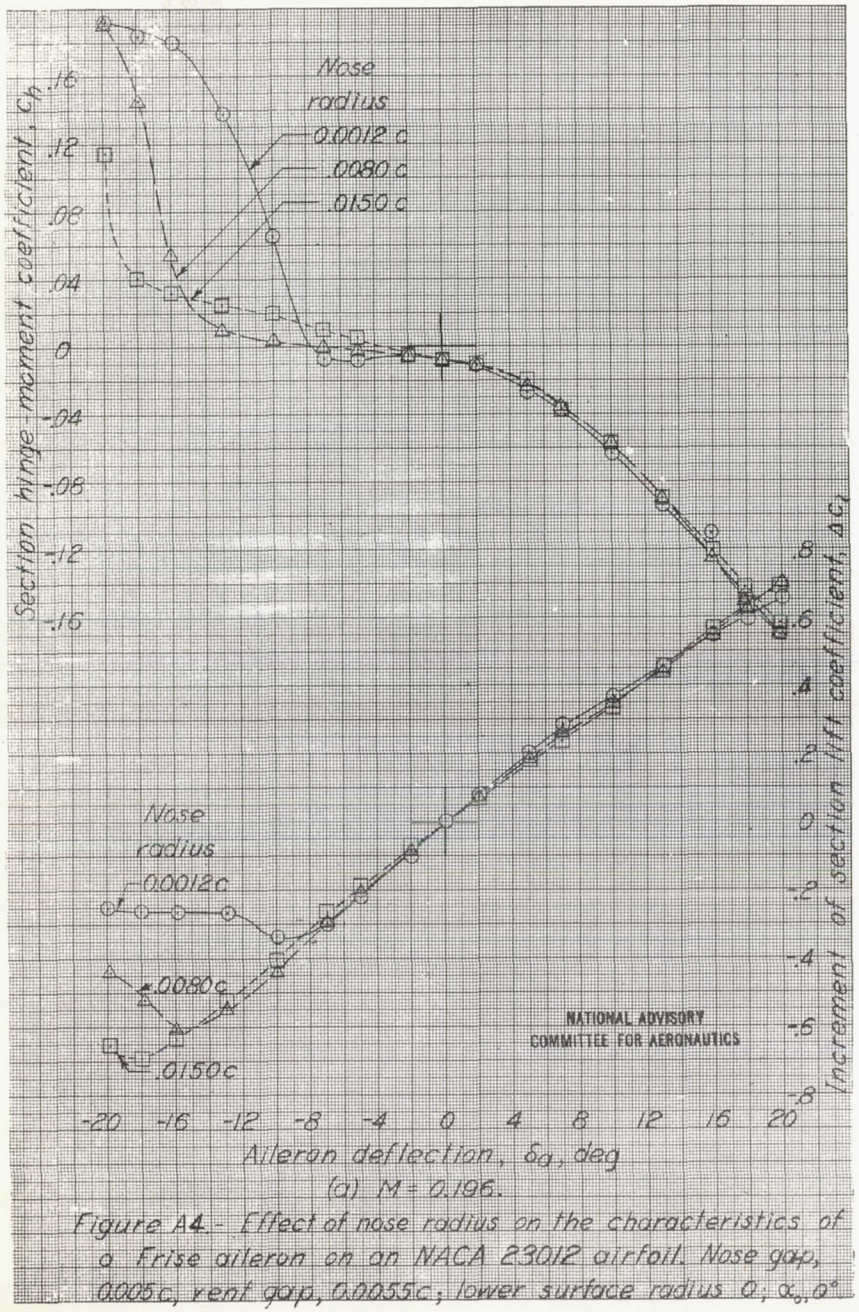

(a) M = 0.196.

Figure A4.- Effect of nose radius on the characteristics of a Frise aileron on an NACA 23012 airfoil. Nose gap, 0.005c, vent gap, 0.0055c, lower surface radius 0; α_a, 0°.

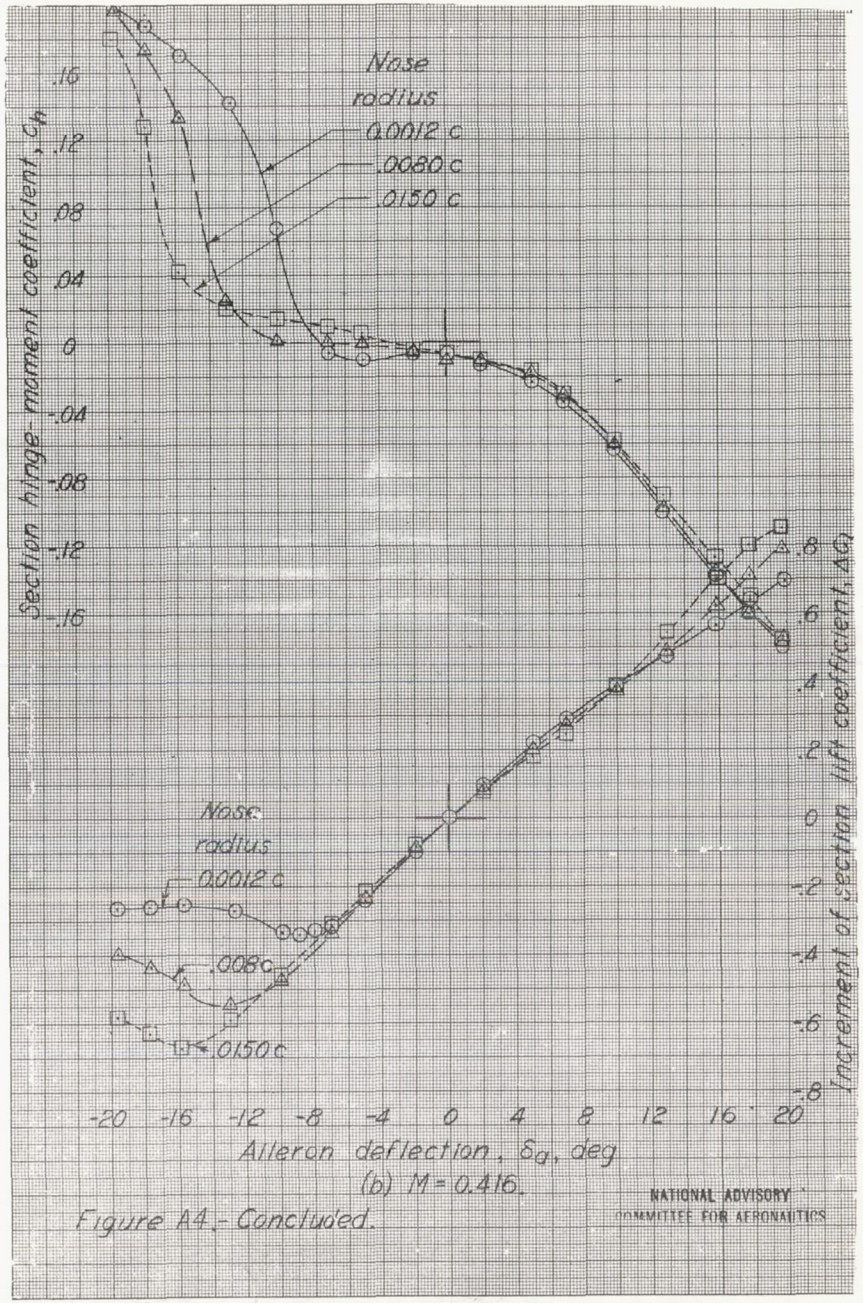

(b) M = 0.416.

Figure A4.- Concluded.

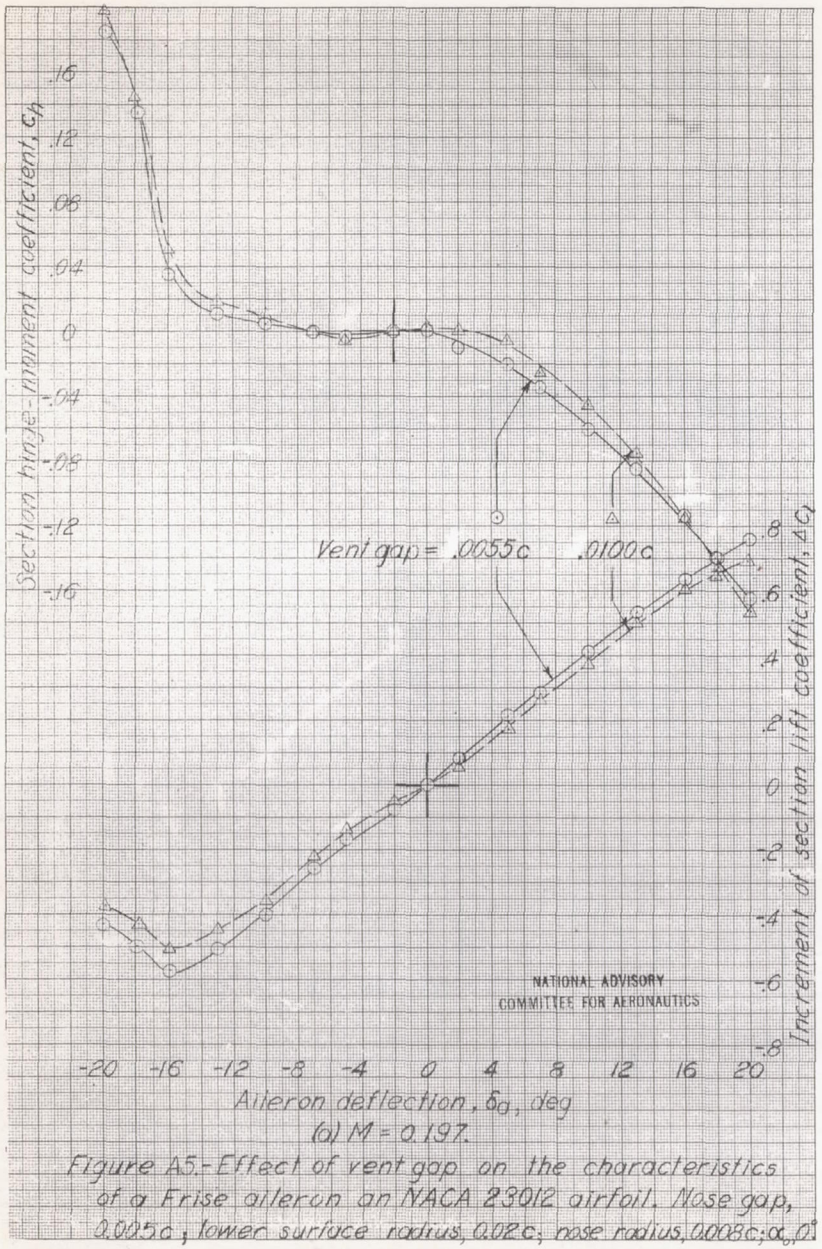

(a) M = 0.197.

Figure A5.- Effect of vent gap on the characteristics of a Frise aileron on NACA 23012 airfoil. Nose gap, 0.005c; lower surface radius, 0.02c; nose radius, 0.008c; α_a, 0°

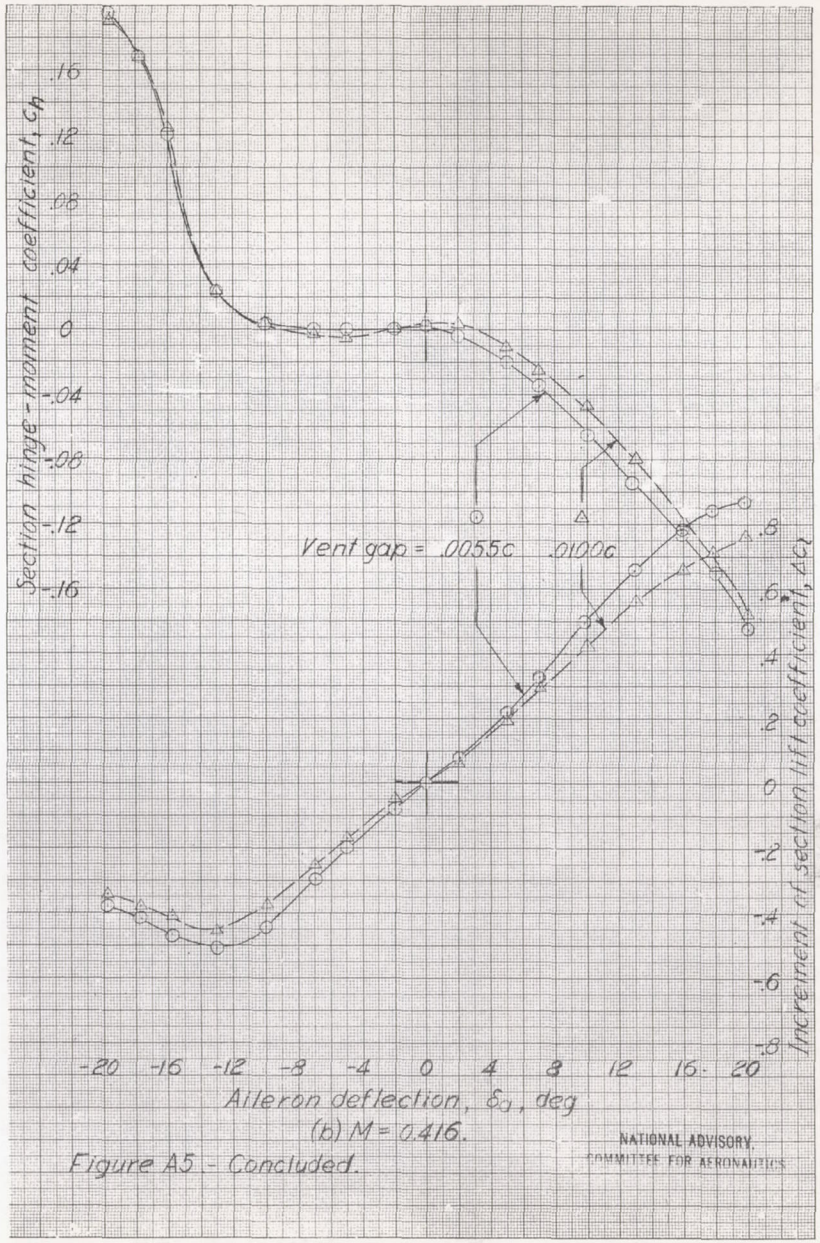

(b) M = 0.416.

Figure A5 - Concluded.

Model A-I

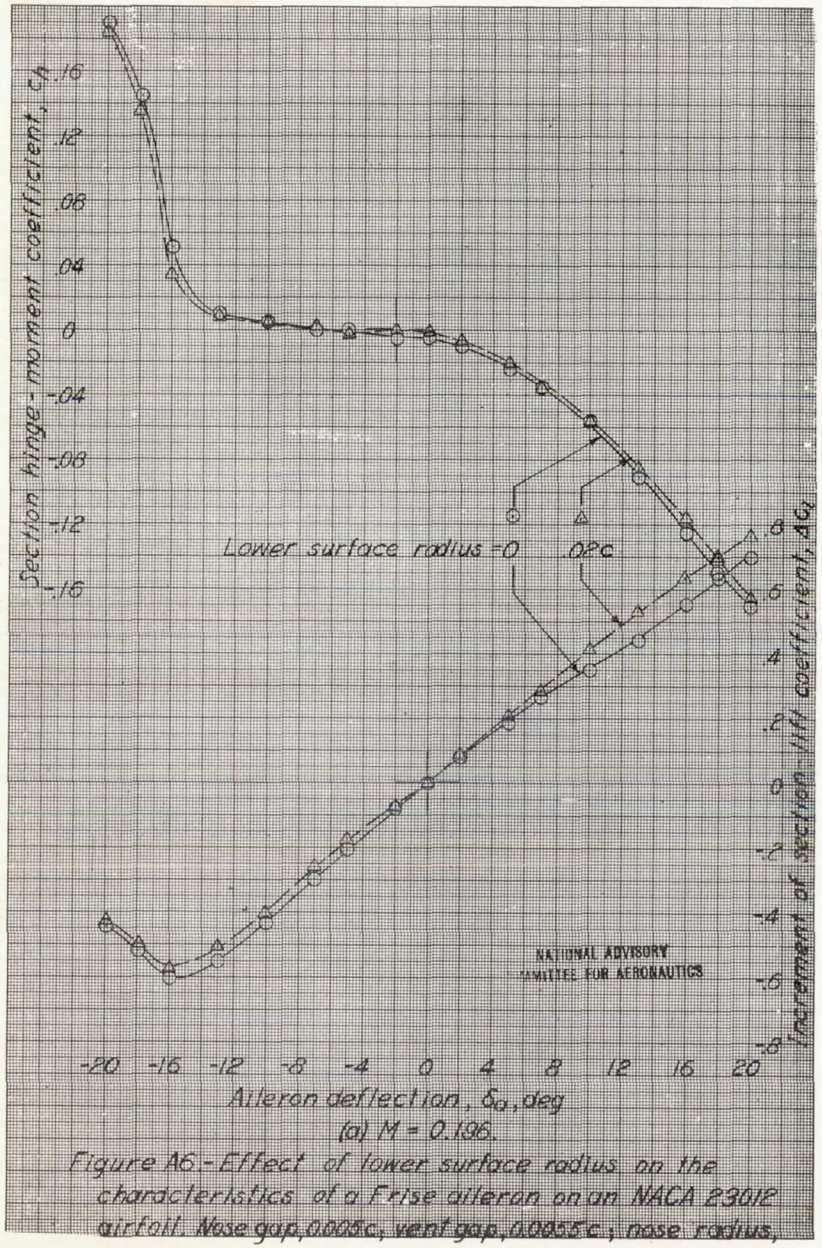

(a) M = 0.196.

Figure A6.- Effect of lower surface radius on the characteristics of a Frise aileron on an NACA 23012 airfoil. Nose gap, 0.005c; vent gap, 0.005c; nose radius, 0.008c; α_o, 0°.

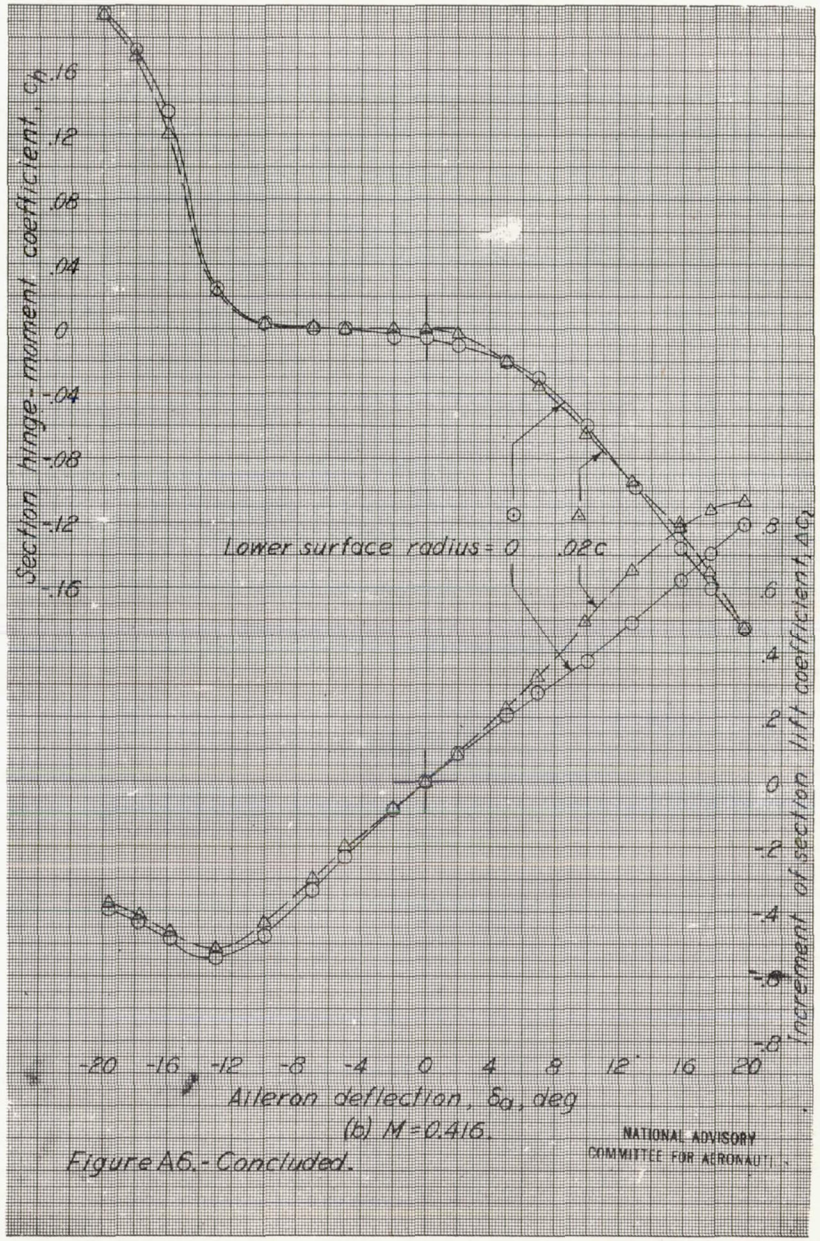

(b) M = 0.416.

Figure A6.- Concluded.

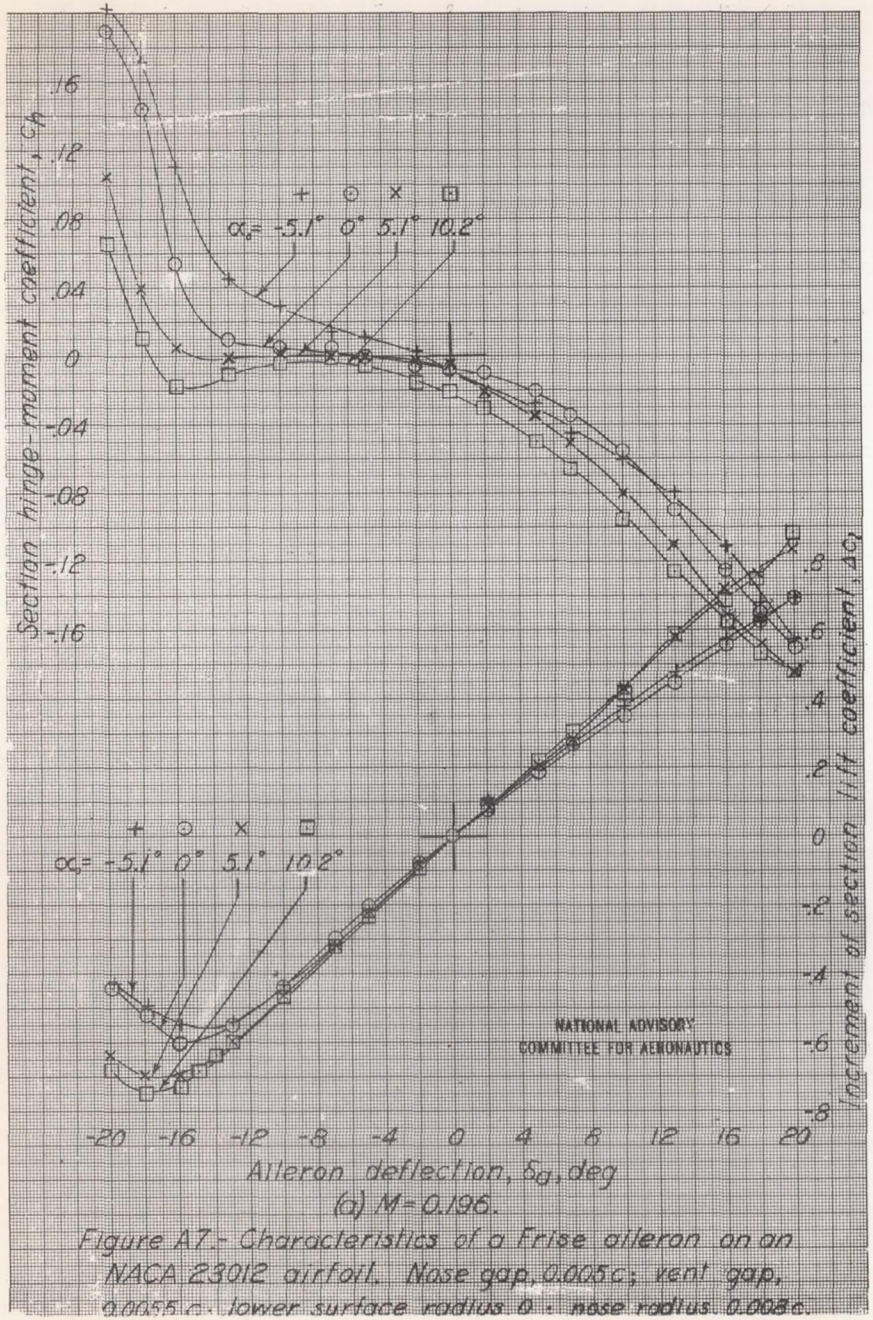

(a) M = 0.196.

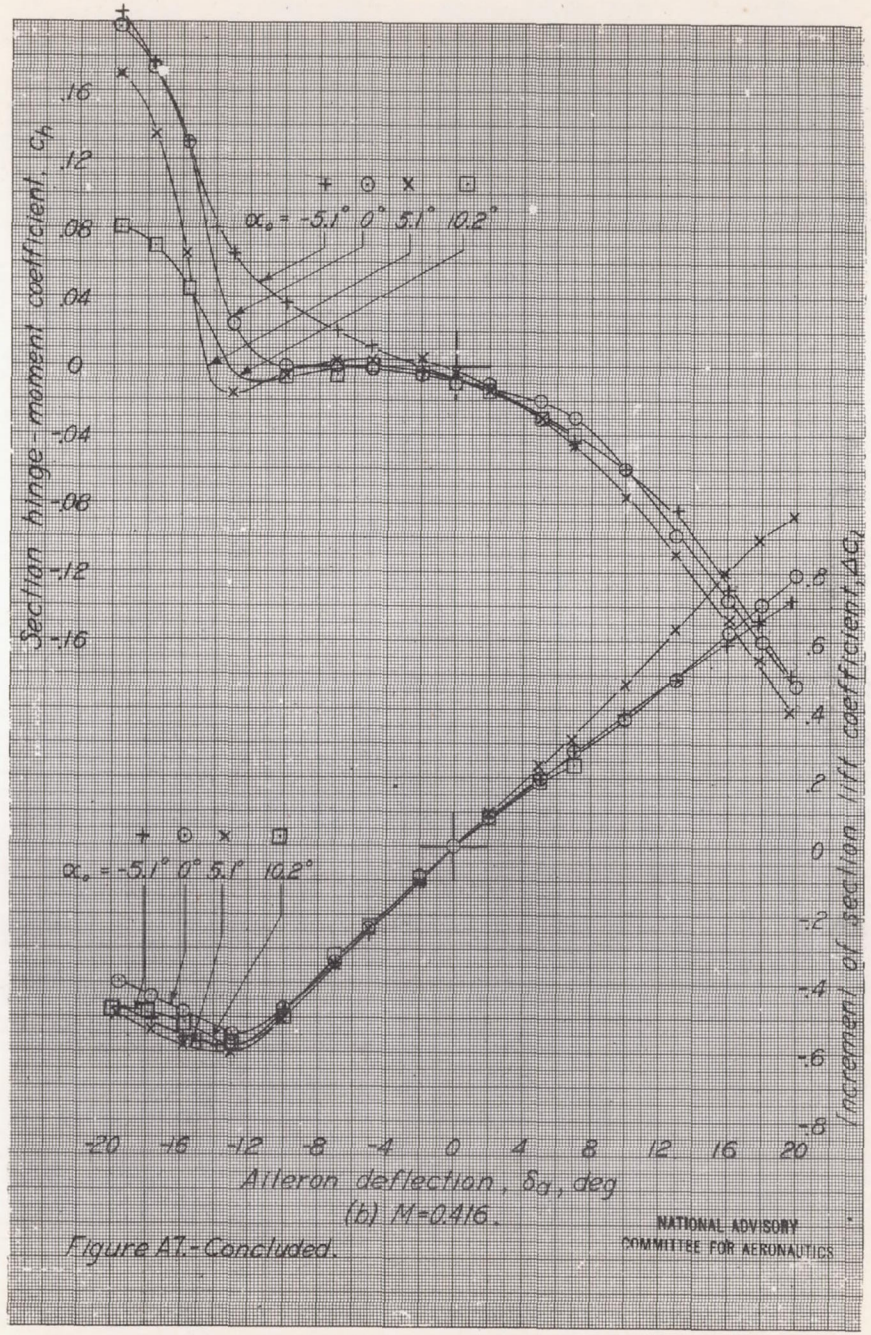

(b) M = 0.416.

Figure A7.- Characteristics of a Frise aileron on an NACA 23012 airfoil. Nose gap, 0.005c; vent gap, 0.0055c; lower surface radius 0; nose radius 0.008c.

Figure A7.- Concluded.

Model A-I

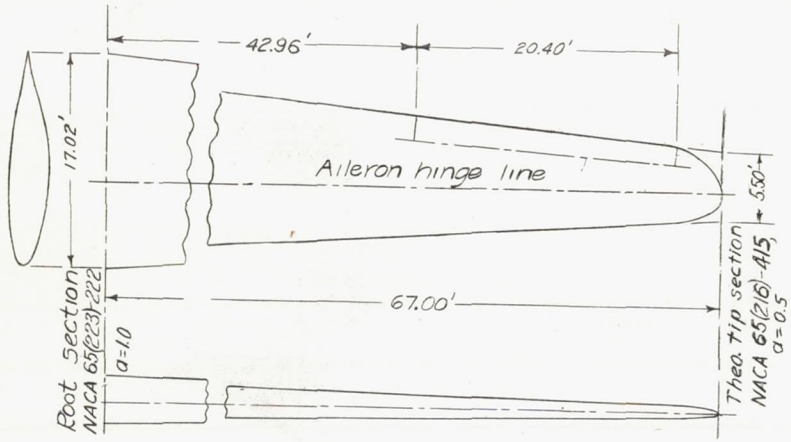

Figure A8.- Plan form of a low-drag wing equipped with Frise ailerons.

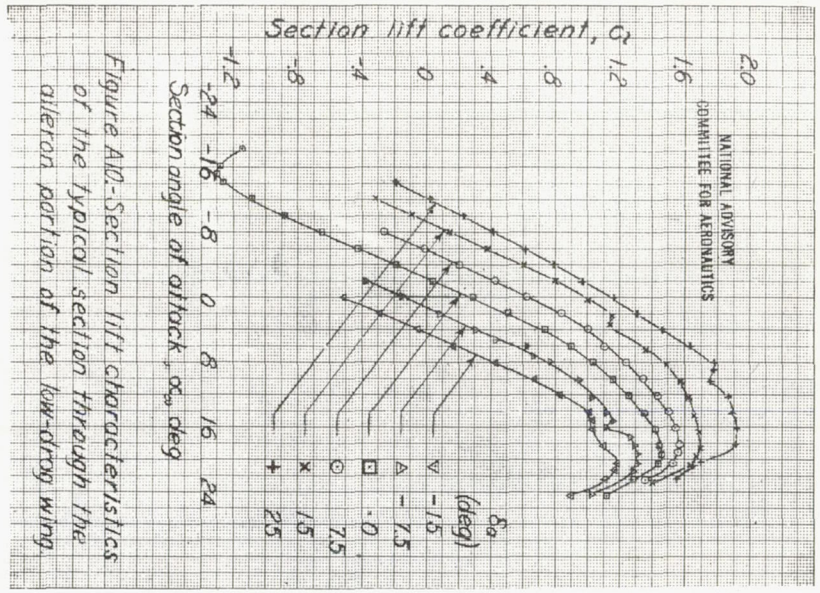

Figure A10.- Section lift characteristics of the typical section through the aileron portion of the low-drag wing.

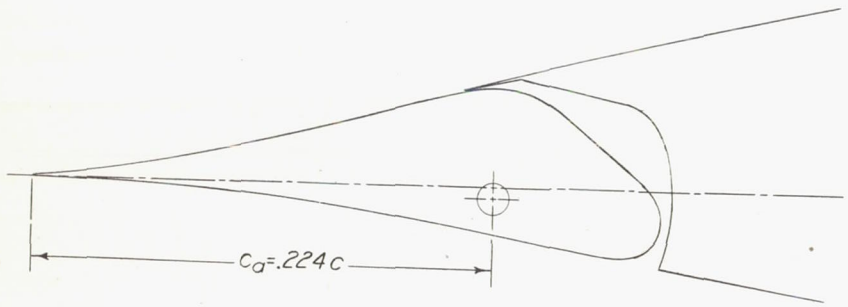

Figure A9.- Typical section through the aileron portion of the low-drag wing tested in two-dimensional low-turbulence pressure tunnel.

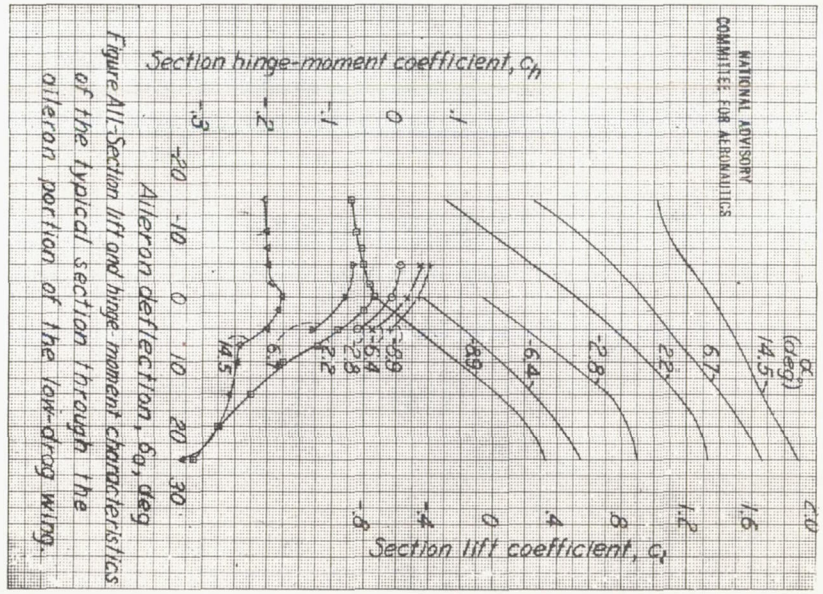

Figure A11.- Section lift and hinge-moment characteristics of the typical section through the aileron portion of the low-drag wing.

Model A-II

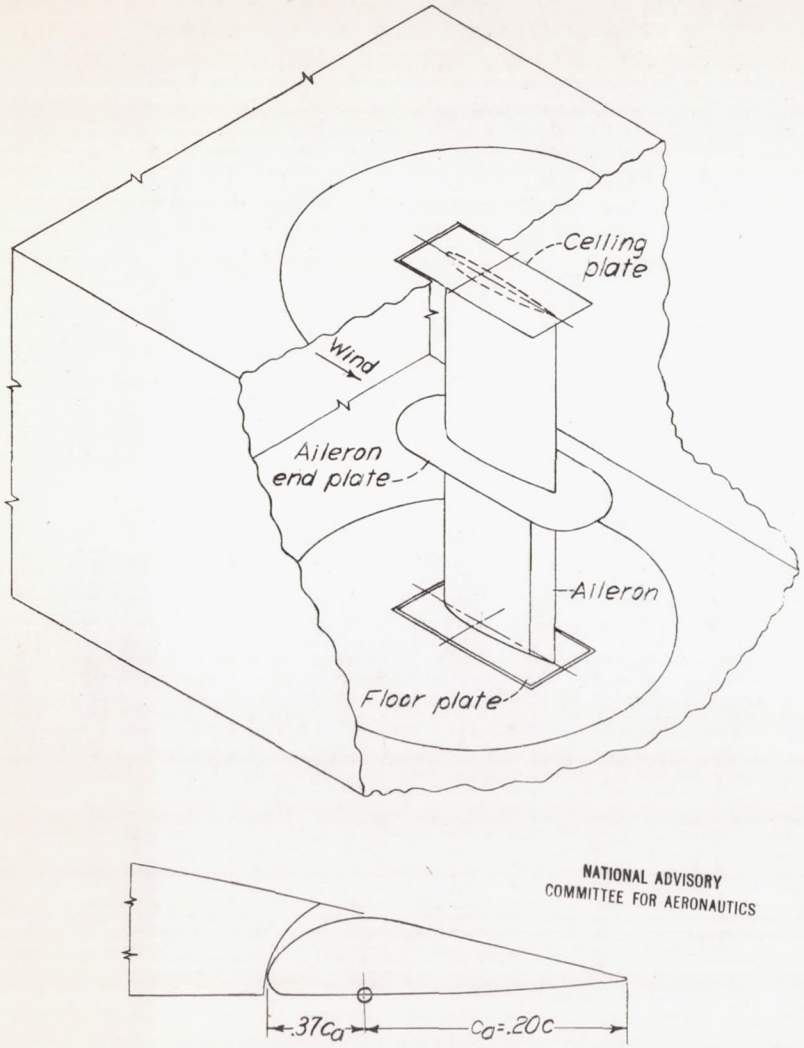

Figure A12.- Two-dimensional test installation and profile of Frise aileron. AAL 7-by 10-foot tunnel.

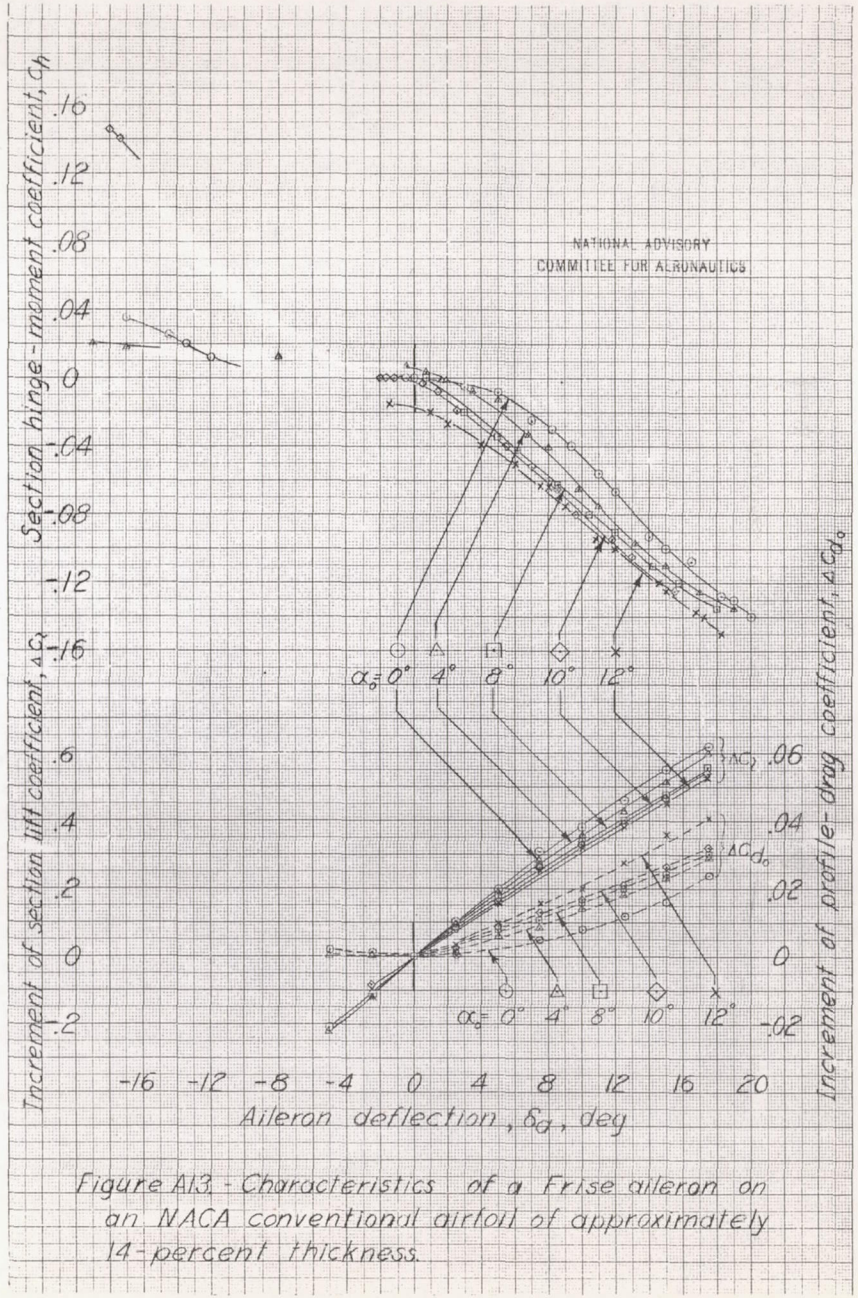

Figure A13.- Characteristics of a Frise aileron on an NACA conventional airfoil of approximately 14-percent thickness.

Model A-III

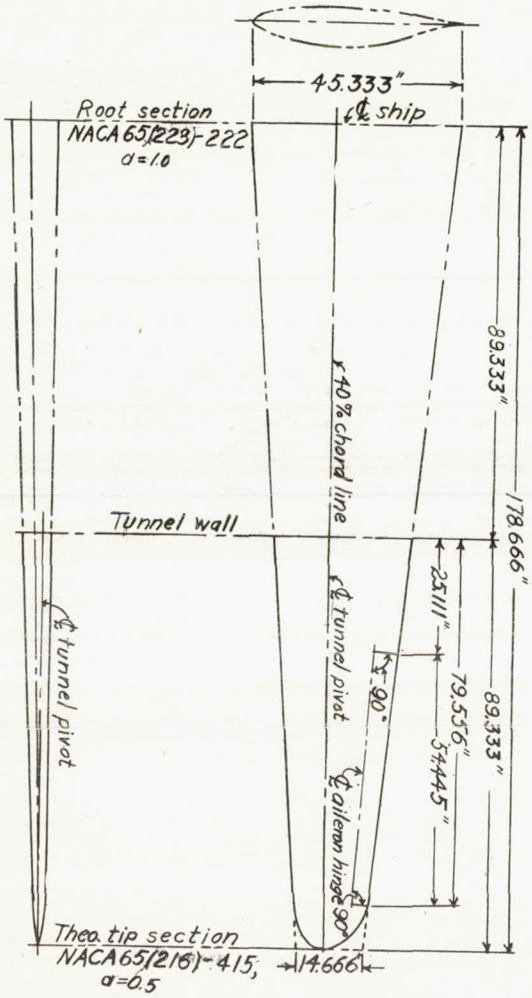

Figure A14.- The 1/4.5-scale model of a tapered low-drag wing. LMAL 7-by 10-foot tunnel.

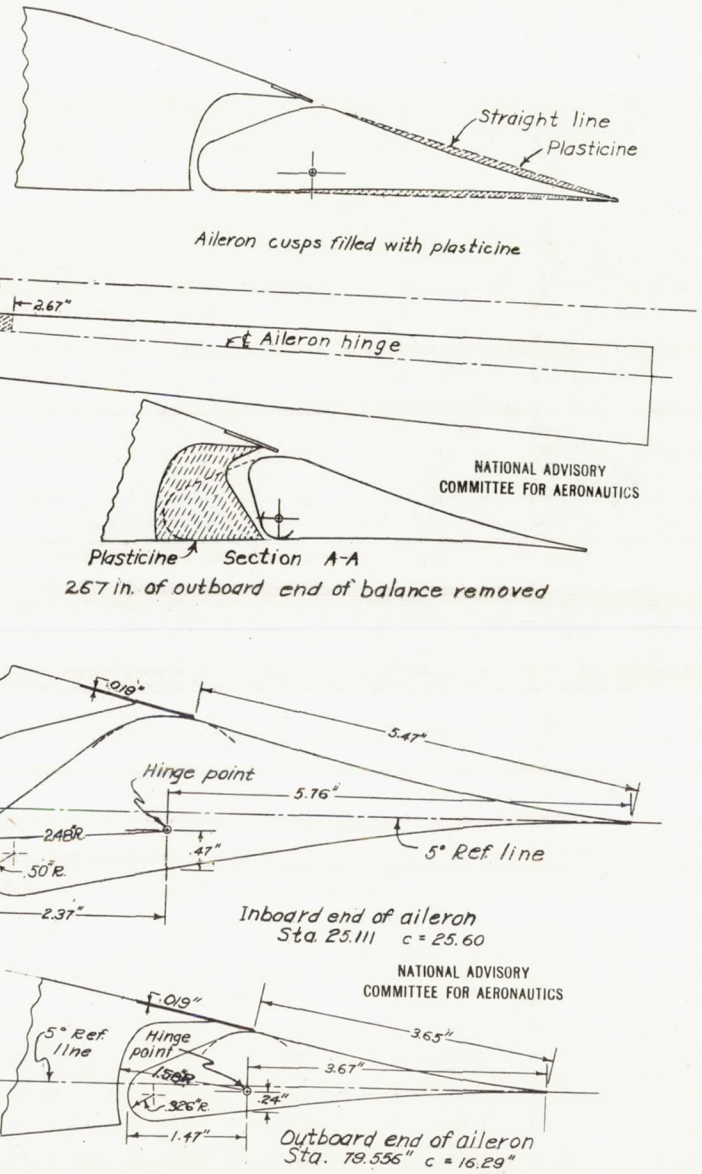

Figure A15.- The Frise ailerons tested on the 1/4.5-scale model of a tapered low-drag wing.

Model A-IV

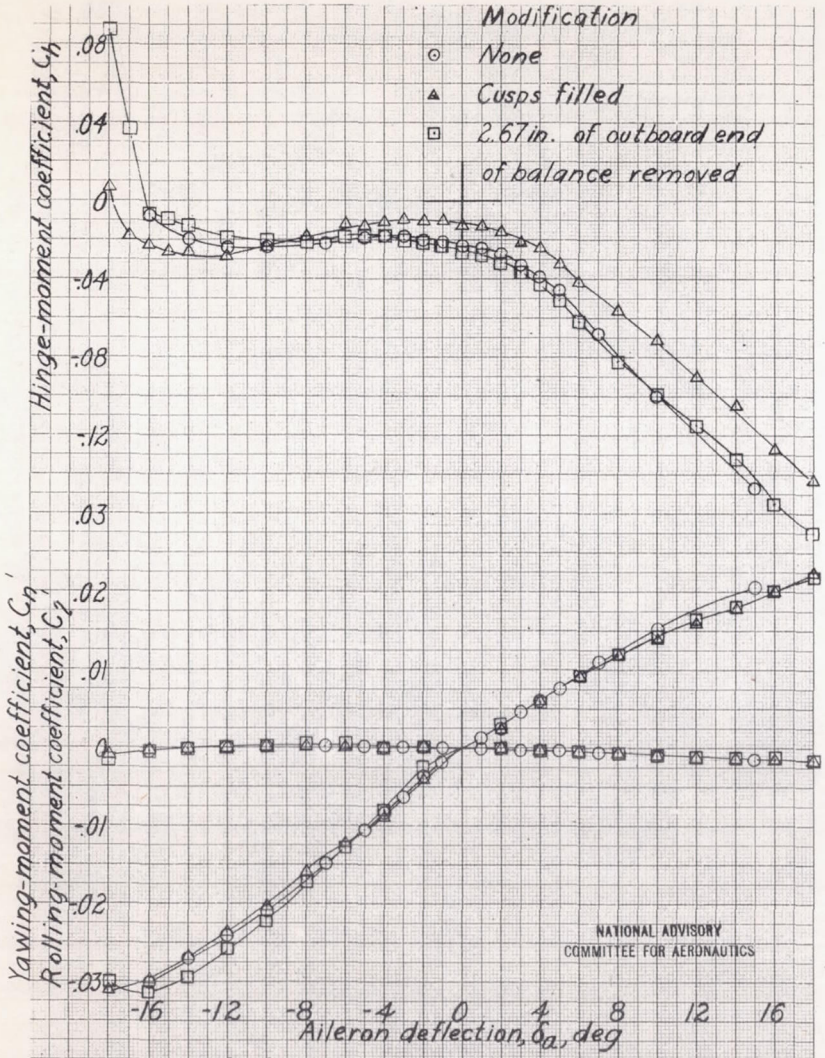

Figure A16.- Effect of modifications on aerodynamic characteristics of a Frise aileron on the 1/4.5-scale model of a tapered low-drag wing. α, 6.6°; C_L, 0.665.

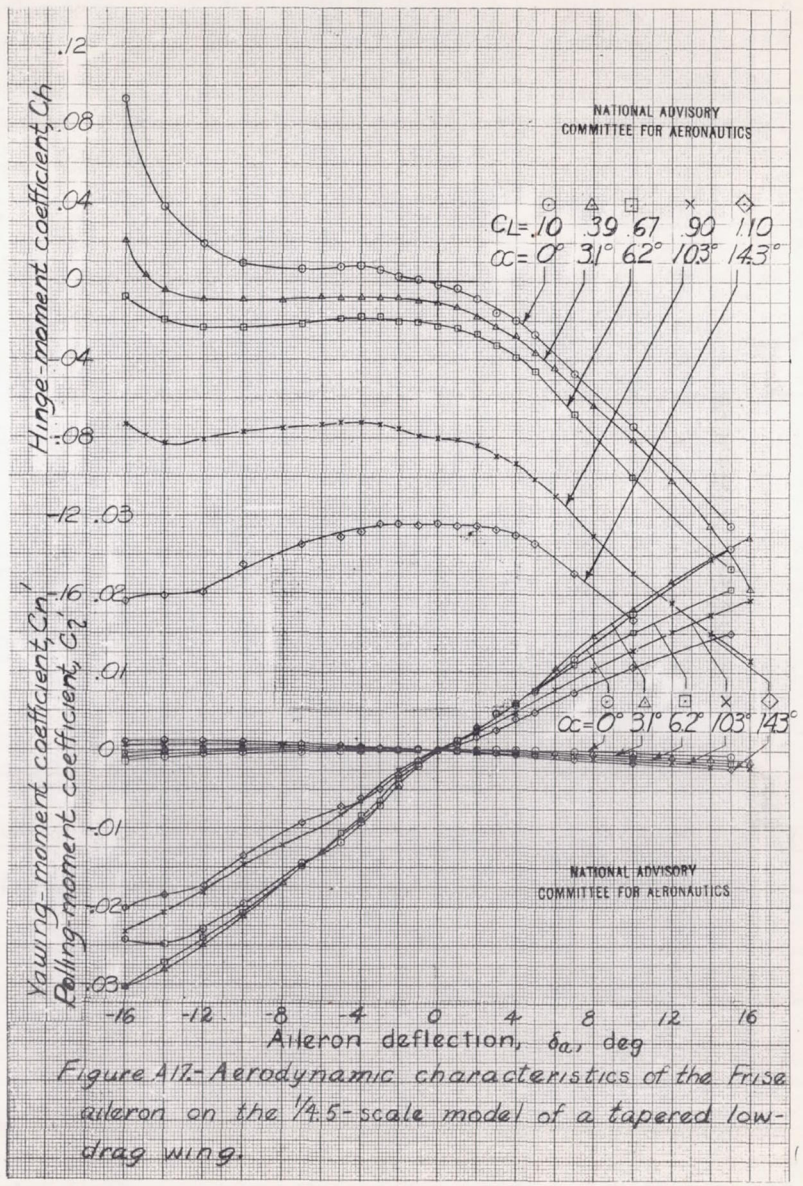

Figure A17.- Aerodynamic characteristics of the Frise aileron on the 1/4.5-scale model of a tapered low-drag wing.

Model A-IV

Model A-V

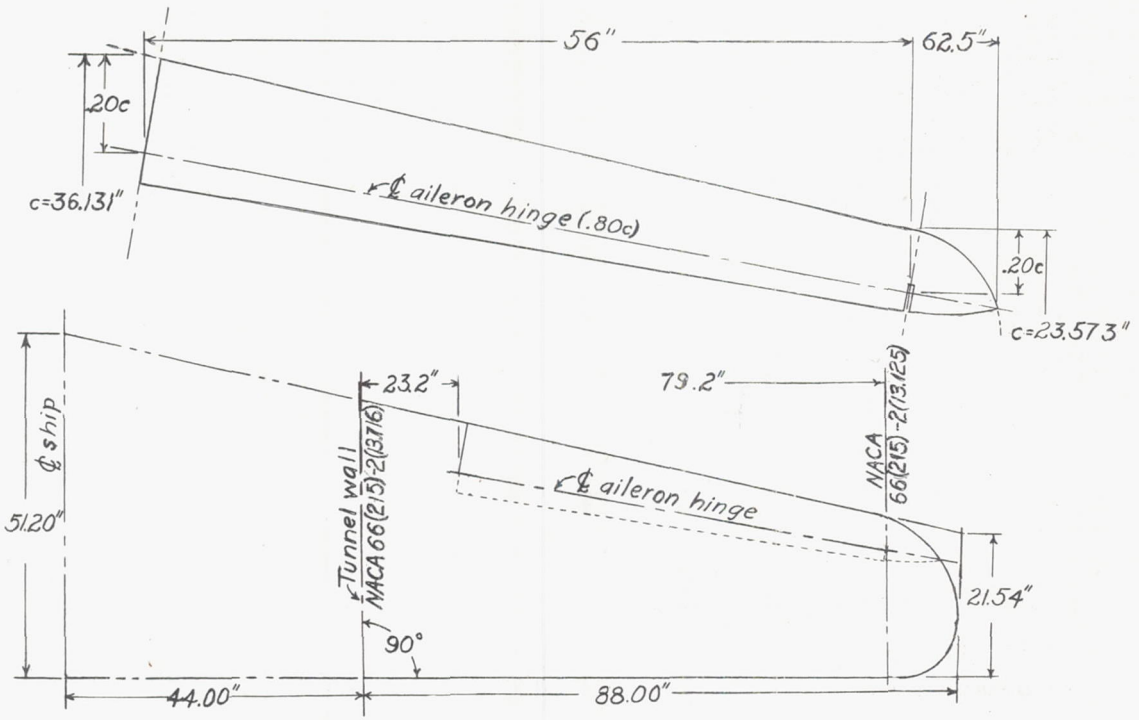

NATIONAL ADVISORY
COMMITTEE FOR AERONAUTICS

Figure A18.-The 0.4-scale model of a tapered low-drag wing. LMAL 7-by 10-foot tunnel.

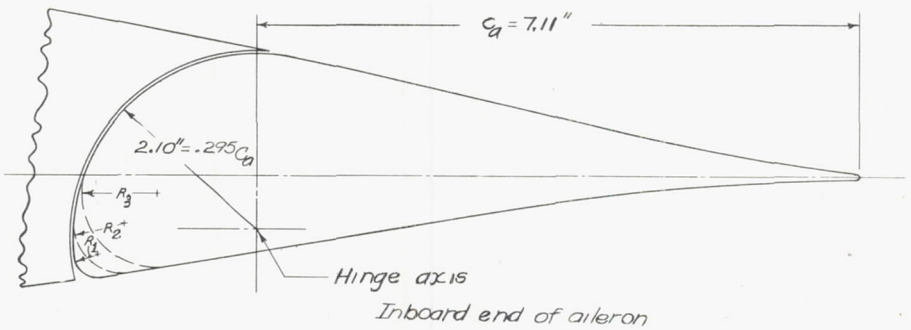

Symbol	Inboard radius	Outboard radius	Average radius
R_1	0.303"	0.198"	Original
R_2	.606"	.395"	0.500"
R_3	.909"	.592"	.750"

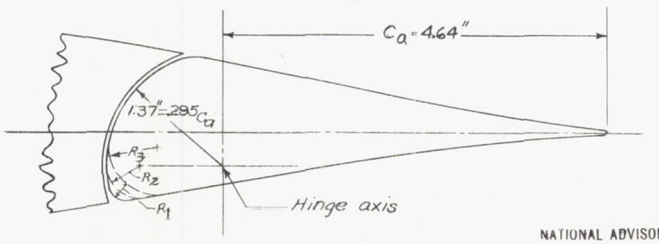

NATIONAL ADVISORY
COMMITTEE FOR AERONAUTICS

Outboard end of aileron

Figure A19. - The 0.295 c_a balance Frise aileron on the 0.4-scale model of a tapered low-drag wing.

Model A-V

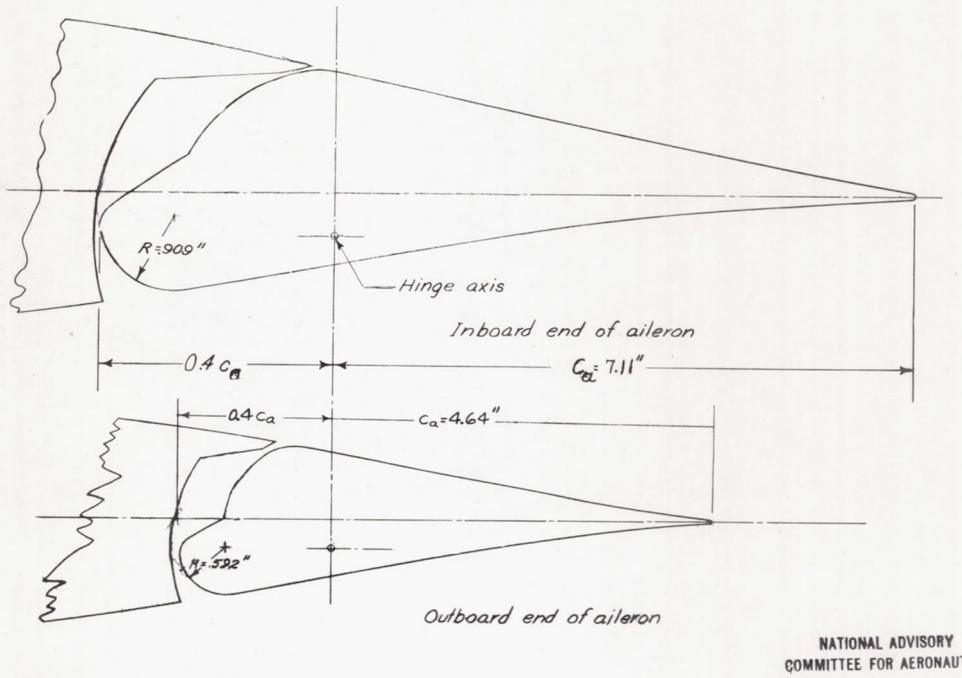

(a) Original.

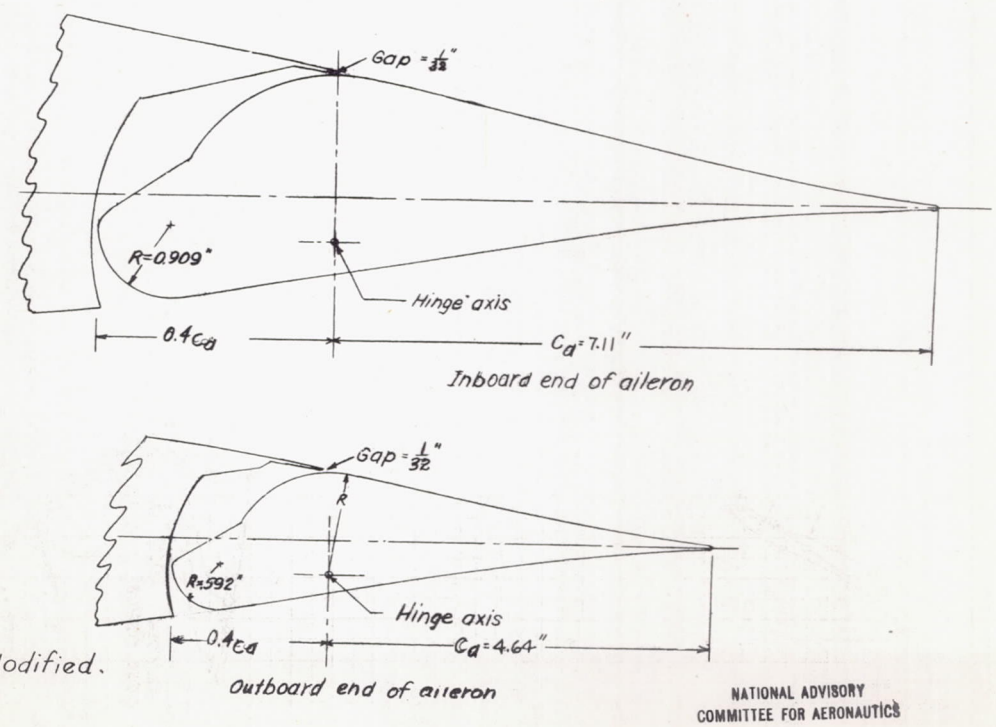

(b) Modified.

Figure A20.- The 0.40c_a balance Frise aileron on the 0.4-scale model of a tapered low-drag wing.

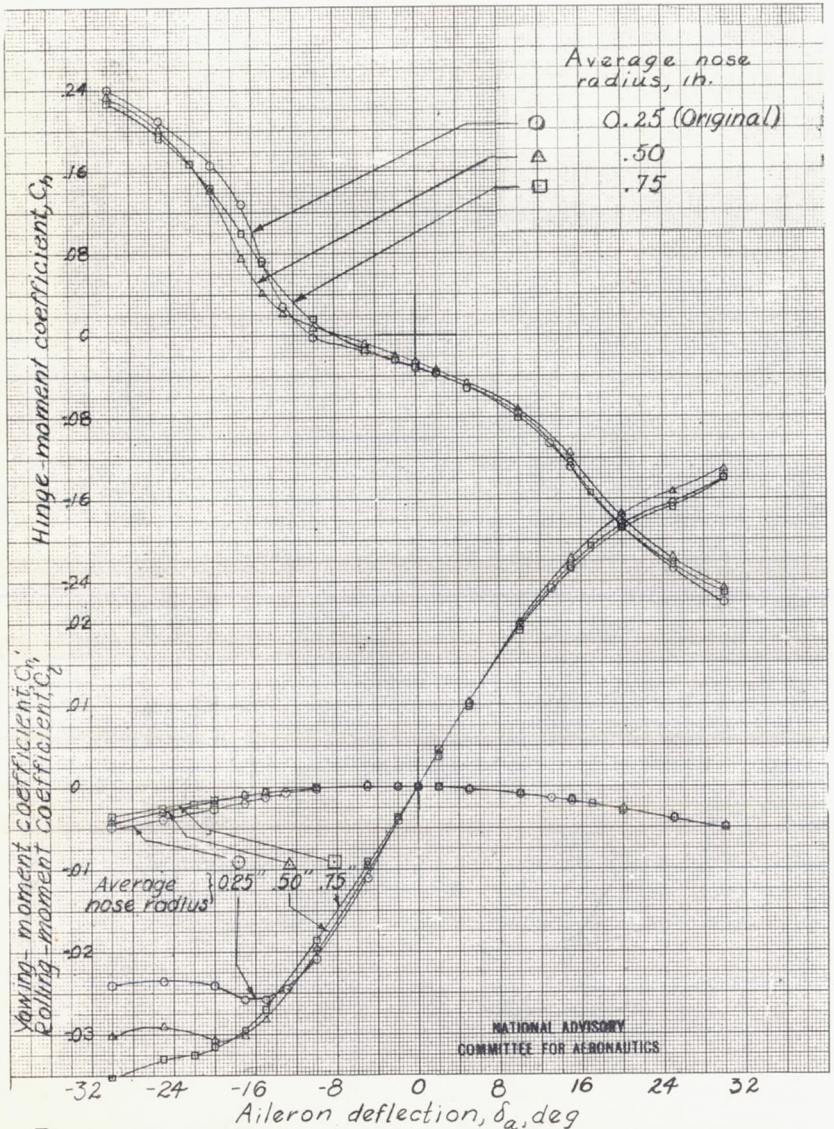

Figure A21.- Effect of nose radius on aerodynamic characteristics of the 0.295 c_a balance Frise aileron on the 0.4-scale model of a tapered low-drag wing. α, 1° ; C_L, 0.17.

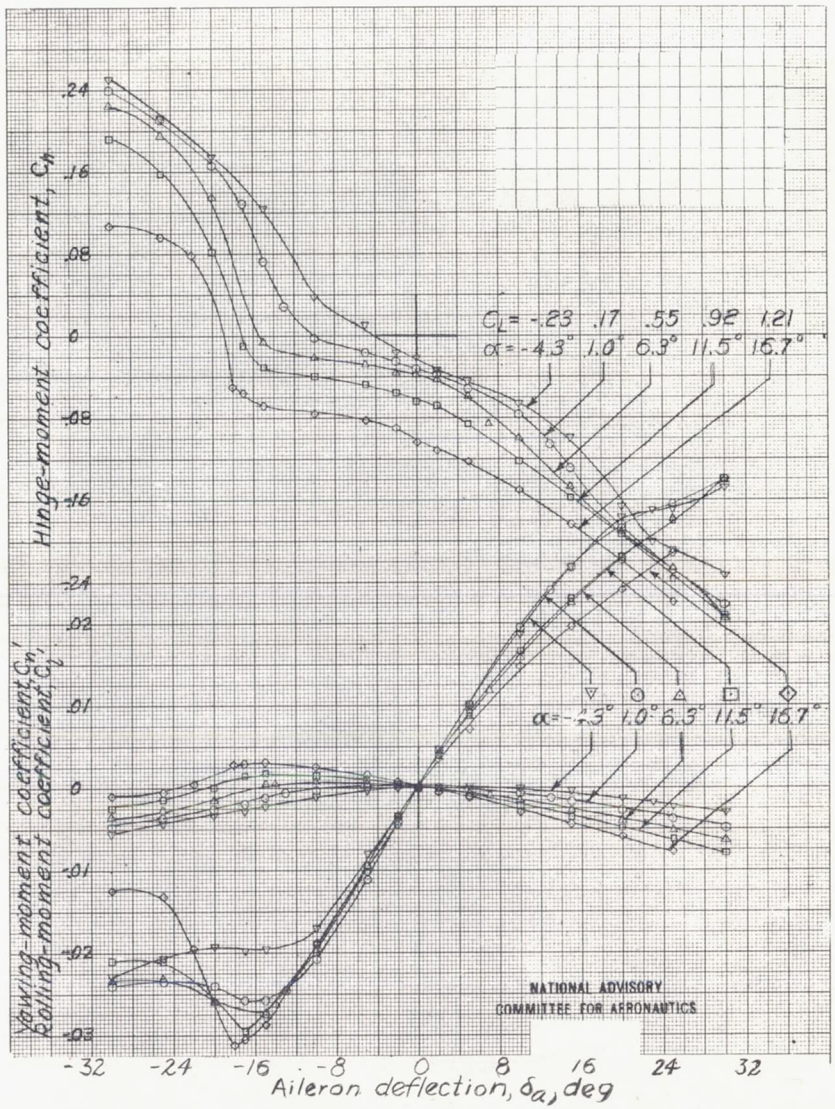

Figure A22.- Aerodynamic characteristics of original 0.295 c_a balance Frise aileron on the 0.4-scale model of a tapered low-drag wing.

Model A-V

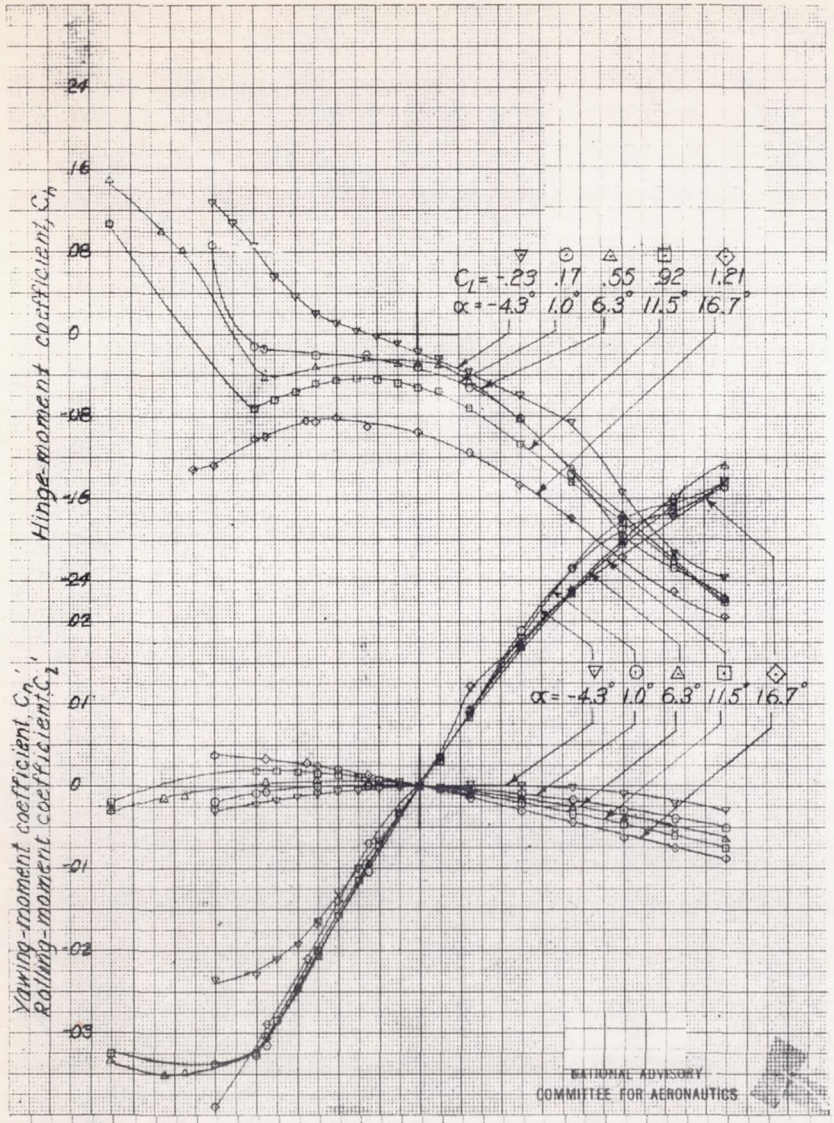

(a) Original.

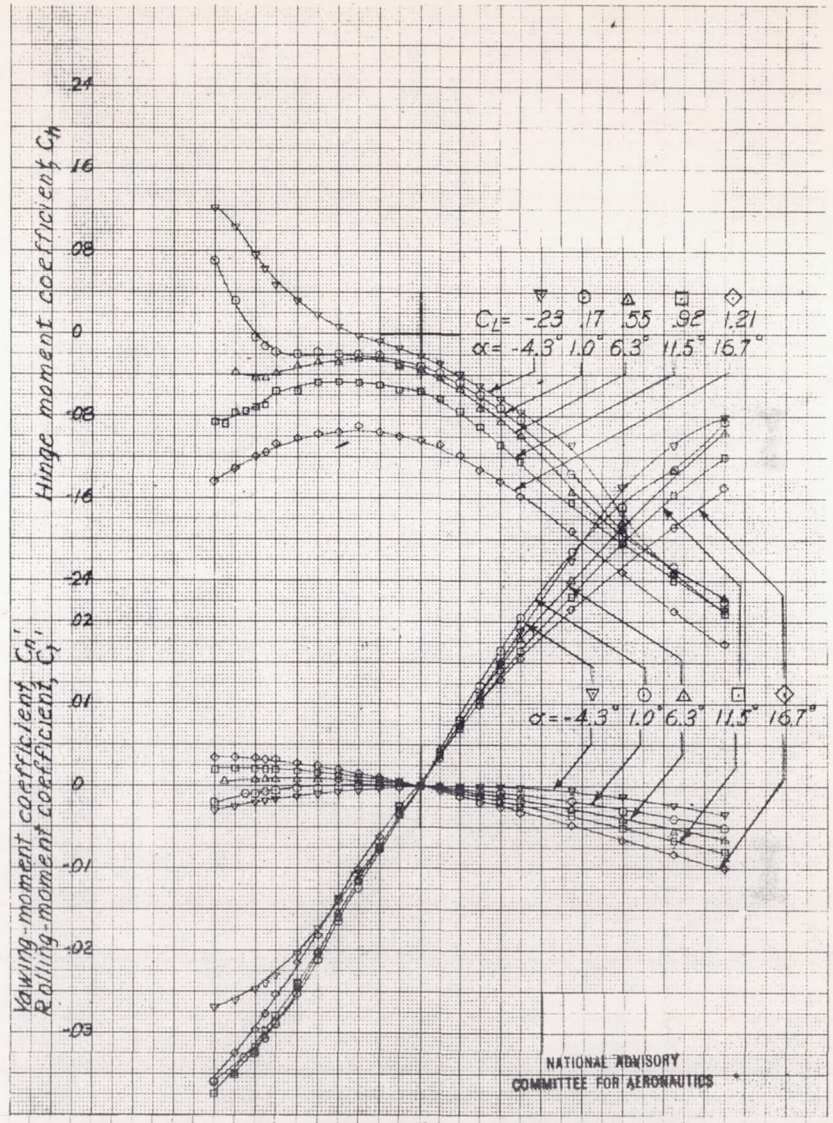

(b) Modified.

Figure A23.- Aerodynamic characteristics of the 0.4c_a balance Frise ailerons on the 0.4-scale model of a tapered low-drag wing.

Model A-1

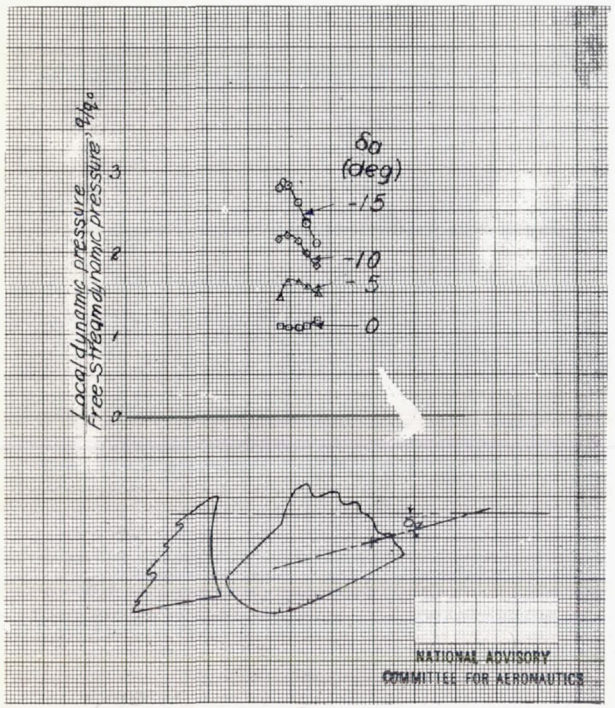

(a) Lower surface, original.

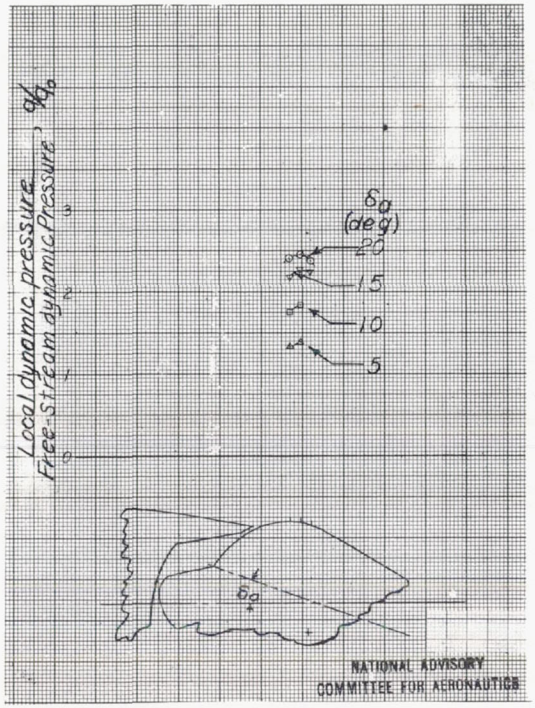

(b) Upper surface, original.

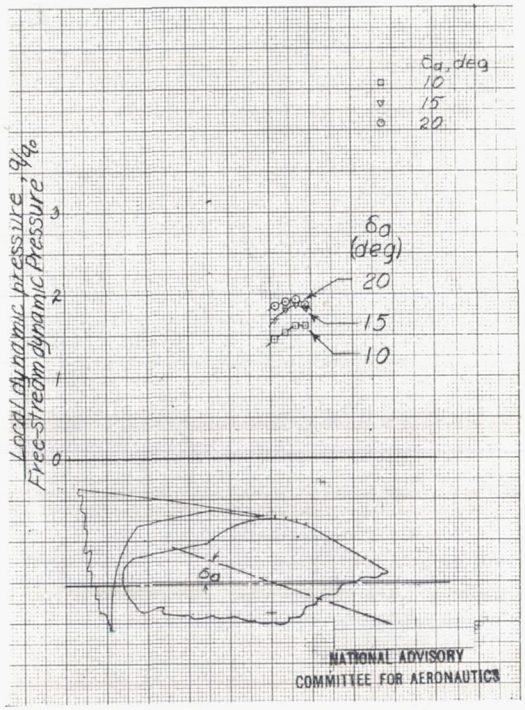

(c) Upper surface, modified.

Figure A24.- Local pressure surveys over the 0.4c_a balance Frise ailerons on the 0.4-scale model of a tapered low-drag wing. α, 1°; C_L, 0.17.

Model A-V

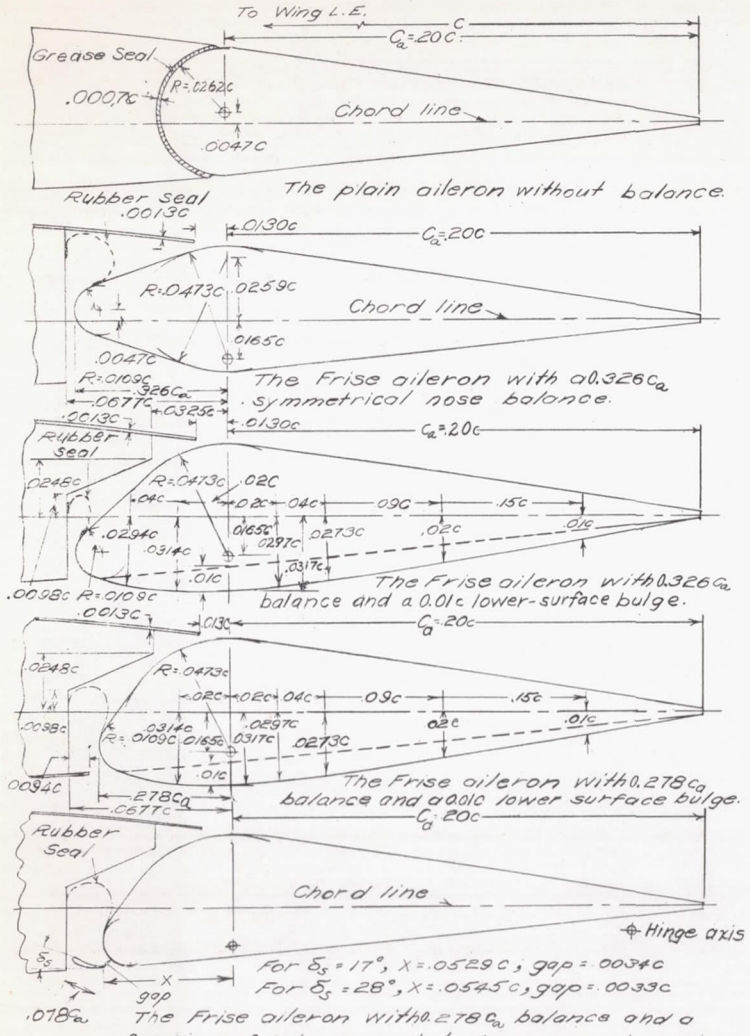

Figure A25.- The 0.20c by 0.37 $\frac{b}{2}$ ailerons tested on the 8-foot semispan NACA 23012 airfoil.

NATIONAL ADVISORY COMMITTEE FOR AERONAUTICS

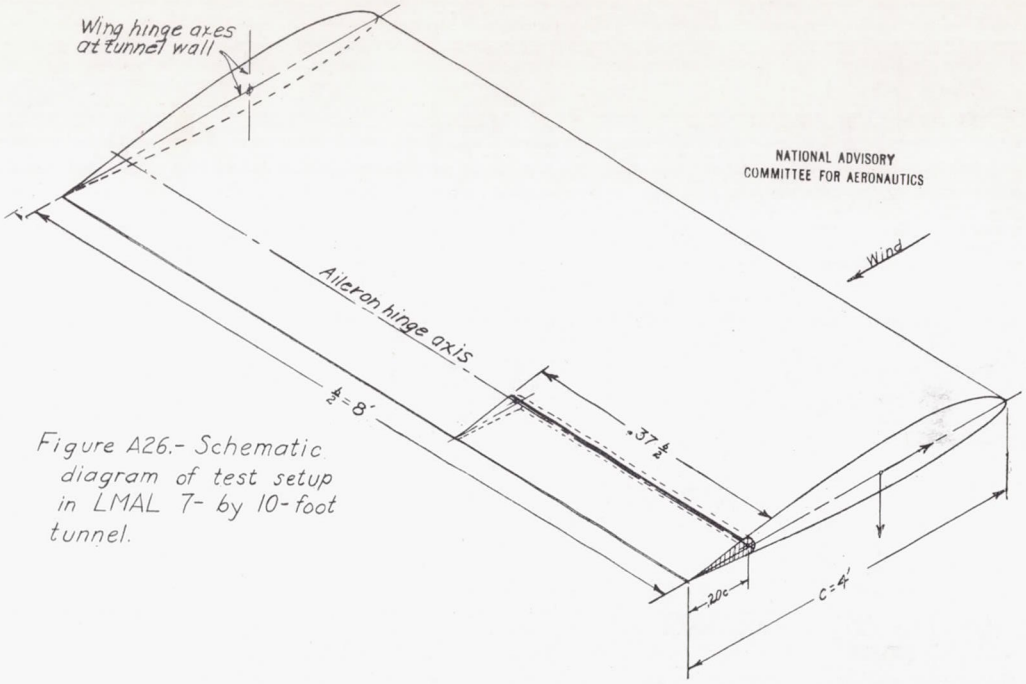

Figure A26.- Schematic diagram of test setup in LMAL 7- by 10-foot tunnel.

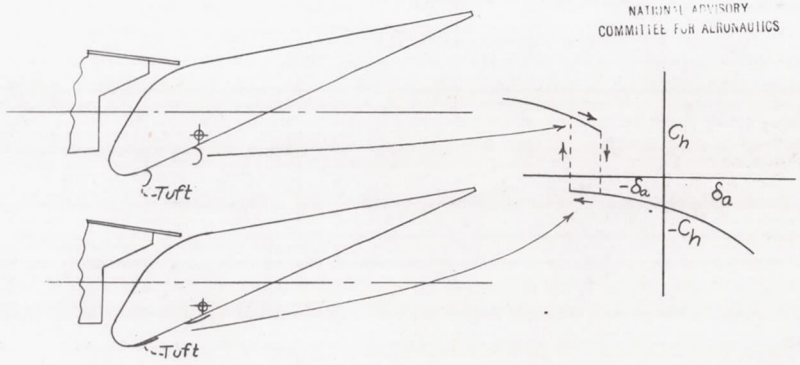

Figure A27.- Tuft action on lower surface of up-deflected Frise aileron, showing cause of oscillation.

Model A-XII

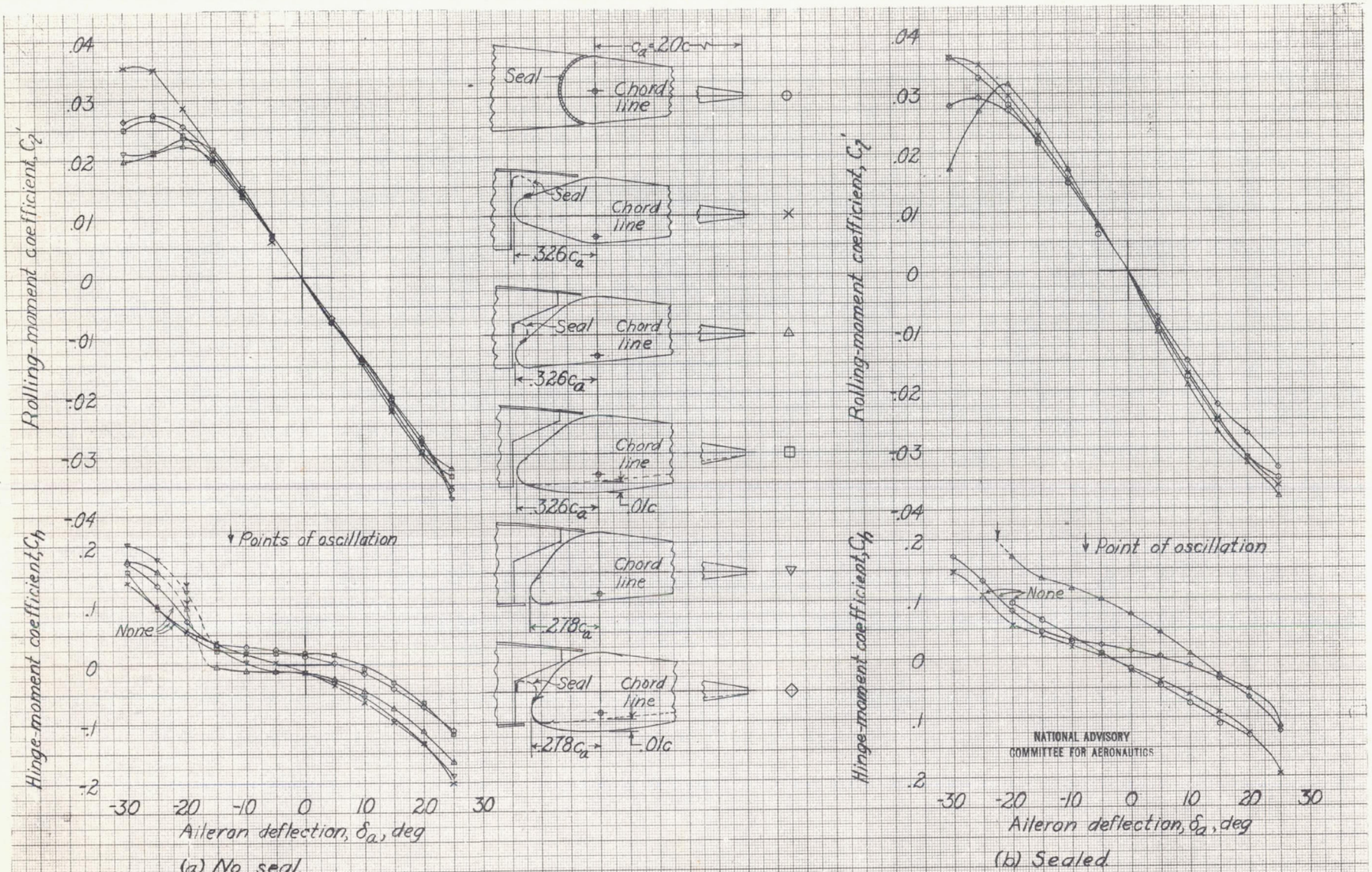

(a) No seal.

(b) Sealed.

Figure A28.-Effect of aileron shape on aerodynamic characteristics of 0.20c by 0.37½ ailerons on an NACA 23012 airfoil. V, 40 mph ; α, 1° ; C_L, 0.18.

Model A-VI

L-414

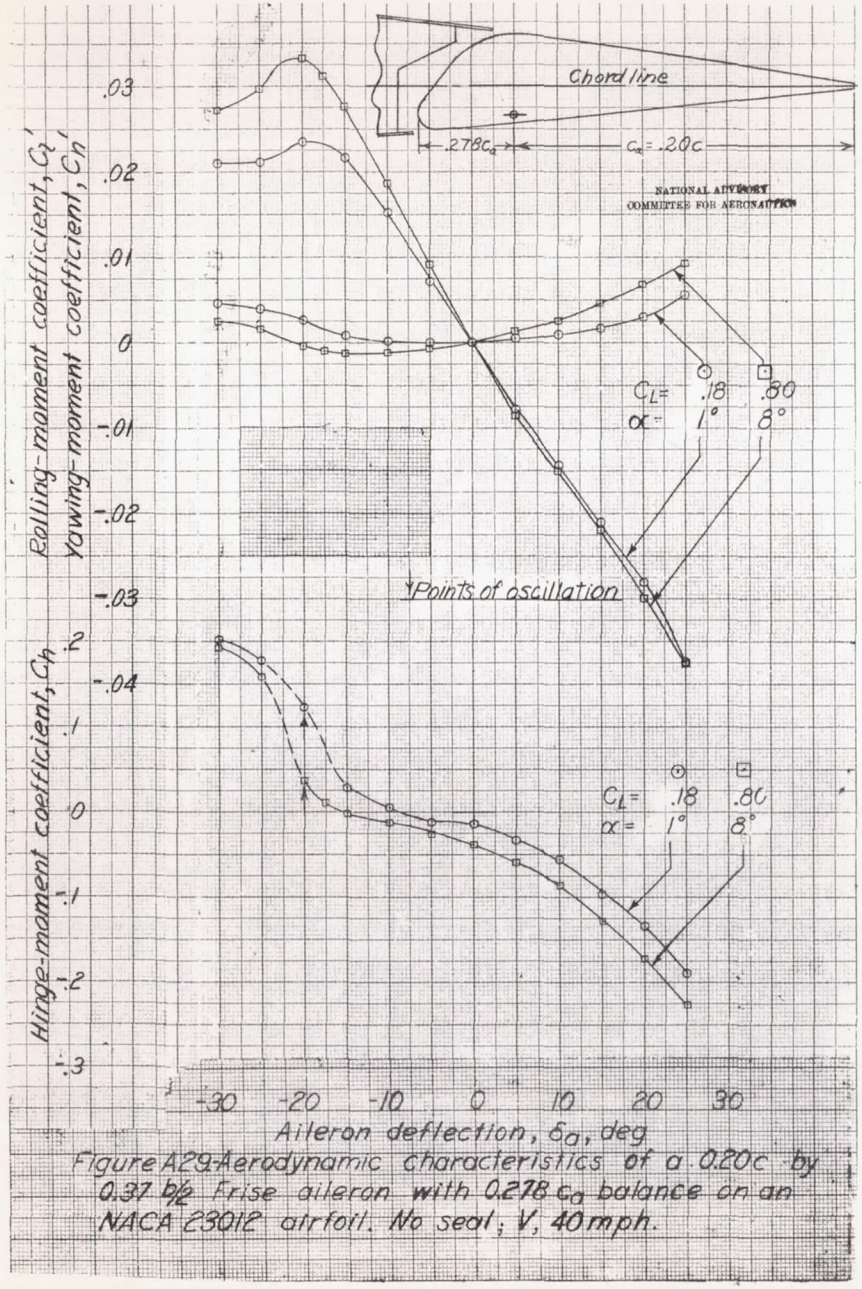

Figure A29-Aerodynamic characteristics of a 0.20c by 0.37 b/2 Frise aileron with 0.278 c_a balance on an NACA 23012 airfoil. No seal; V, 40 mph.

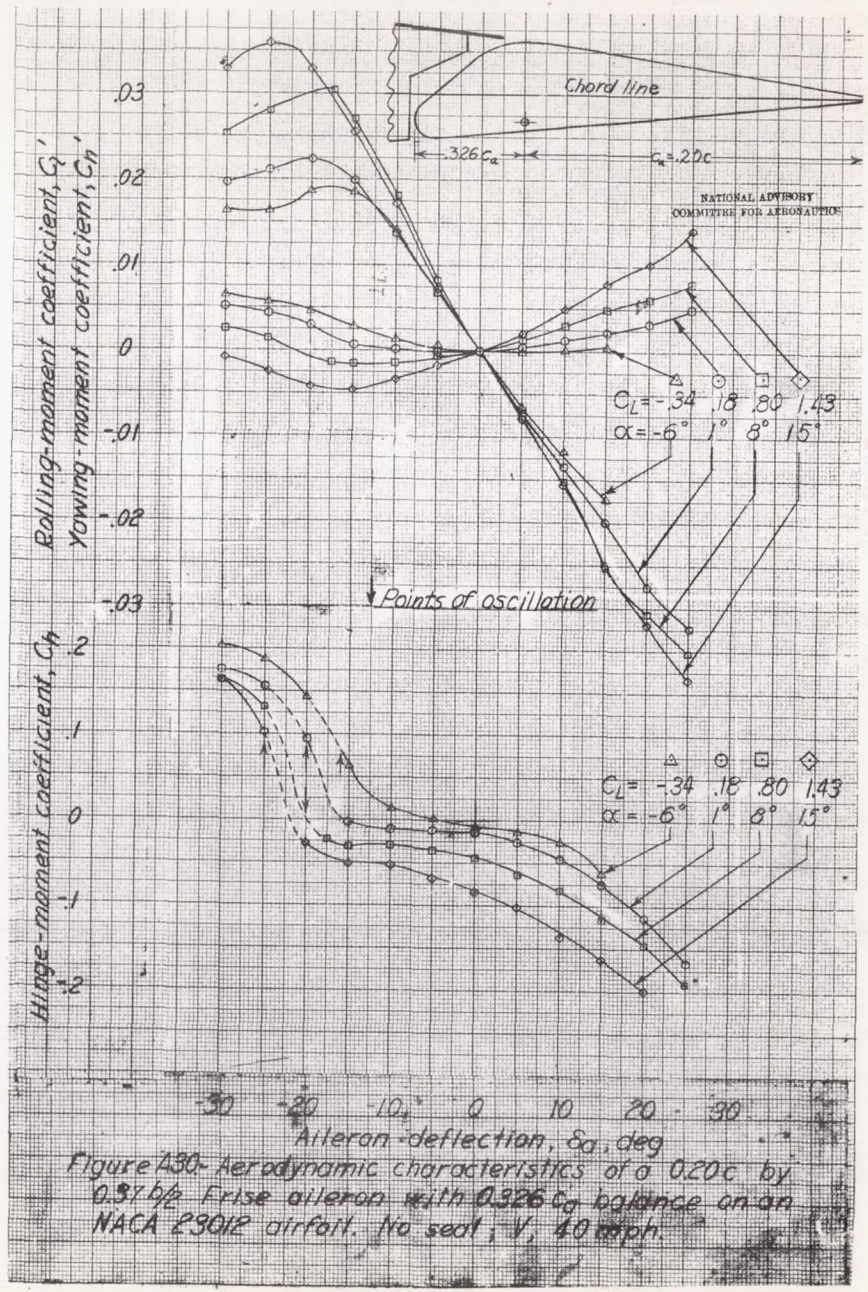

Figure A30- Aerodynamic characteristics of a 0.20c by 0.37 b/2 Frise aileron with 0.326 c_a balance on an NACA 23012 airfoil. No seal; V, 40 mph.

Model A-VI

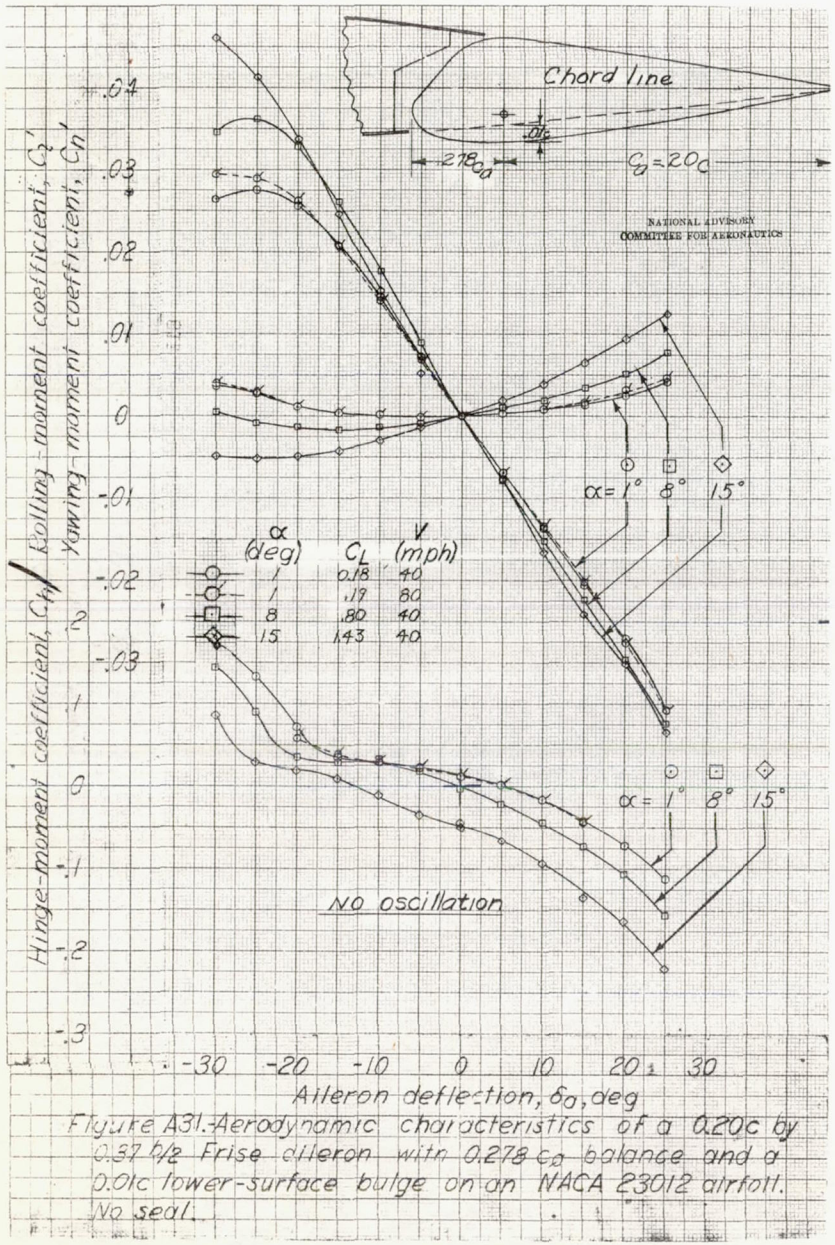

Figure A31.-Aerodynamic characteristics of a 0.20c by 0.37 b/2 Frise aileron with 0.278 c_a balance and a 0.01c lower-surface bulge on an NACA 23012 airfoil. No seal.

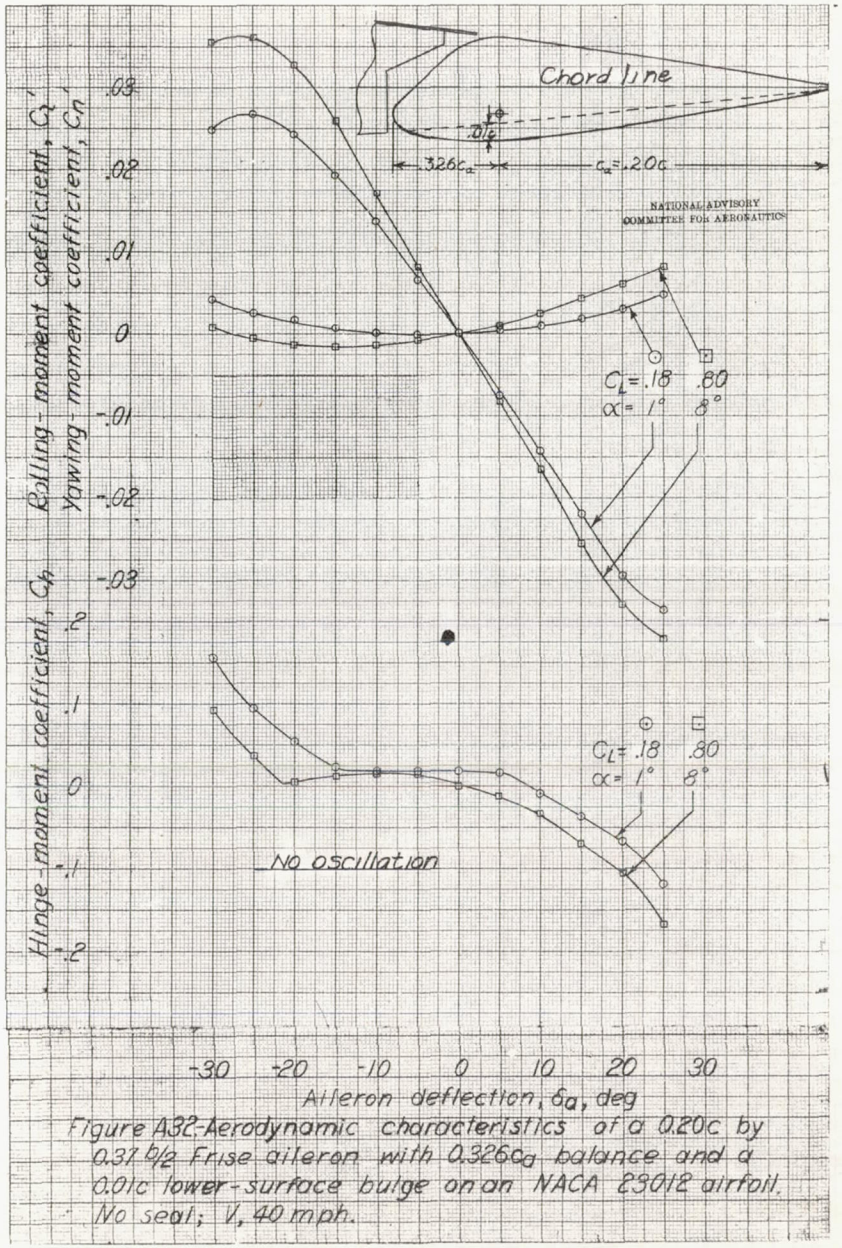

Figure A32-Aerodynamic characteristics of a 0.20c by 0.37 b/2 Frise aileron with 0.326 c_a balance and a 0.01c lower-surface bulge on an NACA 23012 airfoil. No seal; V, 40 mph.

Model A-VI

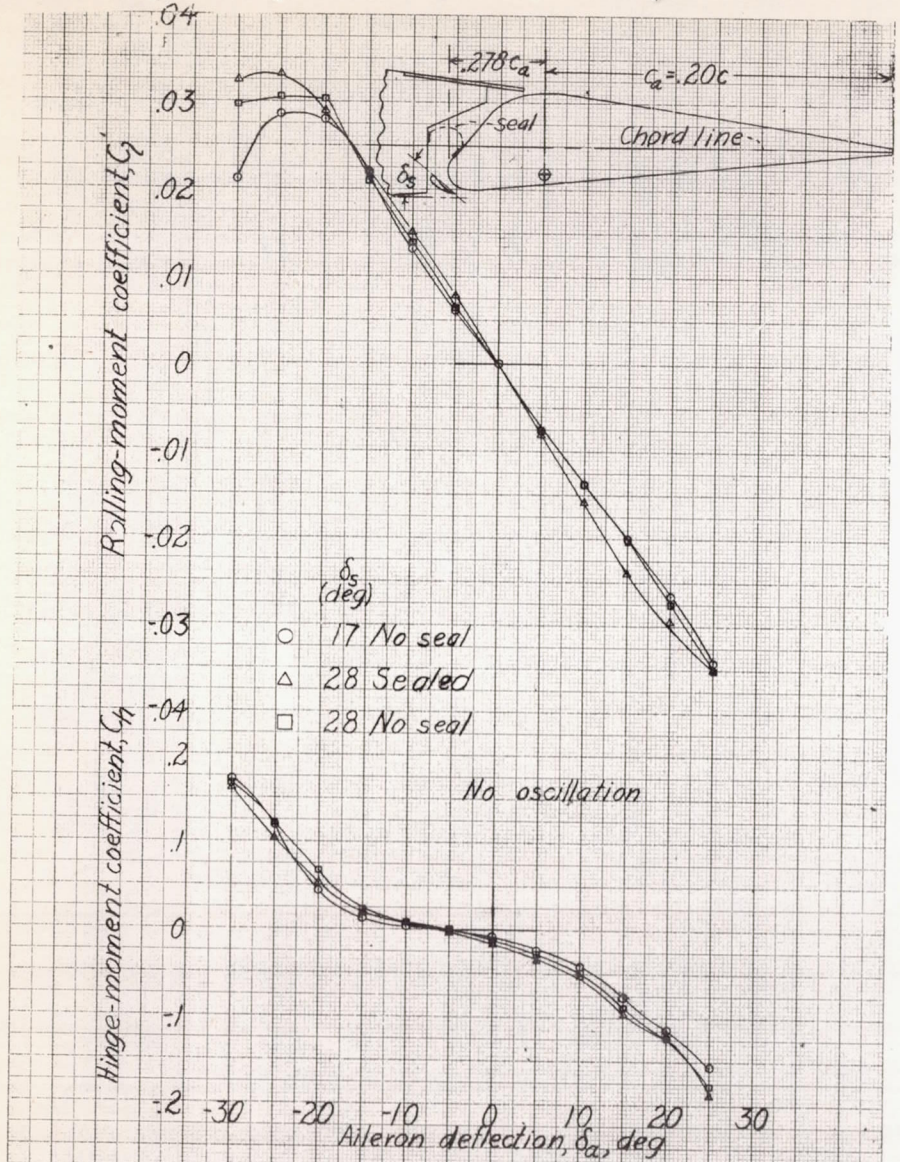

Figure A33.-Effect of slat angle and seal on aerodynamic characteristics of a 0.20c by 0.37 b/2 Frise aileron with 0.278 c_a balance and a centrally located 0.078 c_a by 0.31 b/2 nose slat on an NACA 23012 airfoil. V, 40 mph; α, 1°; C_L, 0.16.

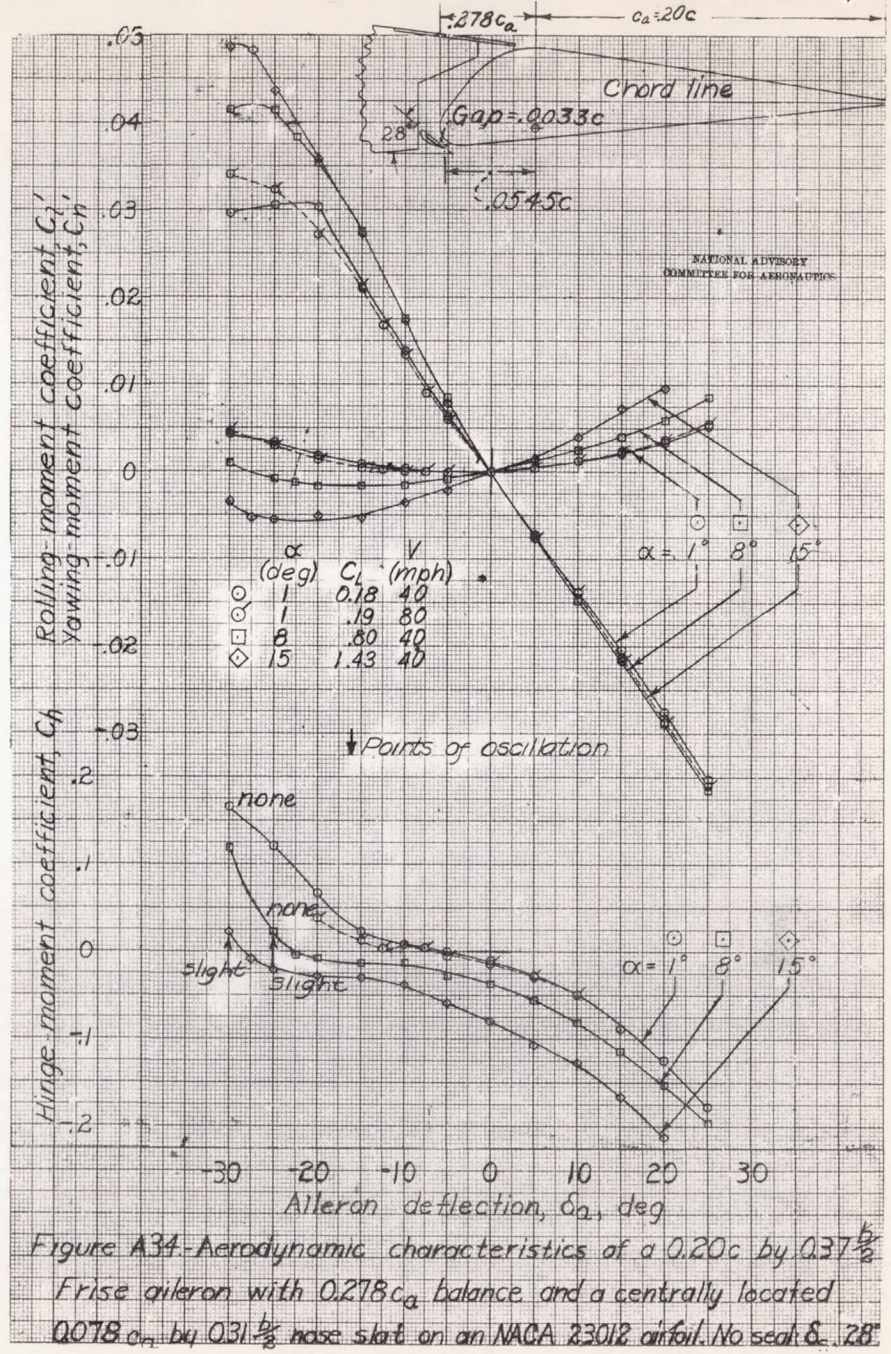

Figure A34.-Aerodynamic characteristics of a 0.20c by 0.37 b/2 Frise aileron with 0.278 c_a balance and a centrally located 0.078 c_a by 0.31 b/2 nose slat on an NACA 23012 airfoil. No seal. δ_s, 28°

Model A-VI

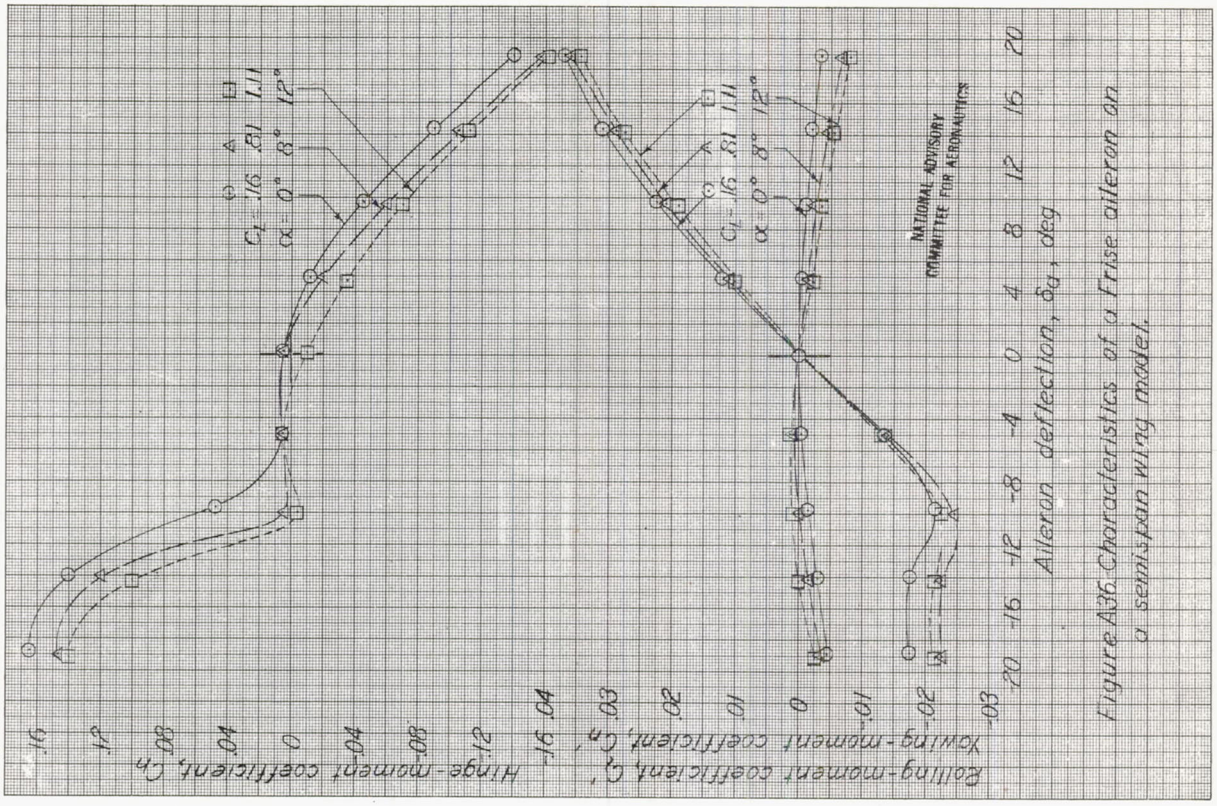

Figure A36.-Characteristics of a Frise aileron on a semispan wing model.

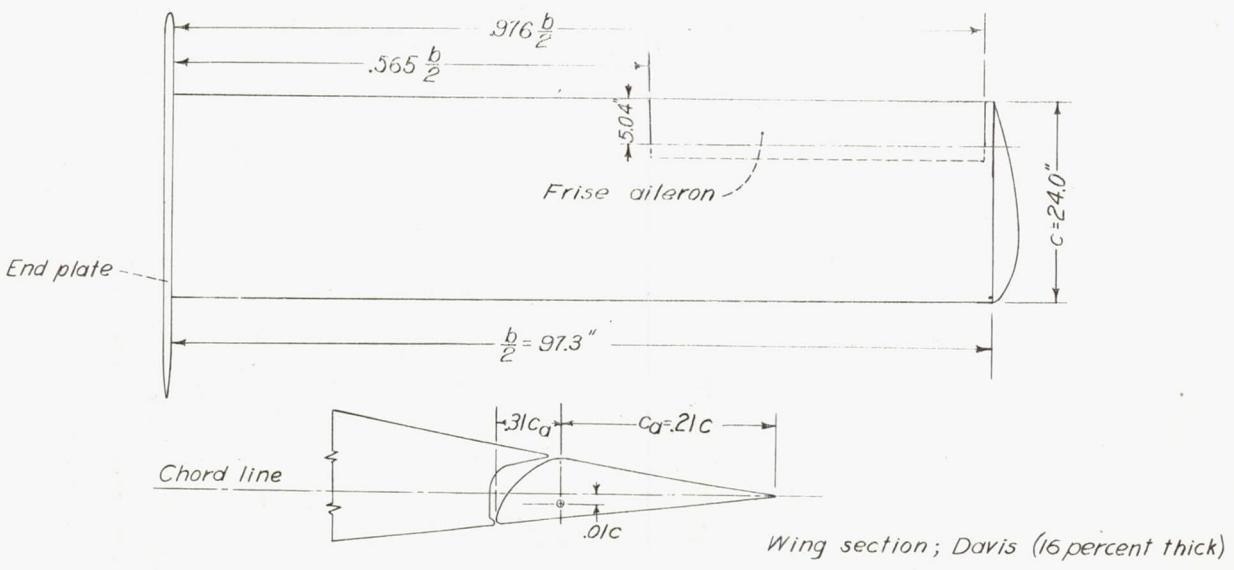

Figure A35.-Plan form of semispan wing model and profile of Frise aileron. AAL 7-by 10-foot tunnel.

Model A-VIII

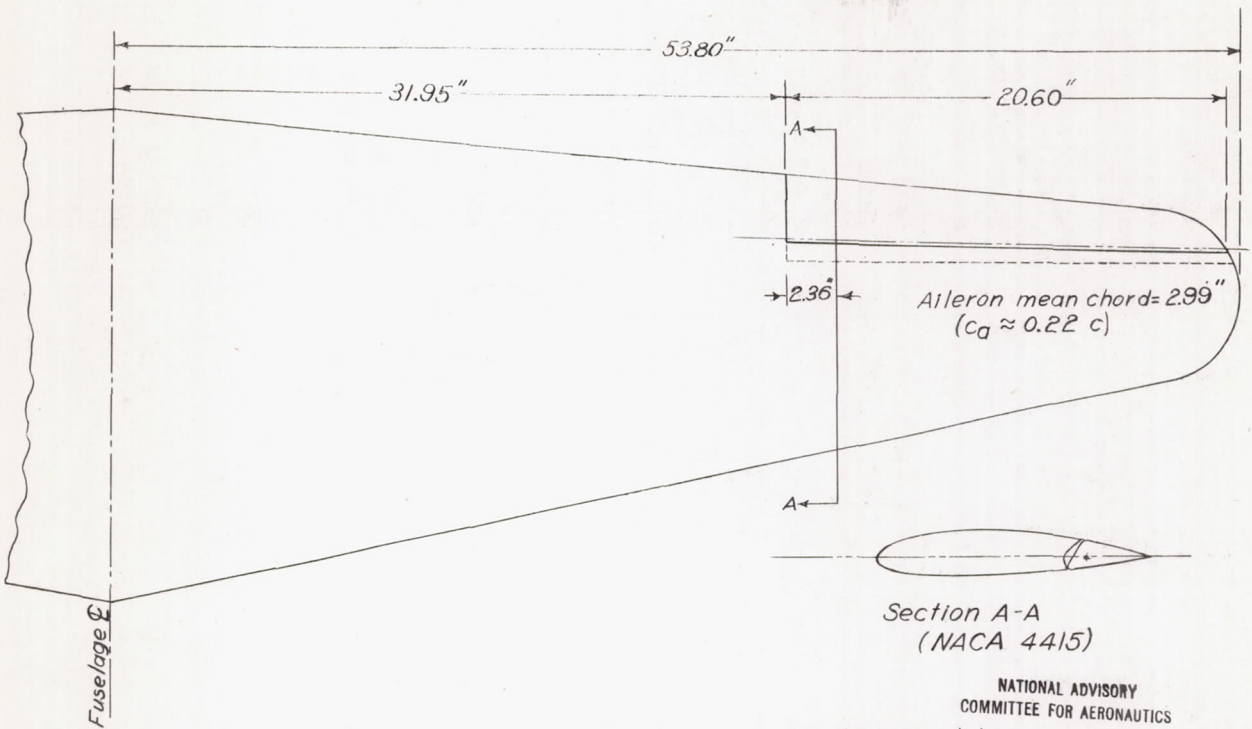

Figure A37.-Planform of wing of 1/13-scale airplane model.

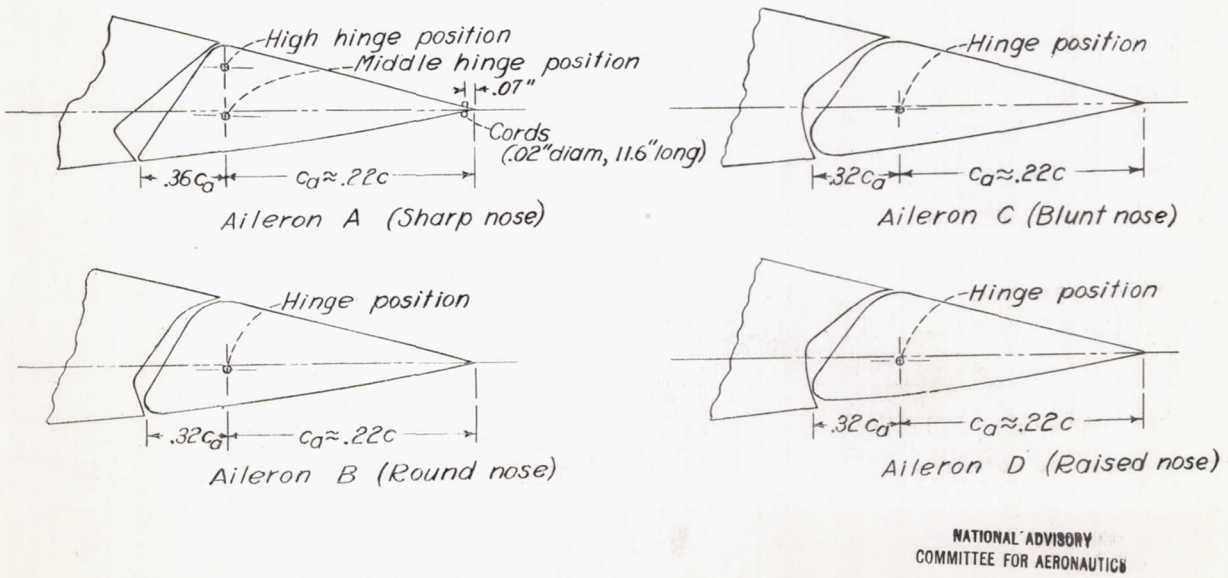

Figure A38.-The various modifications of the aileron of the 1/13-scale airplane model. R.A.E. 11-foot tunnel.

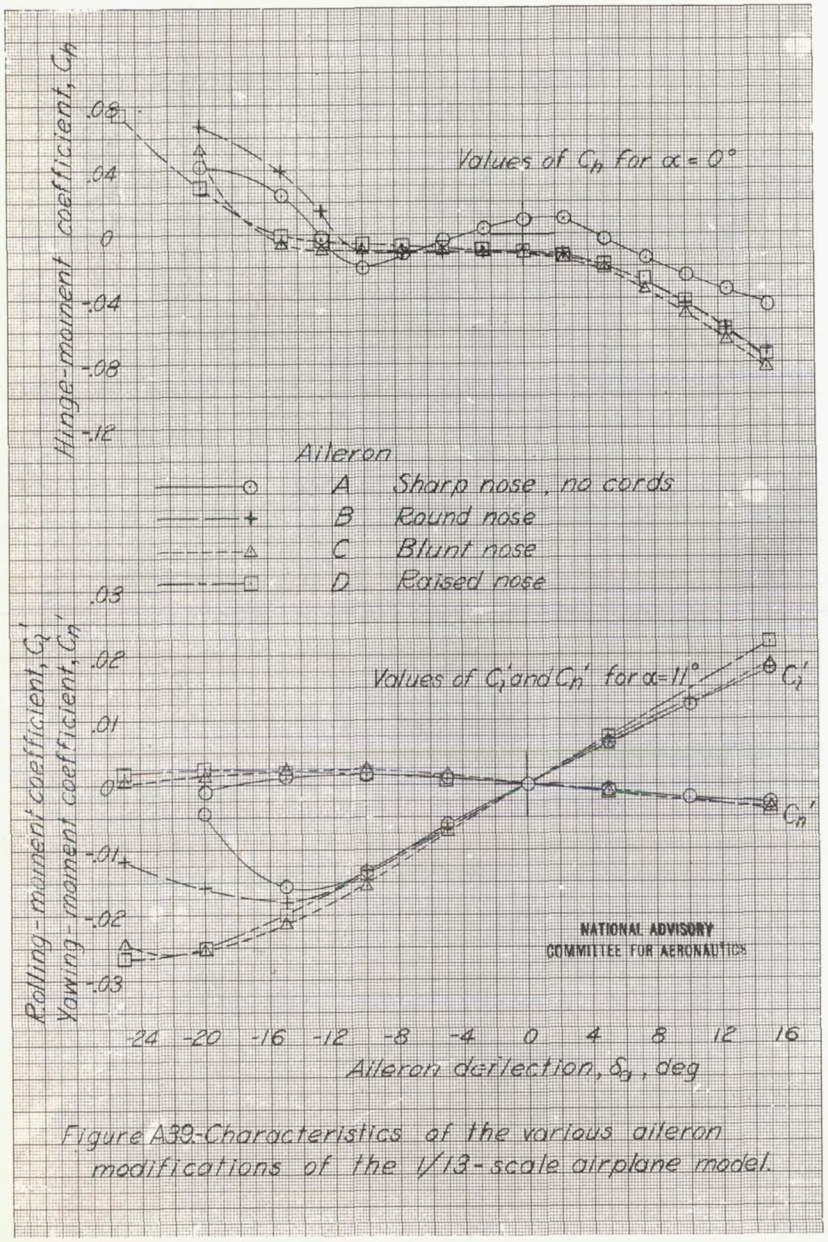

Figure A39.-Characteristics of the various aileron modifications of the 1/13-scale airplane model.

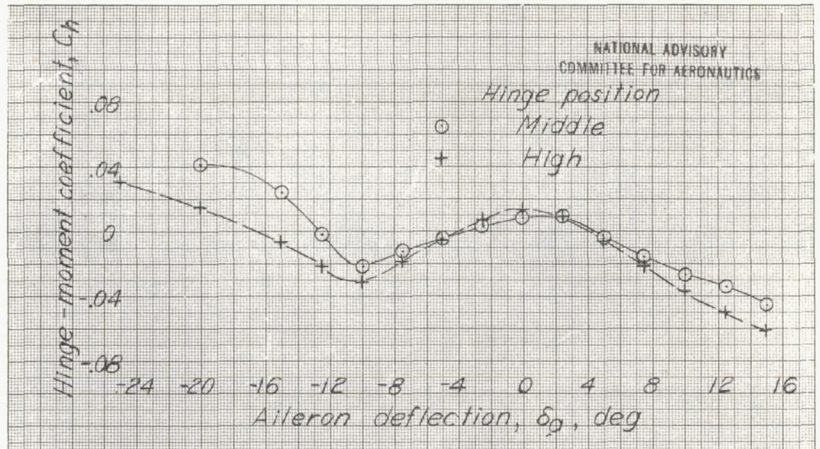

Figure A40.-Effect of vertical position of hinge axis of aileron A of the 1/13-scale airplane model. α, 0°.

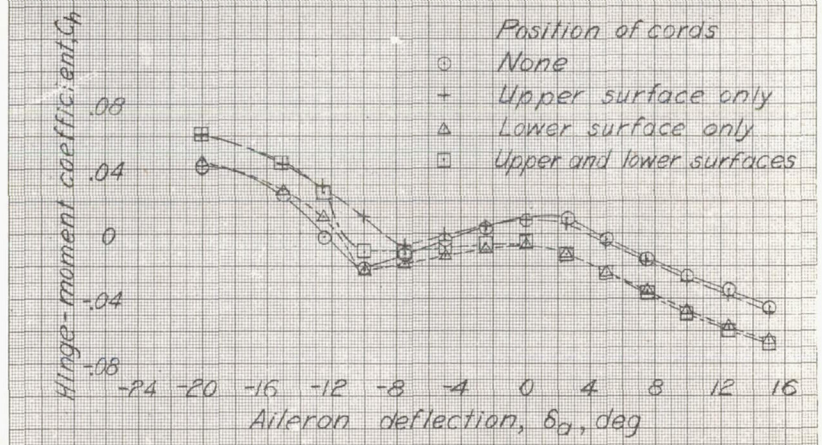

Figure A41.-Effect of cords near the trailing edge of aileron A with middle hinge position of the 1/13-scale airplane model. α, 0°.

Model A-VIII

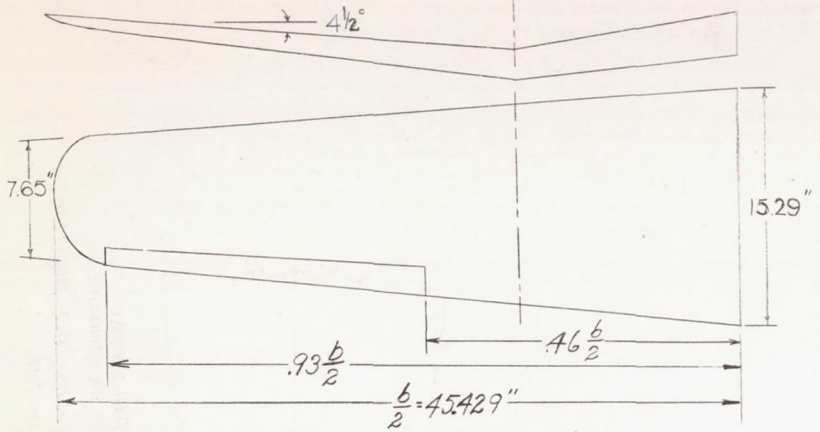

Figure A42.-Plan form of wing of 1/14 - scale airplane model. LMAL 7-by 10-foot tunnel.

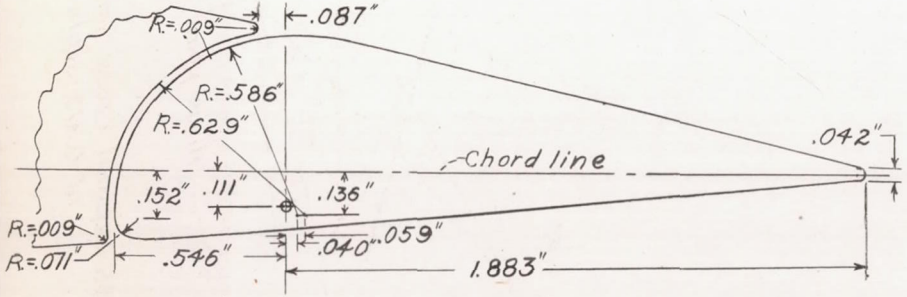

Inboard end

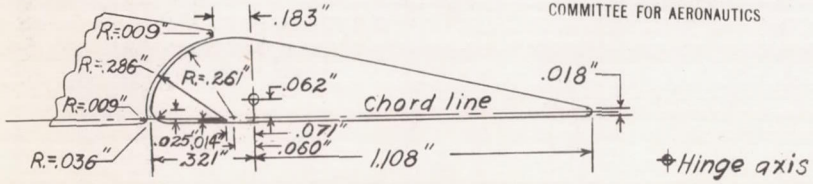

Outboard end

Figure A43.- Details of Frise aileron tested on the 1/14 - scale model of an airplane.

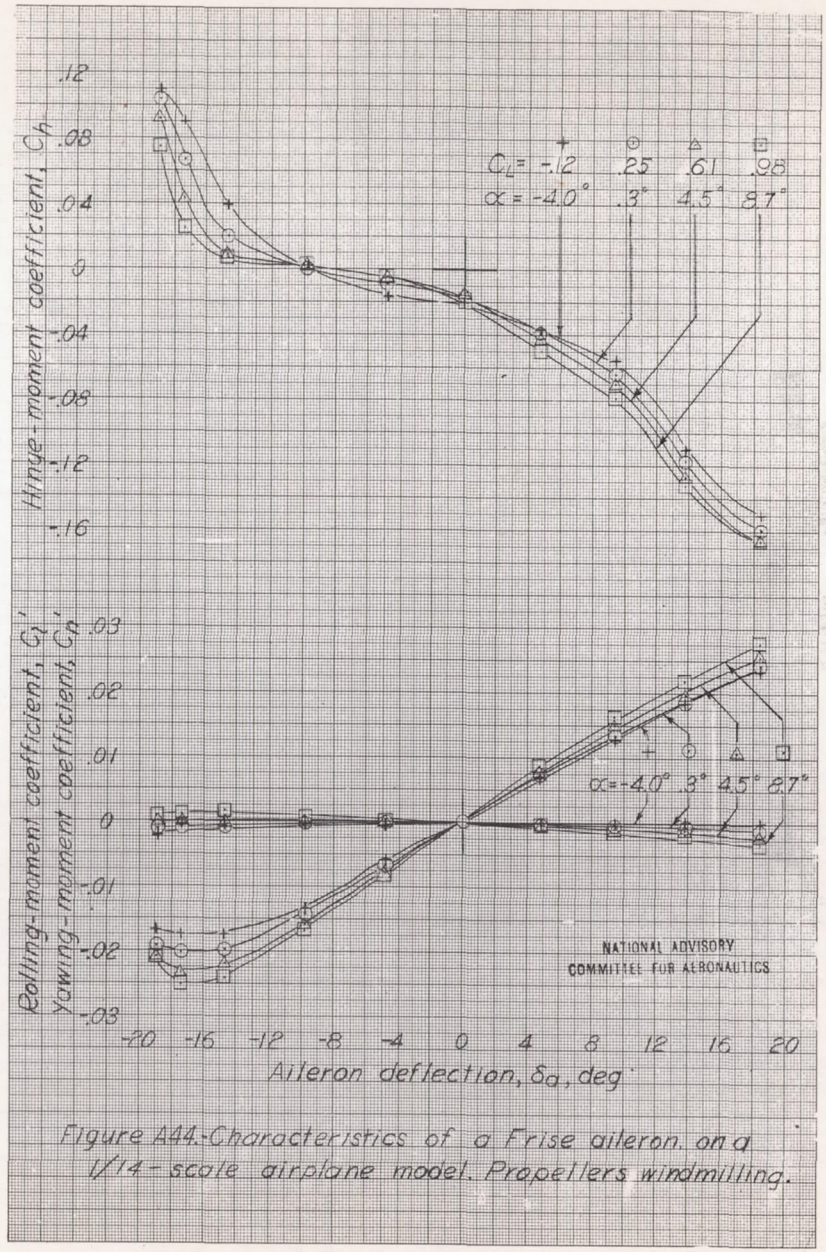

Figure A44.-Characteristics of a Frise aileron on a 1/14 - scale airplane model. Propellers windmilling.

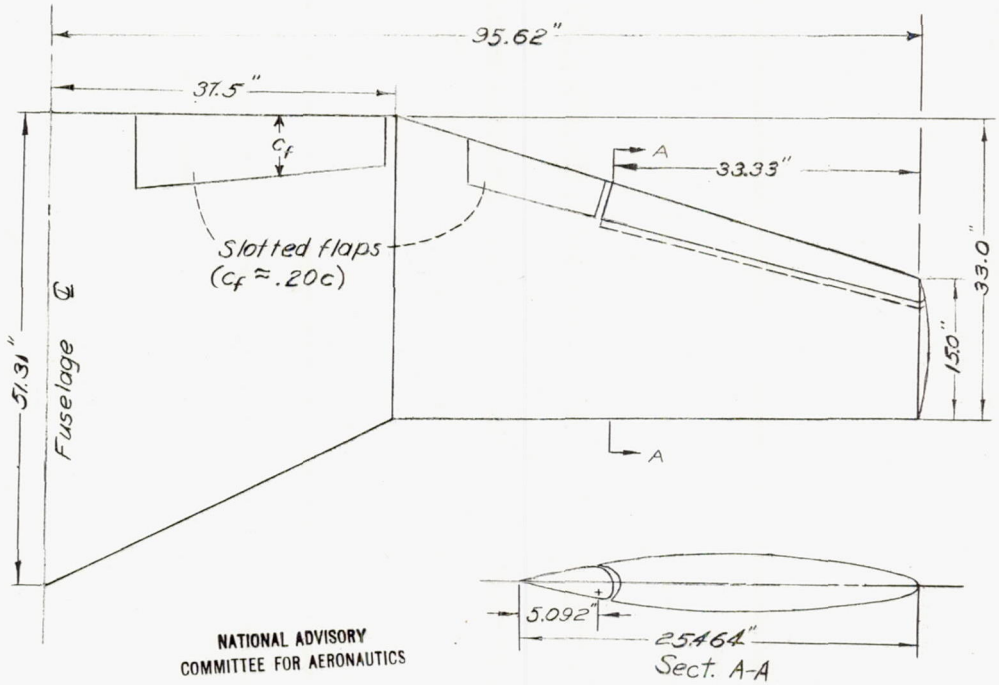

Figure A45.-Plan form of wing of 0.375-scale airplane model.
NACA 19-foot pressure tunnel.

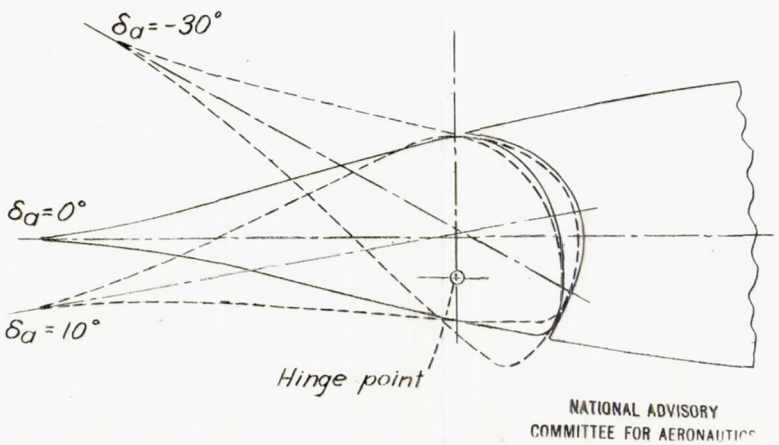

Figure A46.-Typical cross section and deflected positions
of 0.375-scale airplane model.

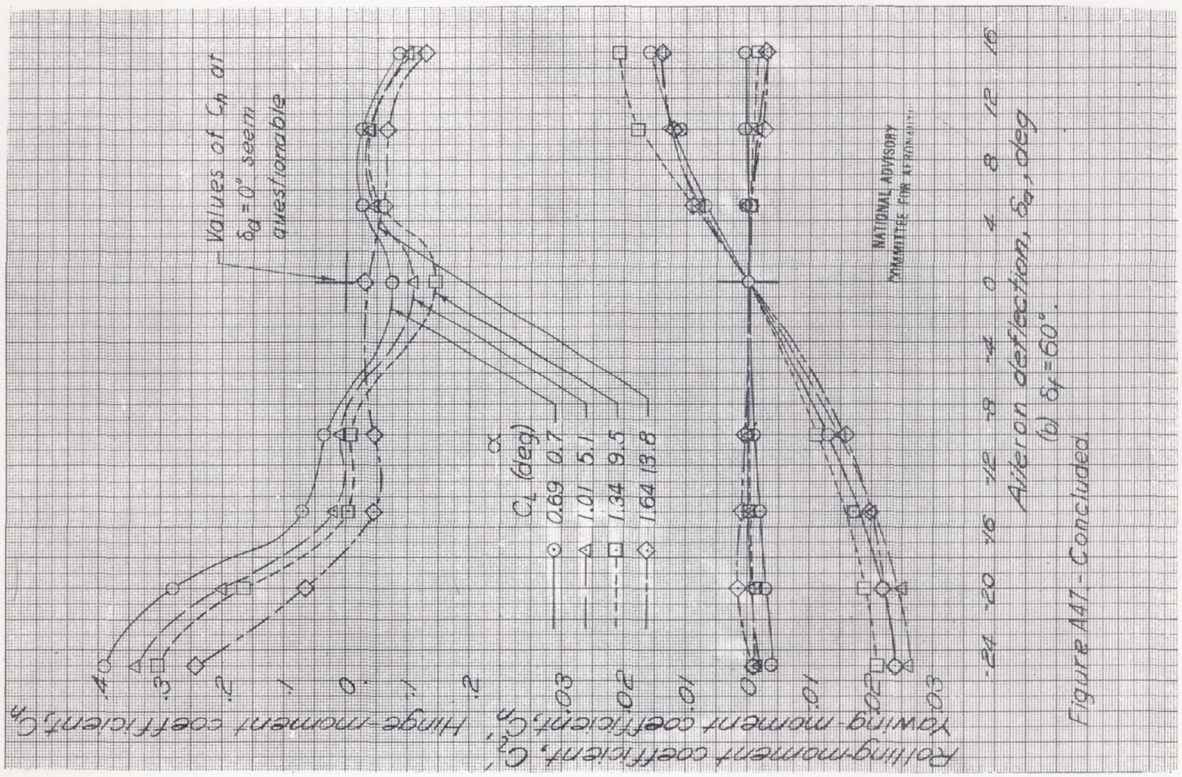

(b) $\delta_f = 60°$.

Figure A47.- Concluded.

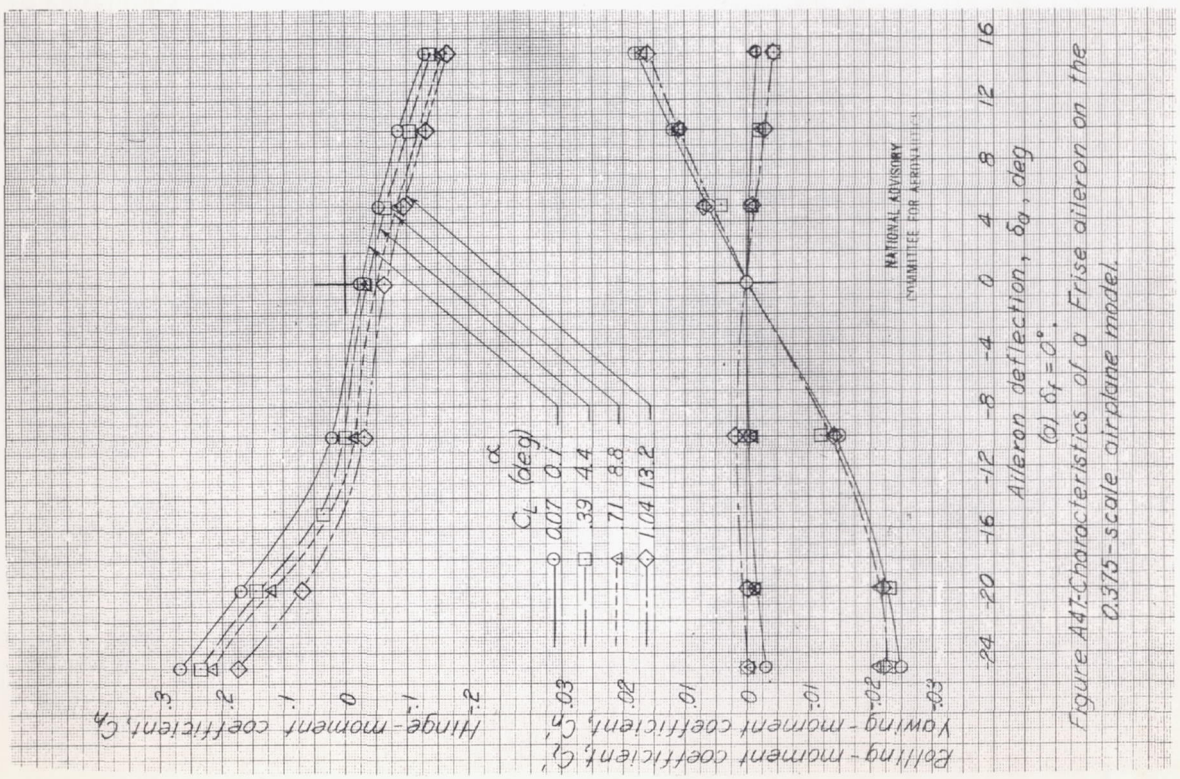

Figure A47.- Characteristics of a Frise aileron on the 0.375-scale airplane model.

(a) $\delta_f = 0°$.

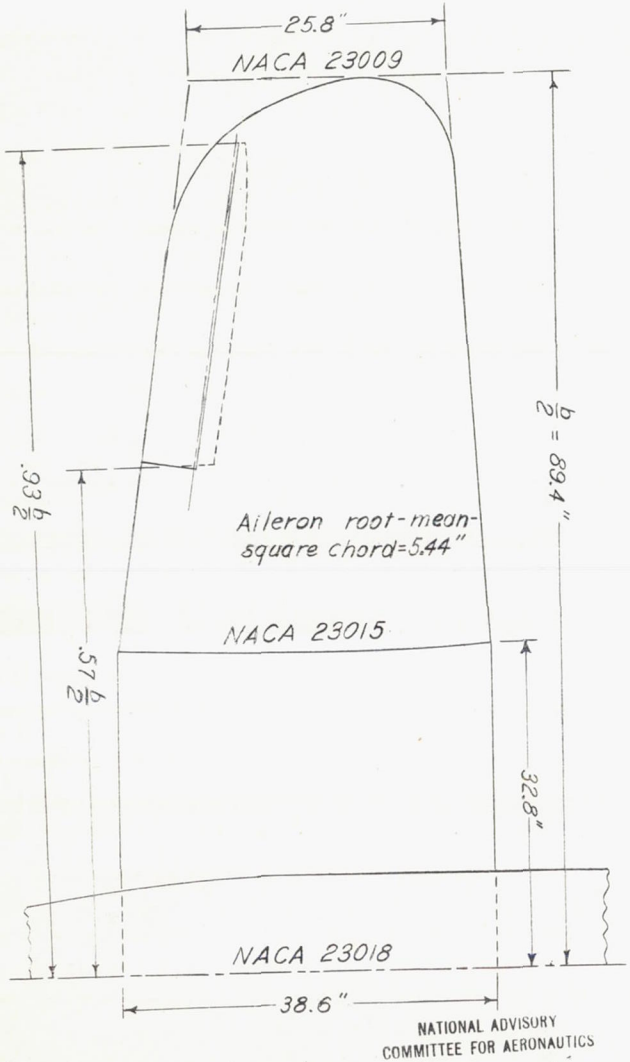

Figure A48.-Plan form of wing of a 1/2.75-scale model of a fighter-type airplane. NACA 19-foot pressure tunnel.

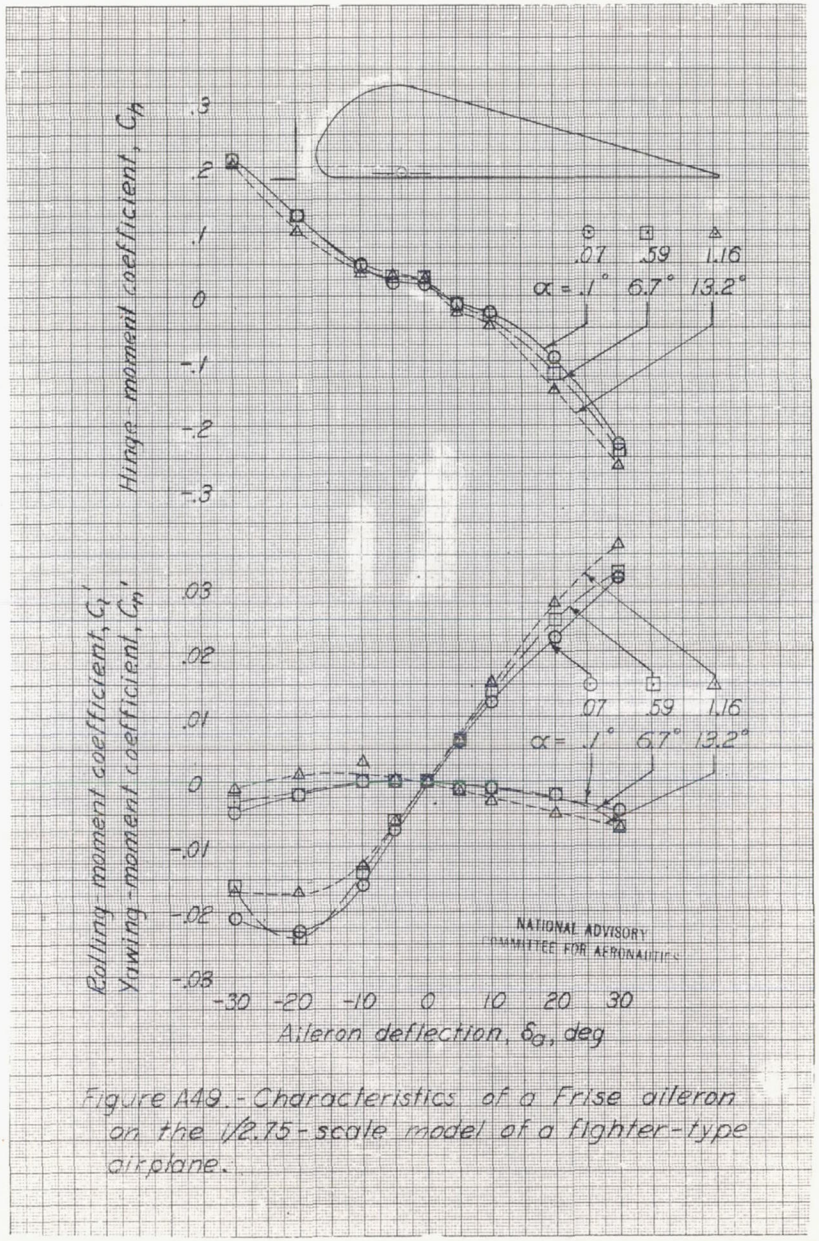

Figure A49.-Characteristics of a Frise aileron on the 1/2.75-scale model of a fighter-type airplane.

Model A-XI

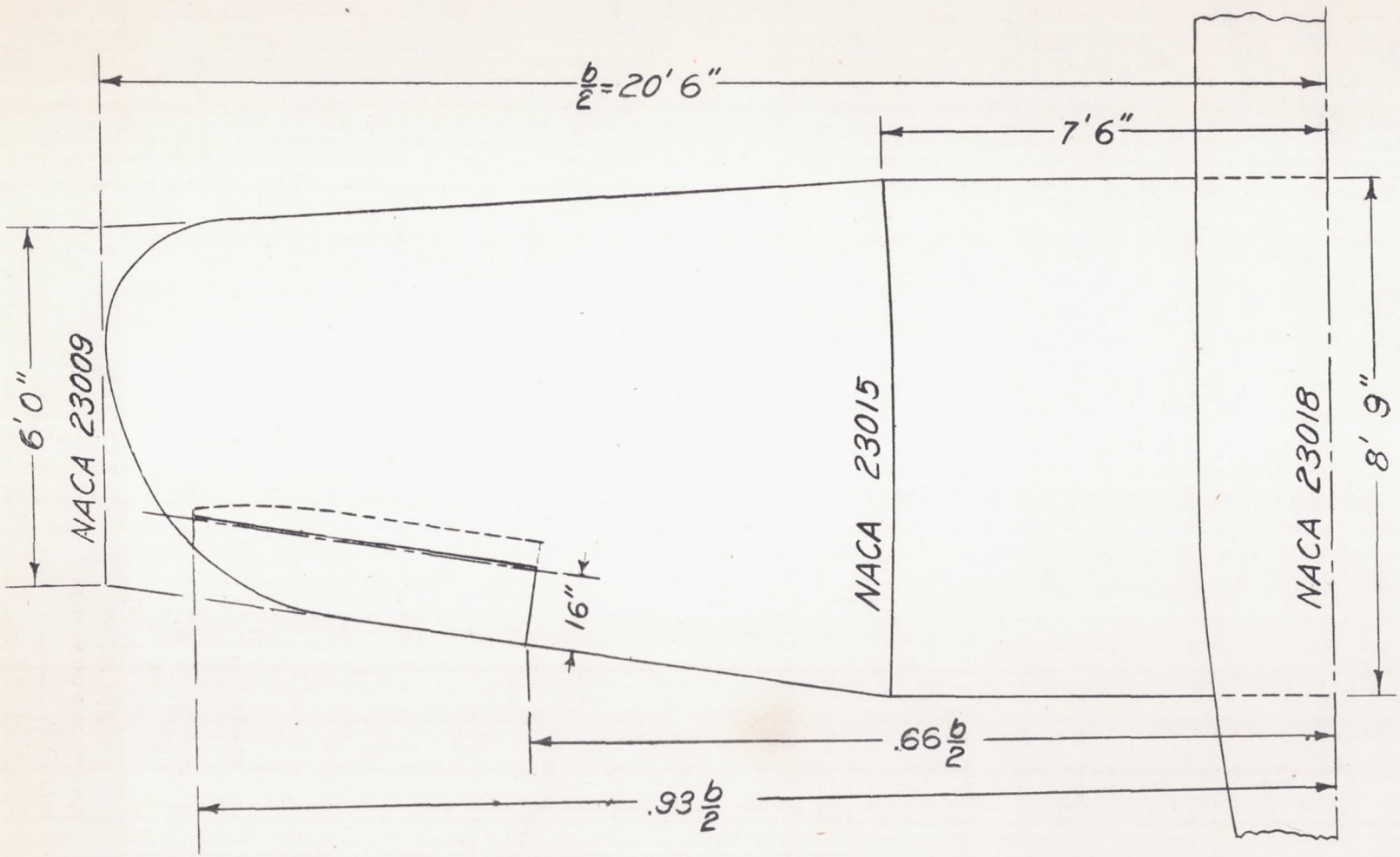

Figure A50.- Plan form of wing of fighter-type airplane tested in flight at LMAL.

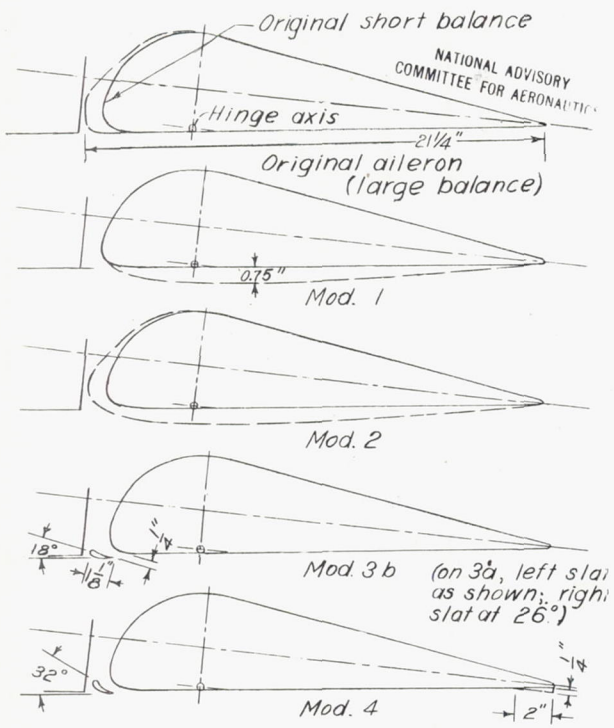

Figure A51.-The various modifications to the aileron section.

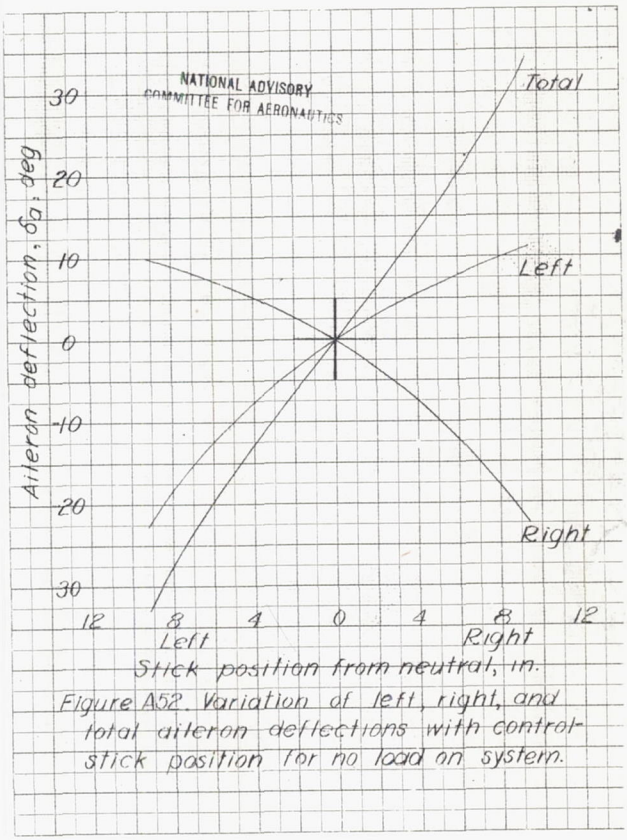

Figure A52. Variation of left, right, and total aileron deflections with control-stick position for no load on system.

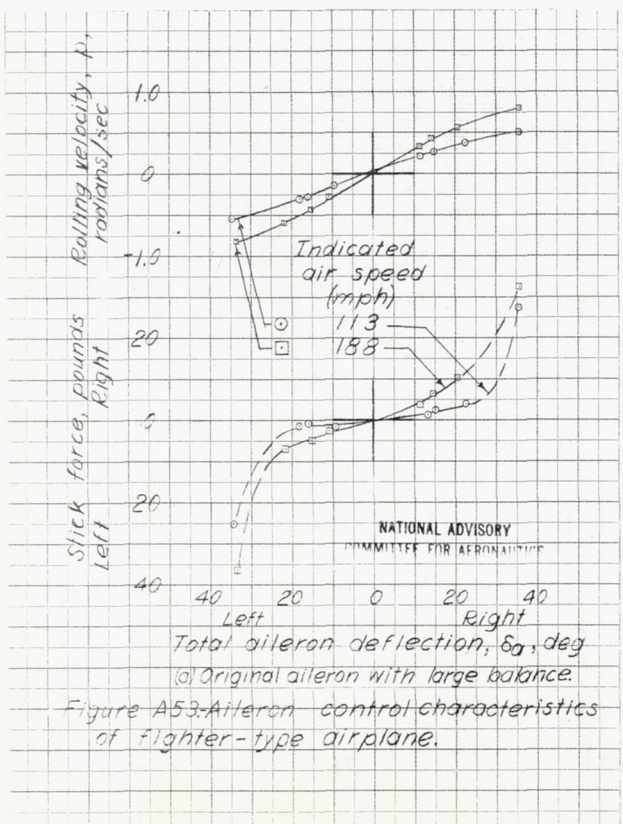

(a) Original aileron with large balance.

Figure A53.-Aileron control characteristics of fighter-type airplane.

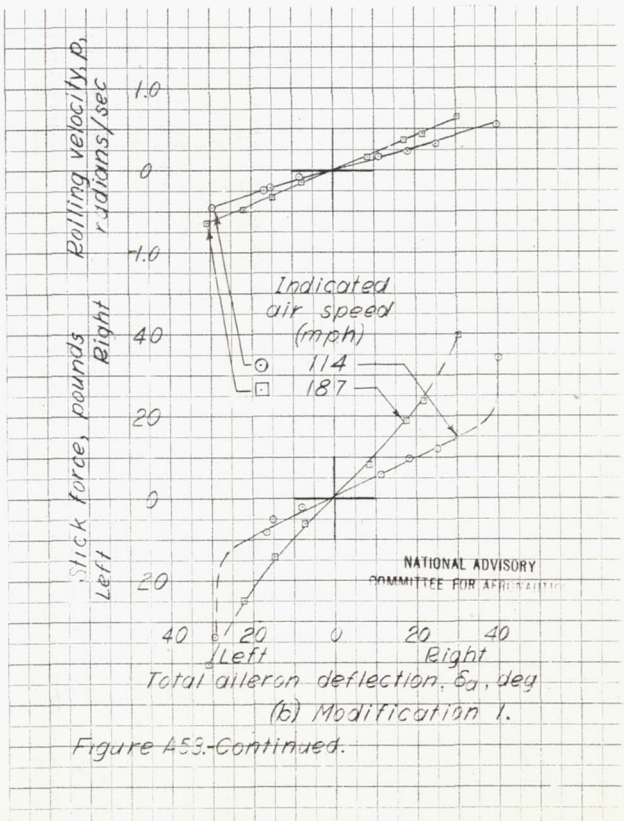

(b) Modification 1.

Figure A53.-Continued.

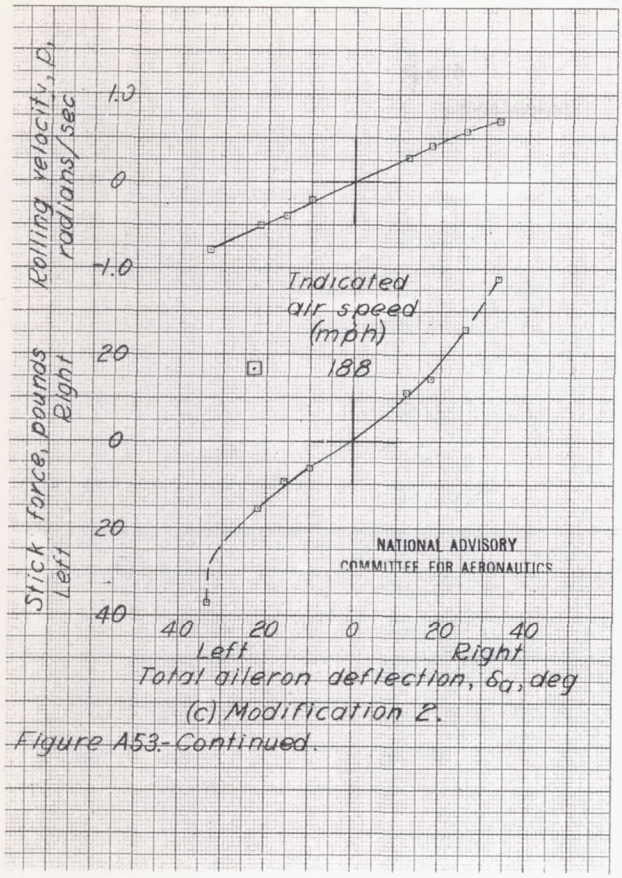

(c) Modification 2.

Figure A53.- Continued.

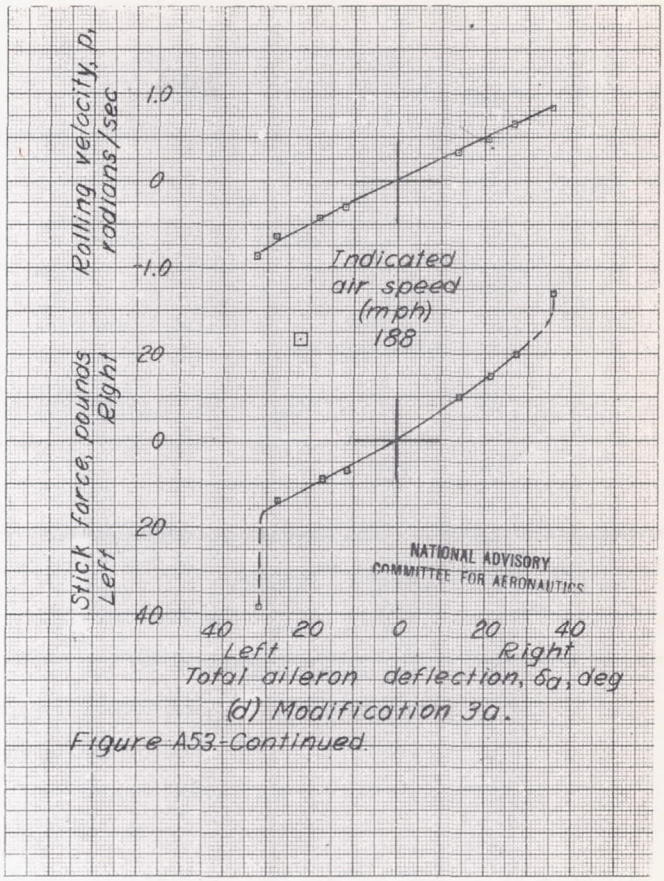

(d) Modification 3a.

Figure A53.- Continued.

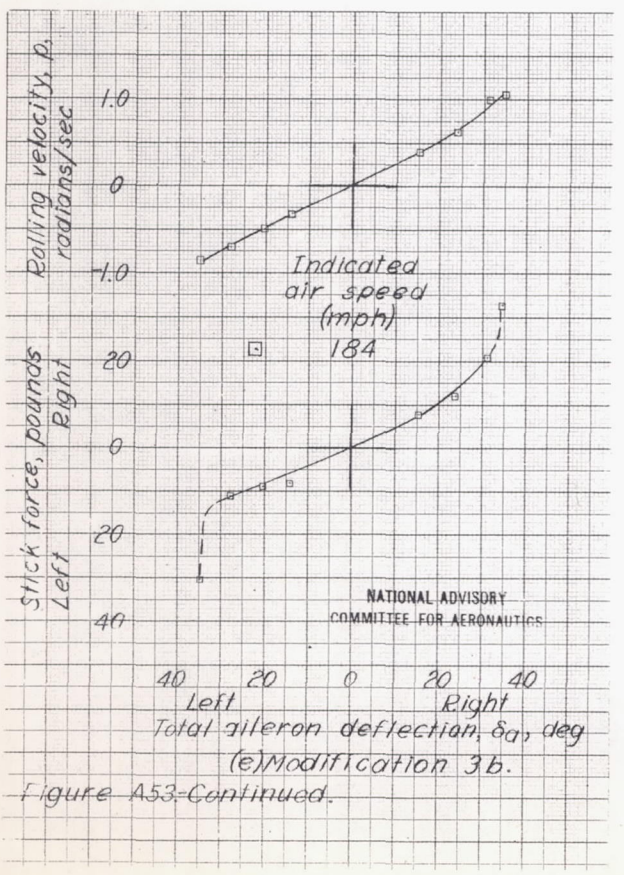

(e) Modification 3b.

Figure A53.- Continued.

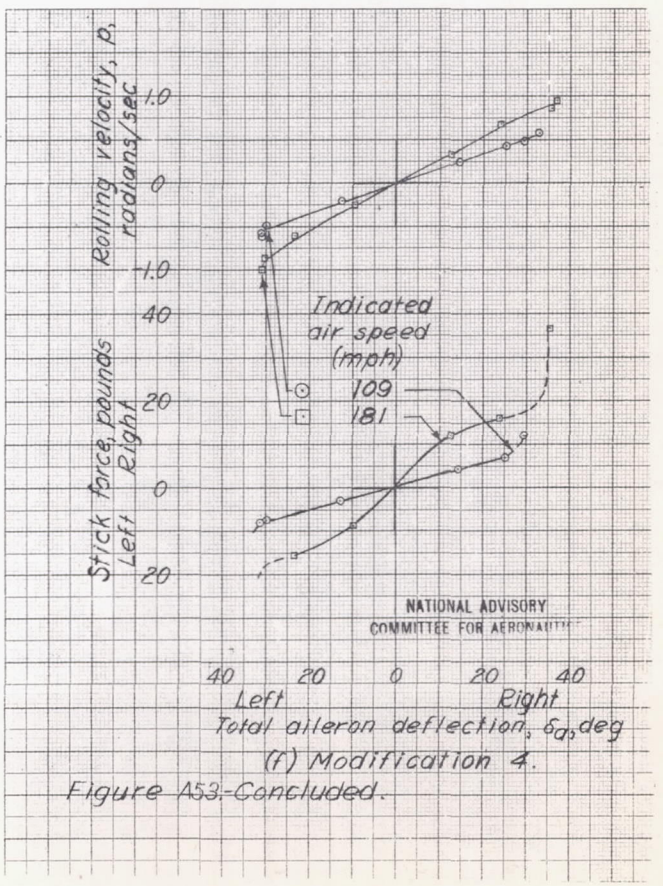

(f) Modification 4.

Figure A53.- Concluded.

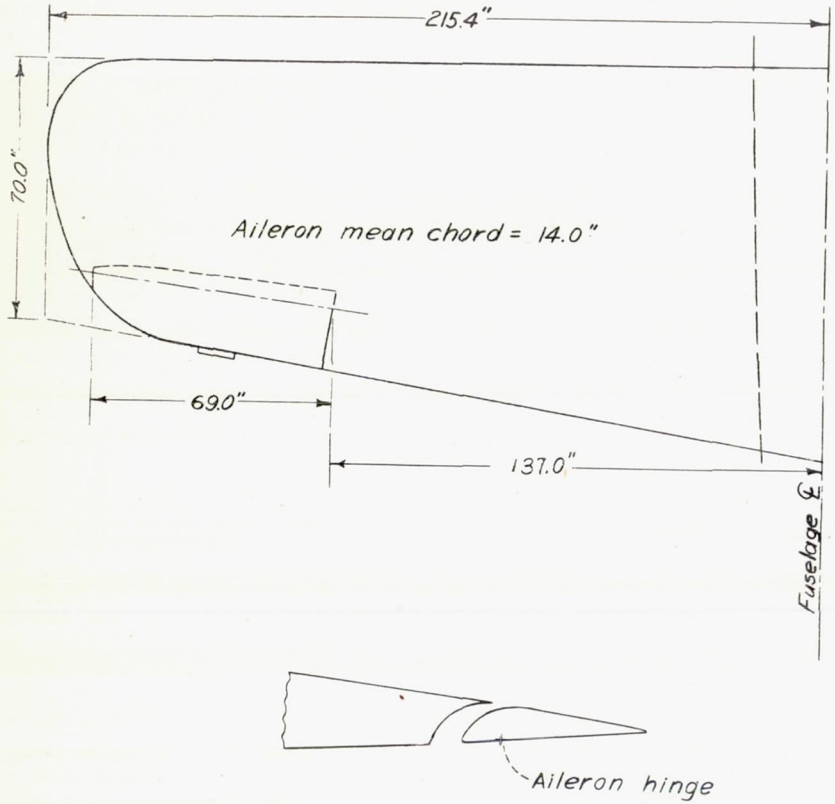

Figure A54.-Wing plan form and typical aileron section of a light scout-type airplane tested in flight at AAL.

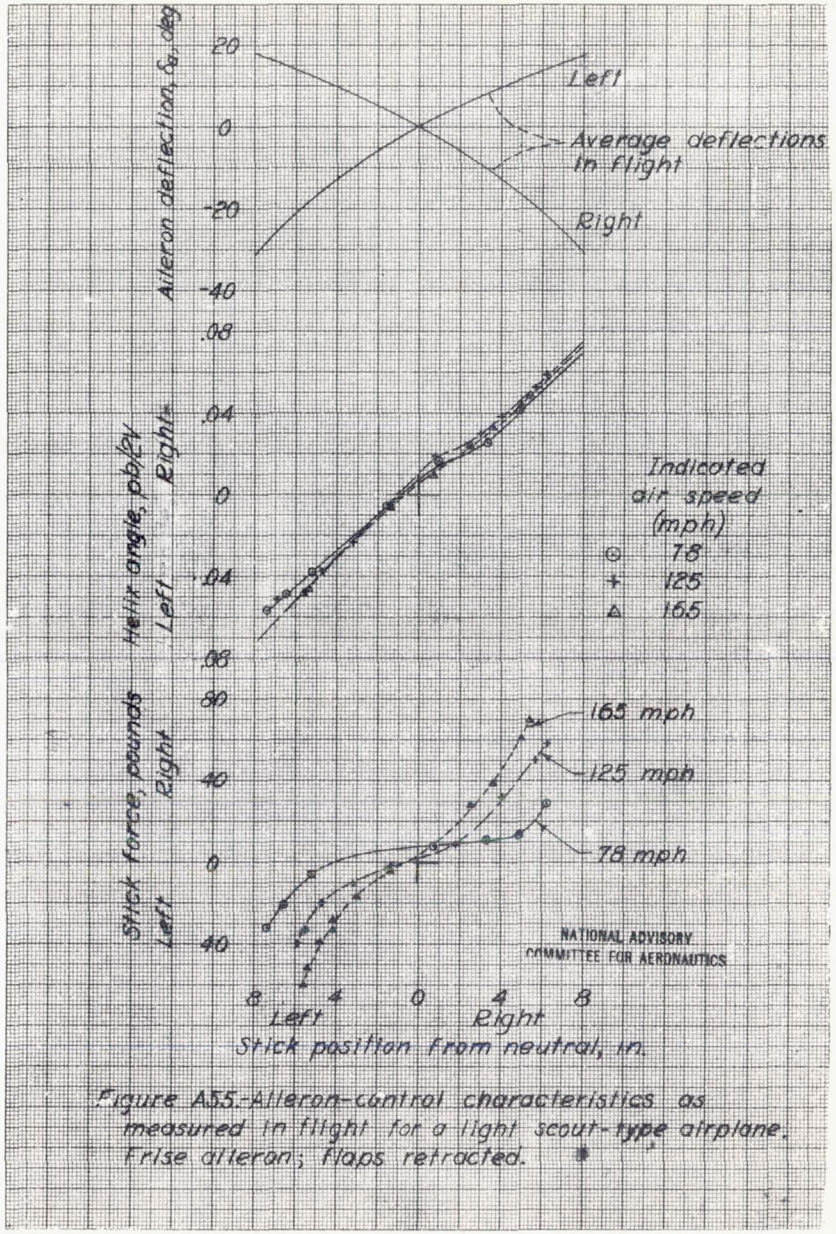

Figure A55.-Aileron-control characteristics as measured in flight for a light scout-type airplane. Frise aileron; flaps retracted.

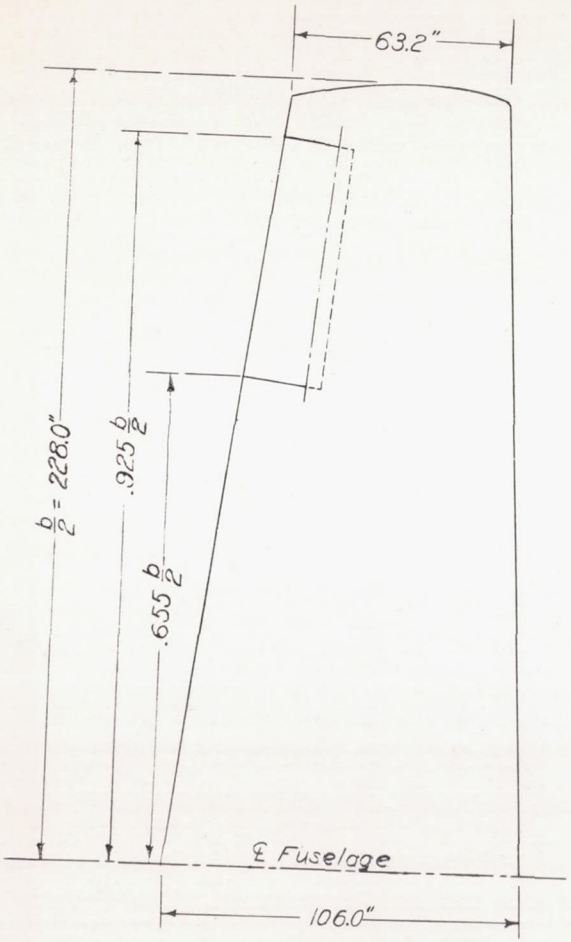

Figure A56.-Plan form of wing of fighter-type airplane tested in flight at LMAL.

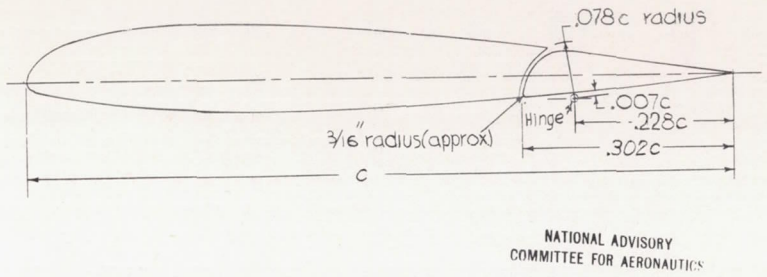

Figure A57.-Typical section through aileron portion of wing of fighter-type airplane. NACA 230-series airfoil.

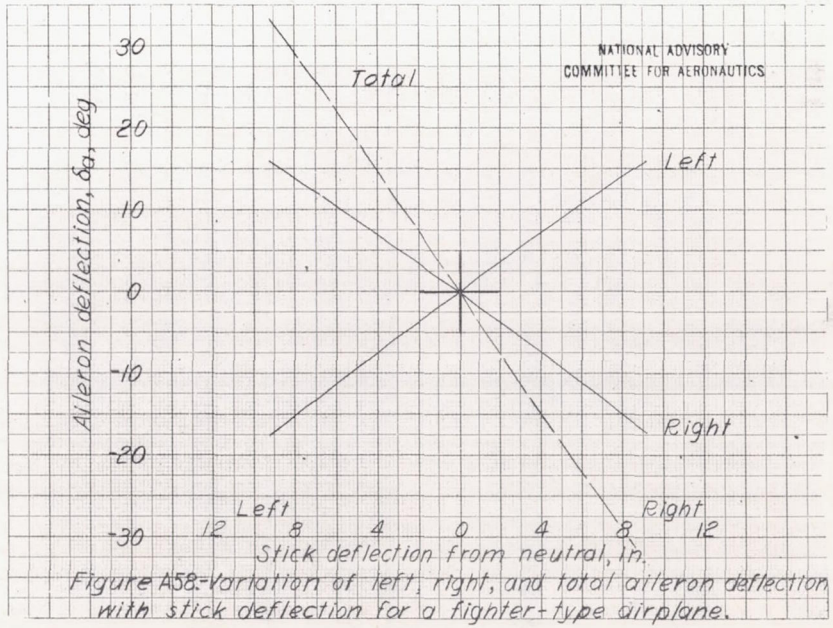

Figure A58.-Variation of left, right, and total aileron deflection with stick deflection for a fighter-type airplane.

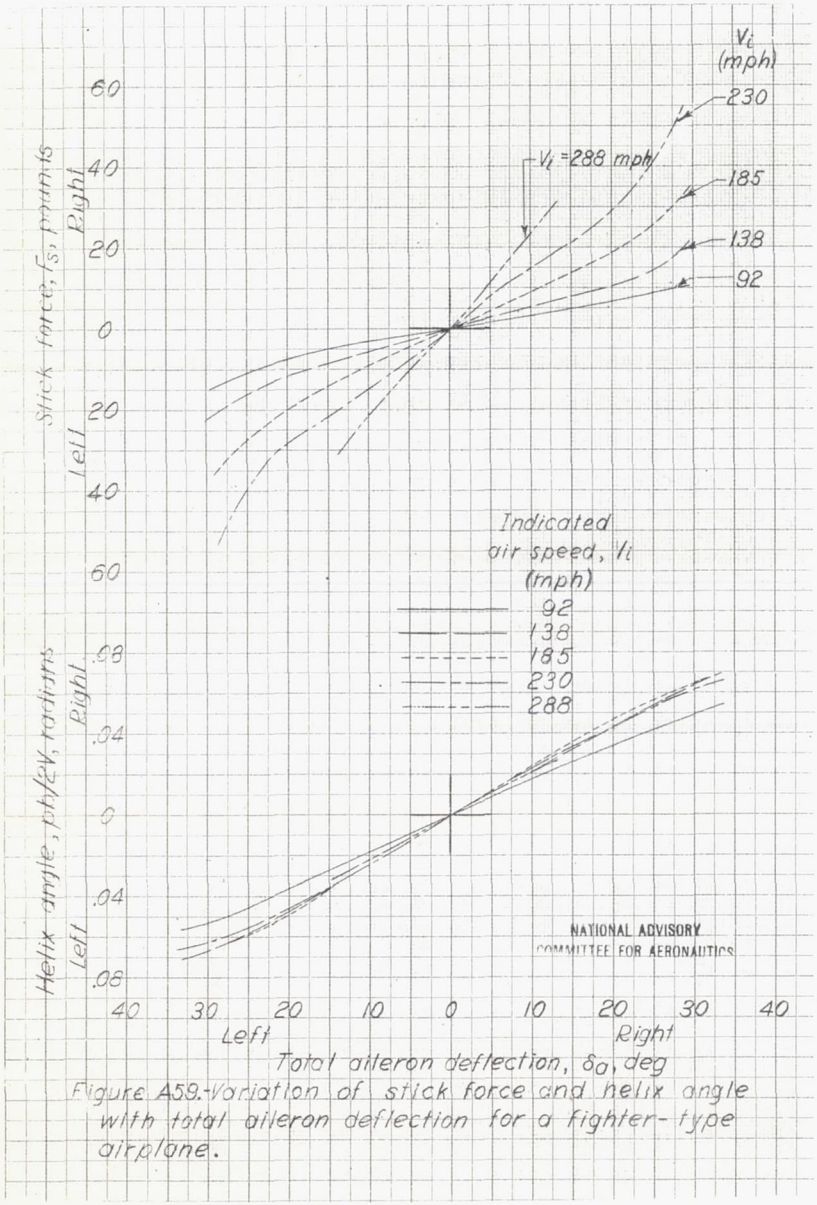

Figure A59.-Variation of stick force and helix angle with total aileron deflection for a fighter-type airplane.

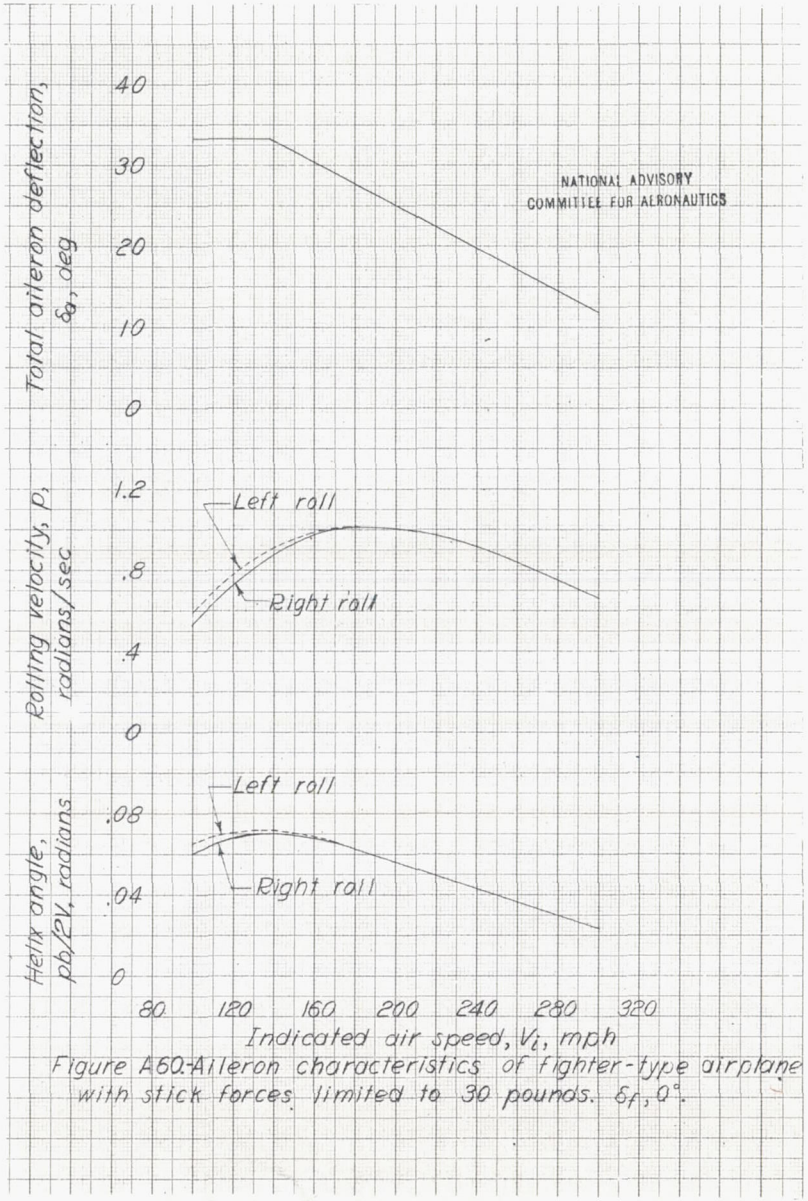

Figure A60.-Aileron characteristics of fighter-type airplane with stick forces limited to 30 pounds. δ_f, 0°.

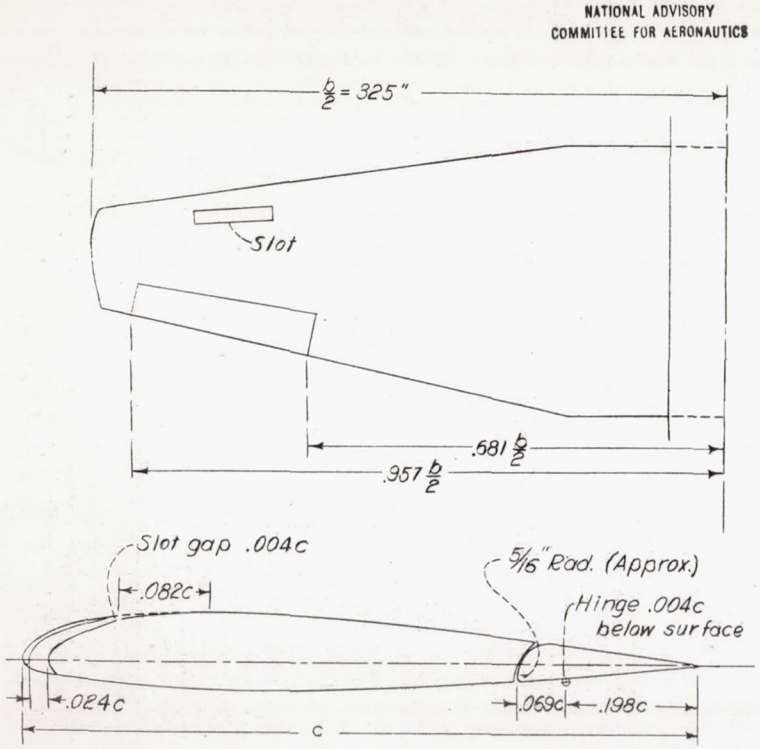

Figure A61.- Plan form of wing and typical section through the aileron portion of the wing of an airplane tested in flight at LMAL.

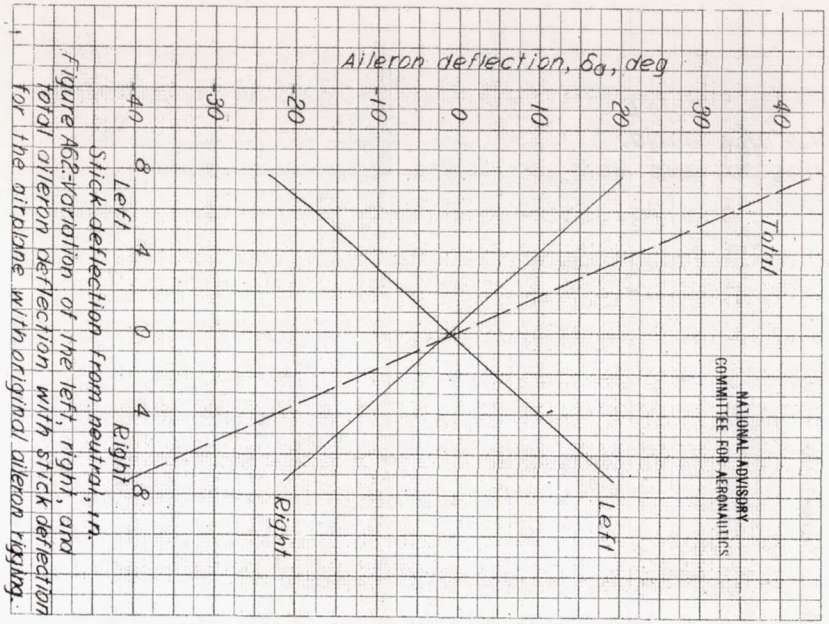

Figure A62.- Variation of the left, right, and total aileron deflection with stick deflection for the airplane with original aileron rigging.

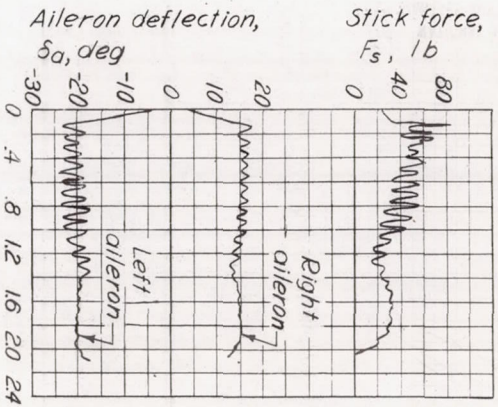

Figure A63.- Time history for an abrupt full left aileron deflection with original aileron rigging. Level flight; wing slots open; V_i, 120 mph; δ_f, 0°.

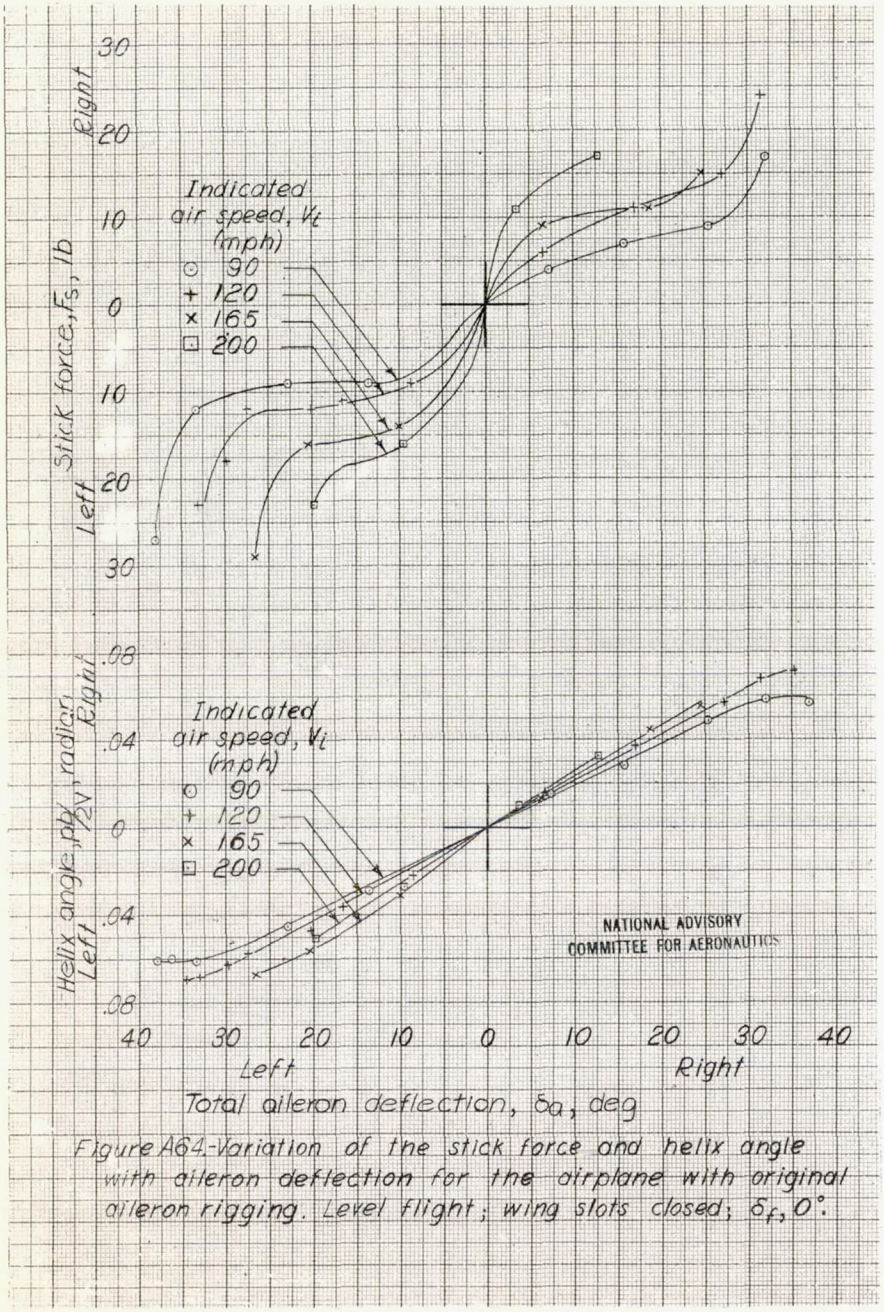

Figure A64-Variation of the stick force and helix angle with aileron deflection for the airplane with original aileron rigging. Level flight; wing slots closed; δ_f, 0°.

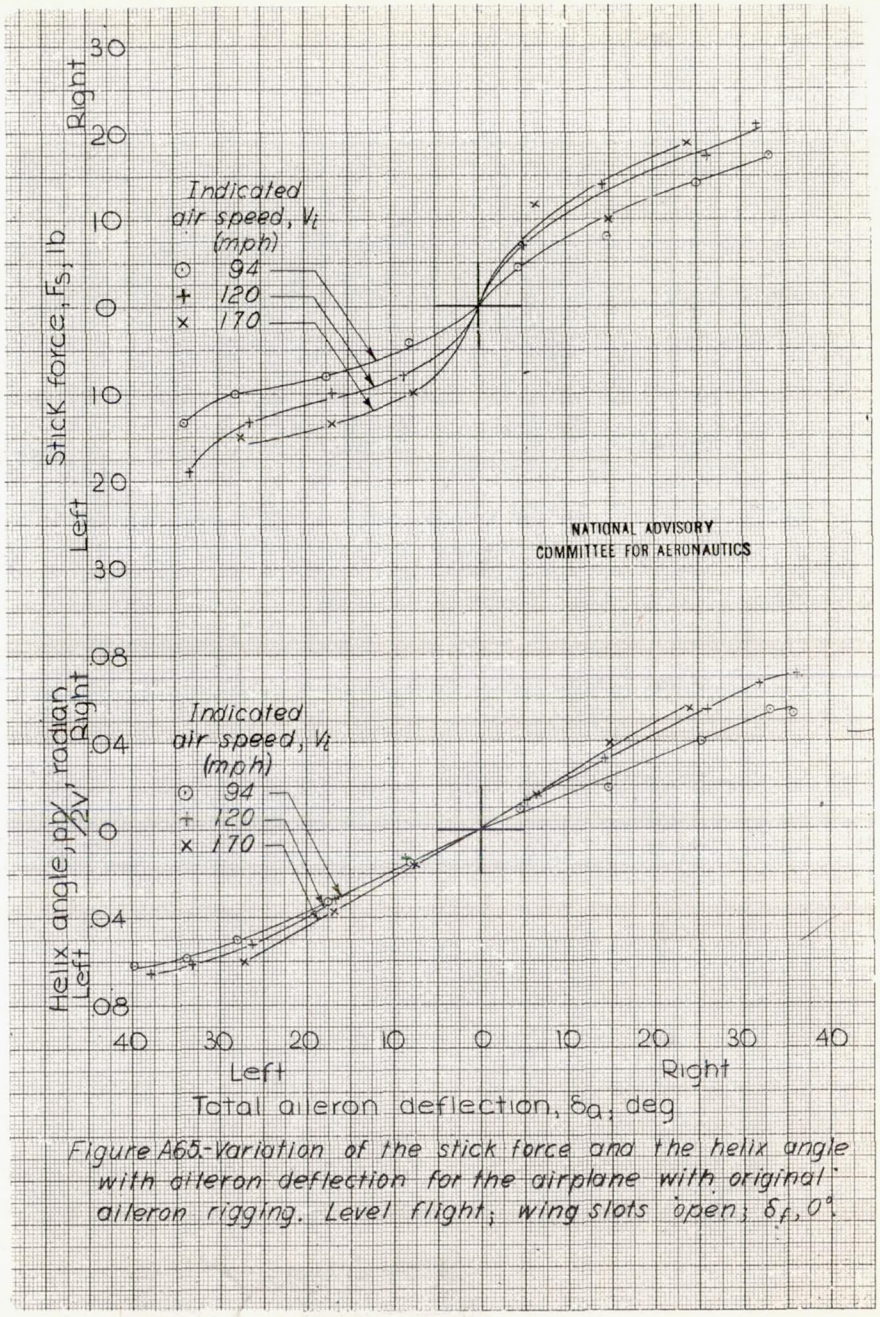

Figure A65-Variation of the stick force and the helix angle with aileron deflection for the airplane with original aileron rigging. Level flight; wing slots open; δ_f, 0°.

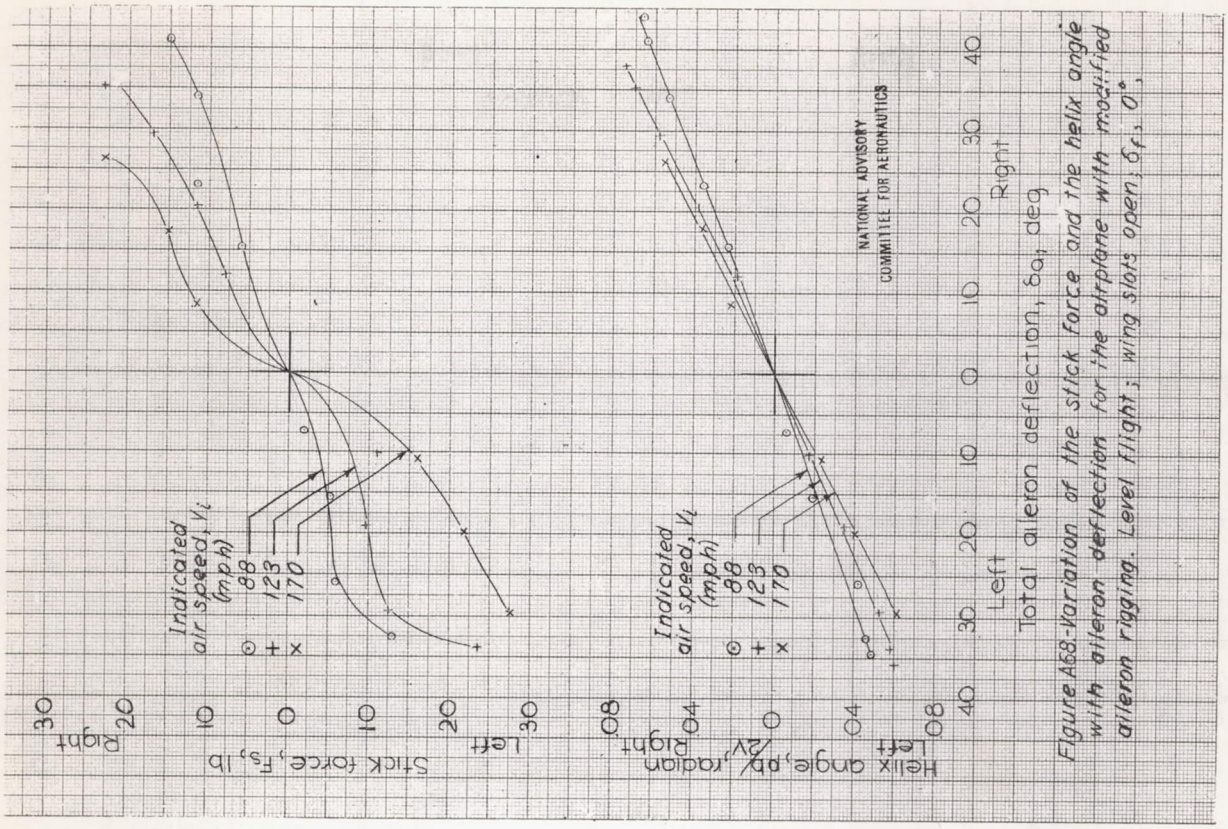

Figure A68.-Variation of the stick force and the helix angle with aileron deflection for the airplane with modified aileron rigging. Level flight; wing slots open; δ_f, 0°.

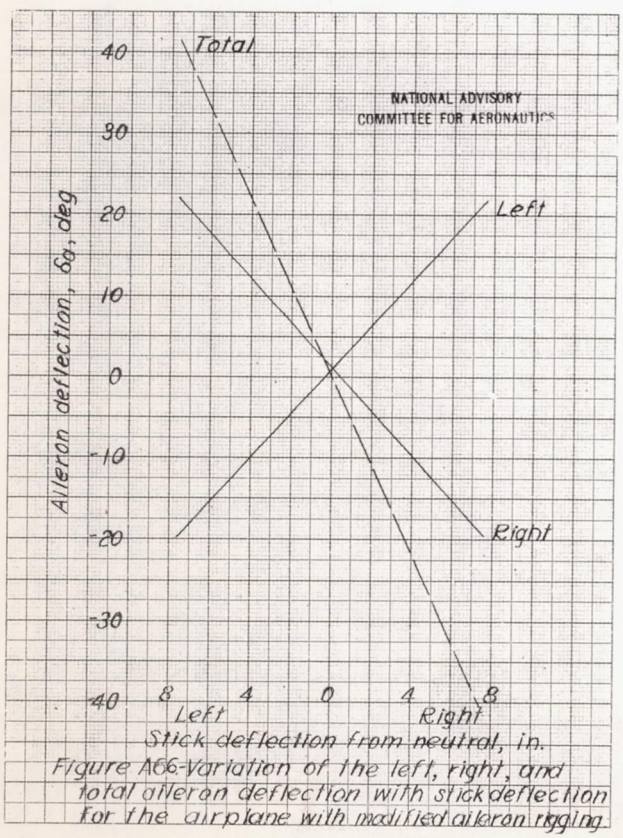

Figure A66.-Variation of the left, right, and total aileron deflection with stick deflection for the airplane with modified aileron rigging.

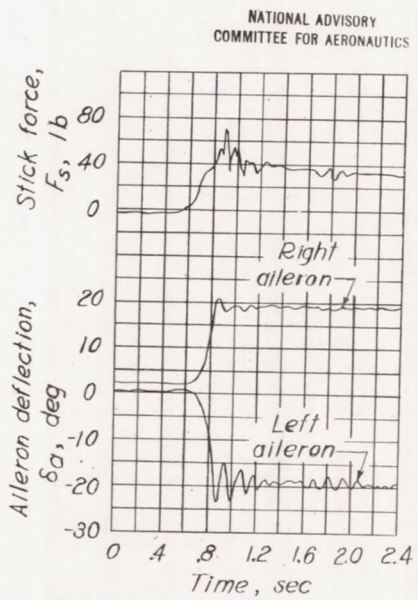

Figure A67.-Time history for an abrupt full left aileron deflection with modified aileron rigging. Level flight; wing slots open; V_i, 120 mph; δ_f, 0°.

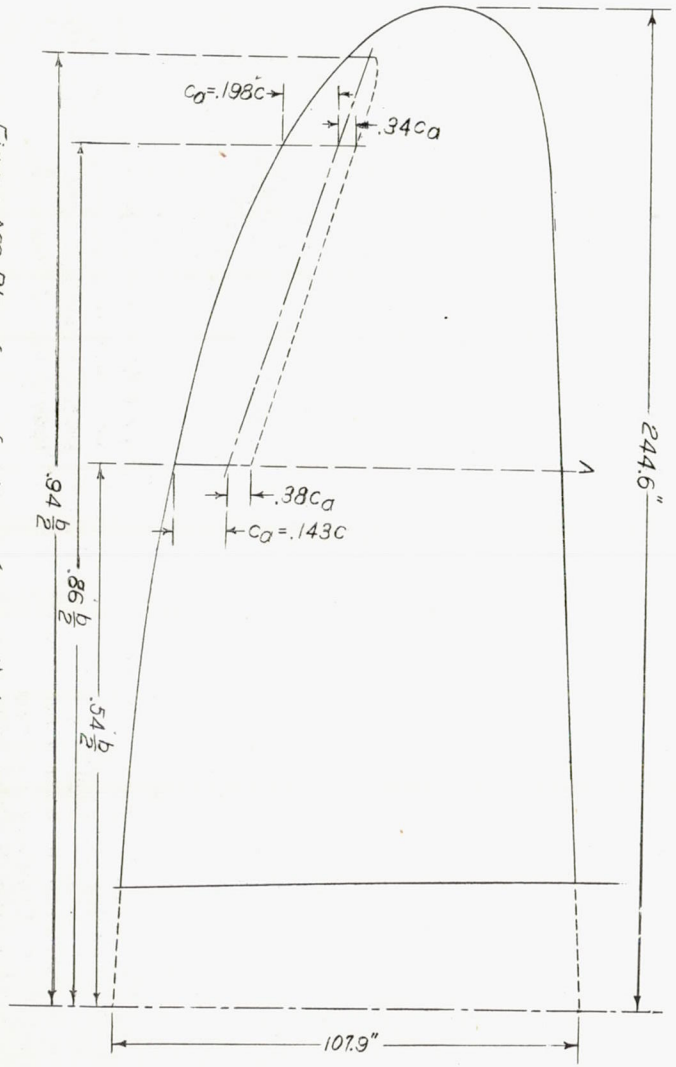

Figure A69.-Plan form of wing of pursuit-type airplane tested in flight at LMAL.

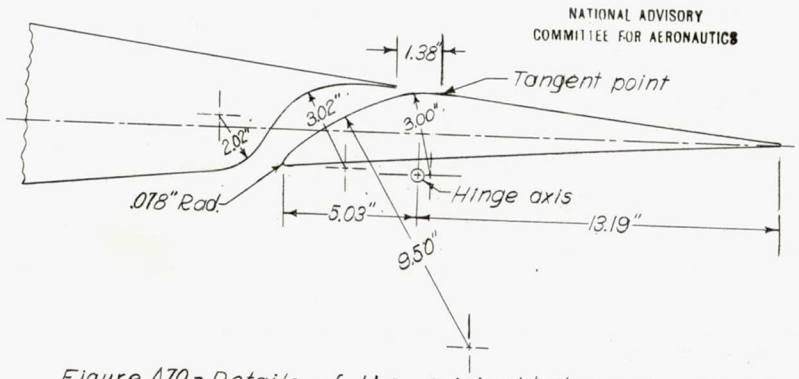

Figure A70.- Details of the original aileron at section A.

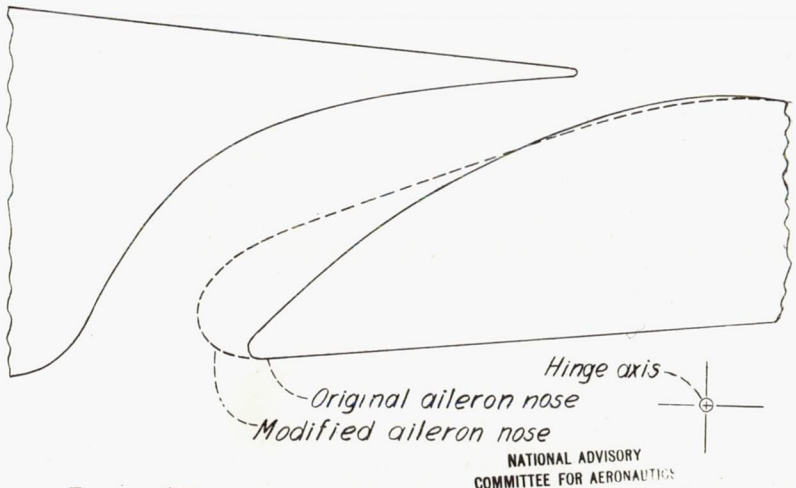

Figure A71.-Original nose and modified nose of the aileron of the pursuit-type airplane.

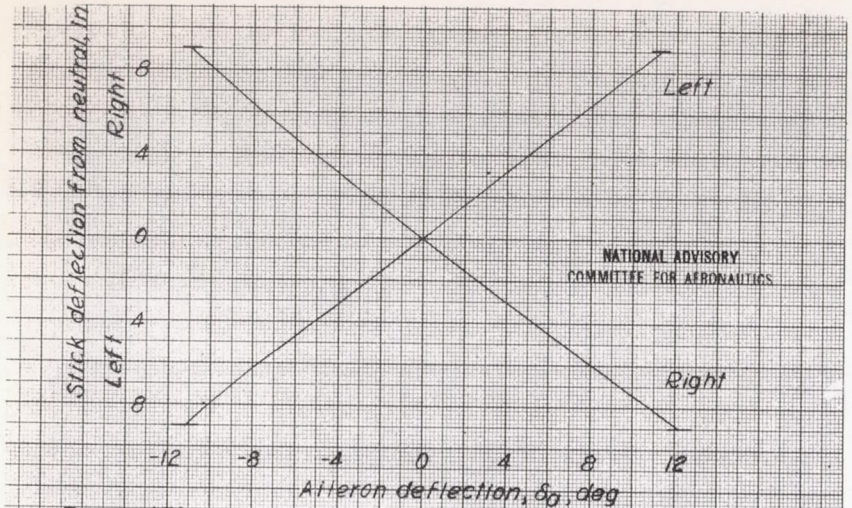

Figure A72.-Variation of the left and right aileron deflection with stick deflection for the pursuit-type airplane. NACA modified ailerons; aileron deflection range, ±11°.

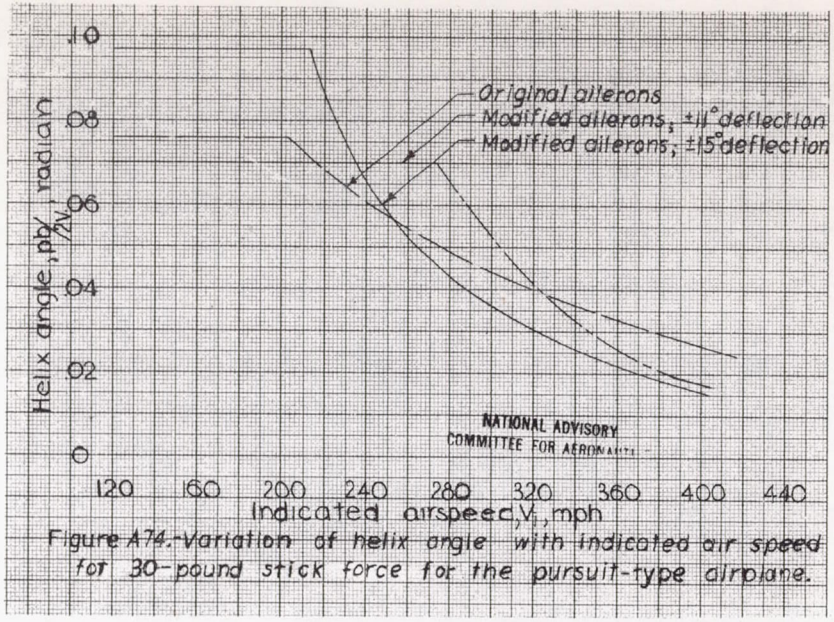

Figure A74.-Variation of helix angle with indicated air speed for 30-pound stick force for the pursuit-type airplane.

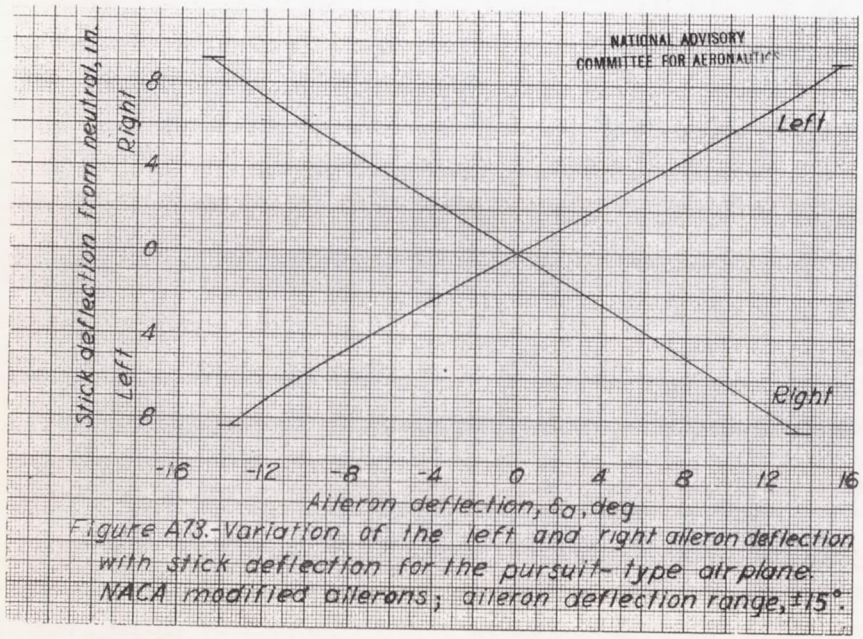

Figure A73.-Variation of the left and right aileron deflection with stick deflection for the pursuit-type airplane. NACA modified ailerons; aileron deflection range, ±15°.

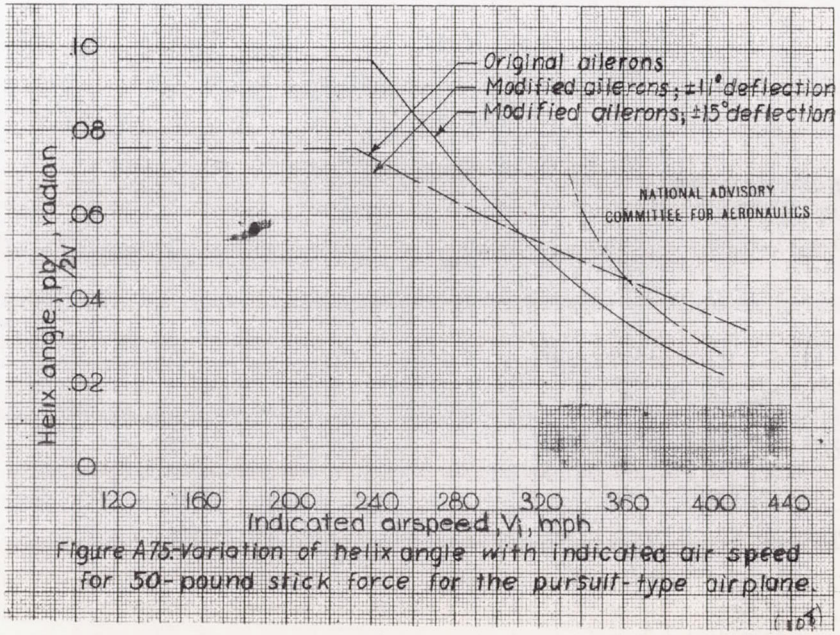

Figure A75.-Variation of helix angle with indicated air speed for 50-pound stick force for the pursuit-type airplane.

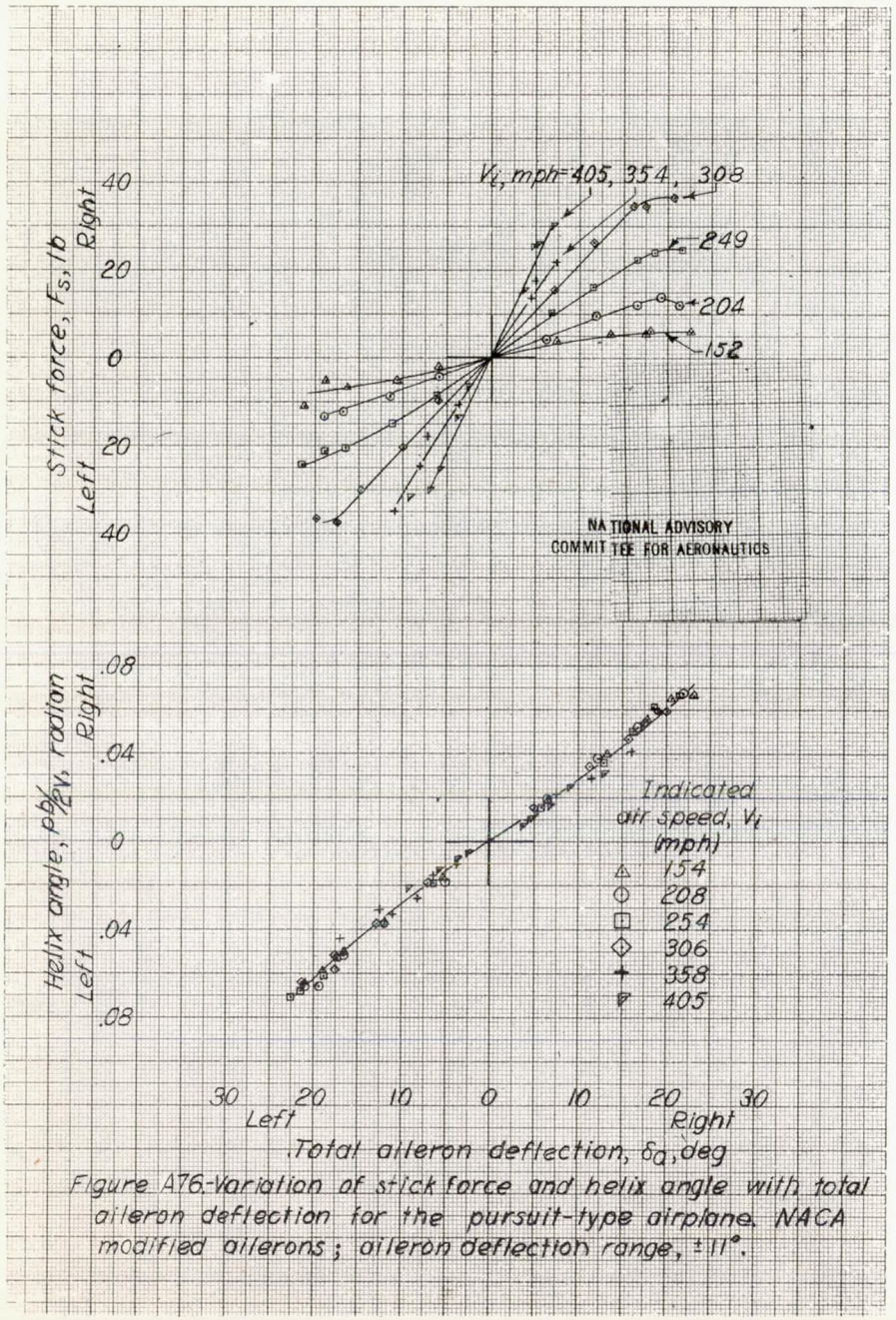

Figure A76.-Variation of stick force and helix angle with total aileron deflection for the pursuit-type airplane. NACA modified ailerons; aileron deflection range, ±11°.

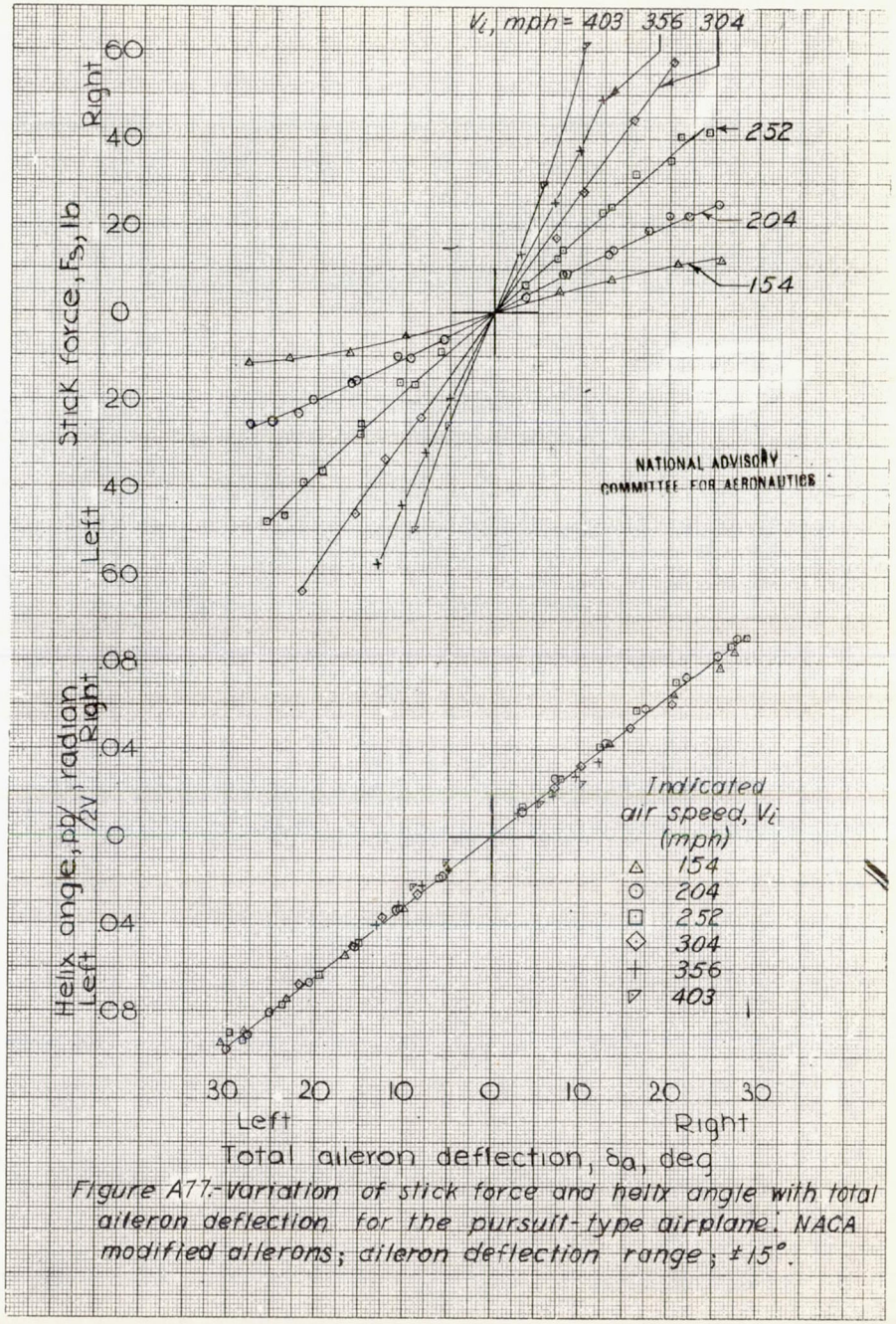

Figure A77.-Variation of stick force and helix angle with total aileron deflection for the pursuit-type airplane. NACA modified ailerons; aileron deflection range, ±15°.

Airplane A-XVI

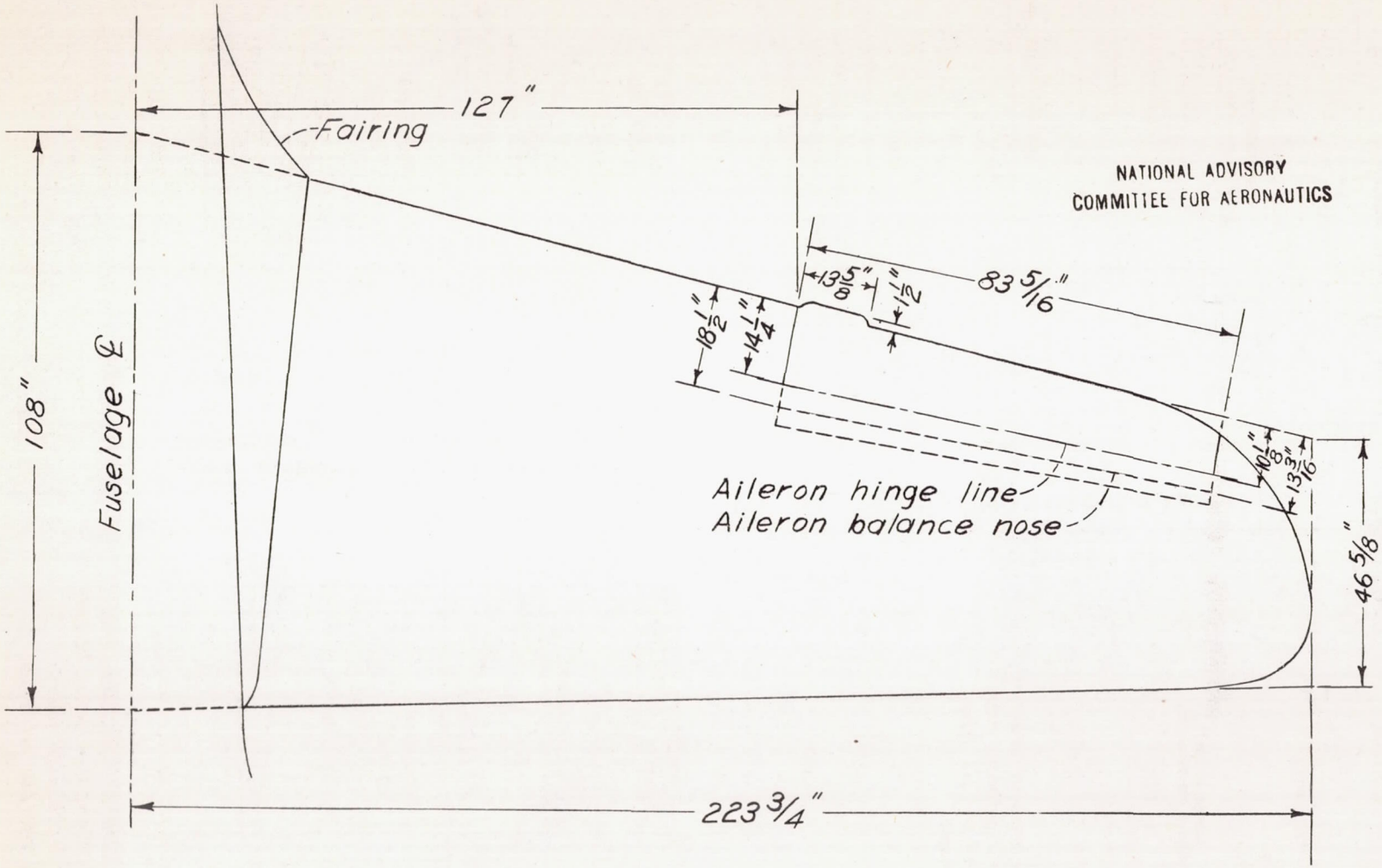

Figure A78.-Plan form of the wing of a pursuit-type airplane tested in flight at LMAL.

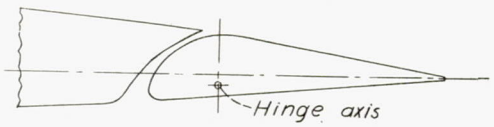

Inboard station

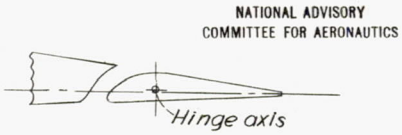

Outboard station

Figure A79.- Aileron sections at stations near the inboard and outboard ends of the aileron of the pursuit-type airplane tested in flight.

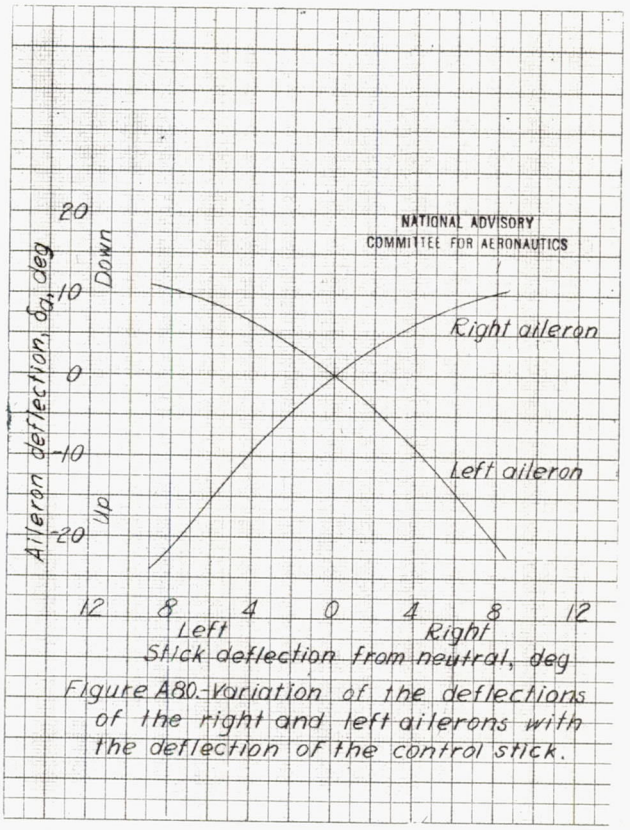

Figure A80.- Variation of the deflections of the right and left ailerons with the deflection of the control stick.

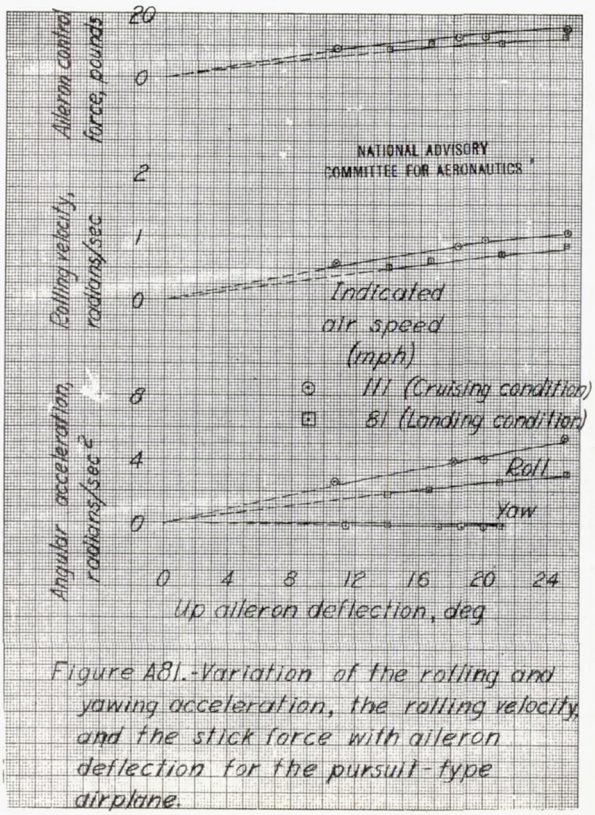

Figure A81.- Variation of the rolling and yawing acceleration, the rolling velocity, and the stick force with aileron deflection for the pursuit-type airplane.

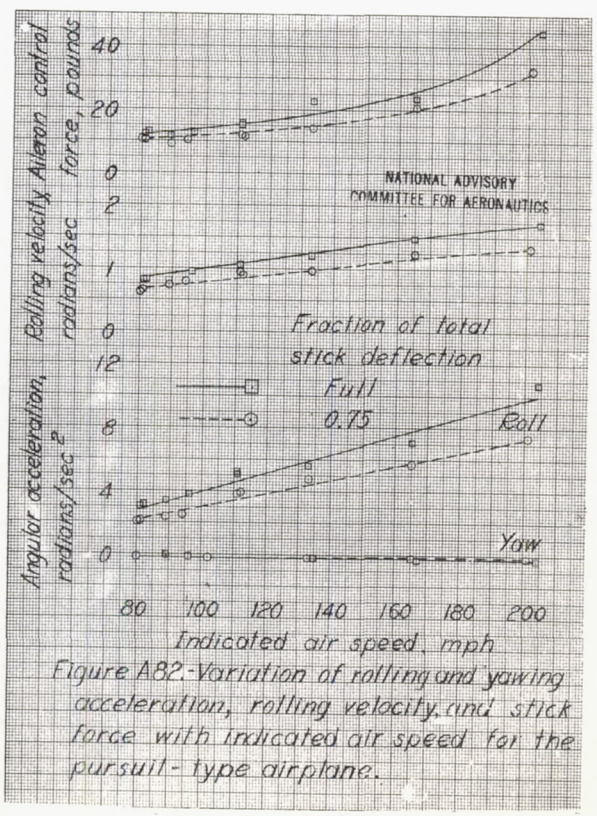

Figure A82.- Variation of rolling and yawing acceleration, rolling velocity, and stick force with indicated air speed for the pursuit-type airplane.

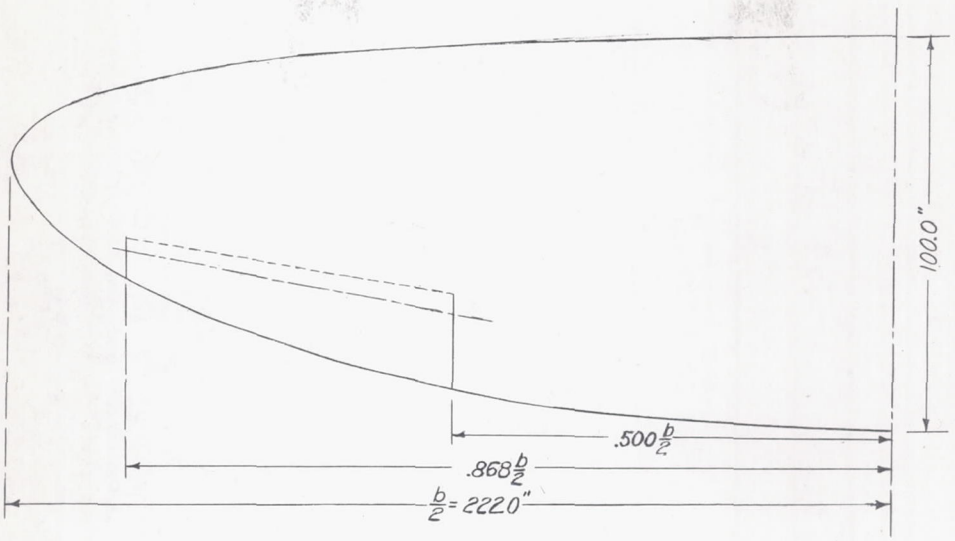

NATIONAL ADVISORY
COMMITTEE FOR AERONAUTICS

Figure A83.- Plan form of wing of Supermarine Spitfire airplane tested in flight at LMAL.

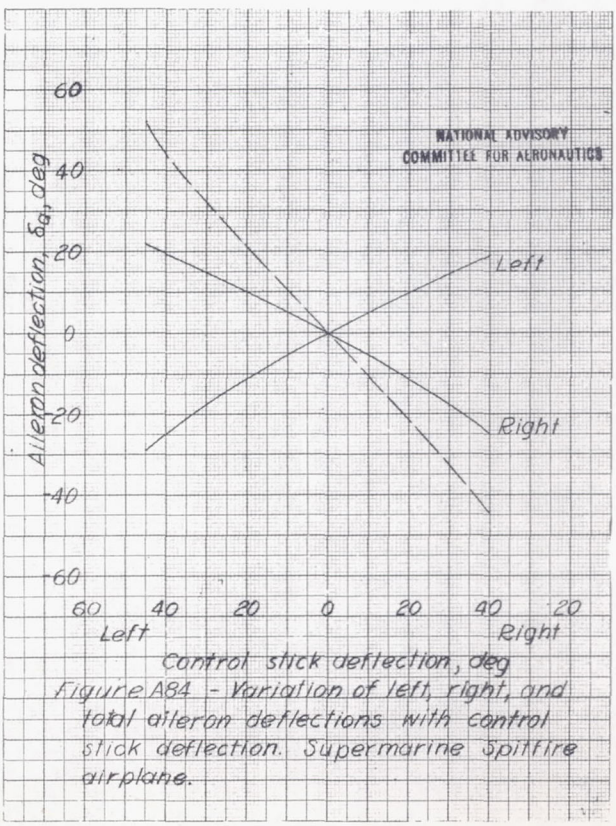

Figure A84 - Variation of left, right, and total aileron deflections with control stick deflection. Supermarine Spitfire airplane.

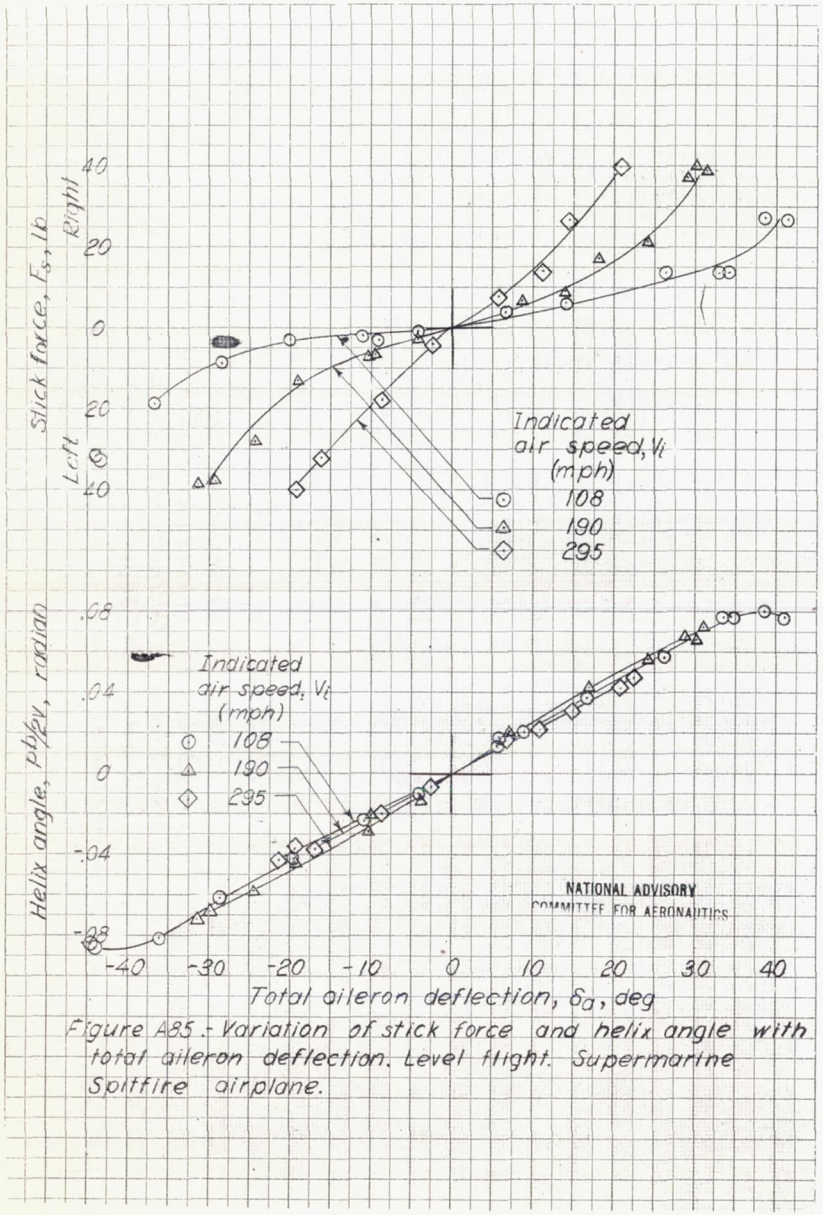

Figure A85.- Variation of stick force and helix angle with total aileron deflection. Level flight. Supermarine Spitfire airplane.

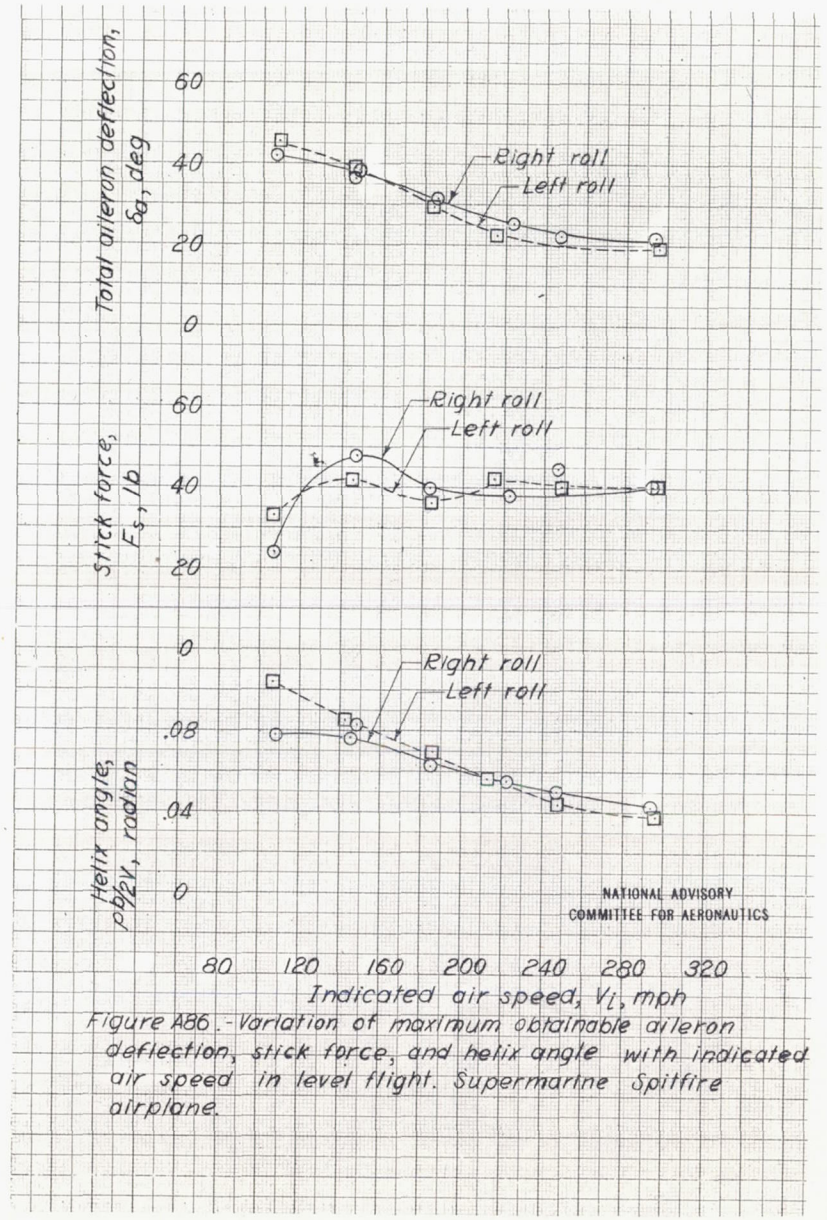

Figure A86.- Variation of maximum obtainable aileron deflection, stick force, and helix angle with indicated air speed in level flight. Supermarine Spitfire airplane.

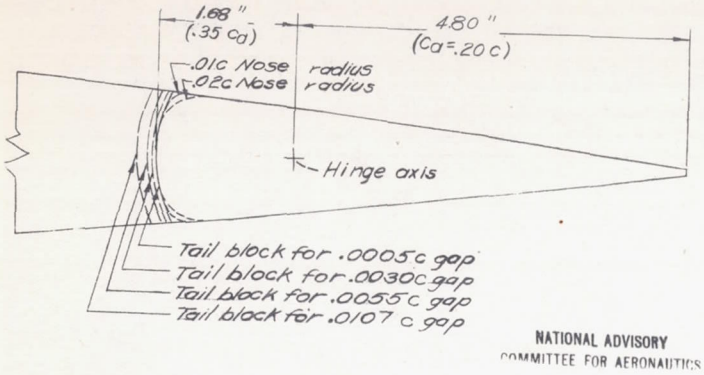

Figure B1.- Aileron section of NACA 23012 airfoil showing modifications to the nose radii and gap. NACA stability tunnel.

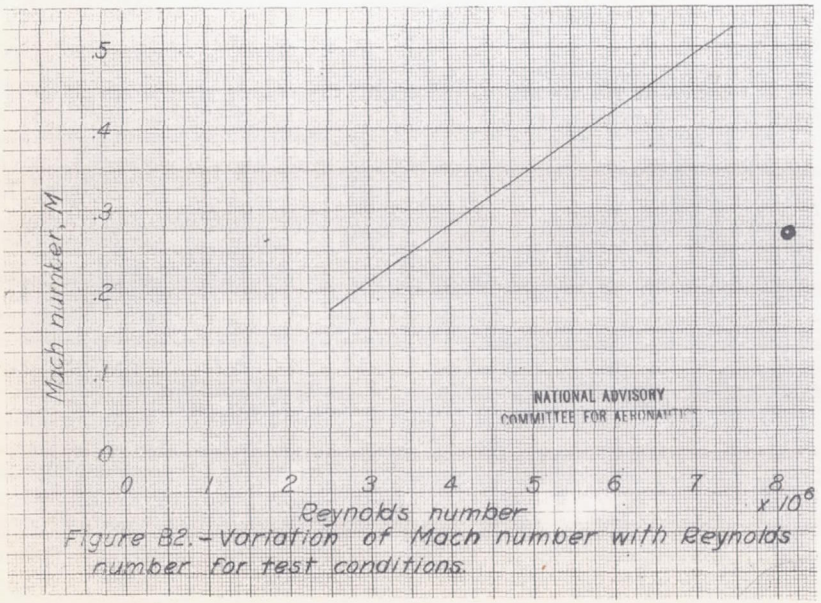

Figure B2.- Variation of Mach number with Reynolds number for test conditions.

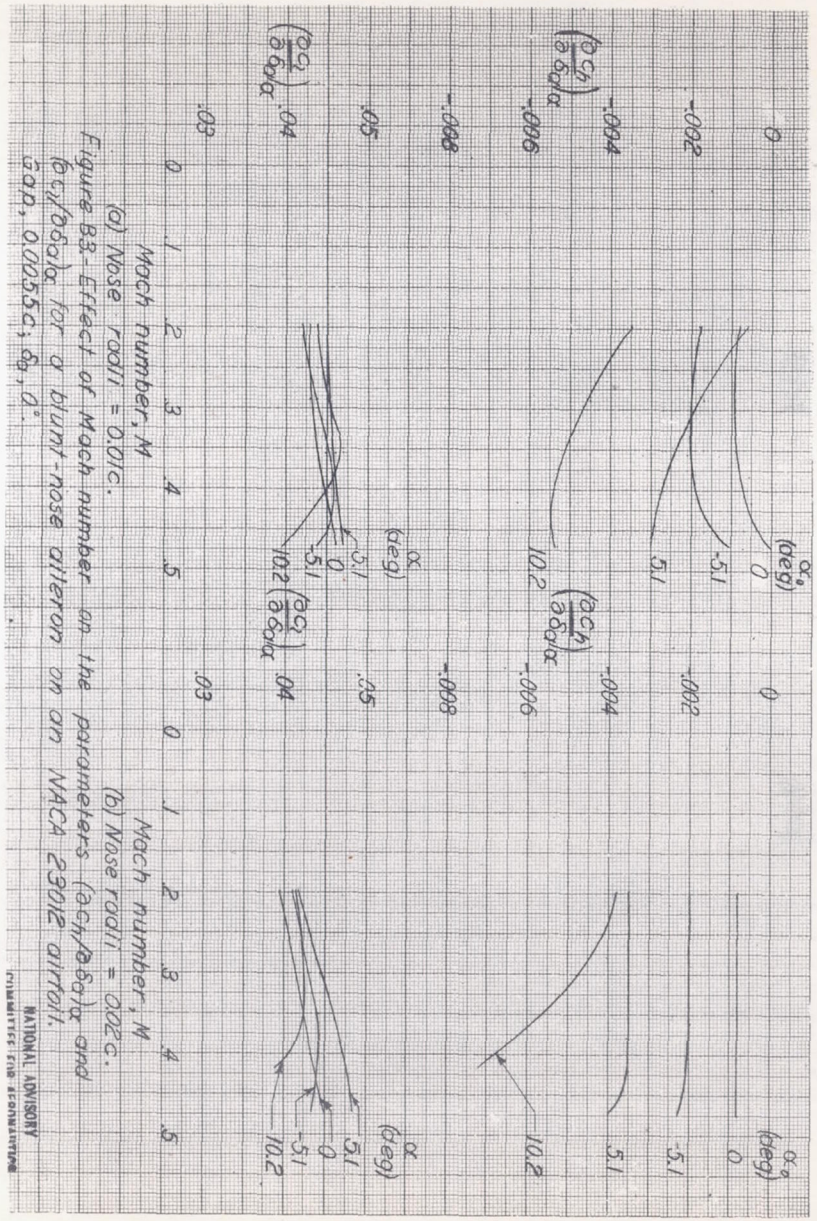

Figure B3.- Effect of Mach number on the parameters $\left(\frac{\partial c_h}{\partial \delta_a \alpha}\right)_\alpha$ and $\left(\frac{\partial c_l}{\partial \delta_a \alpha}\right)_\alpha$ for a blunt-nose aileron on an NACA 23012 airfoil. $\bar{c}_{a_0}$, 0.0055c; δ_a, 0°.

Model B-1

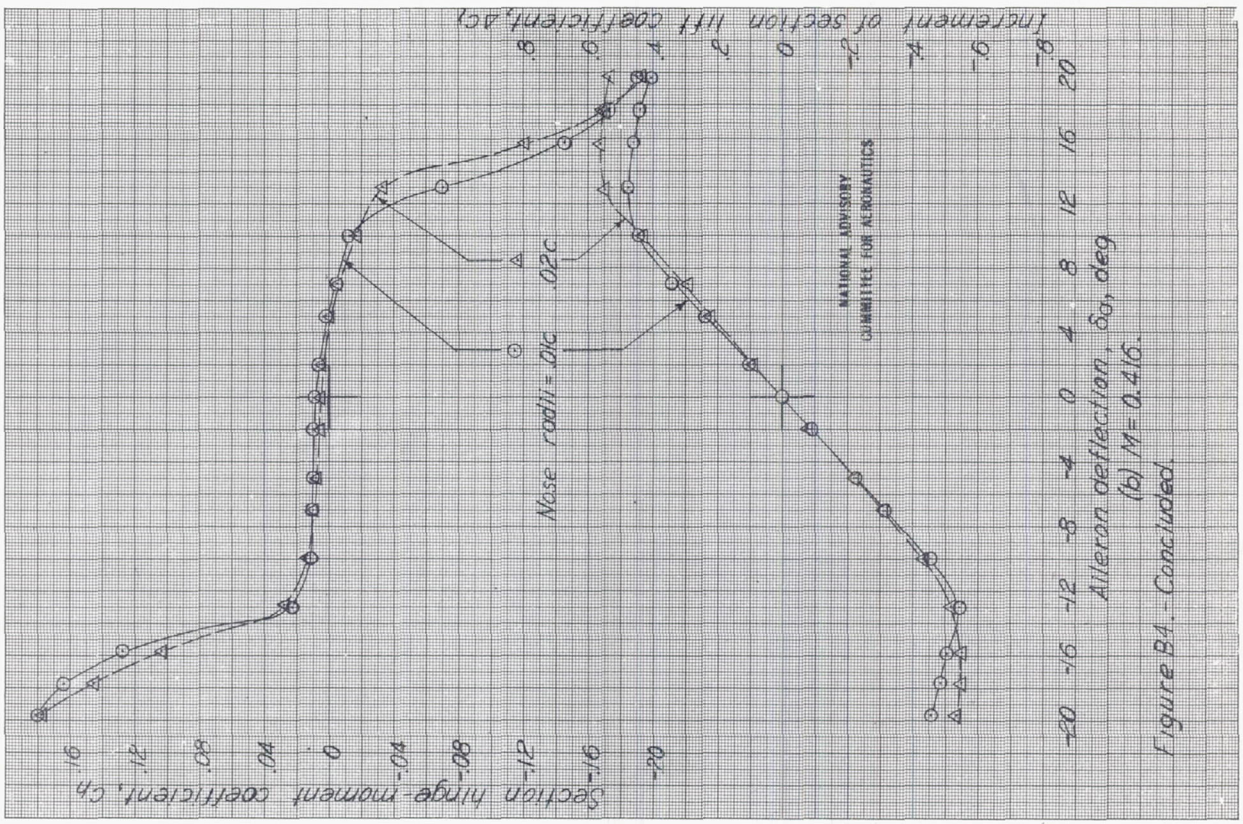

Figure B4.- Concluded.

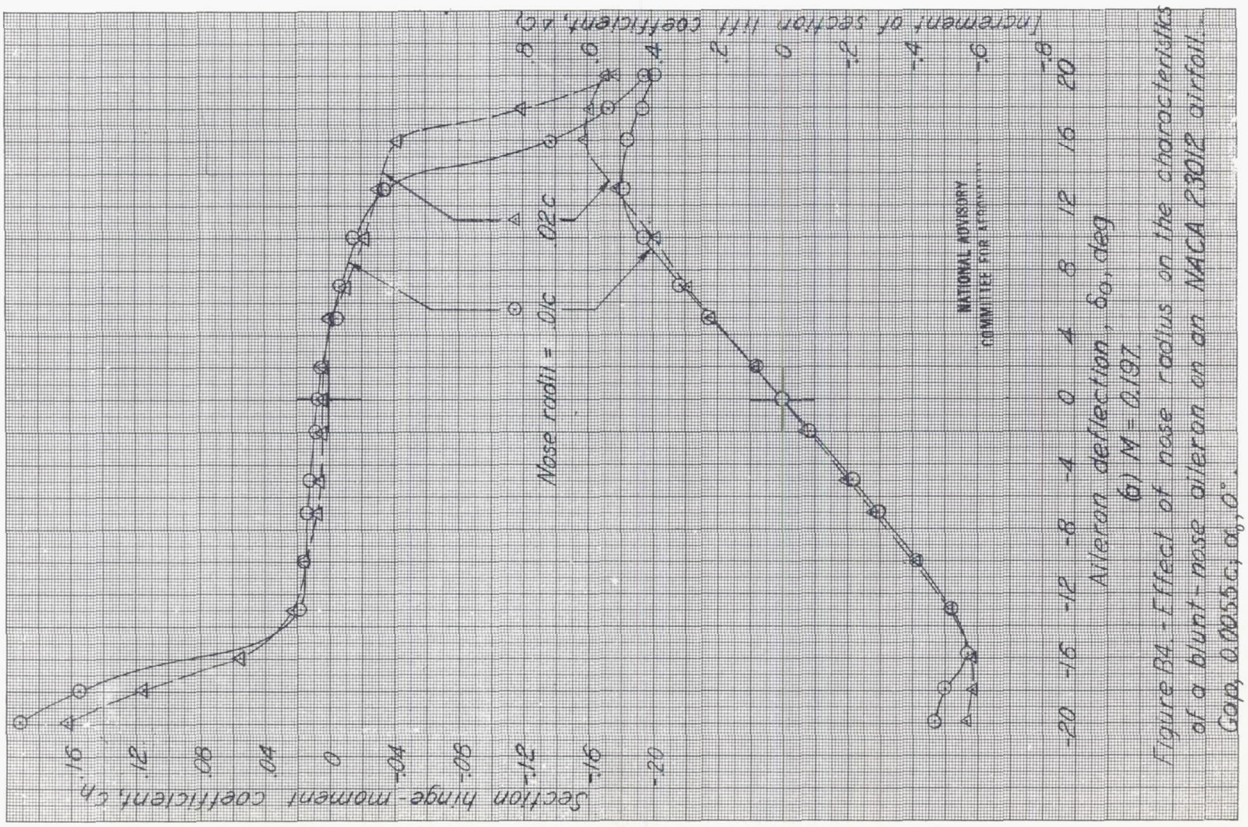

Figure B4.- Effect of nose radius on the characteristics of a blunt-nose aileron on an NACA 23012 airfoil. Gap, 0.005c; α_a, 0°.

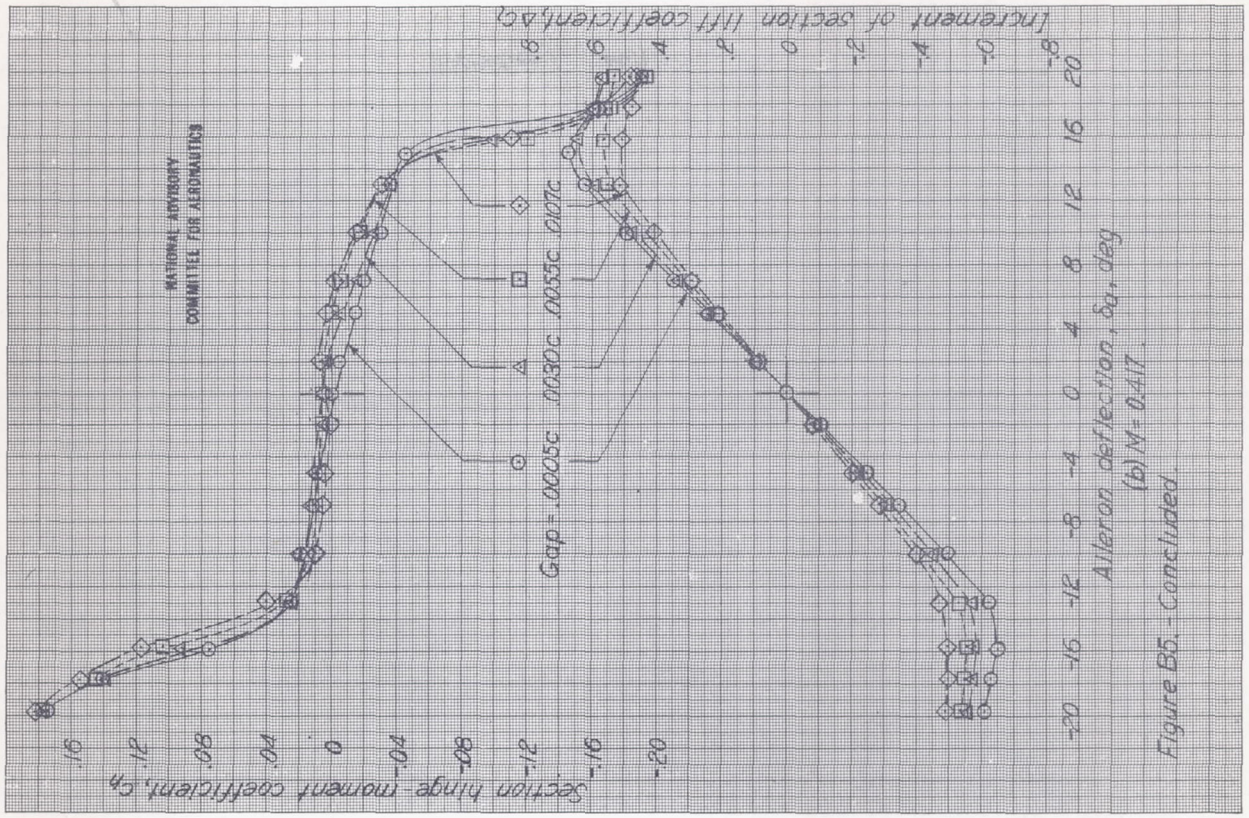

(b) M = 0.417.

Figure B5.- Concluded.

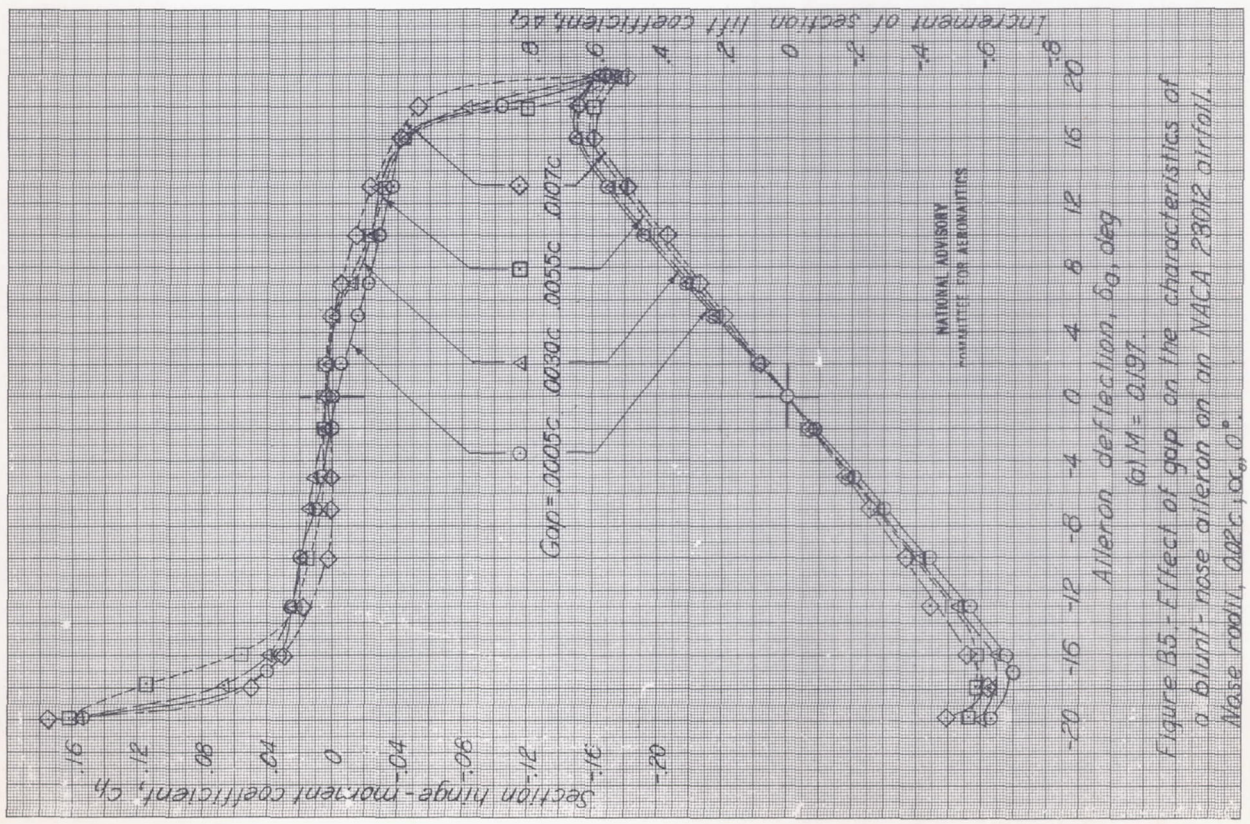

(a) M = 0.197.

Figure B5.- Effect of gap on the characteristics of a blunt-nose aileron on an NACA 23012 airfoil. Nose radius, .002c; α_a, 0°.

Model B- I

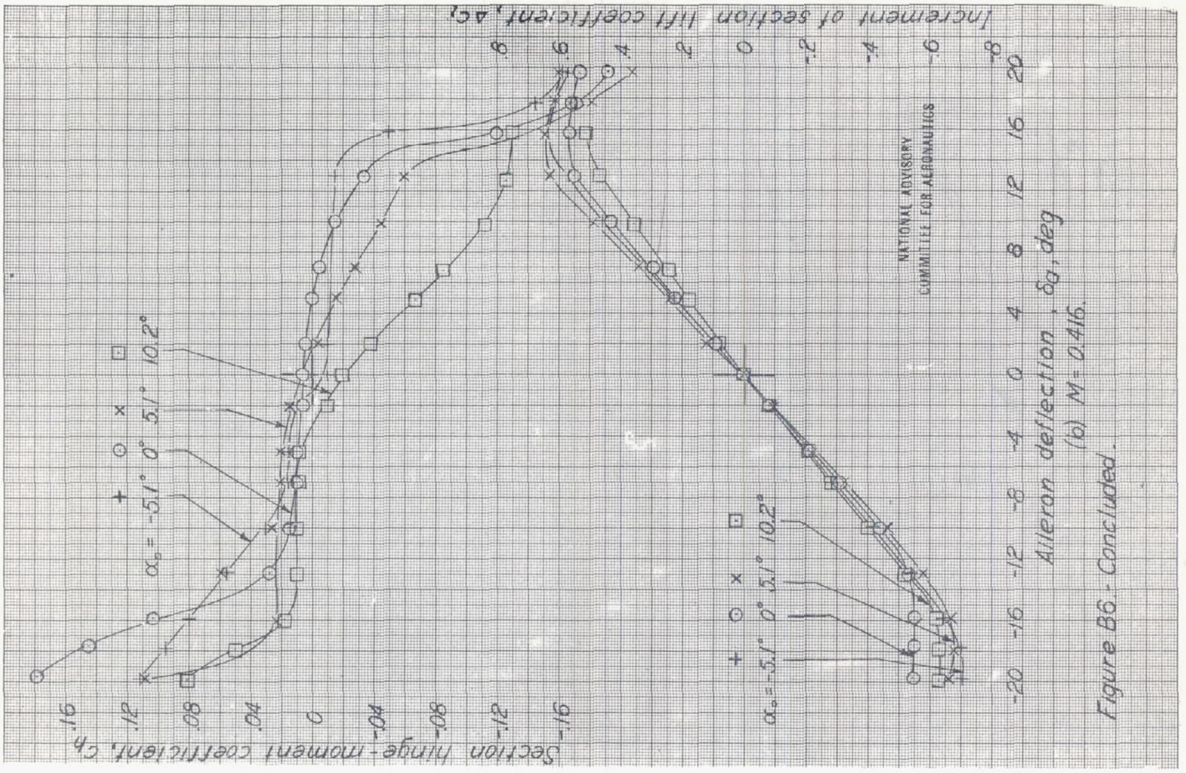

Figure B6.- Concluded.
(b) M = 0.416.

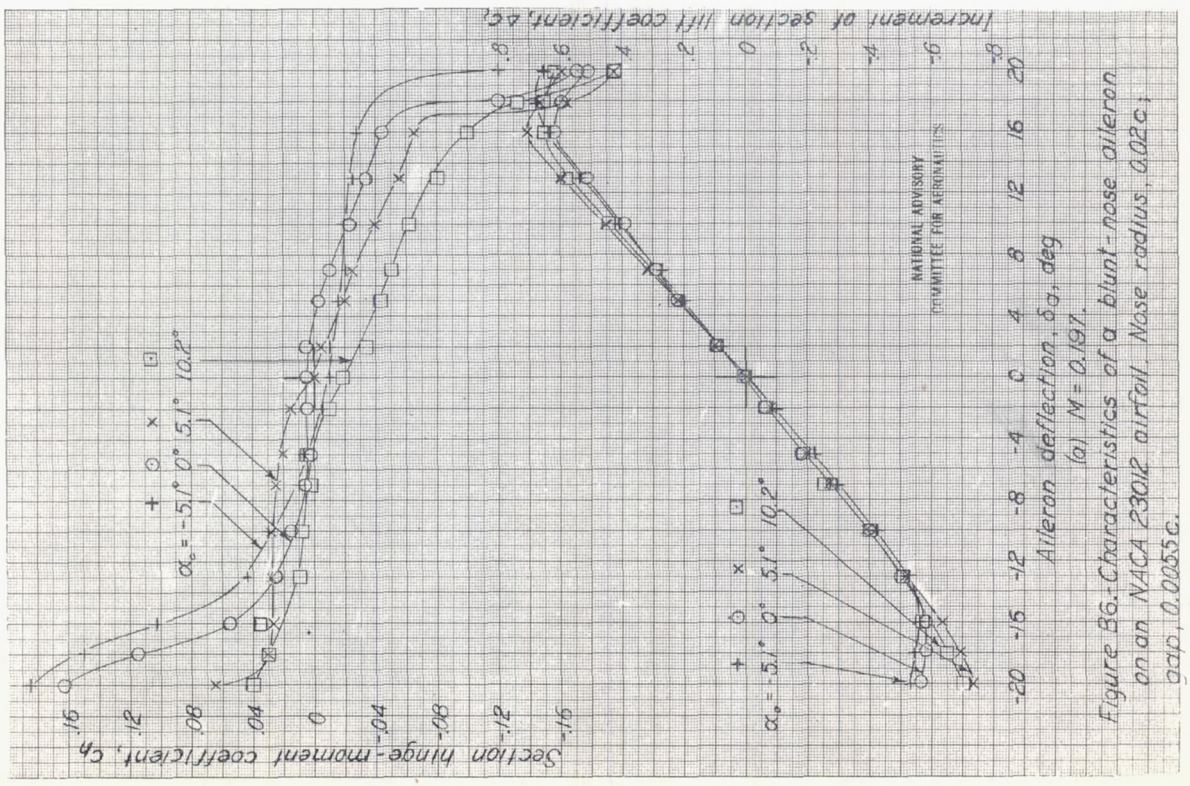

Figure B6.- Characteristics of a blunt-nose aileron on an NACA 23012 airfoil. Nose radius, 0.02c; gap, 0.0055c.
(a) M = 0.197.

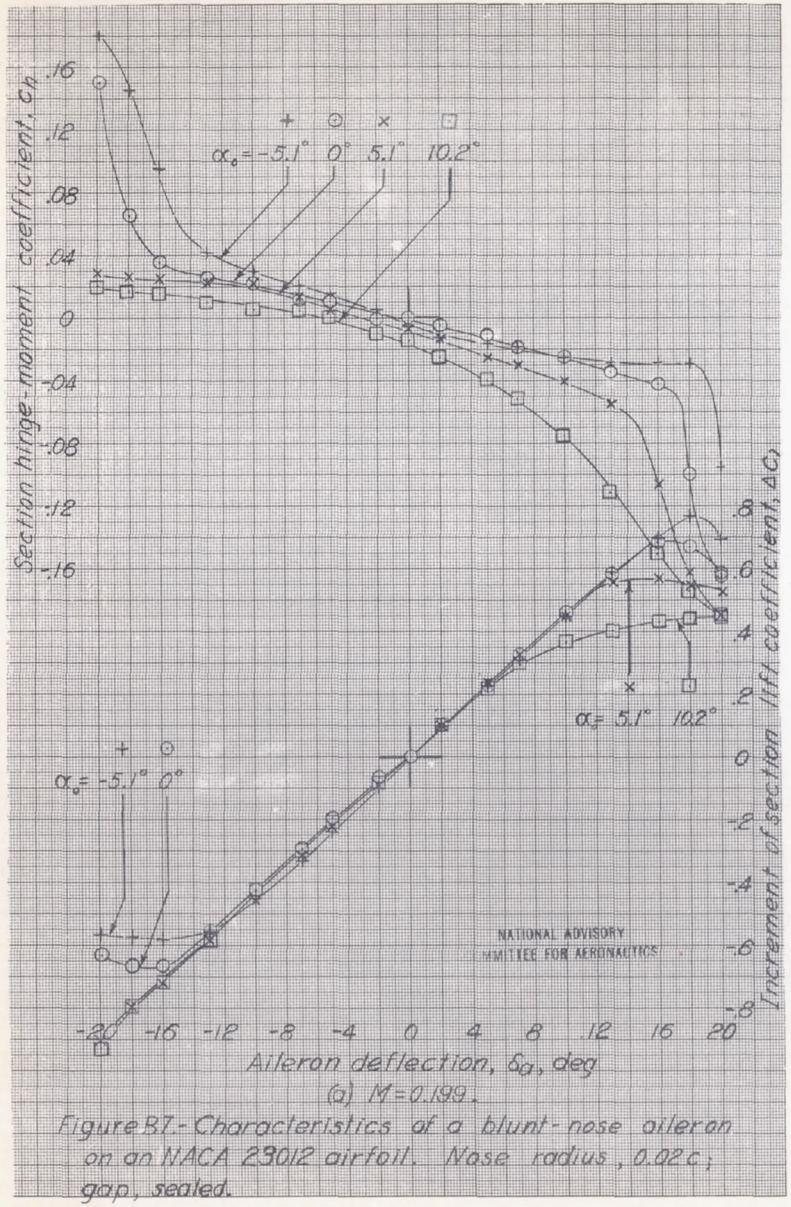

(a) M = 0.199.

Figure B7.- Characteristics of a blunt-nose aileron on an NACA 23012 airfoil. Nose radius, 0.02c; gap, sealed.

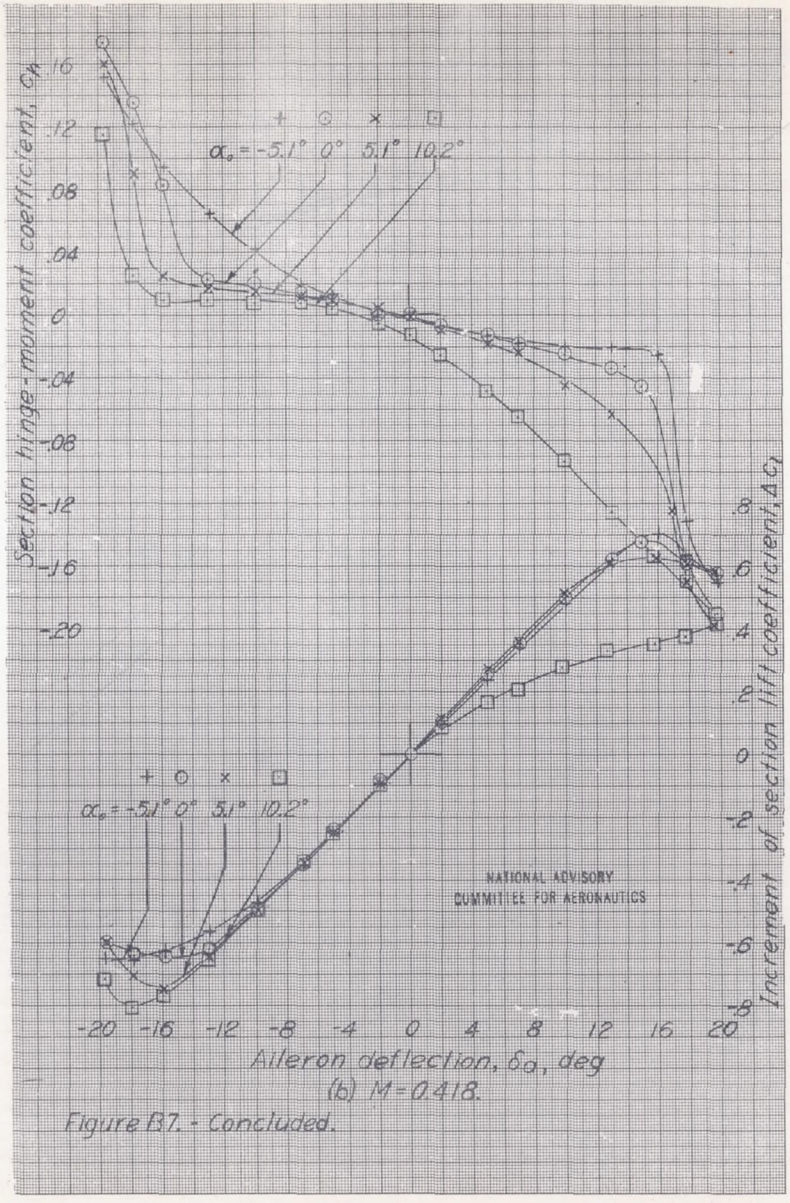

(b) M = 0.418.

Figure B7.- Concluded.

Model B-1

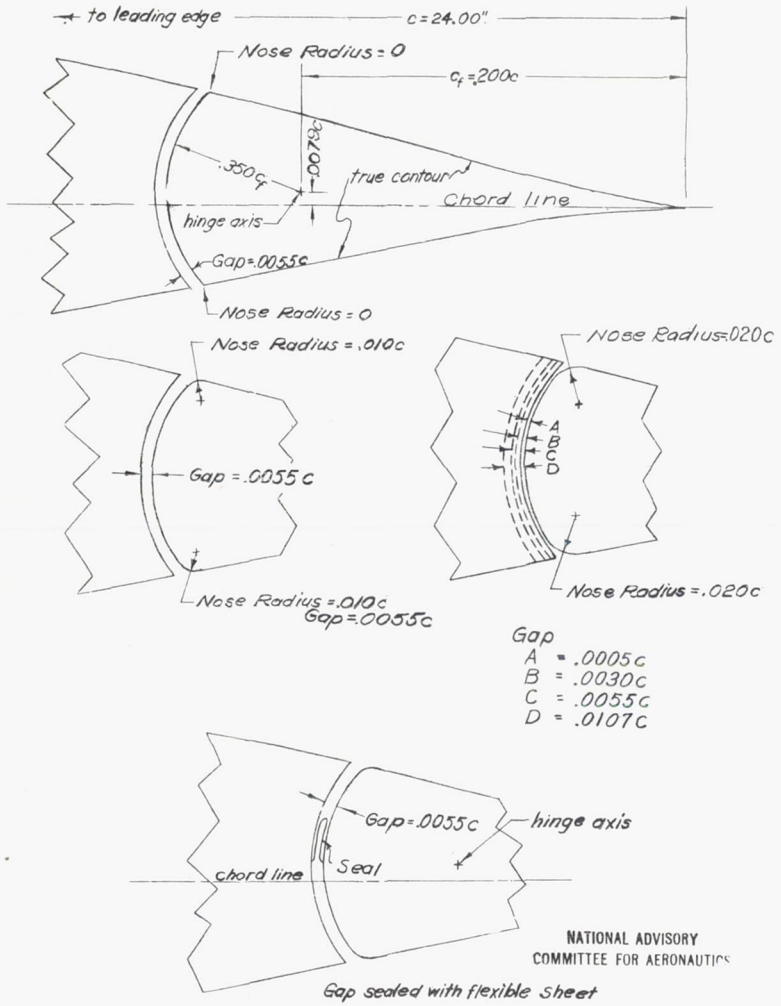

Figure B8.- The various modifications of a blunt-nose aileron on an NACA 66(215)-216, $a = 1.0$ airfoil section tested in two-dimensional flow. NACA stability tunnel.

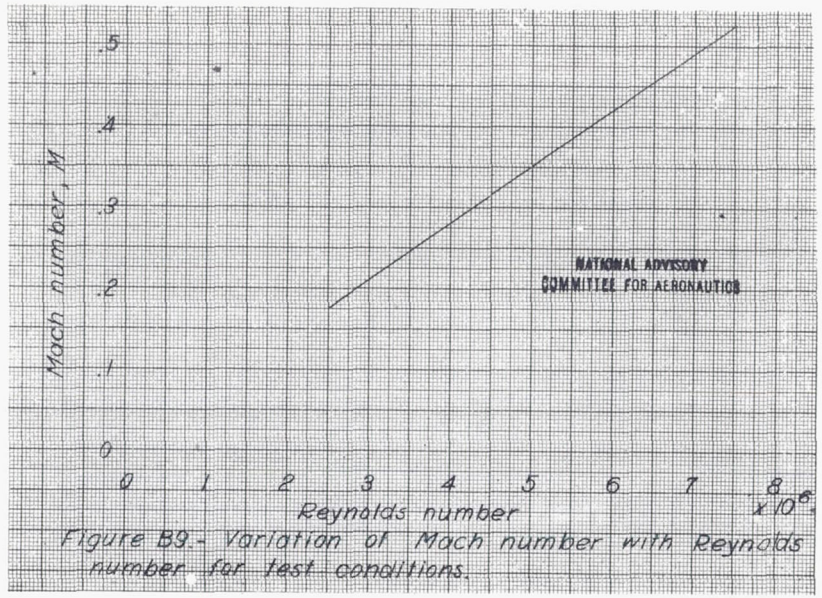

Figure B9.- Variation of Mach number with Reynolds number for test conditions.

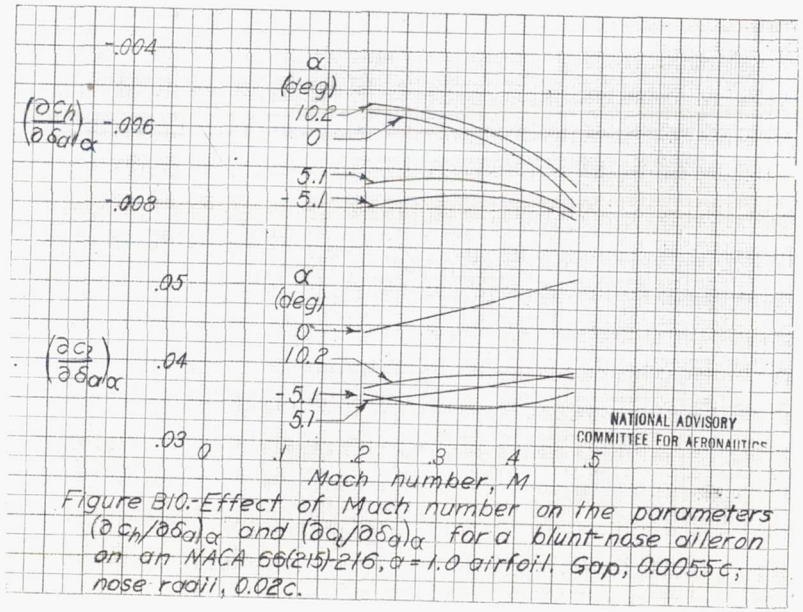

Figure B10.-Effect of Mach number on the parameters $(\partial c_h/\partial \delta_a)_\alpha$ and $(\partial c_l/\partial \delta_a)_\alpha$ for a blunt-nose aileron on an NACA 66(215)-216, $a = 1.0$ airfoil. Gap, 0.0055c; nose radii, 0.02c.

Model B-II

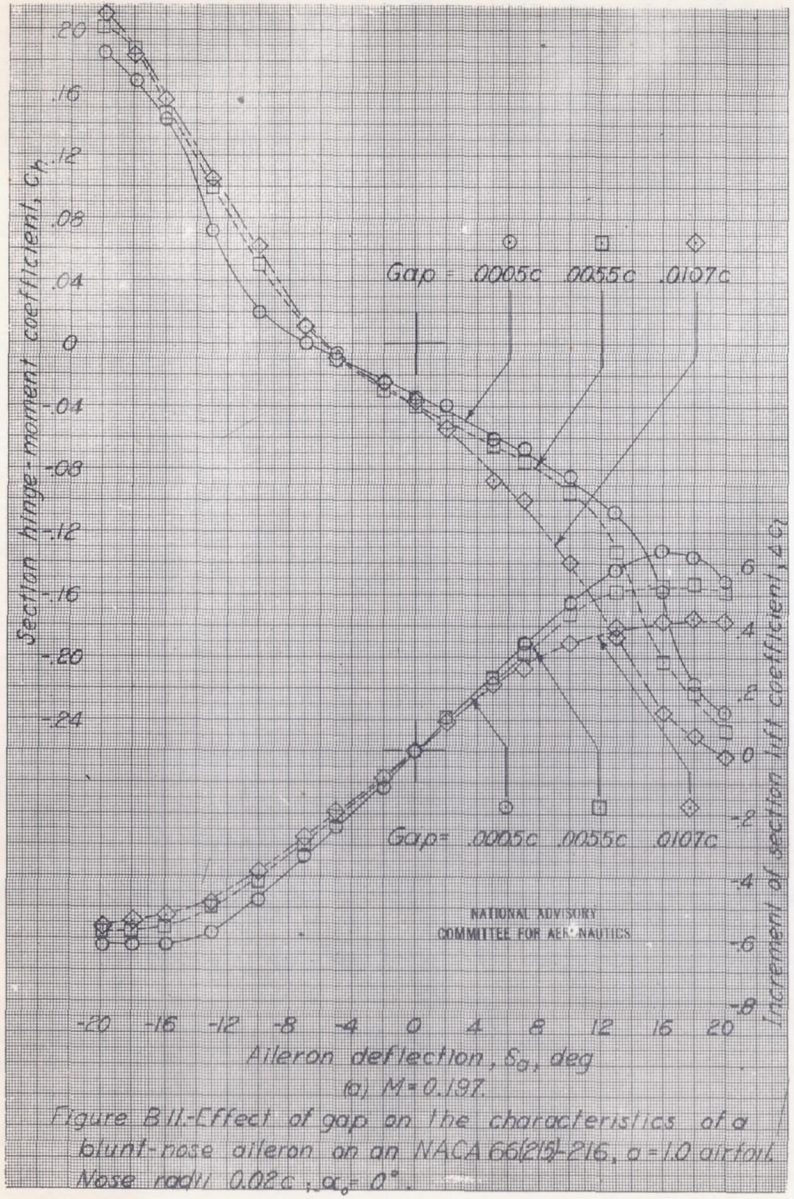

(b) M = 0.197.

Figure B11.-Effect of gap on the characteristics of a blunt-nose aileron on an NACA 66(215)-216, a = 1.0 airfoil. Nose radii 0.02c; $\alpha_a = 0°$.

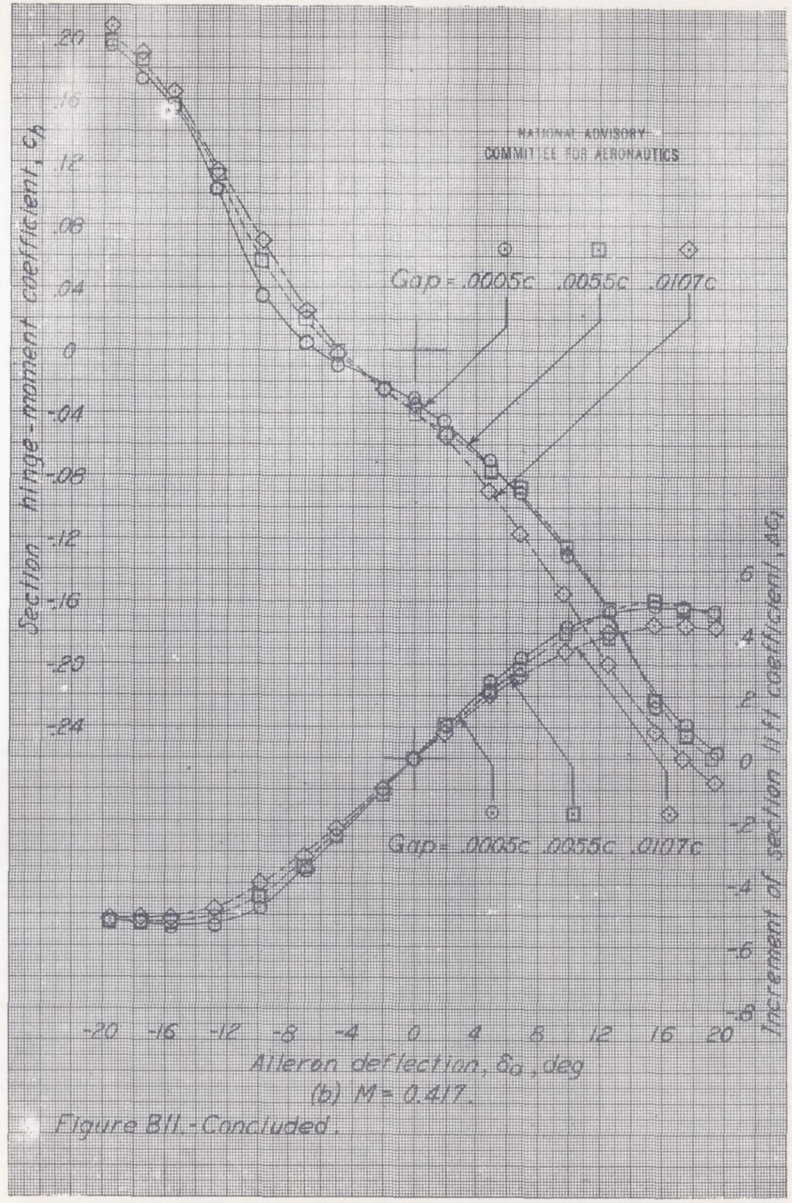

(b) M = 0.417.

Figure B11.-Concluded.

Model B-II

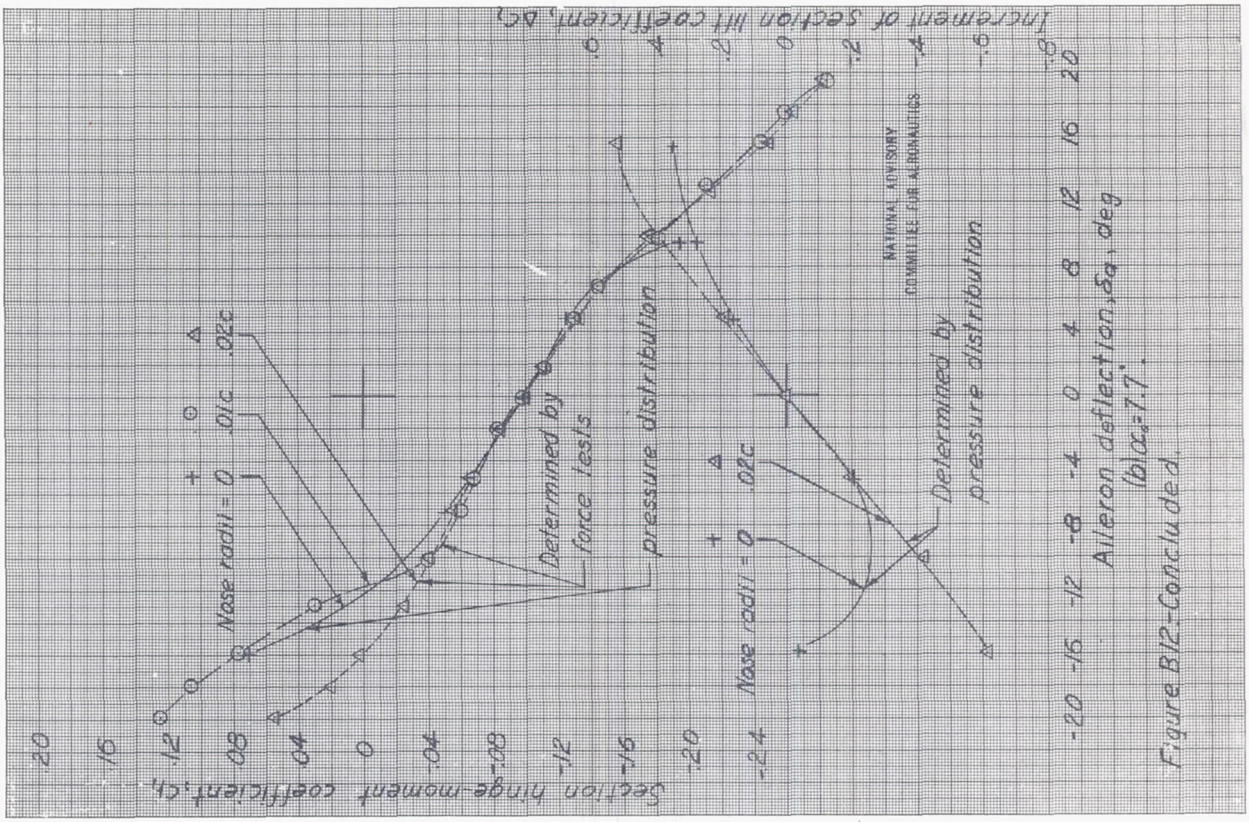

Figure B12.- Concluded.

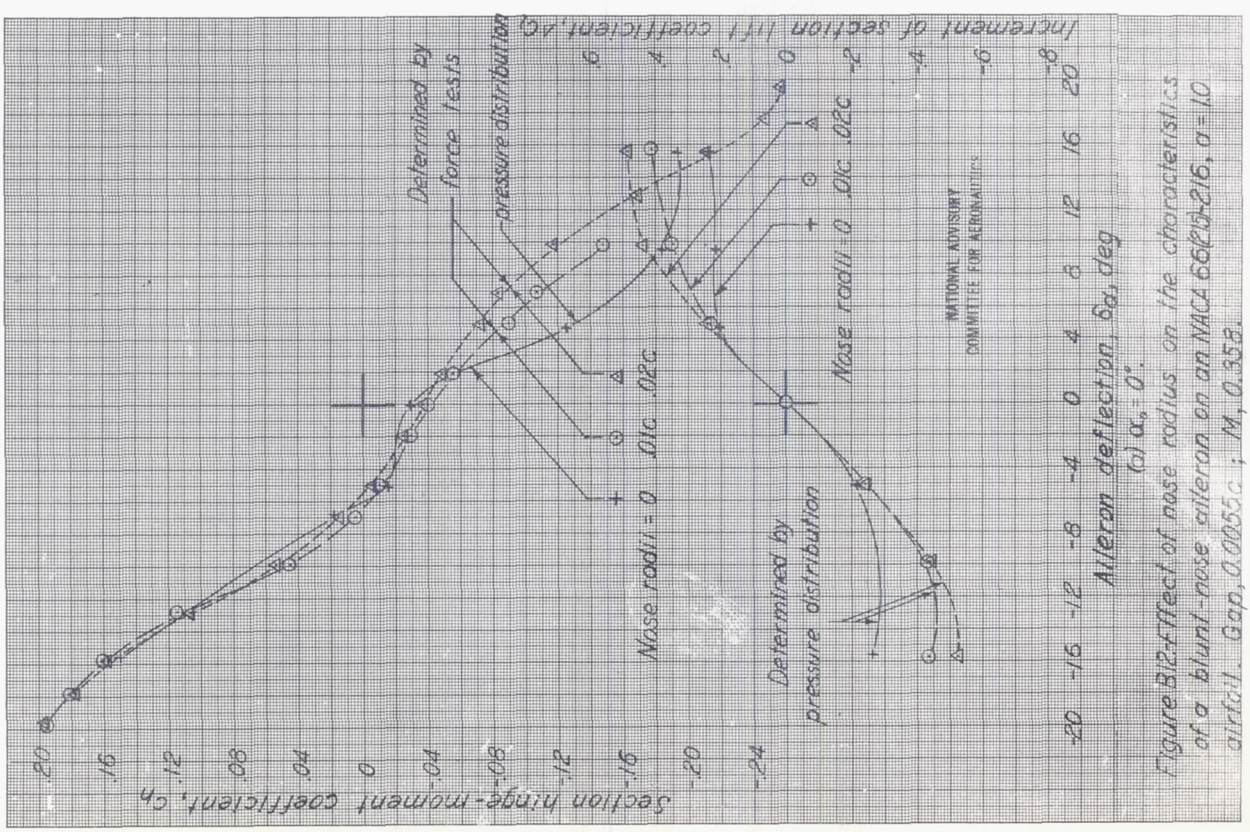

Figure B13.- Effect of nose radius on the characteristics of a blunt-nose aileron on an NACA 66(216)-216, $\alpha = 10$ airfoil. Gap, 0.005c; M, 0.35.

Model B- II

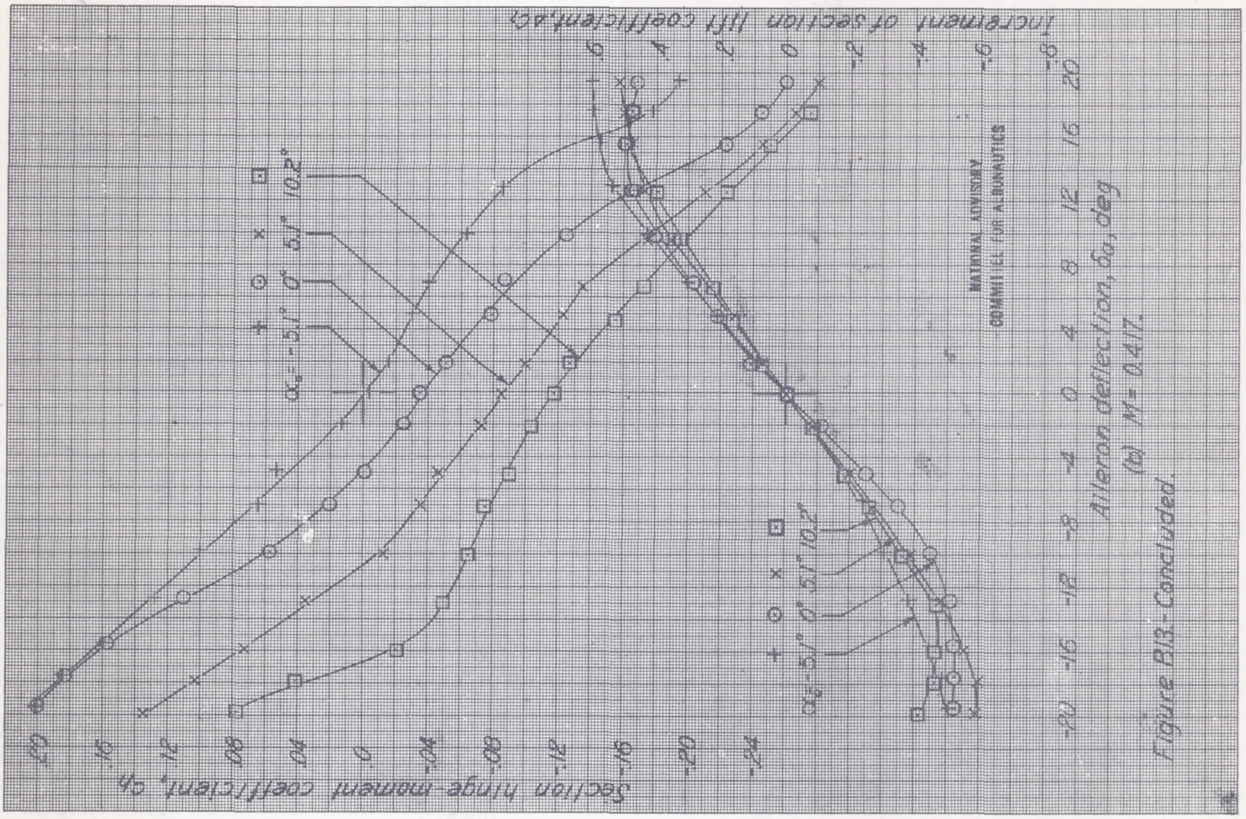

Figure B13-Concluded.
(b) M= 0.417.

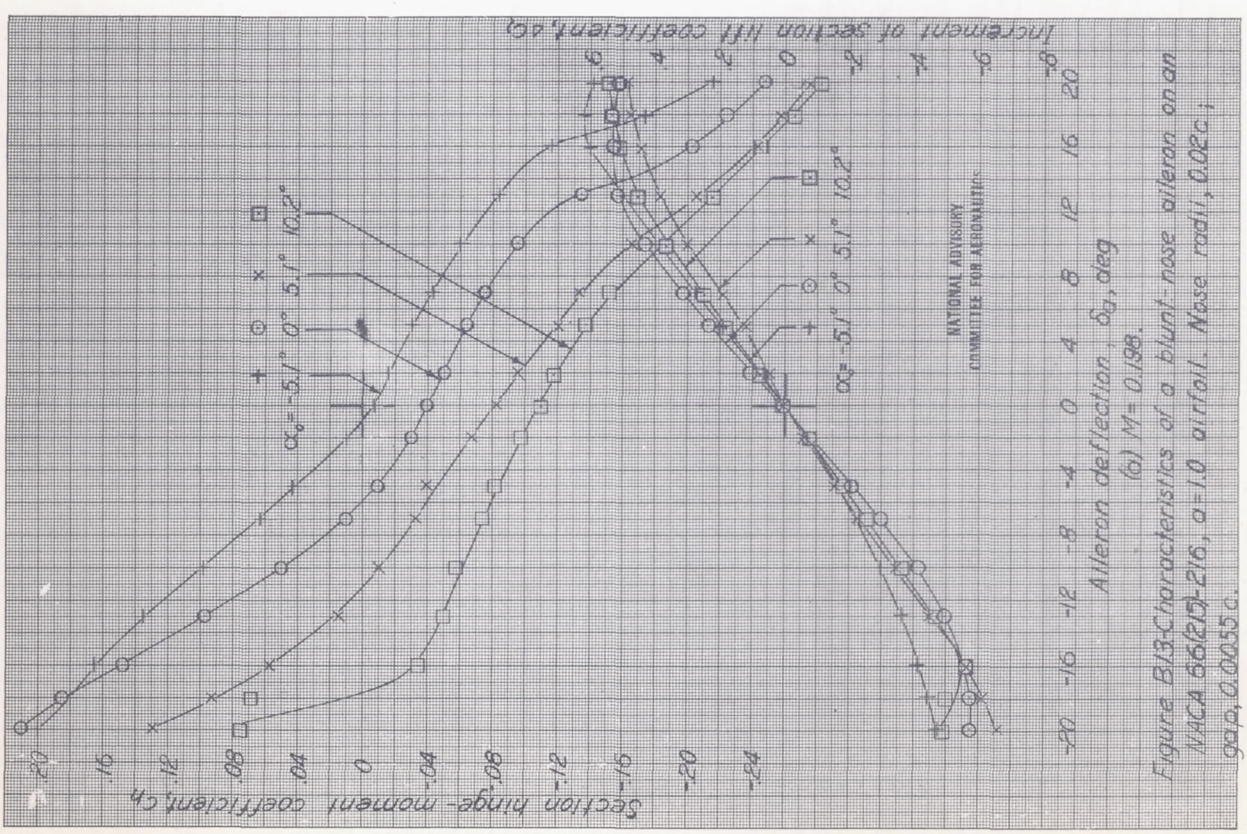

Figure B13-Characteristics of a blunt-nose aileron on an NACA 66(215)-216, a=1.0 airfoil. Nose radii, 0.02c; c_a/c, 0.0055c.
(a) M= 0.198.

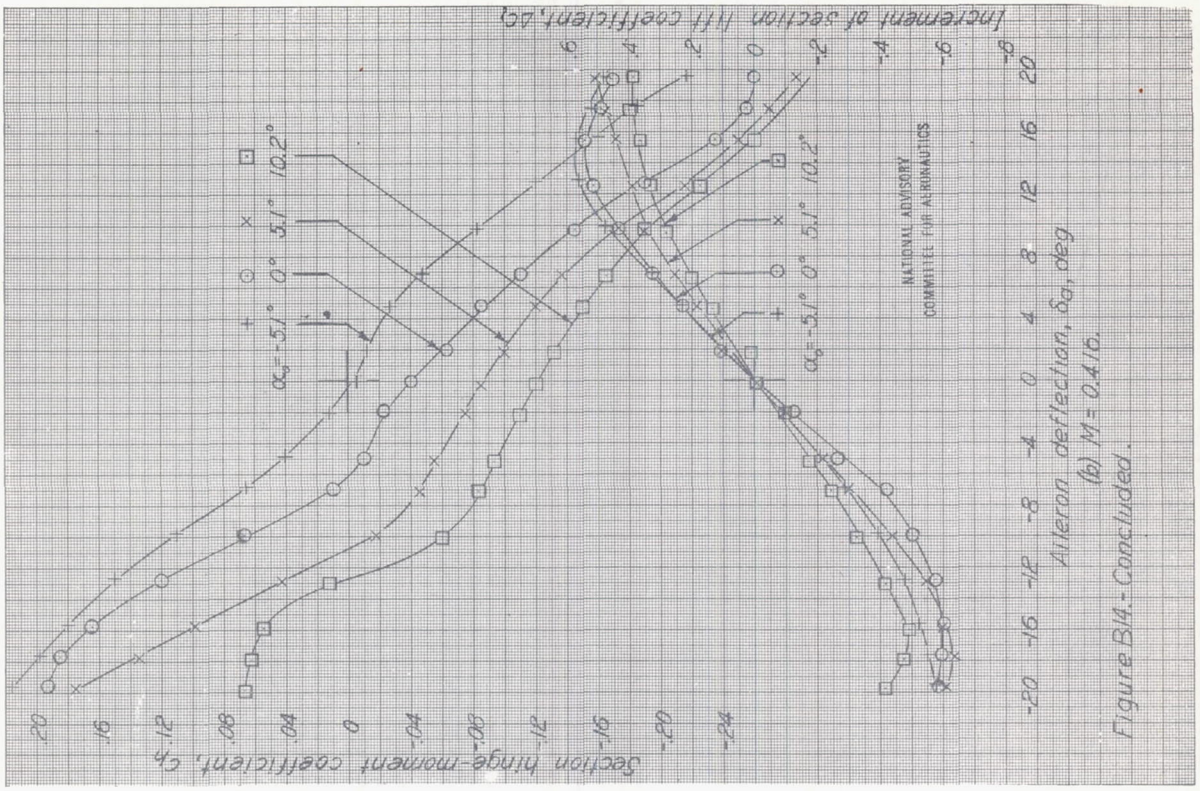

(b) $M = 0.410$.

Figure B14.- Concluded.

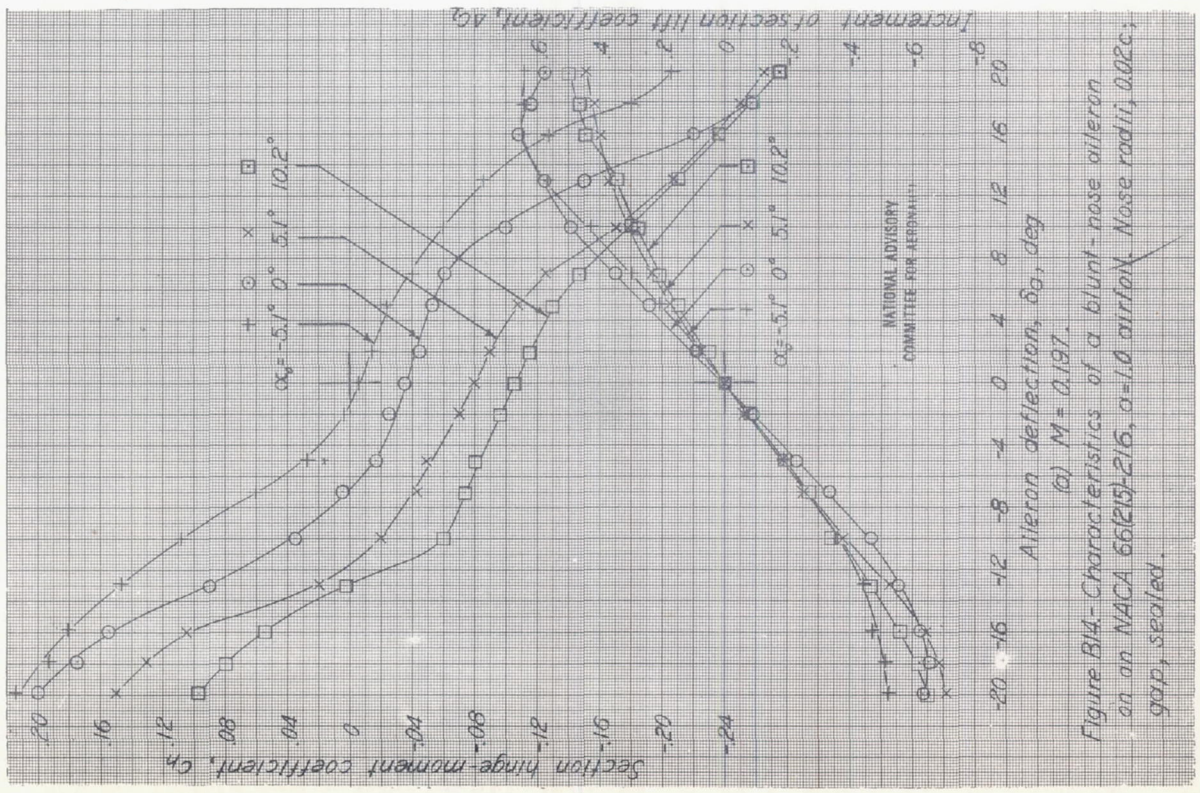

(a) $M = 0.197$.

Figure B14.- Characteristics of a blunt-nose aileron on an NACA 66(215)-216, α=1.0 airfoil. Nose radii, 0.02c; gap, sealed.

Model B-III

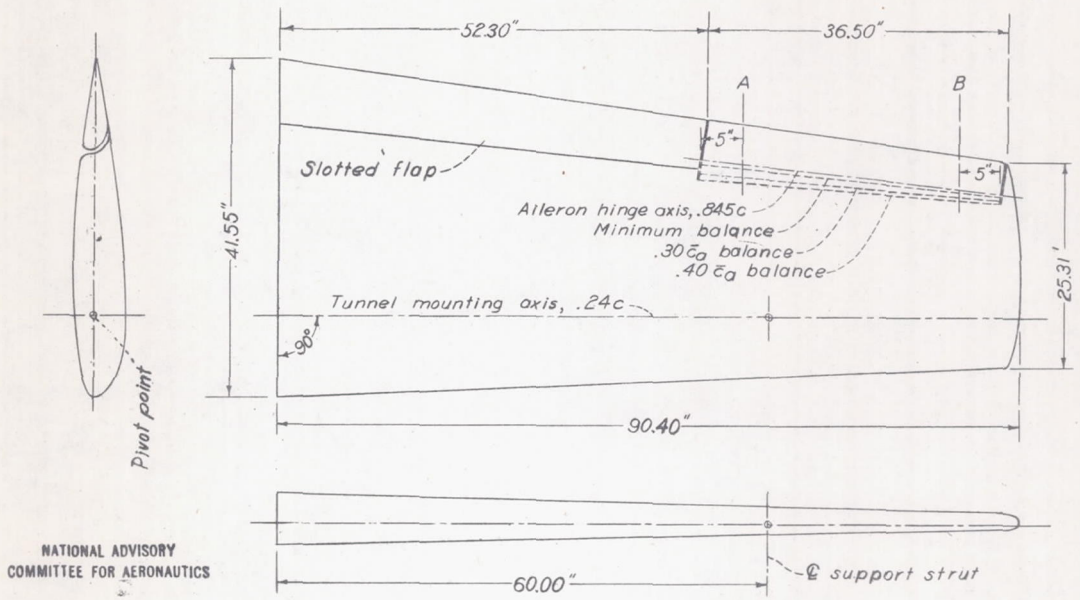

Figure B15 - Semispan model of tapered wing.
LMAL 7-by-10-foot tunnel.

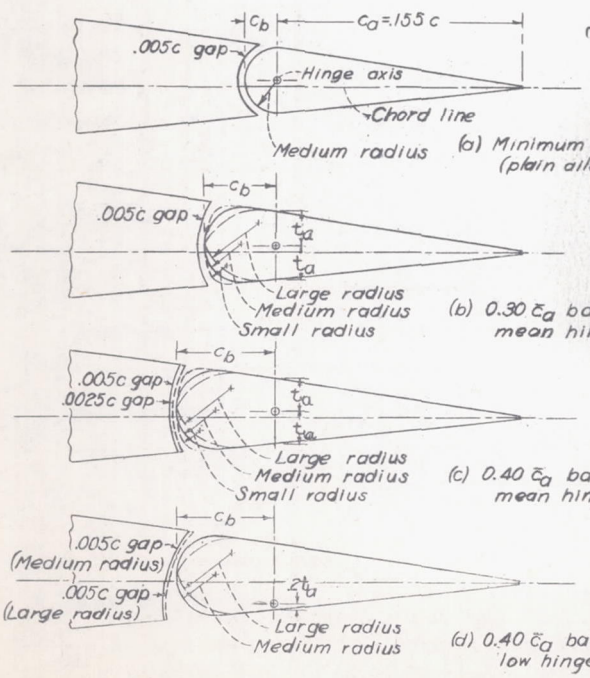

NATIONAL ADVISORY COMMITTEE FOR AERONAUTICS

	Inboard end c = 31.986" c_a = 4.942"	Outboard end c = 25.314" c_a = 3.965"
c_b	0.1315 c_a	0.0878 c_a
Medium radius	.1315 c_a	.0878 c_a
c_b	.3570 c_a	.2175 c_a
Small radius	.0782 c_a	.0492 c_a
Medium radius	.1554 c_a	.0984 c_a
Large radius	.2346 c_a	.1476 c_a
c_b	.4758 c_a	.2896 c_a
Small radius	.0840 c_a	.0517 c_a
Medium radius	.1681 c_a	.1034 c_a
Large radius	.2521 c_a	.1551 c_a
c_b	.4758 c_a	.2896 c_a
Medium radius	.1681 c_a	.1034 c_a
Large radius	.2521 c_a	.1551 c_a

Figure B16 The various 0.155c by 0.405 b/2 ailerons tested on the tapered-wing model.

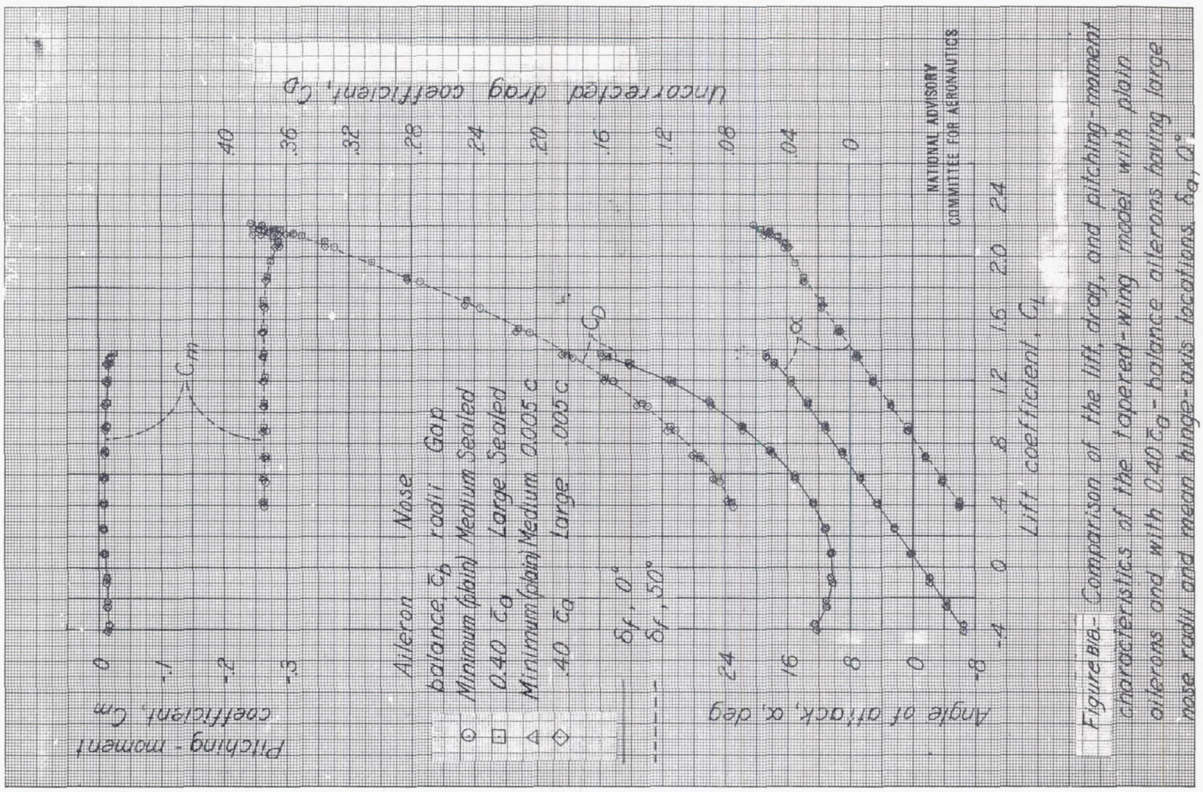

Figure B16.- Comparison of the lift, drag, and pitching-moment characteristics of the tapered-wing model with plain ailerons and with 0.40 $\bar{c}_a$-balance ailerons having large nose radii and mean hinge-axis locations. δ_a, 0°.

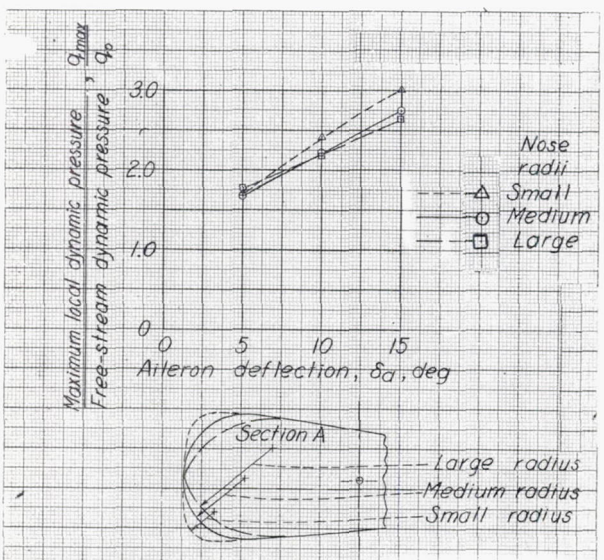

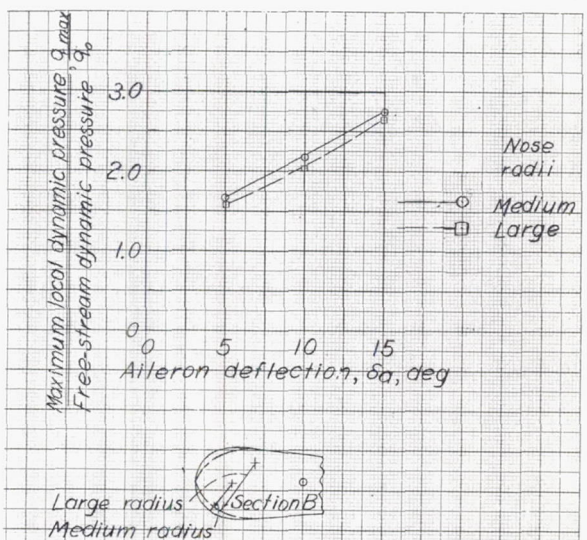

NATIONAL ADVISORY COMMITTEE FOR AERONAUTICS

Figure B17.- Effect of nose radius on the peak dynamic pressures over the nose (at sections A and B of figure B15) of a 0.40 $\bar{c}_a$-balance blunt-nose aileron on the tapered-wing model. Hinge-axis location, mean; gap, 0.005c; δ_f, 0°; α, 0°.

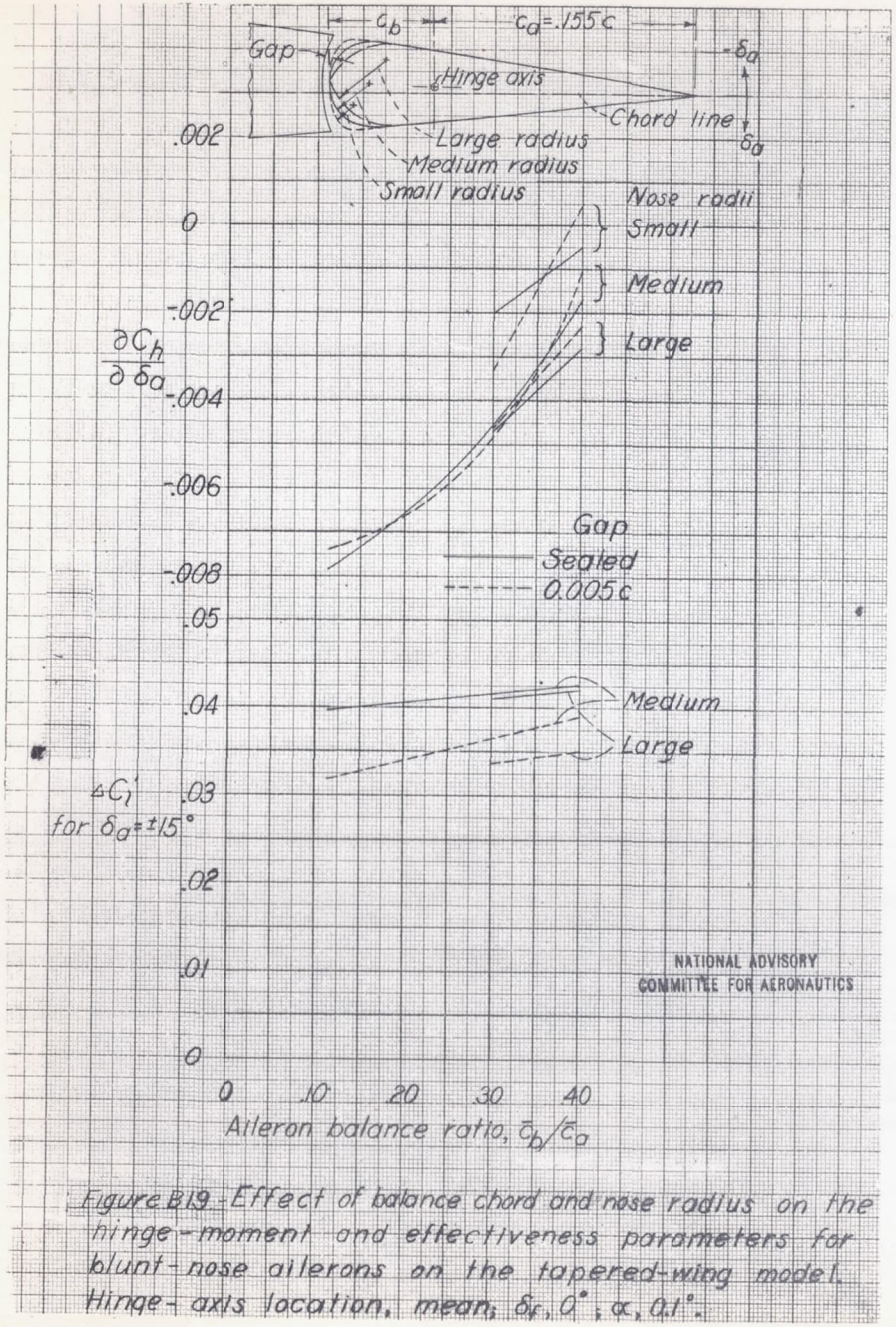

Figure B19.- Effect of balance chord and nose radius on the hinge-moment and effectiveness parameters for blunt-nose ailerons on the tapered-wing model. Hinge-axis location, mean; δ_f, 0°; α, 0.1°.

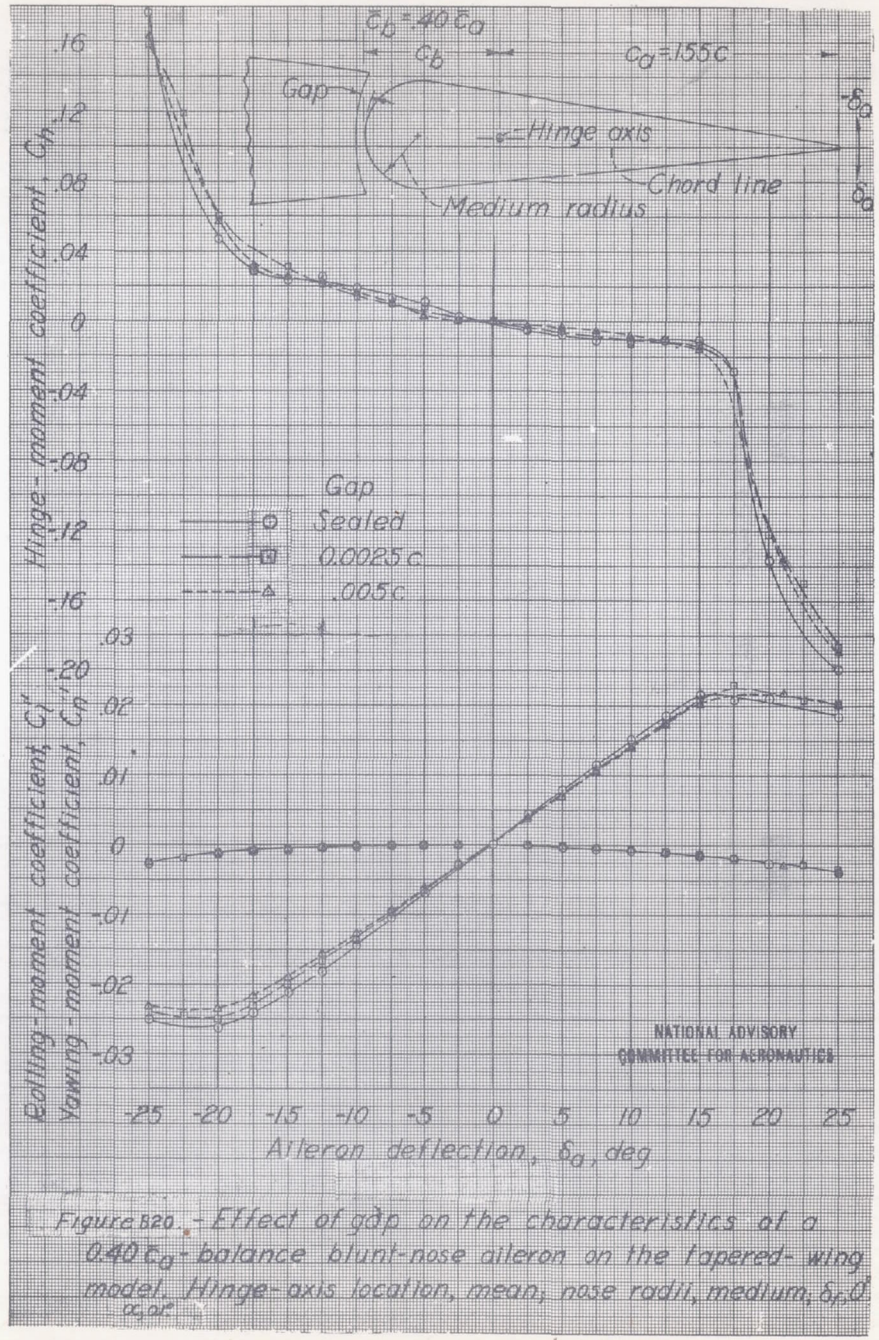

Figure B20.- Effect of gap on the characteristics of a 0.40c_a-balance blunt-nose aileron on the tapered-wing model. Hinge-axis location, mean; nose radii, medium; δ_f, 0°; α, 0°.

Model B-III

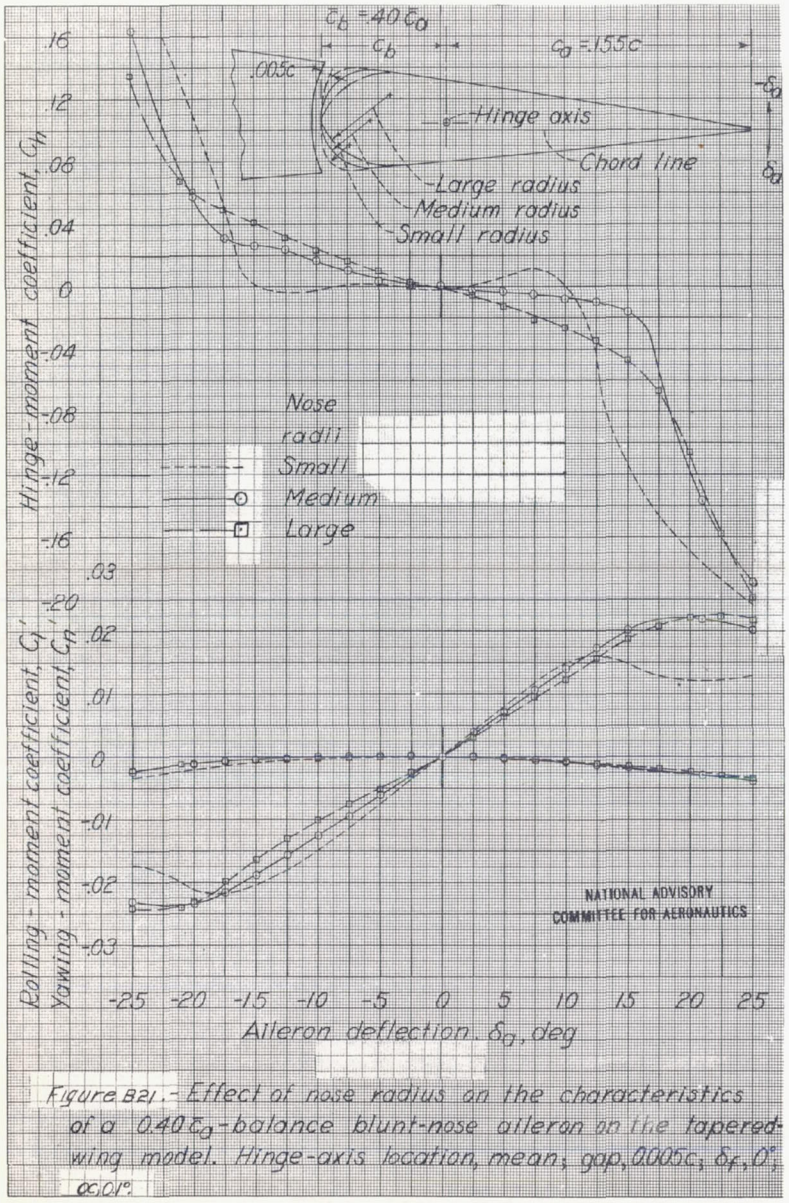

Figure B21. - Effect of nose radius on the characteristics of a $0.40\,c_a$-balance blunt-nose aileron on the tapered-wing model. Hinge-axis location, mean; gap, 0005c; δ_f, 0°; α, 0°.

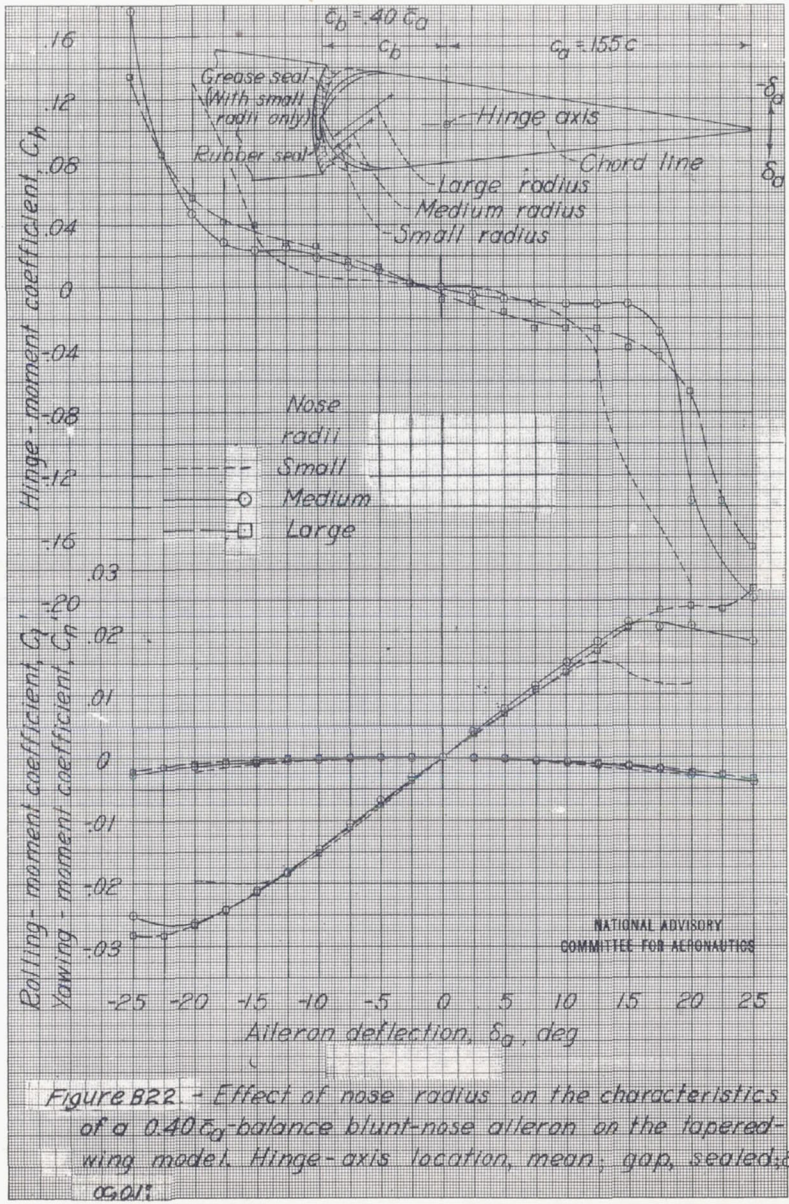

Figure B22. - Effect of nose radius on the characteristics of a $0.40\,c_a$-balance blunt-nose aileron on the tapered-wing model. Hinge-axis location, mean; gap, sealed; δ_f, 0°; α, 0°.

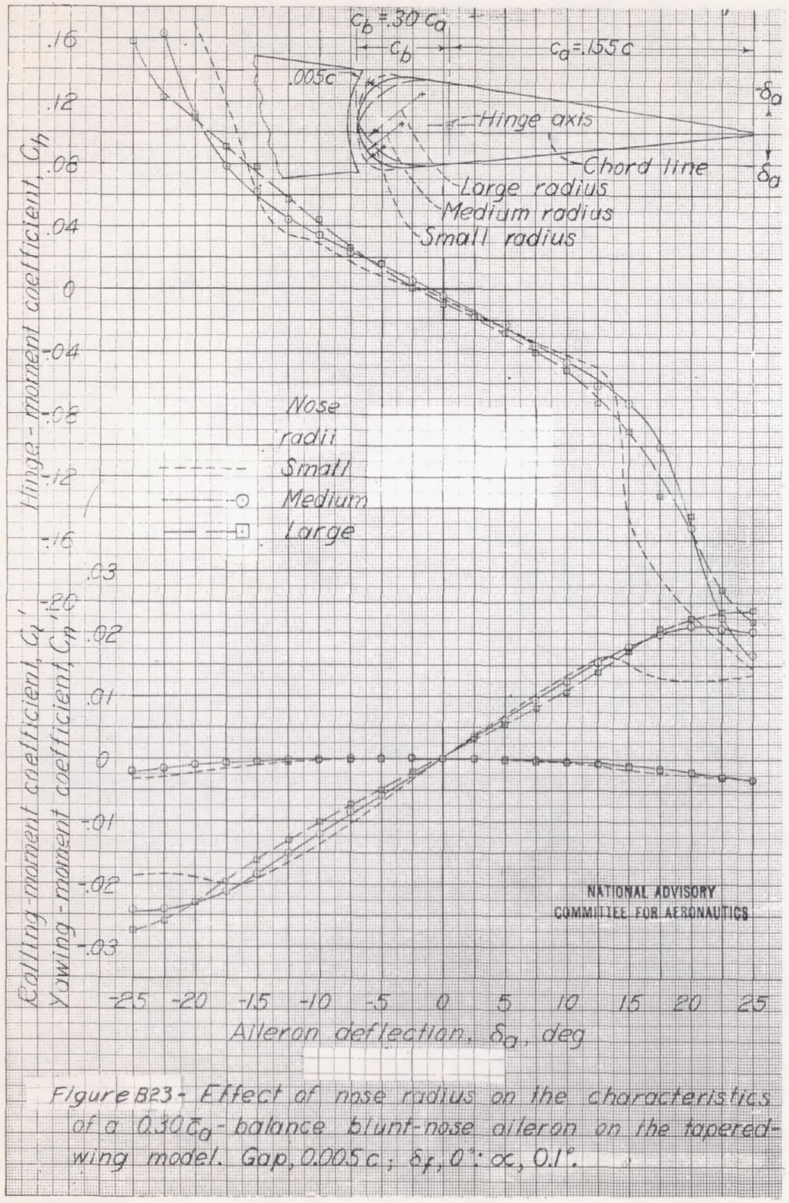

Figure B23 - Effect of nose radius on the characteristics of a $0.30\,c_a$-balance blunt-nose aileron on the tapered-wing model. Gap, 0.005 c; δ_f, 0°; α, 0.1°.

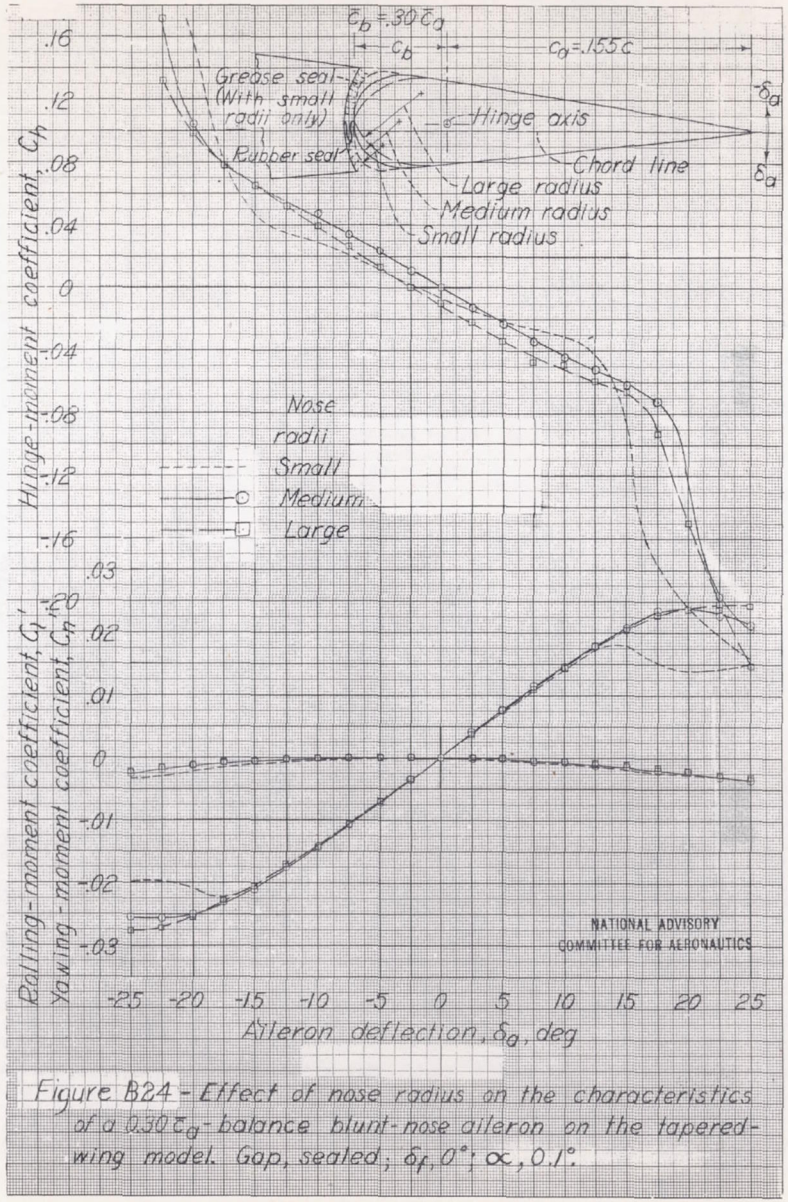

Figure B24 - Effect of nose radius on the characteristics of a $0.30\,c_a$-balance blunt-nose aileron on the tapered-wing model. Gap, sealed; δ_f, 0°; α, 0.1°.

Model B-III

Model B-III

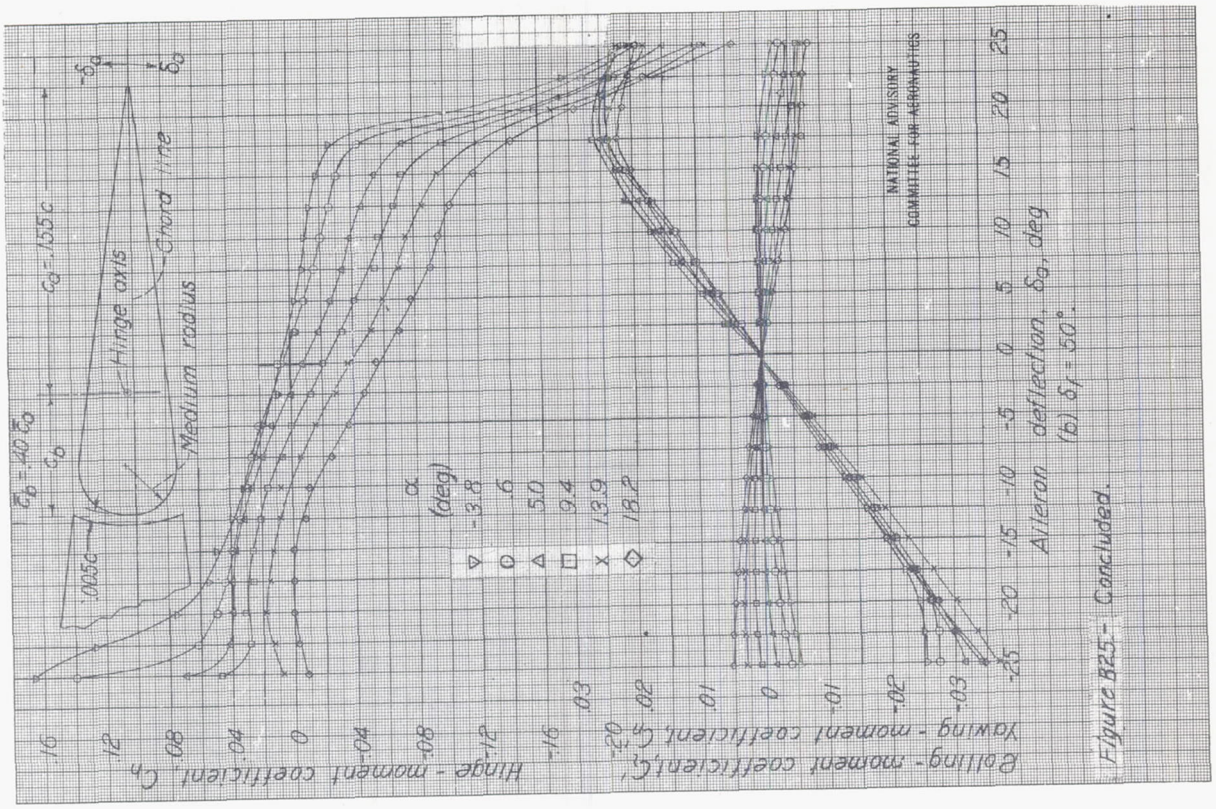

Figure B25.- Concluded.

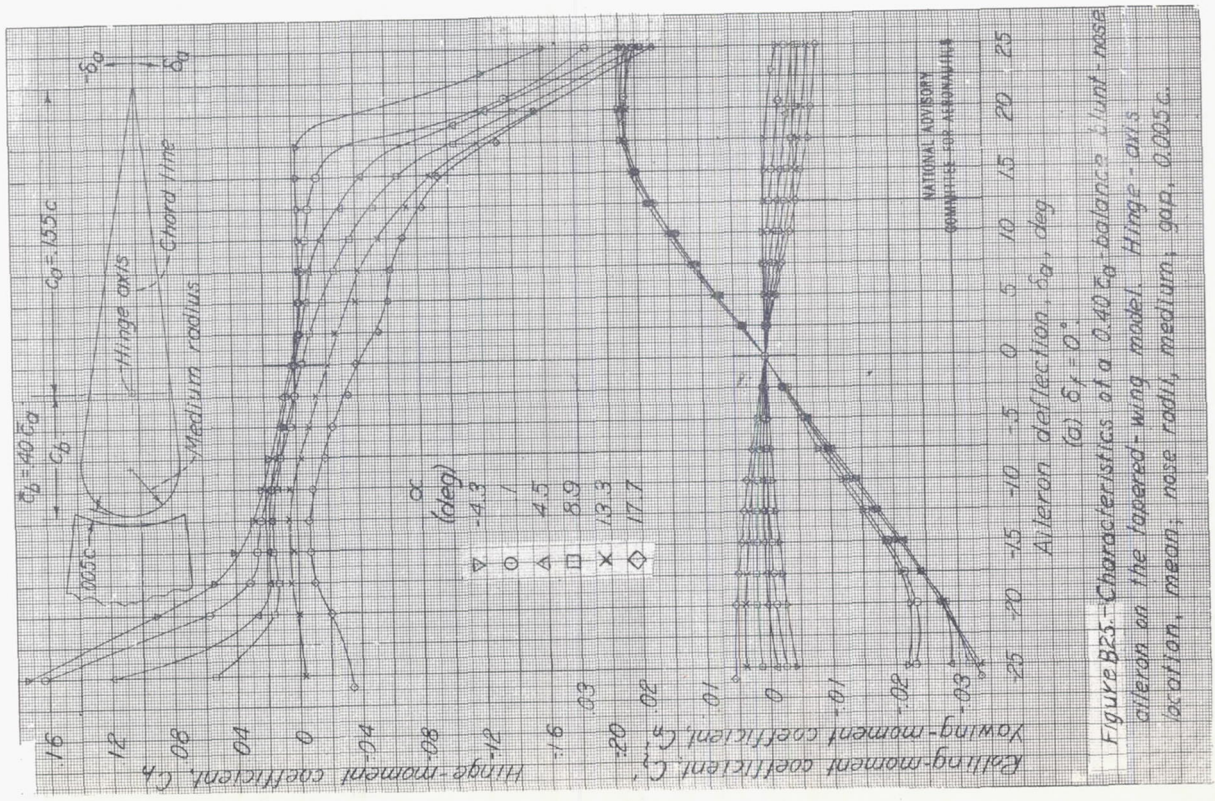

Figure B25.- Characteristics of a 0.40 c_b-balance Hunt nose aileron on the tapered-wing model. Hinge-axis location, mean; nose radii, medium; gap, 0.005c.
(a) $\delta_f = 0°$.

Model B- III

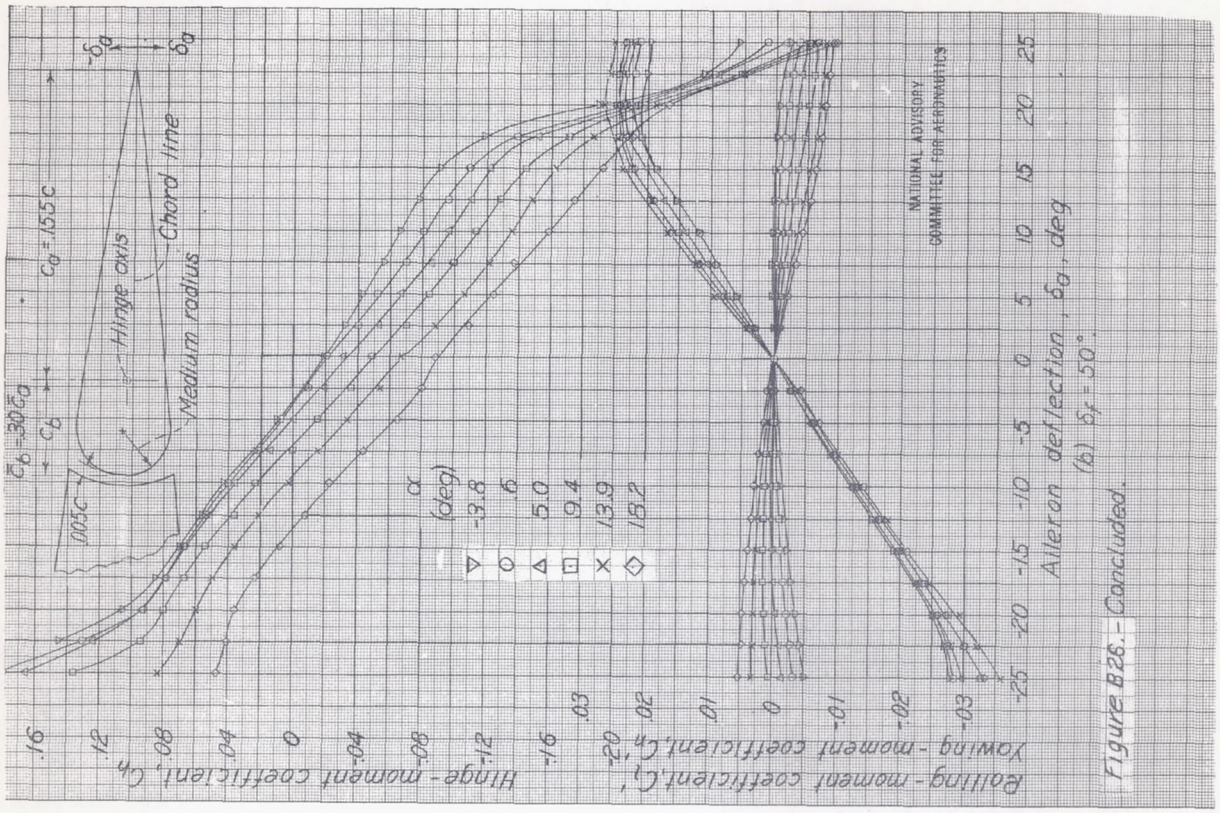

Figure B26.- Concluded.

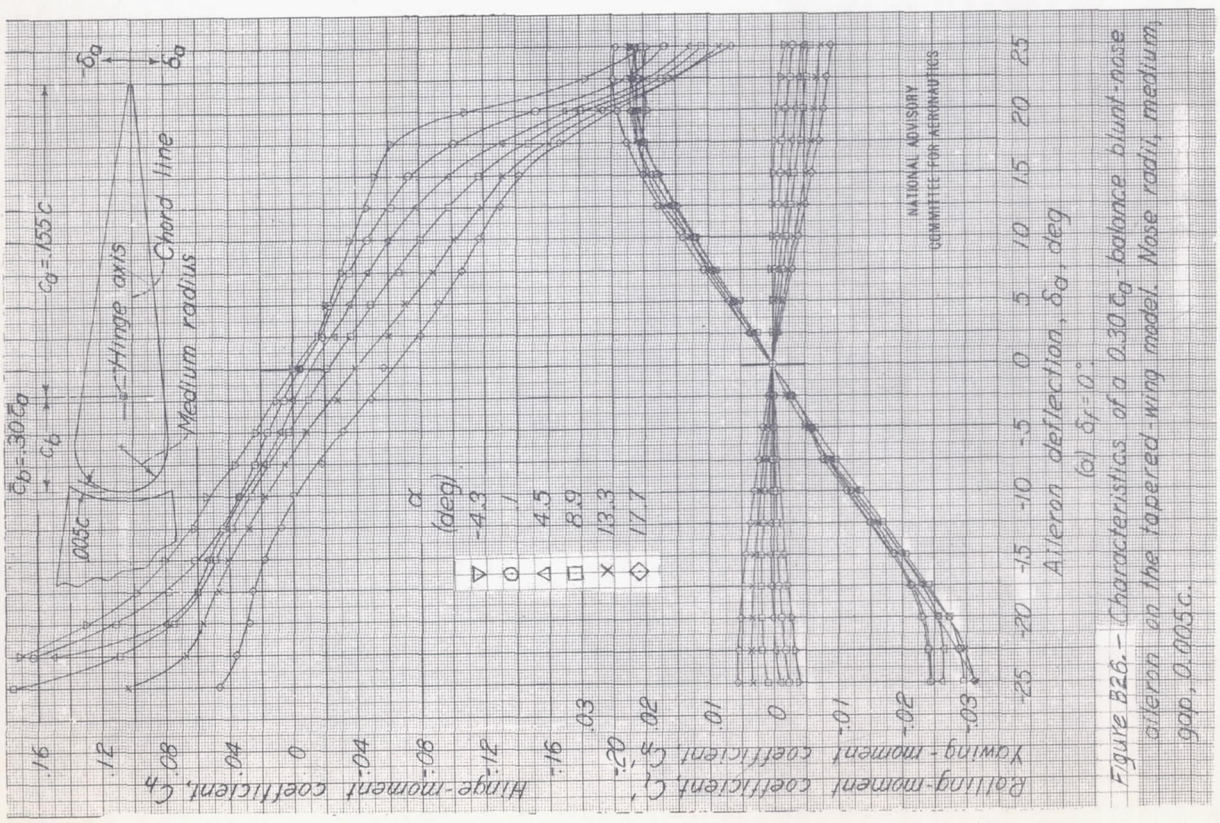

Figure B26.- Characteristics of a 0.30c_b balance blunt-nose aileron on the tapered wing model. Nose radii, medium; gap, 0.005c.

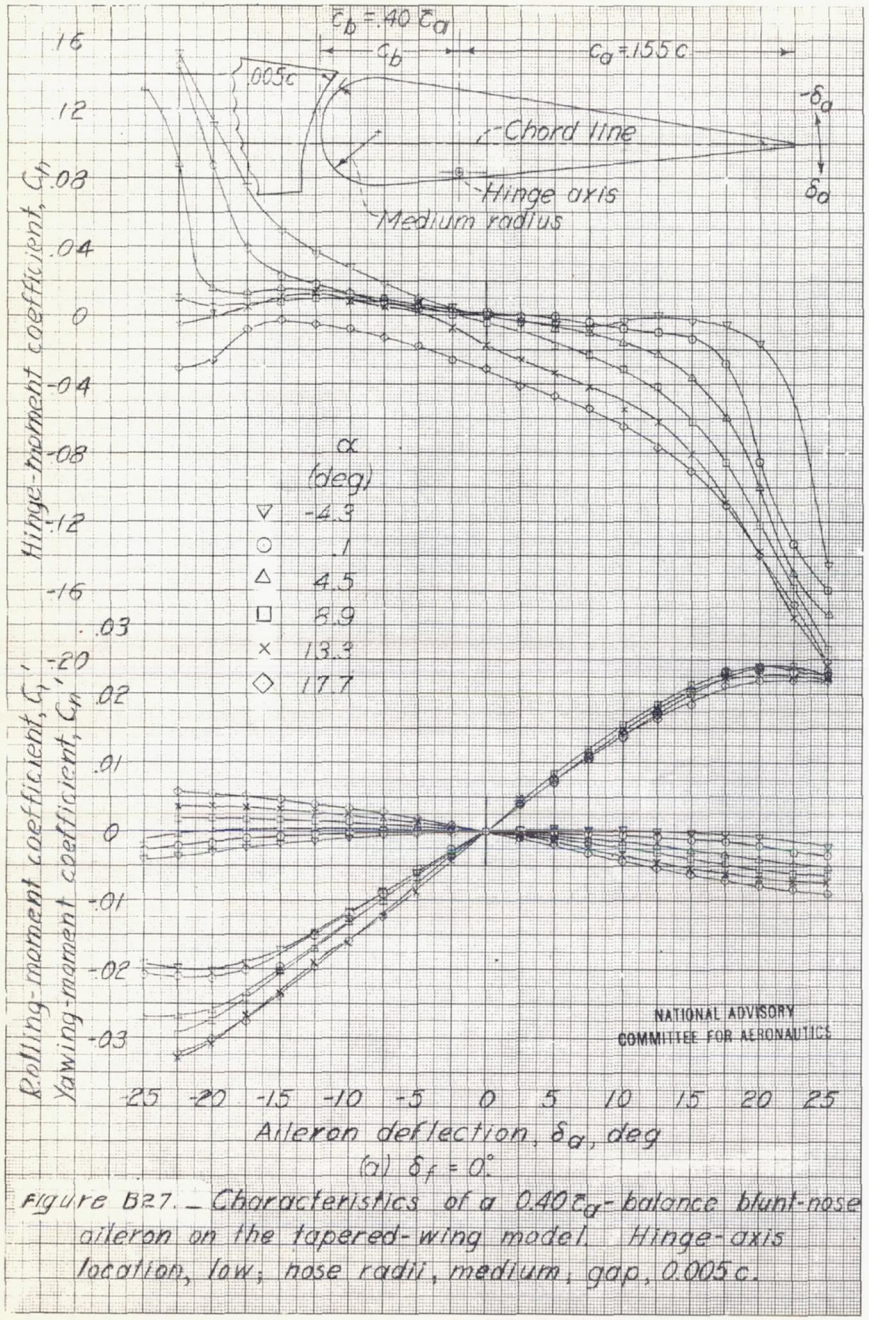

(a) $\delta_f = 0°$.

Figure B27. – Characteristics of a $0.40\bar{c}_a$-balance blunt-nose aileron on the tapered-wing model. Hinge-axis location, low; nose radii, medium; gap, 0.005c.

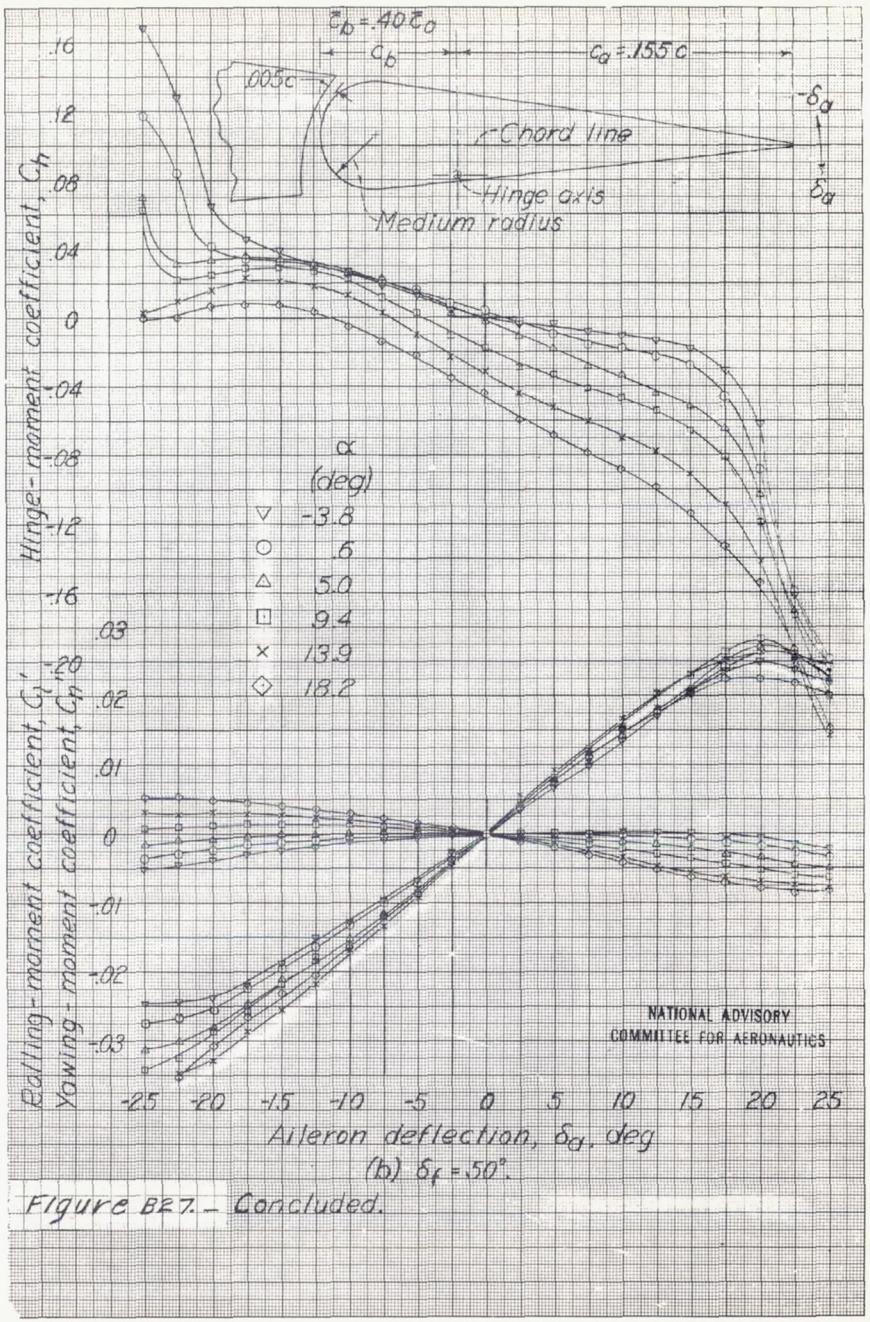

(b) $\delta_f = 50°$.

Figure B27. – Concluded.

Model B-III

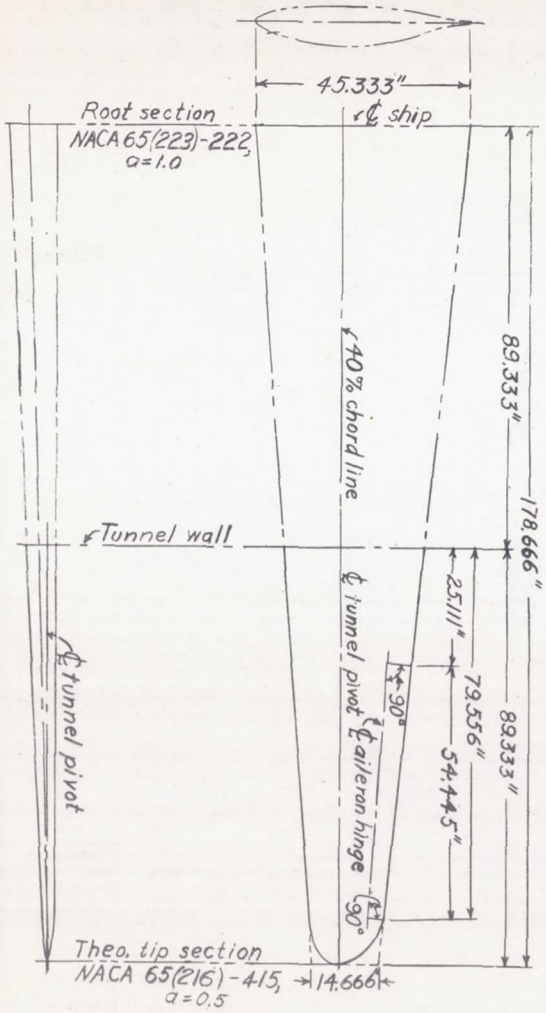

Figure B28:-The 1/4.5-scale model of a tapered low-drag wing.
LMAL 7-by 10-foot tunnel.

NATIONAL ADVISORY
COMMITTEE FOR AERONAUTICS

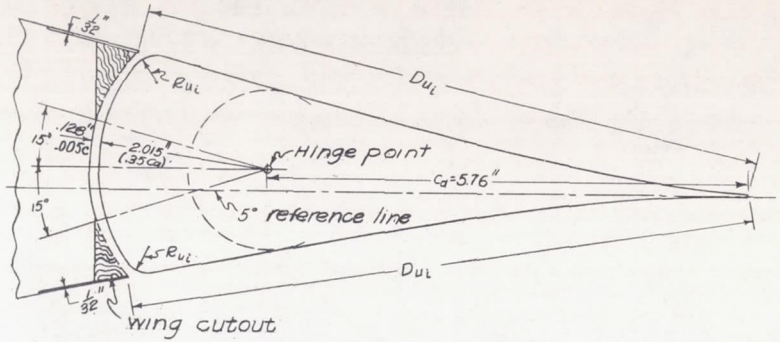

Inboard end of aileron c = 25.60"

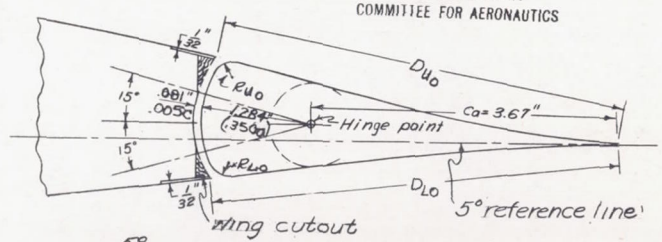

5° Outboard end of aileron c = 16.29"

Modification No.	Nose radii, in.				Dist, Cover plate to T.E., in.				Wing cutouts	Nose seal
	Inboard		Outboard		Inboard		Outboard			
	Rui	Rli	Ruo	Rlo	Dui	Dli	Duo	Dlo		
Original	.250	.250	.163	.163	7.50	7.50	4.89	4.89	Open	None
1	.500	.500	.325	.325	7.50	7.50	4.89	4.89	Open	None
2	.750	.500	.488	.325	7.50	7.50	4.89	4.89	Open	None
3	.750	.500	.488	.325	7.50	7.50	4.89	4.89	Filled with plasticine	None
4	.750	.500	.488	.325	7.50	7.50	4.89	4.89		Grease
5	.750	.500	.488	.325	7.33	7.34	4.80	4.85		None
					Min. gap at $\delta_a = \pm 16°$					

* Equal to original Frise nose radii

Figure B29.- The blunt-nose ailerons tested on the 1/4.5-scale model of a tapered low-drag wing.

Model B-IV

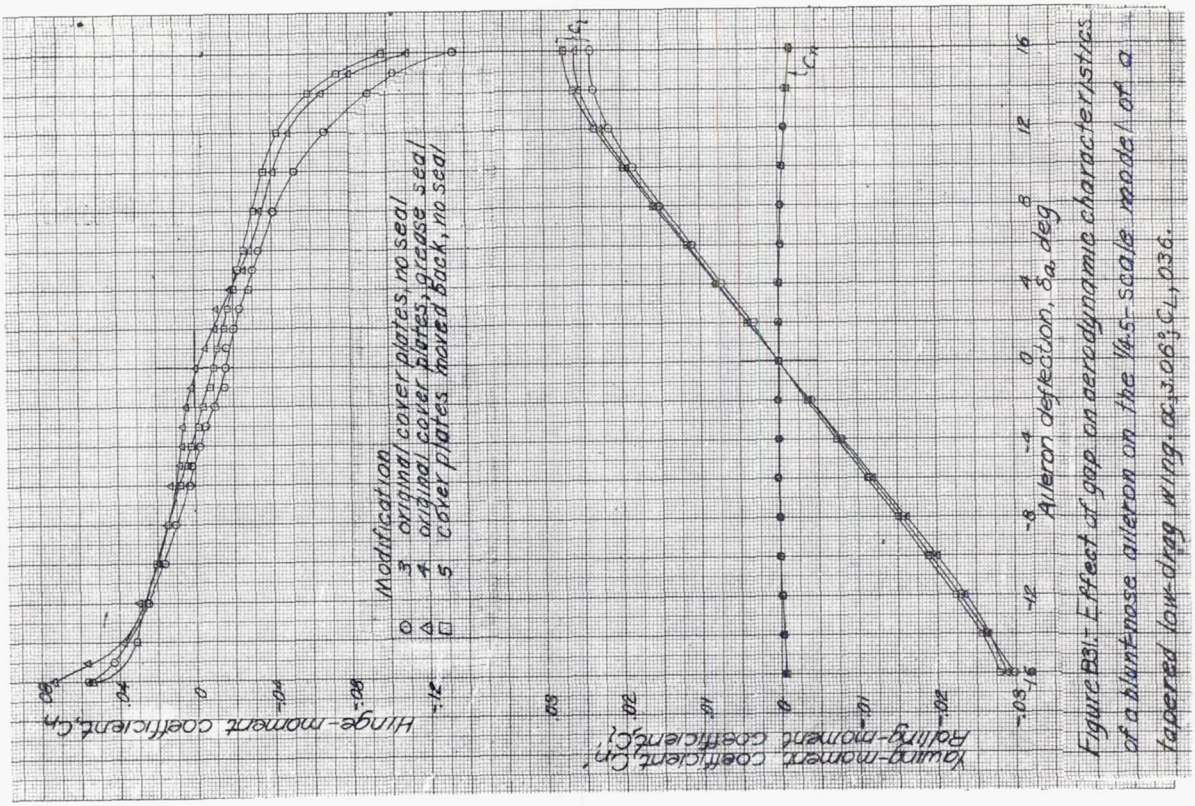

Figure B31.- Effect of gap on aerodynamic characteristics of a blunt-nose aileron on the 1/4.5-scale model of a tapered low-drag wing. a_c, 3.06°; C_L, 0.36.

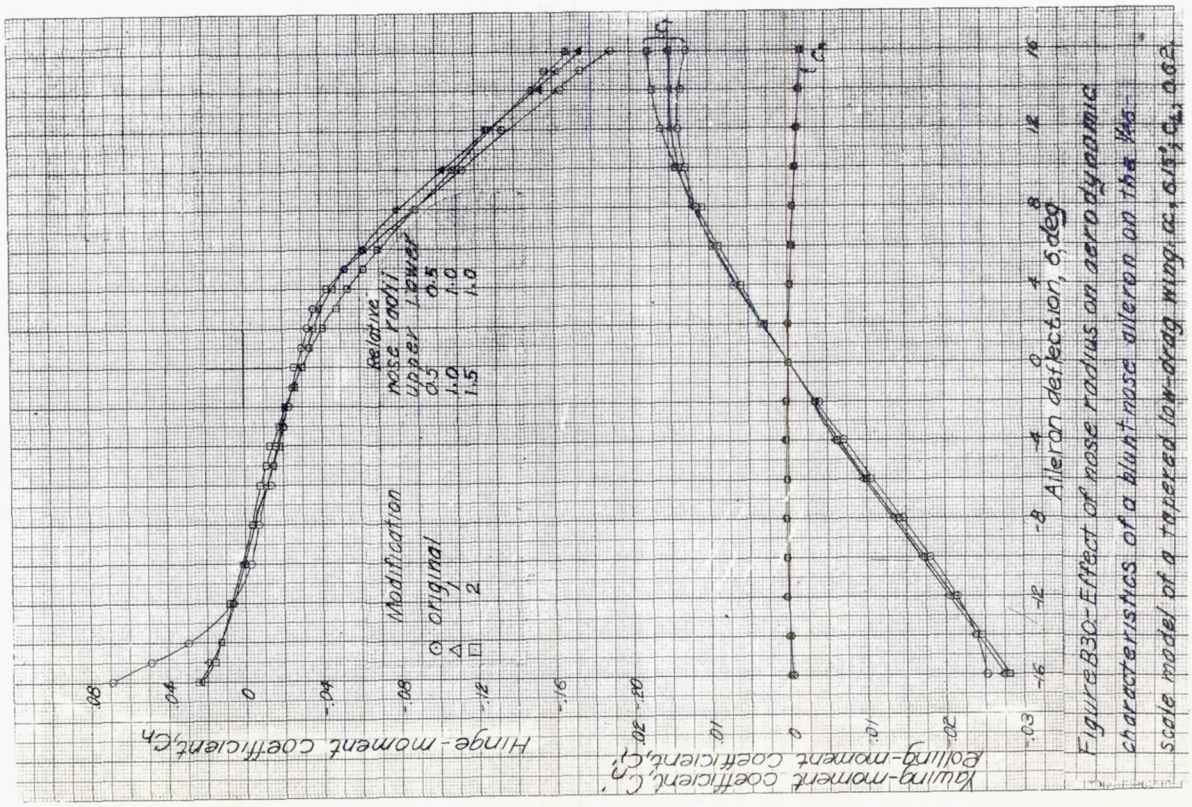

Figure B30.- Effect of nose radius on aerodynamic characteristics of a blunt-nose aileron on the 1/4.5-scale model of a tapered low-drag wing. a_c, 0.15°; C_L, 0.02.

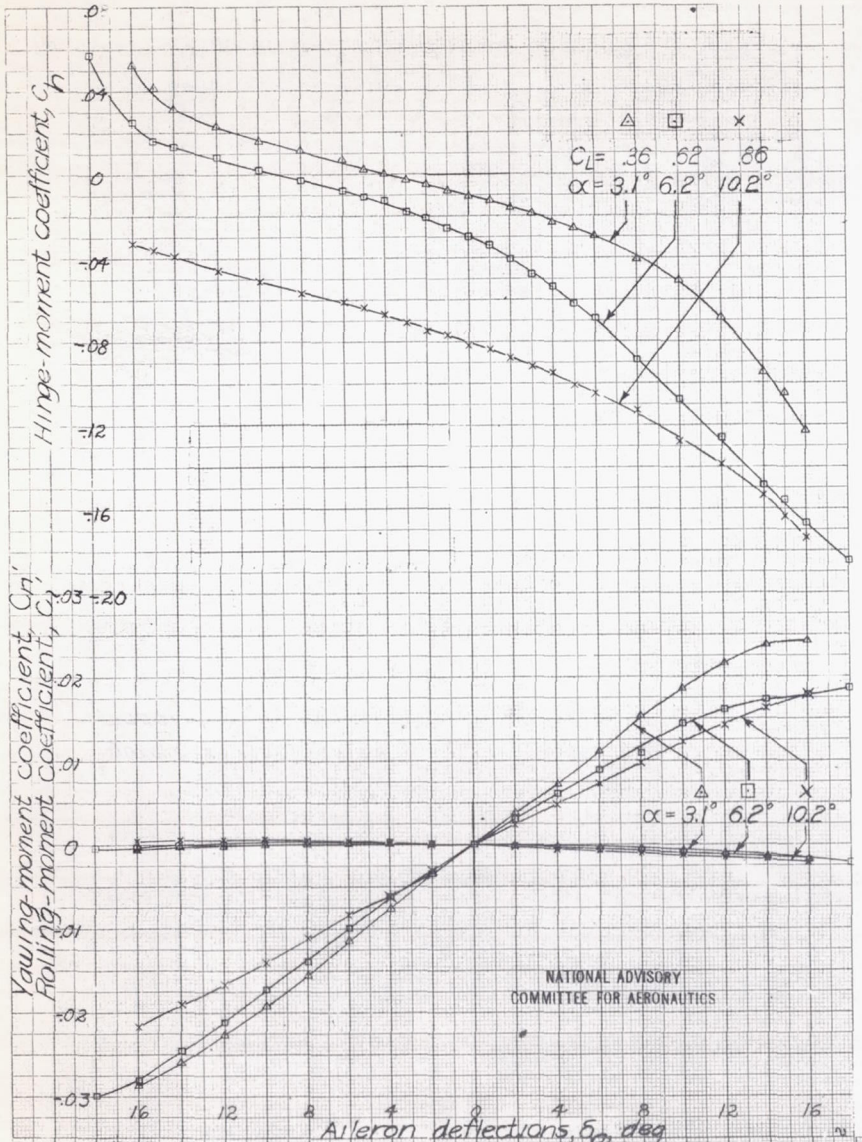

(a) Modification 2.

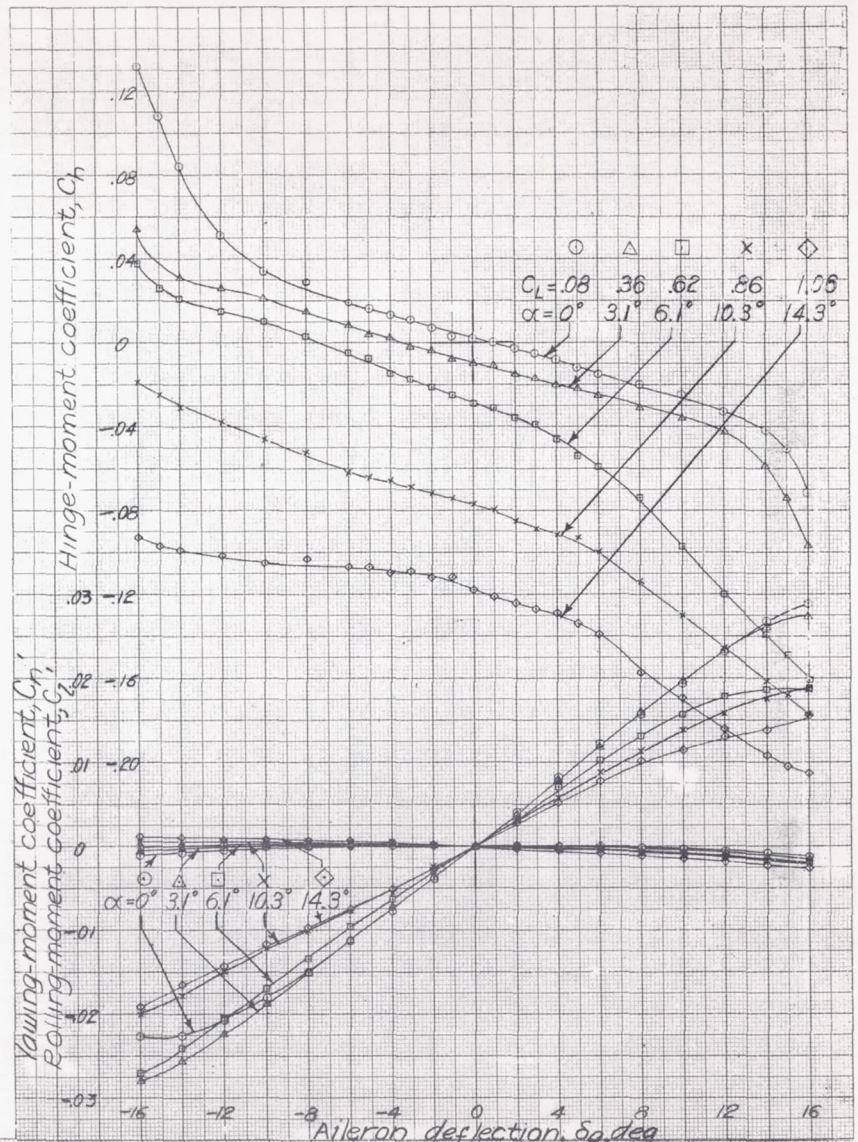

(b) Modification 5.

Figure B32.- Aerodynamic characteristics of blunt-nose ailerons on the $\frac{1}{4.5}$-scale model of a tapered low-drag wing.

Model B-IV

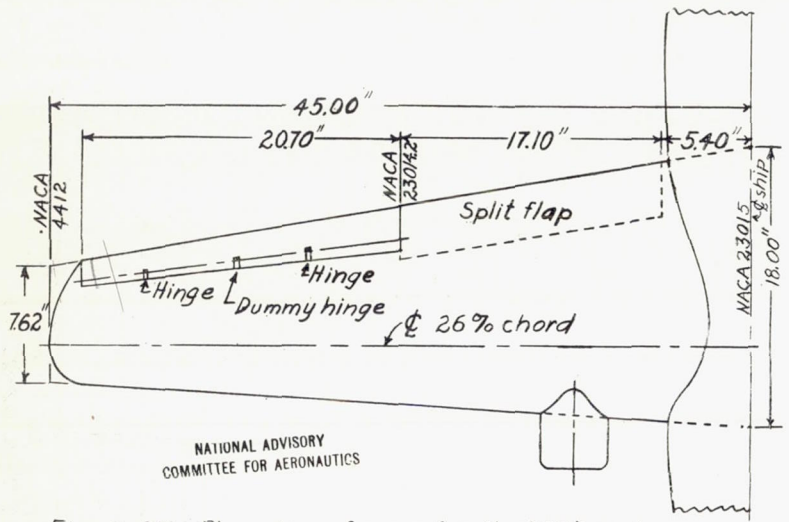

Figure B33.-Plan view of wing for the 0.075-scale model of an airplane. LMAL 7-by 10-foot tunnel.

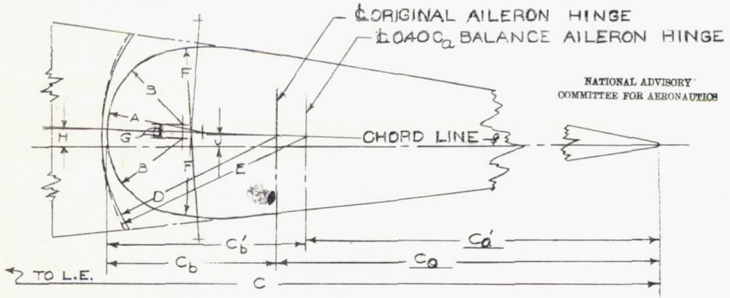

AILERON STATION	RADII (in.)					(in.)												
	A	B	D	E	F	G	H	J	C	c_a	c'_a	c_b	c'_b	$\frac{c_a}{c}$	$\frac{c'_a}{c}$	$\frac{c'_b}{c_b}$	$\frac{c_a}{c_a'}$
INBOARD END	.478	.368	.869	.006	.045	.035	.084	.053	12.672	2.534	2.457	.846	.383	.205	.184	.326	.400
OUTBOARD END	.227	.200	.531	.625	.483	.009	.100	.081	7.698	1.600	1.506	.508	.602	.208	.196	.318	.400

FIGURE B 34.-Details of ailerons tested on the 0.075 scale model of an airplane.

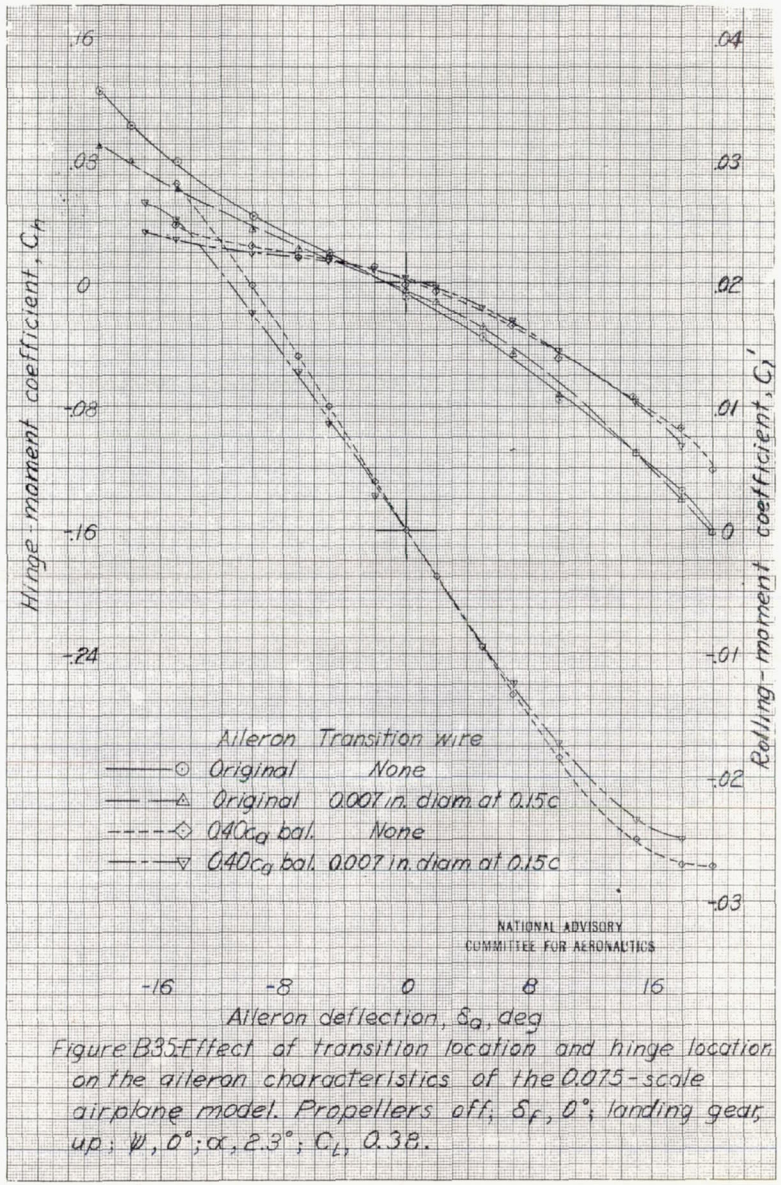

Figure B35.-Effect of transition location and hinge location on the aileron characteristics of the 0.075-scale airplane model. Propellers off, δ_f, 0°; landing gear, up; ψ, 0°; α, 2.3°; C_L, 0.38.

Model B-V

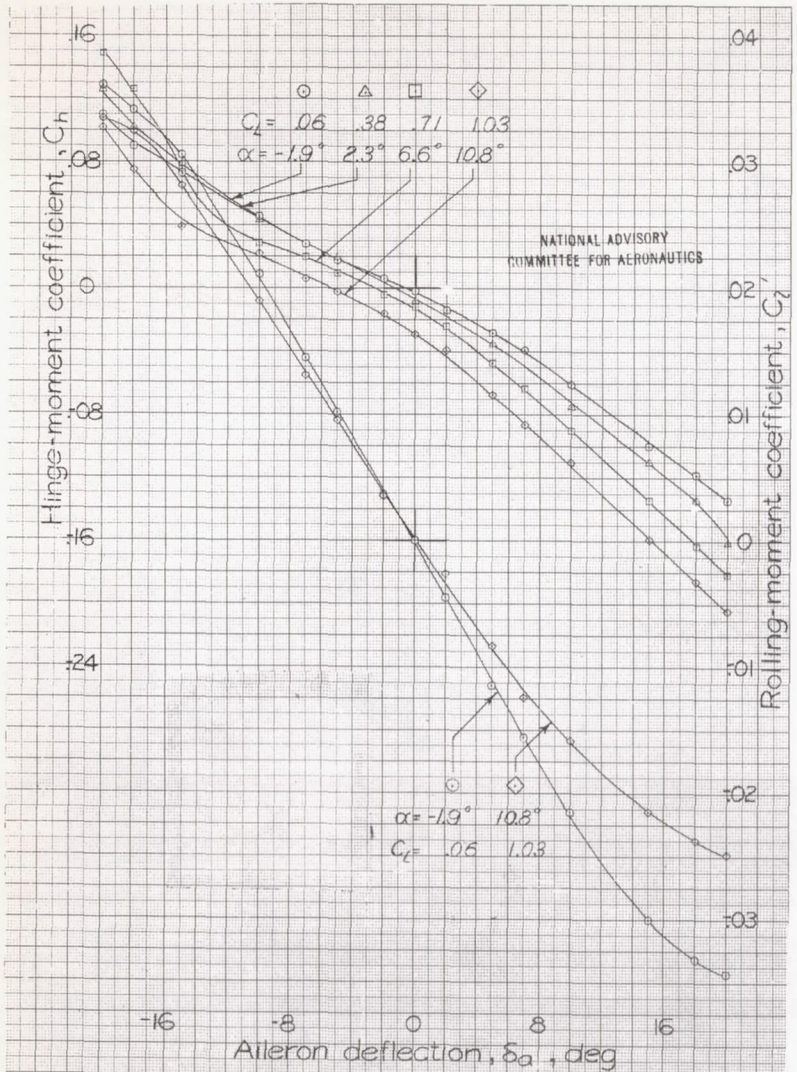

Figure B36 - Characteristics of the original ailerons on the 0.075-scale model of an airplane; complete model minus propellers and tail surfaces; transition not fixed; Ψ=0°; δ_f=0°; landing gear up.

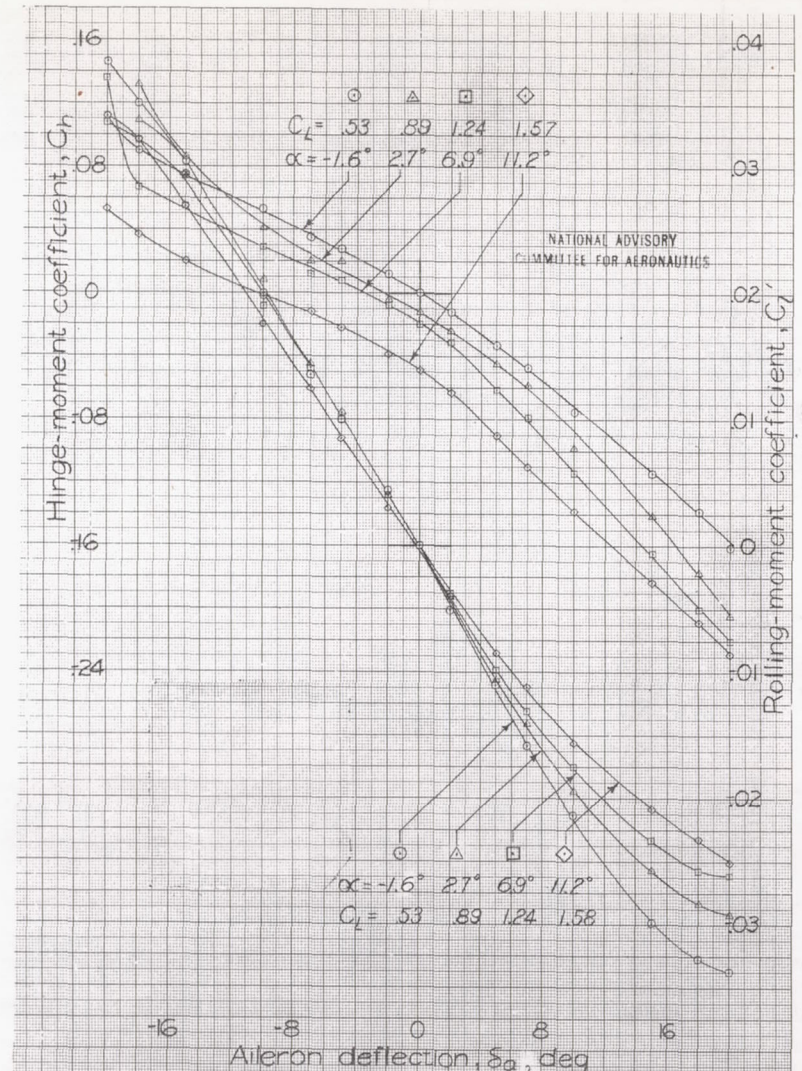

Figure B37 - Characteristics of the original ailerons on the 0.075-scale model of an airplane; complete model minus propellers and tail surfaces; transition not fixed; Ψ=0°; δ_f=50°; landing gear down.

Model B-4

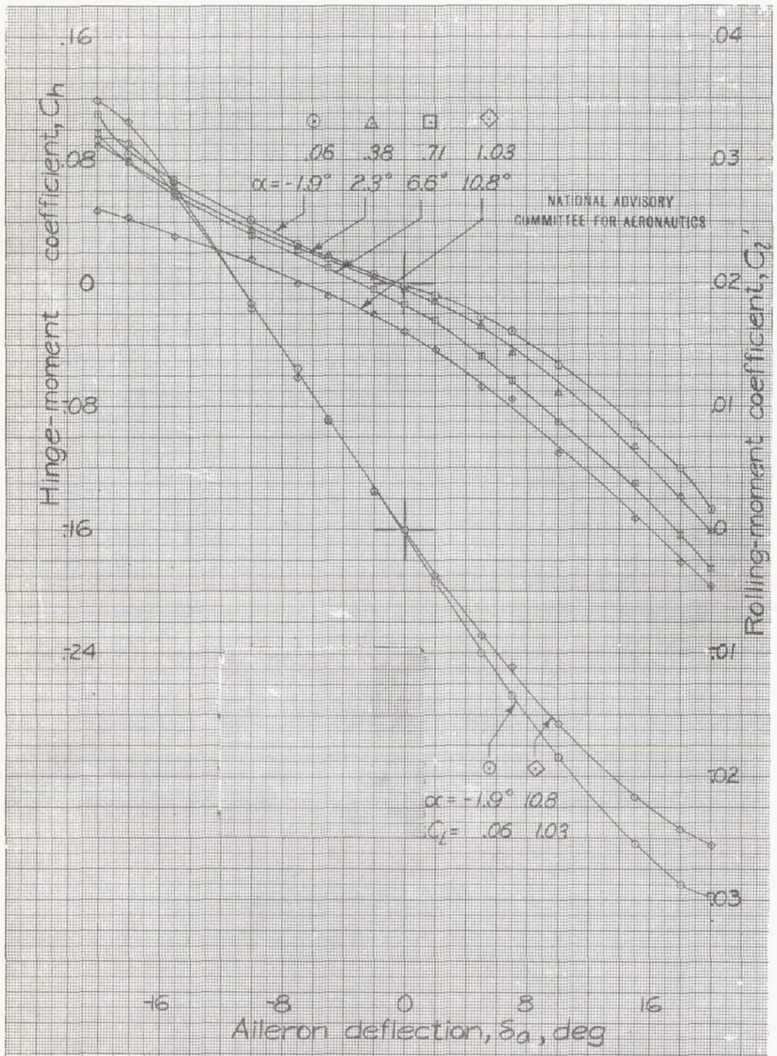

Figure B38.- Characteristics of the original ailerons on the 0.075-scale model of an airplane; complete model minus propellers and tail surfaces; transition fixed at 0.15c; Ψ=0°; δ_f=0°; landing gear up.

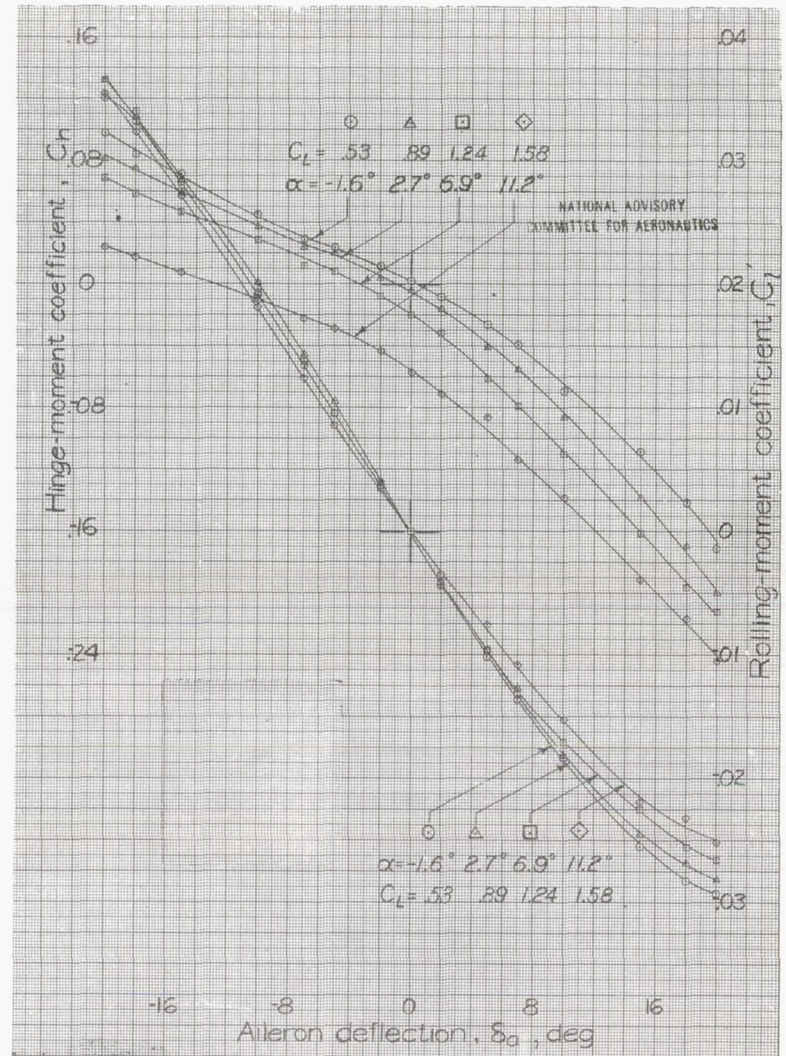

Figure B39.- Characteristics of the original ailerons on the 0.075-scale model of an airplane; complete model minus propellers and tail surfaces; transition fixed at 0.15c; Ψ=0°; δ_f=50°; landing gear down.

Model B-V

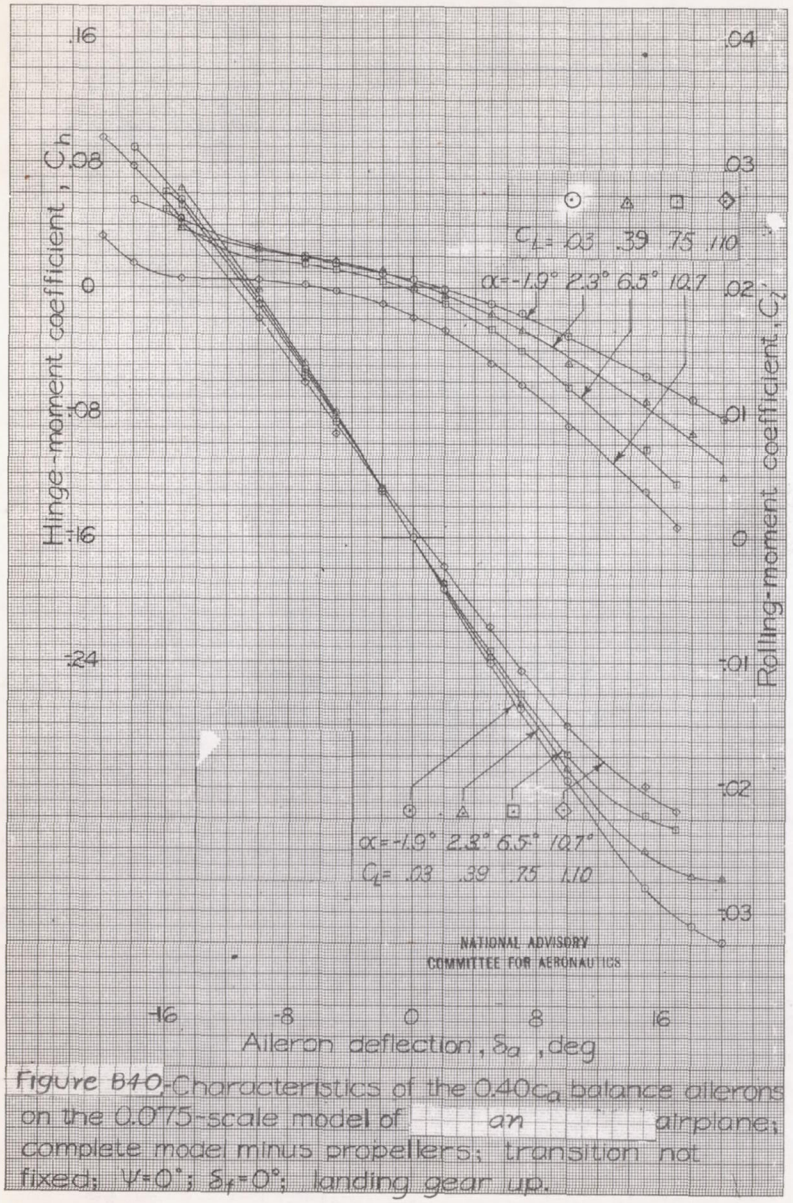

Figure B40.-Characteristics of the 0.40c_a balance ailerons on the 0.075-scale model of an airplane; complete model minus propellers; transition not fixed; Ψ=0°; δ_f=0°; landing gear up.

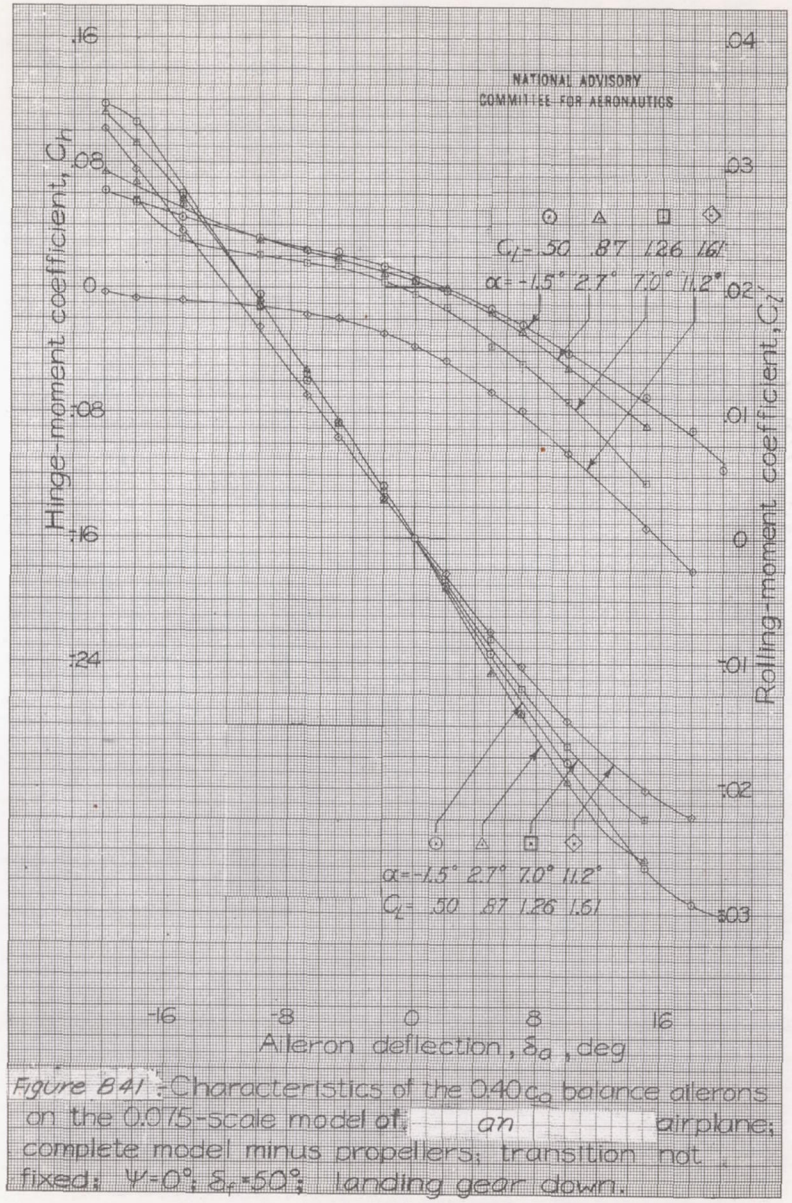

Figure B41.-Characteristics of the 0.40c_a balance ailerons on the 0.075-scale model of an airplane; complete model minus propellers; transition not fixed; Ψ=0°; δ_f=50°; landing gear down.

Model B-V

Model B-V

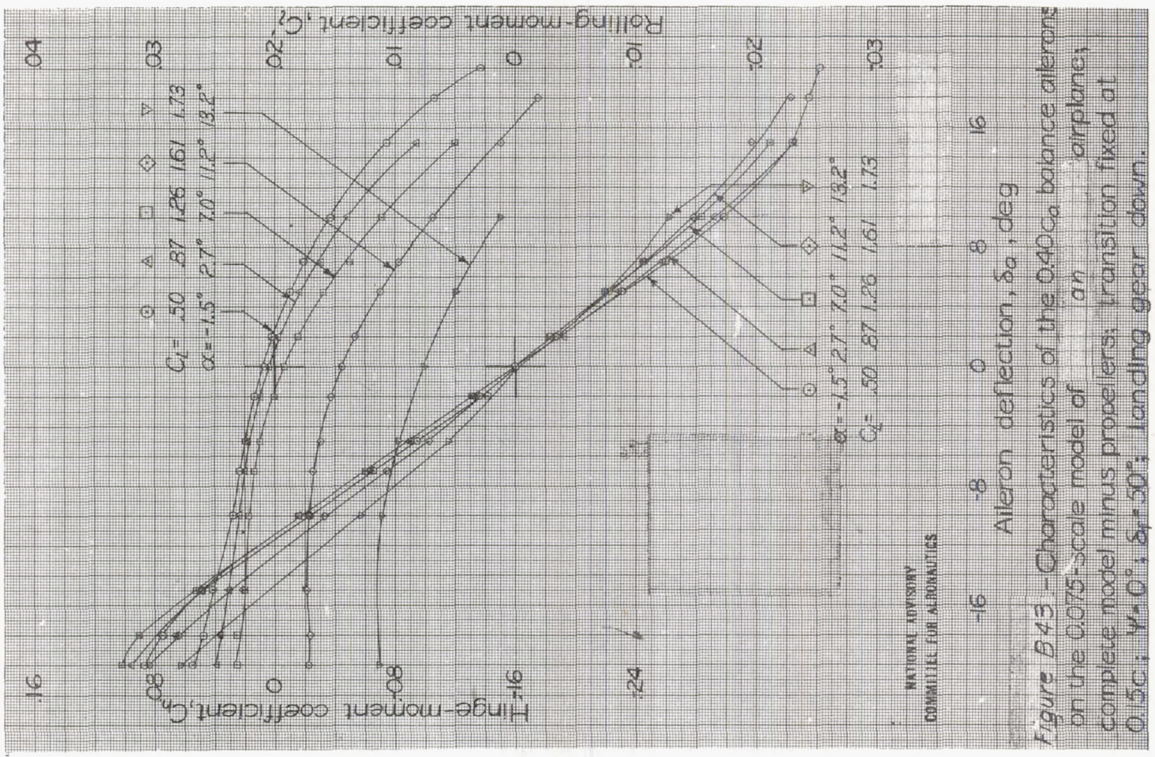

Figure B43.-Characteristics of the 0.40c_a balance ailerons on the 0.075-scale model of an airplane; complete model minus propellers; transition fixed at 0.15c; ψ=0°; δ_t=30°; landing gear down.

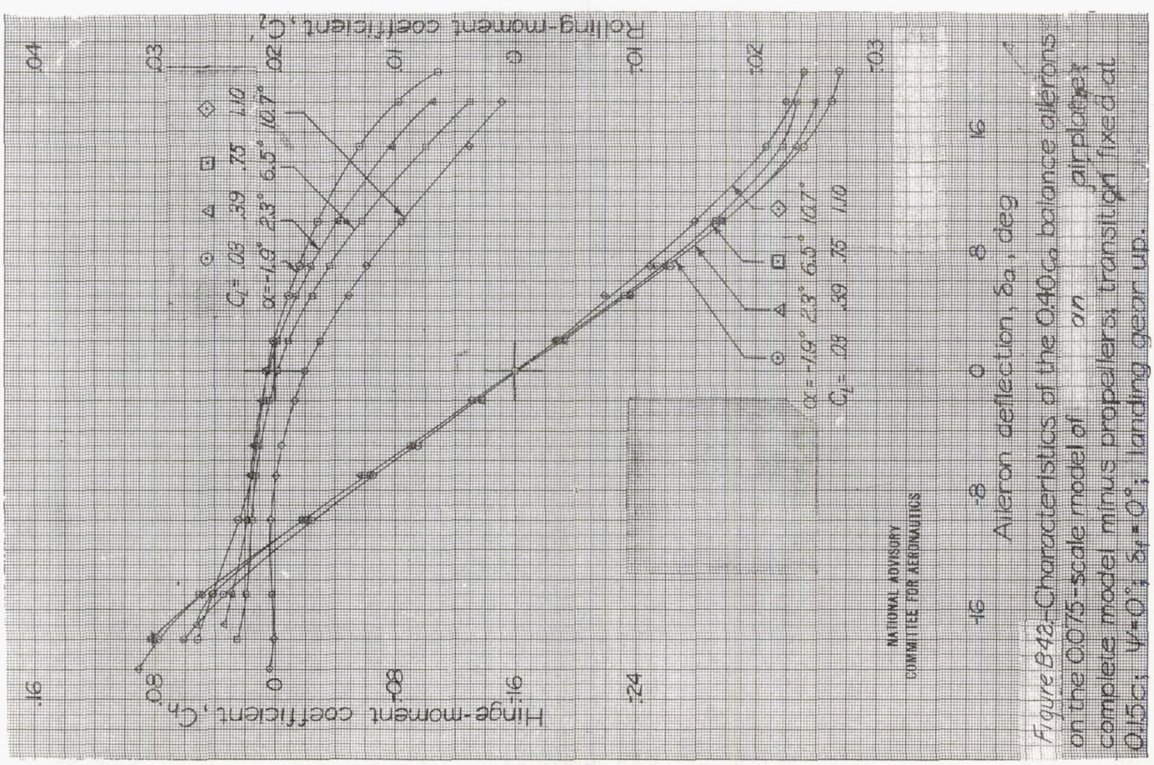

Figure B42.-Characteristics of the 0.40c_a balance ailerons on the 0.075-scale model of an airplane; complete model minus propellers; transition fixed at 0.15c; ψ=0°; δ_t=0°; landing gear up.

Model C-I

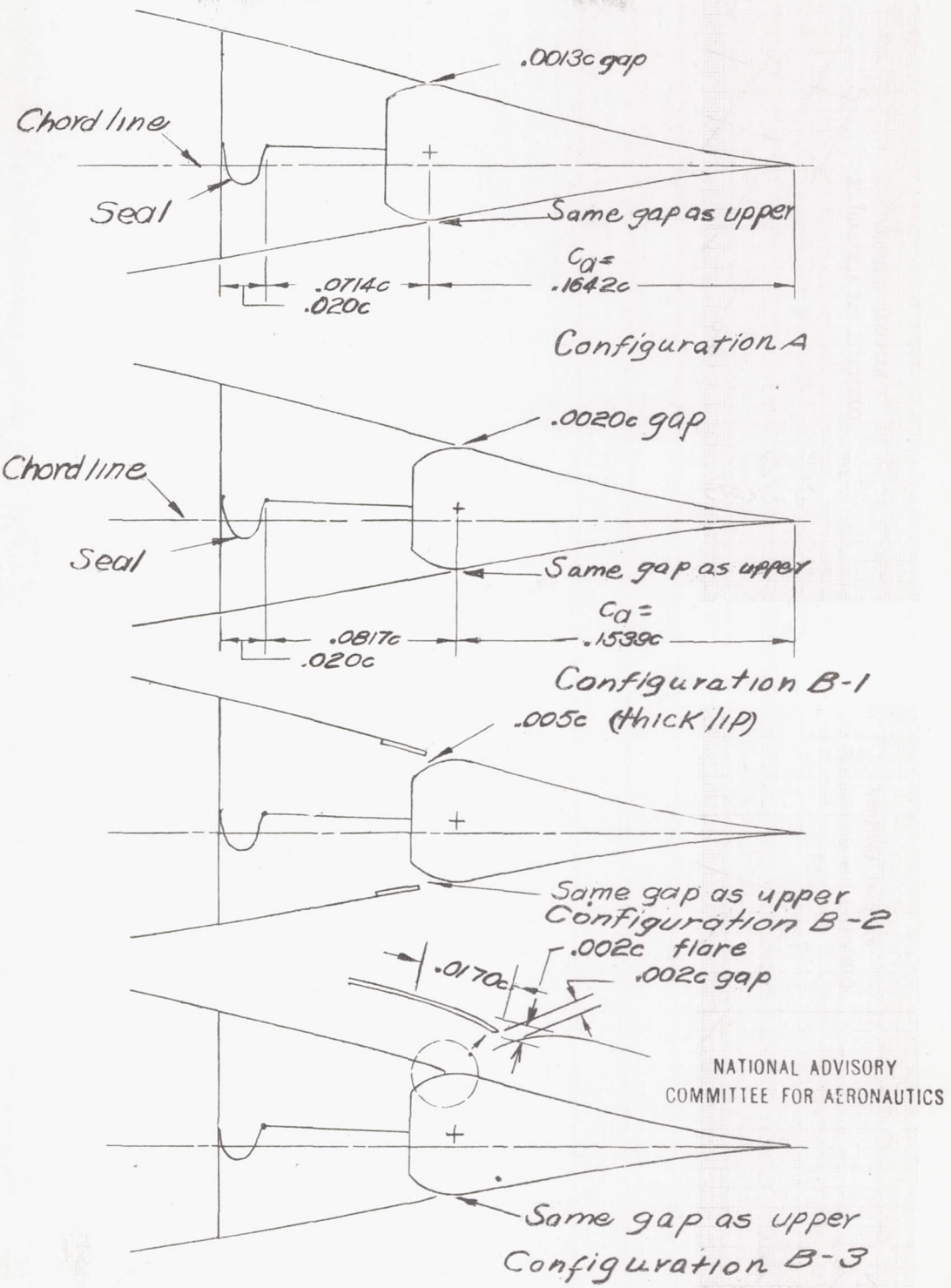

Figure C1 .-Balance configurations tested on the NACA 66(2X15)-216, a=0.6 airfoil section. Two-dimensional-flow tests; 50-inch-chord model C-I ; tests in NACA two-dimensional low-turbulence tunnel.

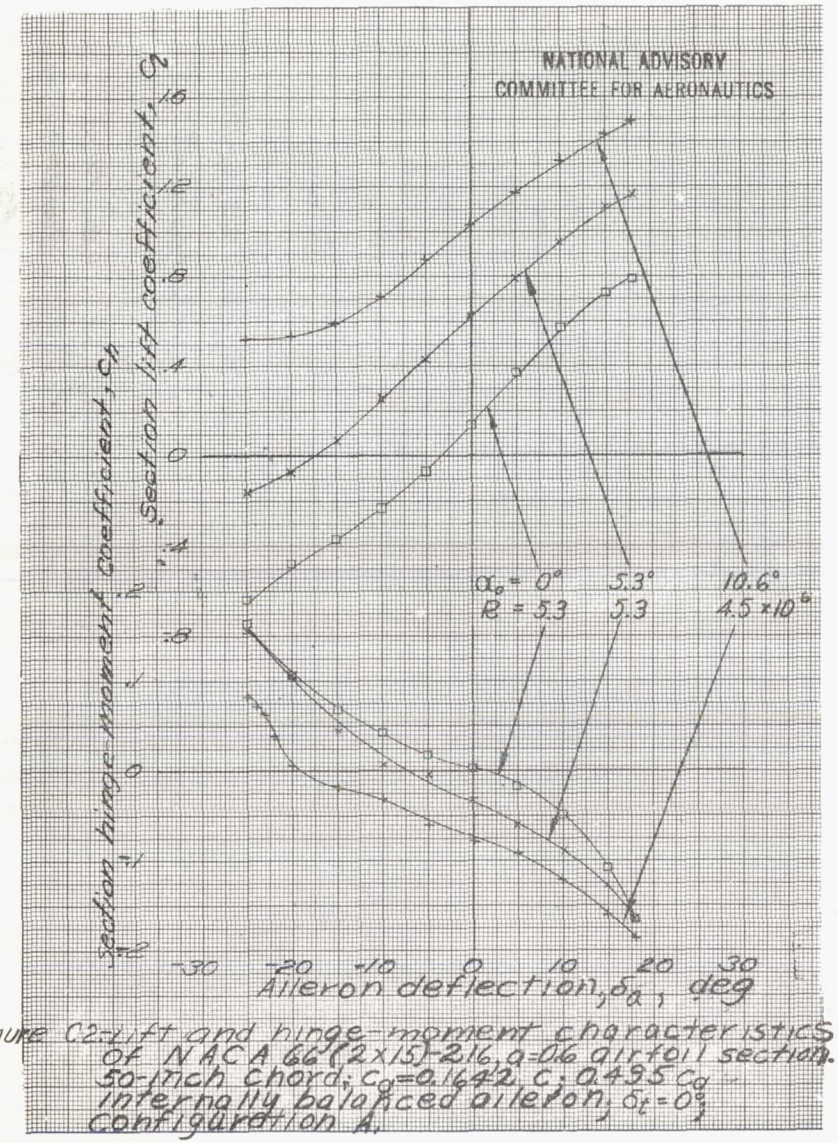

Figure C2-Lift and hinge-moment characteristics of NACA 66(2x15)-216, a=0.6 airfoil section. 50-inch chord; c_a=0.1642 c; 0.435 c_a internally balanced aileron, δ_t=0°; configuration A.

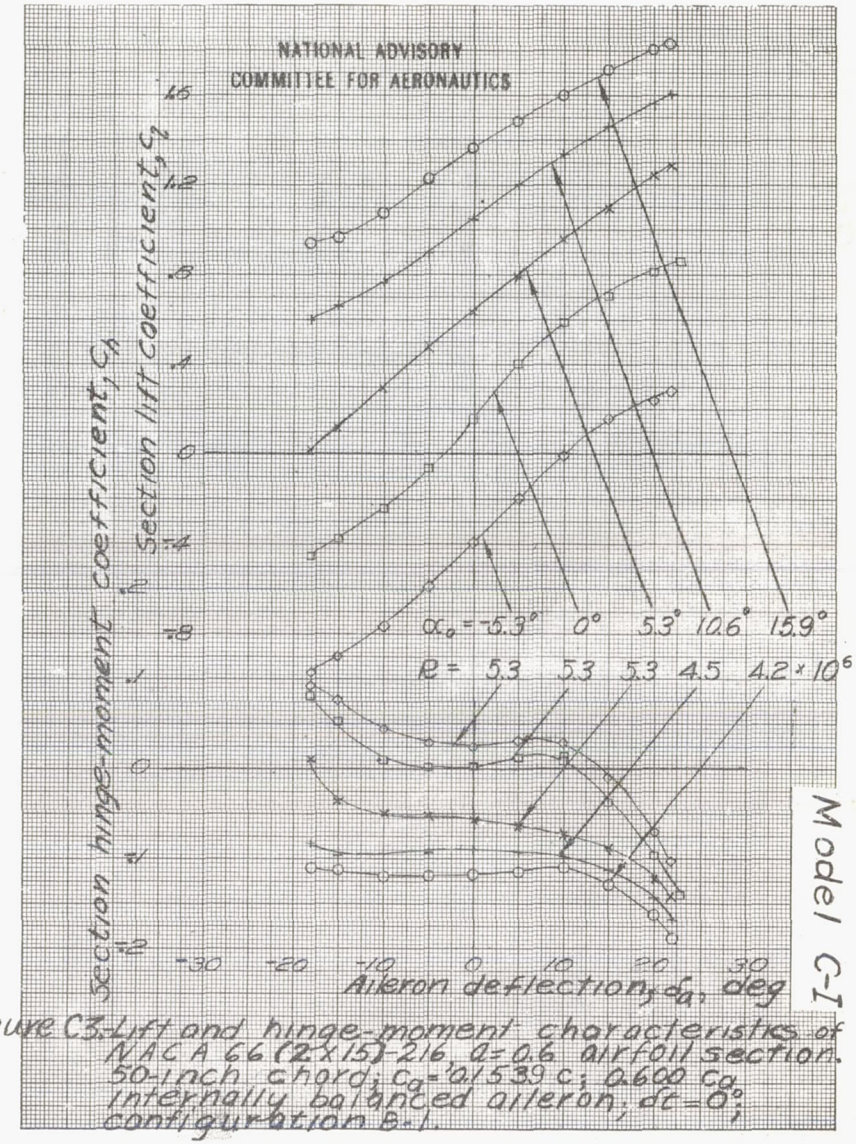

Figure C3-Lift and hinge-moment characteristics of NACA 66(2x15)-216, a=0.6 airfoil section. 50-inch chord; c_a=0.539 c; 0.600 c_a internally balanced aileron, δ_t=0°; configuration B-1.

Model C-1

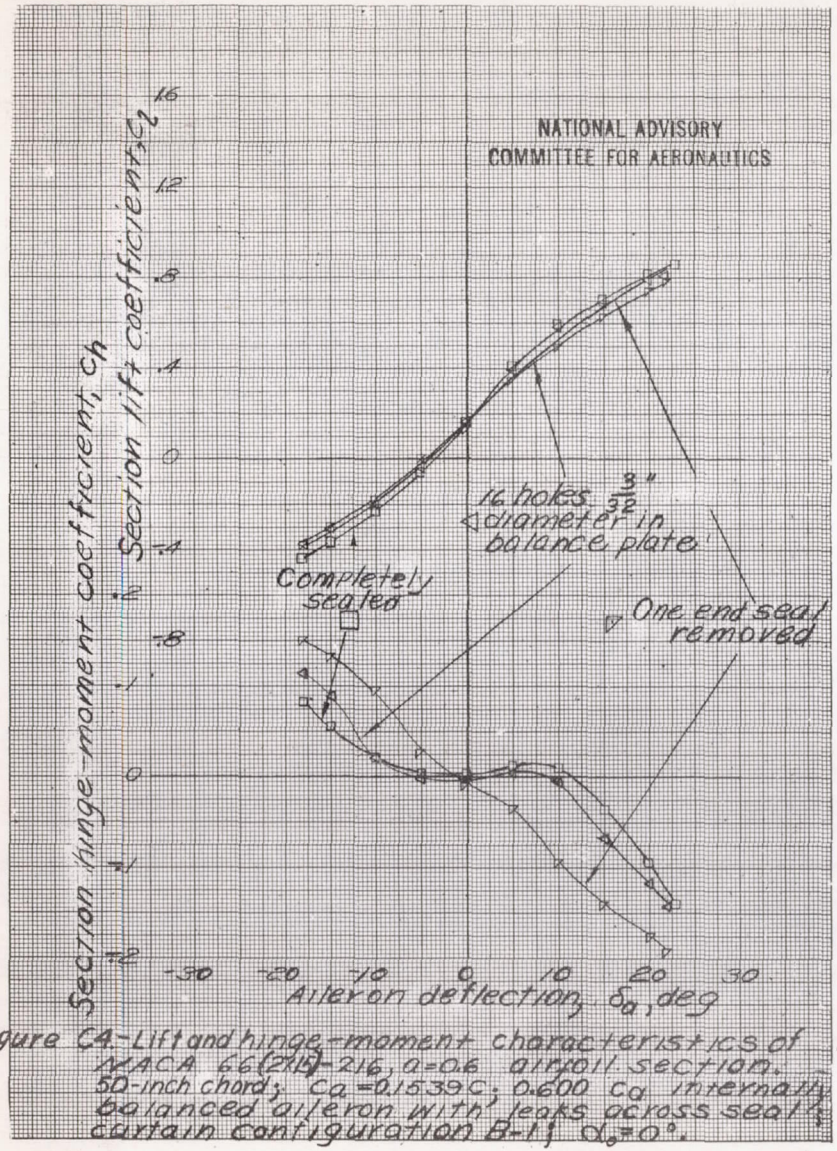

Figure C4.- Lift and hinge-moment characteristics of NACA 66(2x15)-216, a=0.6 airfoil section. 50-inch chord; c_a=0.1539c; 0.600 c_a internally balanced aileron with leaks across seal; certain configuration B-1; α_o=0°.

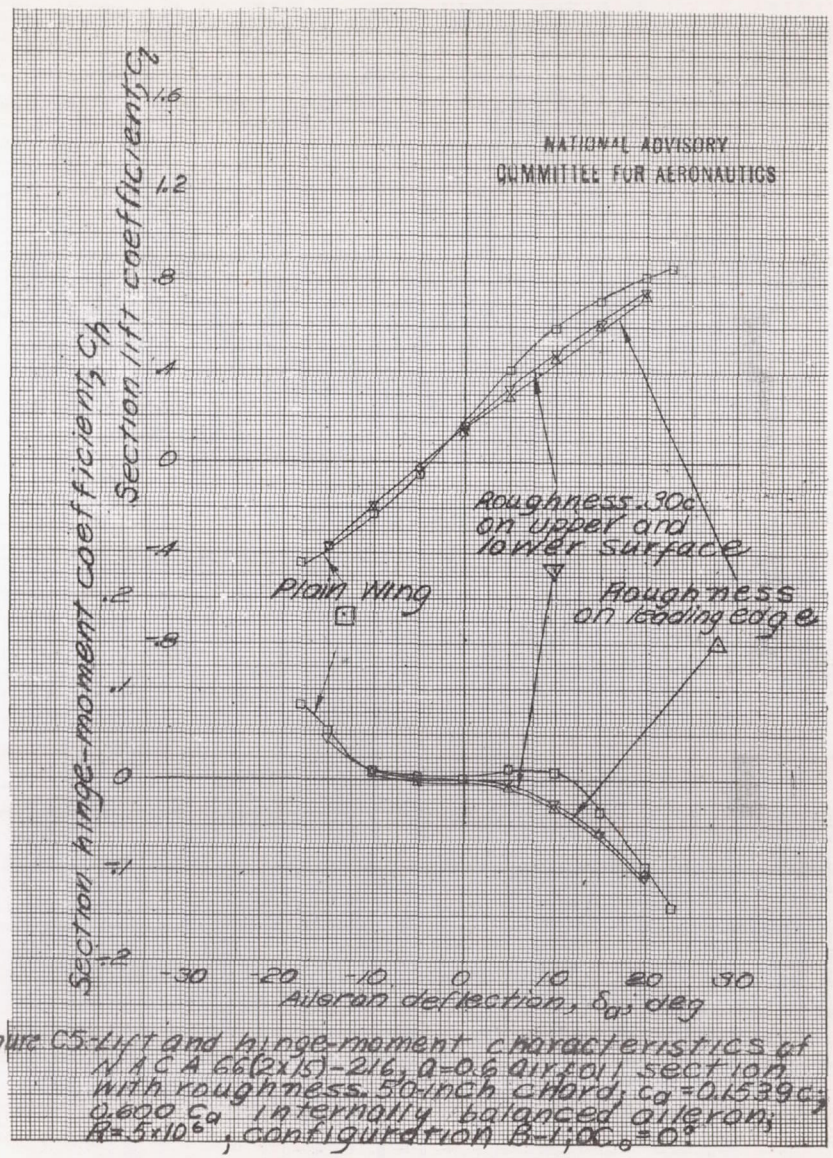

Figure C5.- Lift and hinge-moment characteristics of NACA 66(2x15)-216, a=0.6 airfoil section with roughness. 50-inch chord; c_a=0.1539c; 0.600 c_a internally balanced aileron; R=5x10^6; configuration B-1; α_o=0°.

Model C-I

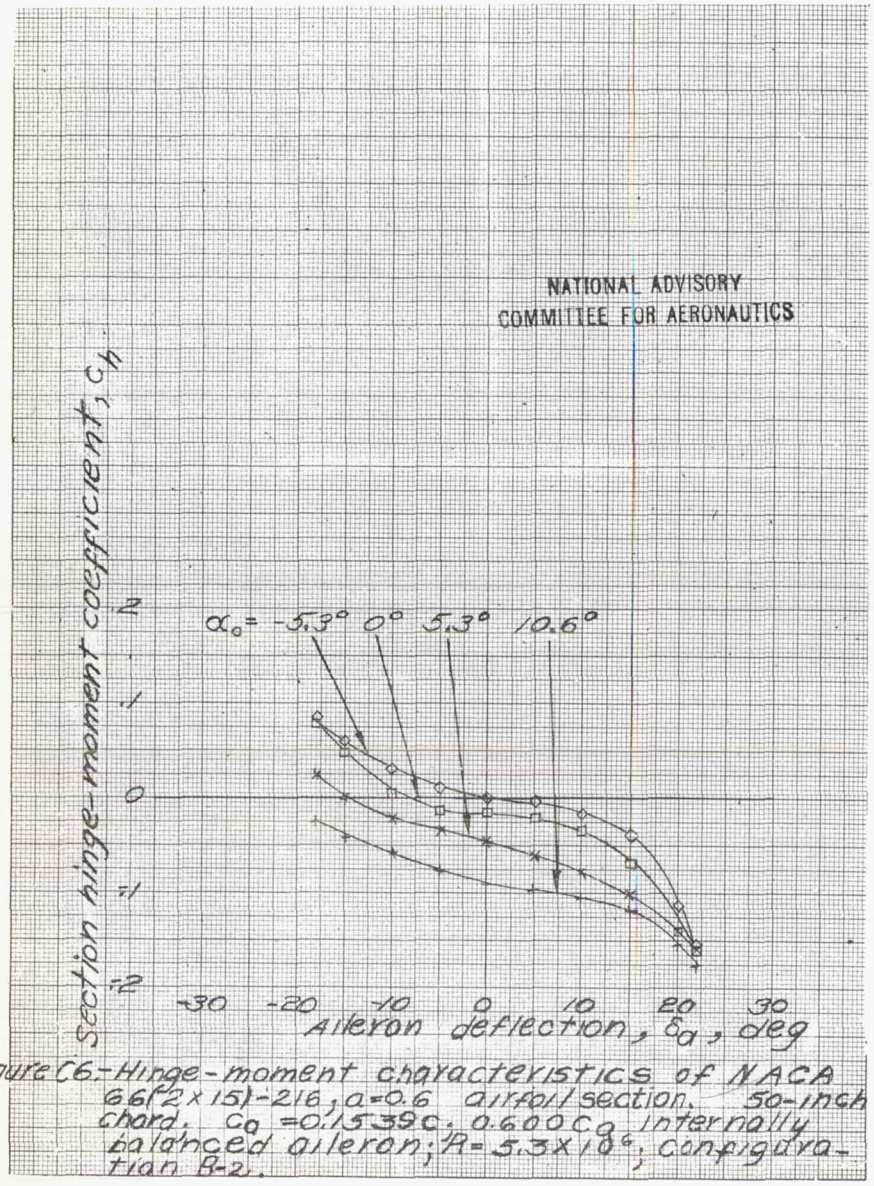

Figure C6.-Hinge-moment characteristics of NACA 66(2x15)-216, a=0.6 airfoil section. 50-inch chord. c_a =0.1539c. 0.600c_a internally balanced aileron; R= 5.3x10^6, configuration B-2.

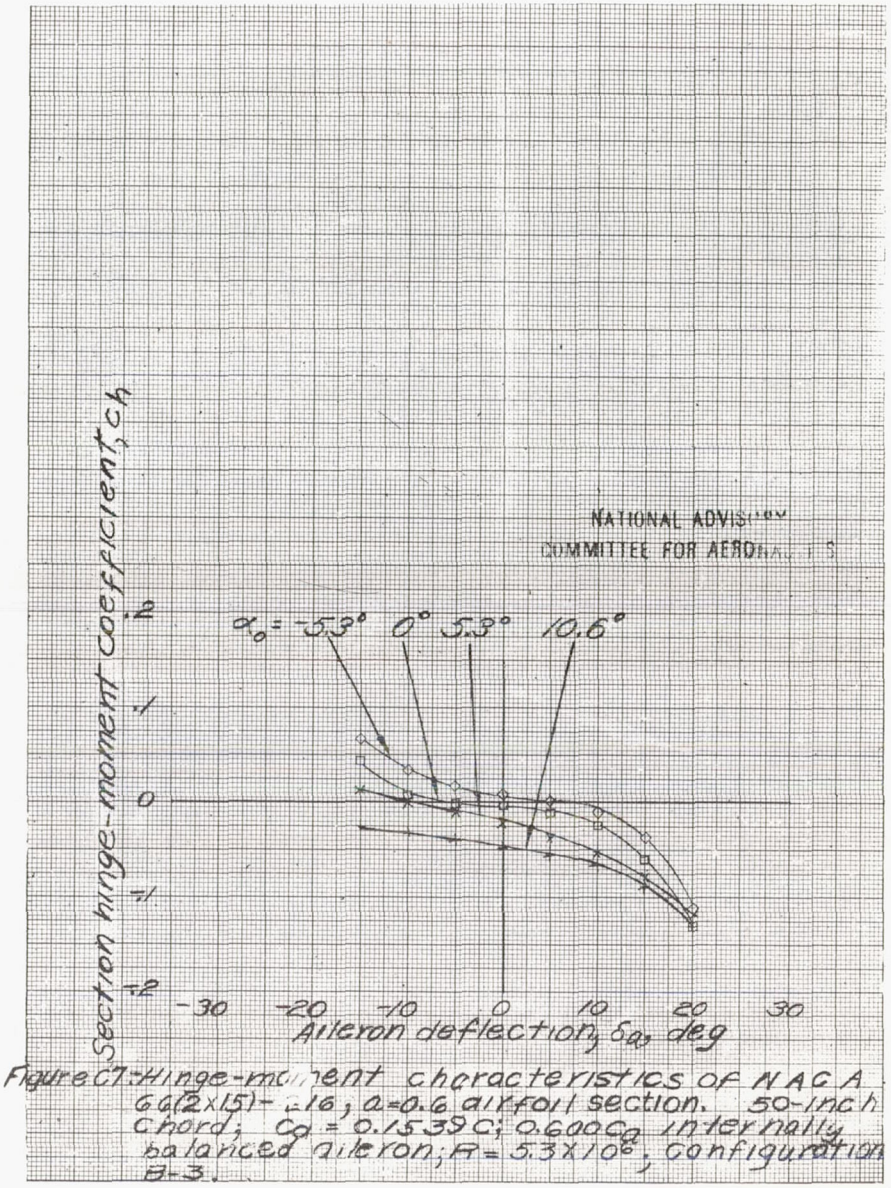

Figure C7.-Hinge-moment characteristics of NACA 66(2x15)-216, a=0.6 airfoil section. 50-inch chord; c_a = 0.1539c; 0.600c_a internally balanced aileron; R= 5.3x10^6, configuration B-3.

Model C-I

L-419

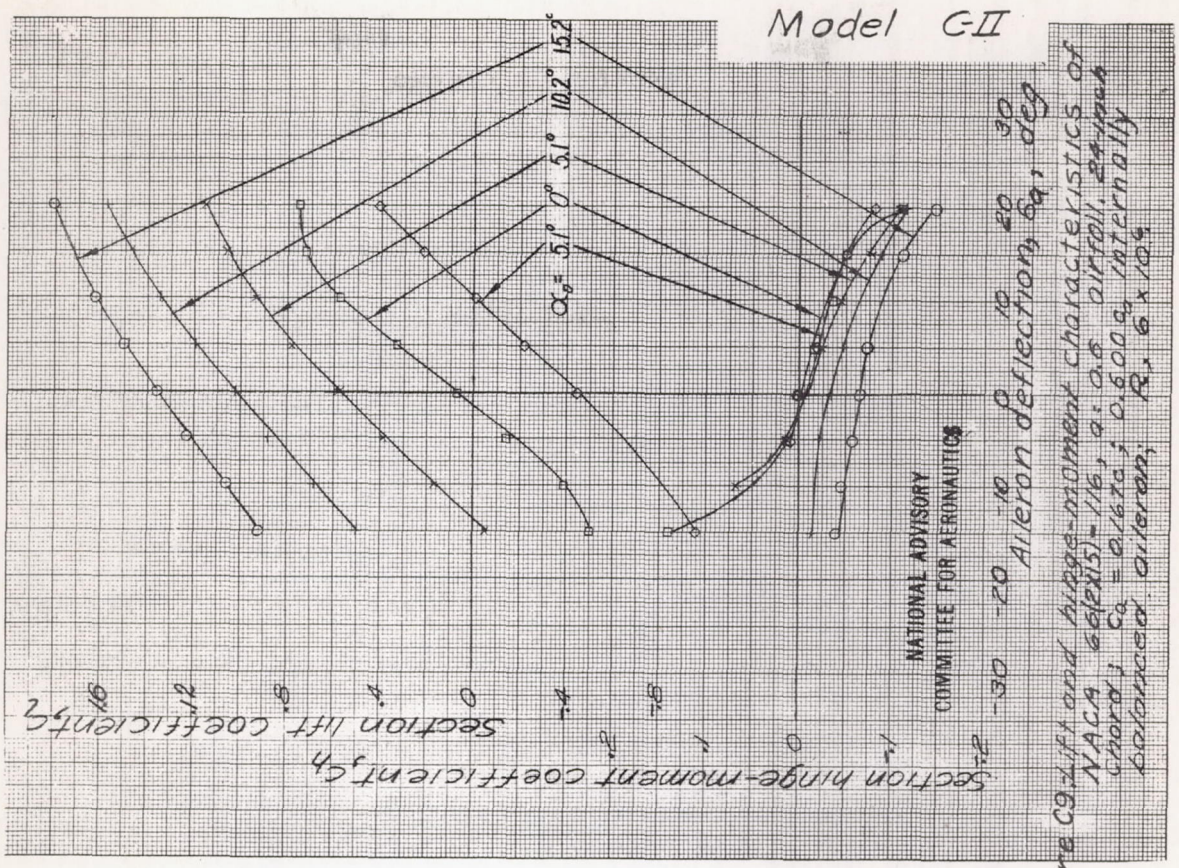

Figure C9.- Lift and hinge-moment characteristics of NACA 66(2X15)-116, a = 0.6 airfoil, 24-inch chord; c_a = 0.167c; 0.600c internally balanced aileron; R, 6×10^6.

NATIONAL ADVISORY
COMMITTEE FOR AERONAUTICS

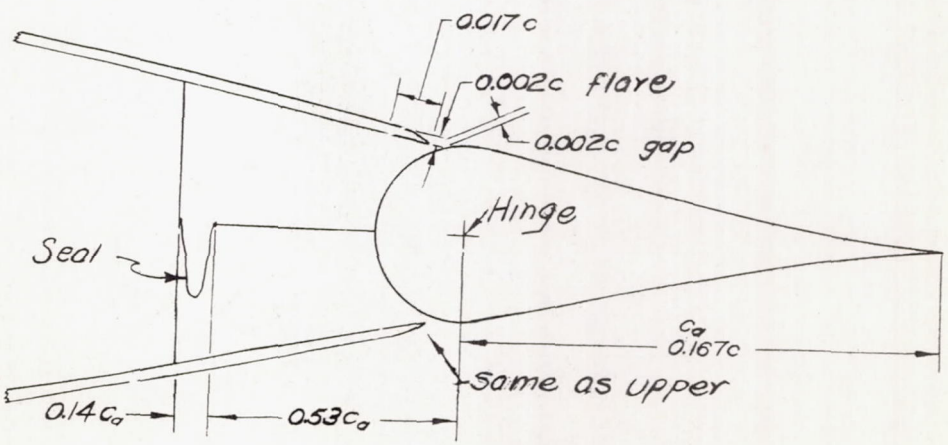

Figure C8.- Balance configuration tested on the NACA 66 (2X15)-116, a= 0.6, airfoil section. Two-dimensional-flow tests; 24-inch-chord model C-II tested in NACA two-dimensional low-turbulence pressure tunnel.

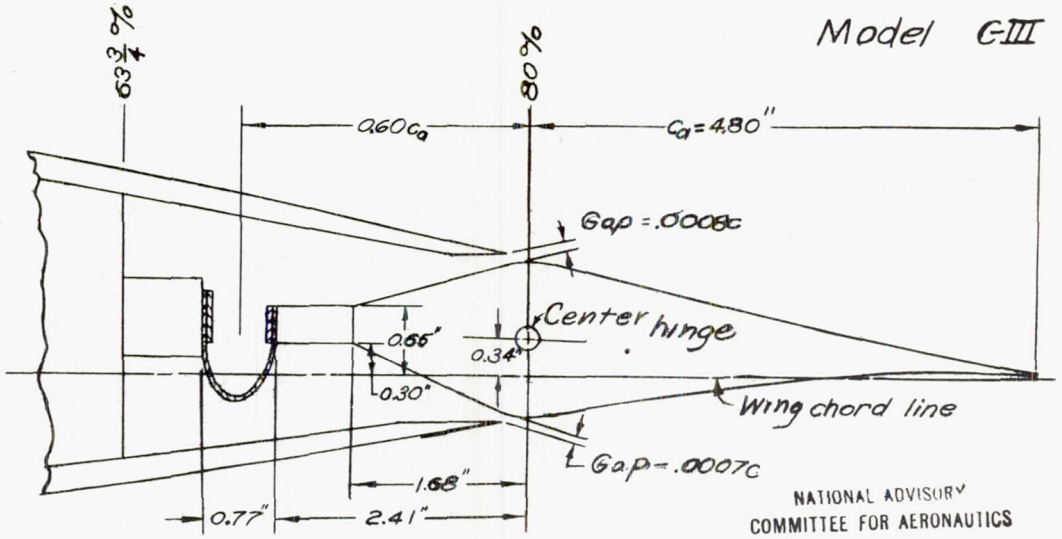

Figure C10.- Aileron and balance configurations on an intermediate section between root - NACA 63(420) -321, a = 1.0 and tip - NACA 65(318) - 415, a = 1.0. Two-dimensional-flow tests. NACA two-dimensional low-turbulence tunnel.

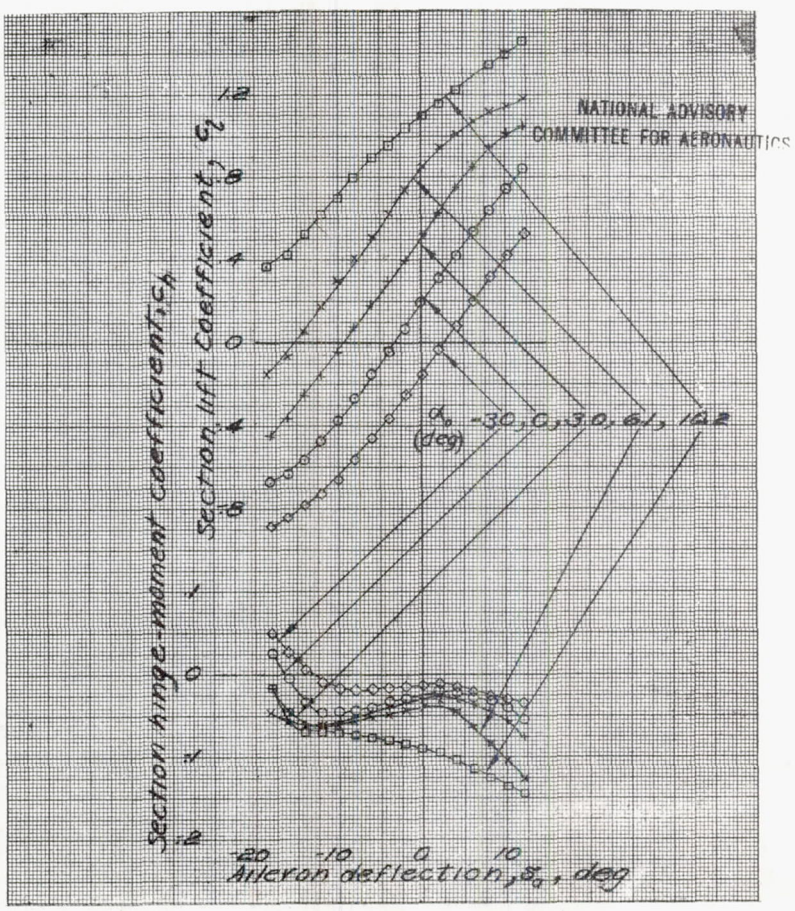

Figure C11.- Characteristics of a completely sealed, 0.60c_a internally balanced 0.20c aileron; R = 2.5 x 10^6. Central hinge position.

Model C-III

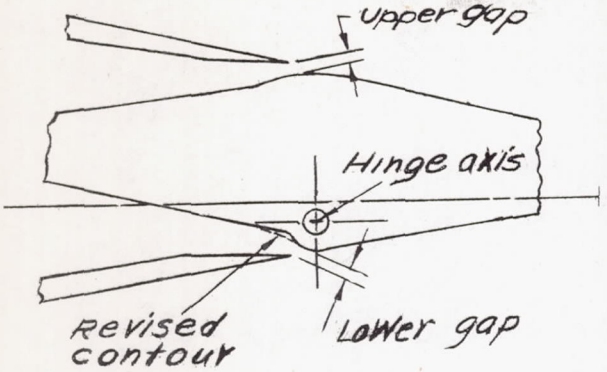

Figure C12.- Characteristics of a completely sealed 0.60 c_a internally balanced 0.20c aileron. Low hinge position; $R = 2.5 \times 10^6$.

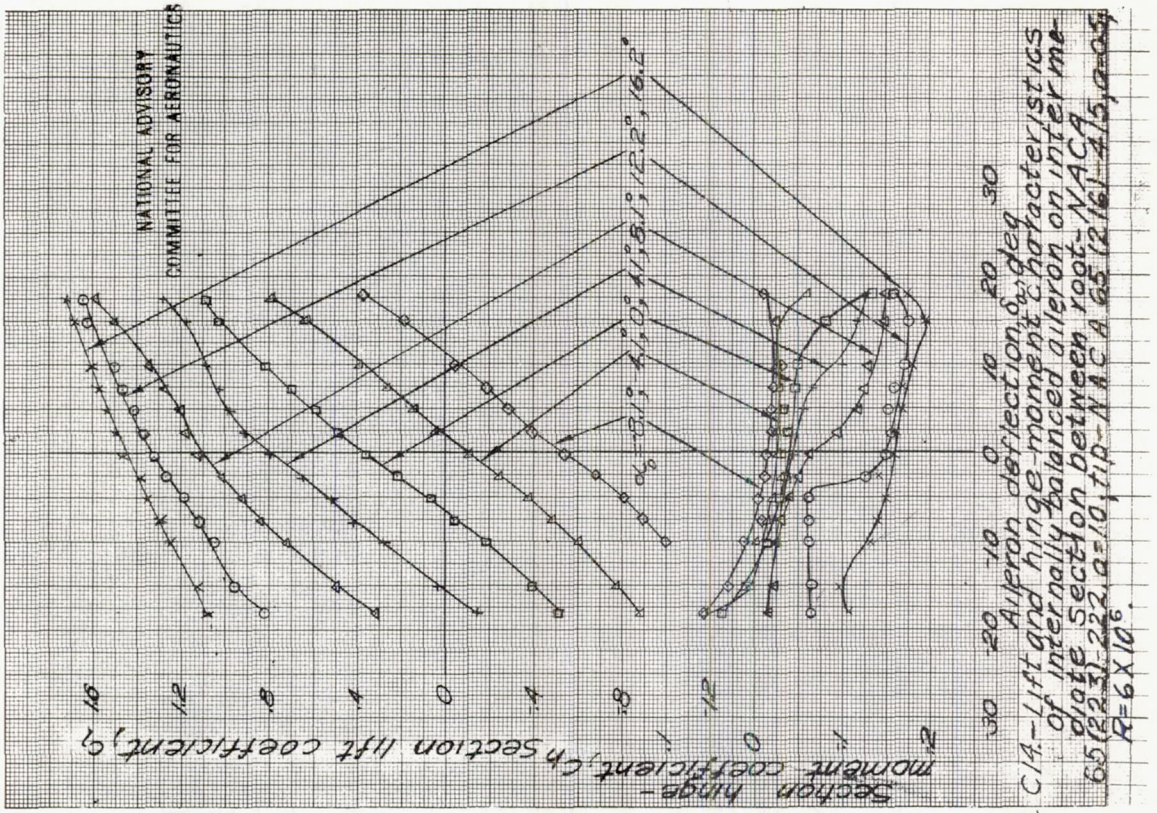

Figure C14.- Lift and hinge-moment characteristics of internally balanced aileron on intermediate section between root - NACA 65(223)-222, a=1.0, tip - NACA 65(216)-415, a=0.5. $R = 6 \times 10^6$.

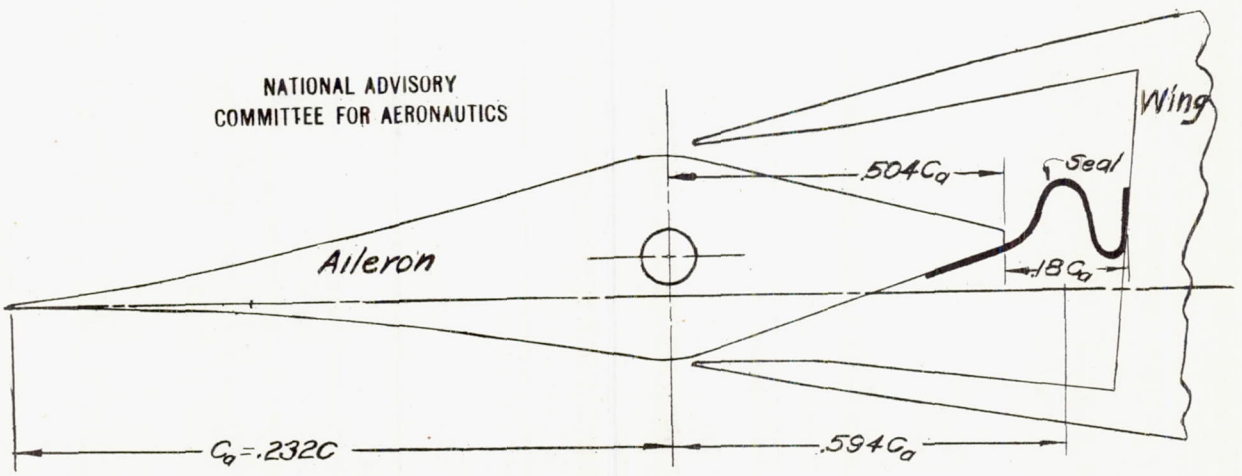

Figure C13.- Aileron and balance setup on intermediate section between root - NACA 65(223)-222, a=1.0 and tip - NACA 65(216)-415, a=0.5. Two-dimensional-flow tests; model C-IV; NACA two-dimensional low-turbulence pressure tunnel.

Model C-V

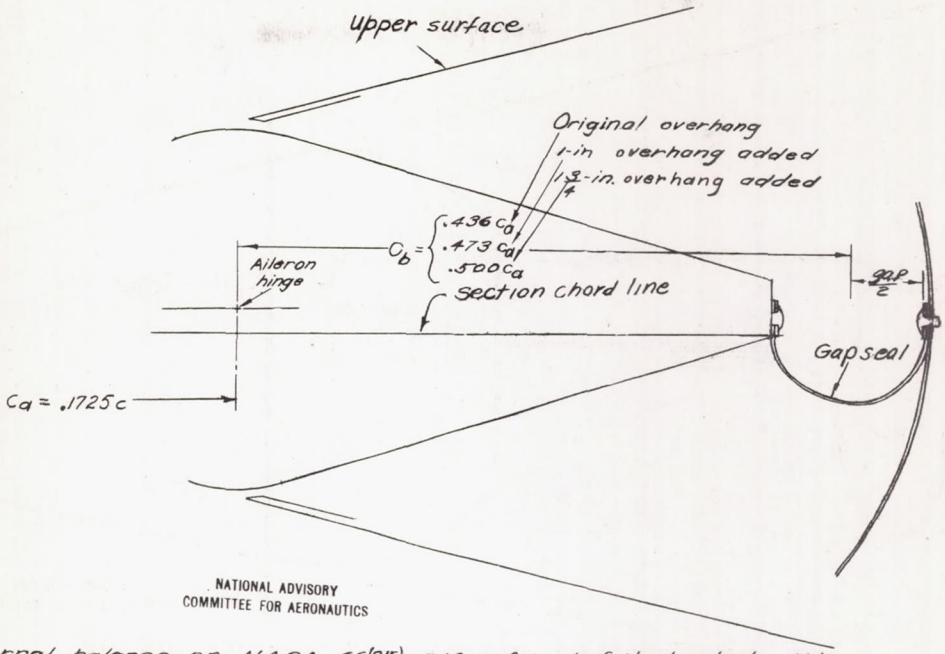

Figure C15.-Internal balance on NACA 66(215)-216, a=0.6 airfoil tested with various amounts of seal and balance. Two-dimensional-flow tests; model C-V; NACA two-dimensional low-turbulence tunnel.

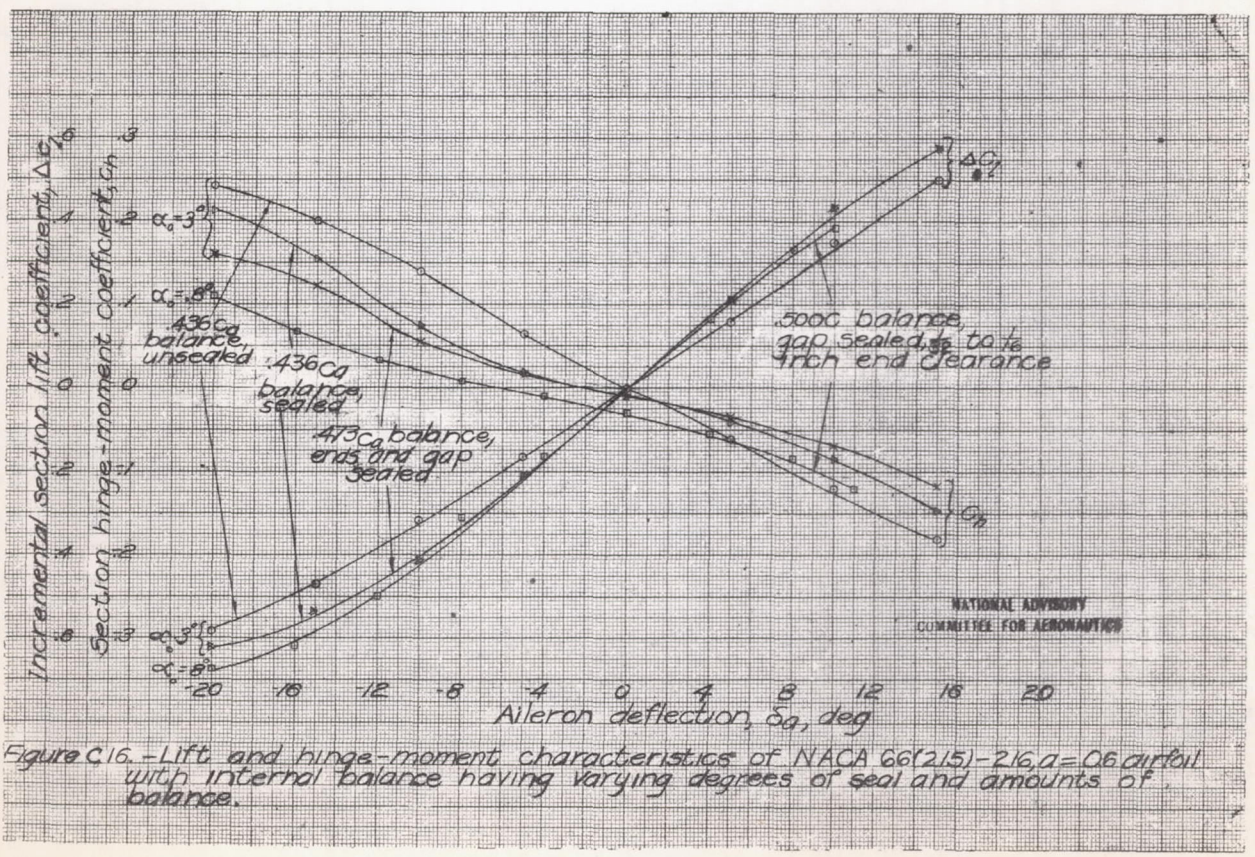

Figure C16.-Lift and hinge-moment characteristics of NACA 66(215)-216, a=0.6 airfoil with internal balance having varying degrees of seal and amounts of balance.

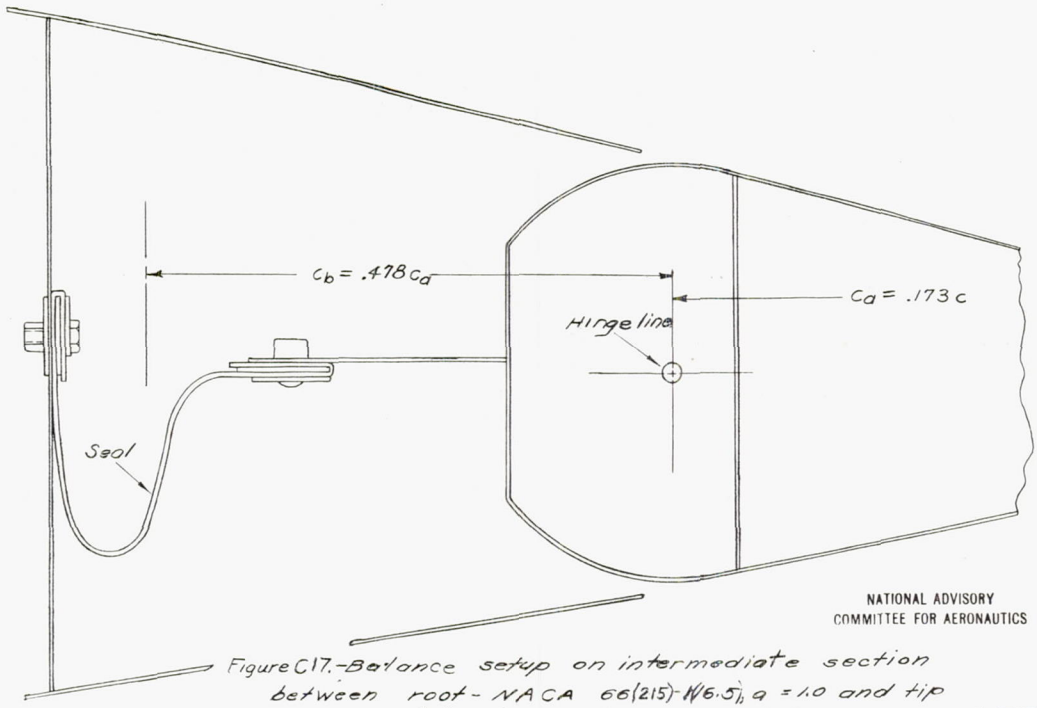

Figure C17.-Balance setup on intermediate section between root-NACA 66(215)-1(16.5)$_1$, a = 1.0 and tip NACA 67(115)-213, a = 0.7. Two-dimensional-flow tests; model C-VII; NACA Two-dimensional low-turbulence tunnel.

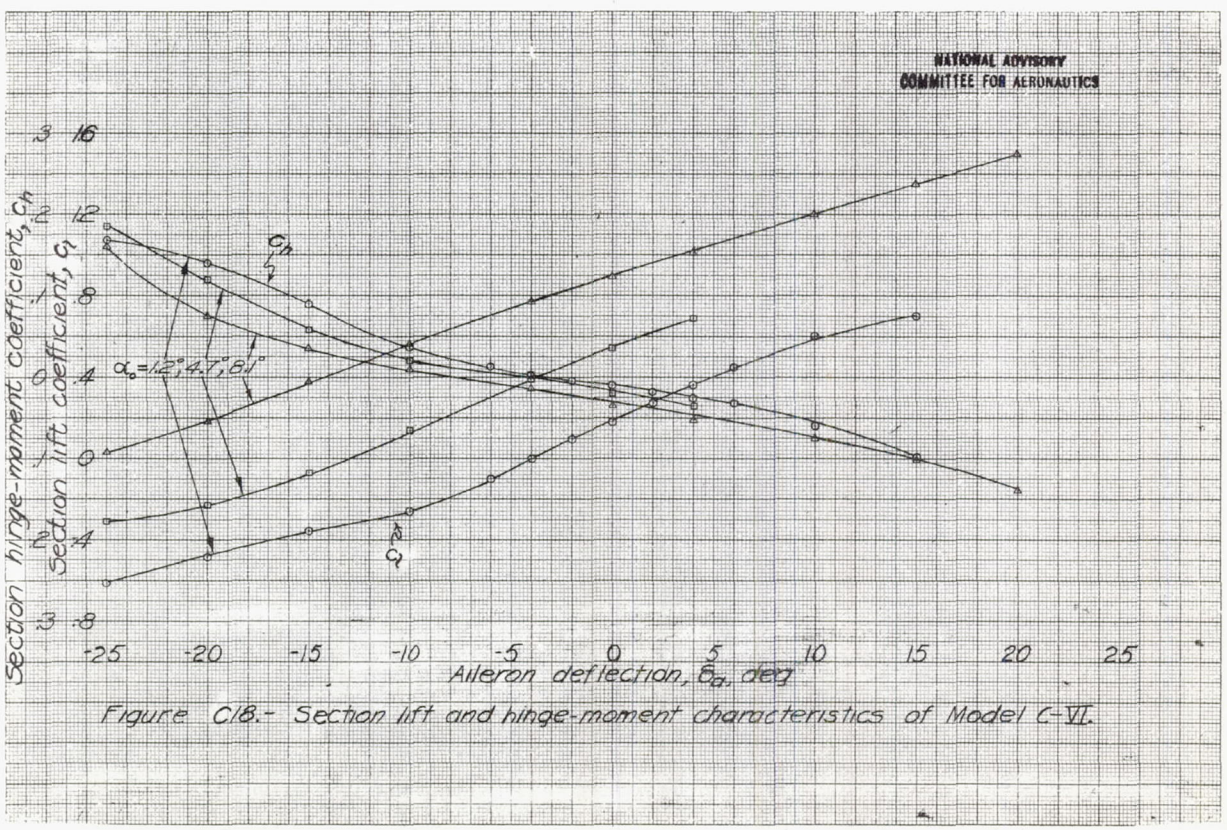

Figure C18.- Section lift and hinge-moment characteristics of Model C-VII.

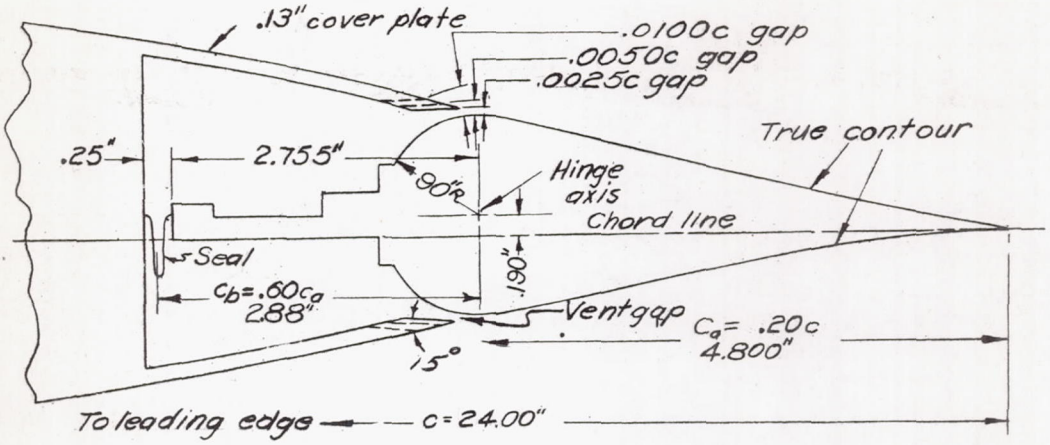

Figure C19.- Aileron section of the NACA 66(215)-216, a = 1.0 airfoil tested with a 0.20c sealed internally balanced aileron of true contour. Model C-VII; c_b=0.60c_a; NACA stability tunnel.

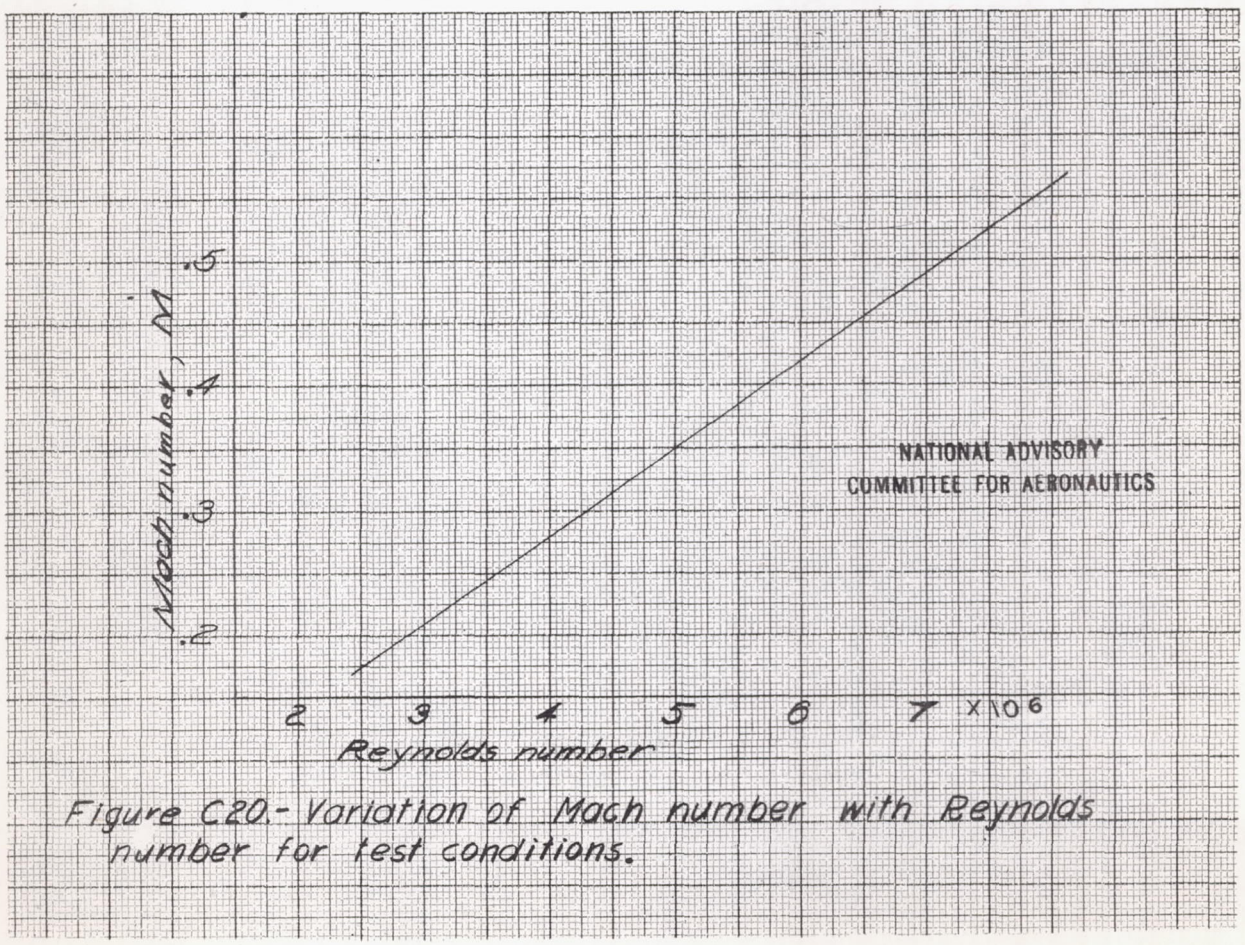

Figure C20.- Variation of Mach number with Reynolds number for test conditions.

Model C-VII

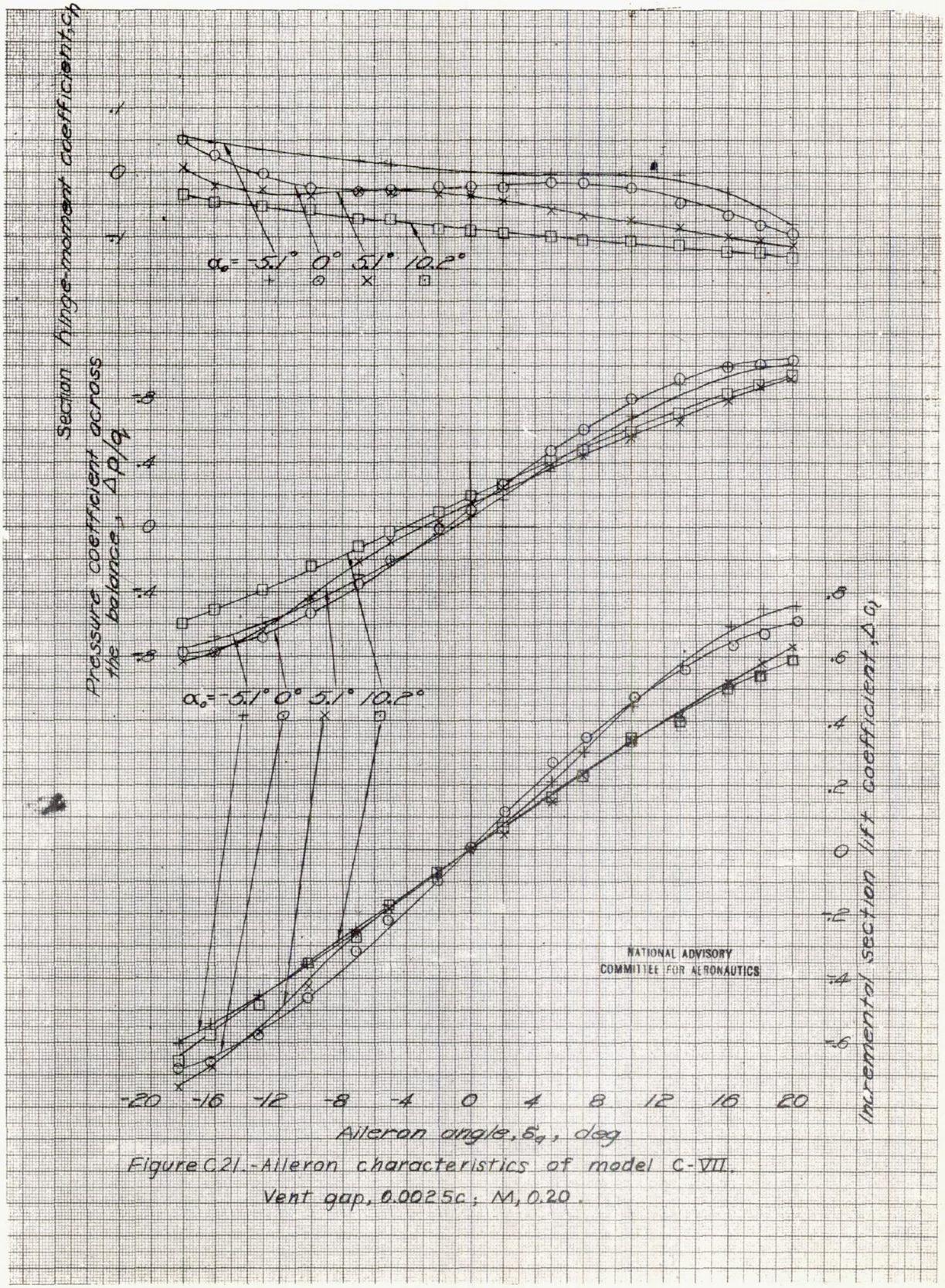

Figure C.21.-Aileron characteristics of model C-VII. Vent gap, 0.0025c; M, 0.20.

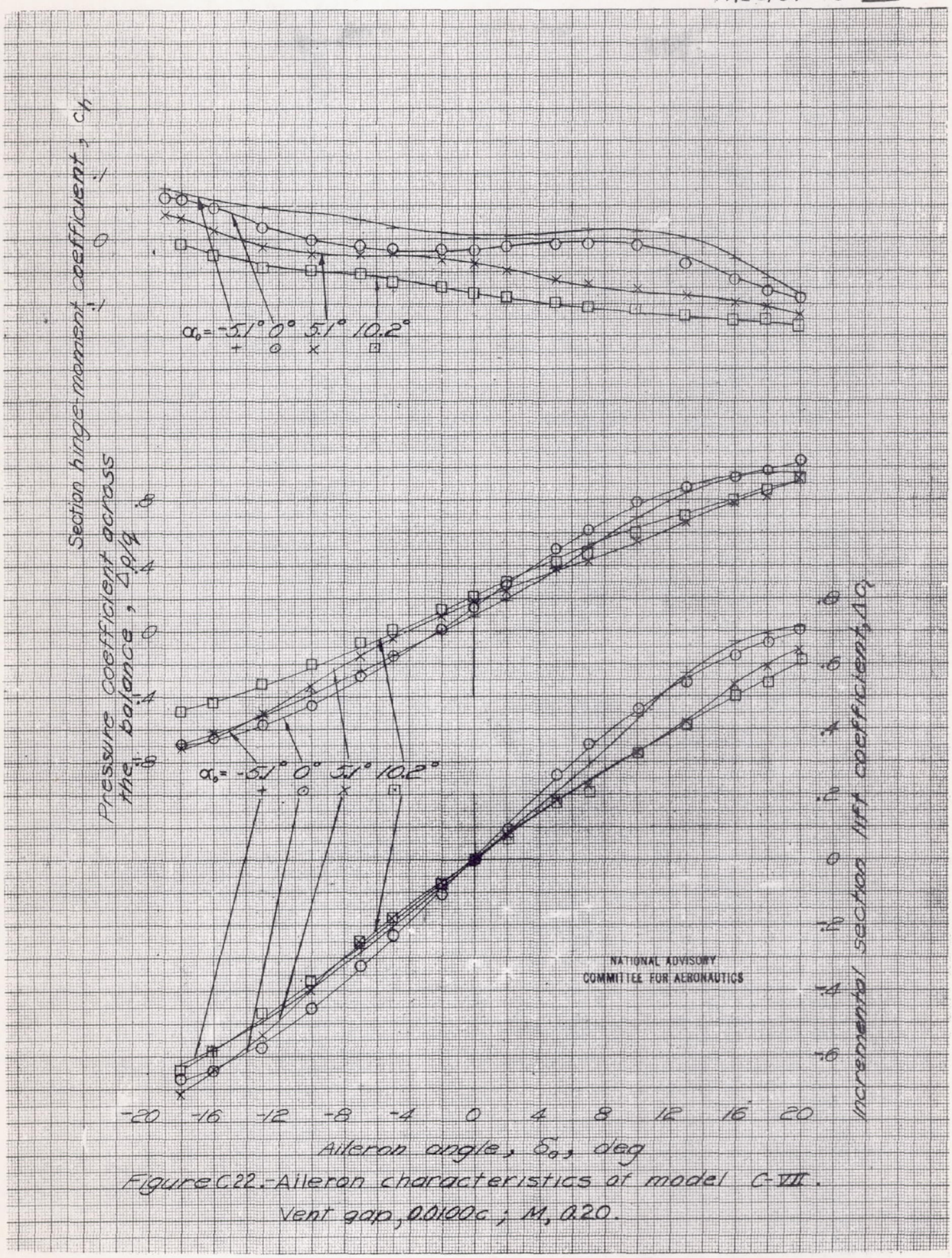

Figure C22.- Aileron characteristics of model C-VII.
Vent gap, 0.0100c; M, 0.20.

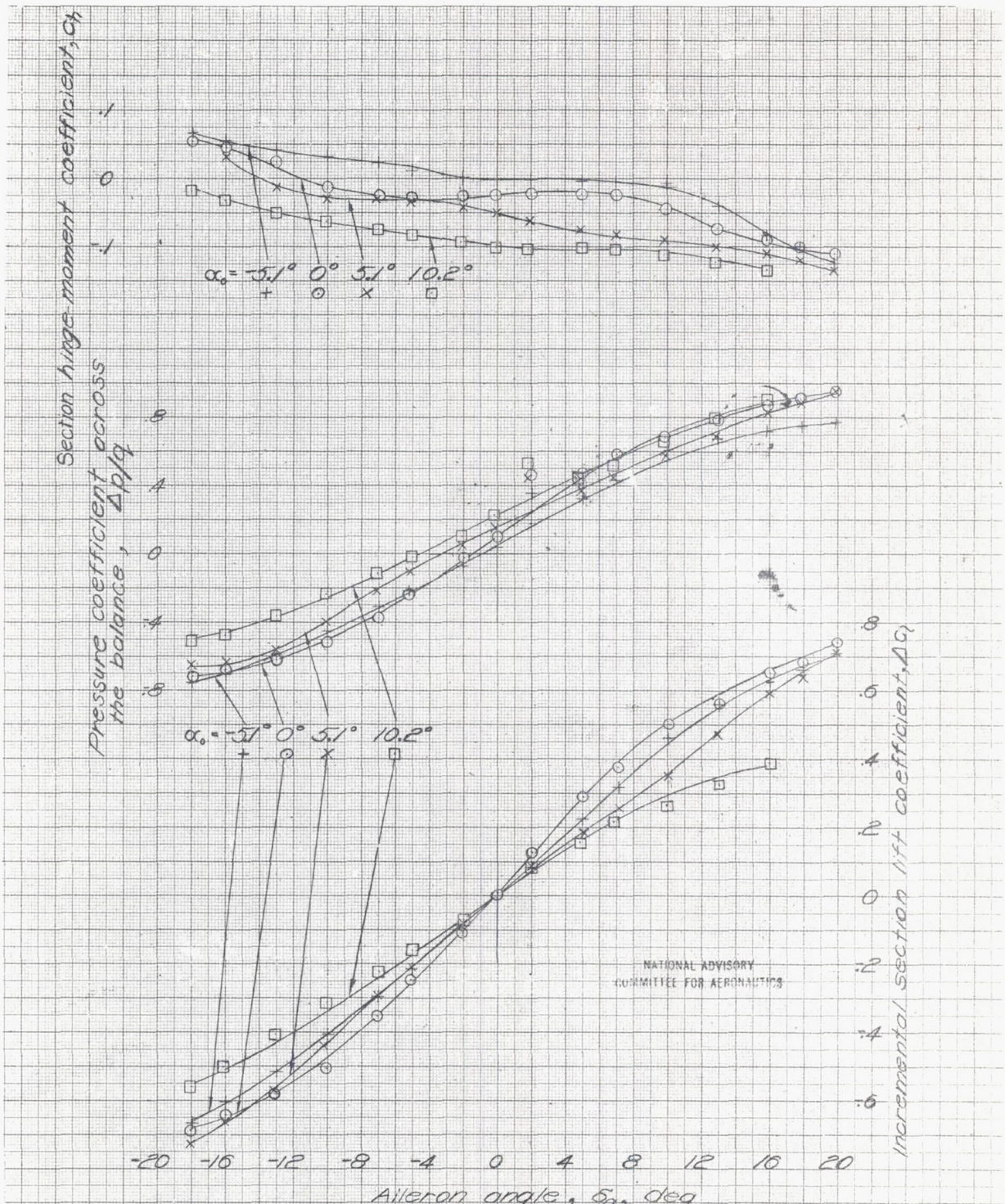

Figure C23.-Aileron characteristics of model C-VII. Vent gap, 0.0025c ; M, 0.42.

Model C-VII

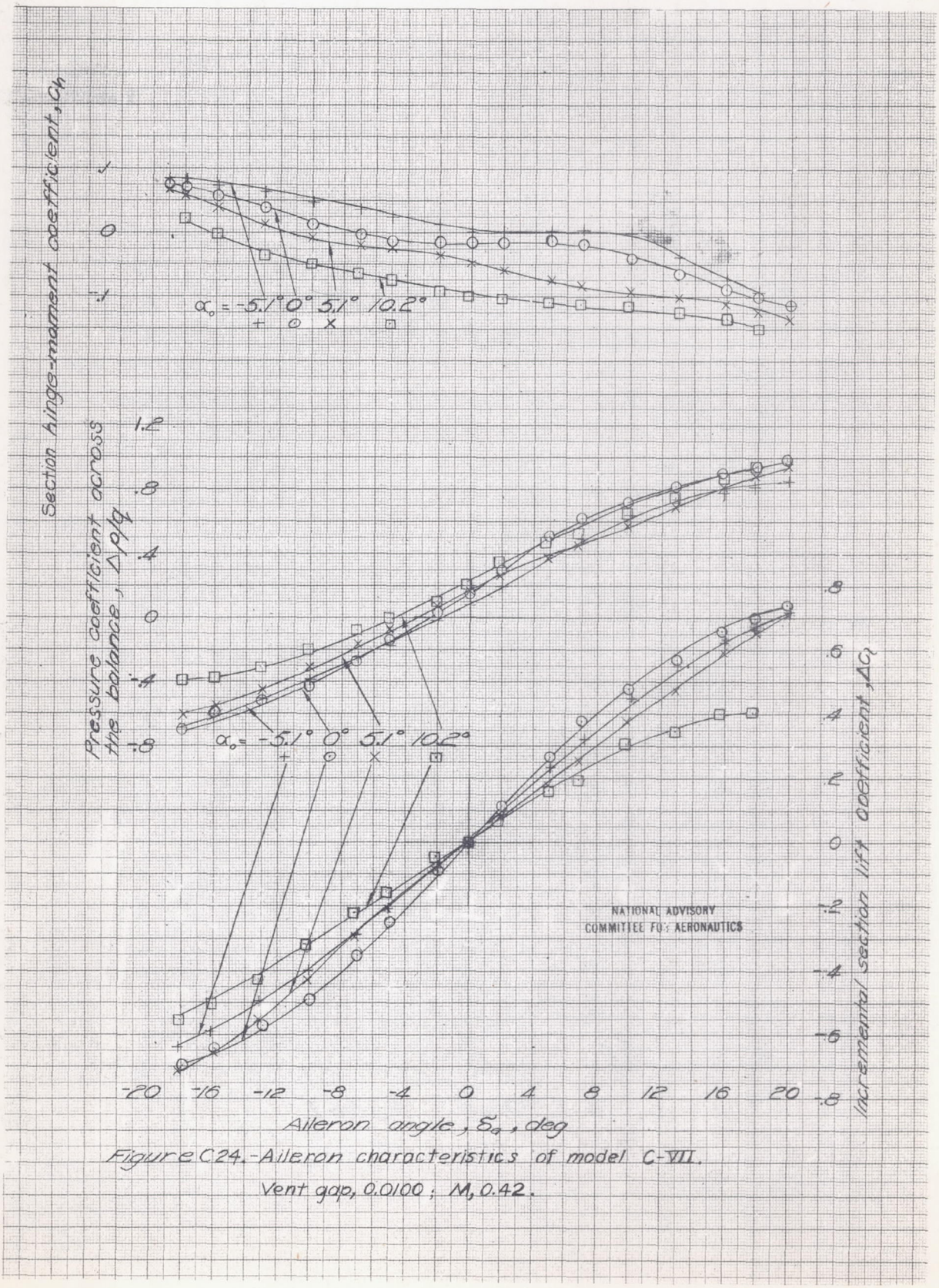

Figure C24.-Aileron characteristics of model C-VII.
Vent gap, 0.0100; M, 0.42.

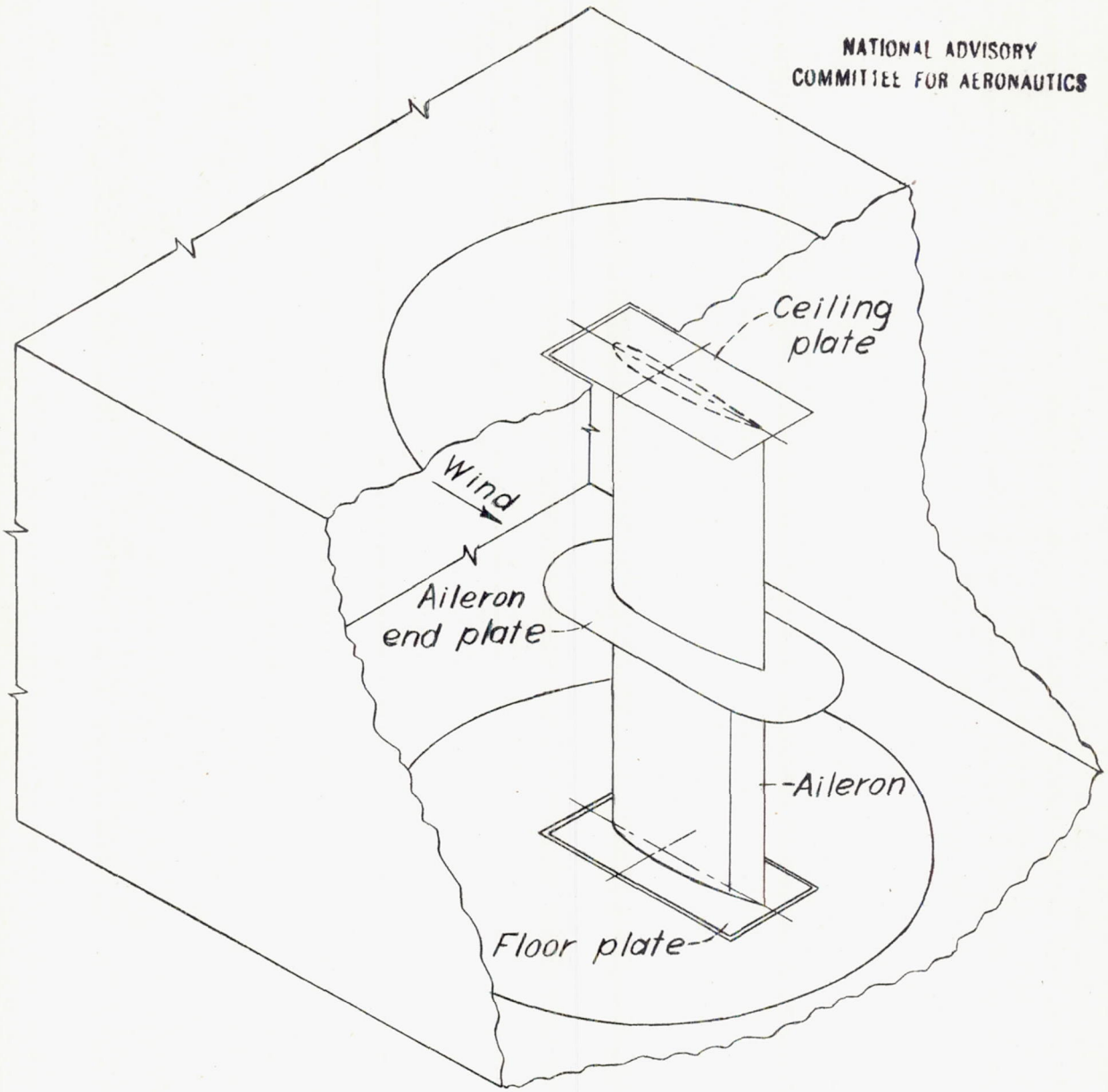

Figure C25.-Test setup for intermediate section of a wing between root NACA 23017 and tip NACA 4409 R. Model C-VIII; AAL 7- by 10-foot tunnel.

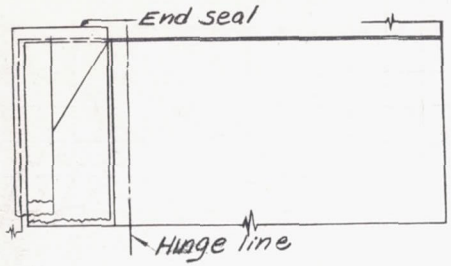

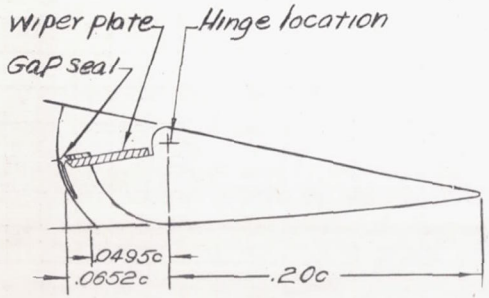

Figure C26.-The aileron and balance with end and gap seals.

NATIONAL ADVISORY
COMMITTEE FOR AERONAUTICS

NATIONAL ADVISORY
COMMITTEE FOR AERONAUTICS

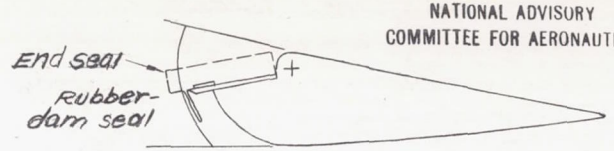

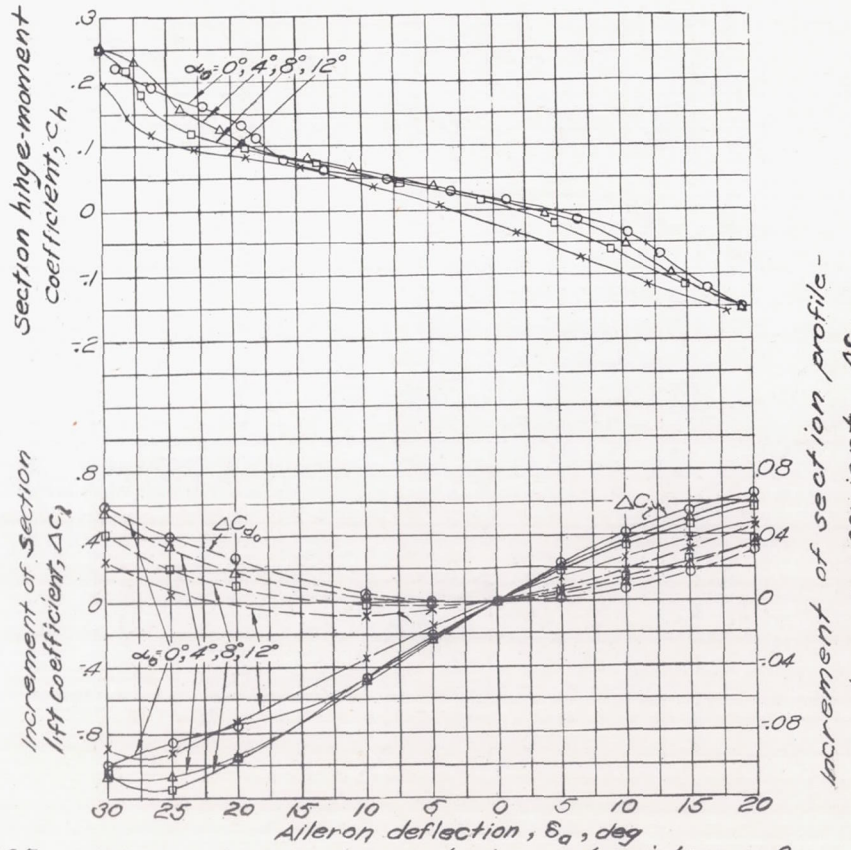

Figure C27.-Lift and hinge-moment characteristics of aileron with gap and ends sealed.

Model C-VIII

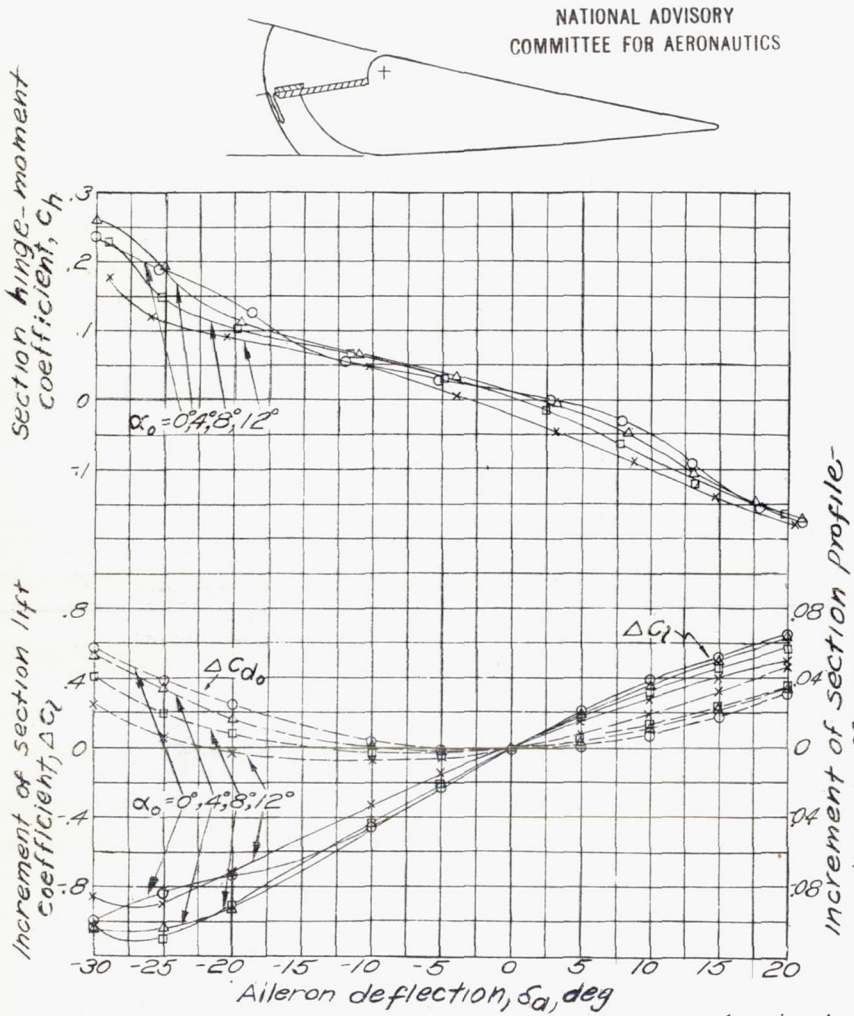

Figure C28.- Lift and hinge-moment characteristics of aileron with ends unsealed.

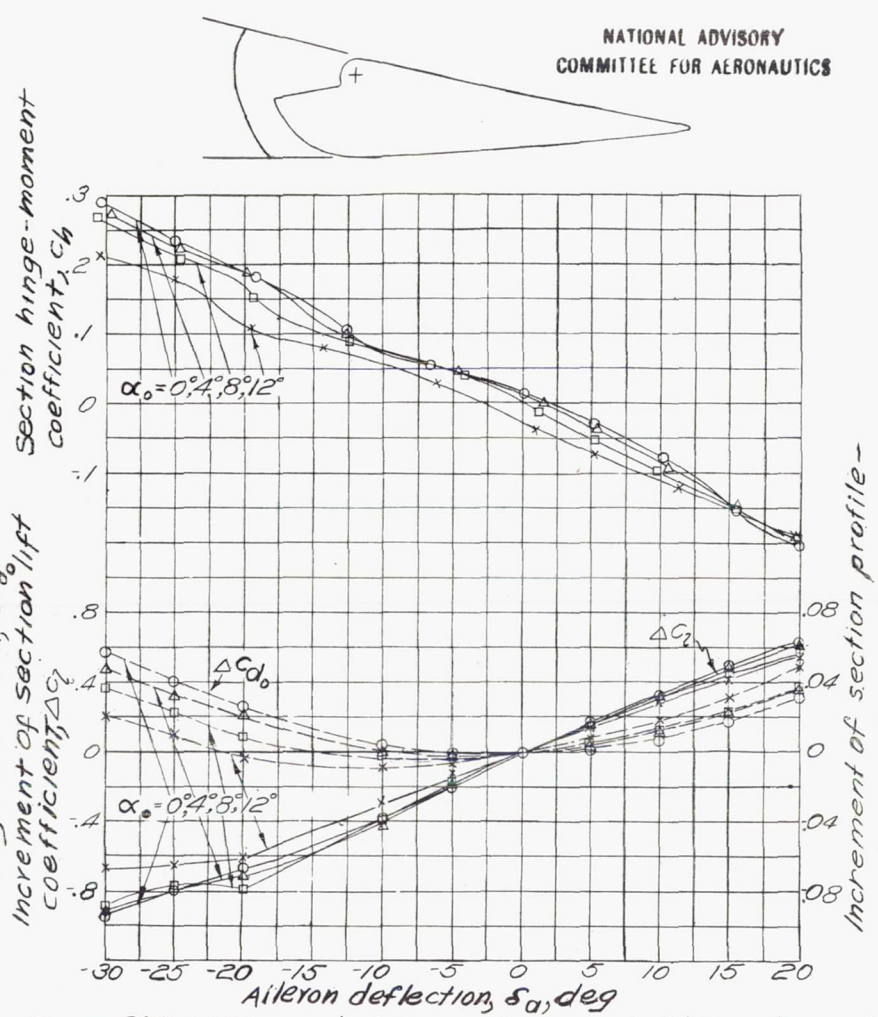

Figure C29.- Lift and hinge-moment characteristics of aileron with seals and overhang plate removed.

Model C-III

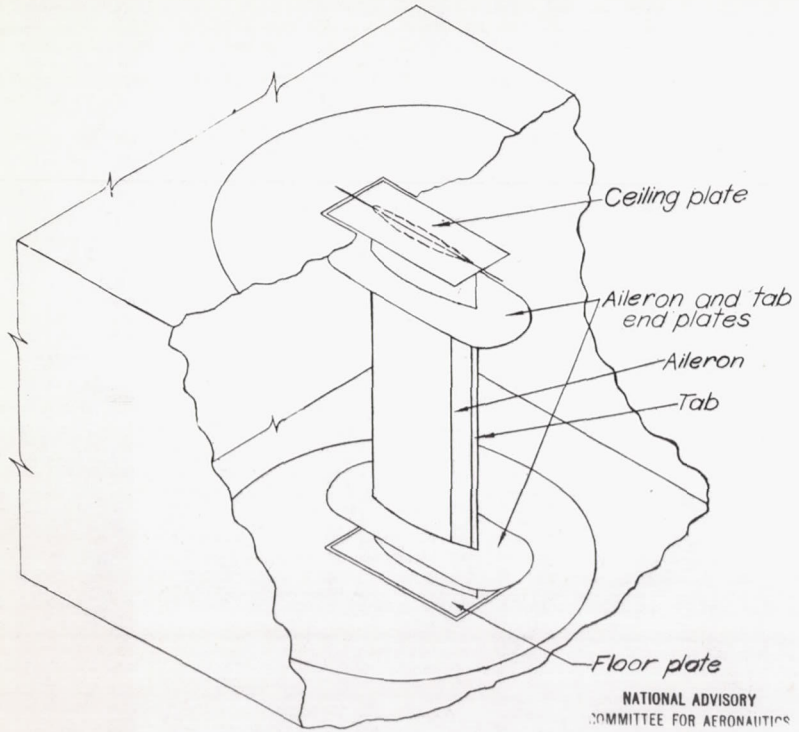

Figure C30.-Test installation for NACA 66(215)-216, a=0.6 airfoil with aileron. Model C-IX; AAL 7-by 10-foot tunnel.

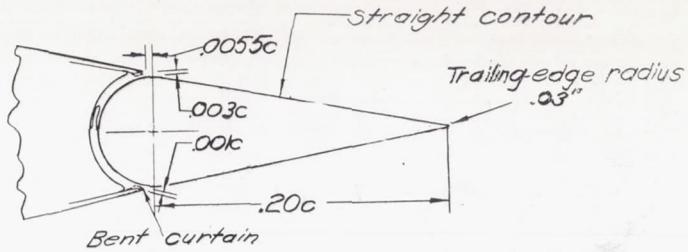

(a) Plain aileron with plain and bent curtains.

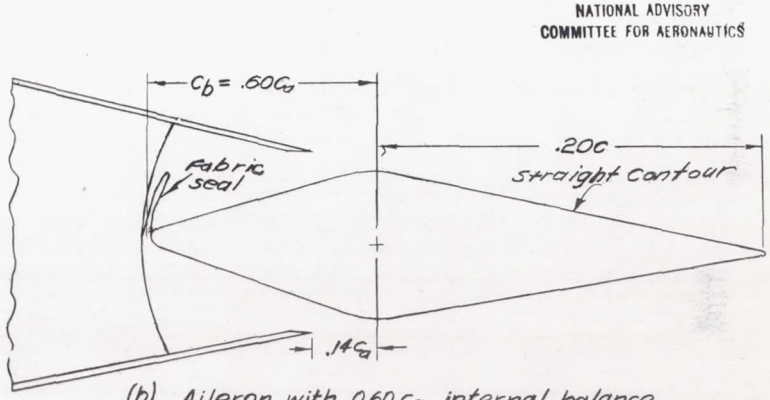

(b) Aileron with 0.60 c_a internal balance.

Figure C31.-Typical sections of ailerons tested on model C-IX.

Model C-IX

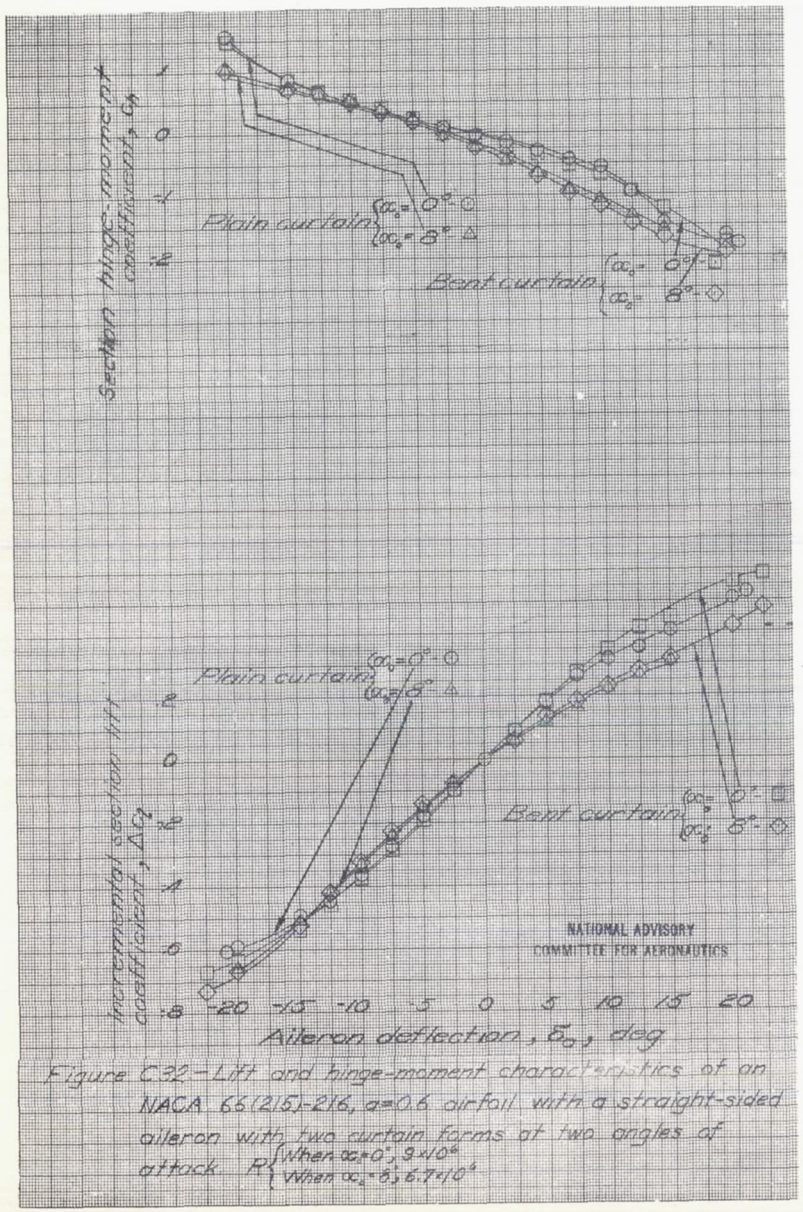

Figure C32.—Lift and hinge-moment characteristics of an NACA 65(215)-216, a=0.6 airfoil with a straight-sided aileron with two curtain forms at two angles of attack. R {When α_2=0°, 9×10⁶ / When α_2=8°, 6.7×10⁶}

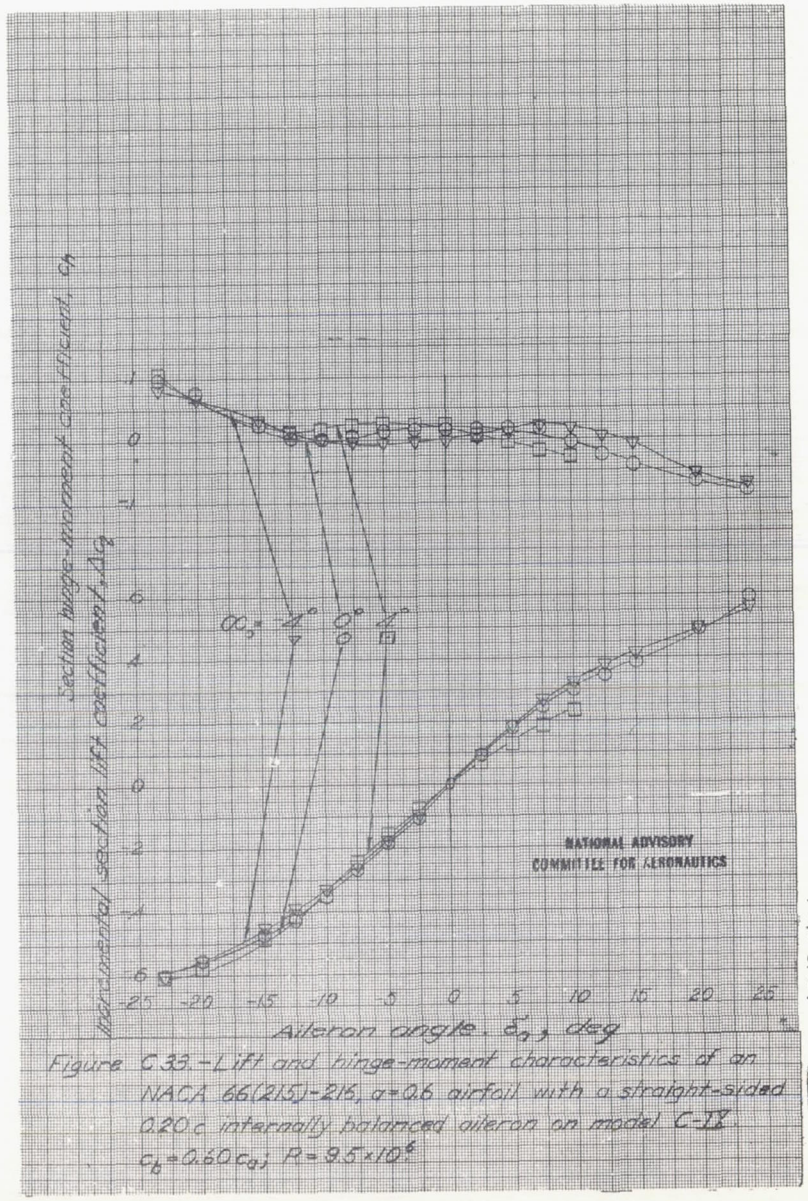

Figure C33.—Lift and hinge-moment characteristics of an NACA 66(215)-216, a=0.6 airfoil with a straight-sided 0.20c internally balanced aileron on model C-IX. c_b=0.60 c_{a_2}; R=9.5×10⁶.

Model C-IX

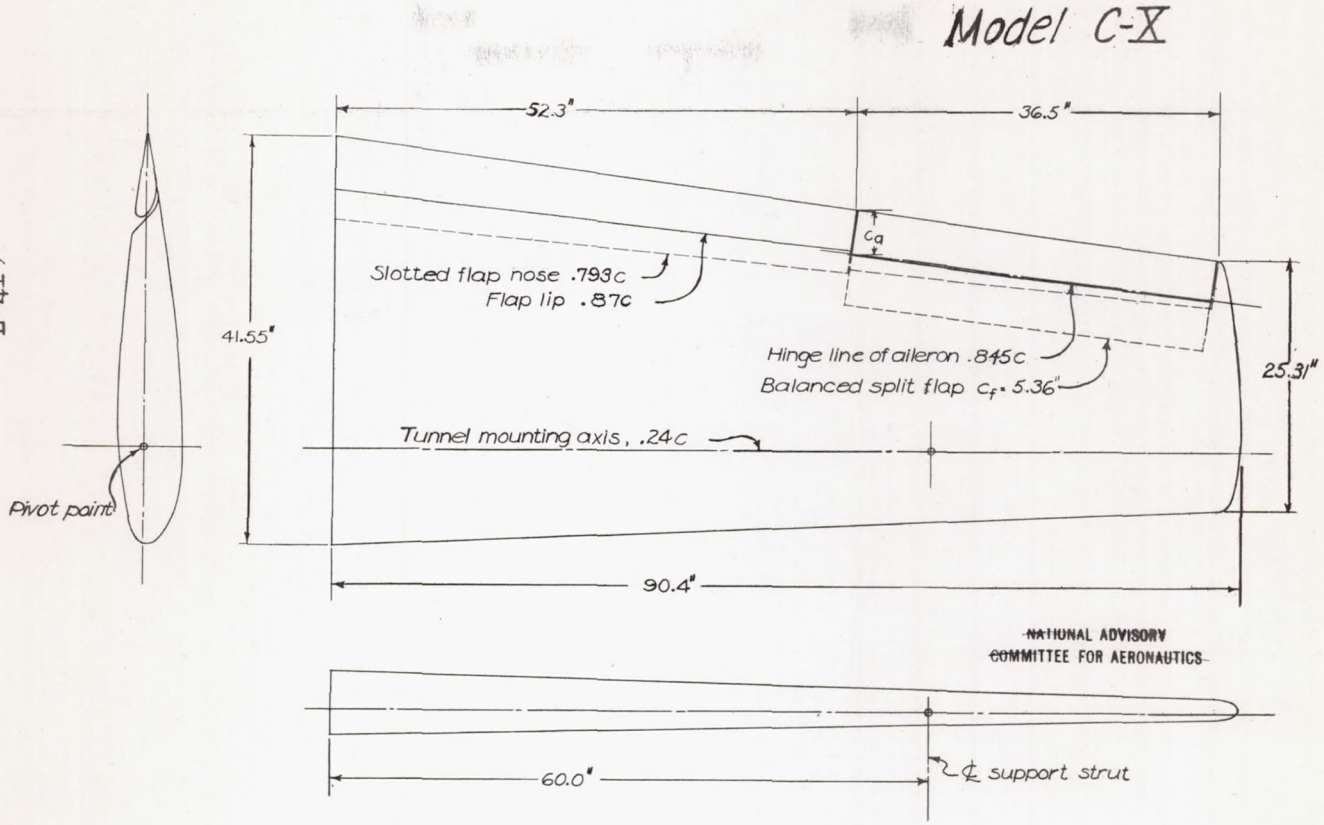

Figure C34.-Semispan wing model C-X. Tested in LMAL 7 by 10-foot tunnel.

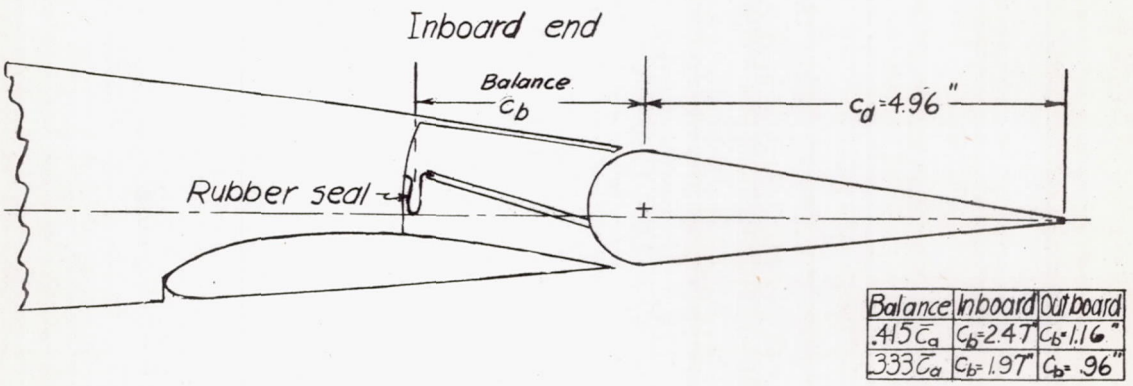

Balance	Inboard	Outboard
.415 $\bar{c}_a$	c_b = 2.47"	c_b = 1.16"
.333 $\bar{c}_a$	c_b = 1.97"	c_b = .96"

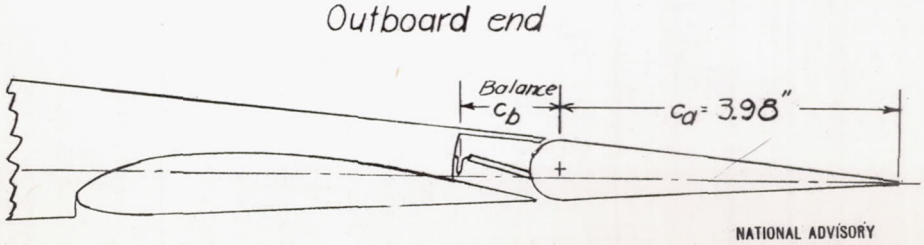

Figure C35.-Profile of the balance arrangement of model C-X.

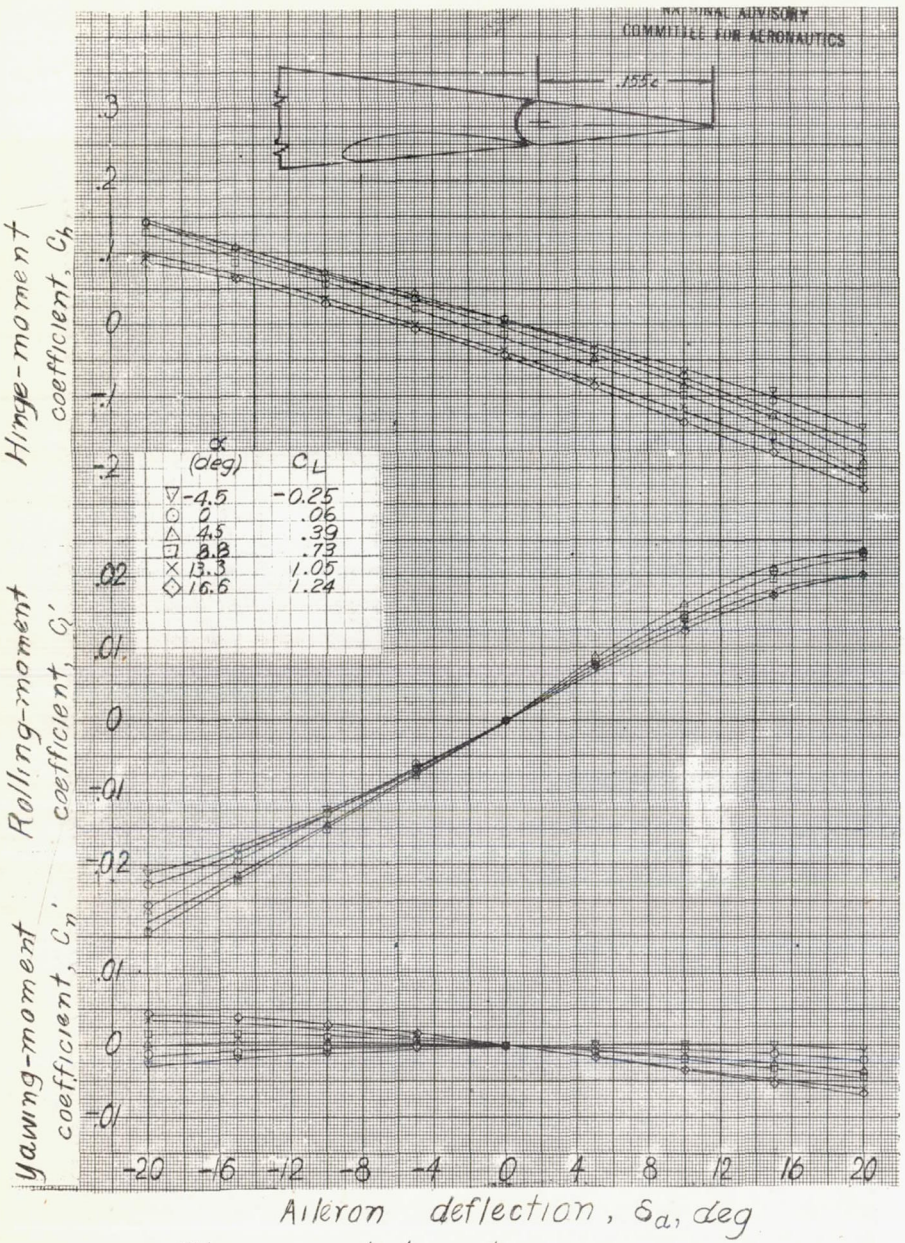

(a) Plain sealed aileron.

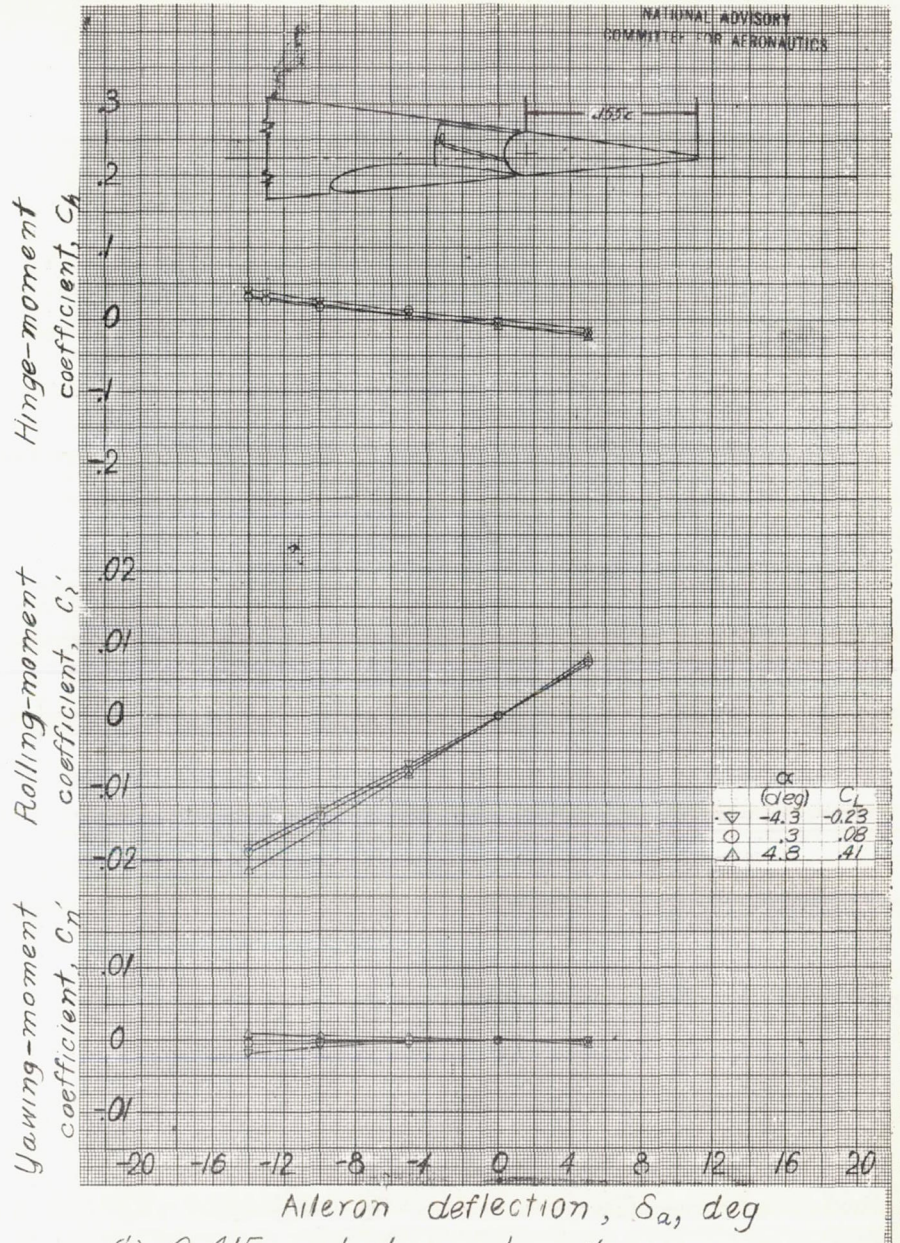

(b) 0.415c_a balanced aileron.

Figure C36.-Aileron characteristics of model C-X with flaps retracted

Model C-X

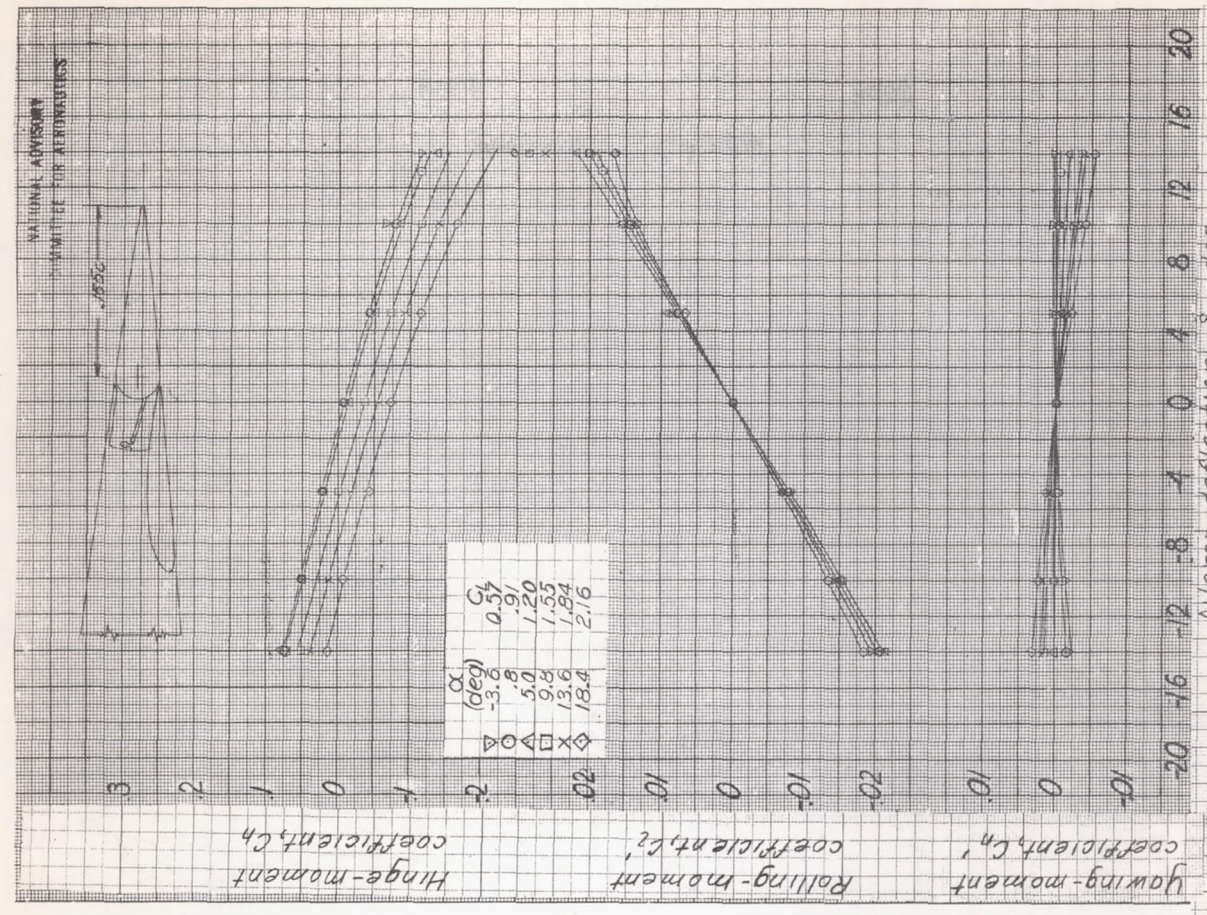

(b) Inboard flap, 50°; outboard flap, retracted.

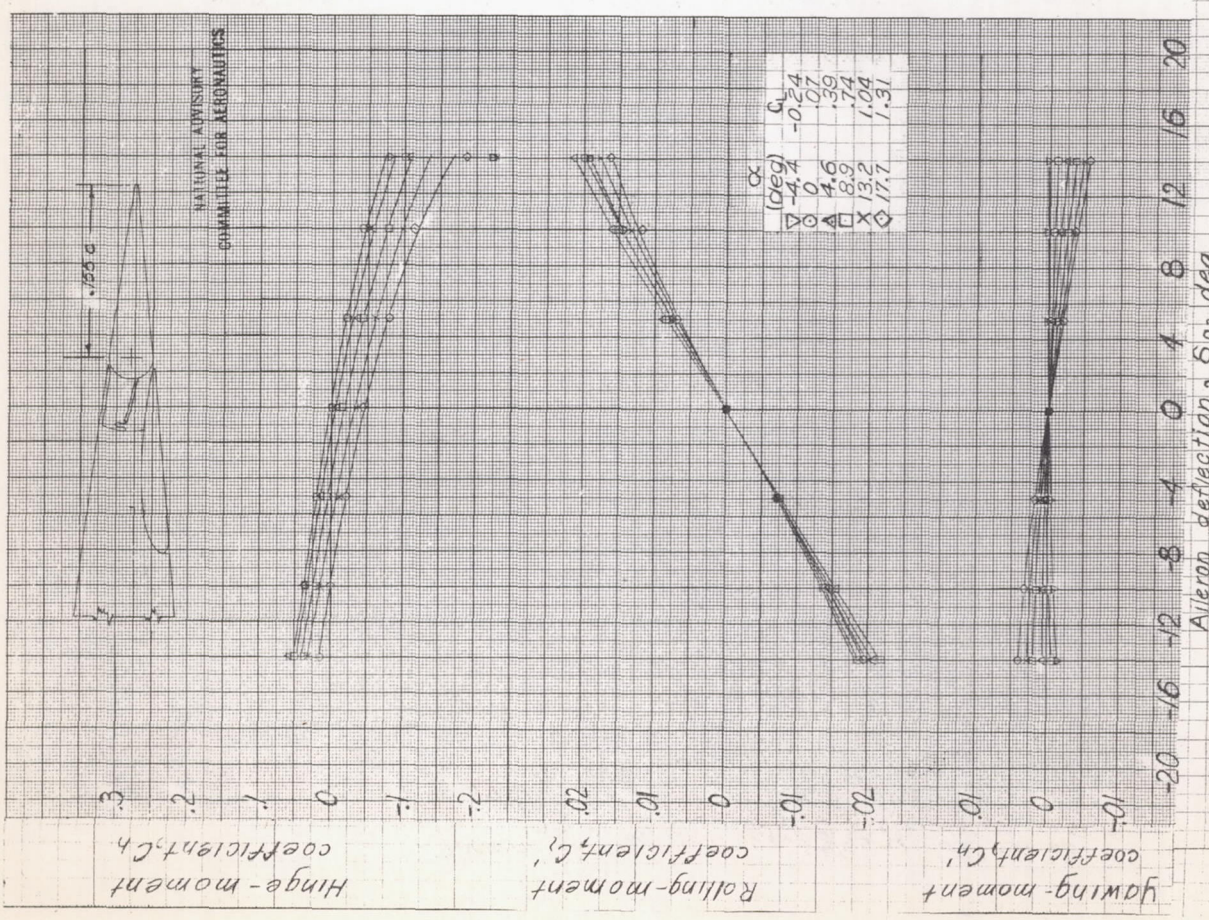

(a) Flaps retracted.

Figure C 37.- Aileron characteristics of model C-X with 0.333 c_a balanced aileron.

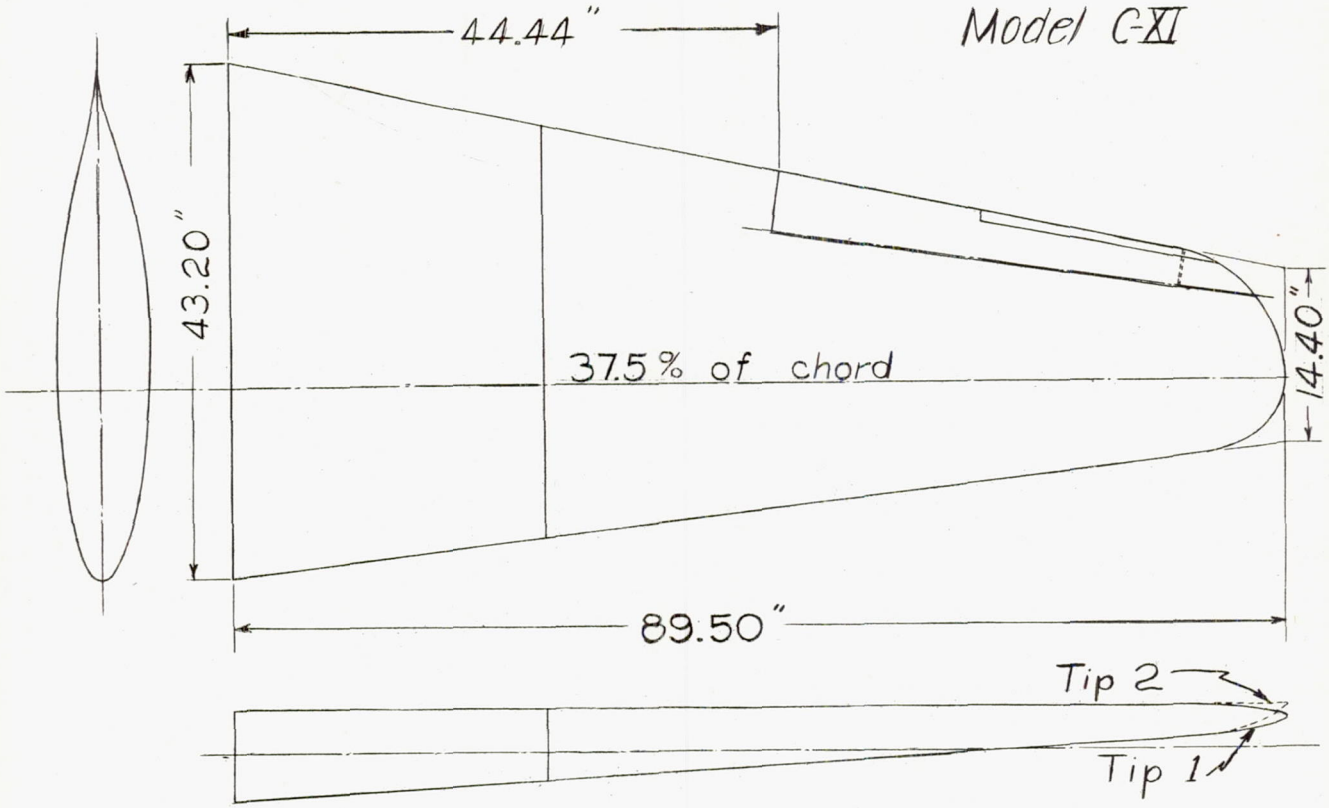

Figure C38. - Semispan wing model C-XI.

NATIONAL ADVISORY COMMITTEE FOR AERONAUTICS

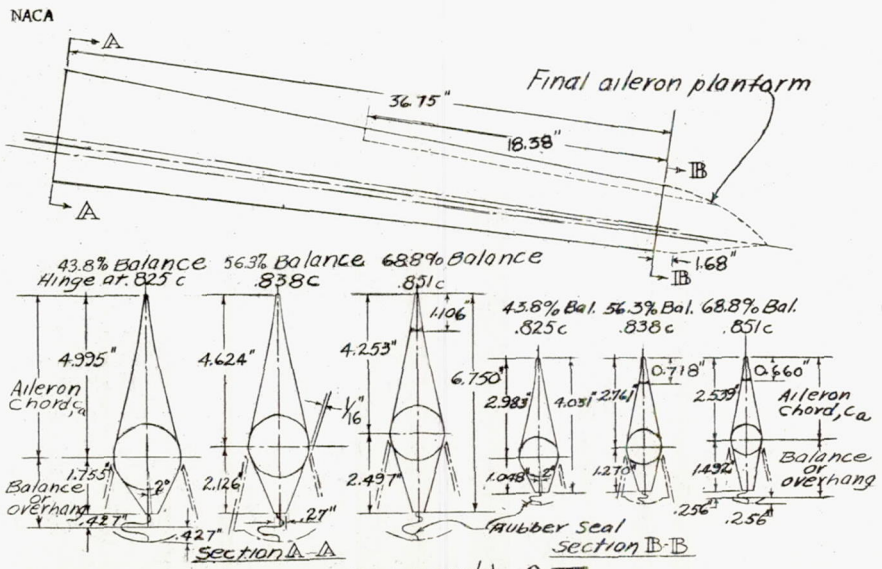

Figure C39.- Ailerons of semispan wing model C-XI as tested in the LMAL 7.6Y 10-foot tunnel.

Model C-XI

L-419

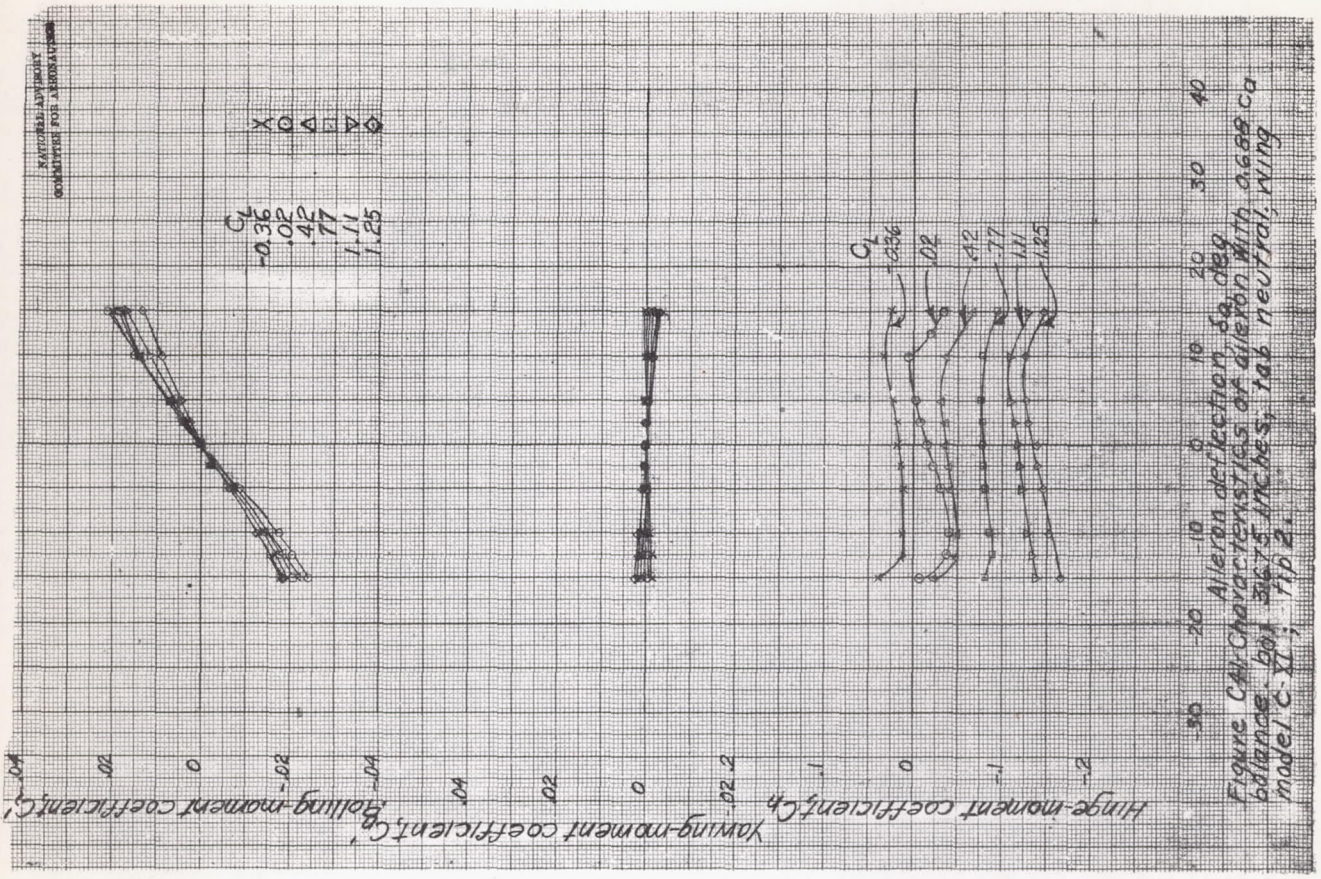

Figure C40.- Characteristics of aileron with C_a 0.688 balance; δ_a, 36.75 inches; 1.46 neutral; wing model C-XI; Fig 2.

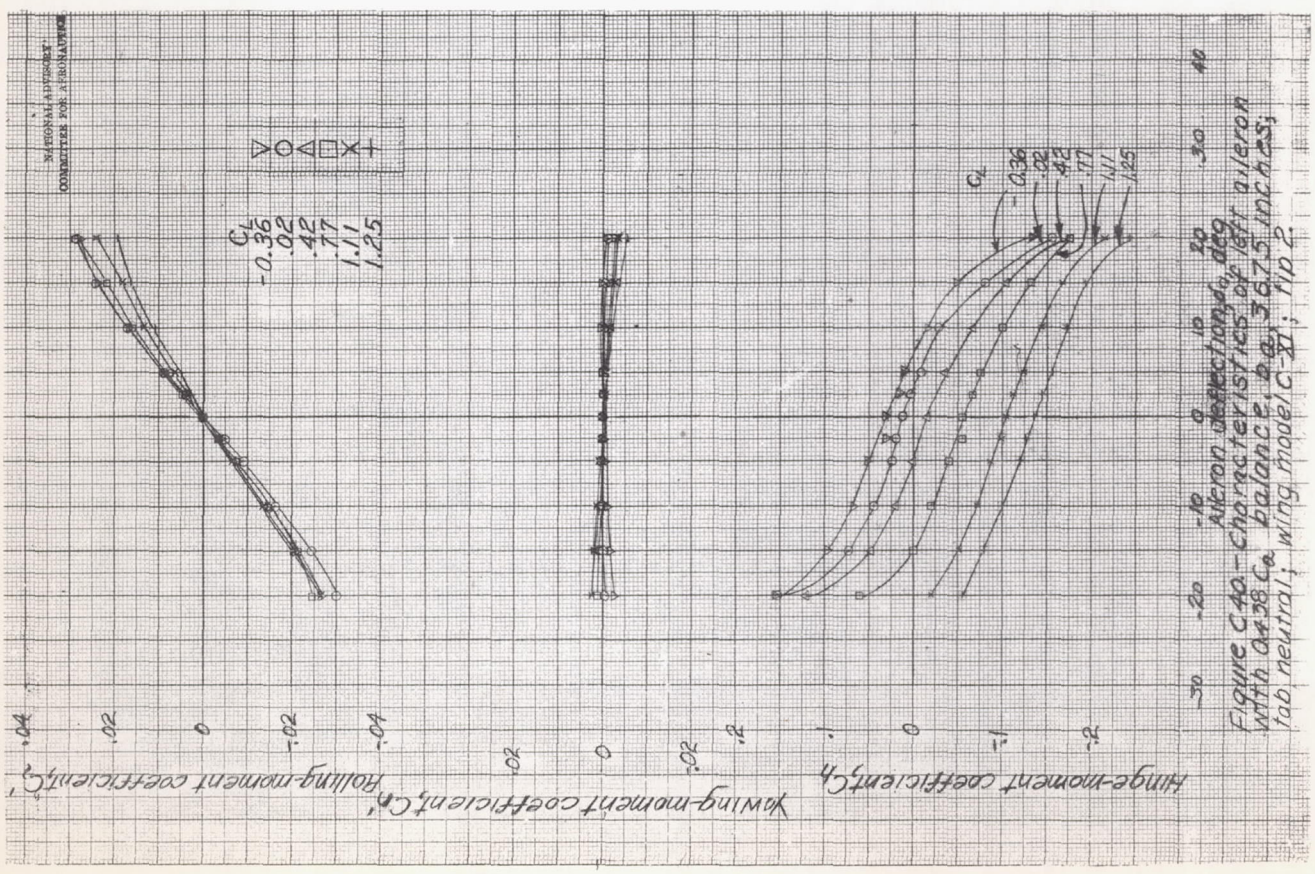

Figure C40 - Characteristics of left aileron with C_a 0.38 balance; δ_a, 36.75 inches; tab neutral; wing model C-XI; Fig 2.

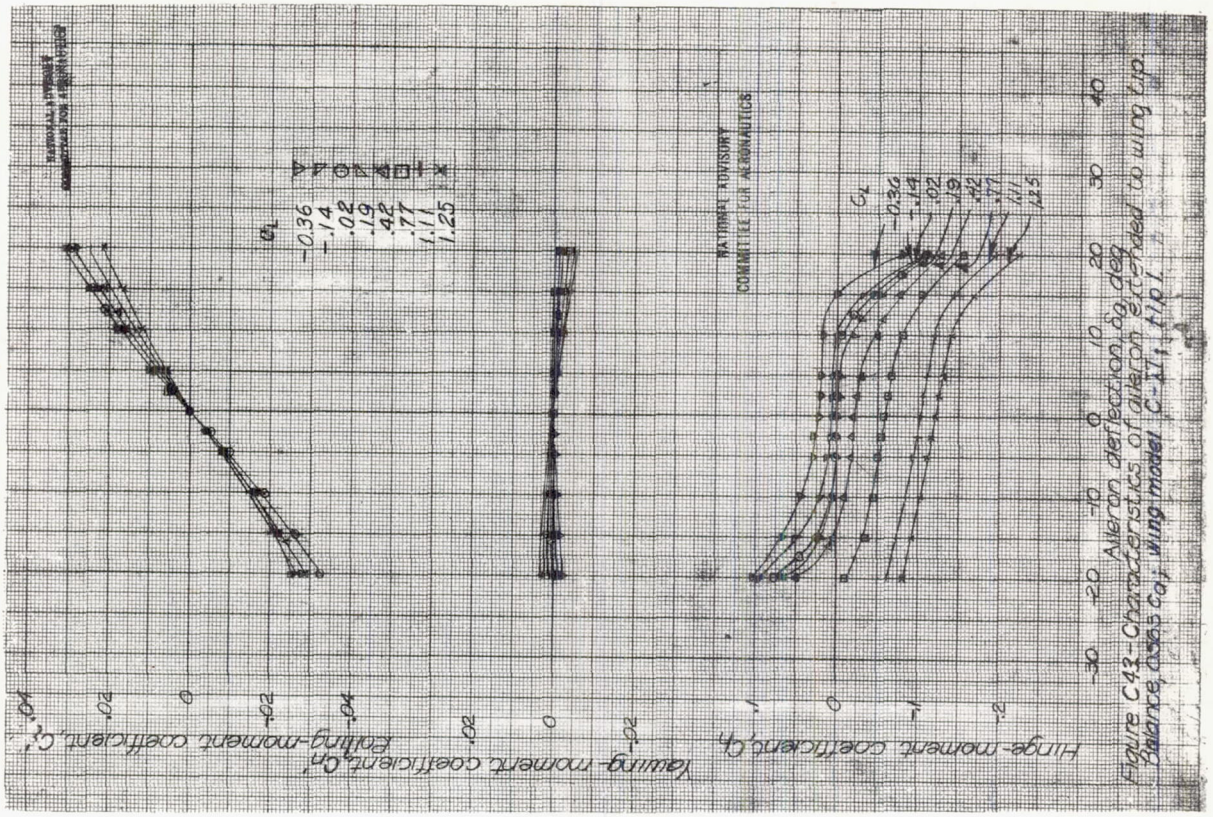

Figure C43 - Characteristics of aileron extended to wing tip. Balance, 0.365 c_a; wing model C-XI, tip 1.

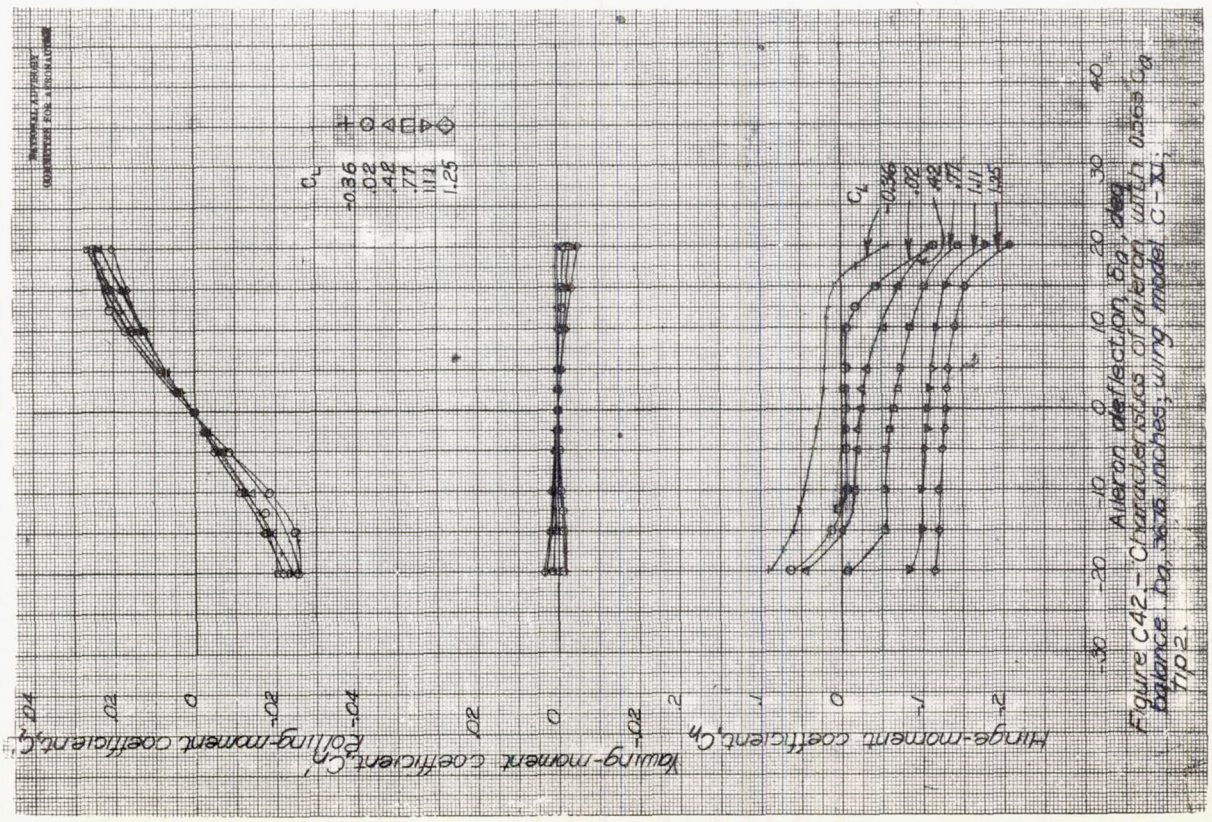

Figure C42 - Characteristics of aileron with 0.365 c_a balance. b_a, 36.6 inches; wing model C-XI, tip 2.

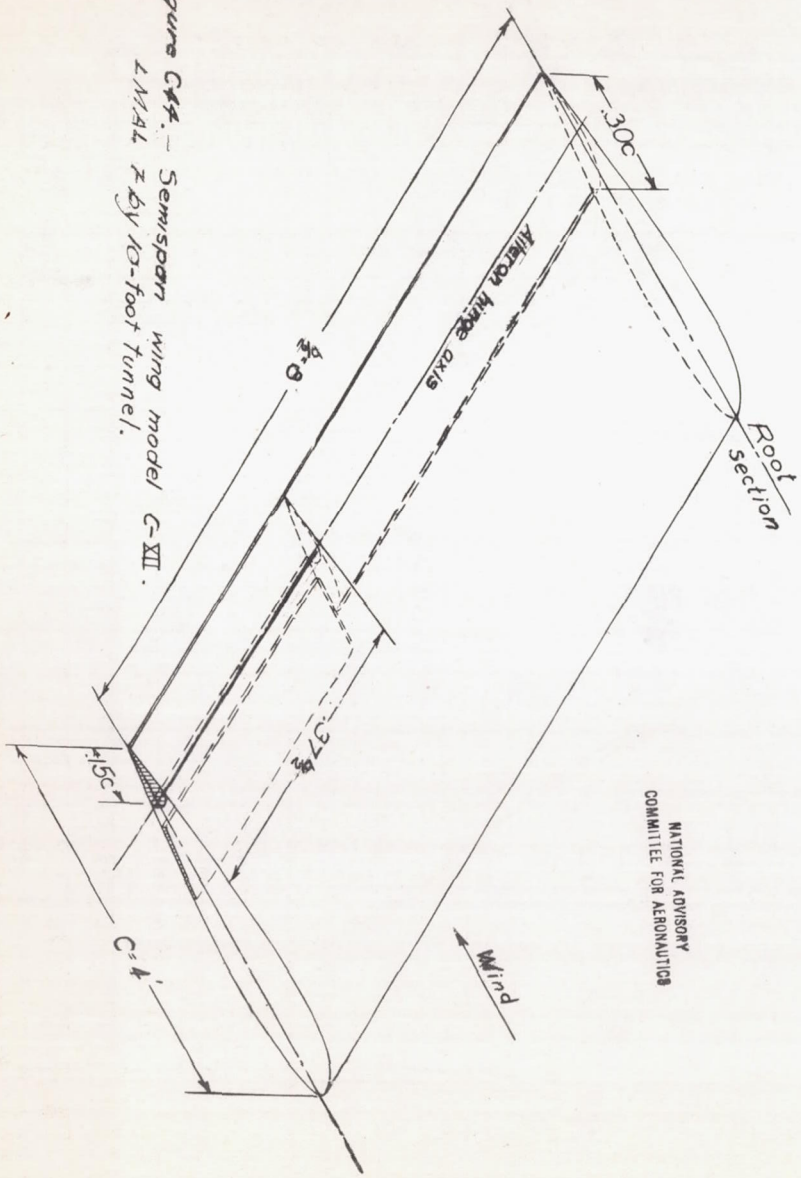

Figure C44.- Semispan wing model C-XII. Aerial view in 10-foot tunnel.

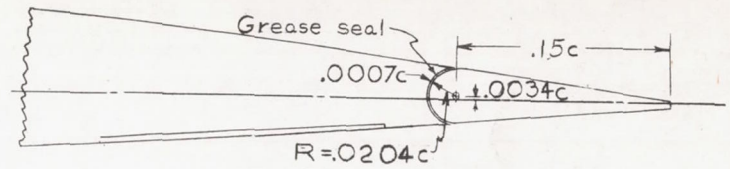

(a) 0.15c by 0.37$b/2$ outboard plain sealed aileron.

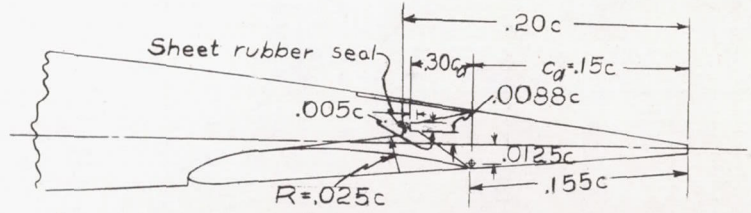

(b) 0.15c by 0.37$b/2$ outboard sealed aileron with 0.30c_a overhang.

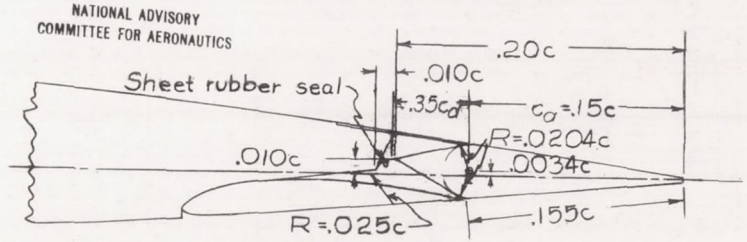

(c) 0.15c by 0.37$b/2$ outboard sealed aileron with 0.35c_a overhang.

Figure C45.-Profile of ailerons of semispan wing model C-XII.

Model C-XII

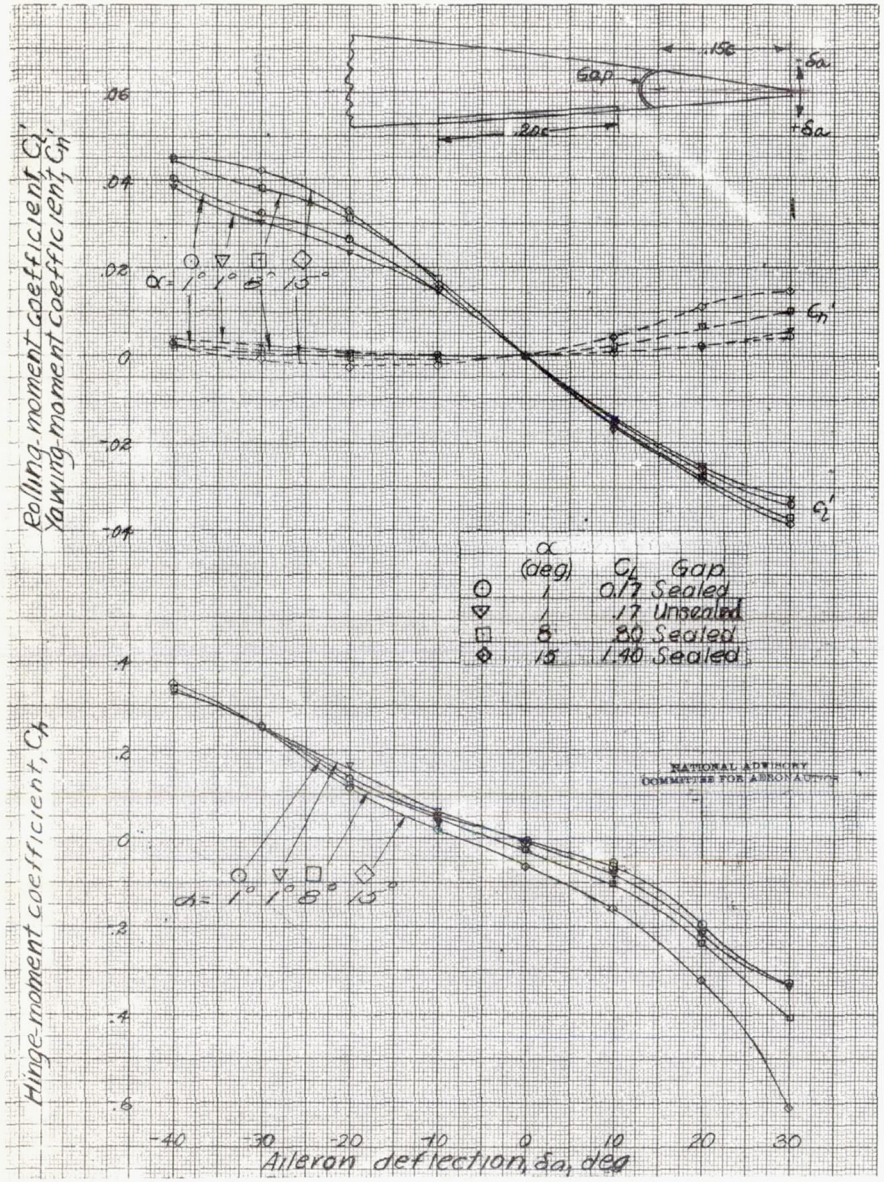

(a) Plain unbalanced aileron.

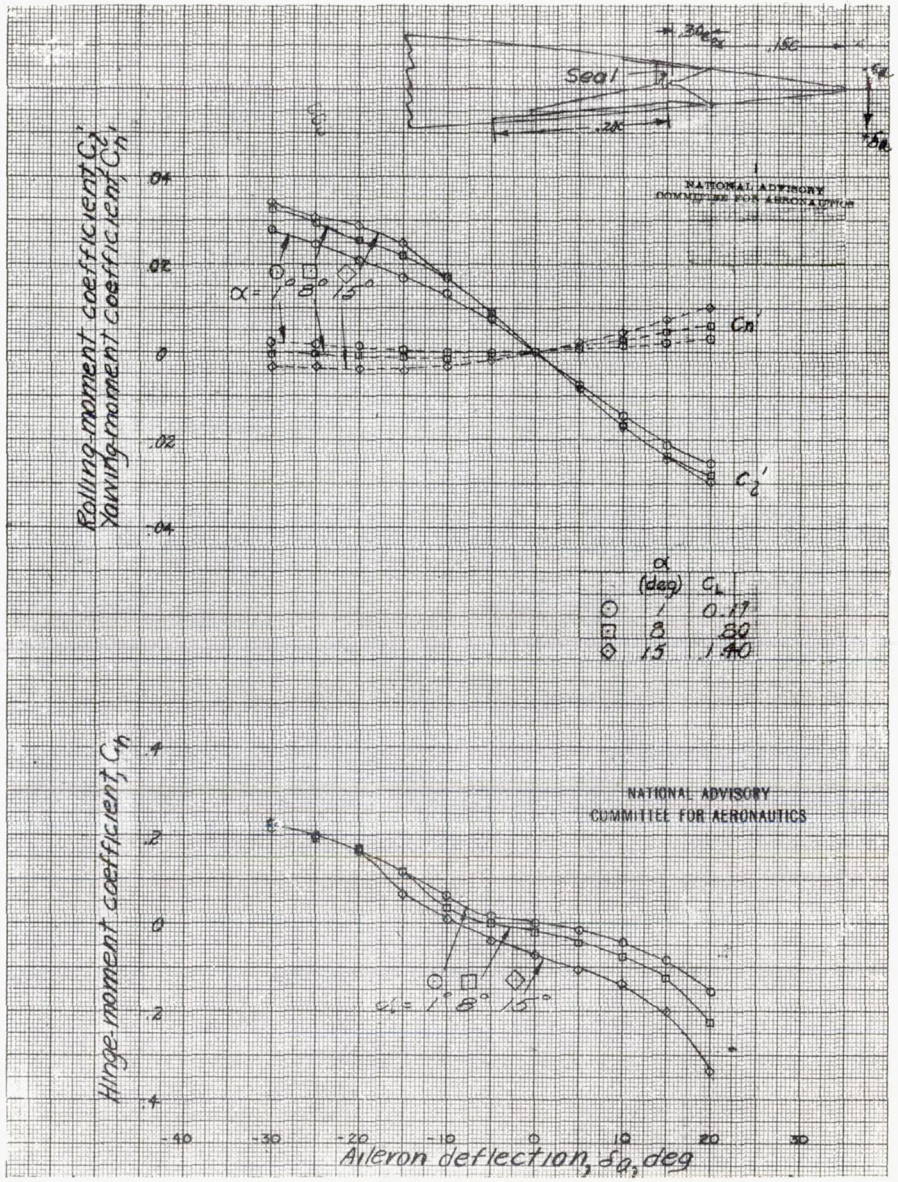

(b) Aileron with 0.30 c_a overhang sealed.

Figure C46. - Aileron characteristics of model C-XII with flaps retracted.

Model C-XII

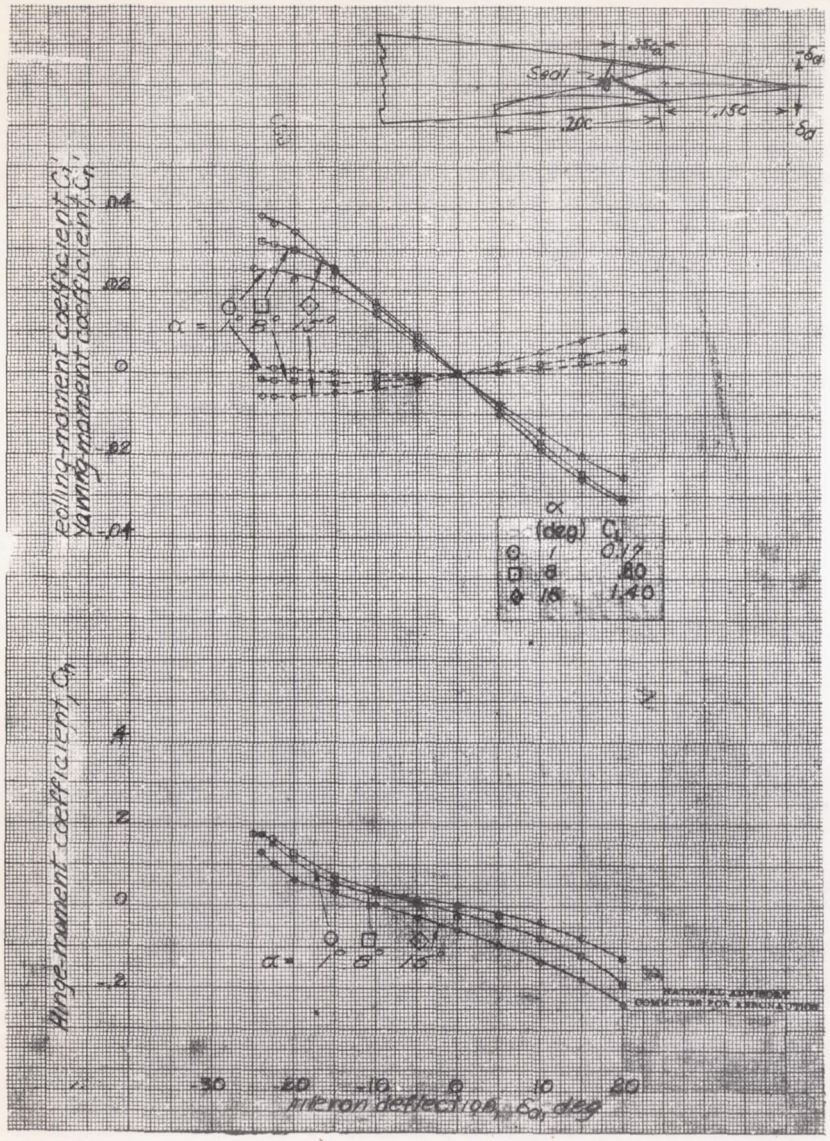

(a) Flaps retracted.

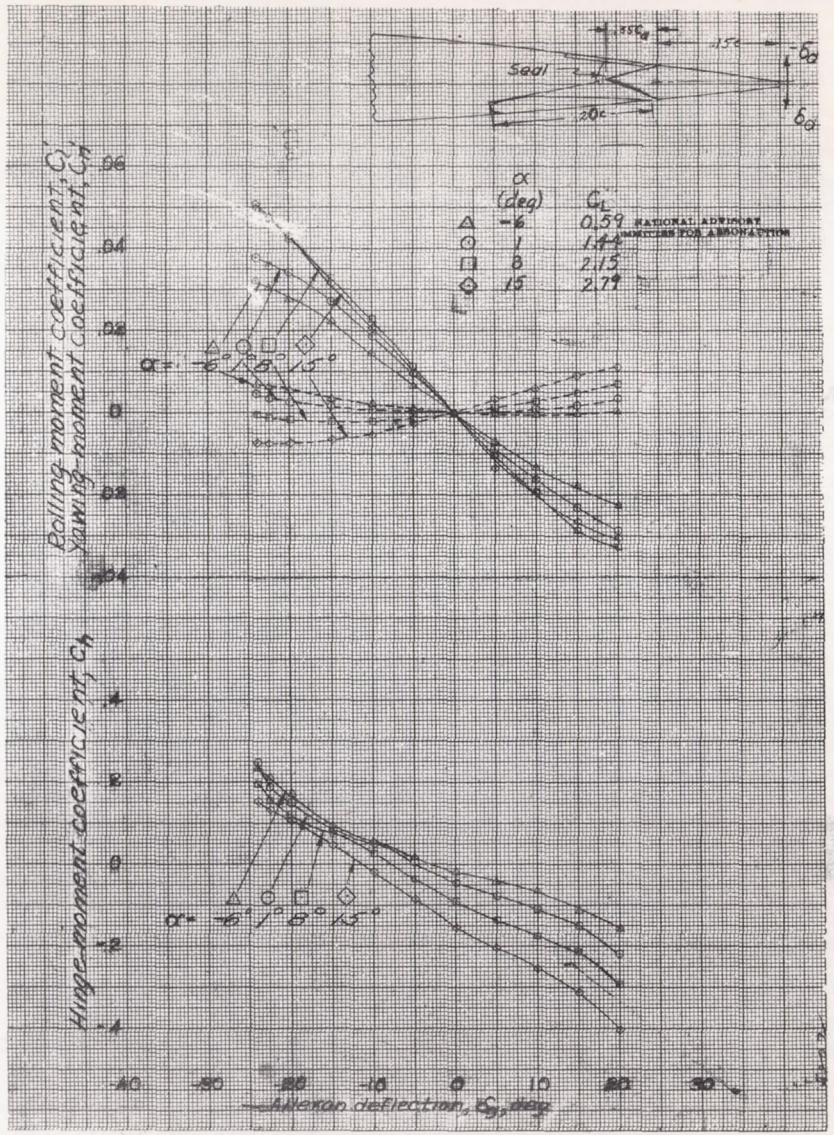

(b) Inboard flap, 40°; outboard flap retracted.

Figure C-47.- Aileron characteristics of model C-XII with 0.35 c_a overhang.

Model C-XII

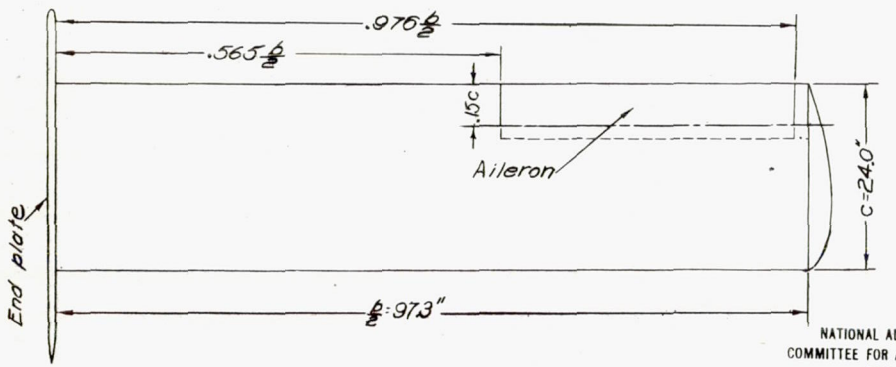

Figure C48:Plan form of semispan wing model C-XIII

Airfoil - Davis (16%-thick). Tested in AAL 7-by 10-foot tunnel.

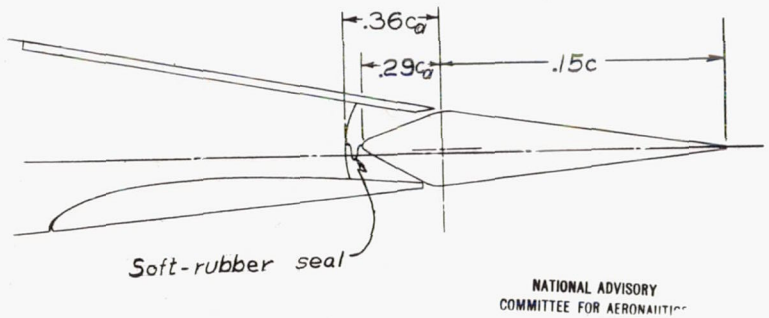

Figure C49.- Balance arrangement of model C-XIII

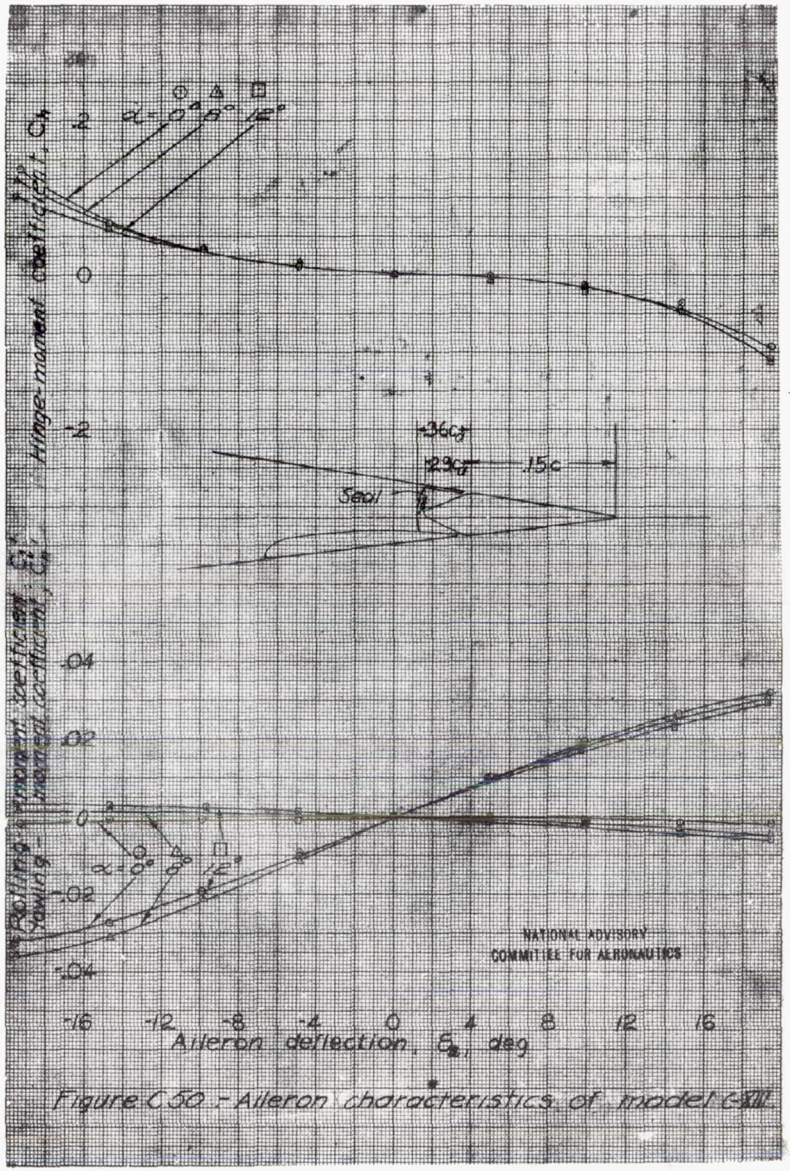

Figure C50.- Aileron characteristics of model C-XIII

Model C-XIII

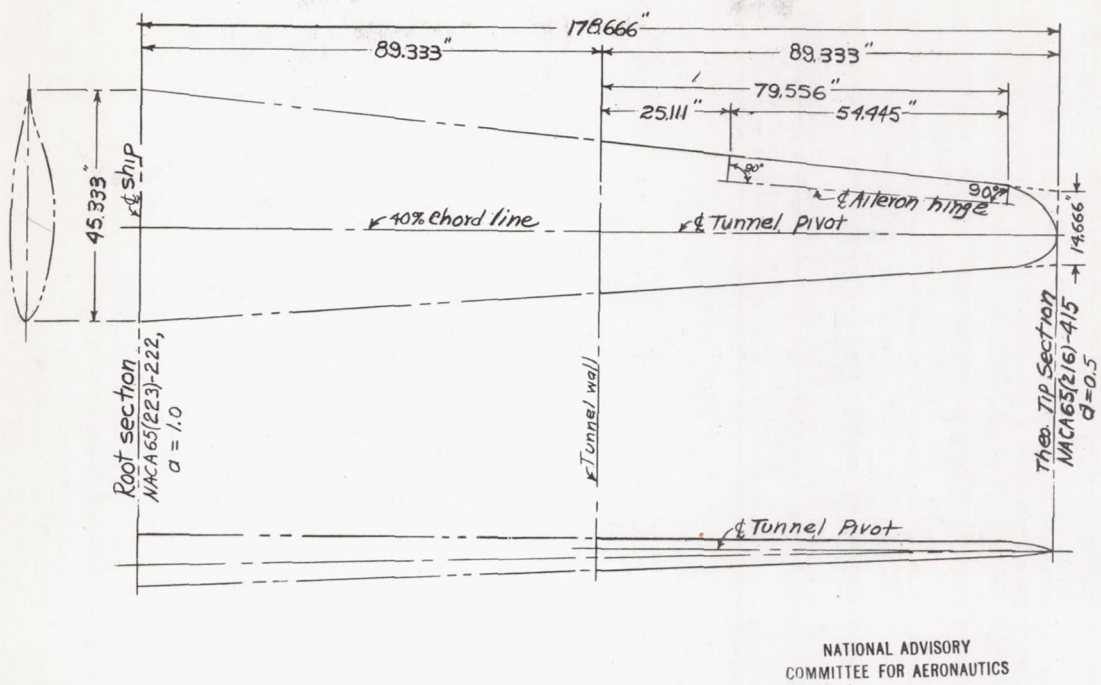

Figure C51.- Quarter-span wing model C-XIV

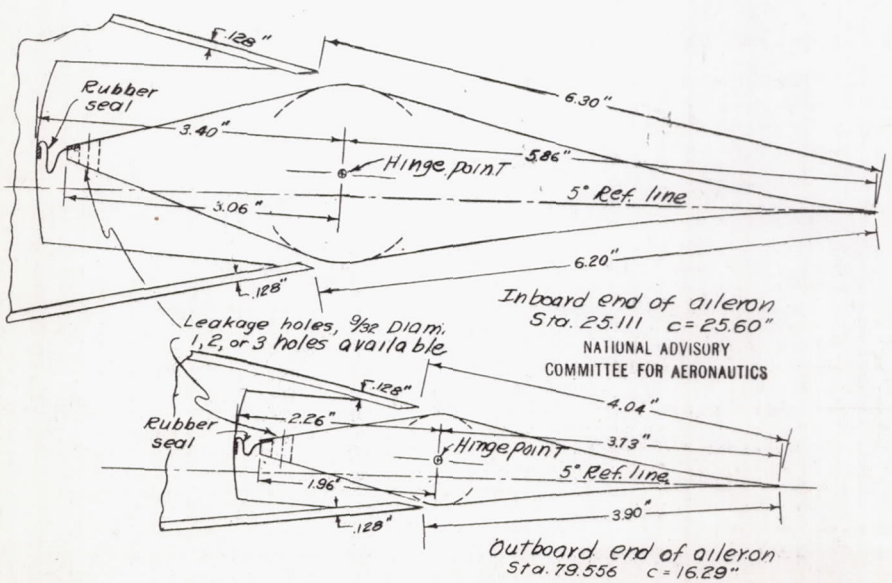

Figure C52.- End sections of aileron on quarter-span wing model C-XIV. LMAL 7-by 10-foot tunnel.

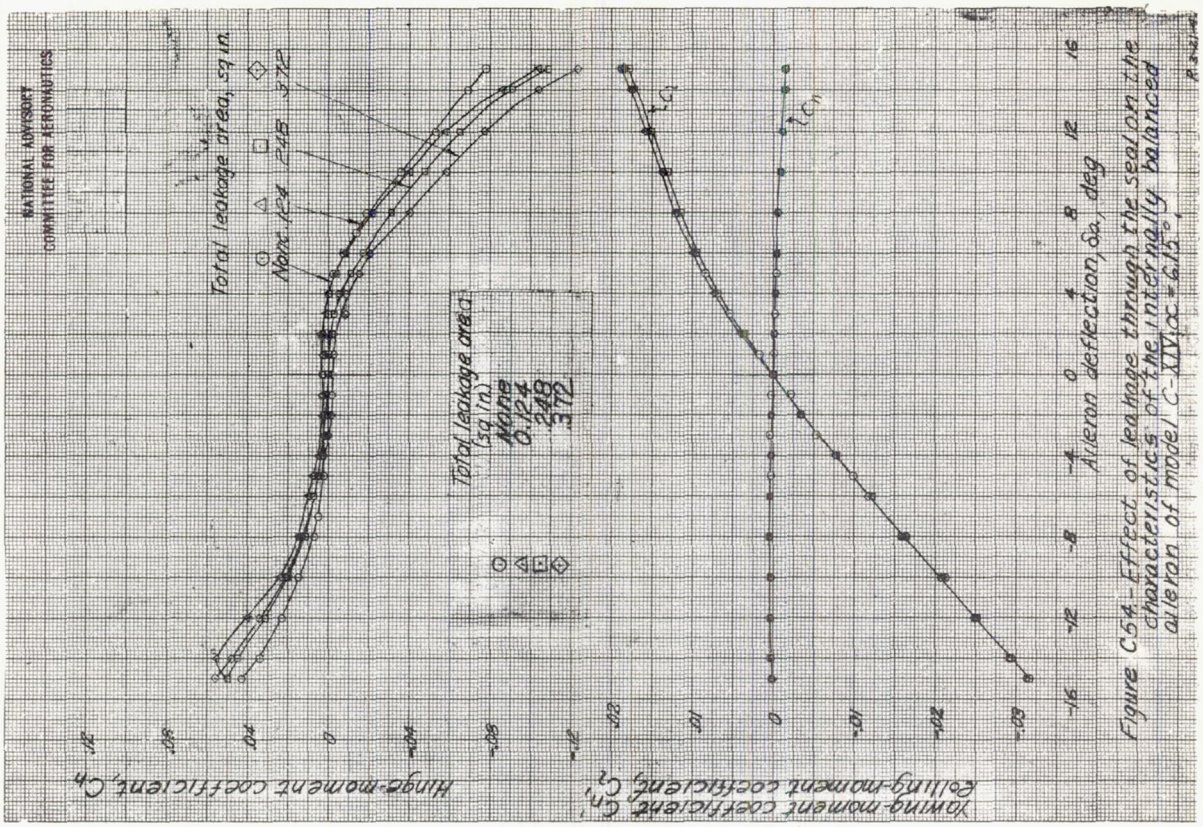

Figure C54.- Effect of leakage through the seal on the characteristics of the internally balanced aileron of model C-XIV ($c_a/c = 0.15$).

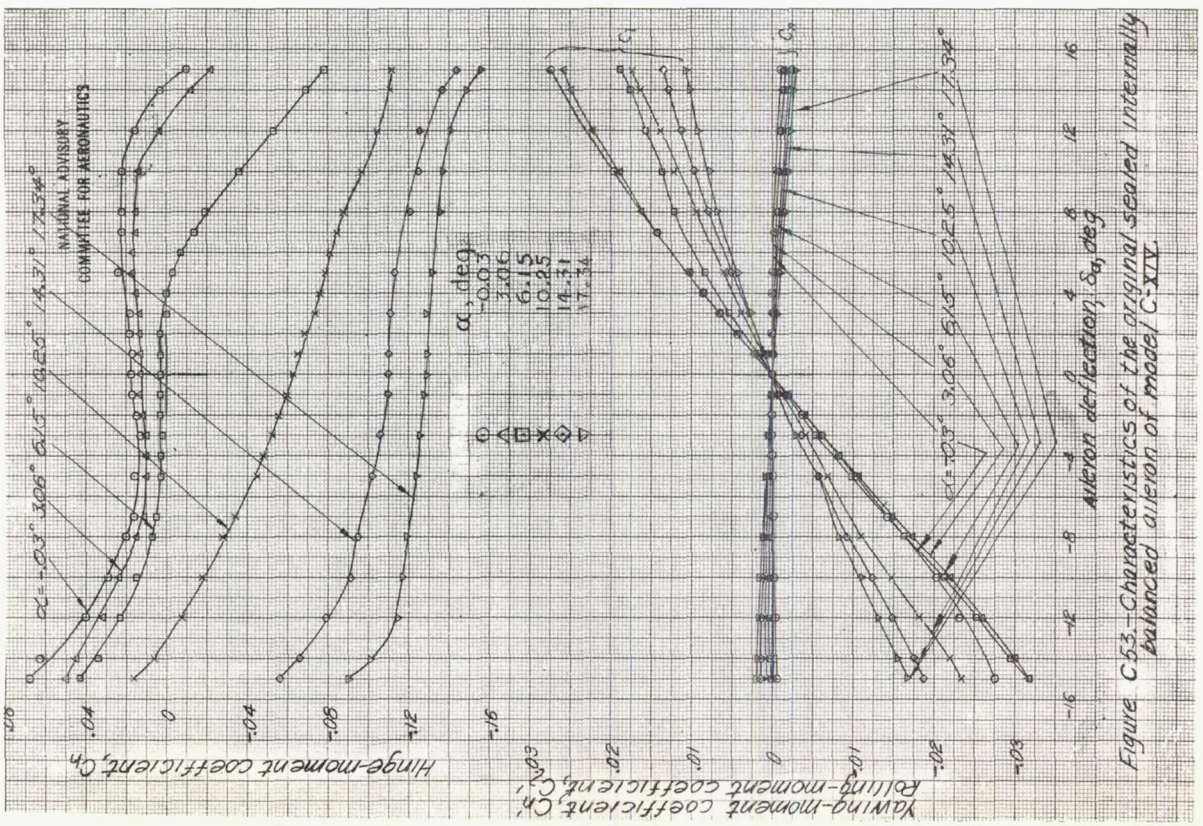

Figure C53.- Characteristics of the original sealed internally balanced aileron of model C-XIV.

Model C-XV

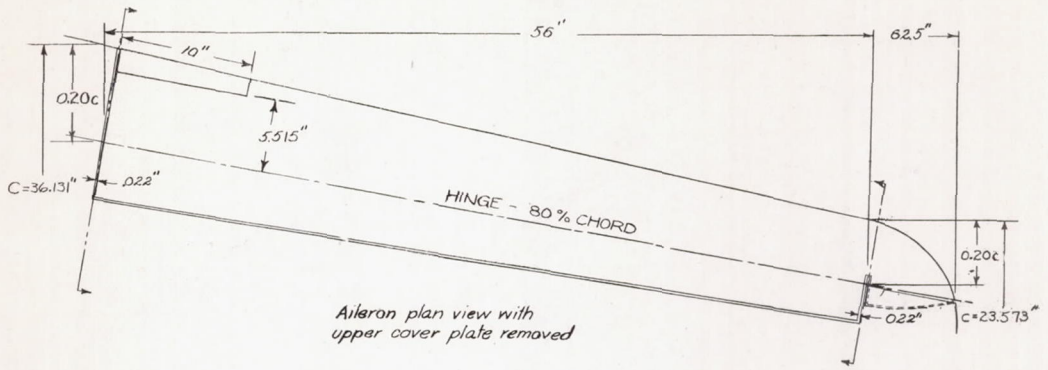

Aileron plan view with upper cover plate removed

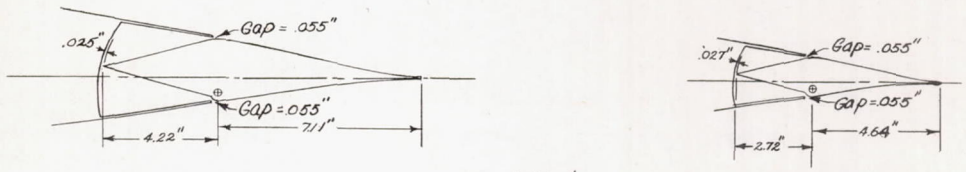

Original

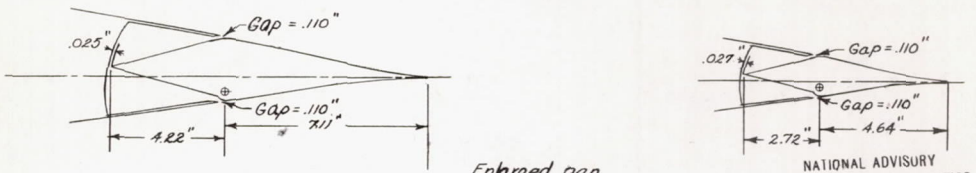

Enlarged gap

NATIONAL ADVISORY COMMITTEE FOR AERONAUTICS

INBOARD END

OUTBOARD END

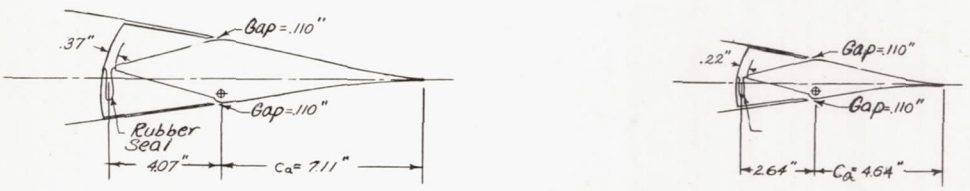

0.57 c_a sealed balance

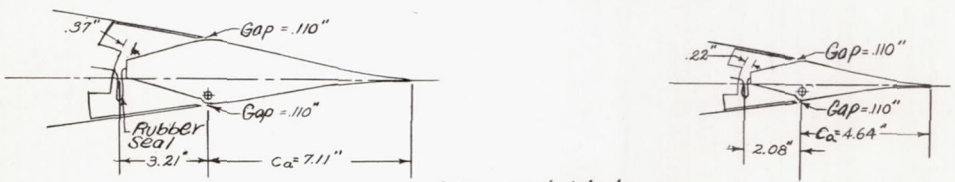

0.45 c_a sealed balance

0.505 c_a sealed balance

NATIONAL ADVISORY COMMITTEE FOR AERONAUTICS

Figure C55.-Internally balanced ailerons on partial-span wing model C-XV. LMAL 7-by 10-foot tunnel.

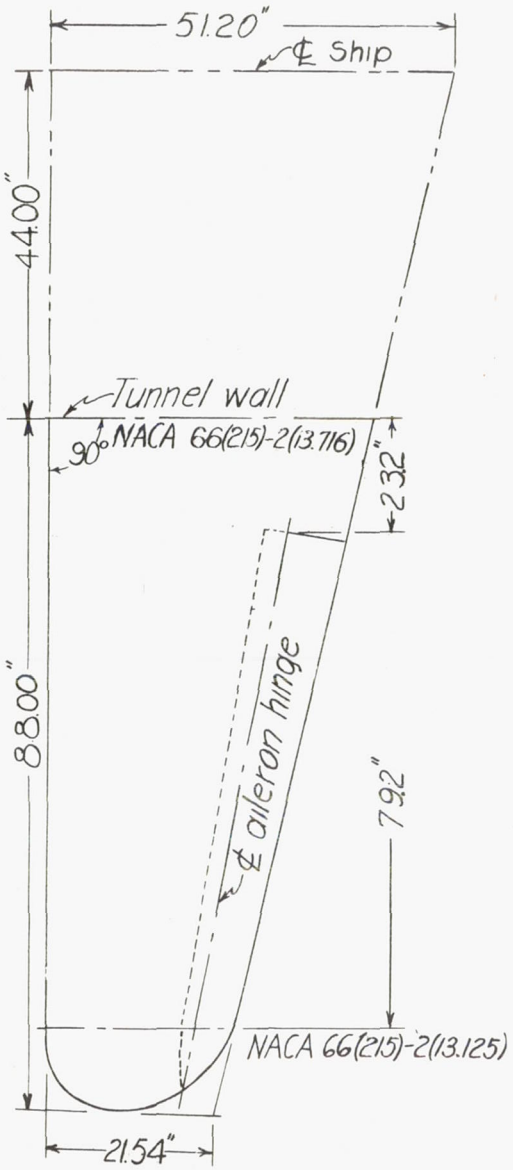

Figure C56.- Partial-span wing model C-XV.

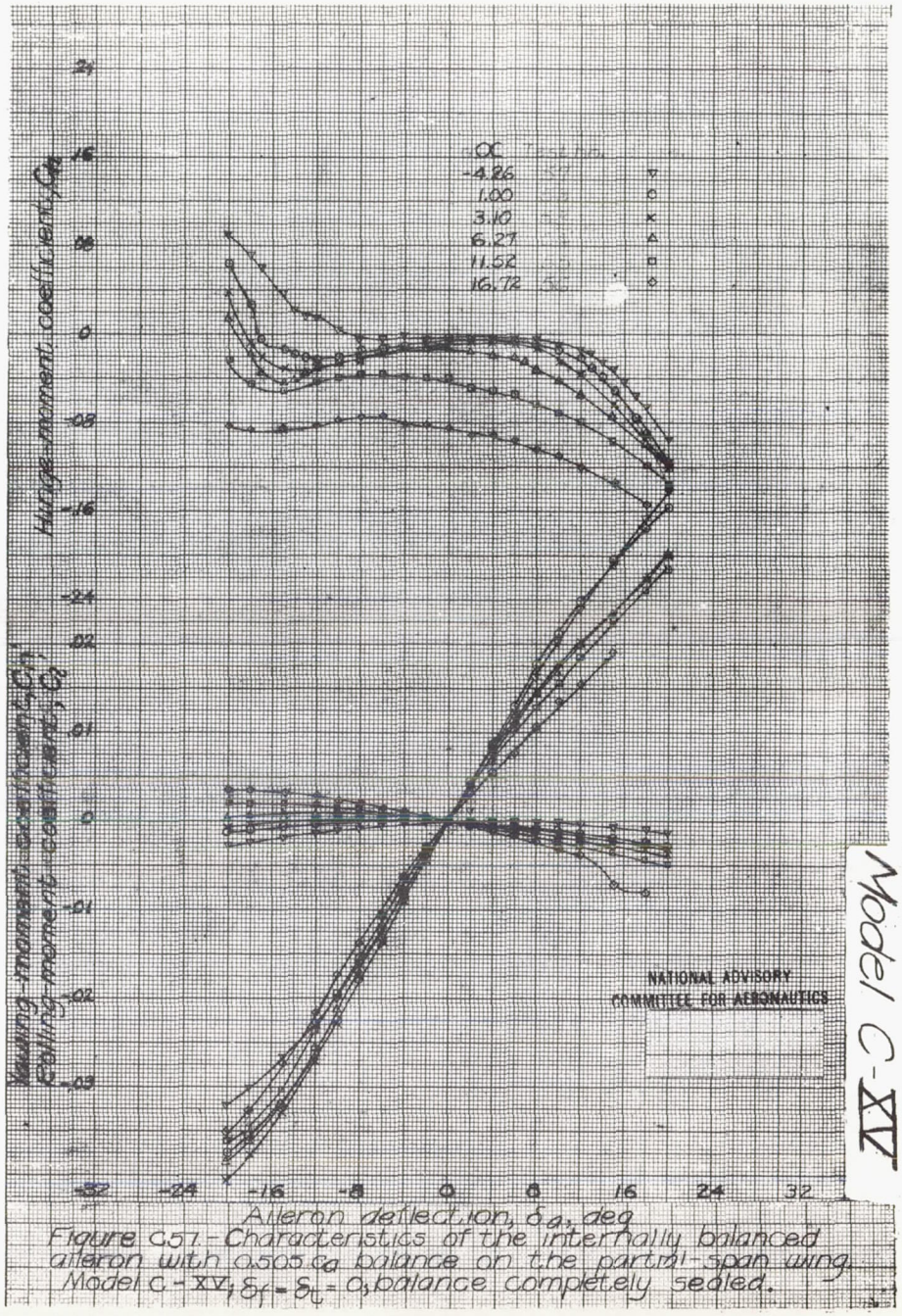

Figure C57.- Characteristics of the internally balanced aileron with 0.505 c_a balance on the partial-span wing. Model C-XV, $\delta_f = \delta_t = 0$, balance completely sealed.

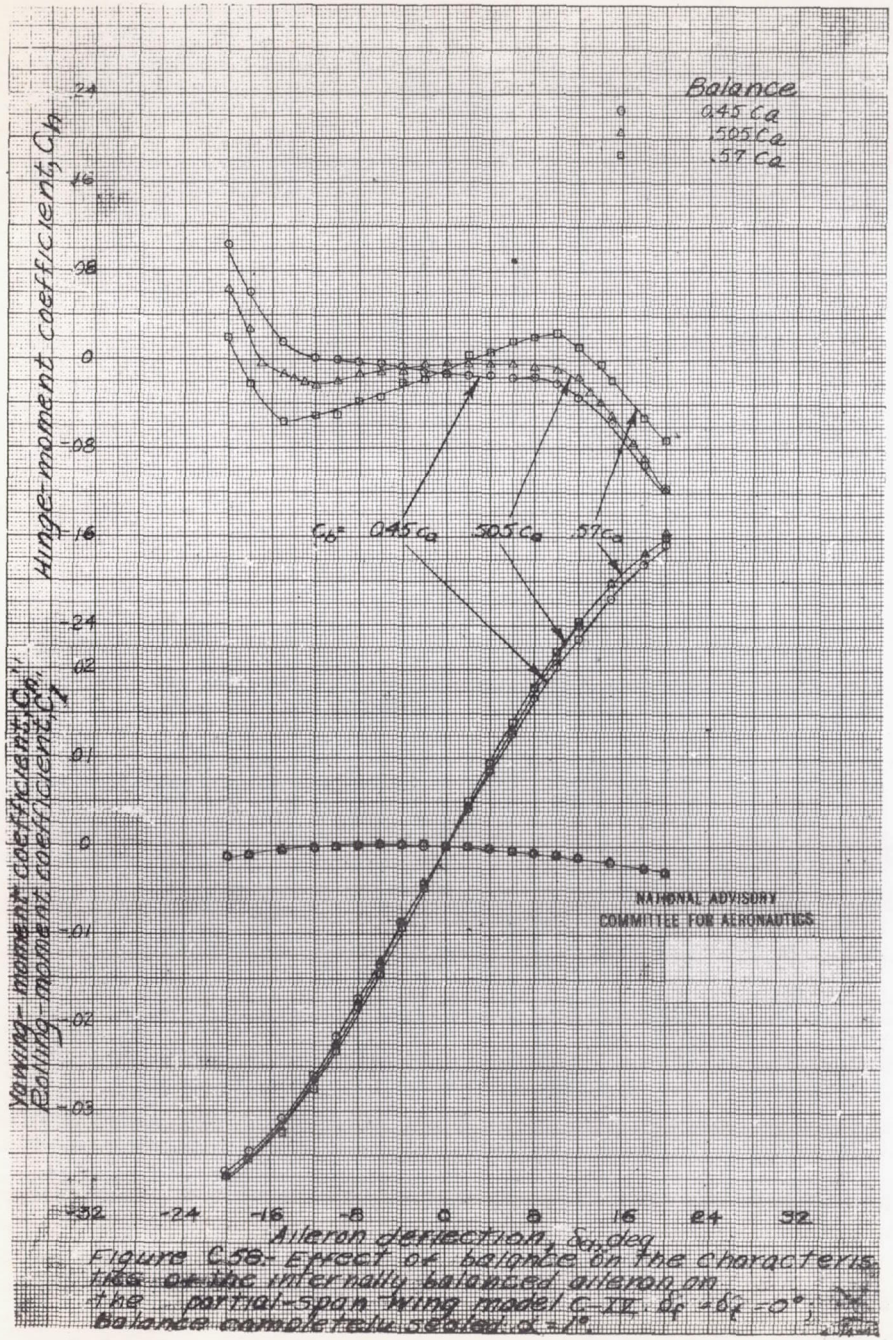

Figure C-58.- Effect of balance on the characteristics of the internally balanced aileron on the partial-span wing model C-XV. δ_f 46; δ_f -0°; balance completely sealed; α 1°.

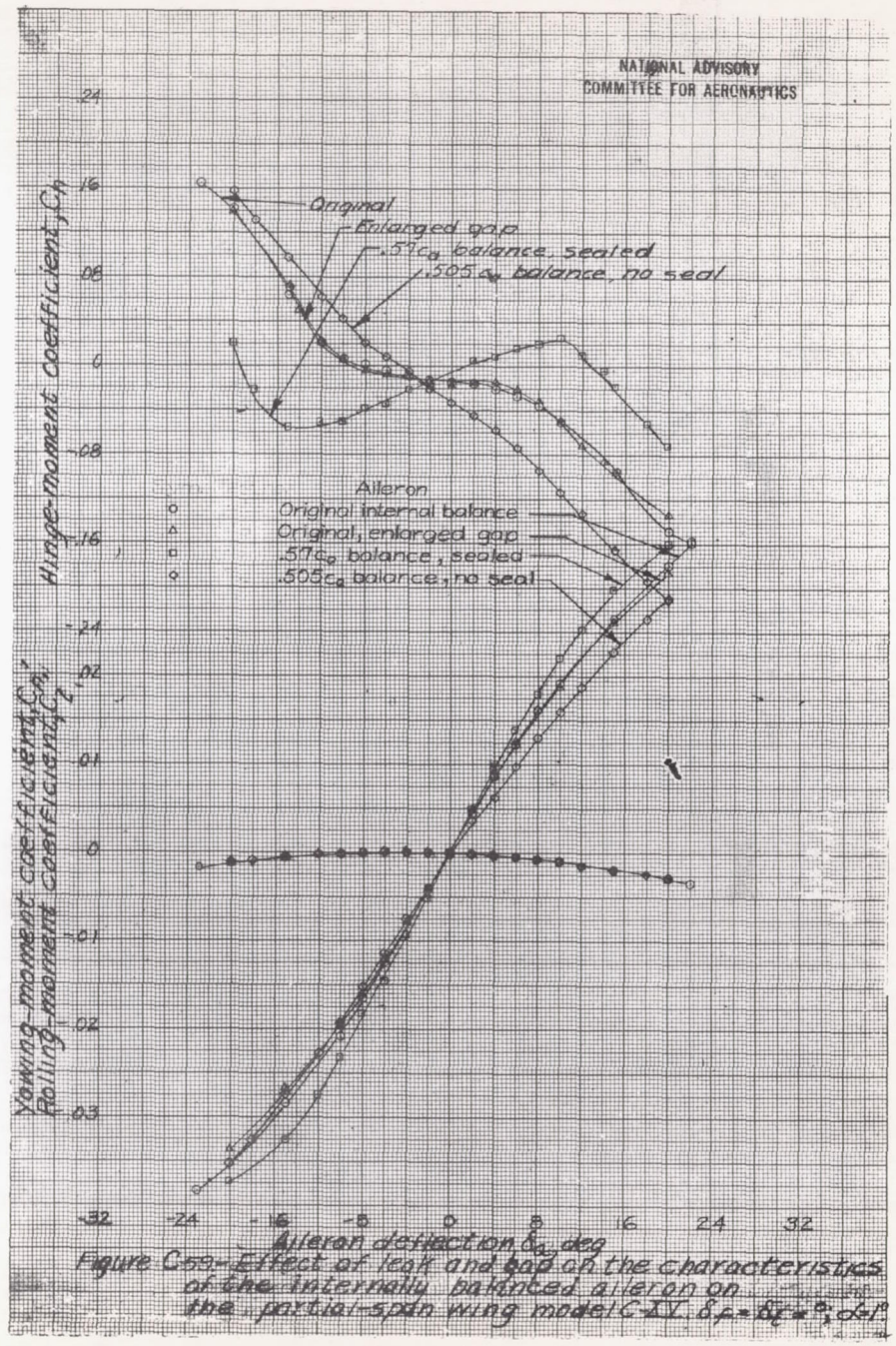

Figure C-59.- Effect of leak and gap on the characteristics of the internally balanced aileron on the partial-span wing model C-XV. $\delta_f = \delta_f = 0°, 61°$

Model C-XV

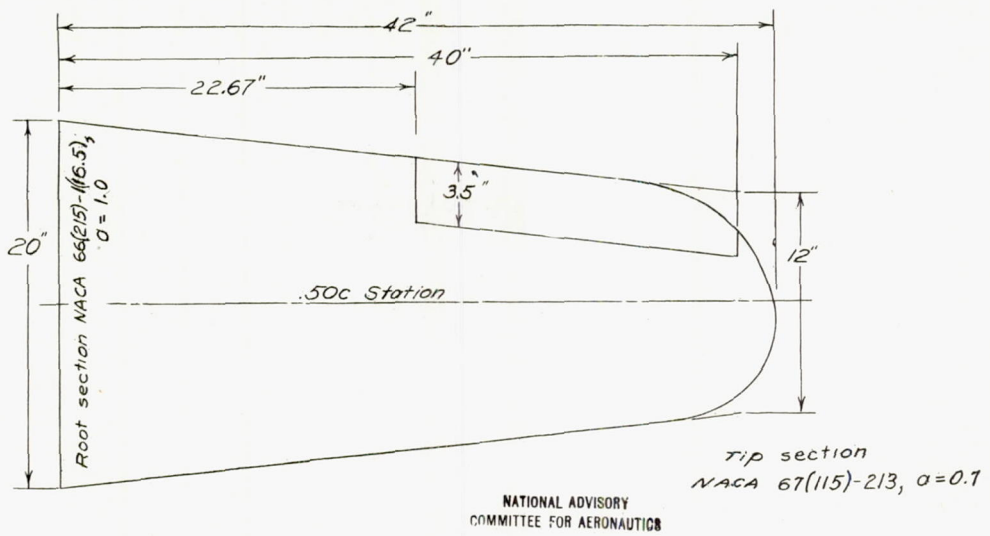

Figure C60.- Semispan plan form of complete model C-XVI.

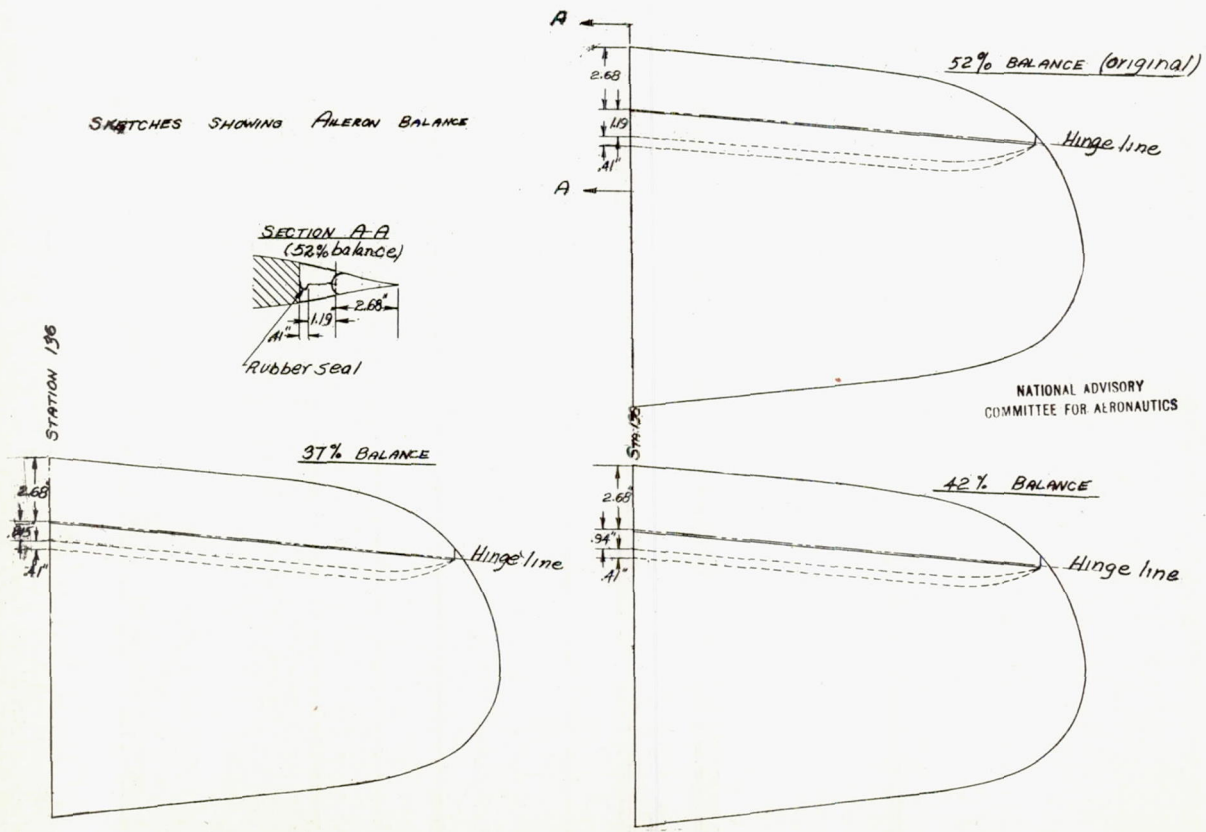

Figure C61.- Ailerons tested on model C-XVI in LMAL 7-by10-foot tunnel.

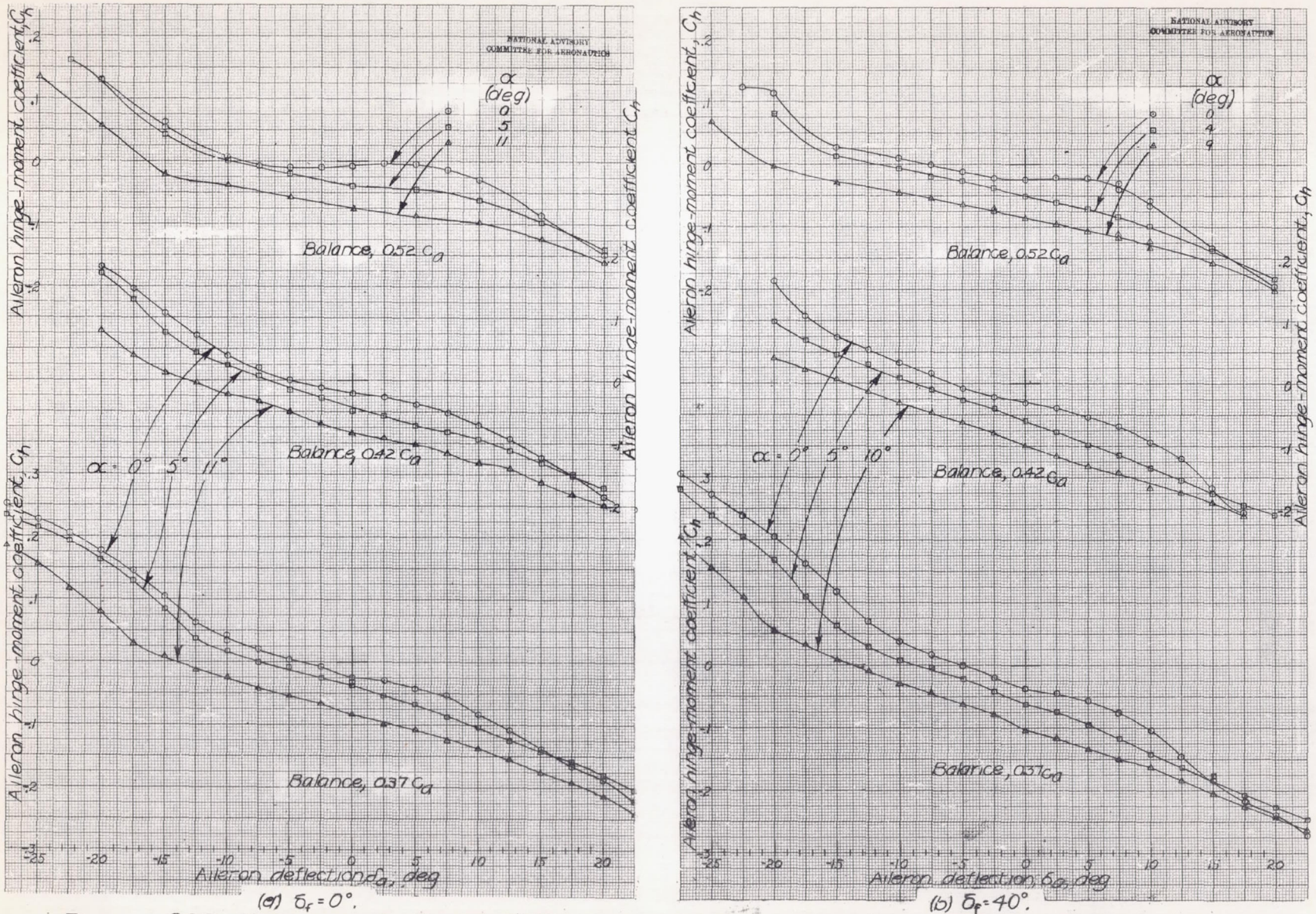

Figure C62.- Hinge-moment characteristics of aileron of complete model C-XVI.

Model C-XVI

Model C-XVII

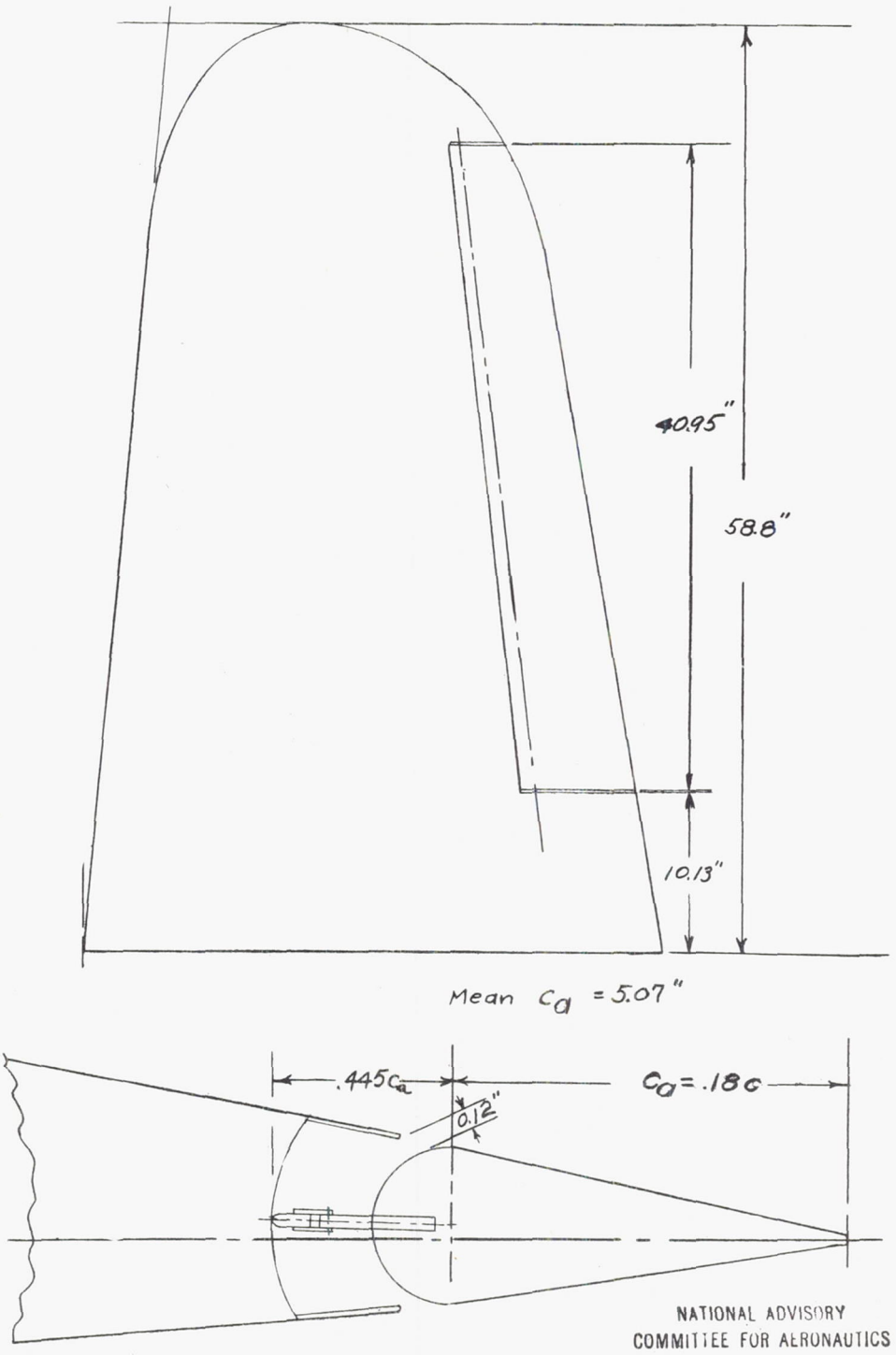

Figure C63.- Partial-span wing model CXVII tested in the N.P.L. NO. 2 wind tunnel.

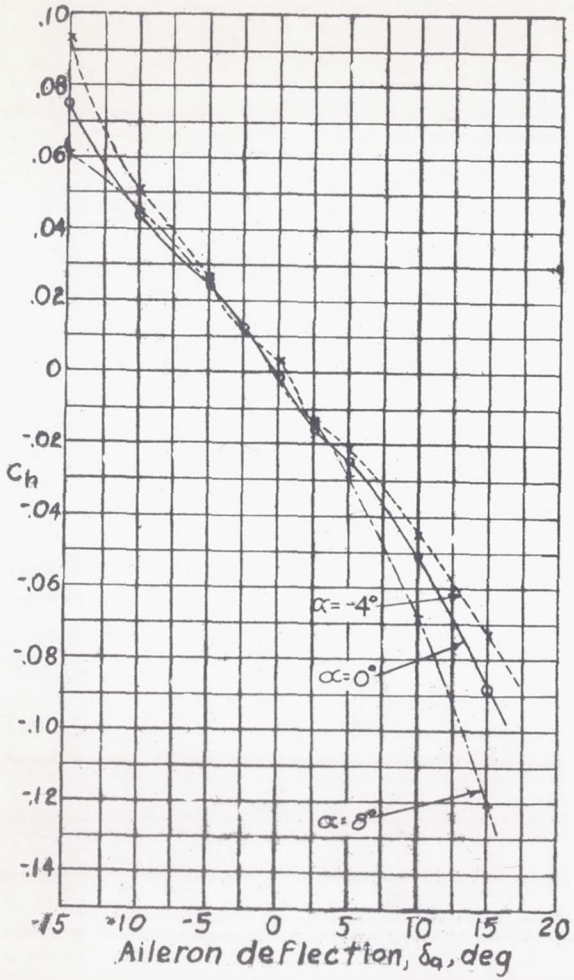

NATIONAL ADVISORY
COMMITTEE FOR AERONAUTICS

Figure C64.- Hinge-moment characteristics of unbalanced aileron. Model C-XVII; nose gap sealed.

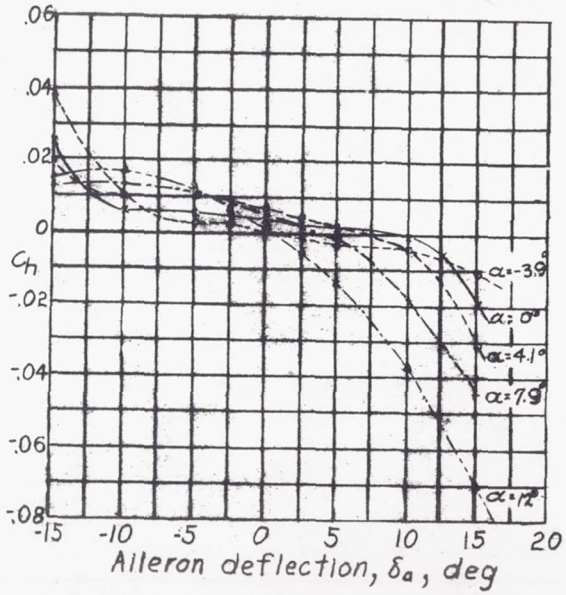

NATIONAL ADVISORY
COMMITTEE FOR AERONAUTICS

Figure C65.- Hinge-moment characteristics of 0.445 c_a internally balanced aileron. Model C-XVII, nose gap sealed.

Model C-XVII

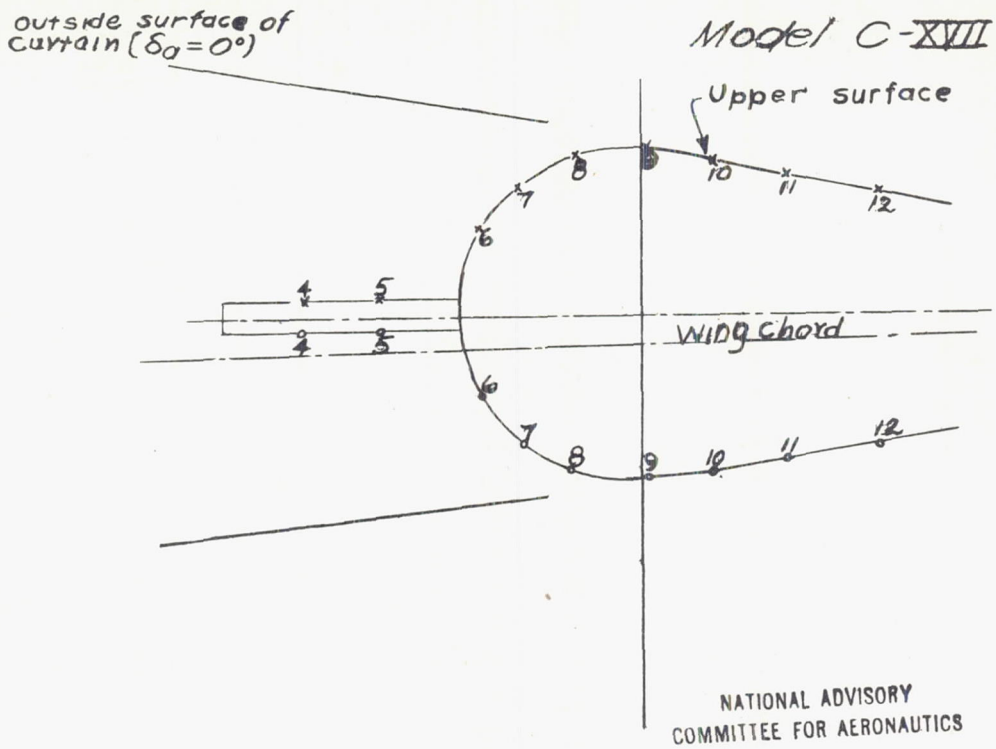

NATIONAL ADVISORY COMMITTEE FOR AERONAUTICS

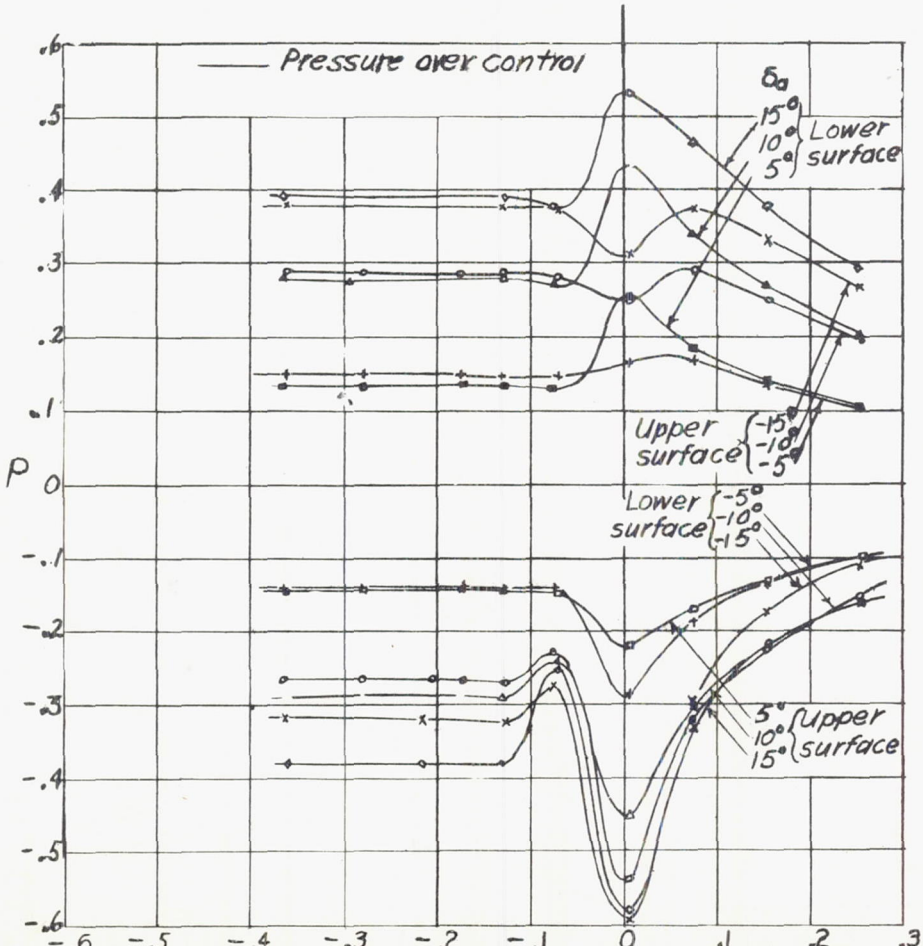

Figure C66.- Pressure distribution over aileron.
Nose gap sealed.

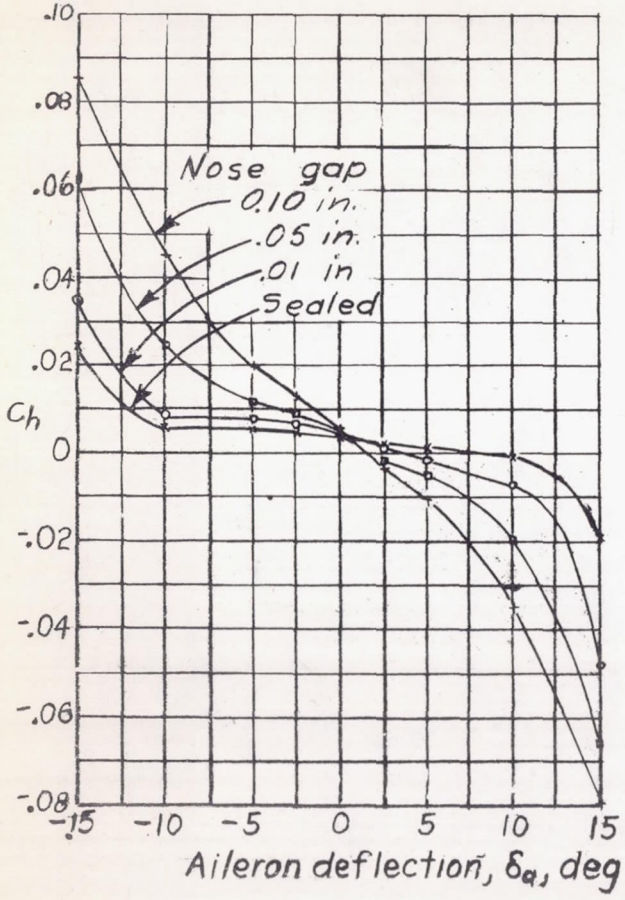

Figure C67.-Effect of nose gap on aileron hinge-moment coefficient. $\alpha = 0°$

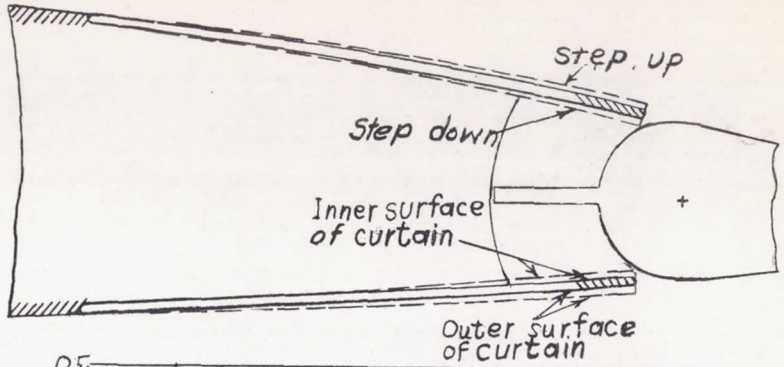

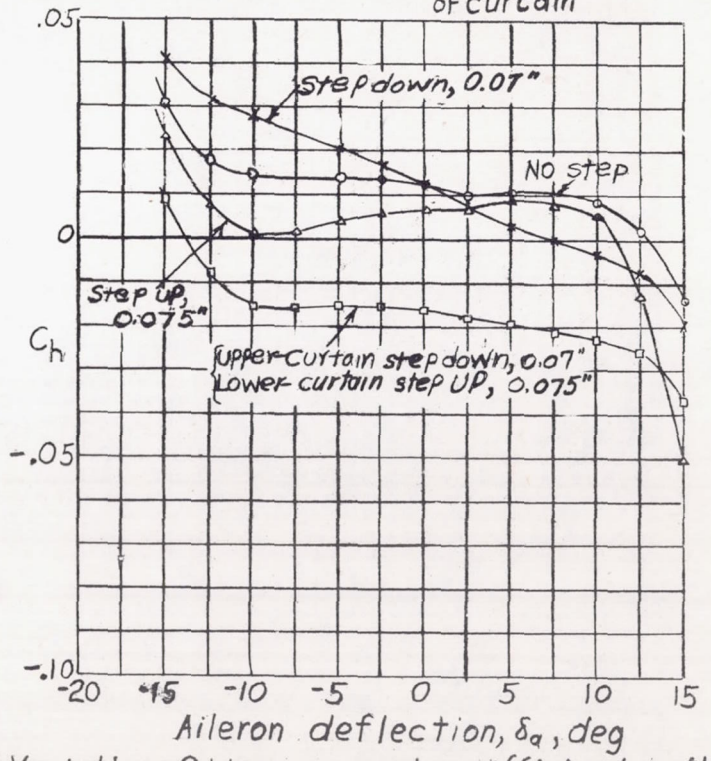

Figure C68.-Variation of hinge-moment coefficient with vertical position of curtain trailing edge. $\alpha = 0°$; nose gap sealed.

Model C-XIII

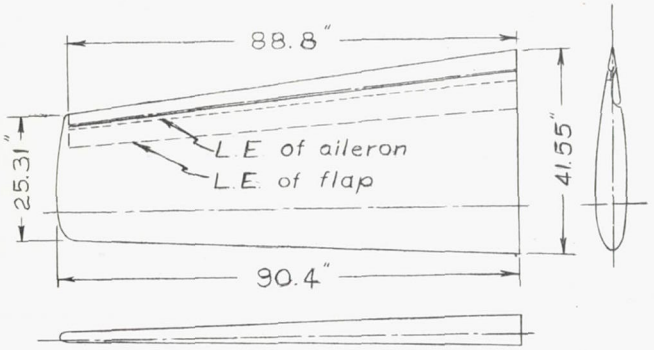

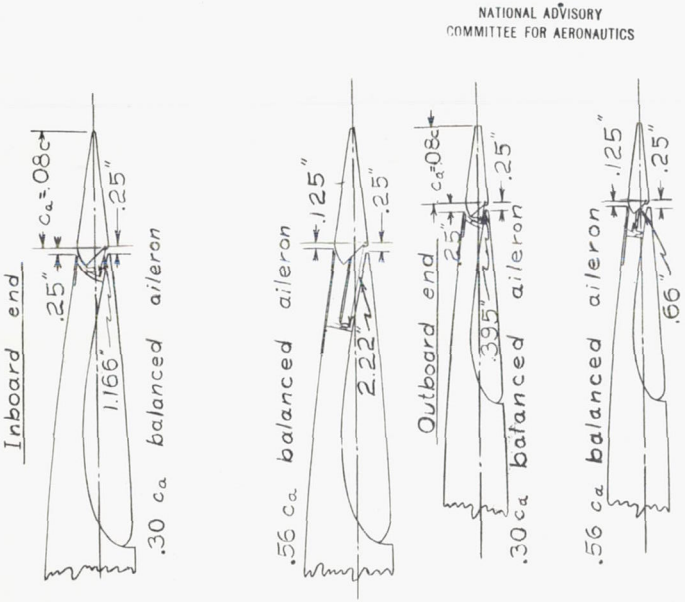

Figure C69.- Semispan wing model C-XVIII LMAL 7-by 10-foot tunnel.

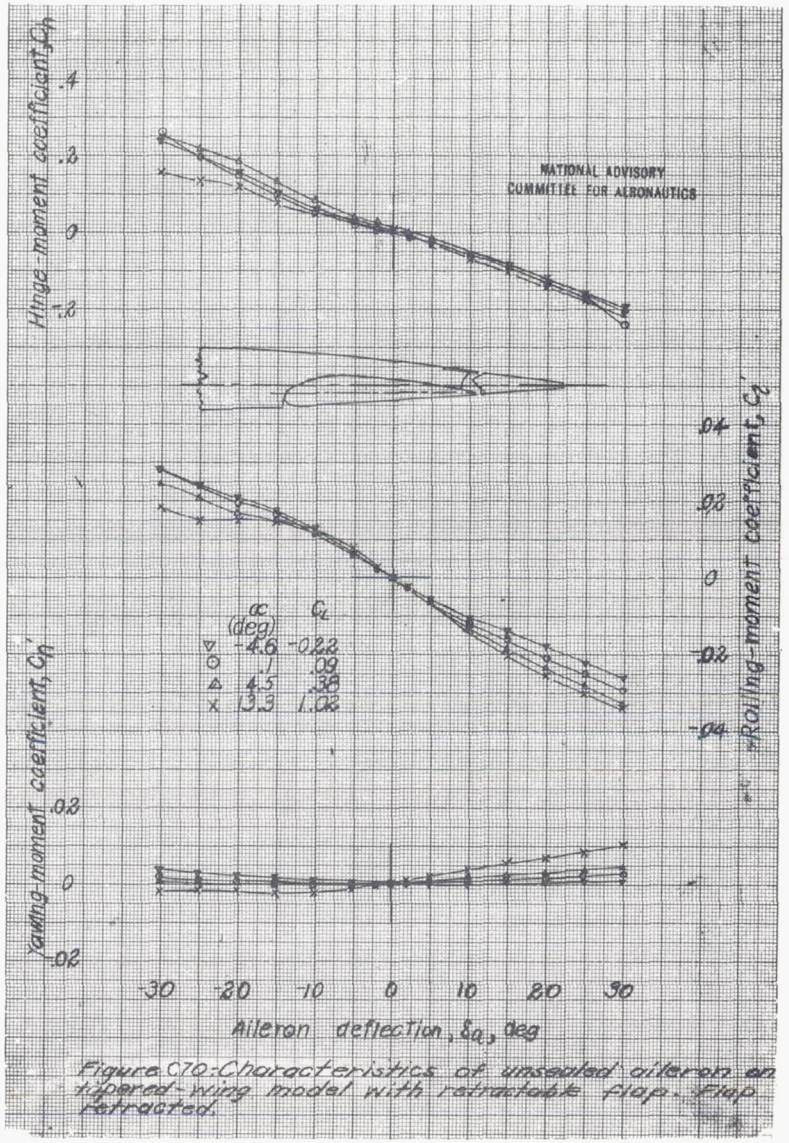

Figure C70:Characteristics of unsealed aileron on tapered wing model with retractable flap. Flap retracted.

Model C-XVIII

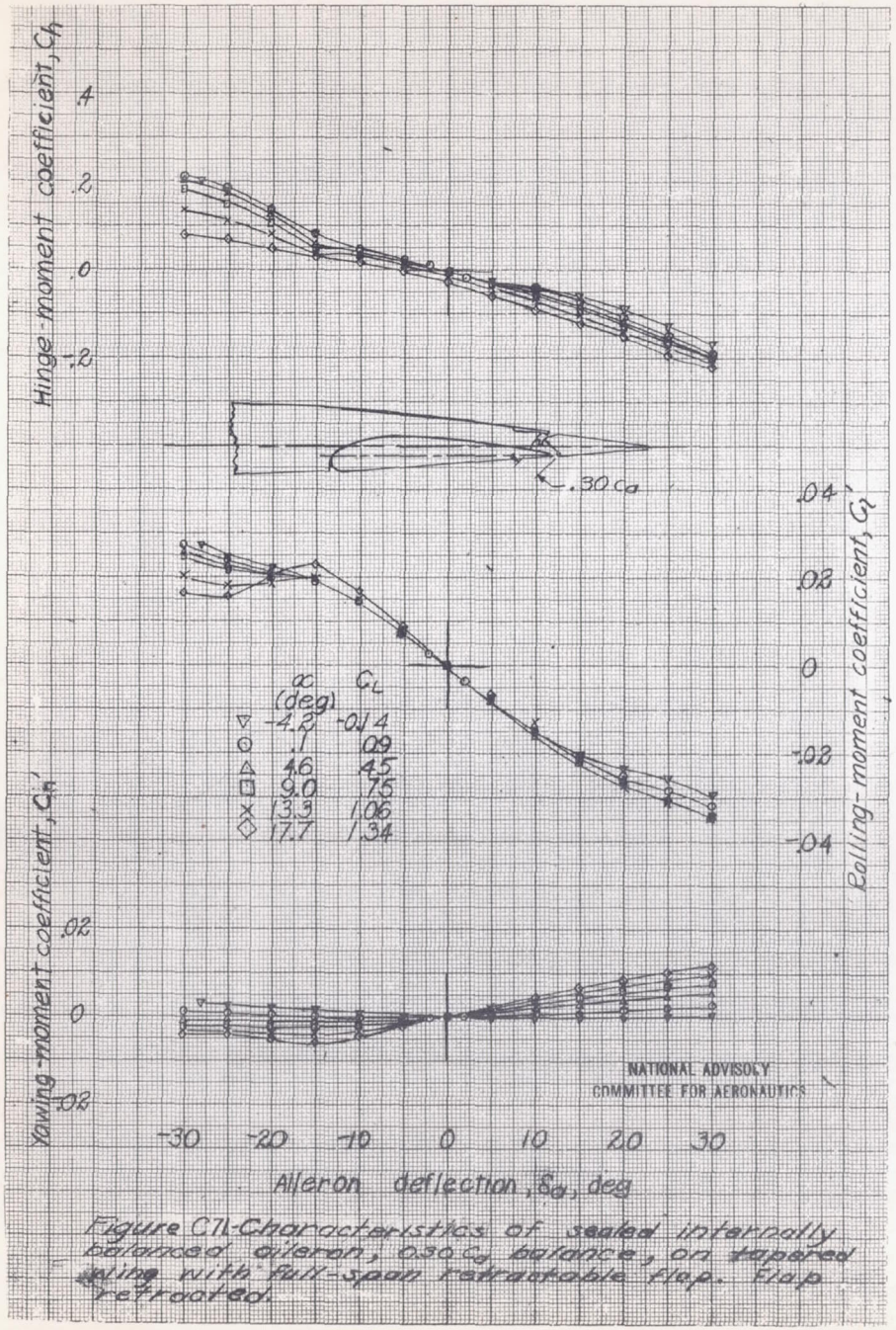

Figure C11.-Characteristics of sealed internally balanced aileron, 0.30 c_a balance, on tapered wing with full-span retractable flap. Flap retracted.

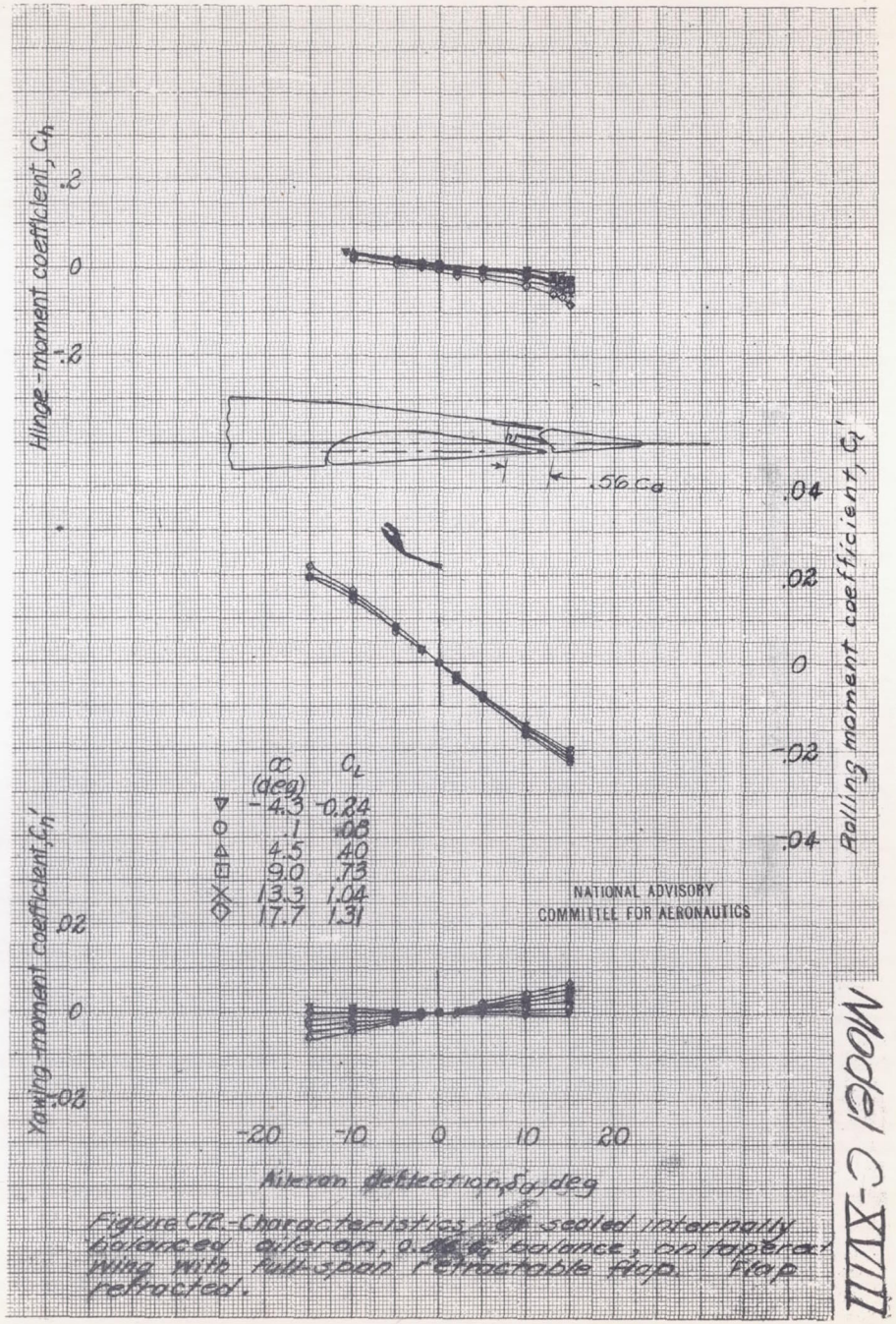

Figure C12.-Characteristics of sealed internally balanced aileron, 0.56 c_a balance, on tapered wing with full-span retractable flap. Flap retracted.

Model C-XIII

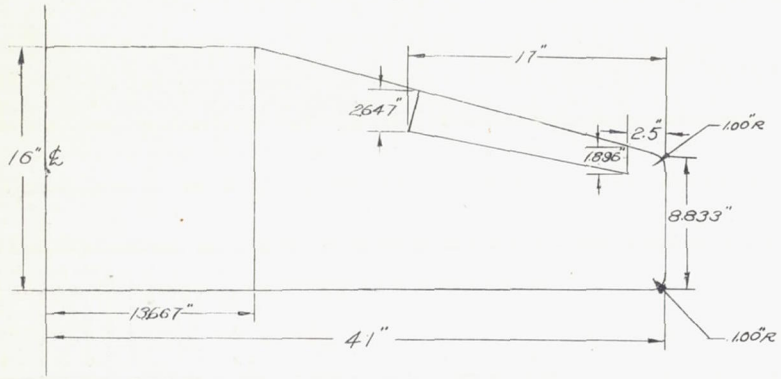

Figure C73:Wing plan form of complete model C-XIX.
Airfoils: root-NACA-23017, tip-NACA 23010.
LMAL 7- by 10-foot tunnel.

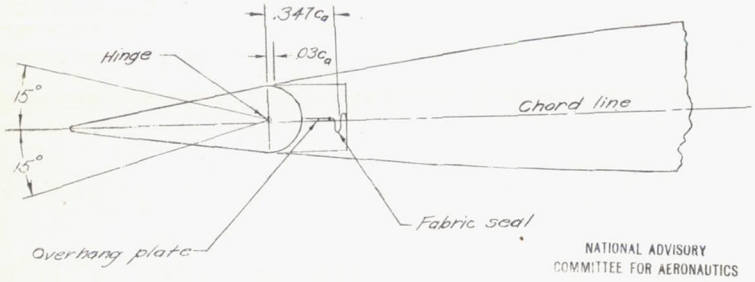

Figure C74:Balance arrangement of model C-XIX.

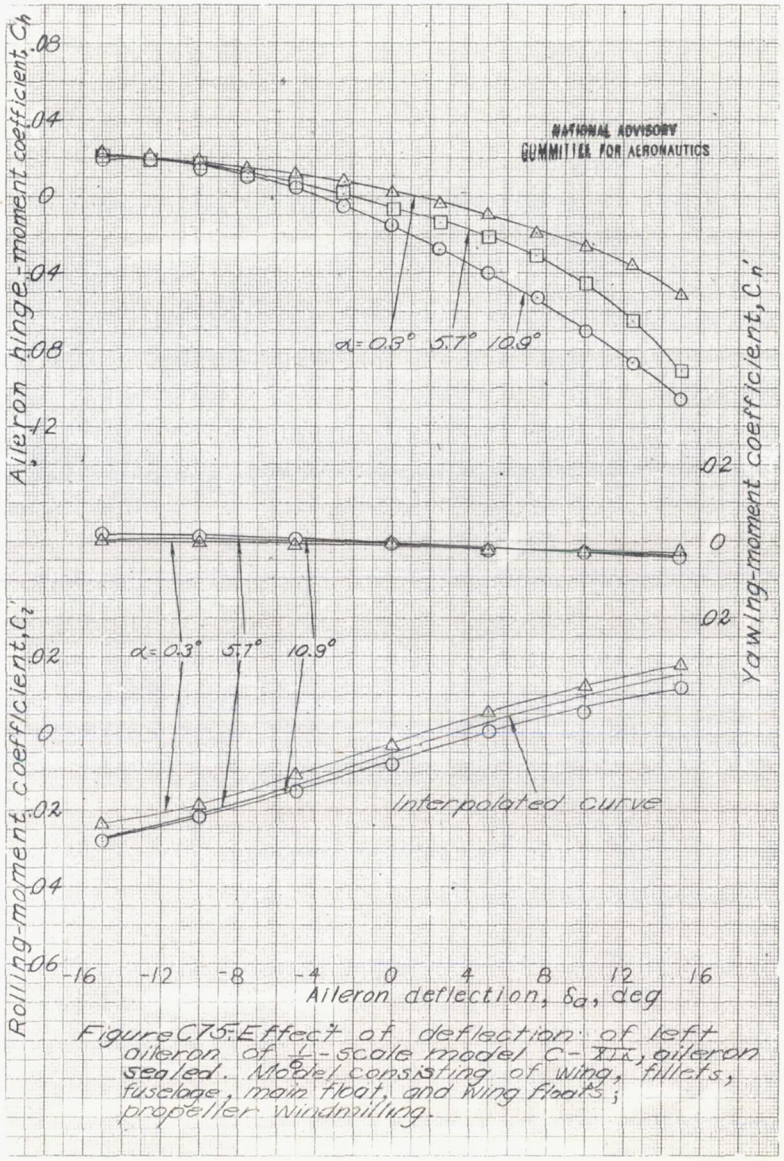

Figure C75:Effect of deflection of left aileron of ¼-scale model C-XIX, aileron sealed. Model consisting of wing, fillets, fuselage, main float, and wing floats; propeller windmilling.

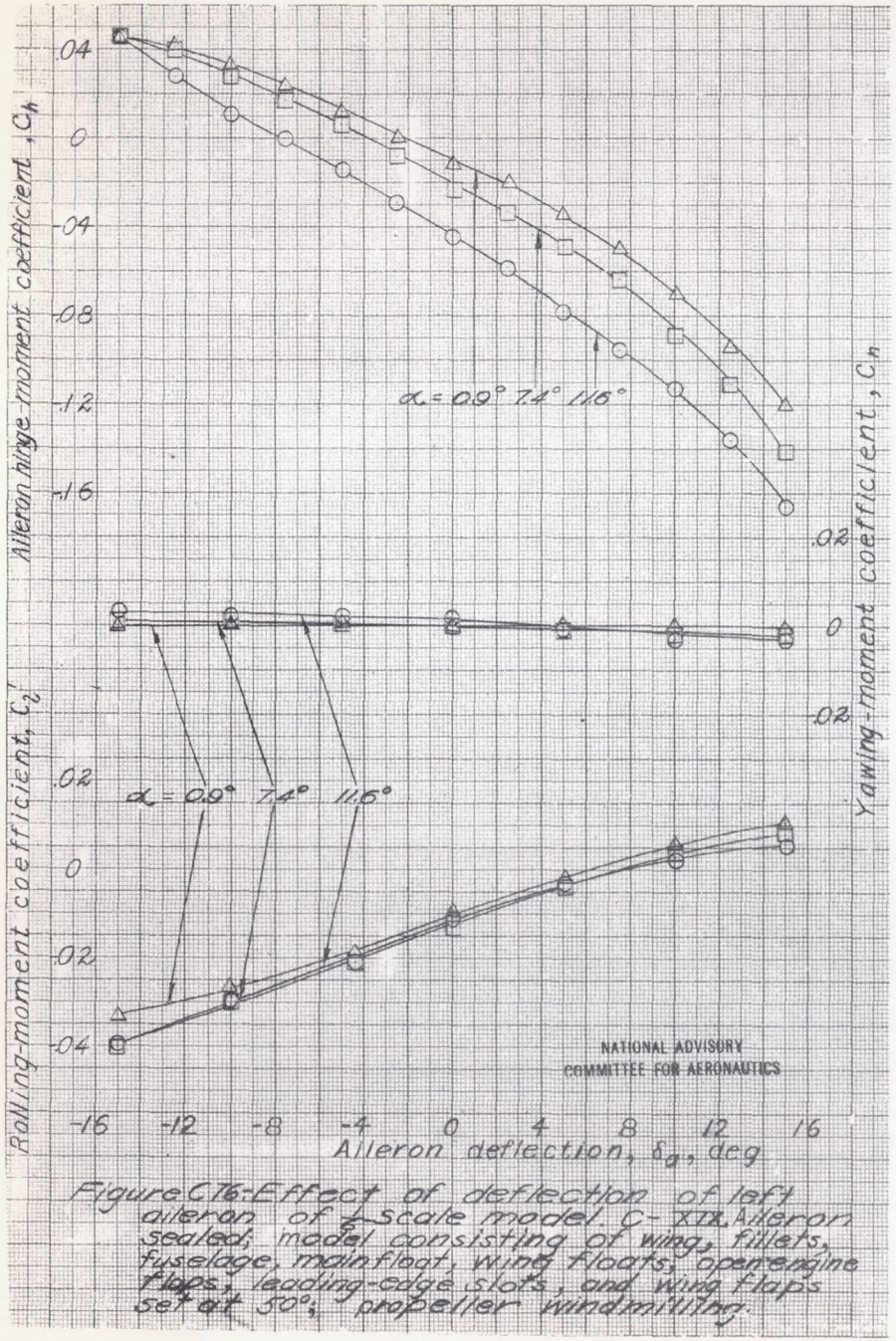

Figure C16.-Effect of deflection of left aileron of ¼-scale model C-XIX. Aileron sealed; model consisting of wing, fillets, fuselage, main float, wing floats, opposite engine flaps, leading-edge slots, and wing flaps set at 50°; propeller windmilling.

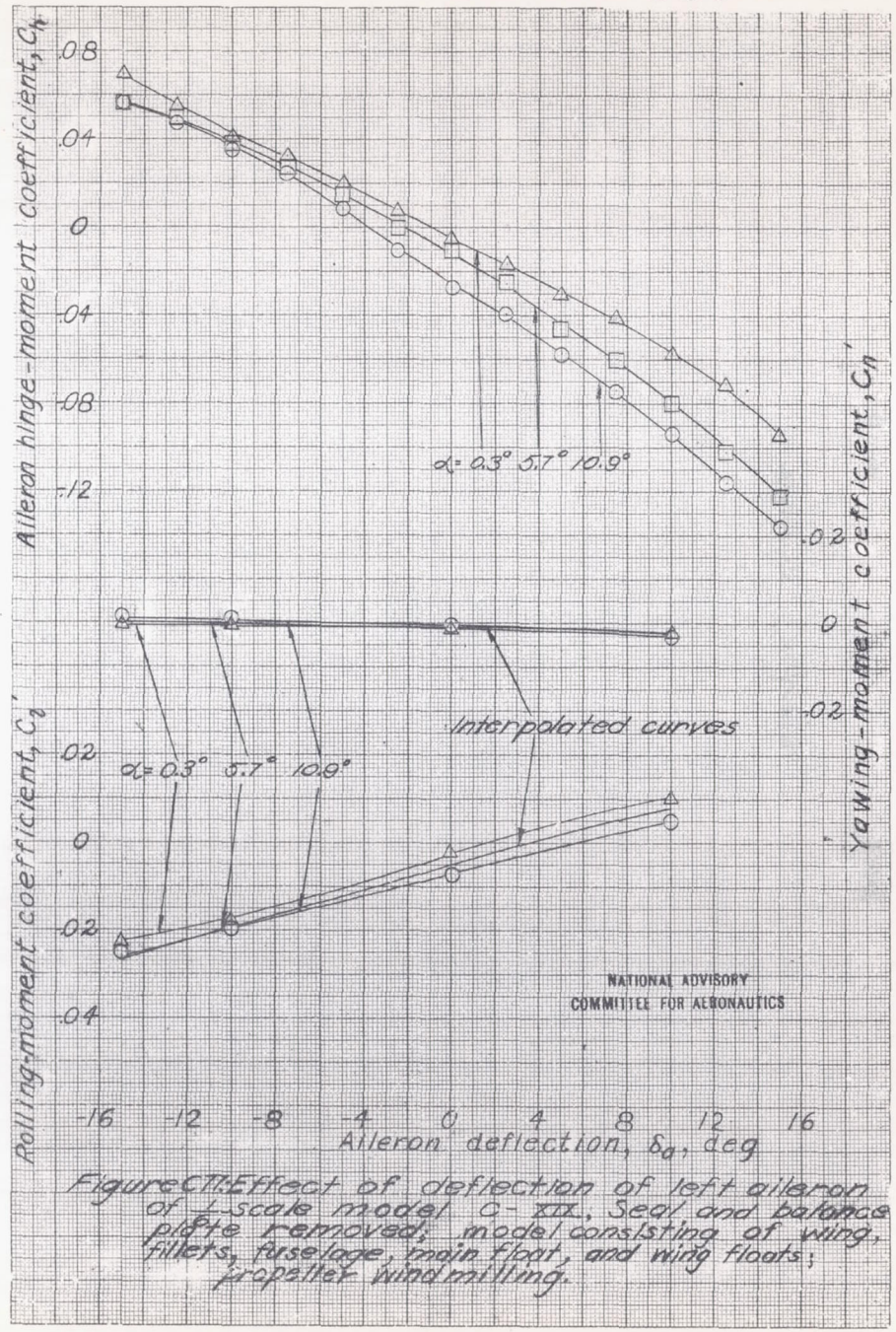

Figure C17.-Effect of deflection of left aileron of ¼-scale model C-XIX. Seal and balance plate removed; model consisting of wing, fillets, fuselage, main float, and wing floats; propeller windmilling.

Model C-XIX

Airplane C-XX

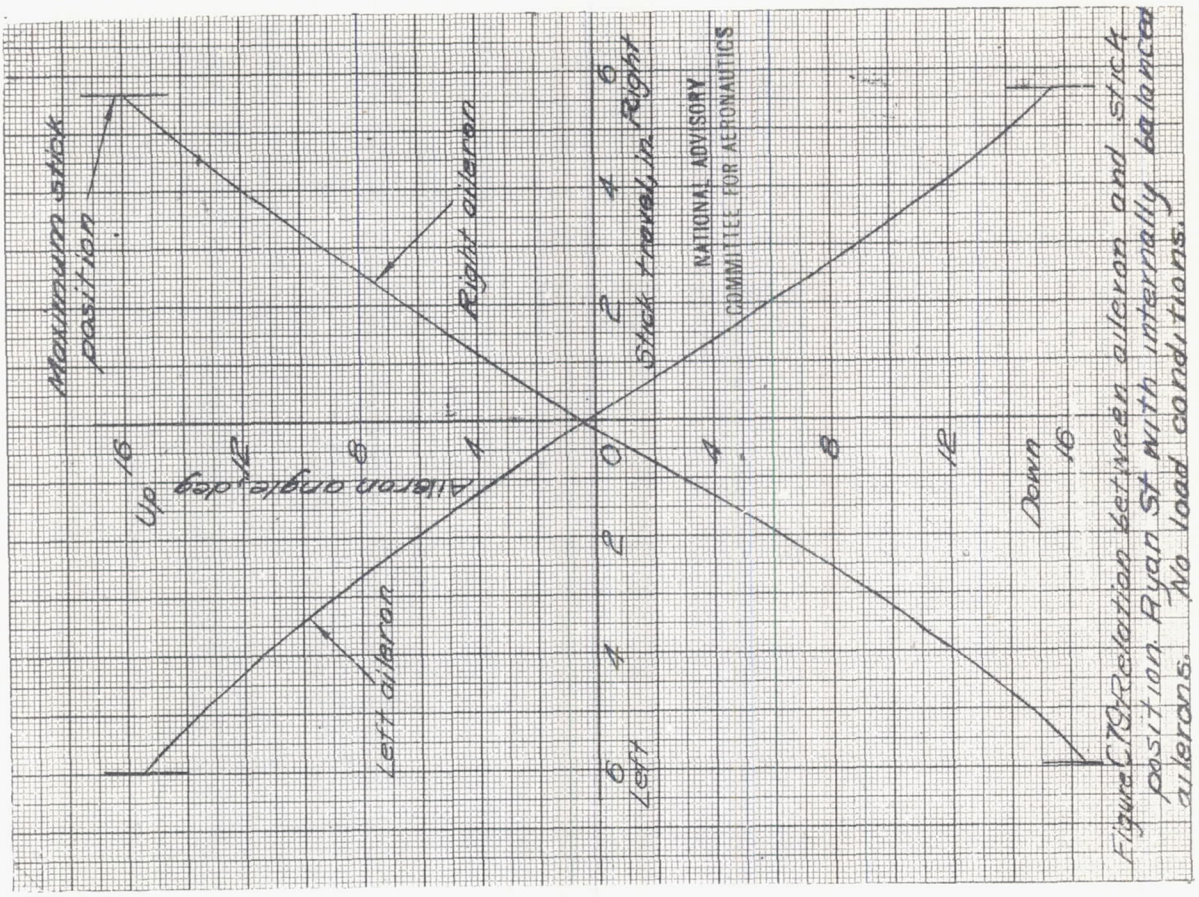

Figure C79.-Relation between aileron and stick position Ryan ST with internally balanced ailerons. No load conditions.

NATIONAL ADVISORY
COMMITTEE FOR AERONAUTICS

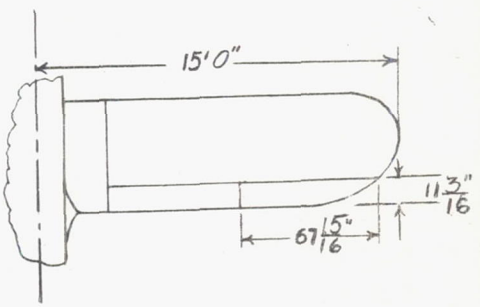

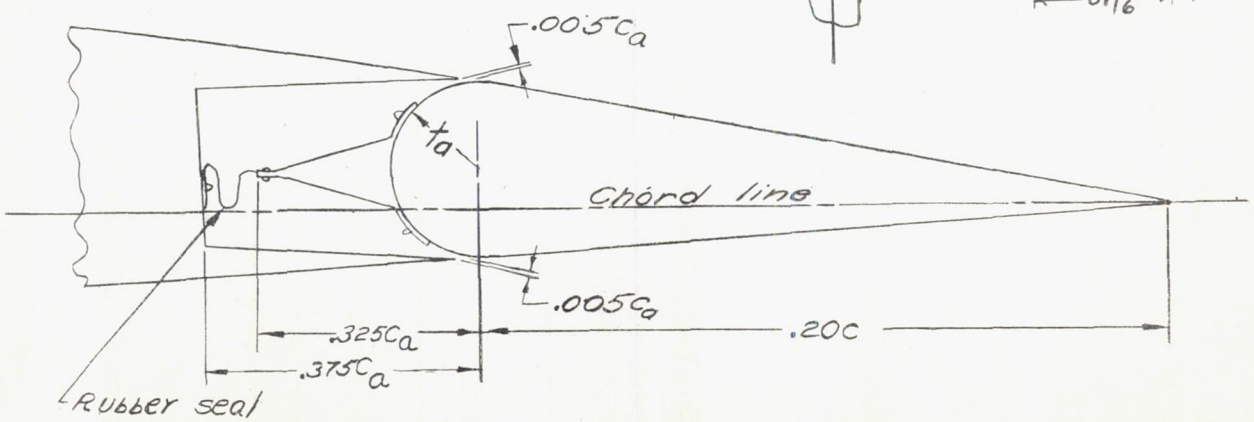

Figure C78.-Sealed and balanced aileron as tested on the Ryan ST airplane in flight at LMAL.

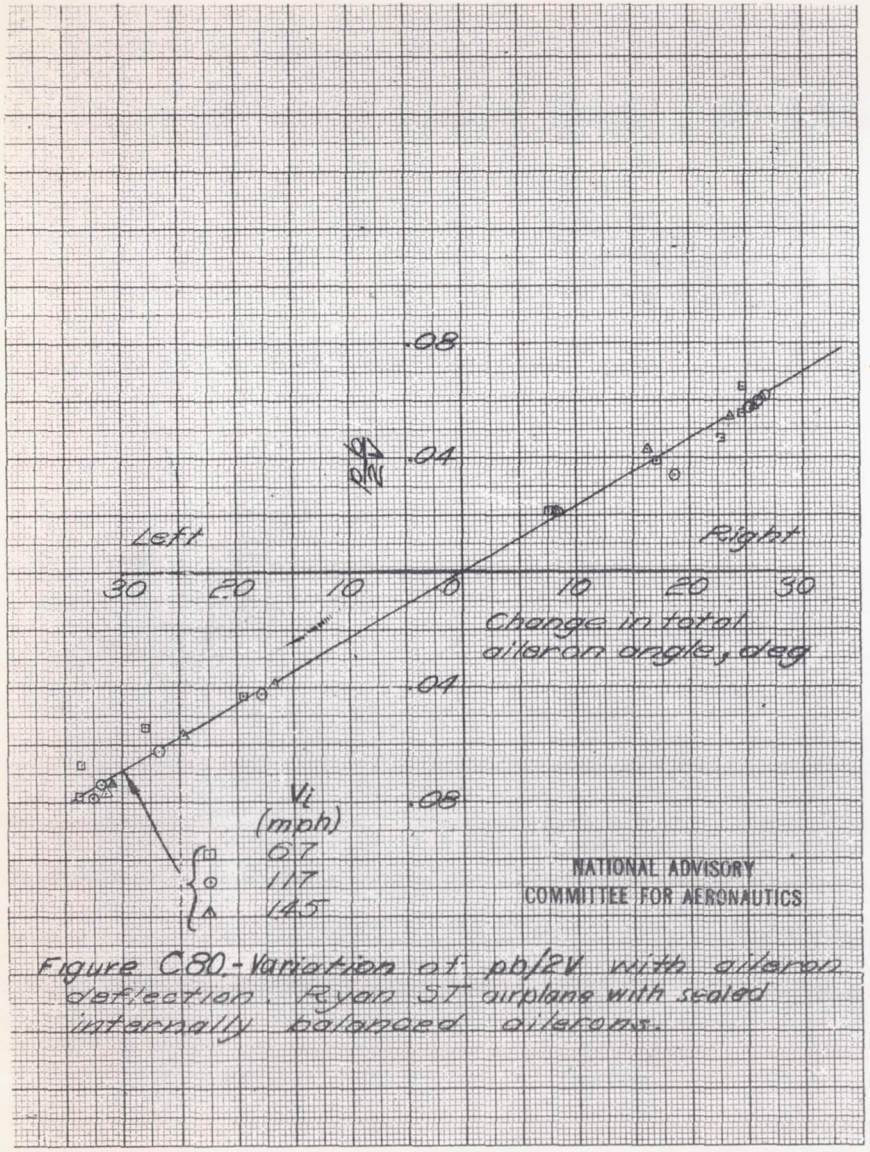

Figure C80.- Variation of $pb/2V$ with aileron deflection. Ryan ST airplane with sealed internally balanced ailerons.

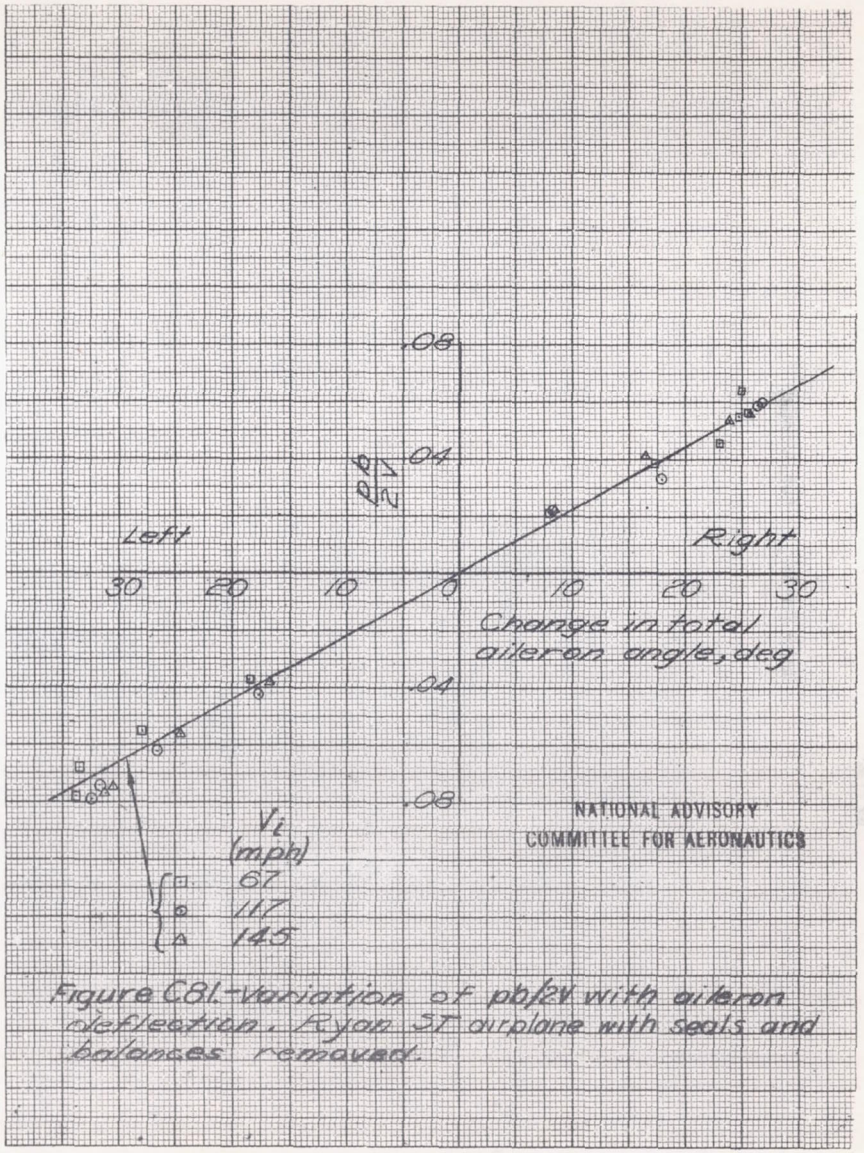

Figure C81.- Variation of $pb/2V$ with aileron deflection. Ryan ST airplane with seals and balances removed.

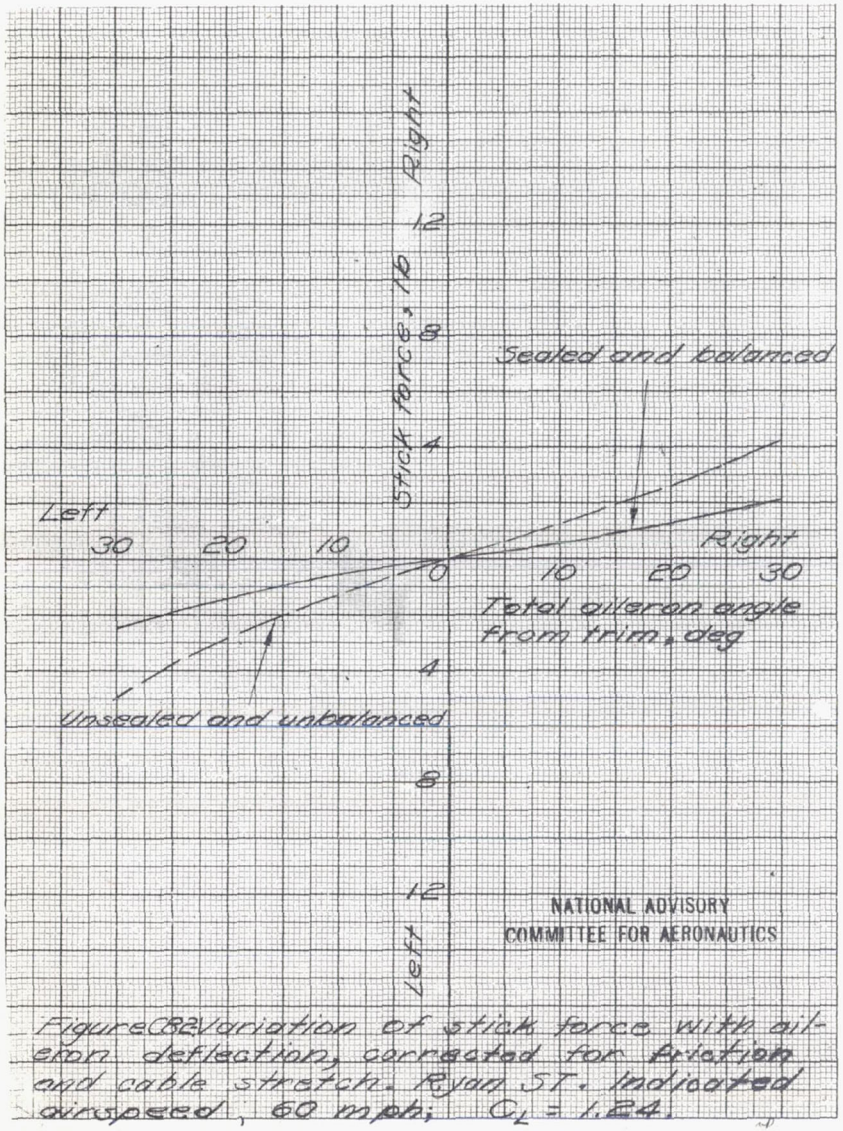

Figure C82. Variation of stick force with aileron deflection, corrected for friction and cable stretch. Ryan ST. Indicated airspeed, 60 mph; C_L = 1.24.

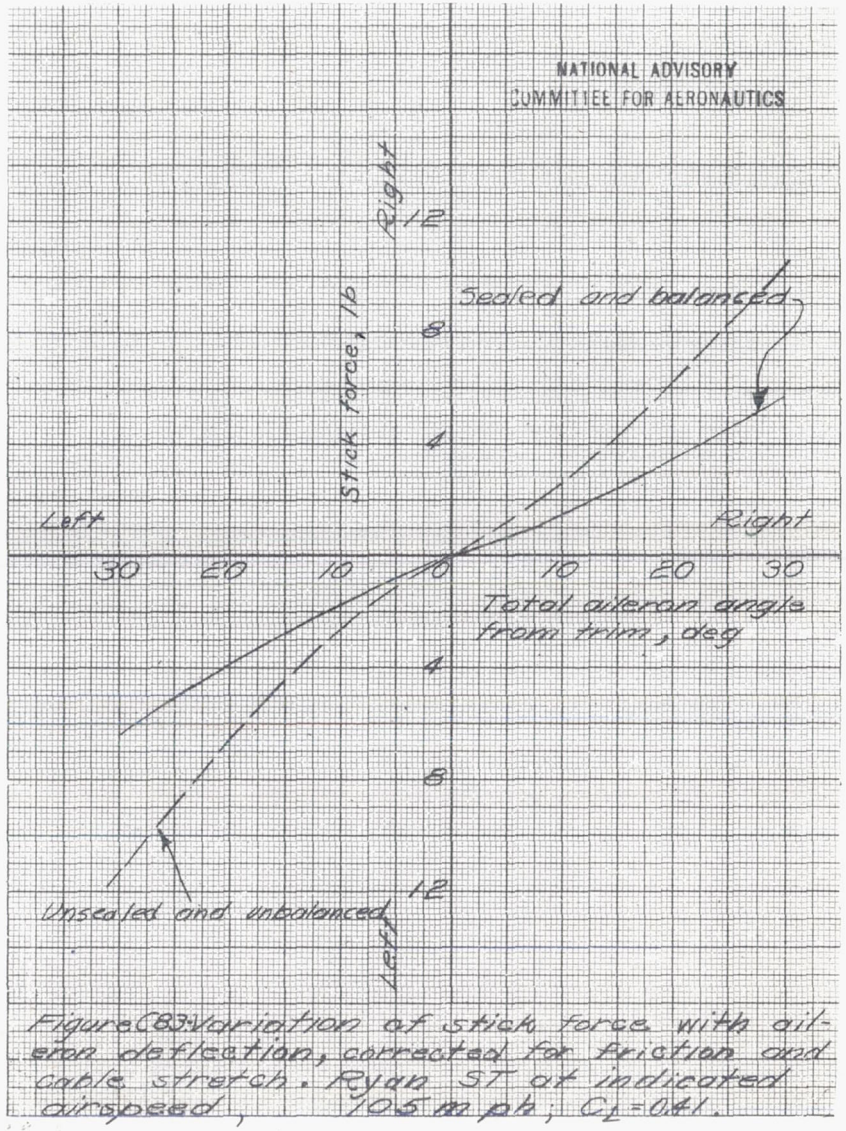

Figure C83. Variation of stick force with aileron deflection, corrected for friction and cable stretch. Ryan ST at indicated airspeed, 105 mph; C_L = 0.41.

Airplane C-XX

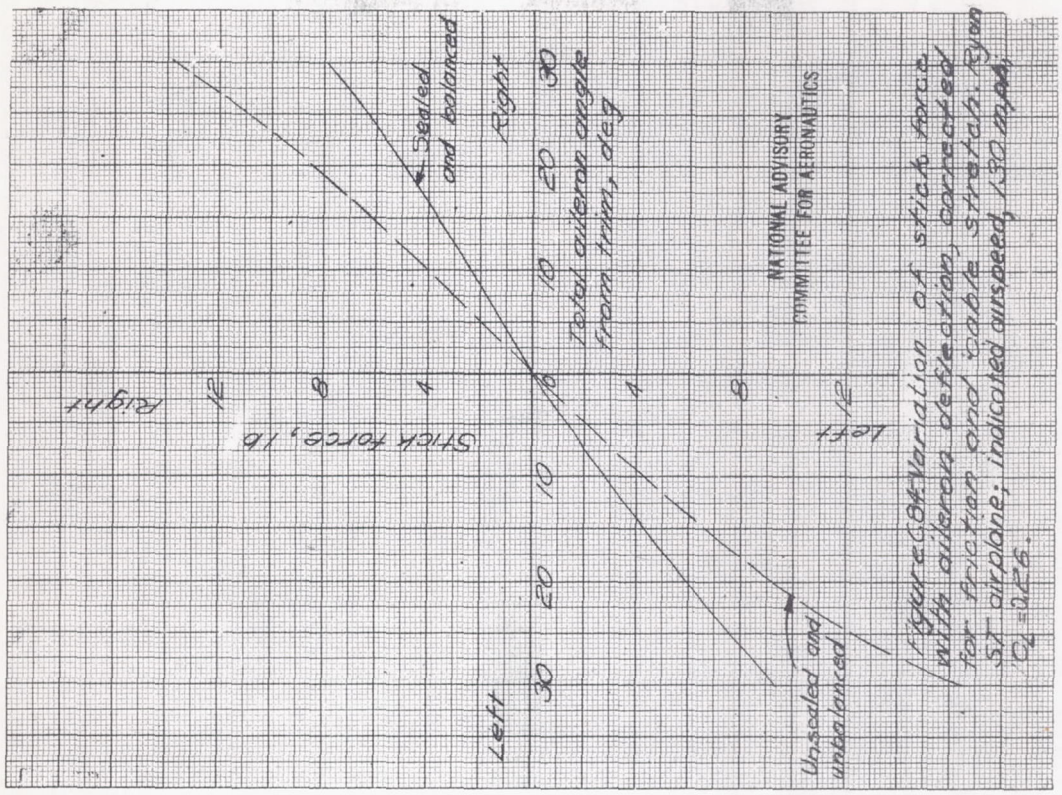

Figure C84.-Variation of stick forces with aileron deflection, corrected for friction and cable stretch. Ryan ST airplane; indicated airspeed, 130 mph; $C_L = 0.26$.

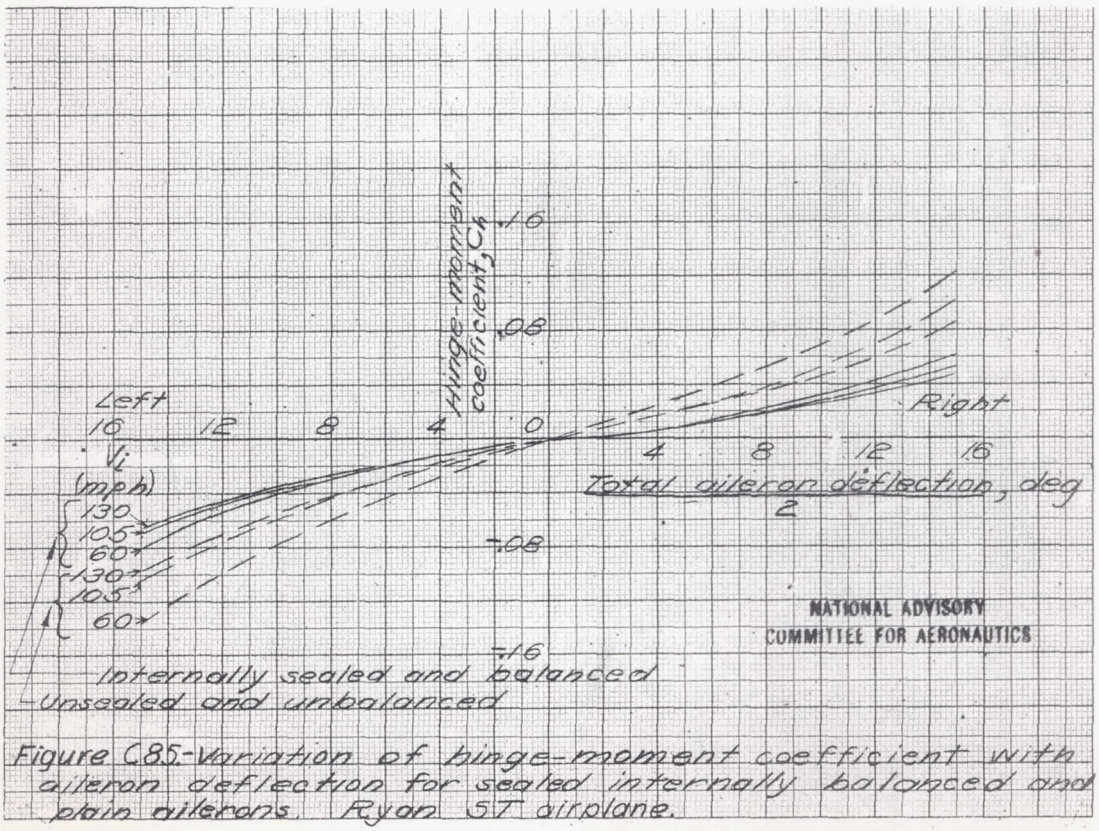

Figure C85.-Variation of hinge-moment coefficient with aileron deflection for sealed internally balanced and plain ailerons. Ryan ST airplane.

Airplane C-XXI

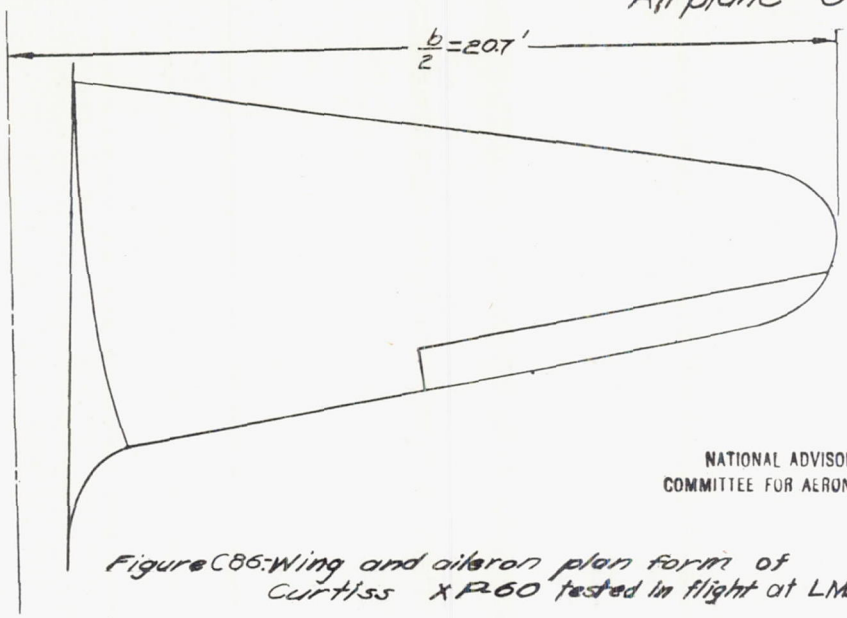

Figure C86: Wing and aileron plan form of Curtiss XP-60 tested in flight at LMAL.

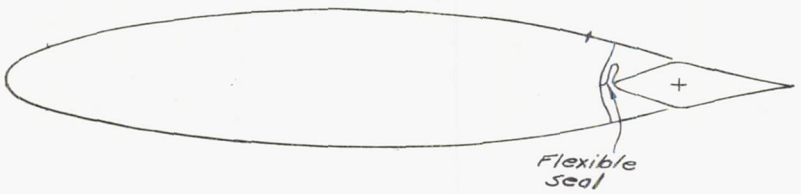

Figure C87:- Schematic view of the internally balanced and sealed aileron on low-drag wing of Curtiss XP-60.

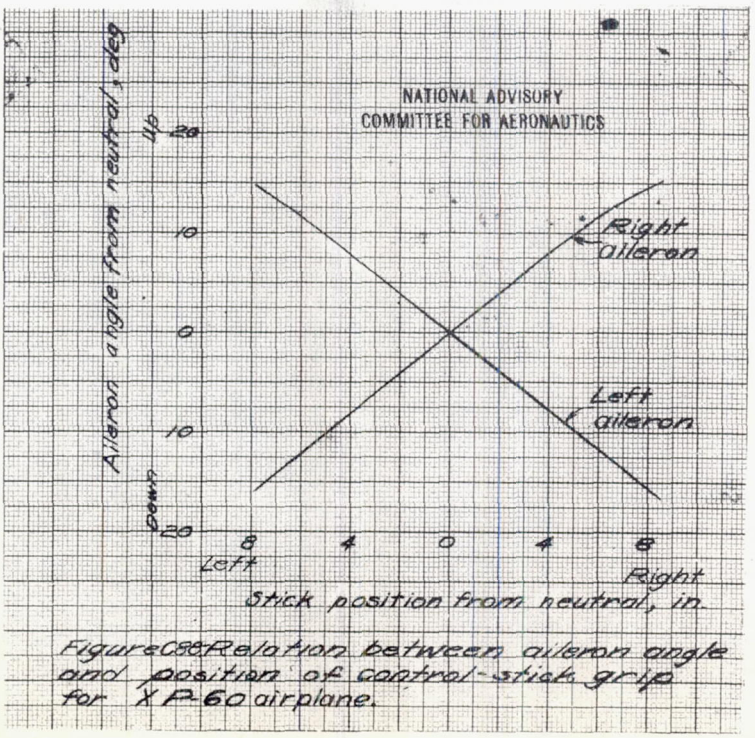

Figure C88: Relation between aileron angle and position of control-stick grip for XP-60 airplane.

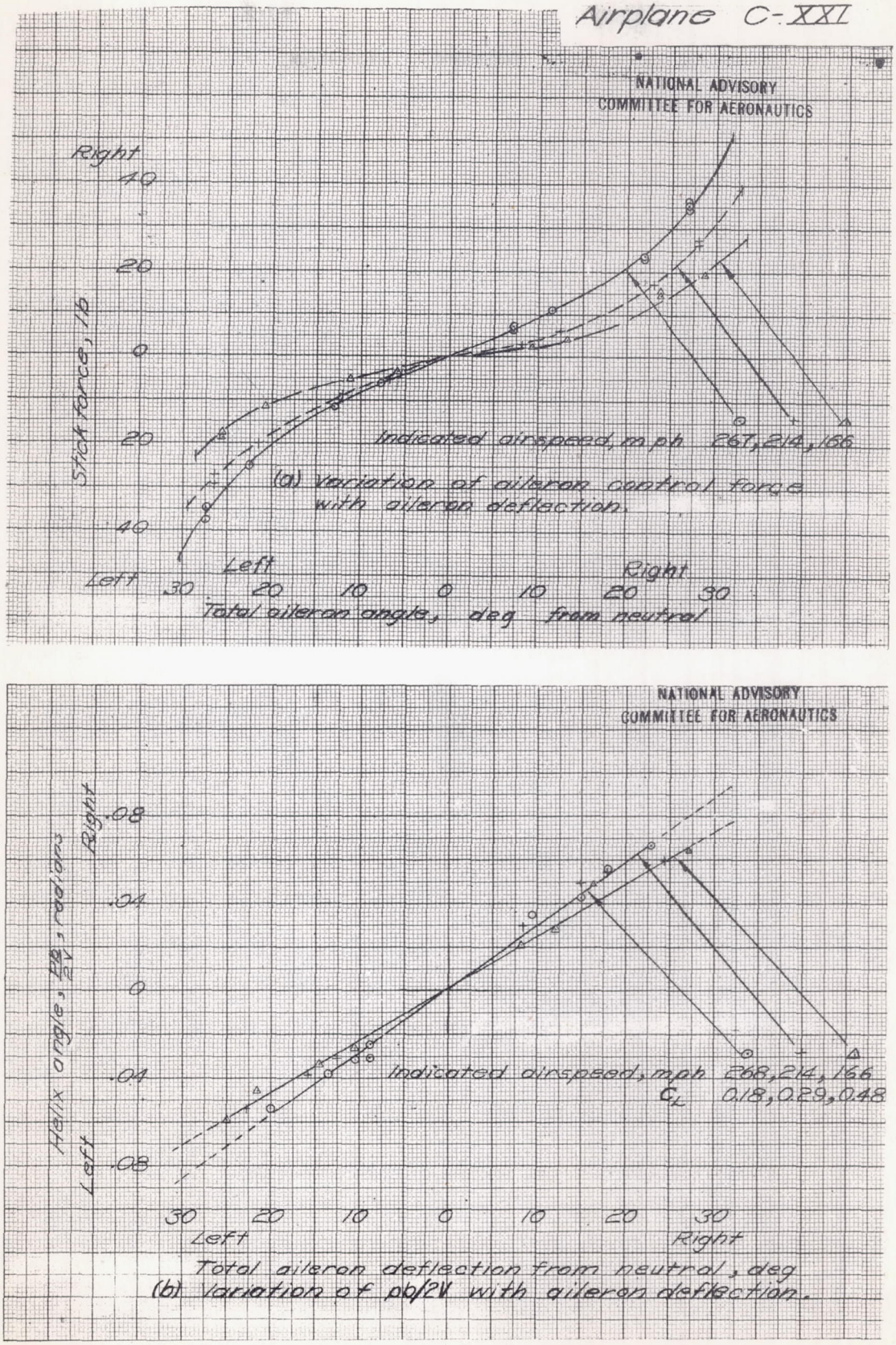

Figure C89.- Aileron control characteristics of Curtiss XP-60 airplane.

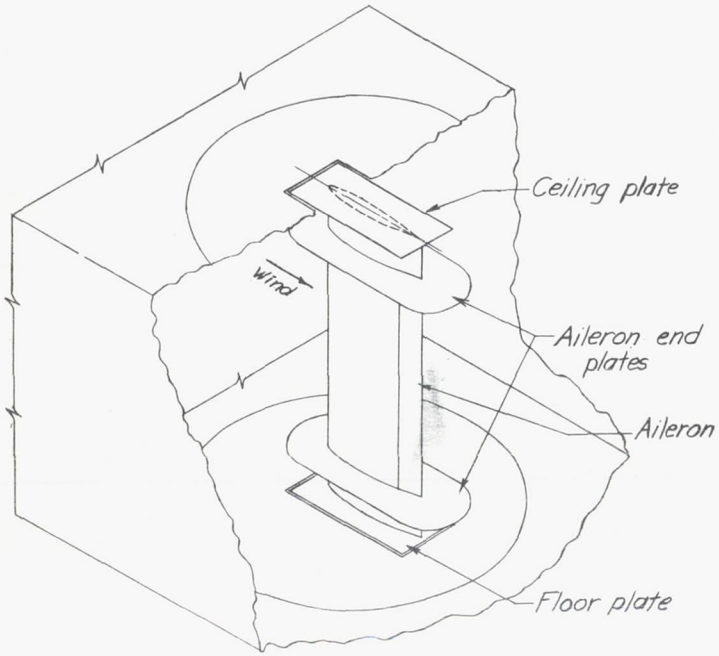

Figure D1.- Two-dimensional model installation of an NACA 66(215)-216, a=0.6 airfoil with a 0.15c and a 0.20c aileron. AAL 7-by 10-foot tunnel.

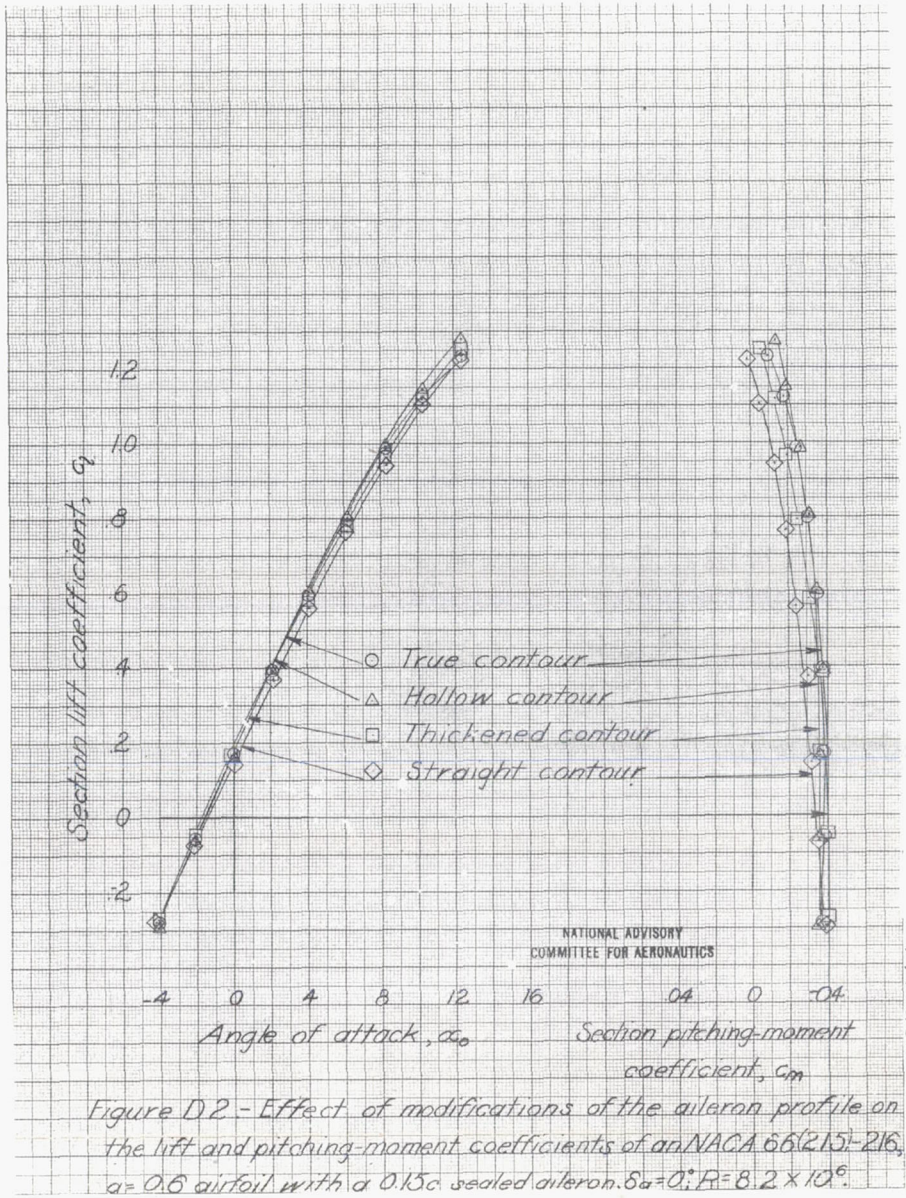

Figure D2 - Effect of modifications of the aileron profile on the lift and pitching-moment coefficients of an NACA 66(215)-216, a=0.6 airfoil with a 0.15c sealed aileron. δ_a=0°; R=8.2 x 10^6.

Model D-1

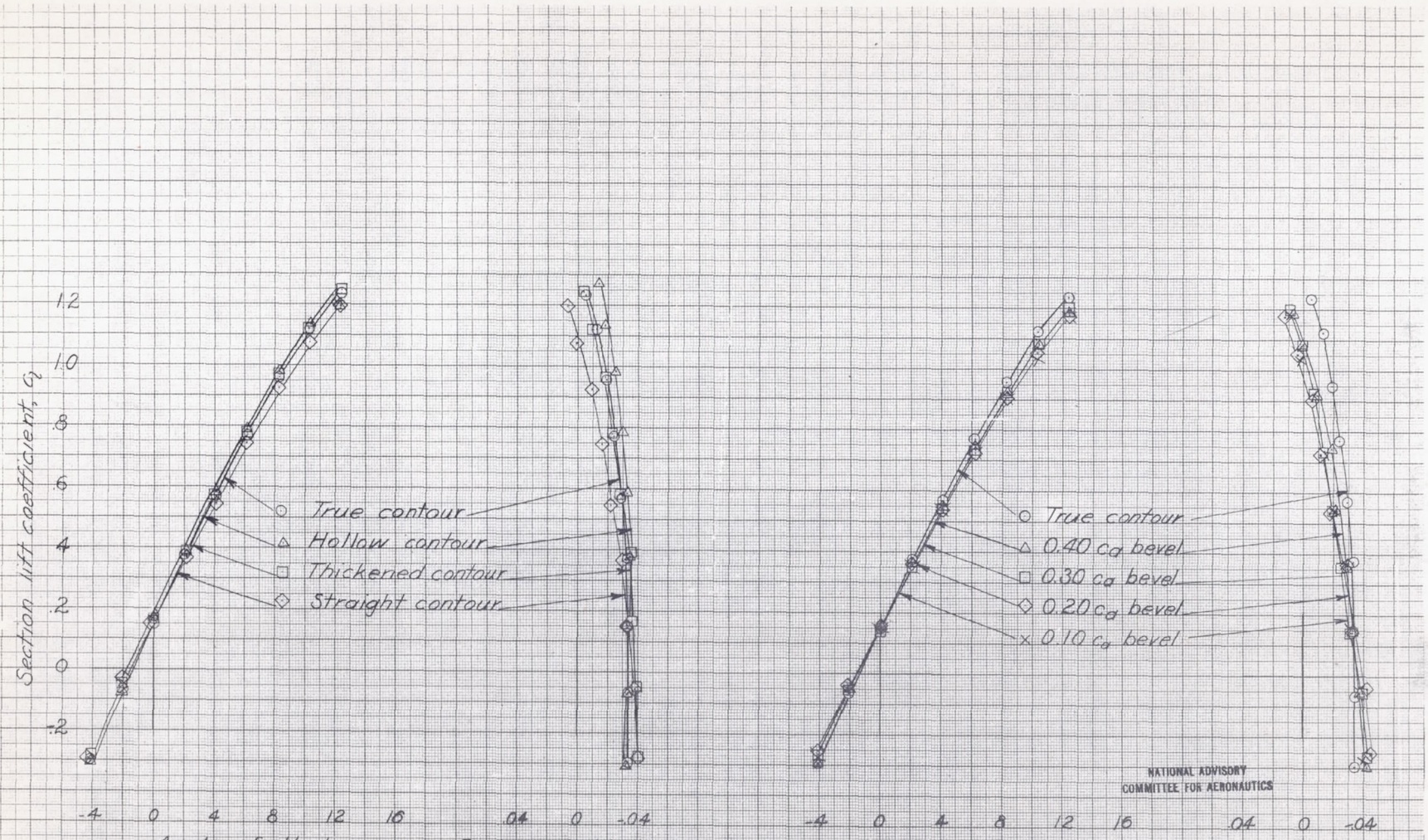

Figure D 13.- Effect of modifications of the aileron profile on the lift and pitching-moment coefficients of an NACA 66(215)-216, $a=0.6$ airfoil with a 0.20c sealed aileron. $\delta_a=0°$; $R=8.2\times10^6$.

Model D-I

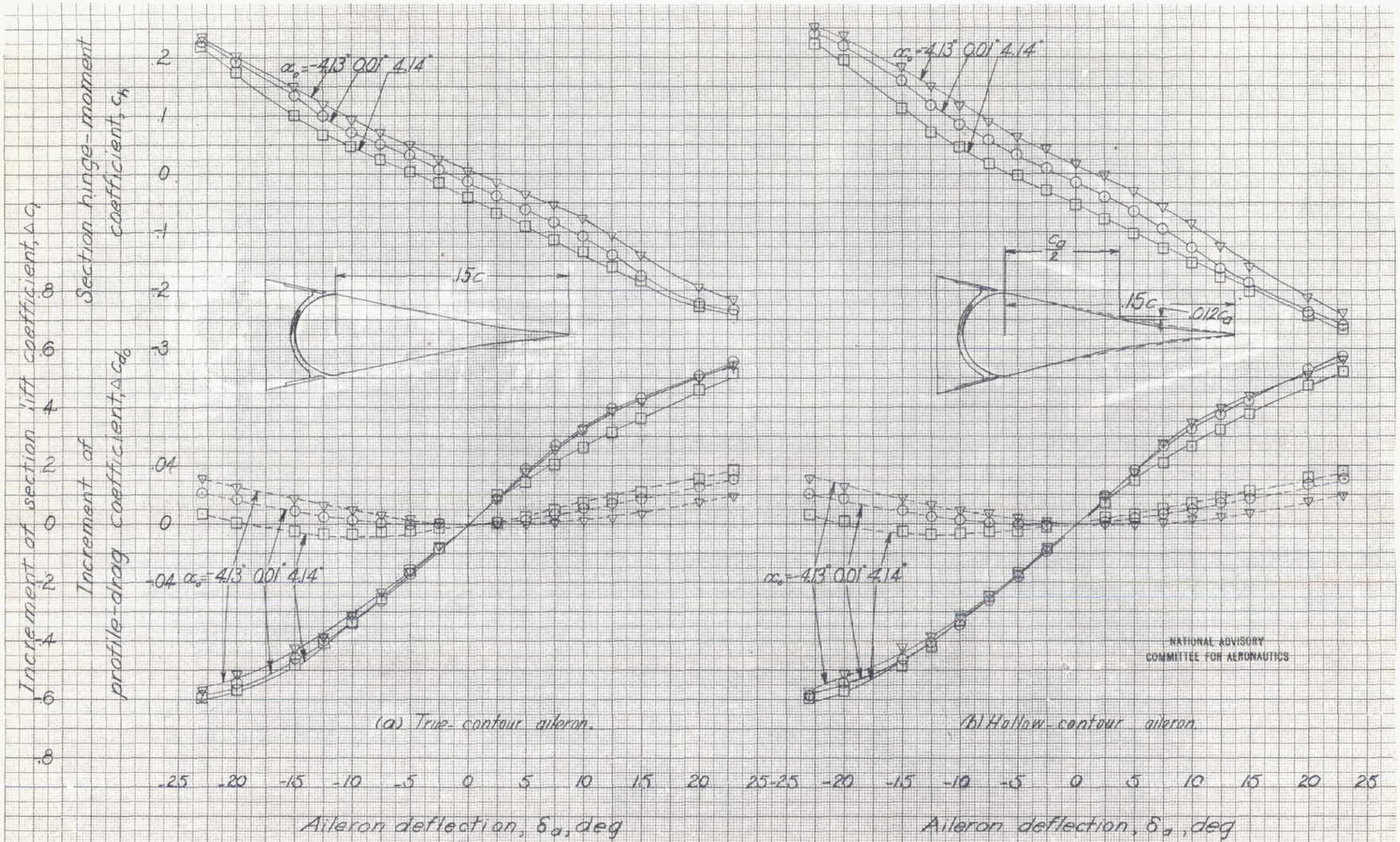

Figure D4.- Section aerodynamic characteristics of a 0.15c sealed aileron with various contour modifications on an NACA 66(215)-216, $a = 0.6$ airfoil. $R = 9.0 \times 10^6$.

Model D-1

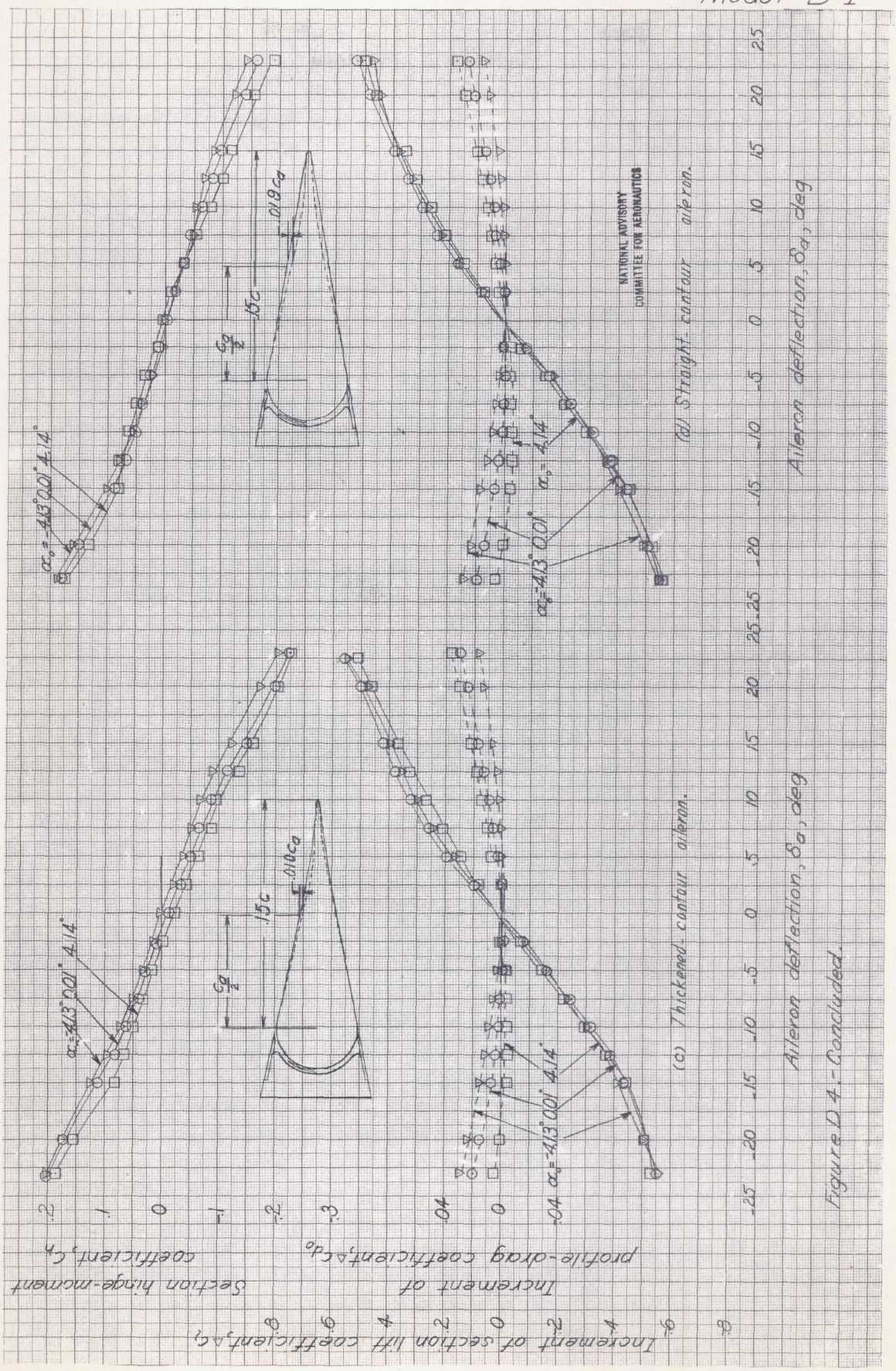

Figure D 4.- Concluded.

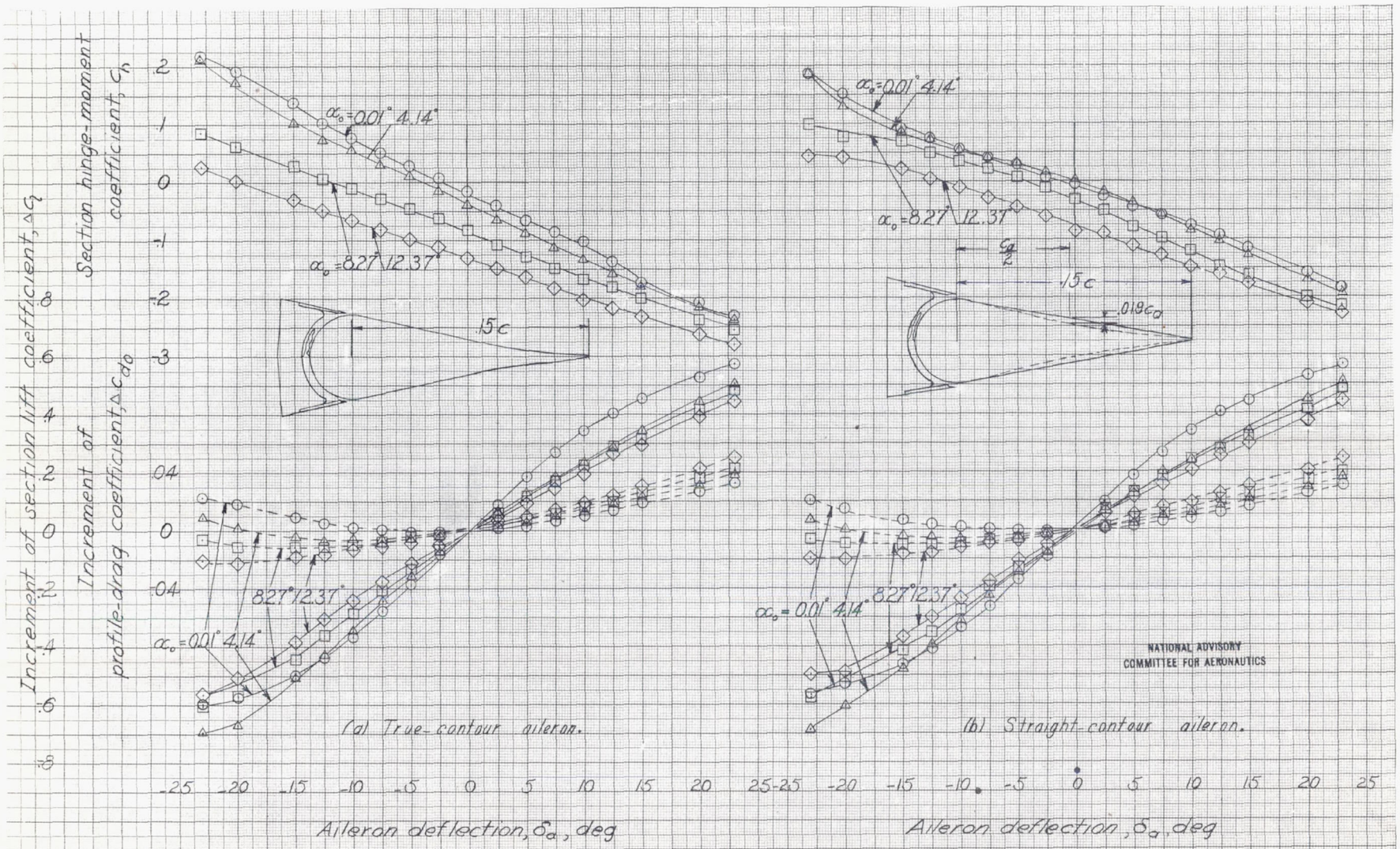

Figure D.5.- Section aerodynamic characteristics of a 0.15c sealed aileron with true contour and straight contour on an NACA 66(215)-216, $a=0.6$ airfoil. $R=3.8\times10^6$.

Model D-I

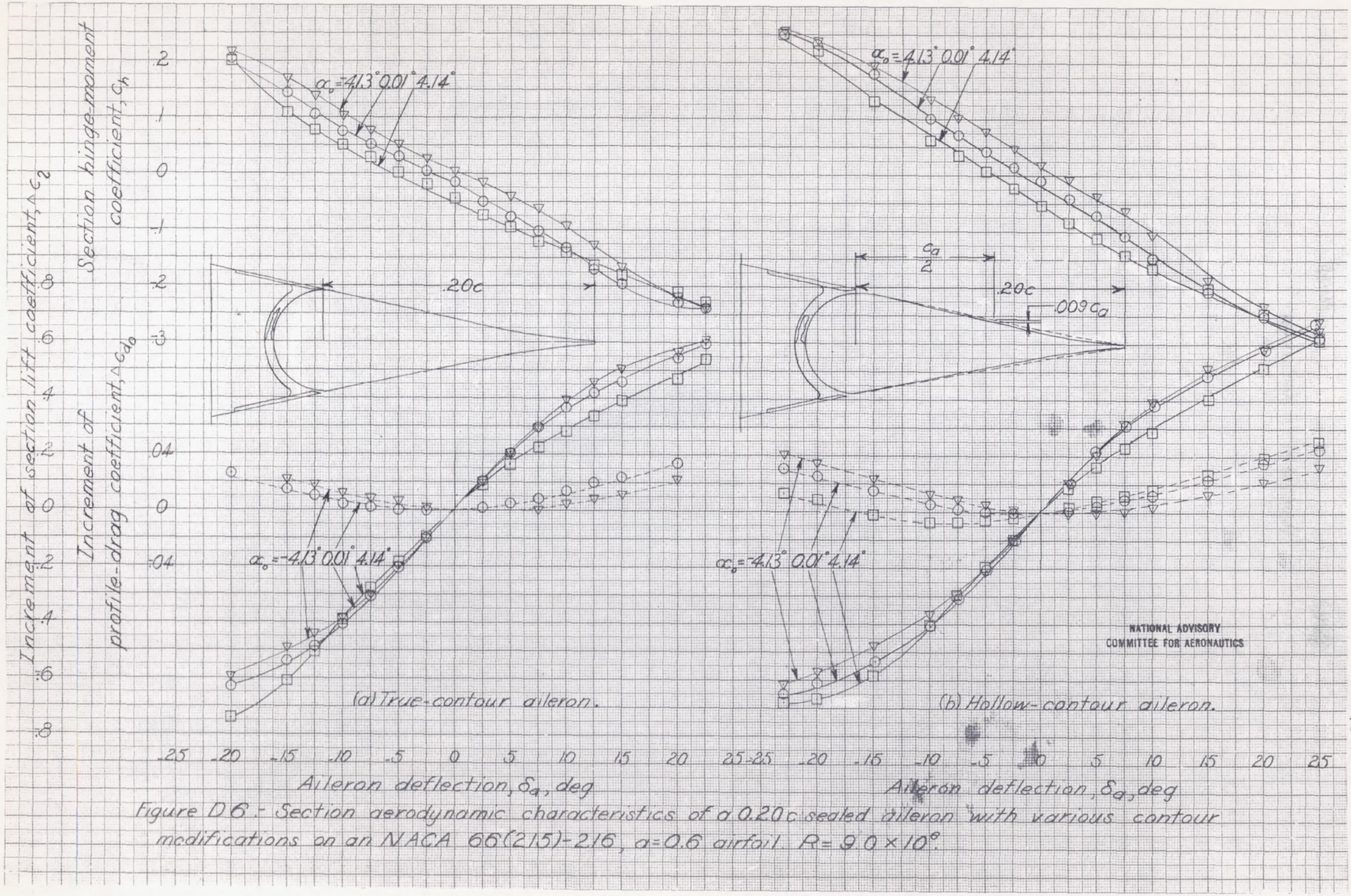

Figure D6.- Section aerodynamic characteristics of a 0.20c sealed aileron with various contour modifications on an NACA 66(215)-216, $a = 0.6$ airfoil. $R = 9.0 \times 10^6$.

Model D-I

Model D-I

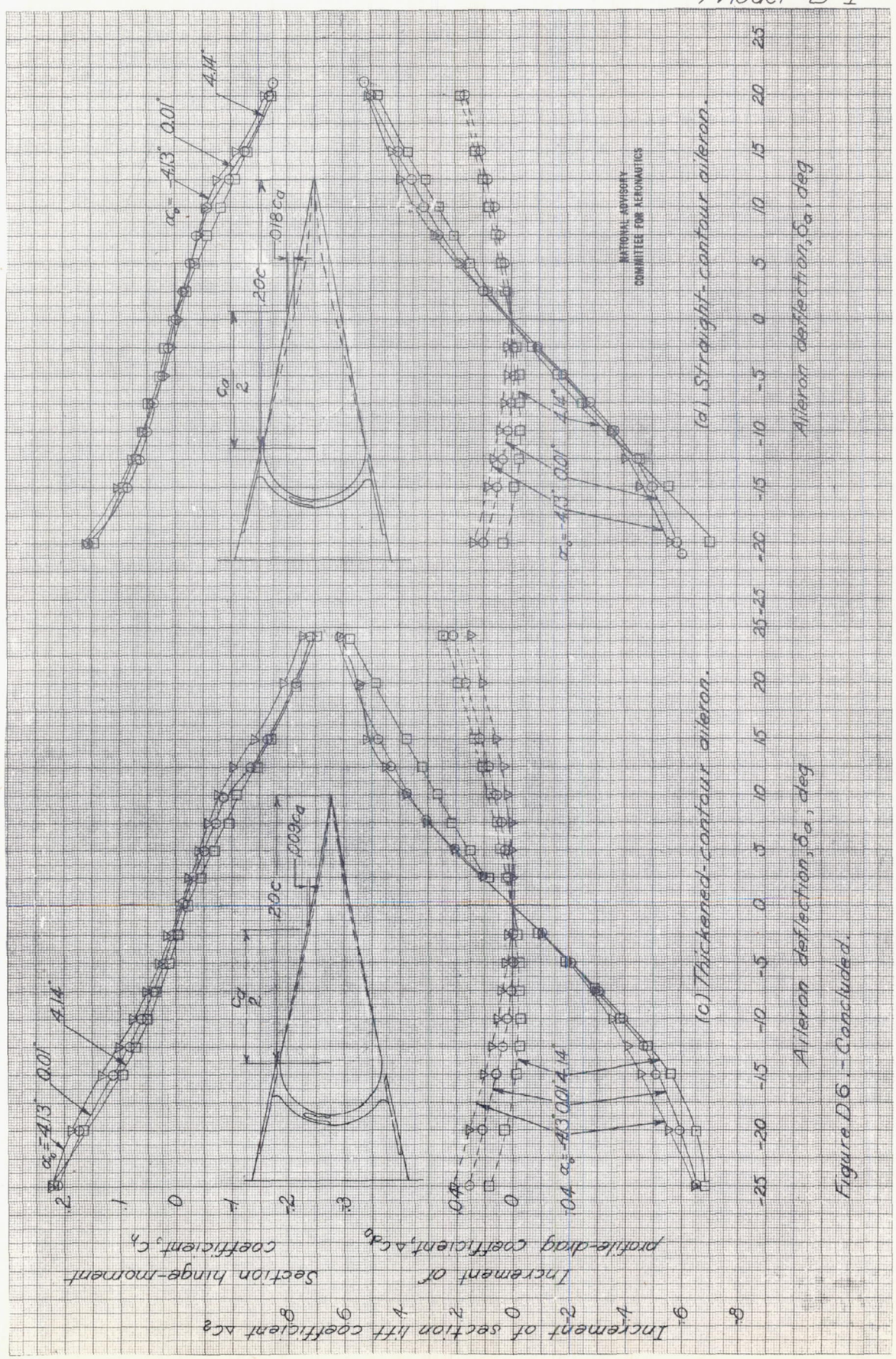

Figure D6.- Concluded.

Model D-I

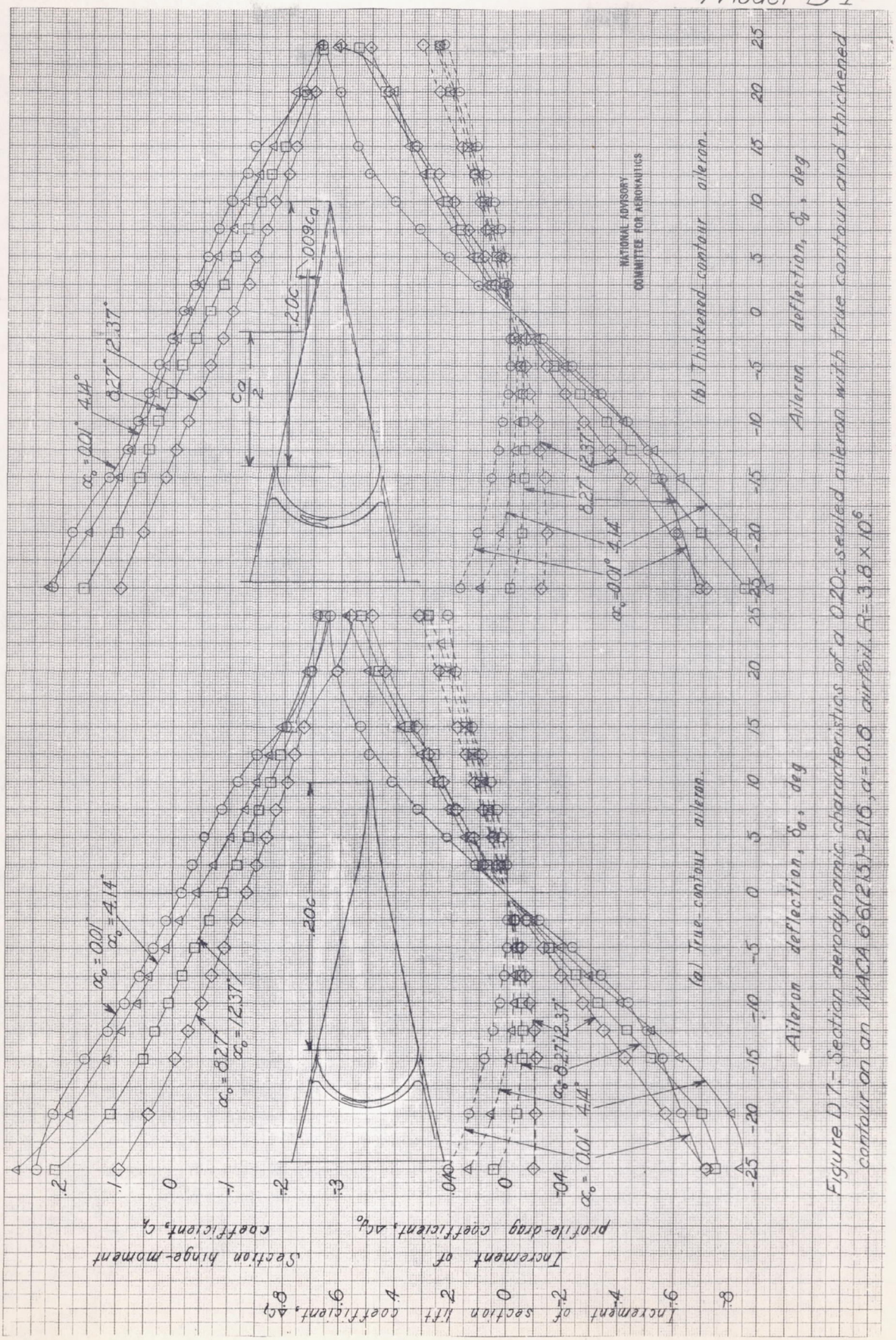

Figure D 1.- Section aerodynamic characteristics of a 0.20c sealed aileron with true contour and thickened contour on an NACA 66(215)-216, $a = 0.8$ airfoil. $R = 3.8 \times 10^6$.

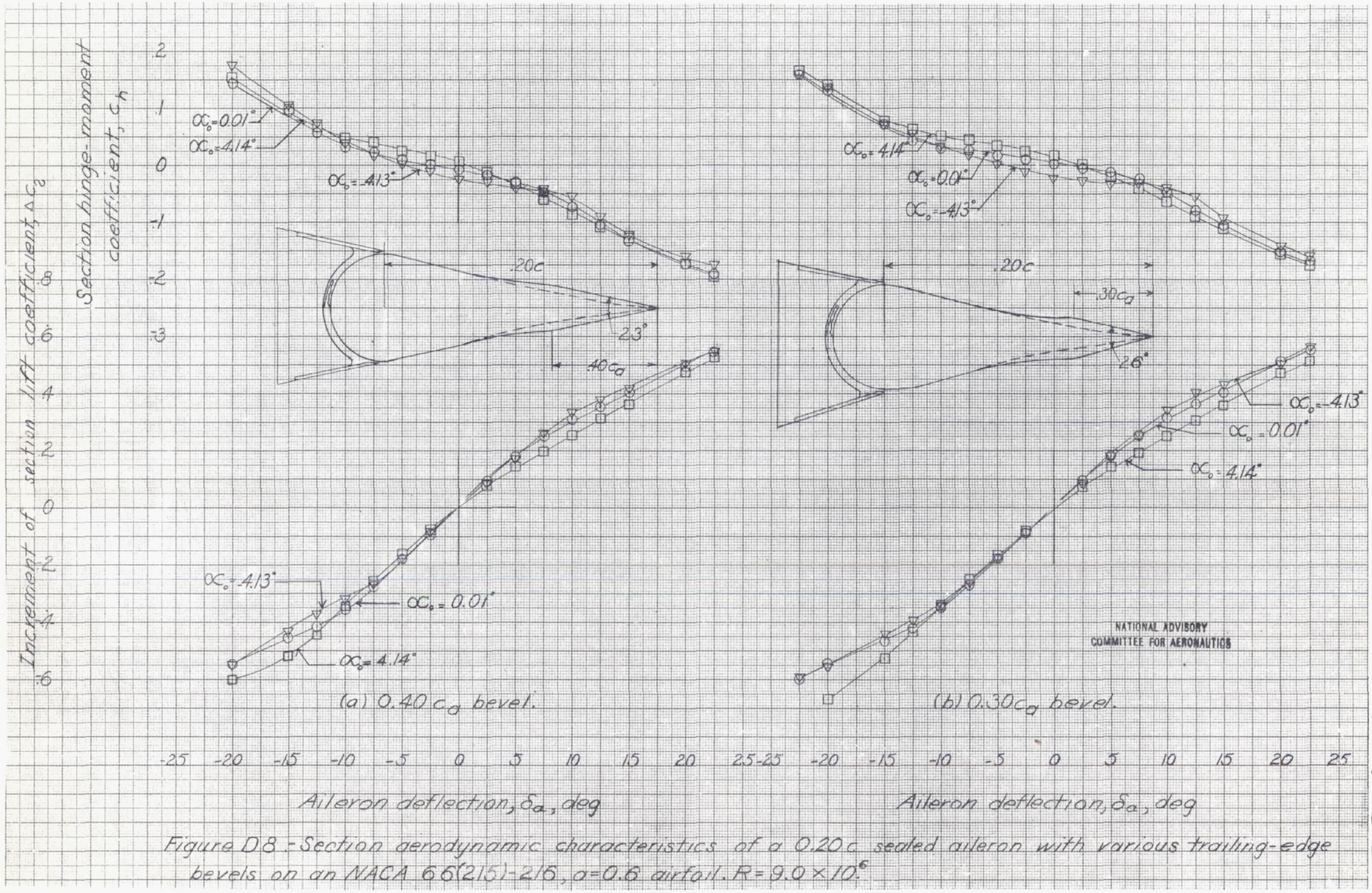

Figure D.8 - Section aerodynamic characteristics of a 0.20c sealed aileron with various trailing-edge bevels on an NACA 66(215)-216, a=0.6 airfoil. R = 9.0 × 10⁶.

Model D-I

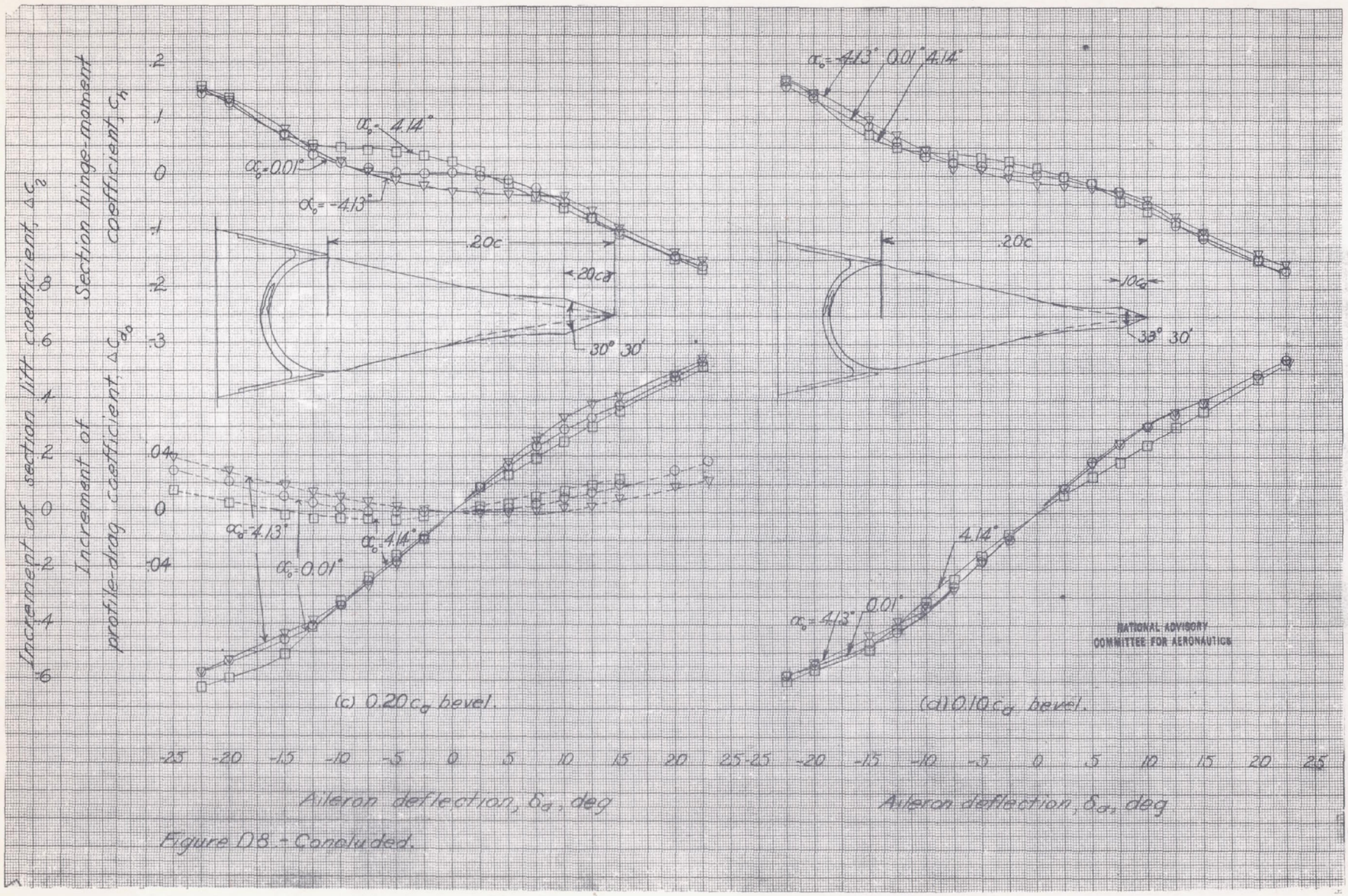

Figure 18.- Concluded.

Model D-I

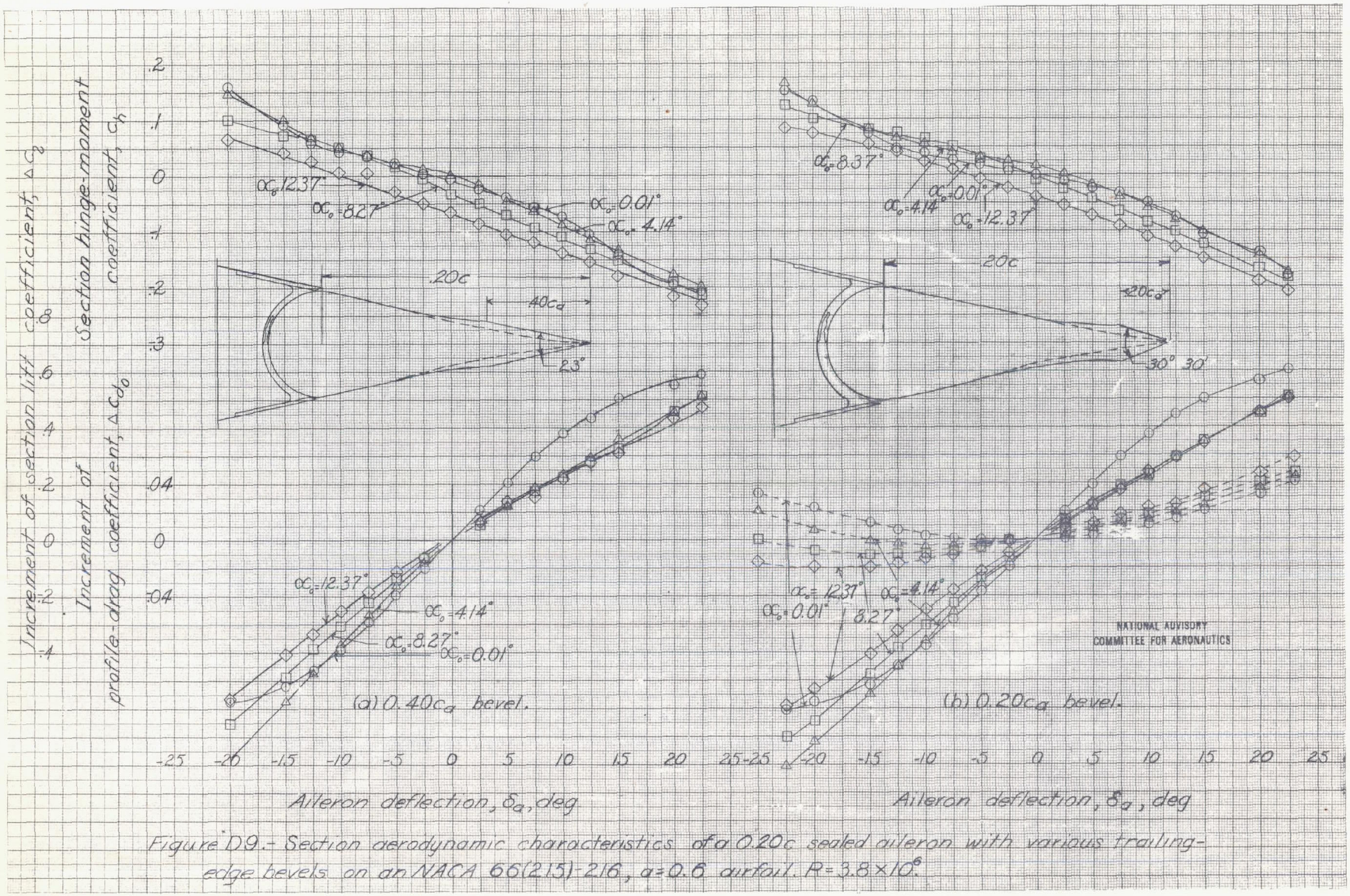

Figure D9.- Section aerodynamic characteristics of a 0.20c sealed aileron with various trailing-edge bevels on an NACA 66(215)-216, a=0.6 airfoil. $R = 3.8 \times 10^6$.

Model D-I

Model D-II

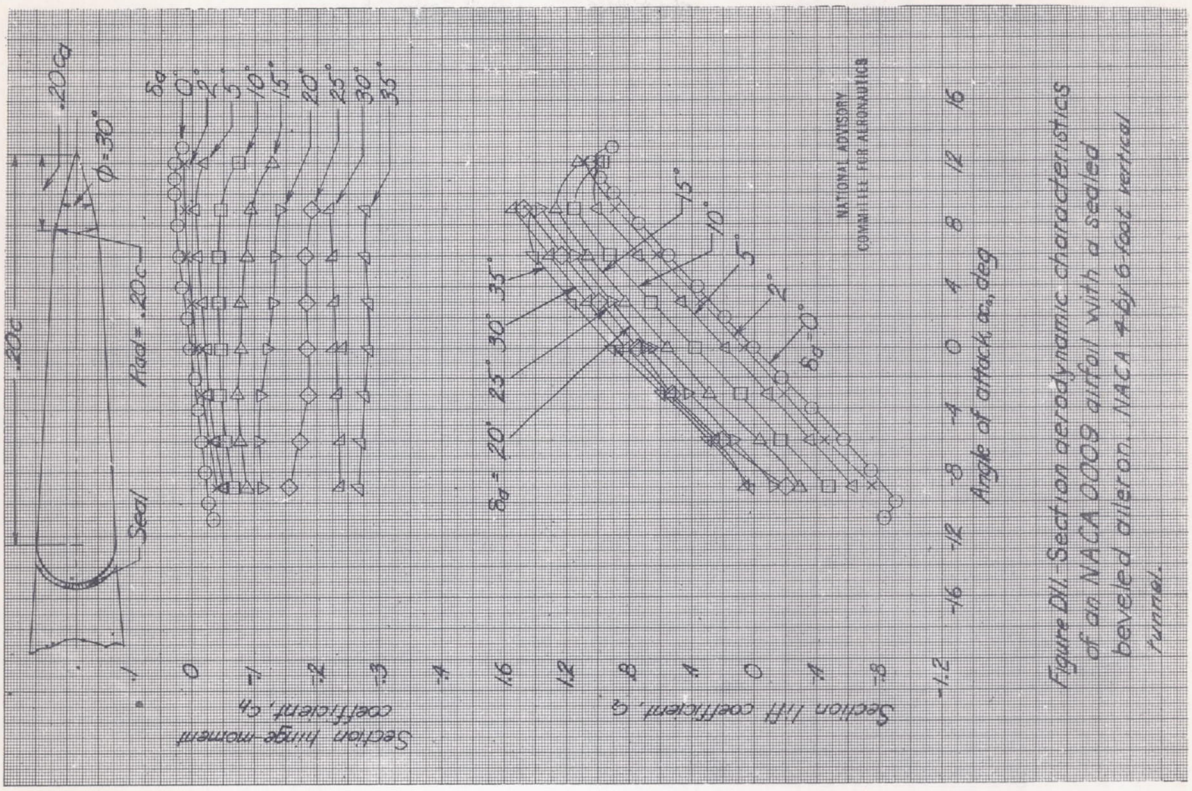

Figure DII.-Section aerodynamic characteristics of an NACA 0009 airfoil with a sealed beveled aileron. NACA 4-by-6-foot vertical tunnel.

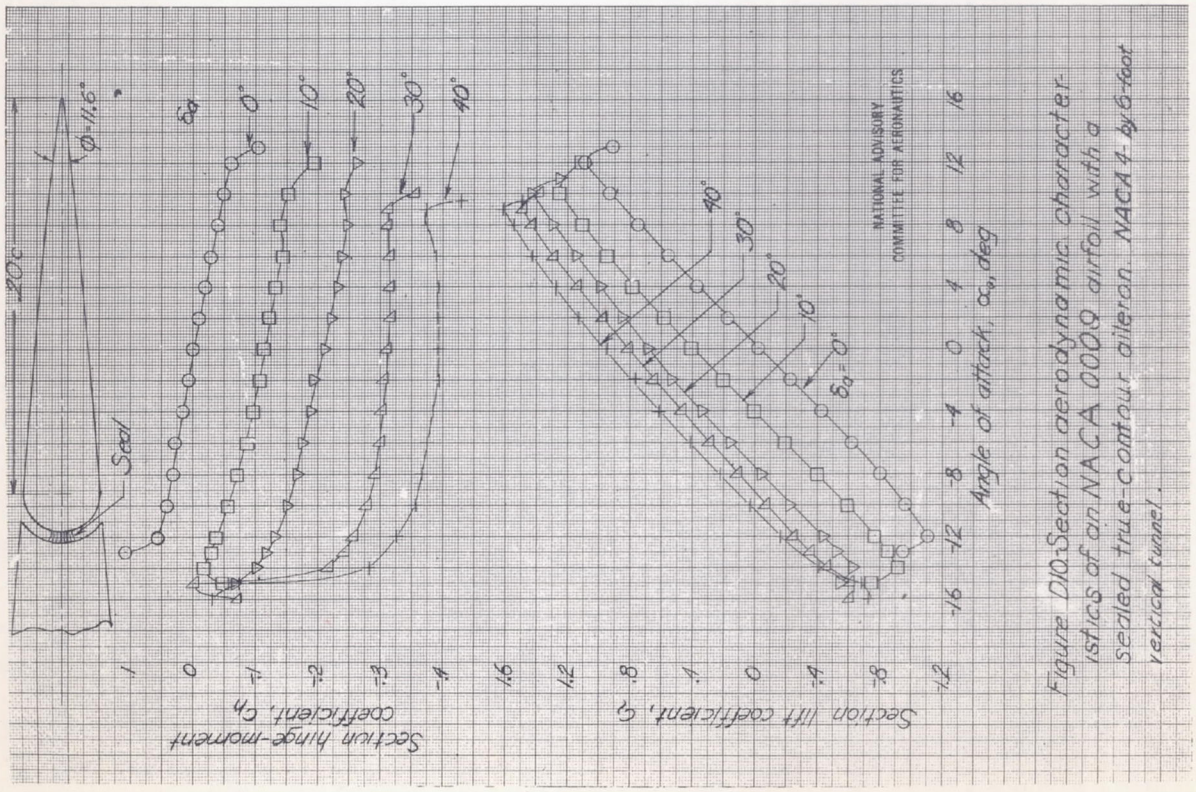

Figure DIO.-Section aerodynamic characteristics of an NACA 0009 airfoil with a sealed true-contour aileron. NACA 4-by-6-foot vertical tunnel.

Model D-II

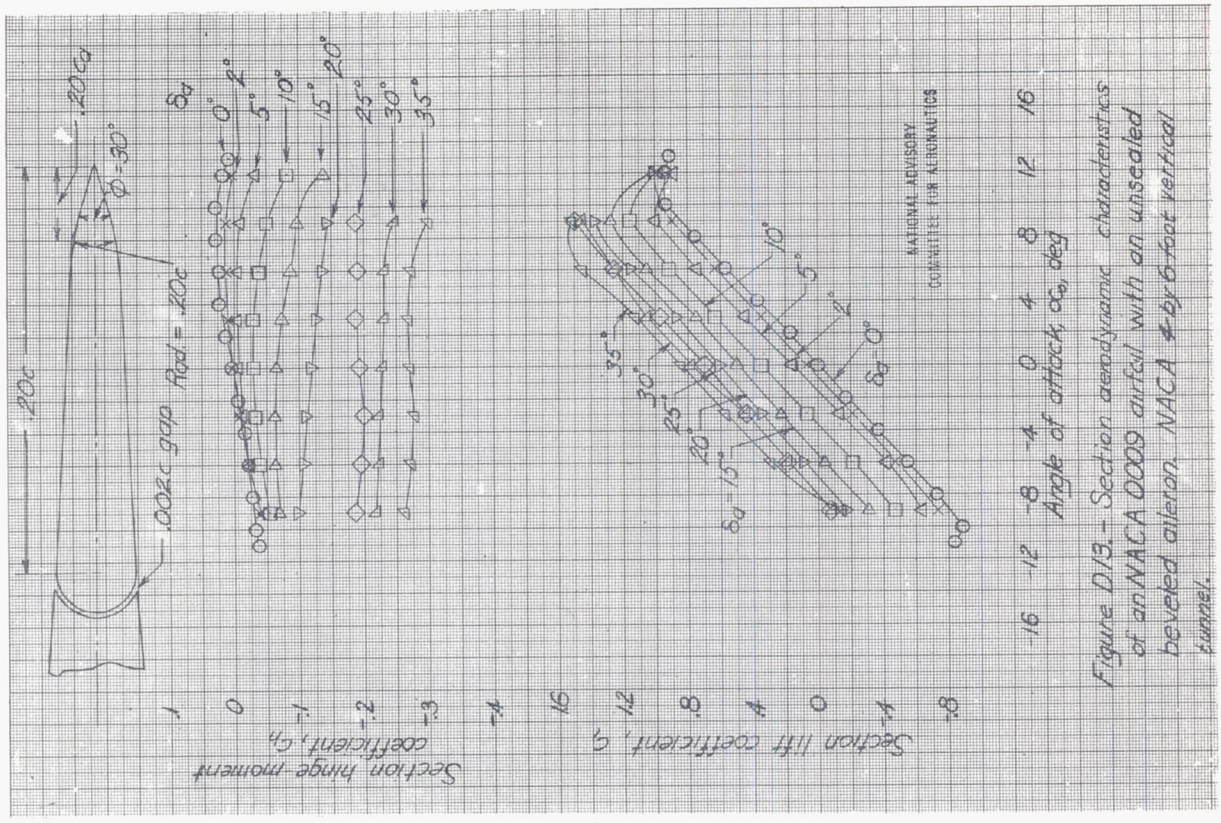

Figure D13.- Section aerodynamic characteristics of an NACA 0009 airfoil with an unsealed beveled aperon. NACA 4-by-6-foot vertical tunnel.

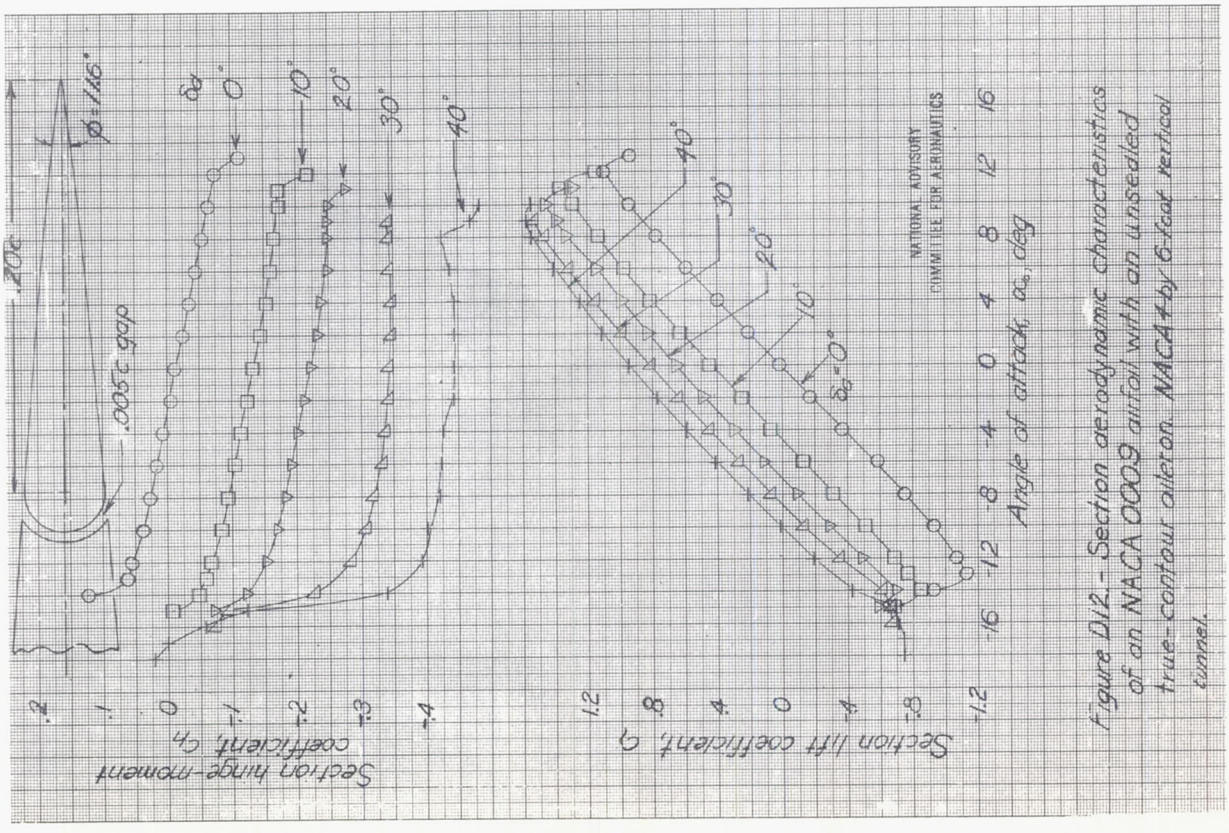

Figure D12.- Section aerodynamic characteristics of an NACA 0009 airfoil with an unsealed true-contour aperon. NACA 4-by-6-foot vertical tunnel.

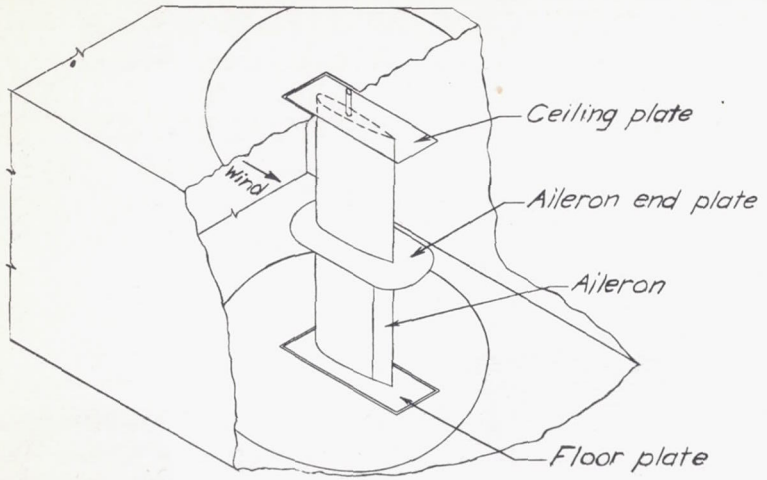

Figure D 14. - Two-dimensional model installation and airfoil section with 0.20c aileron. AAL 7-by 10-foot tunnel.

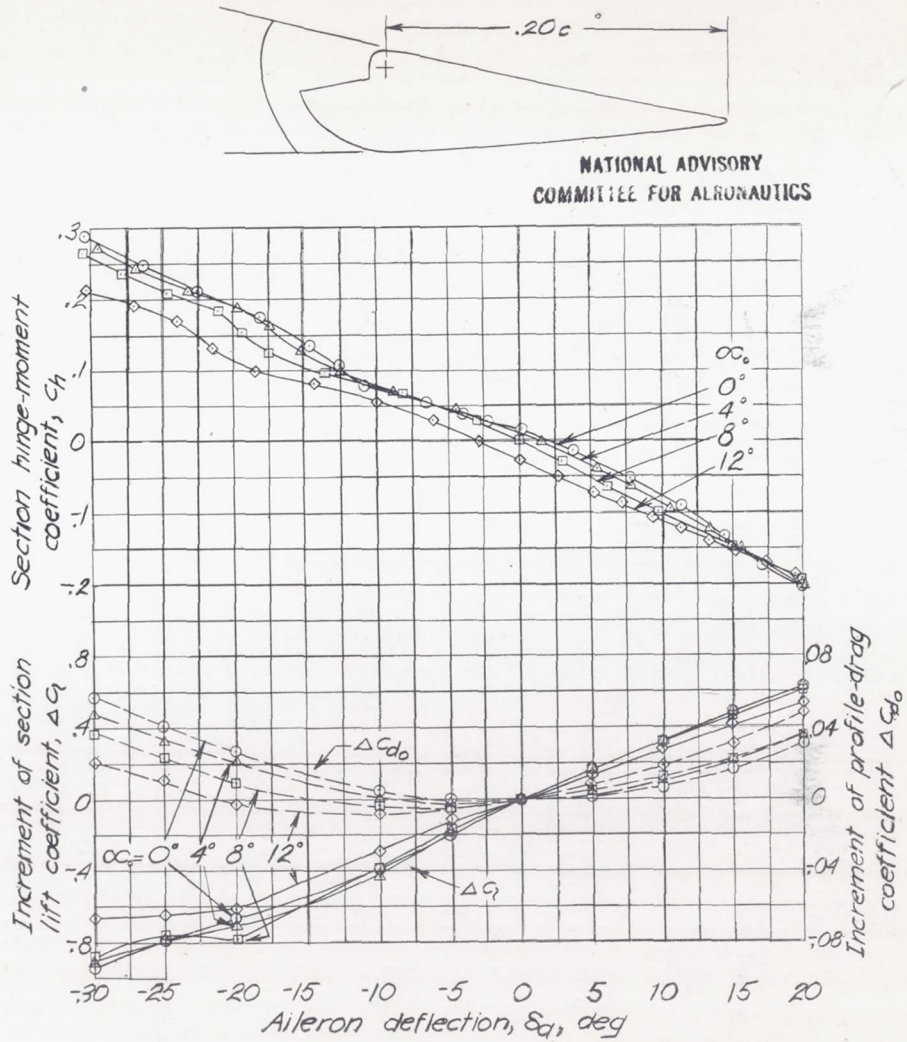

Figure D 15. - Section aerodynamic characteristics of an unsealed true-contour aileron.

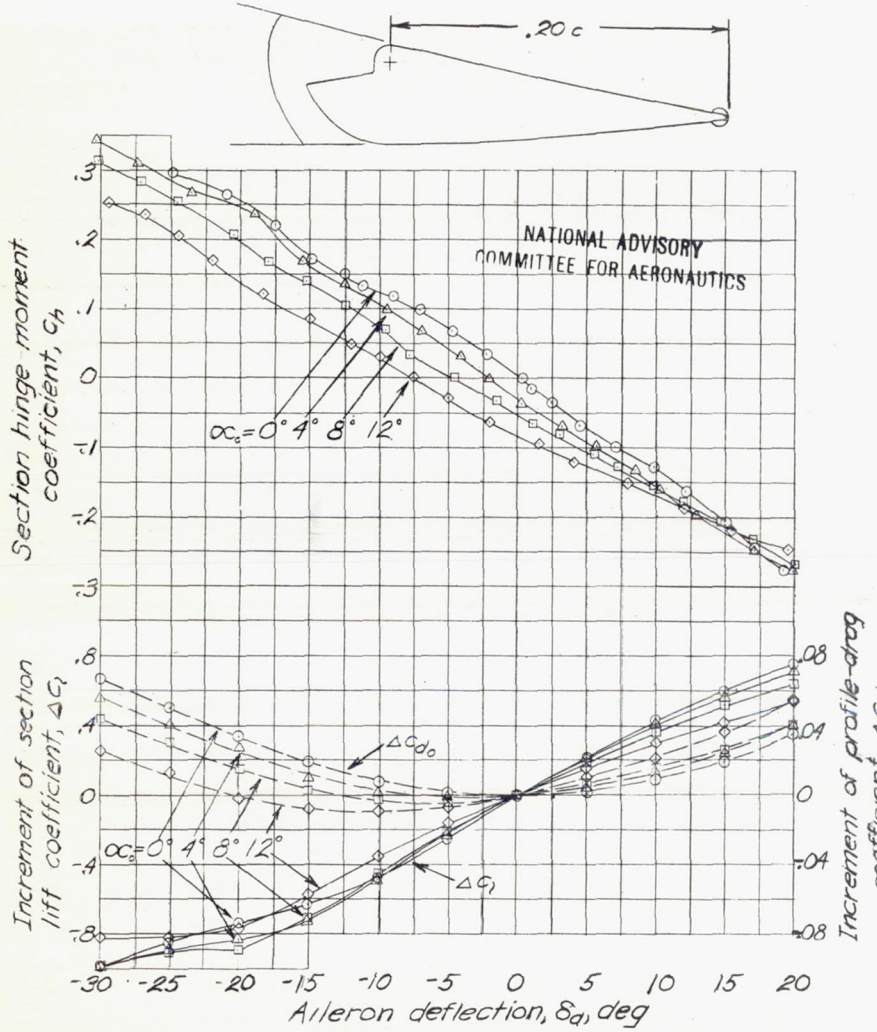

Figure D16.-Section aerodynamic characteristics of an unsealed true-contour aileron with beaded trailing edge.

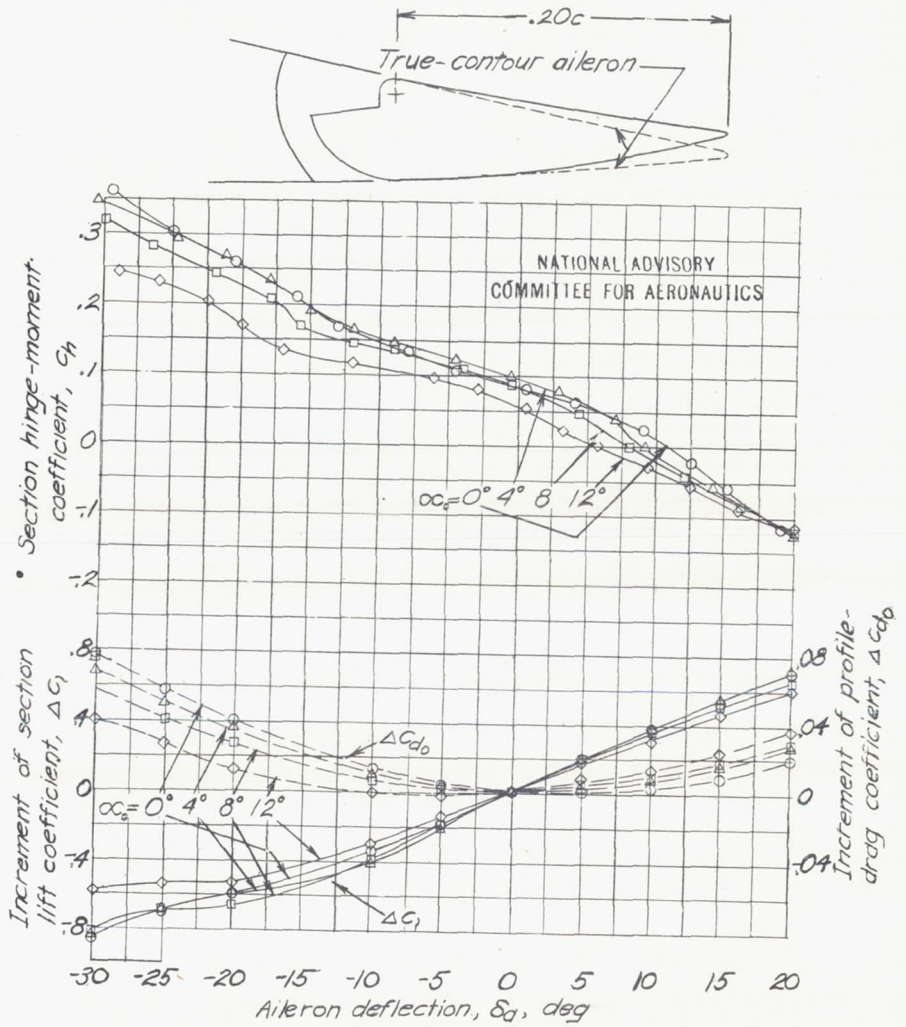

Figure D17.-Section aerodynamic characteristics of an unsealed aileron with reflexed trailing edge.

Model D-IV

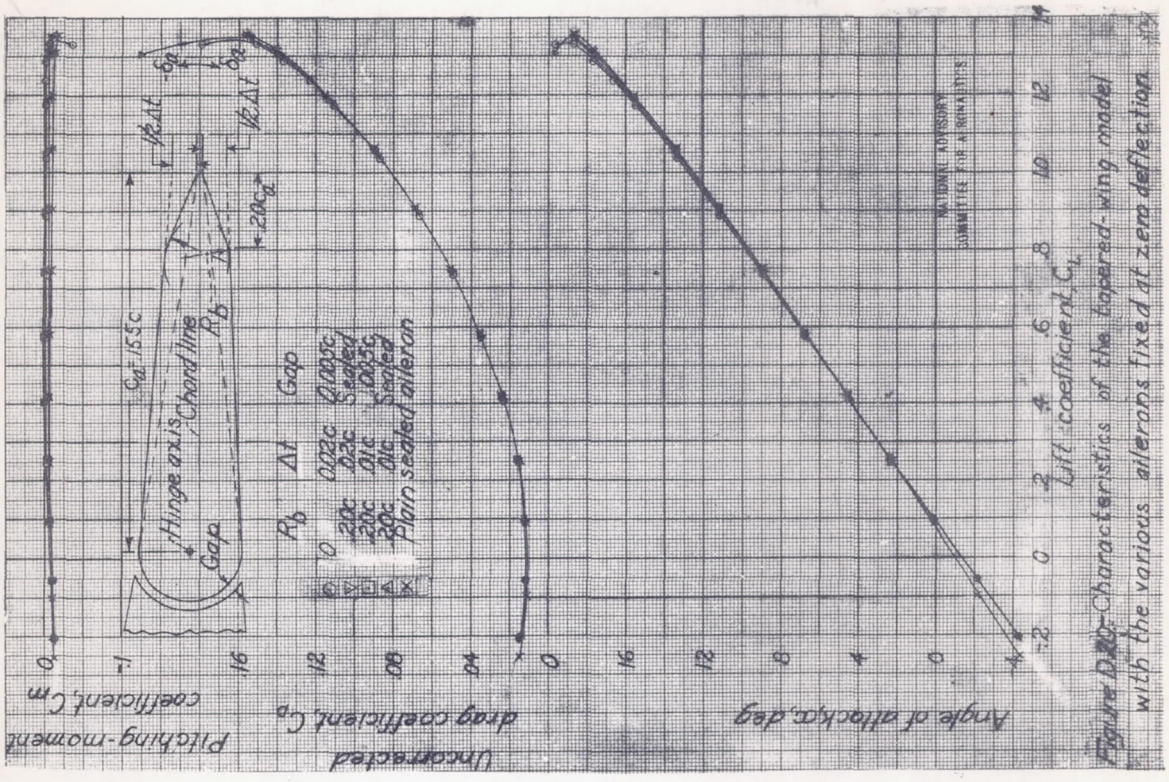

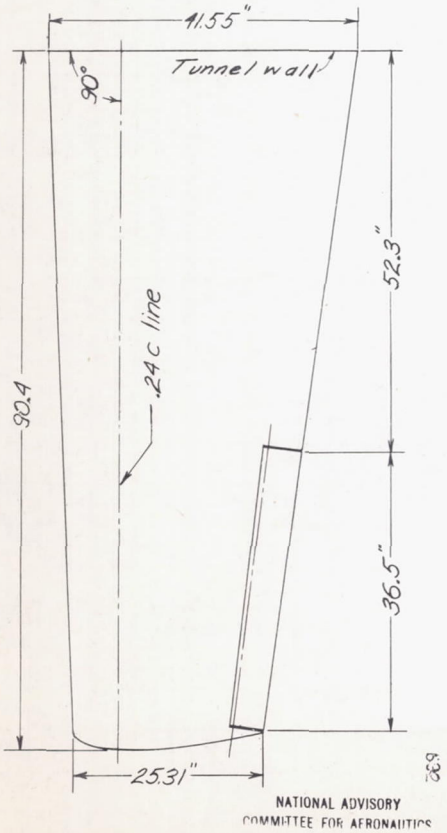

Figure D18.- Semispan model of tapered wing. LMAL 7-by 10-foot tunnel.

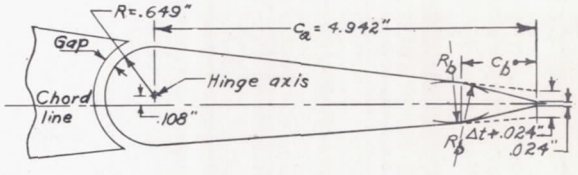

(a) Inboard end; wing chord c=31.986".

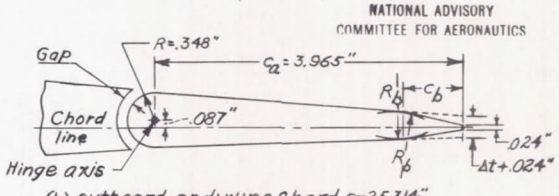

(b) outboard end; wing chord c=25.314".

Trailing-edge angle, deg	c_a percent c		Δt, percent c
	Inboard	Outboard	
40.2	20	20	2.0
27.0	32.6	35.5	2.0
27.0	20	20	1.0
19.0	32.6	35.5	1.0

Gap and R_b were varied during tests and are noted on figures that show test results

Figure D19.- The 0.155c by 0.405 b/2 beveled ailerons tested on the tapered-wing model.

Model D-IV

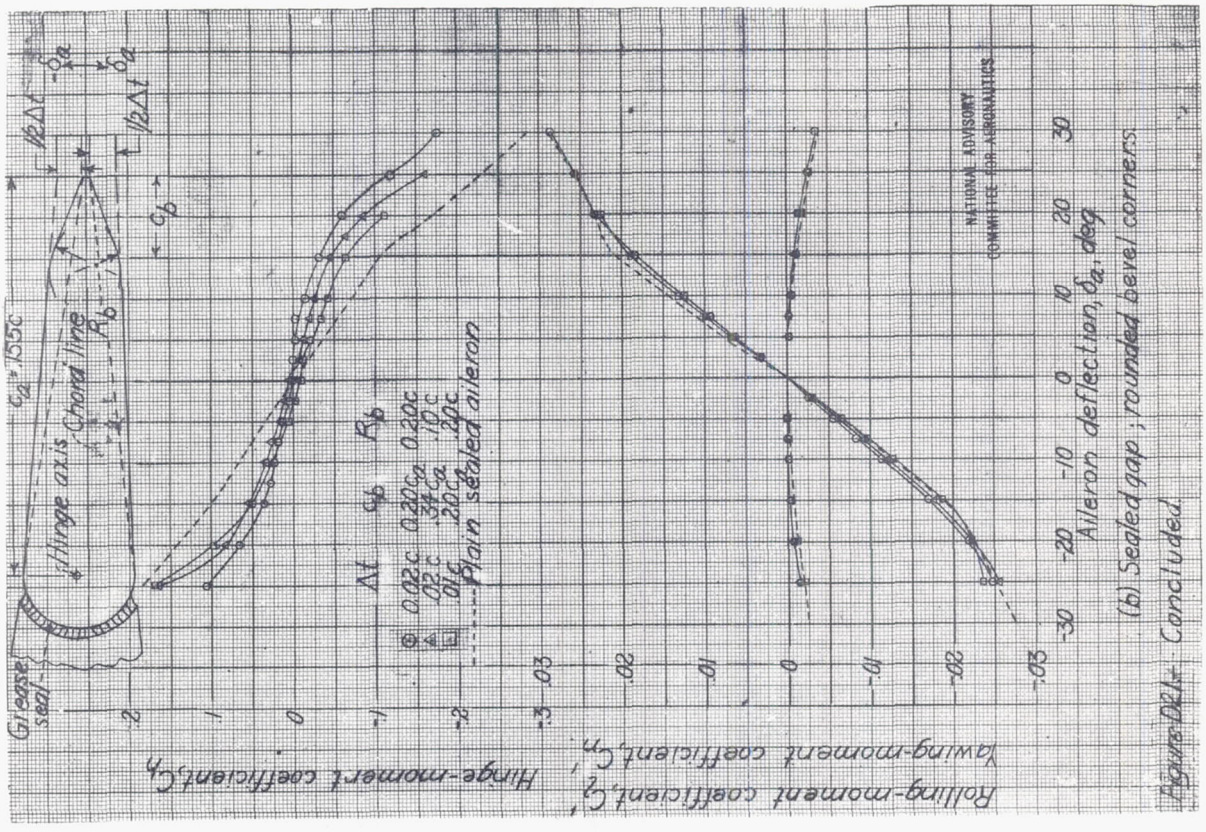

Figure D24.- Concluded.
(b) Sealed gap; rounded bevel corners.

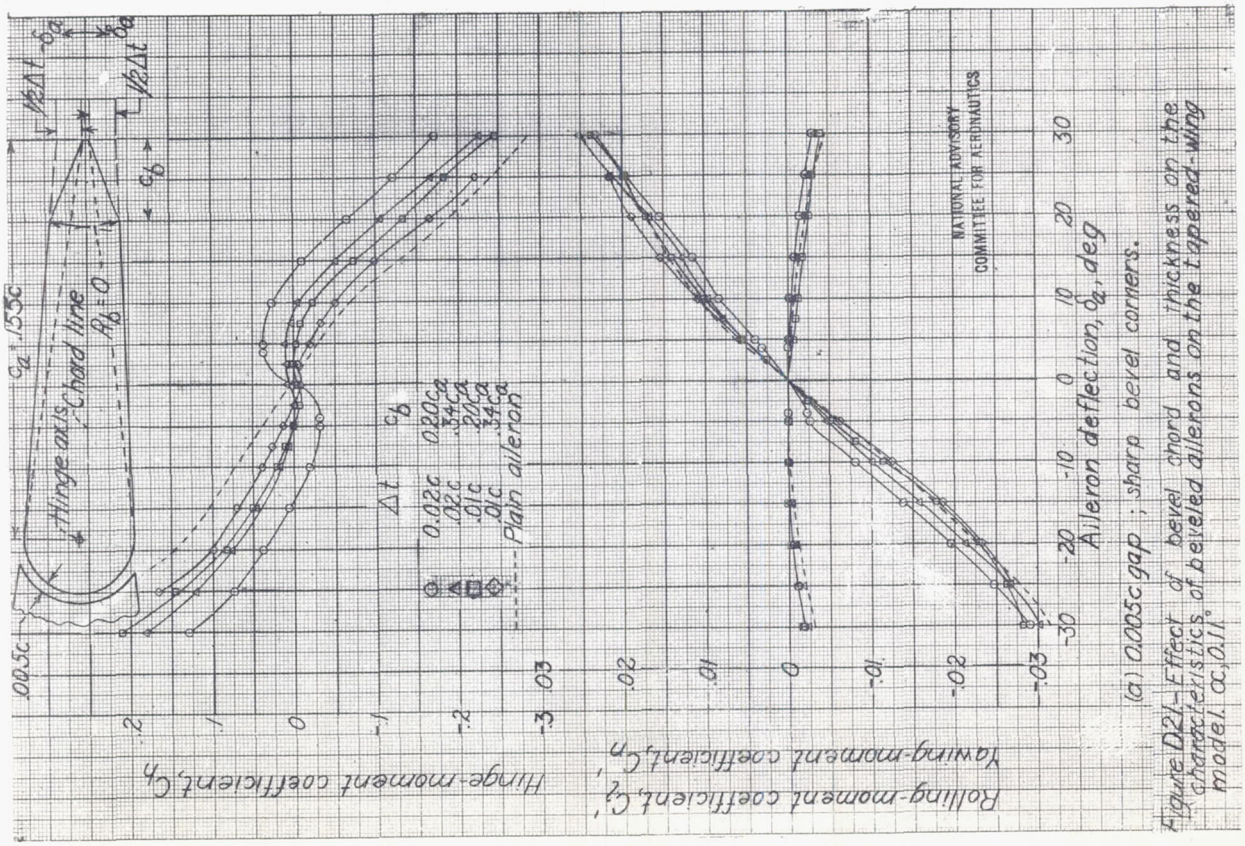

Figure D25.- Effect of bevel chord and thickness on the characteristics of beveled ailerons on the tapered-wing model. α, 0.11°.
(a) 0.005c gap; sharp bevel corners.

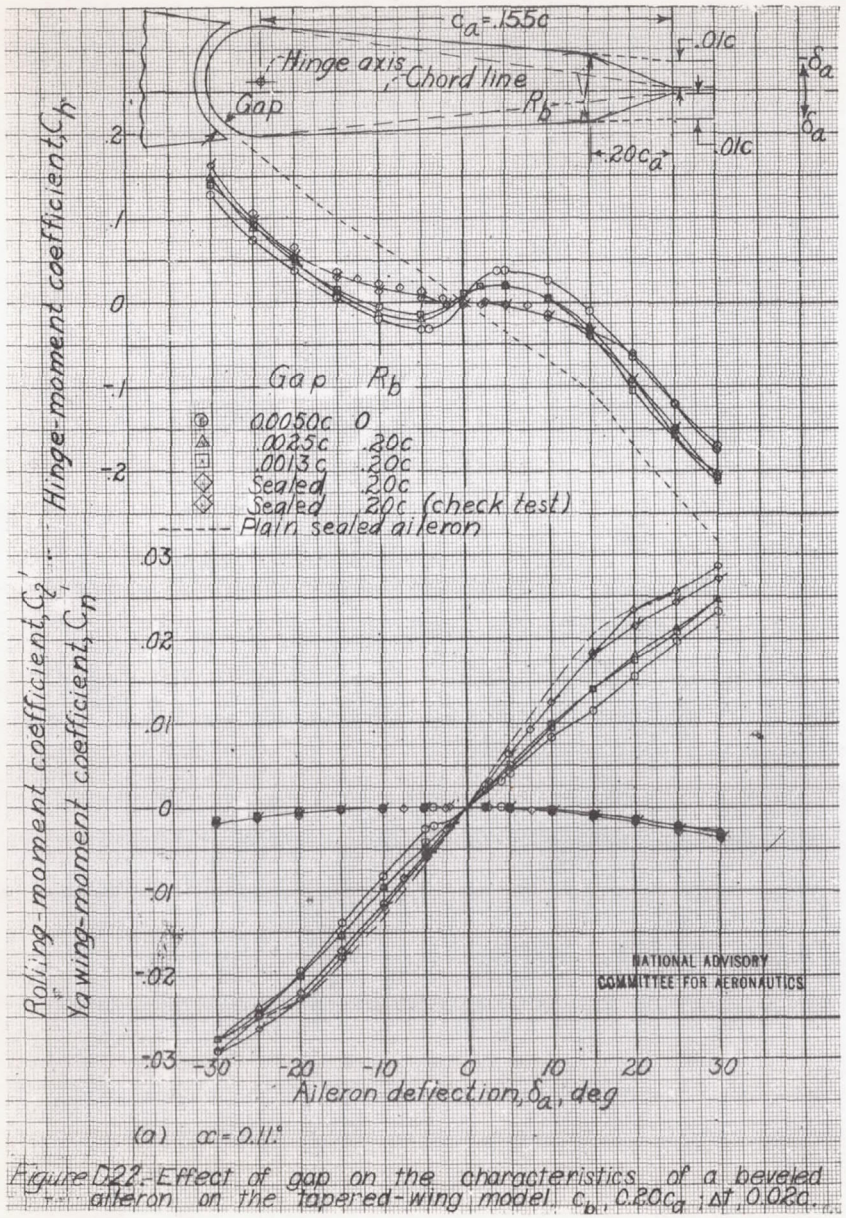

(a) α = 0.11°.

Figure D22.- Effect of gap on the characteristics of a beveled aileron on the tapered-wing model. c_b, 0.20c_a; Δt, 0.02c.

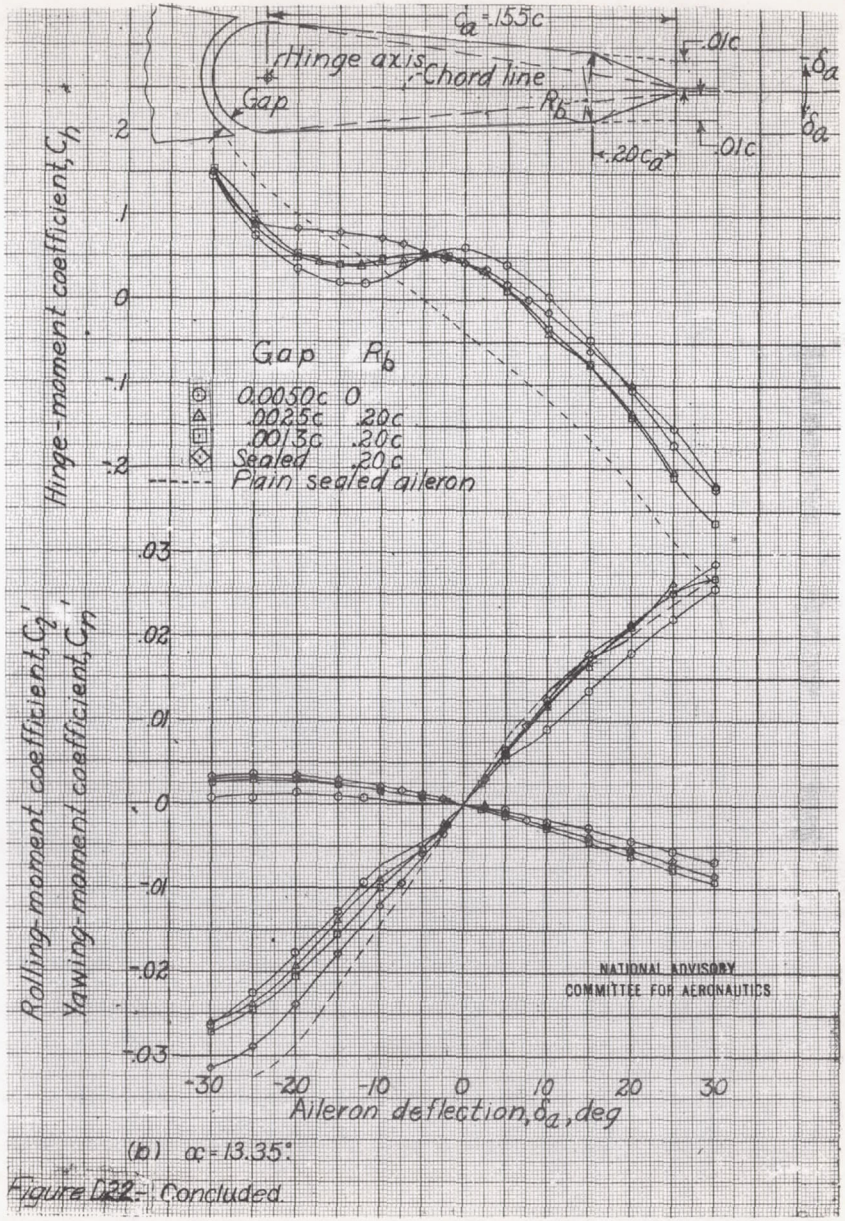

(b) α = 13.35°.

Figure D22.- Concluded.

Model D-IX

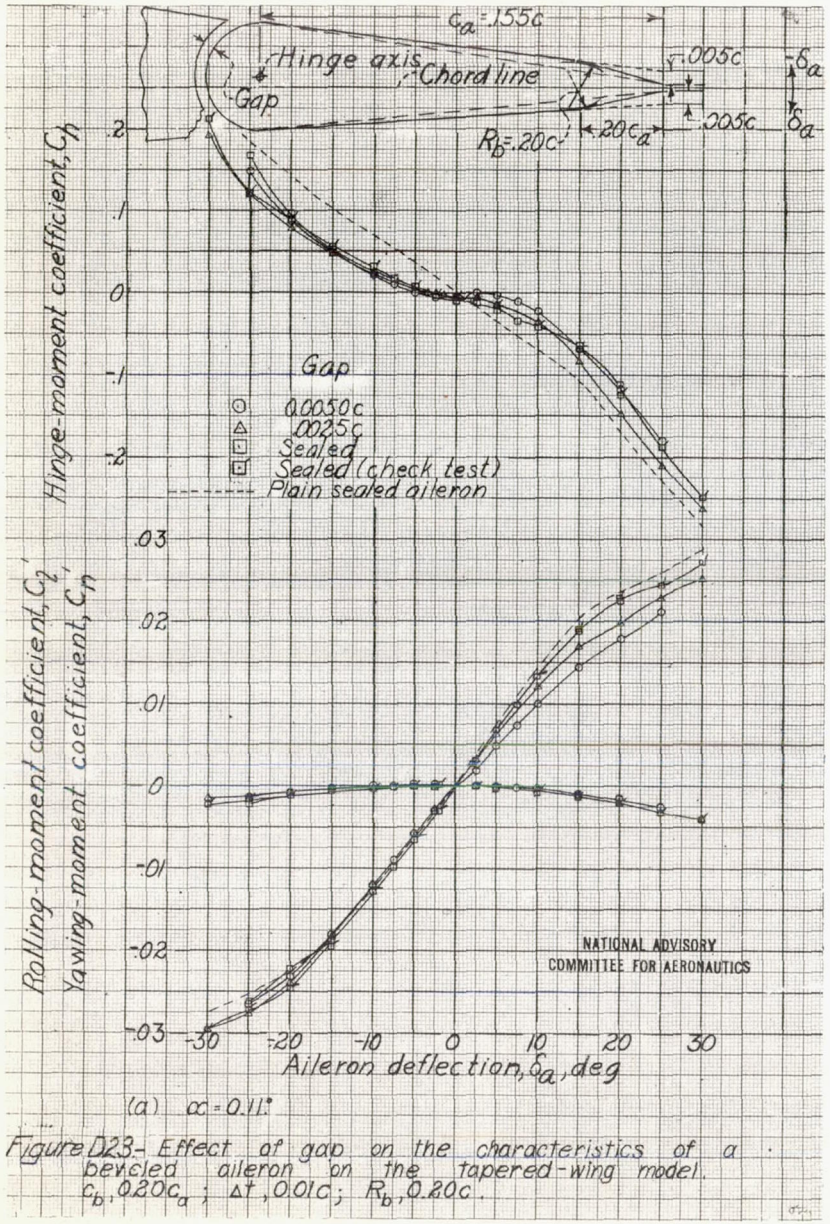

(a) $\alpha = 0.11°$

Figure D23.- Effect of gap on the characteristics of a beveled aileron on the tapered-wing model. c_b, 0.20c_a; Δt, 0.01c; R_b, 0.20c.

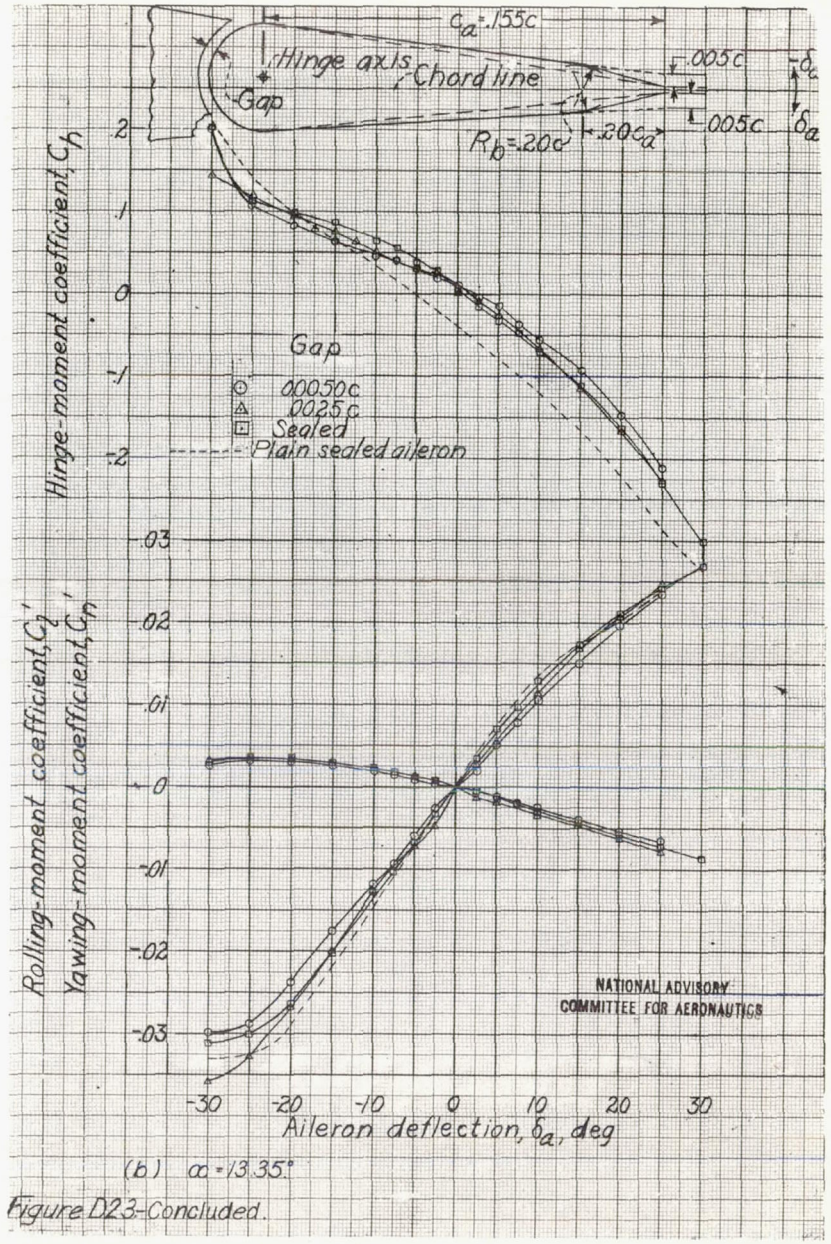

(b) $\alpha = 13.35°$

Figure D23.-Concluded.

Model D-IV

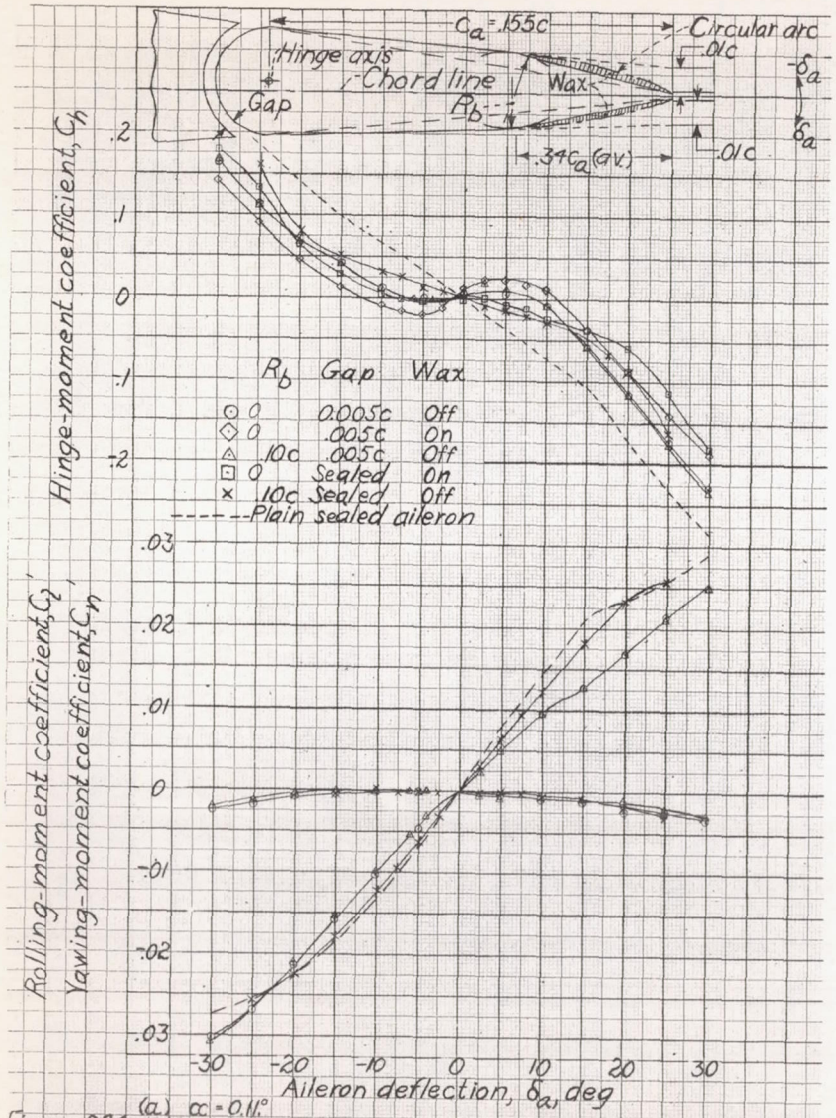

Figure D24.- Effect of gap and bevel radius on the characteristics of a beveled aileron on the tapered-wing model. c_b, 0.34c_a ; Δt, 0.02c .

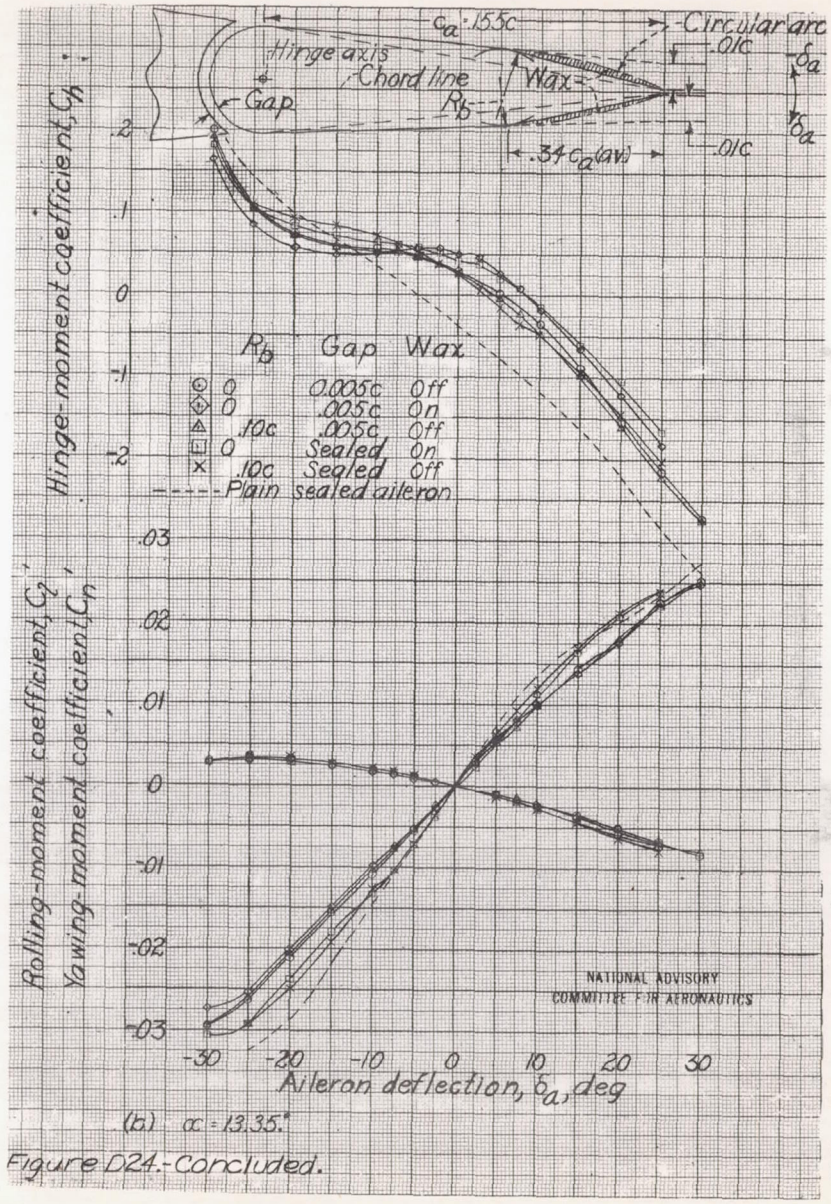

Figure D24.- Concluded.

Model D-IV

Figure 025.- Concluded.

(b) $\alpha = 13.35°$

Figure 025.- Effect of bevel radius on the characteristics of a beveled aileron on the tapered-wing model. C_a, 0.20C_a; ΔT, 0.01c.

(a) $\alpha = 0.11°$.

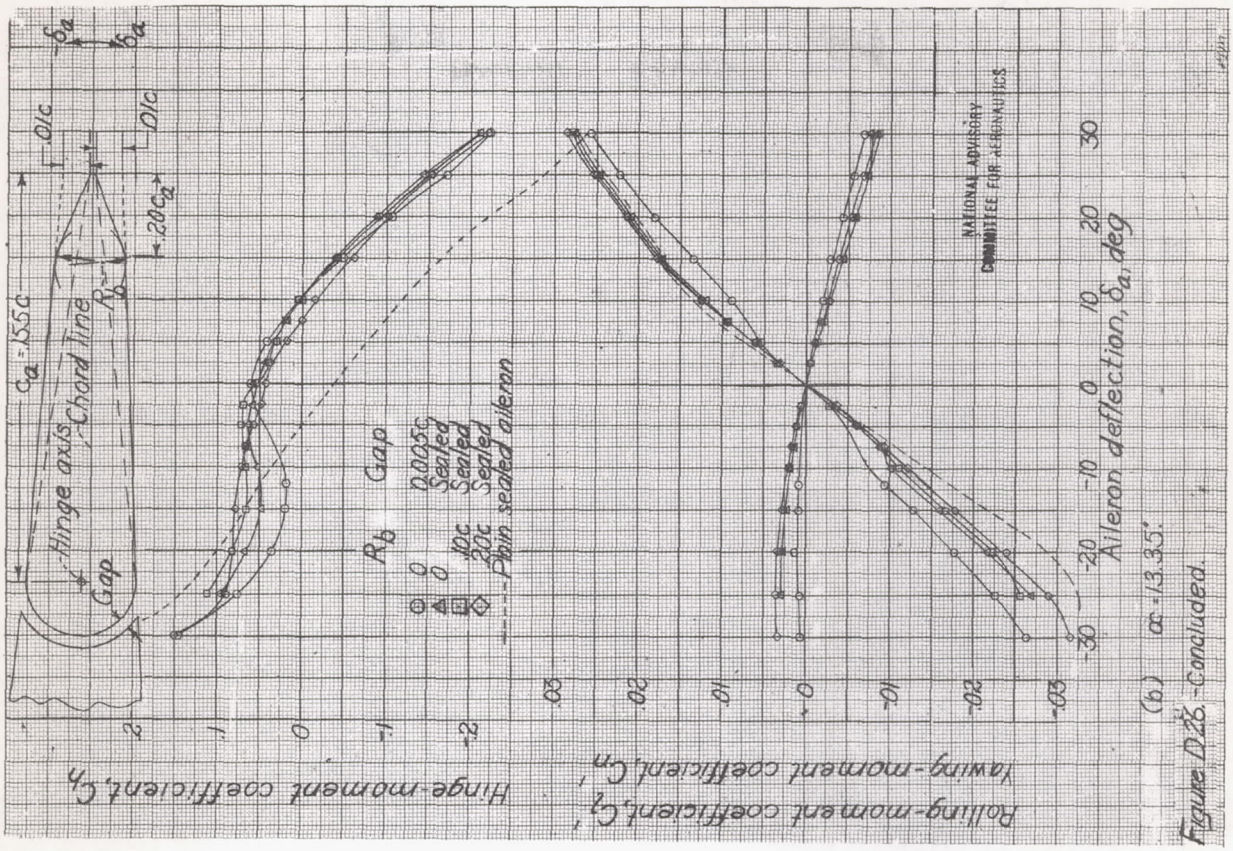

Figure D-25.- Concluded.

(b) $\alpha = 13.3°$.

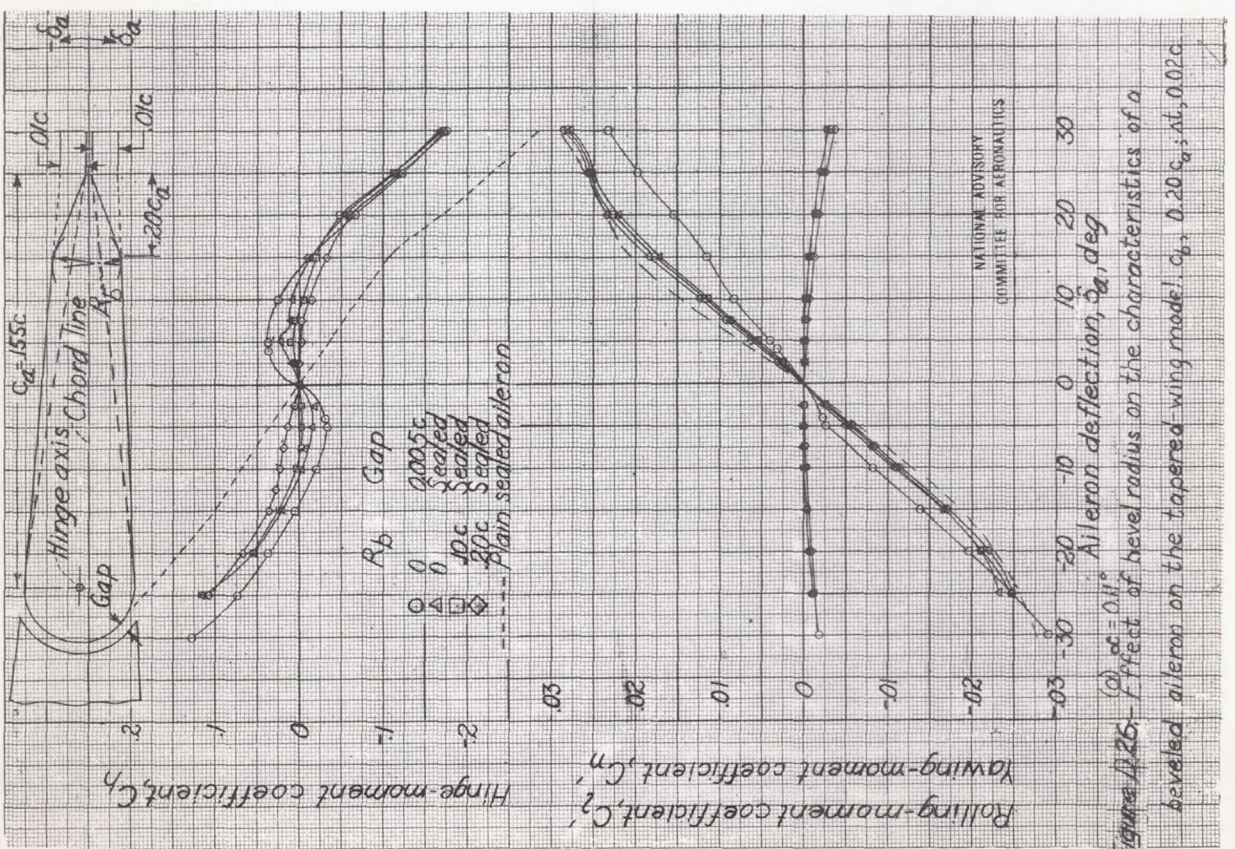

Figure D-26.- Effect of bevel radius on the characteristics of a beveled aileron on the tapered wing model. c_b, 0.20 c_a; Δl, 0.02c.

(a) $\alpha = 0°$.

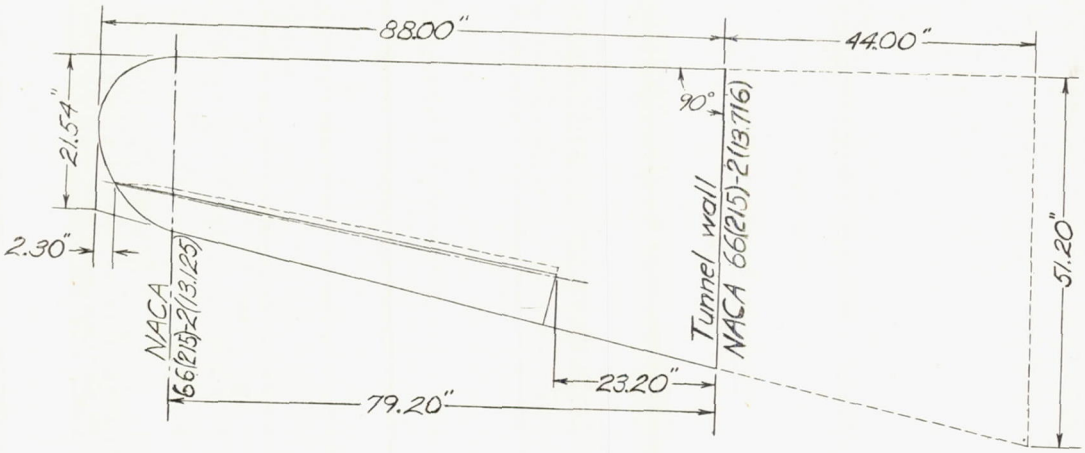

NATIONAL ADVISORY COMMITTEE FOR AERONAUTICS

Figure D27.-The 0.40-scale model of a tapered low-drag wing tested in the LMAL 7-by 10-foot tunnel.

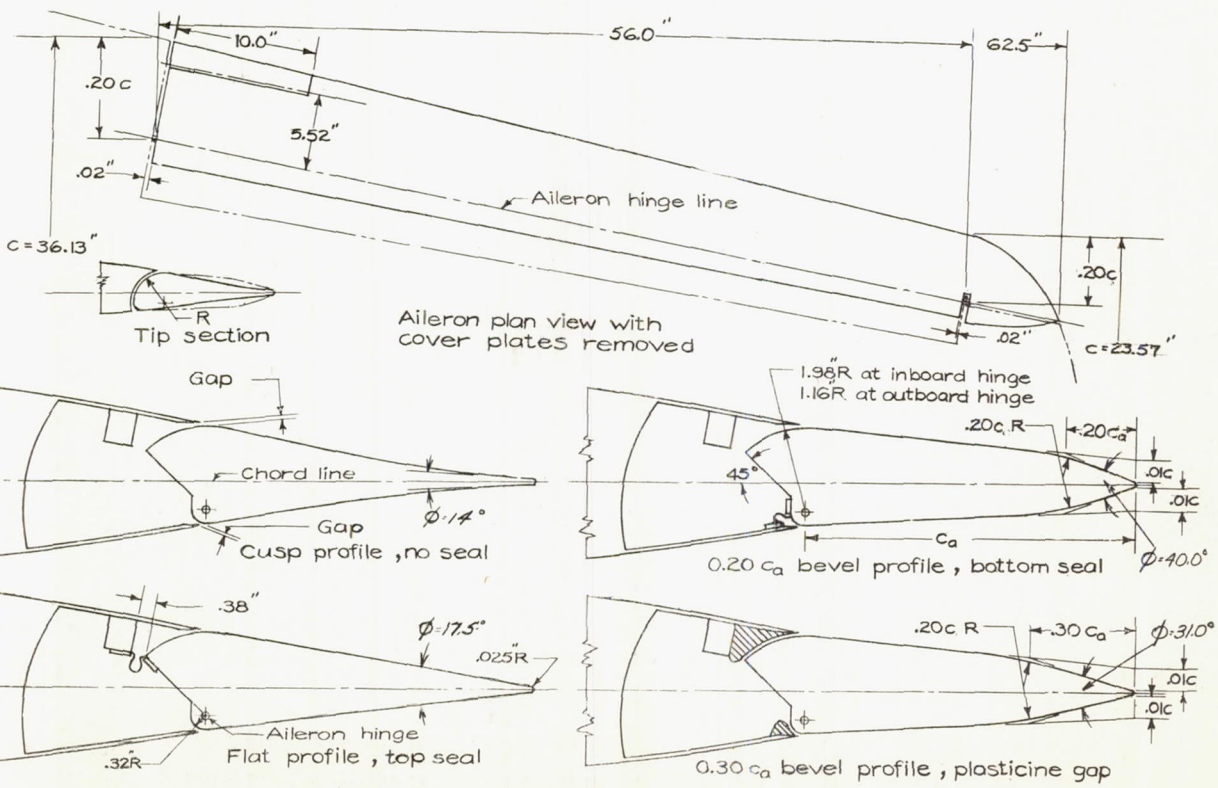

Figure D28.-Aileron with typical profile modifications tested on 0.40-scale partial-span model of a low-drag wing.

NATIONAL ADVISORY COMMITTEE FOR AERONAUTICS

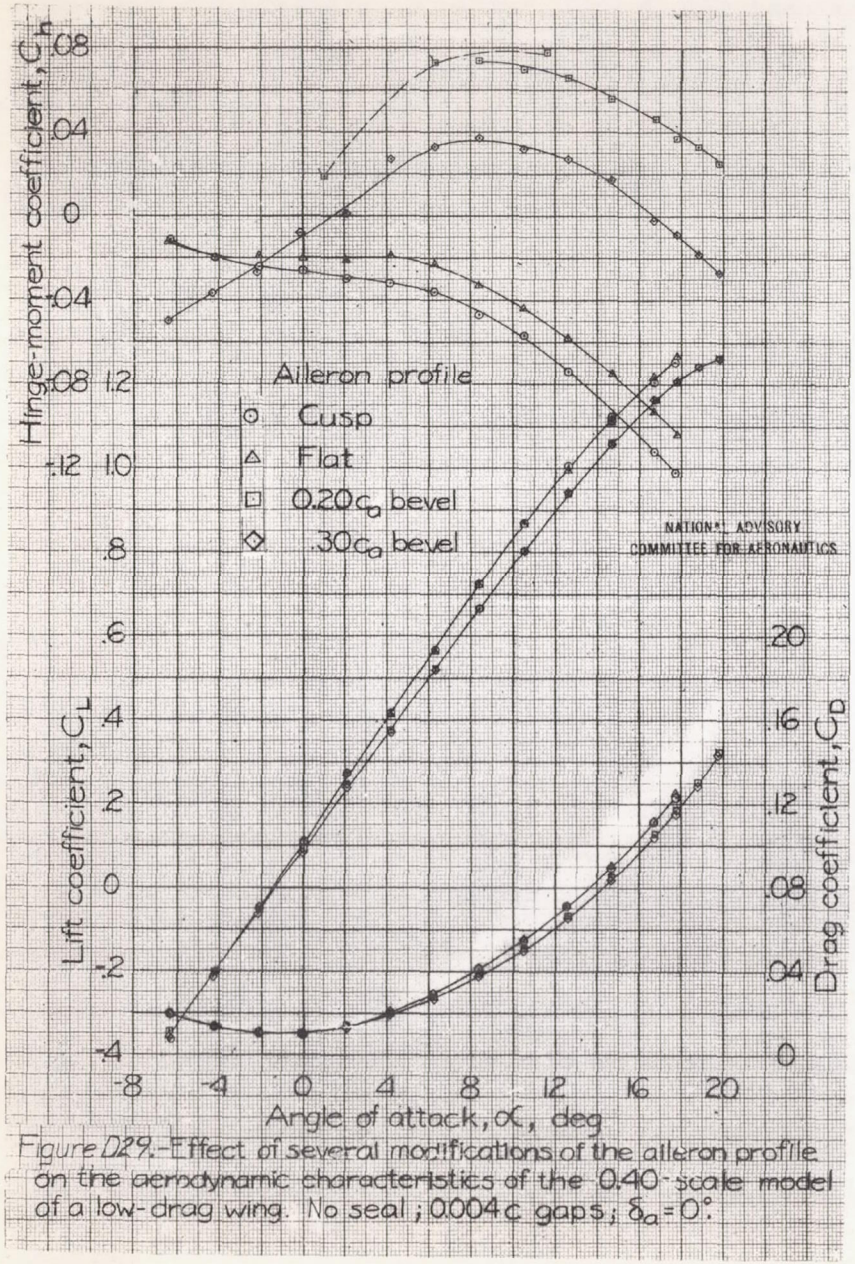

Figure D29.-Effect of several modifications of the aileron profile on the aerodynamic characteristics of the 0.40-scale model of a low-drag wing. No seal; 0.004c gaps; $\delta_a = 0°$.

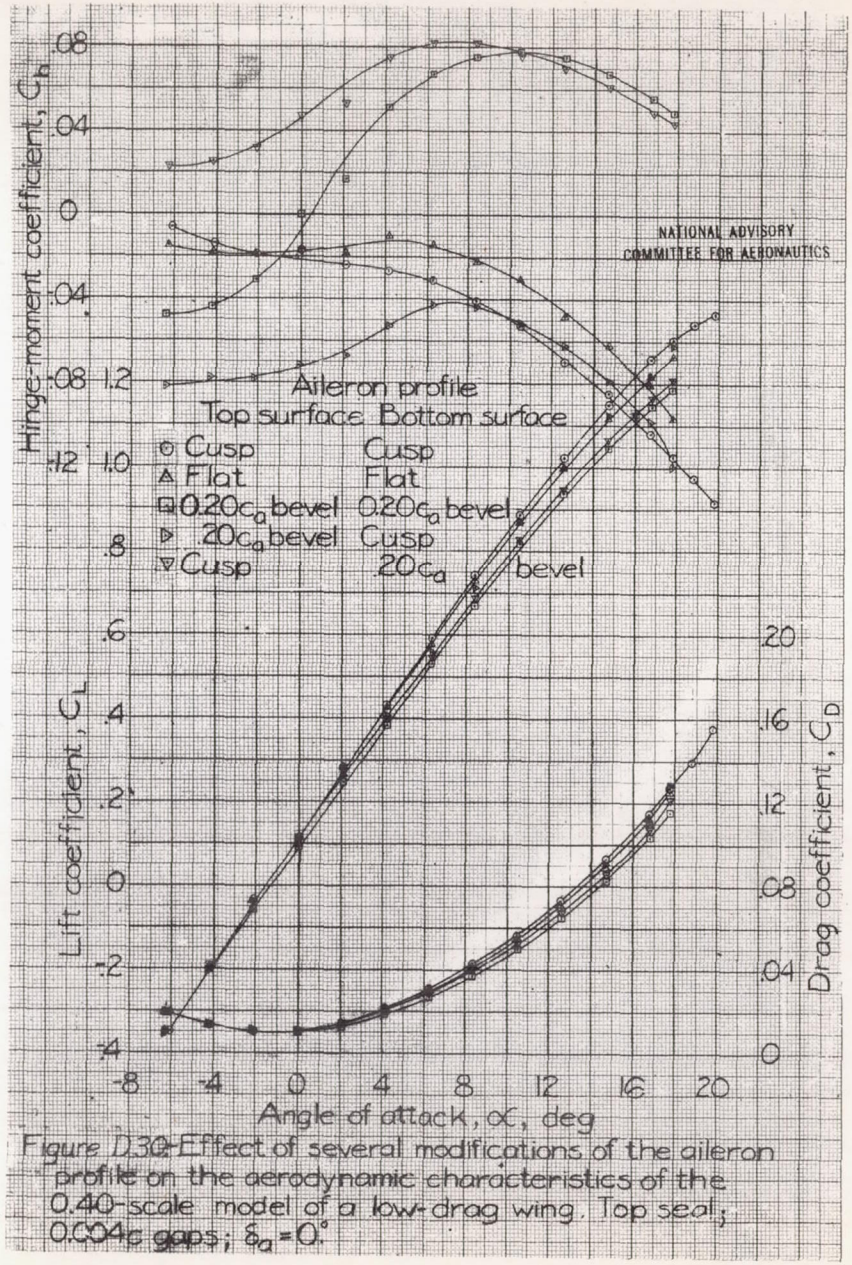

Figure D30-Effect of several modifications of the aileron profile on the aerodynamic characteristics of the 0.40-scale model of a low-drag wing. Top seal; 0.004c gaps; $\delta_a = 0°$.

Model D-Y

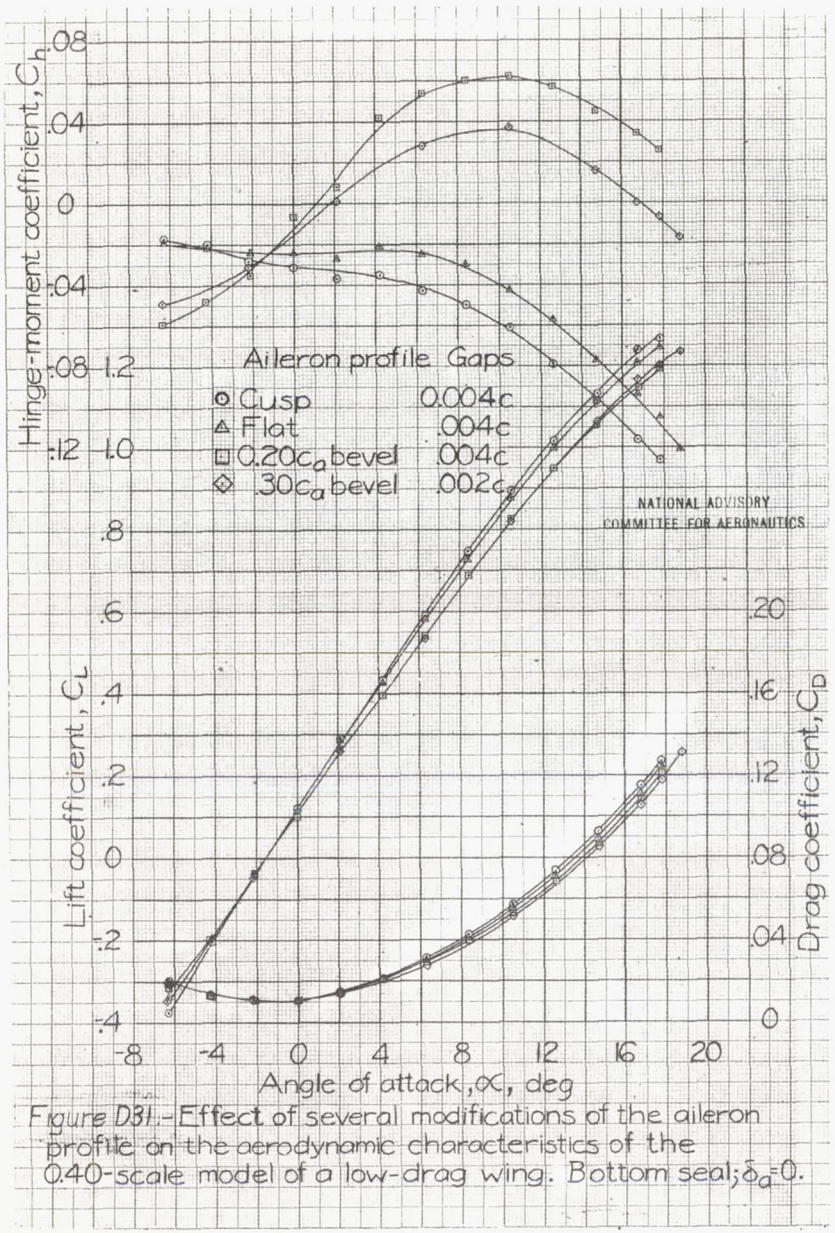

Figure D31.- Effect of several modifications of the aileron profile on the aerodynamic characteristics of the 0.40-scale model of a low-drag wing. Bottom seal; δ_a=0.

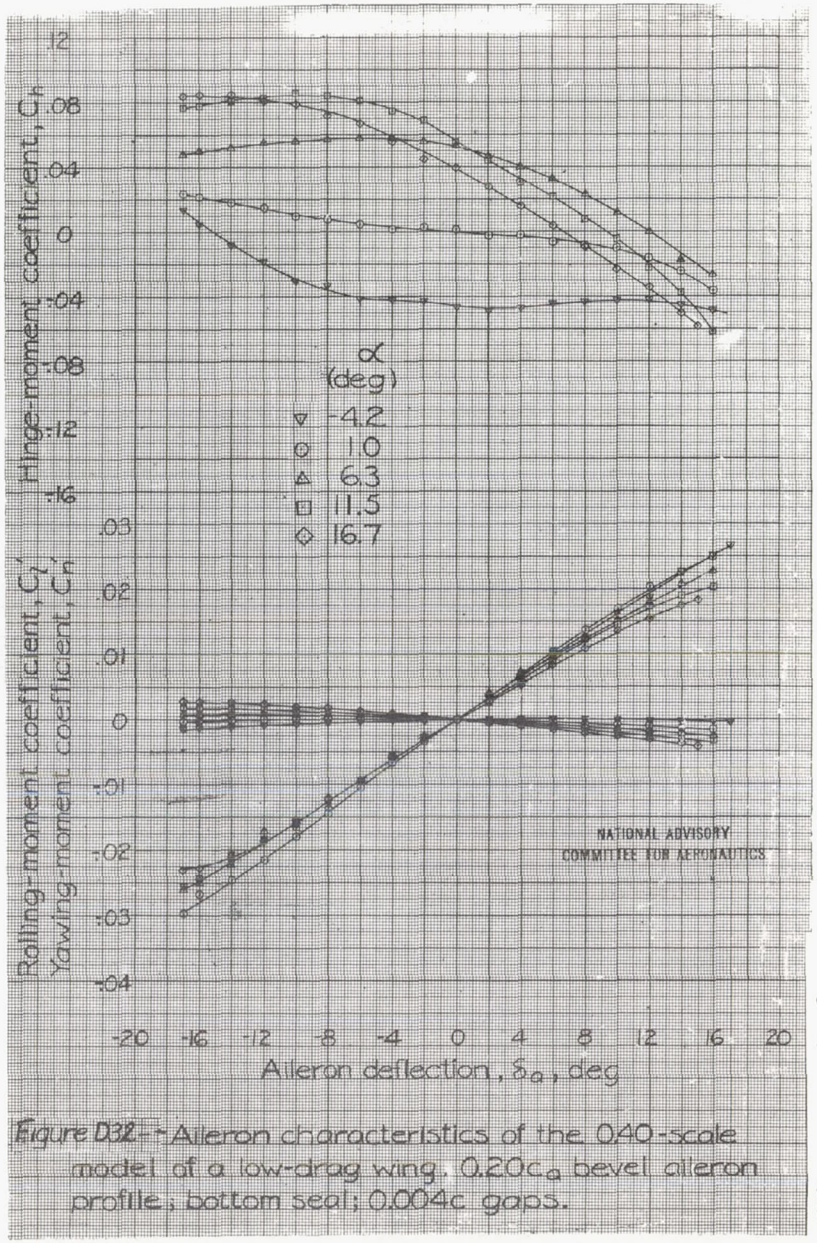

Figure D32.- Aileron characteristics of the 0.40-scale model of a low-drag wing. 0.20c_a bevel aileron profile; bottom seal; 0.004c gaps.

Model D-V

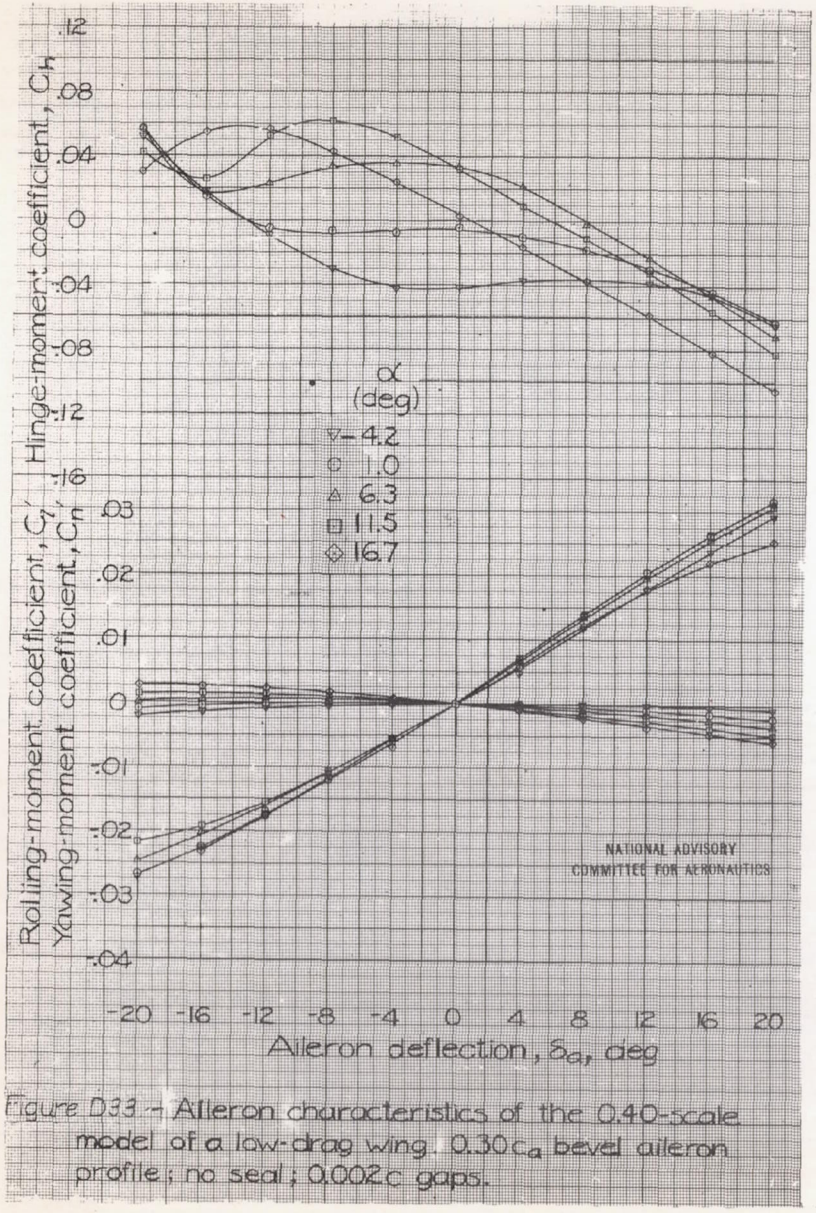

Figure D33 - Aileron characteristics of the 0.40-scale model of a low-drag wing. 0.30c_a bevel aileron profile; no seal; 0.002c gaps.

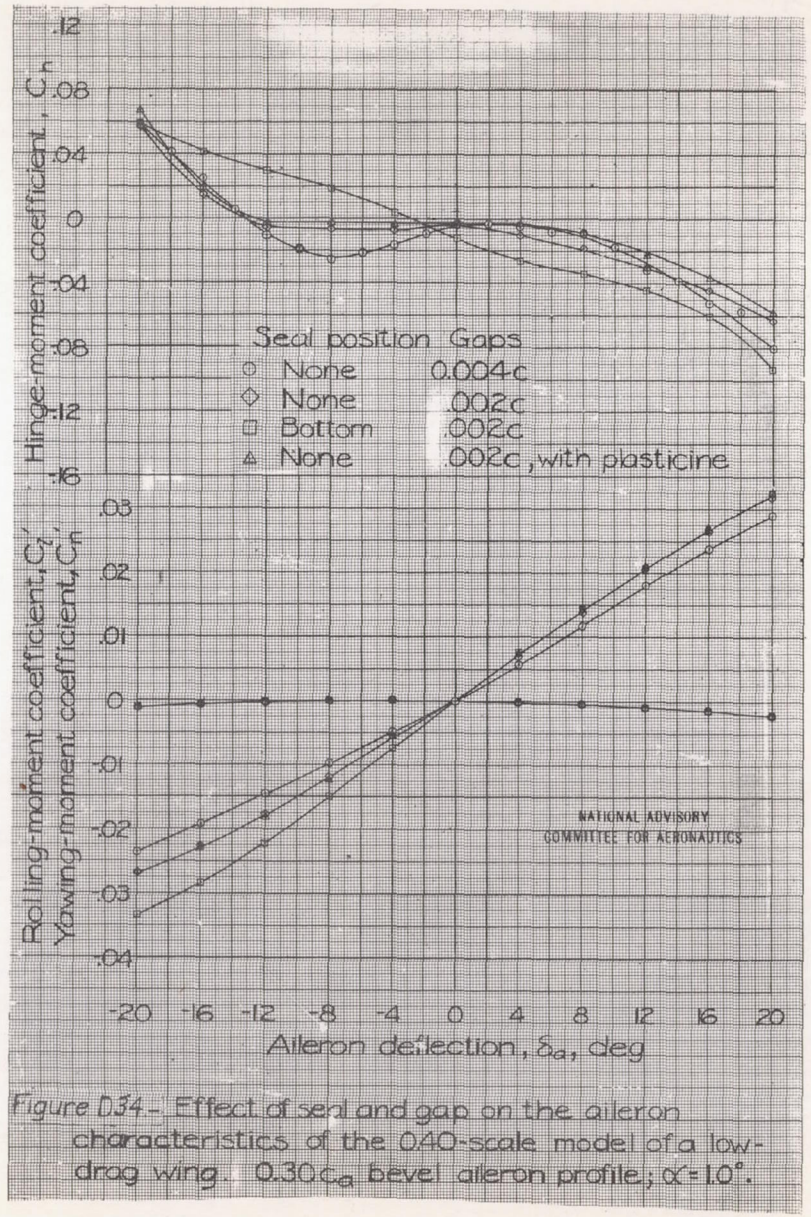

Figure D34 - Effect of seal and gap on the aileron characteristics of the 0.40-scale model of a low-drag wing. 0.30c_a bevel aileron profile; $\alpha = 1.0°$.

Model D-II

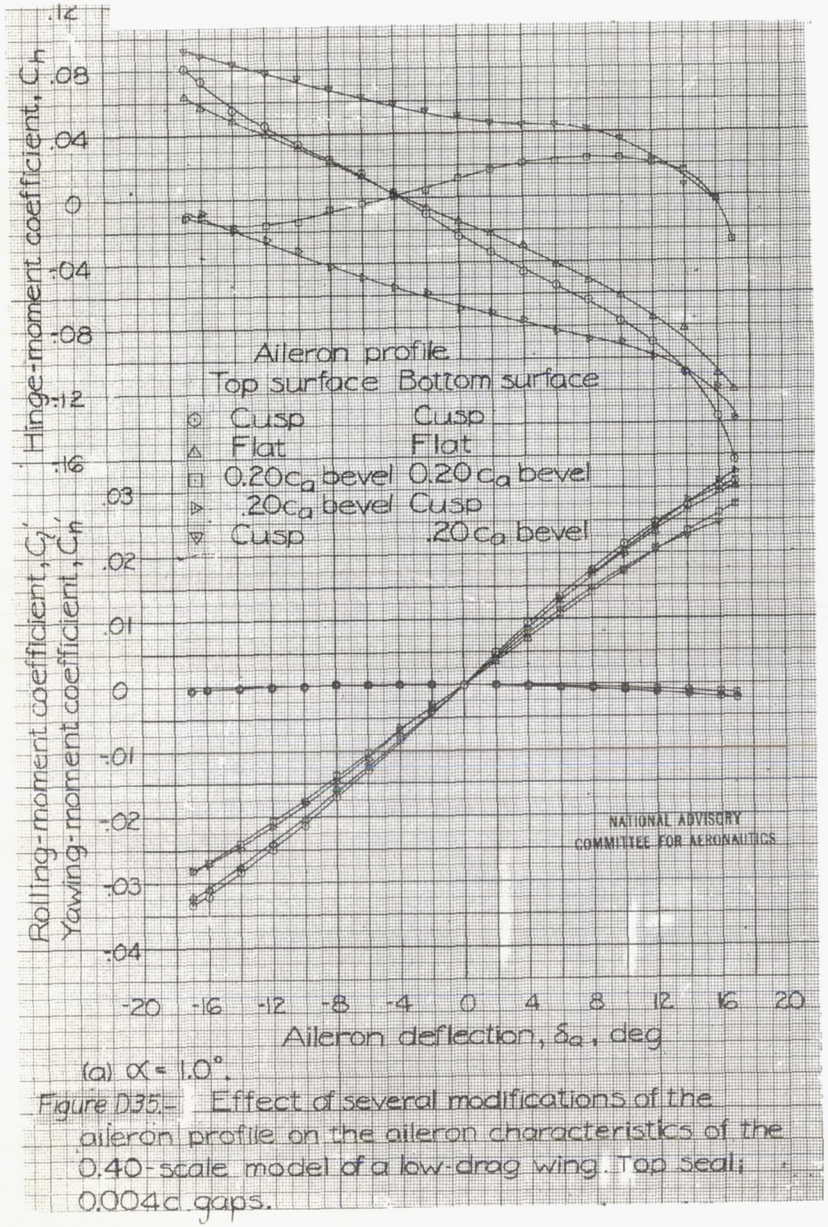

(a) $\alpha = 1.0°$.

Figure D35.- Effect of several modifications of the aileron profile on the aileron characteristics of the 0.40-scale model of a low-drag wing. Top seal; 0.004c gaps.

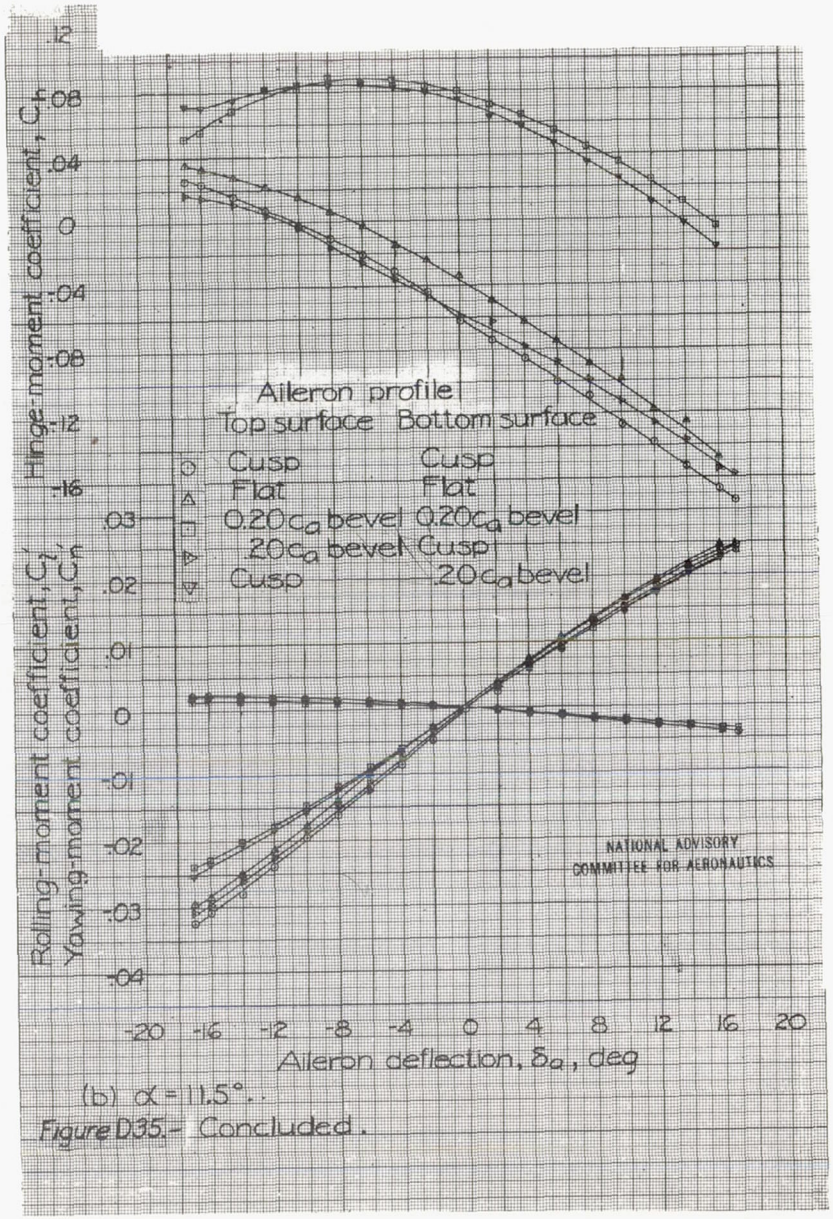

(b) $\alpha = 11.5°$.

Figure D35.- Concluded.

Model D-V

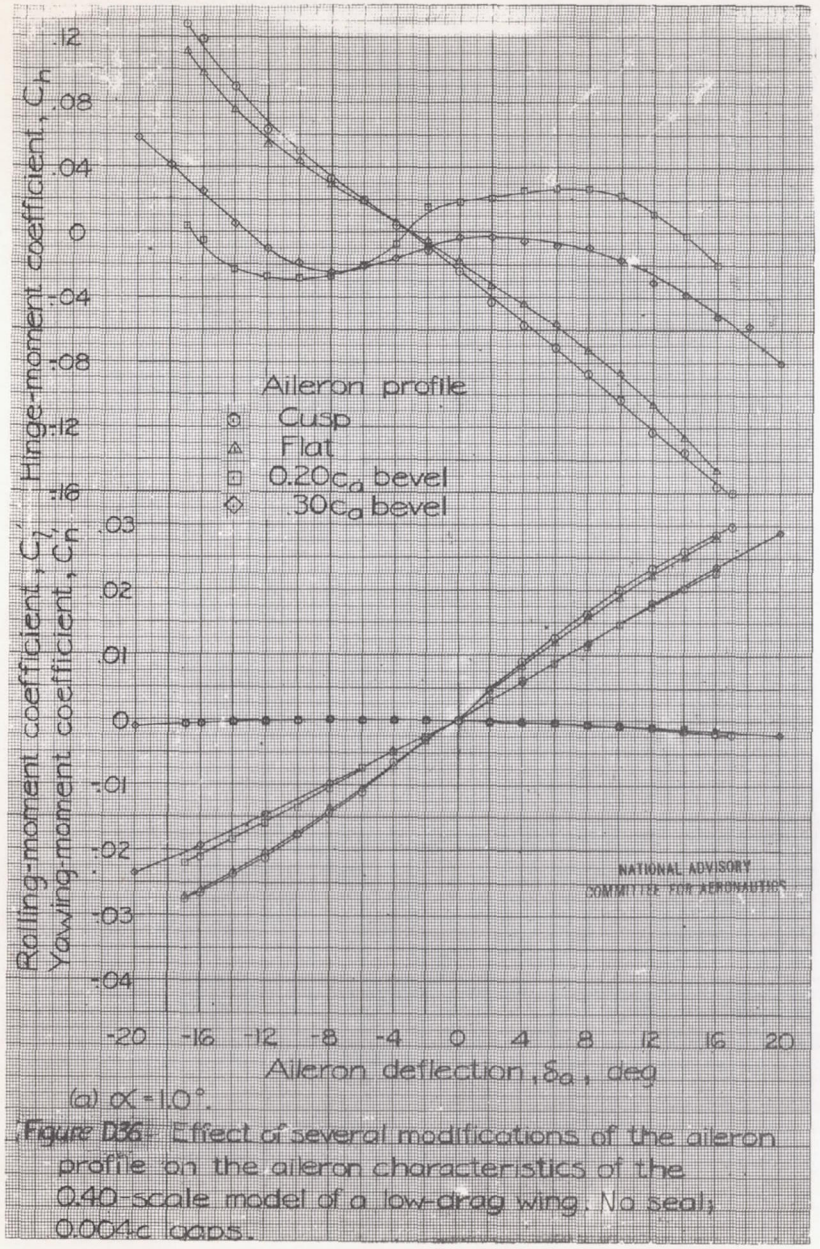

Figure D36.- Effect of several modifications of the aileron profile on the aileron characteristics of the 0.40-scale model of a low-drag wing. No seal; 0.004c gaps.

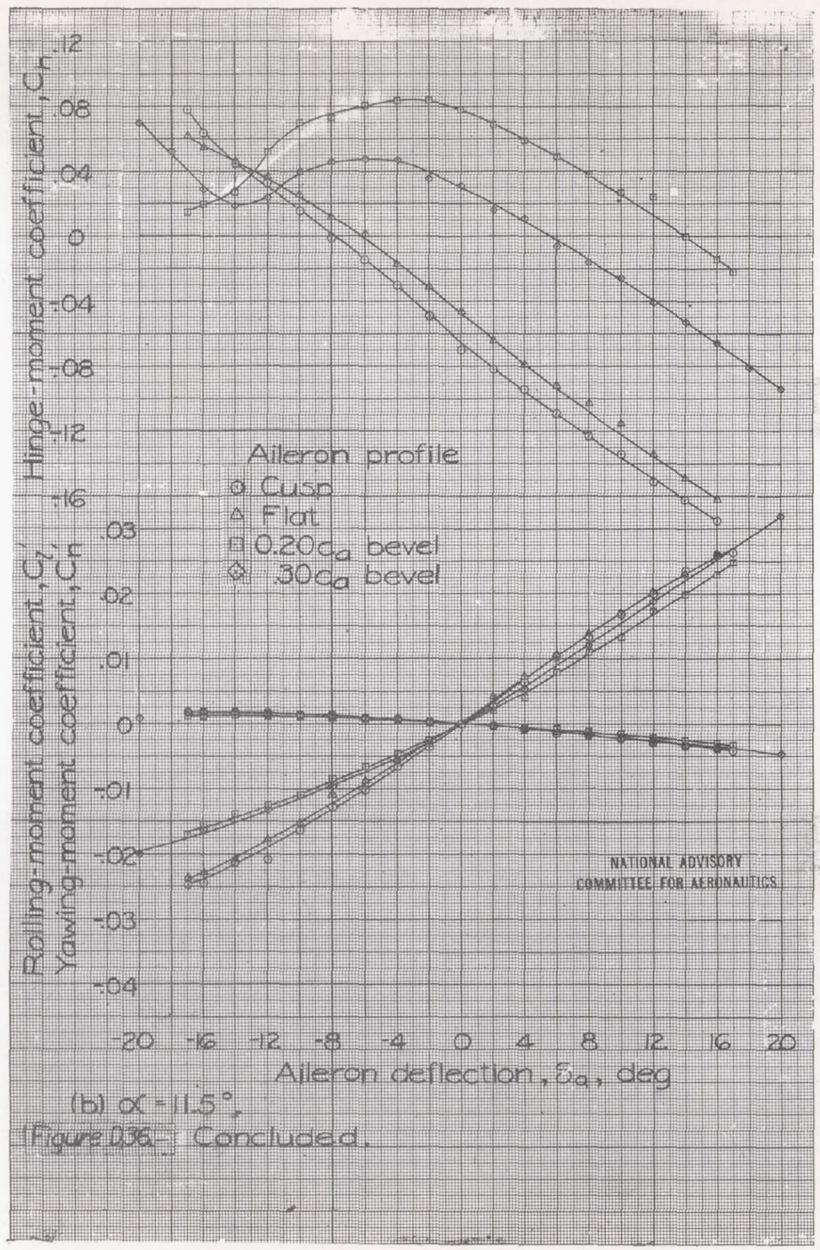

Figure D36.- Concluded.

Model D-V

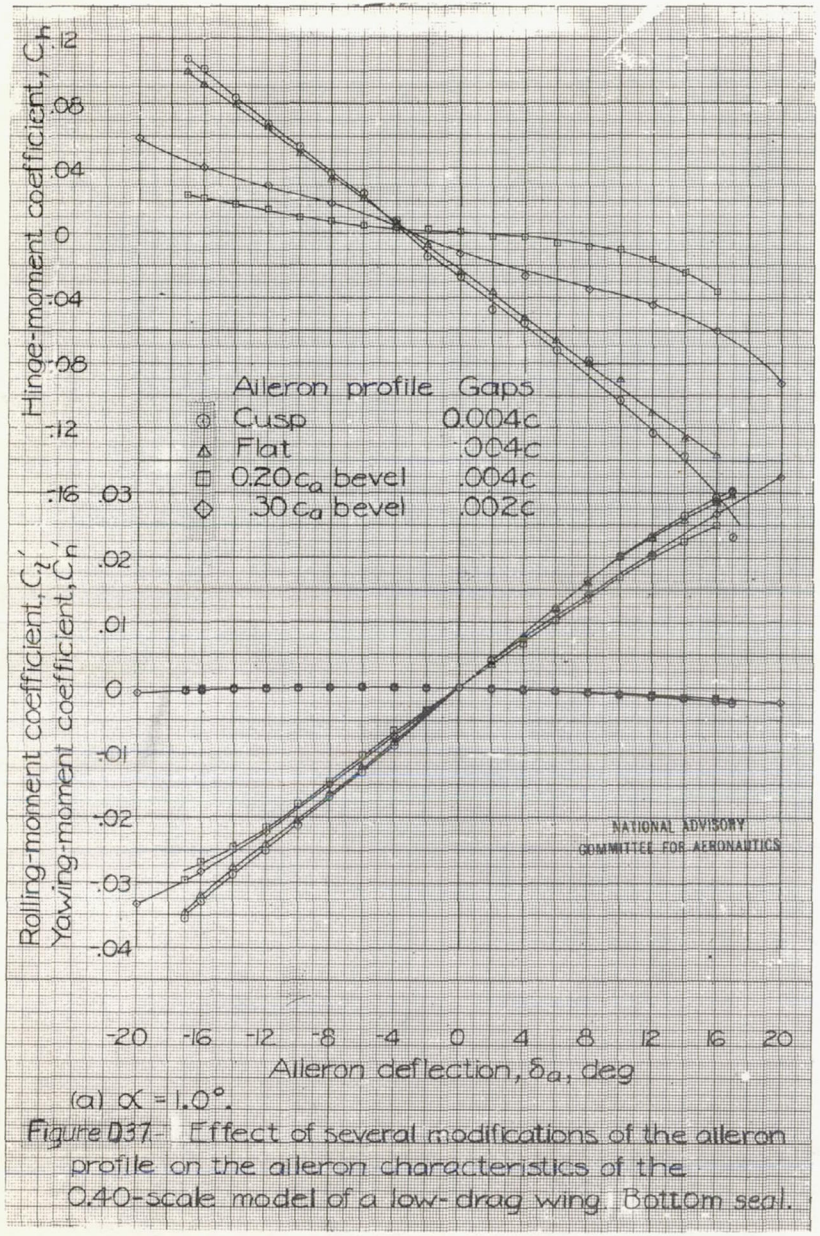

(a) α = 1.0°.

Figure D37.- Effect of several modifications of the aileron profile on the aileron characteristics of the 0.40-scale model of a low-drag wing. Bottom seal.

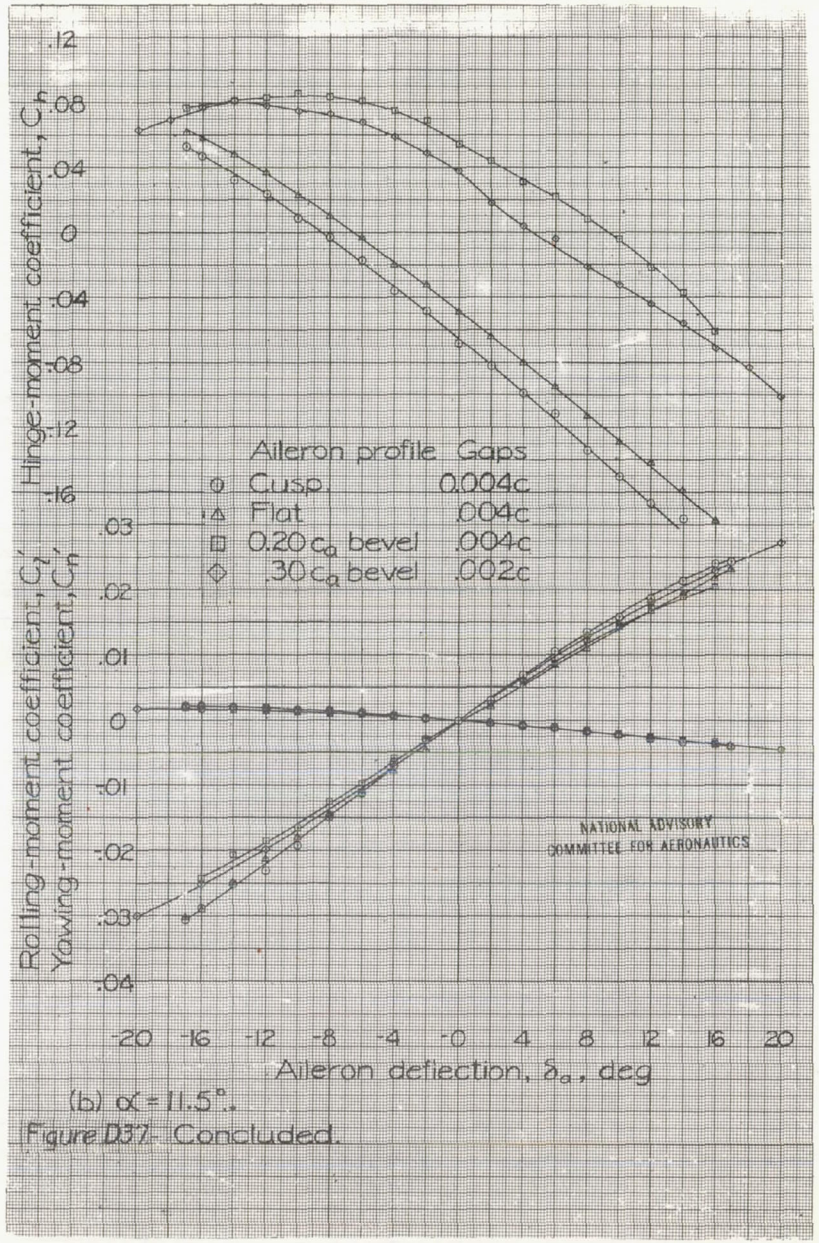

(b) α = 11.5°.

Figure D37.- Concluded.

Model D-IX

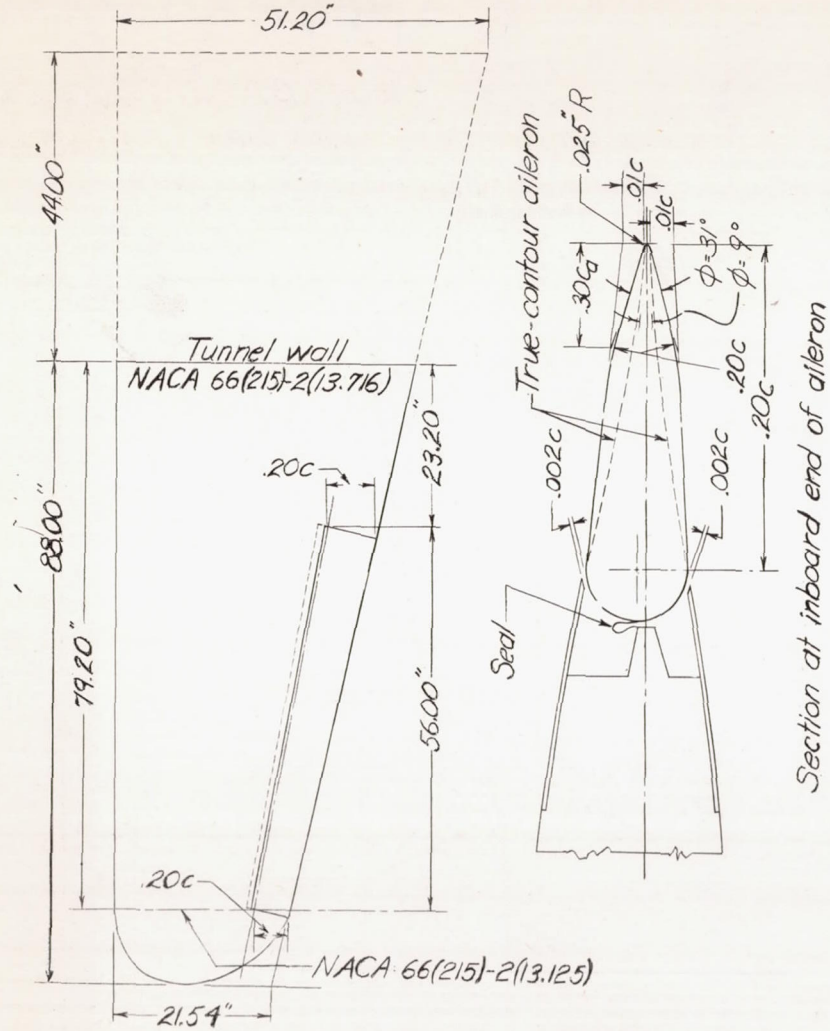

Figure D38.-The 0.40-scale model of a tapered low-drag wing with round-nose ailerons. LMAL 7-by 10-foot tunnel.

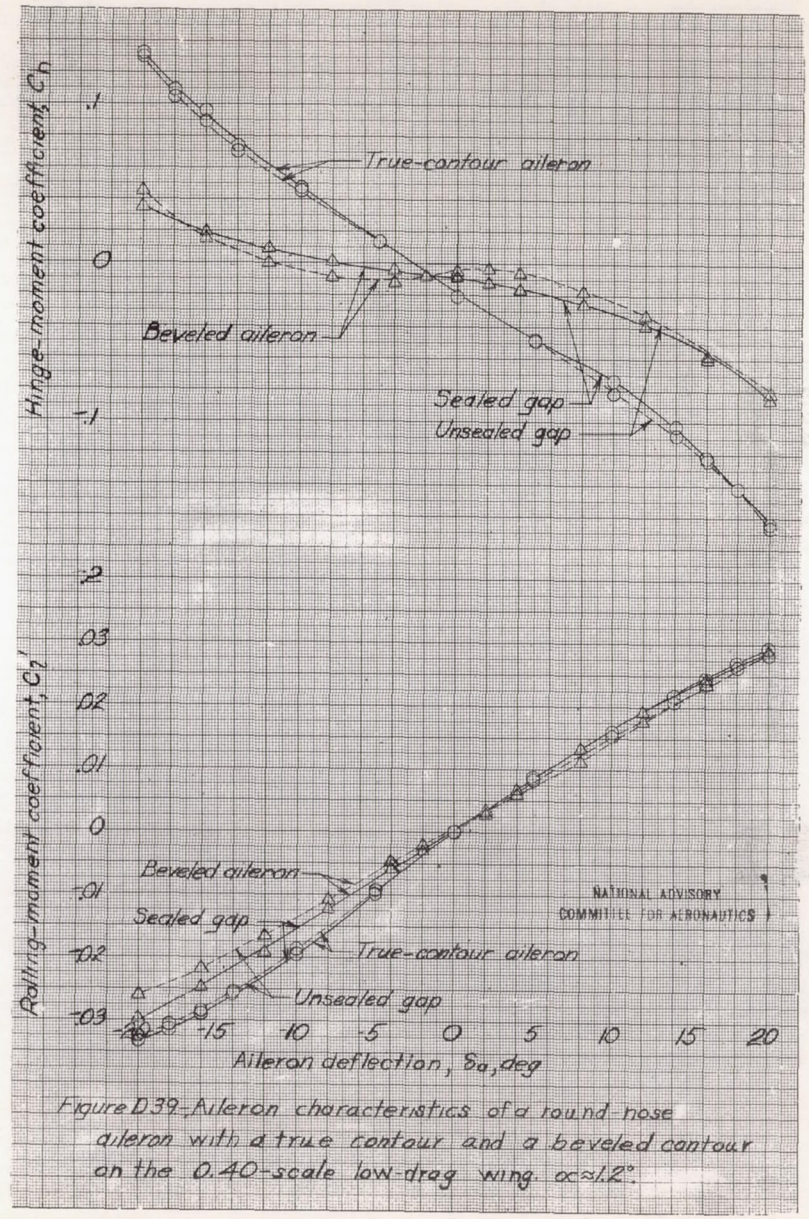

Figure D39.-Aileron characteristics of a round nose aileron with a true contour and a beveled contour on the 0.40-scale low-drag wing. $\alpha \approx 1.2°$.

Model D-VI

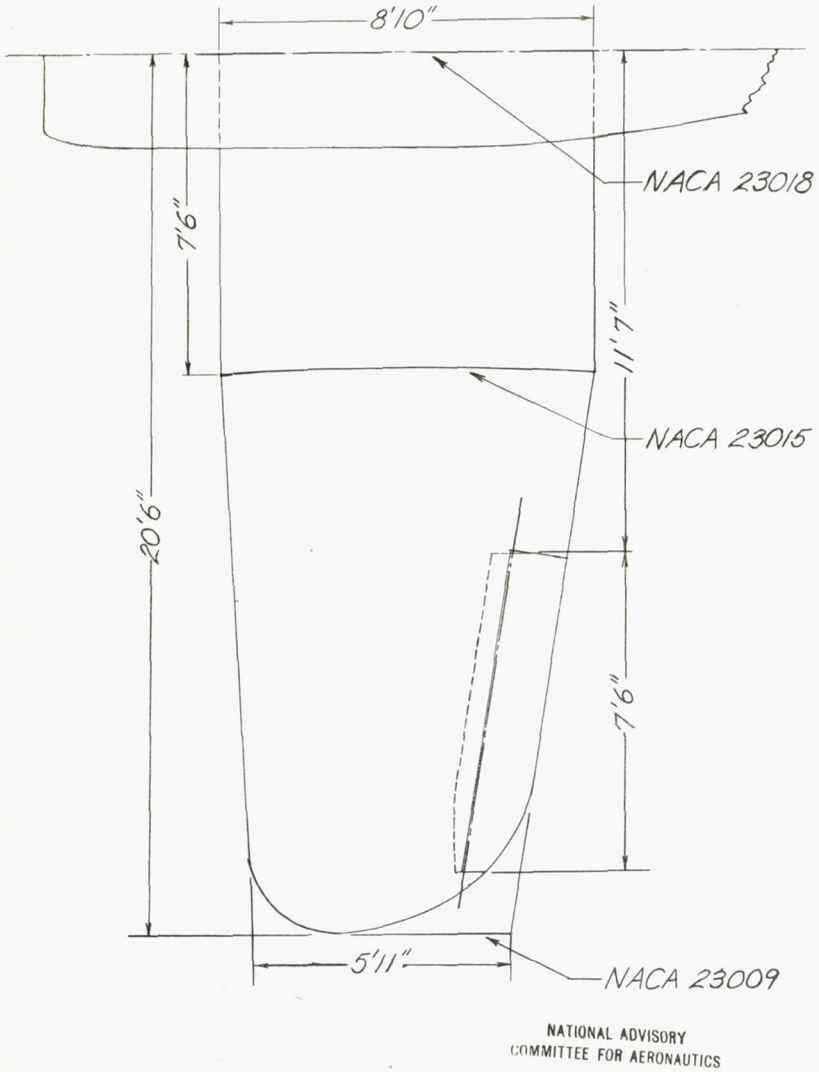

Figure D40.-Left wing panel of the airplane tested in the NACA full-scale tunnel.

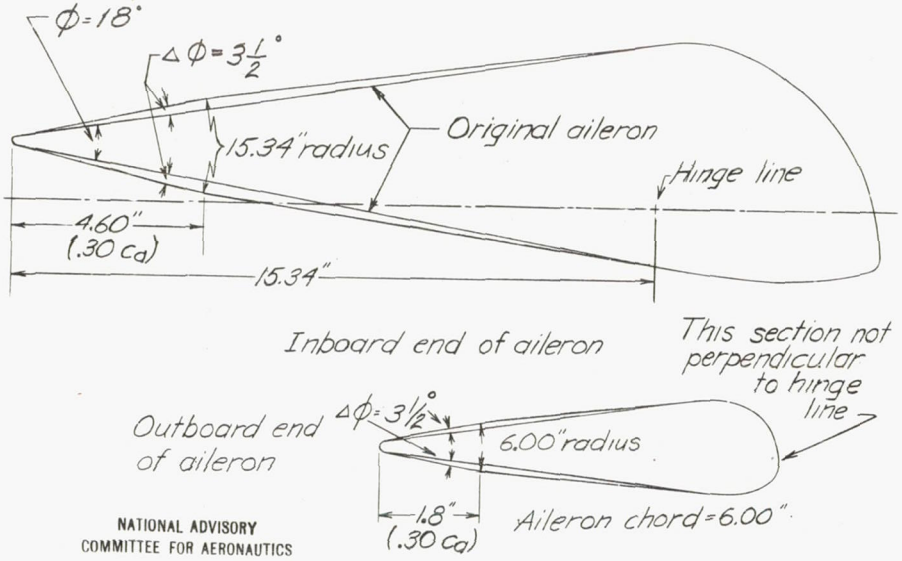

Figure D41.-Aileron sections of the full-scale airplane.

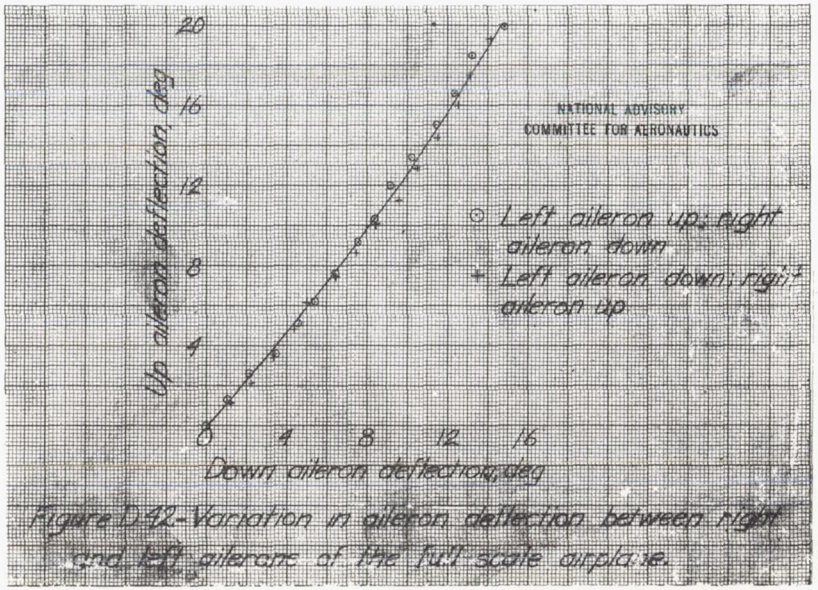

Figure D42.-Variation in aileron deflection between right and left ailerons of the full-scale airplane.

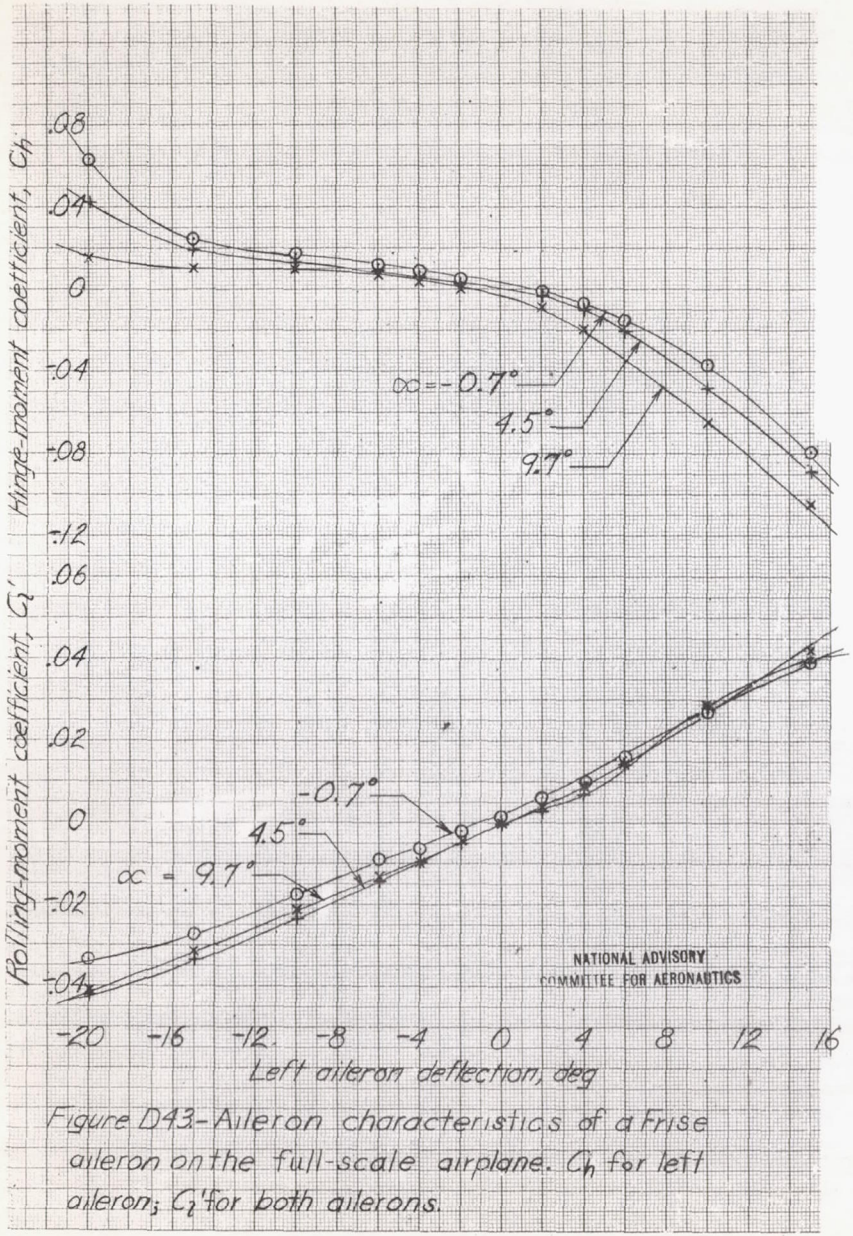

Figure D43- Aileron characteristics of a frise aileron on the full-scale airplane. C_h for left aileron; C_l' for both ailerons.

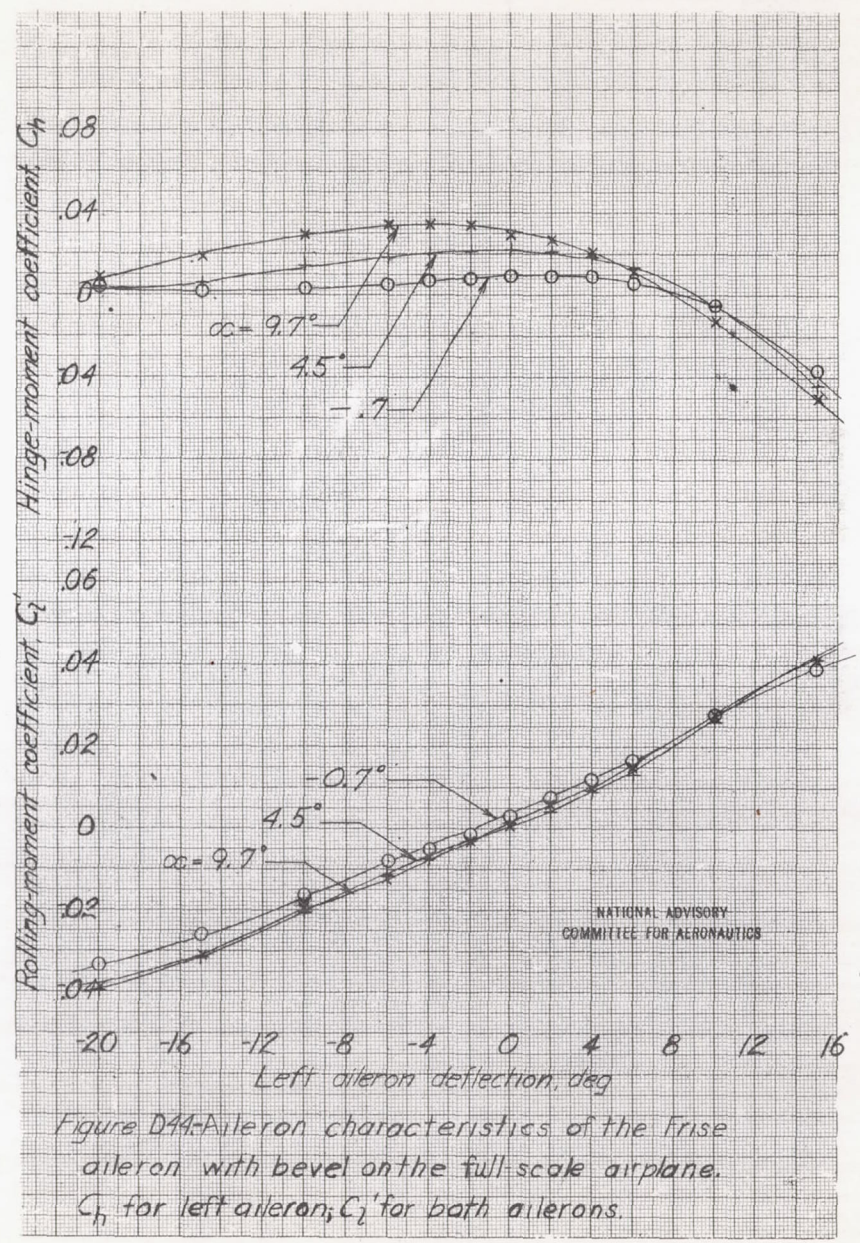

Figure D44-Aileron characteristics of the frise aileron with bevel on the full-scale airplane. C_h for left aileron; C_l' for both ailerons.

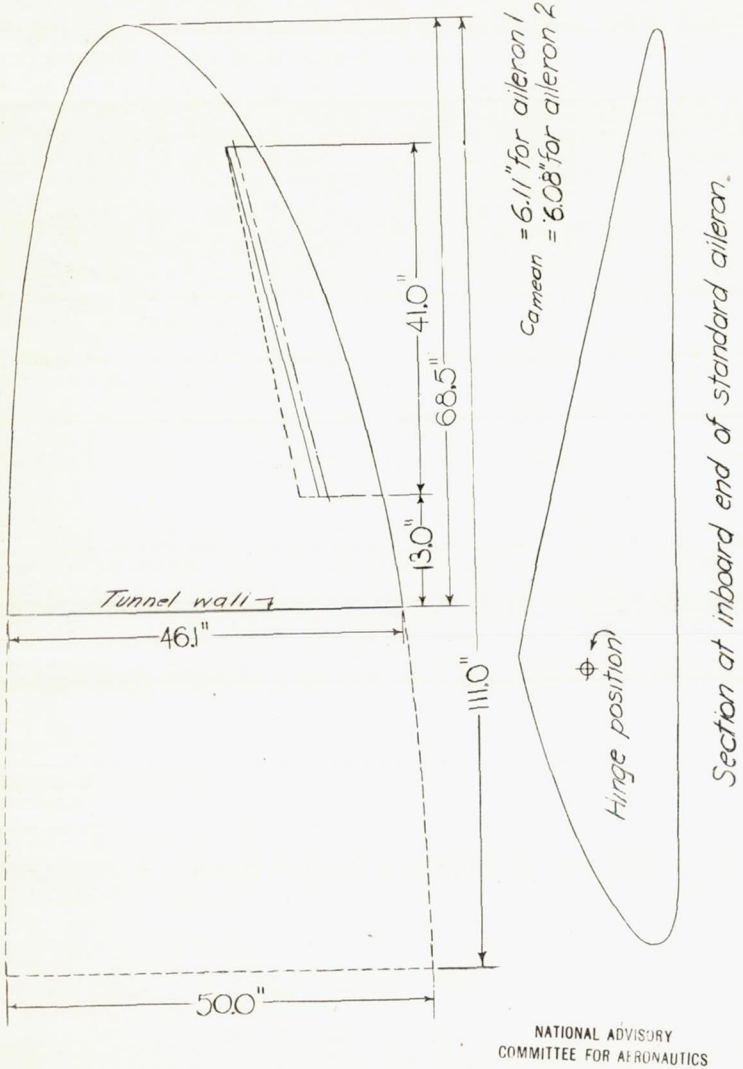

Figure D45.-The 0.50-scale model of an elliptical wing with the standard Frise aileron. N.P.L. Duplex tunnel.

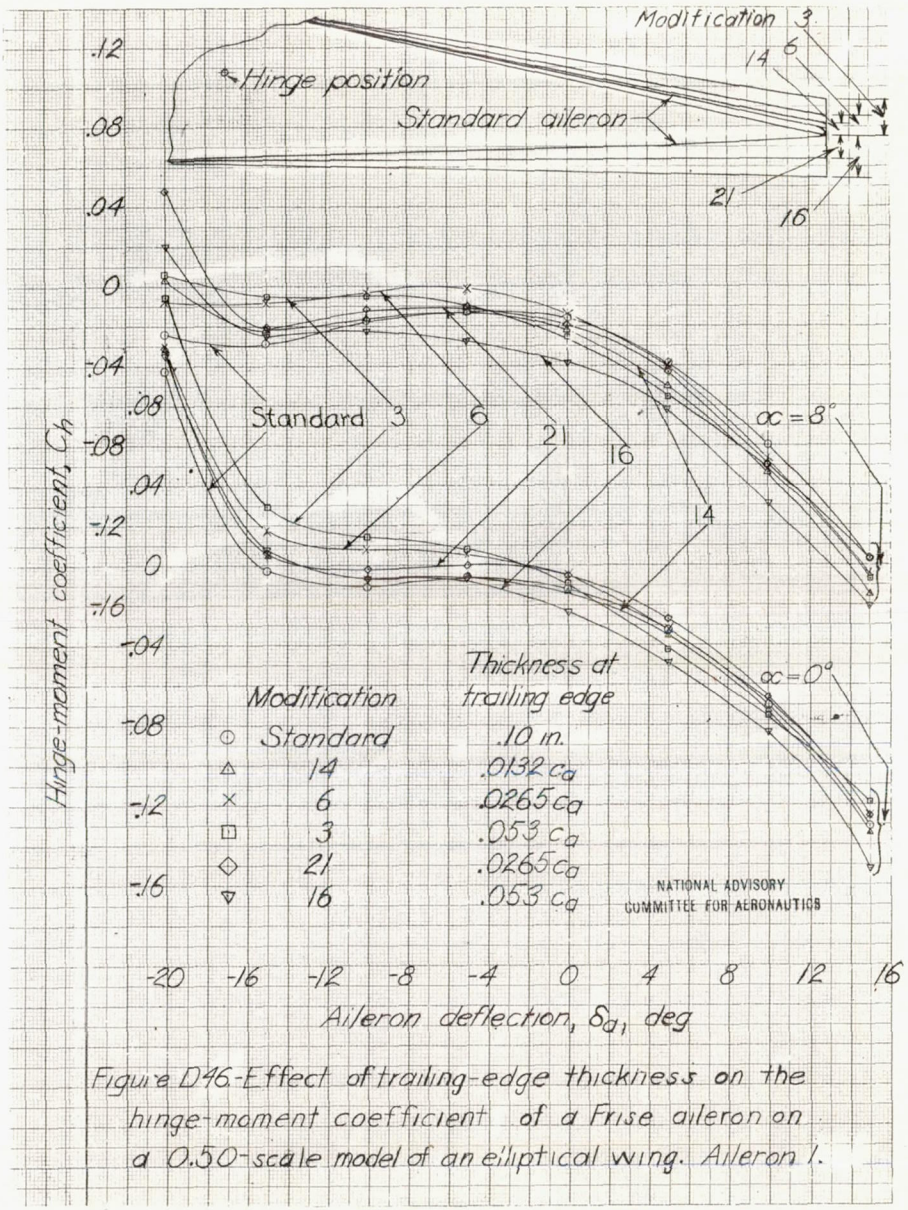

Figure D46.-Effect of trailing-edge thickness on the hinge-moment coefficient of a Frise aileron on a 0.50-scale model of an elliptical wing. Aileron 1.

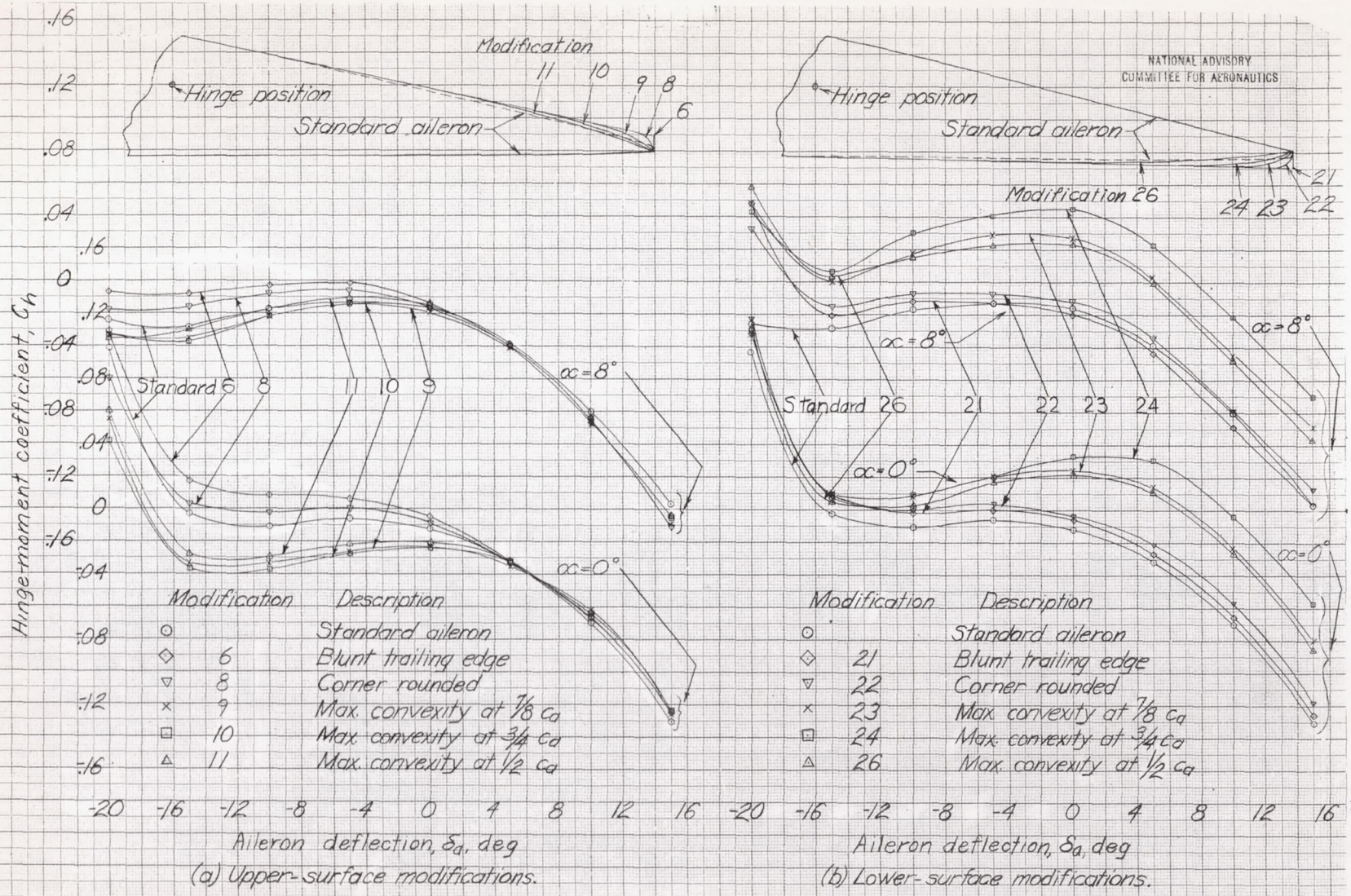

Figure D47.-Effect of modifications of the upper and lower surfaces on the hinge-moment coefficients of a Frise aileron on the 0.50-scale model of an elliptical wing. Aileron 1.

Model D-VIII

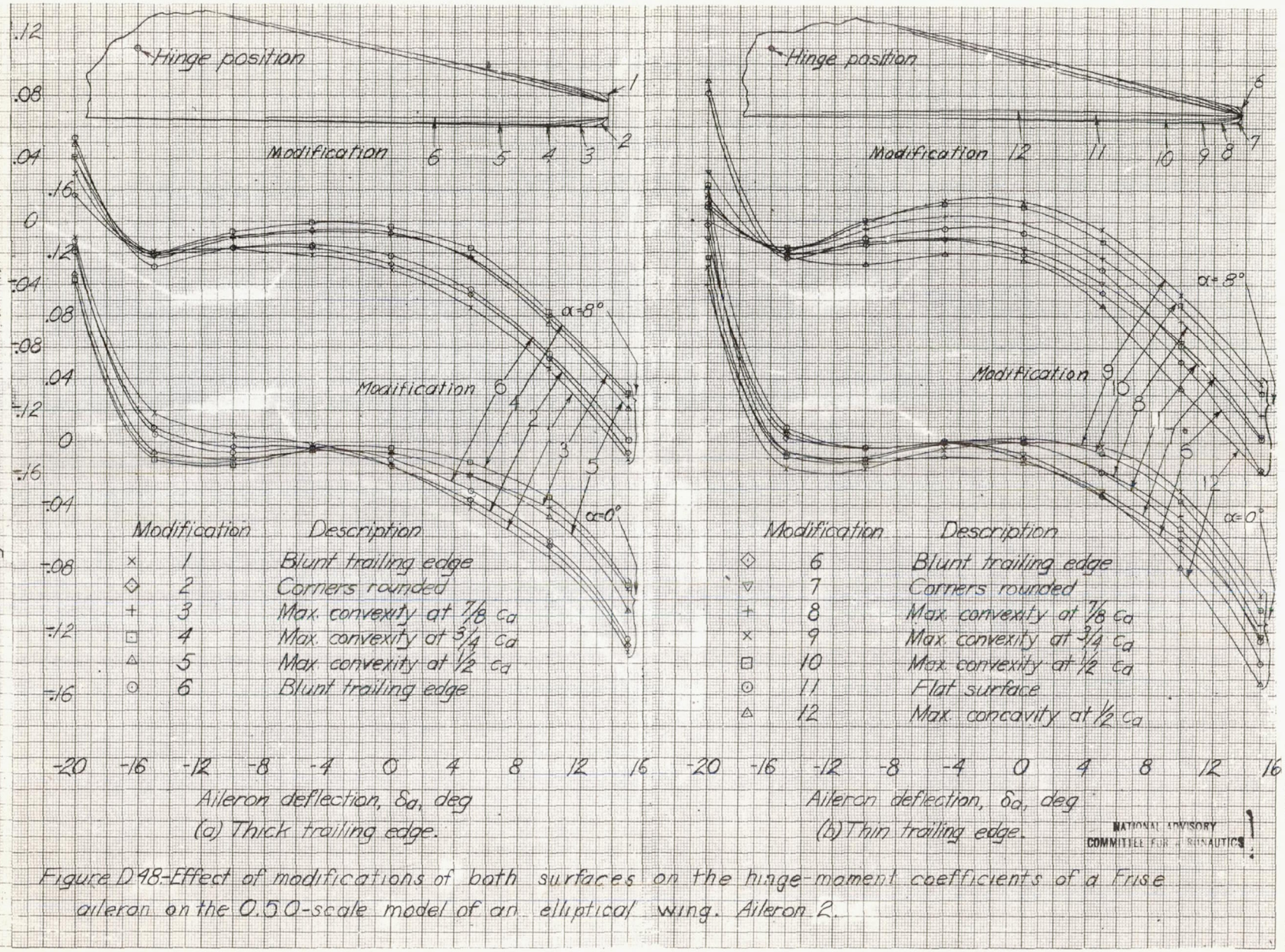

Figure D48.-Effect of modifications of both surfaces on the hinge-moment coefficients of a Frise aileron on the 0.50-scale model of an elliptical wing. Aileron 2.

Model D-VIII

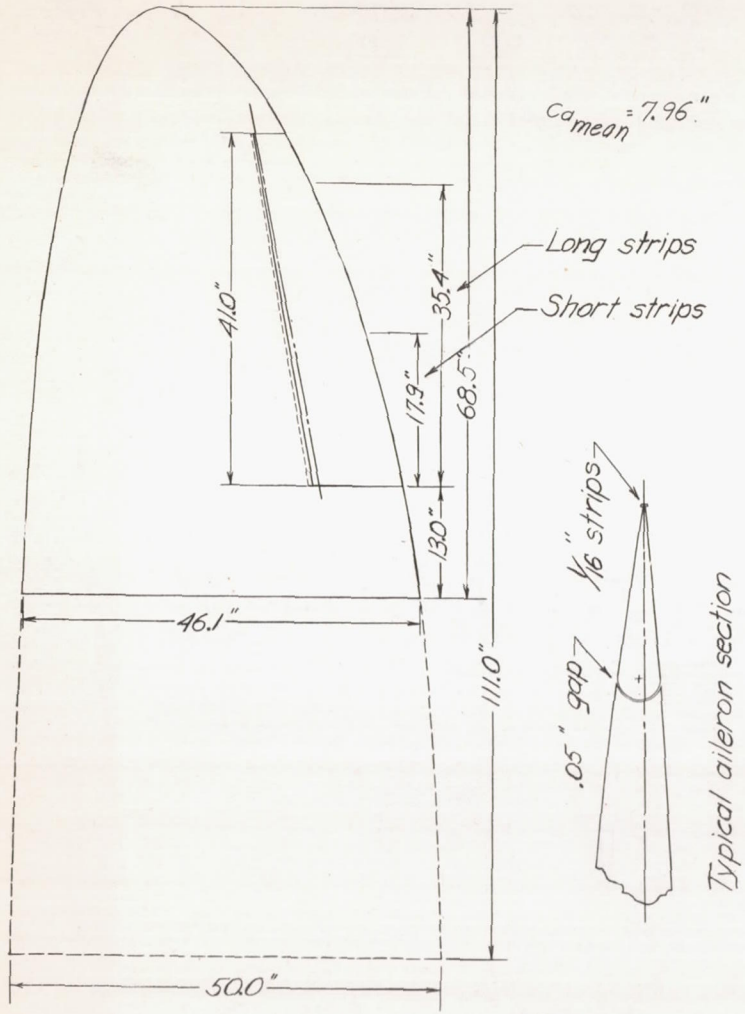

Figure D49-Plain aileron on a 0.50-scale model of an elliptical wing. N.P.L. 7-foot tunnel.

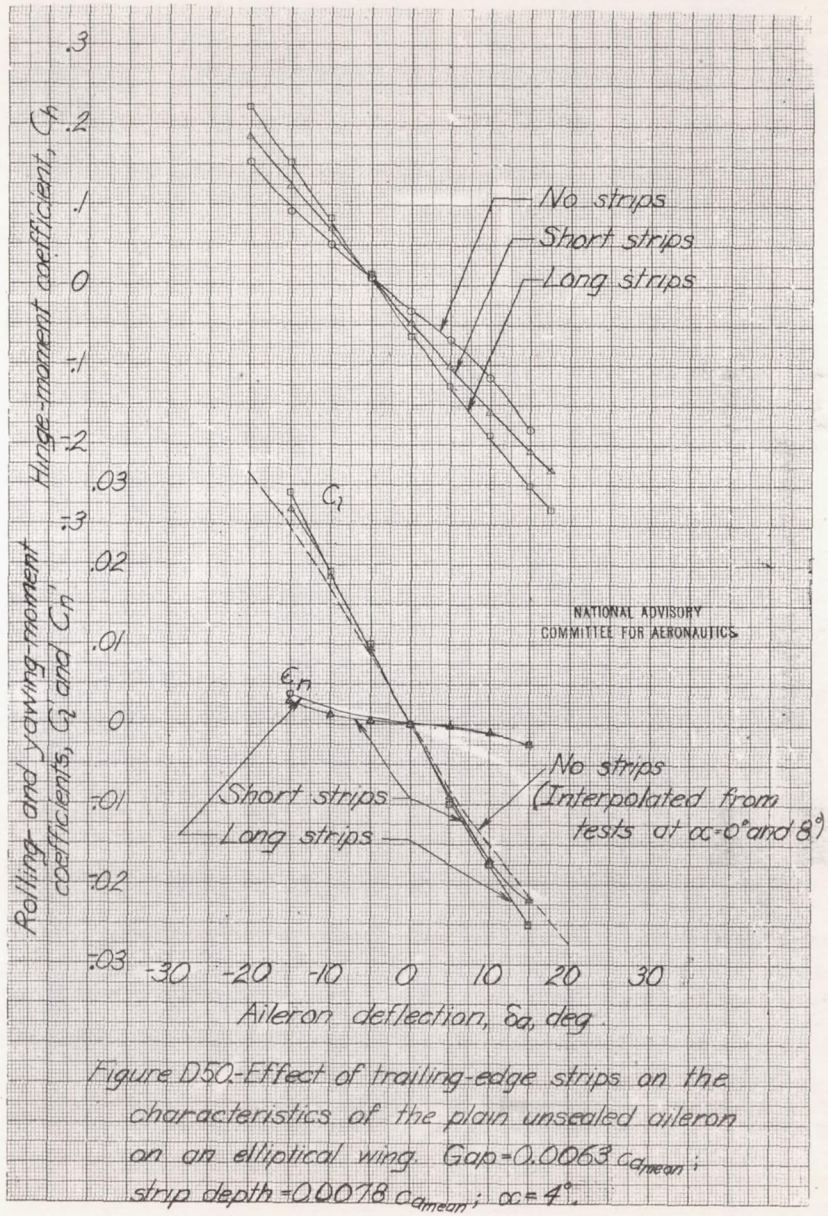

Figure D50-Effect of trailing-edge strips on the characteristics of the plain unsealed aileron on an elliptical wing. Gap=0.0063 $c_{a_{mean}}$; strip depth=0.0078 $c_{a_{mean}}$; α=4°.

Model D-IX

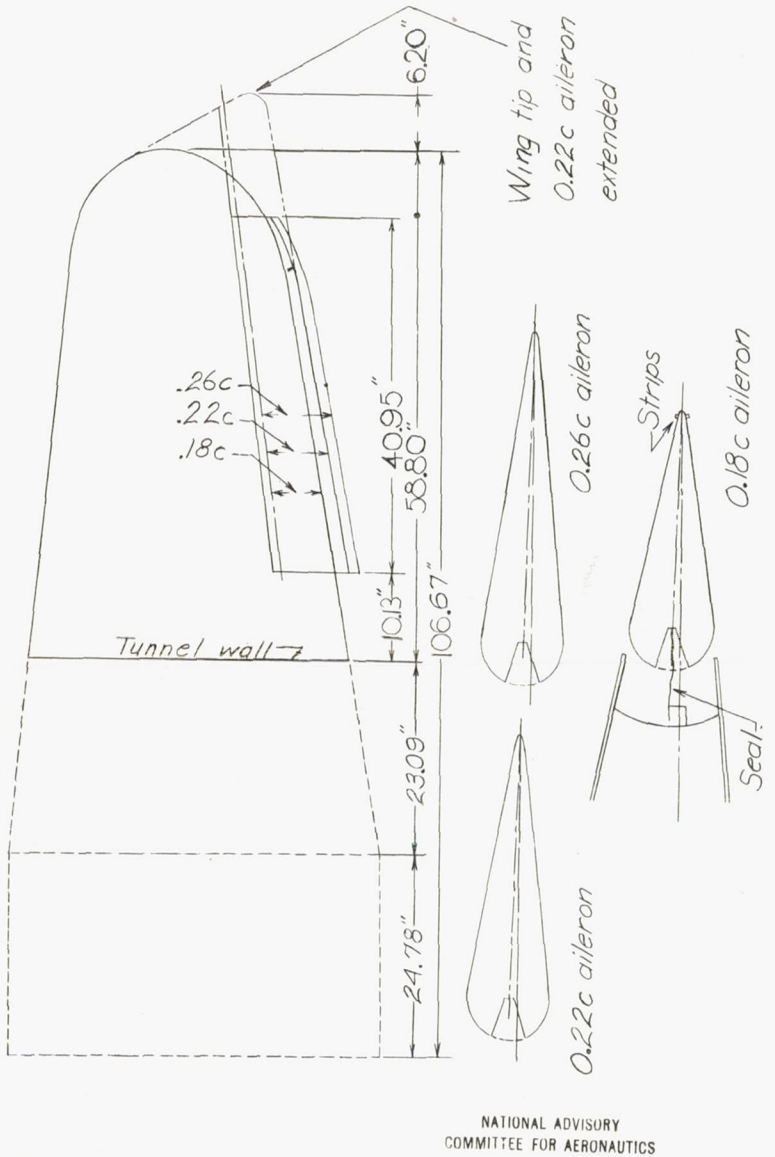

Figure D51.-The $\frac{1}{2.25}$-scale tapered-wing model and aileron sections. N.P.L. 7-foot No. 2 tunnel.

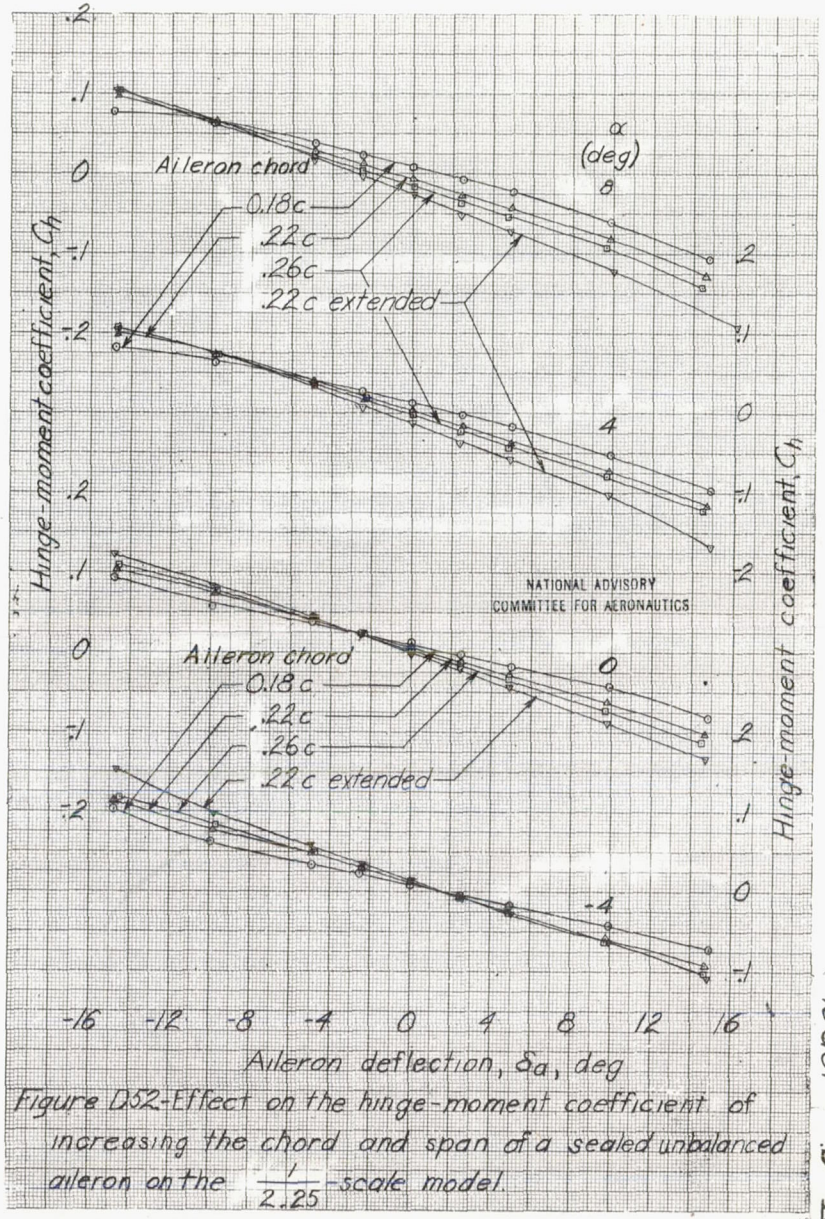

Figure D52.-Effect on the hinge-moment coefficient of increasing the chord and span of a sealed unbalanced aileron on the $\frac{1}{2.25}$-scale model.

Model D-X

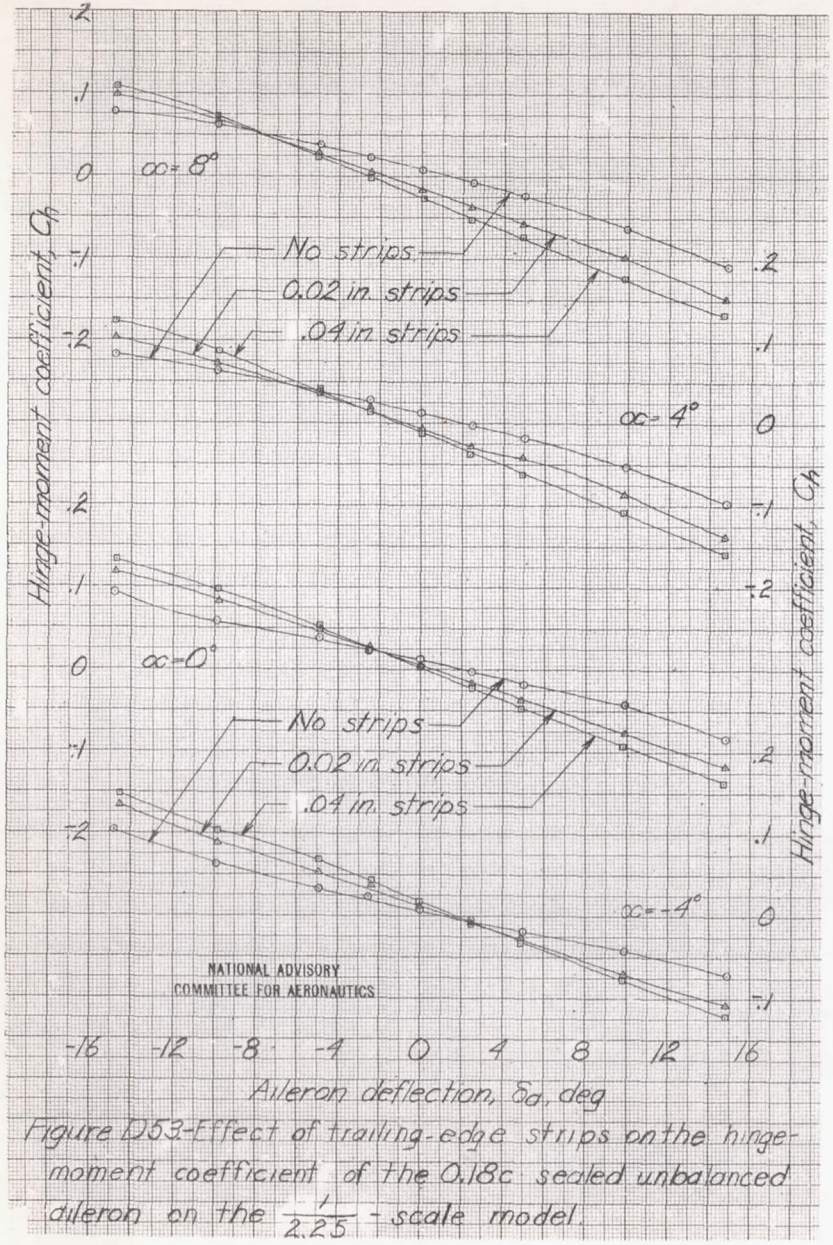

Figure D53-Effect of trailing-edge strips on the hinge-moment coefficient of the 0.18c sealed unbalanced aileron on the $\frac{1}{2.25}$ - scale model.

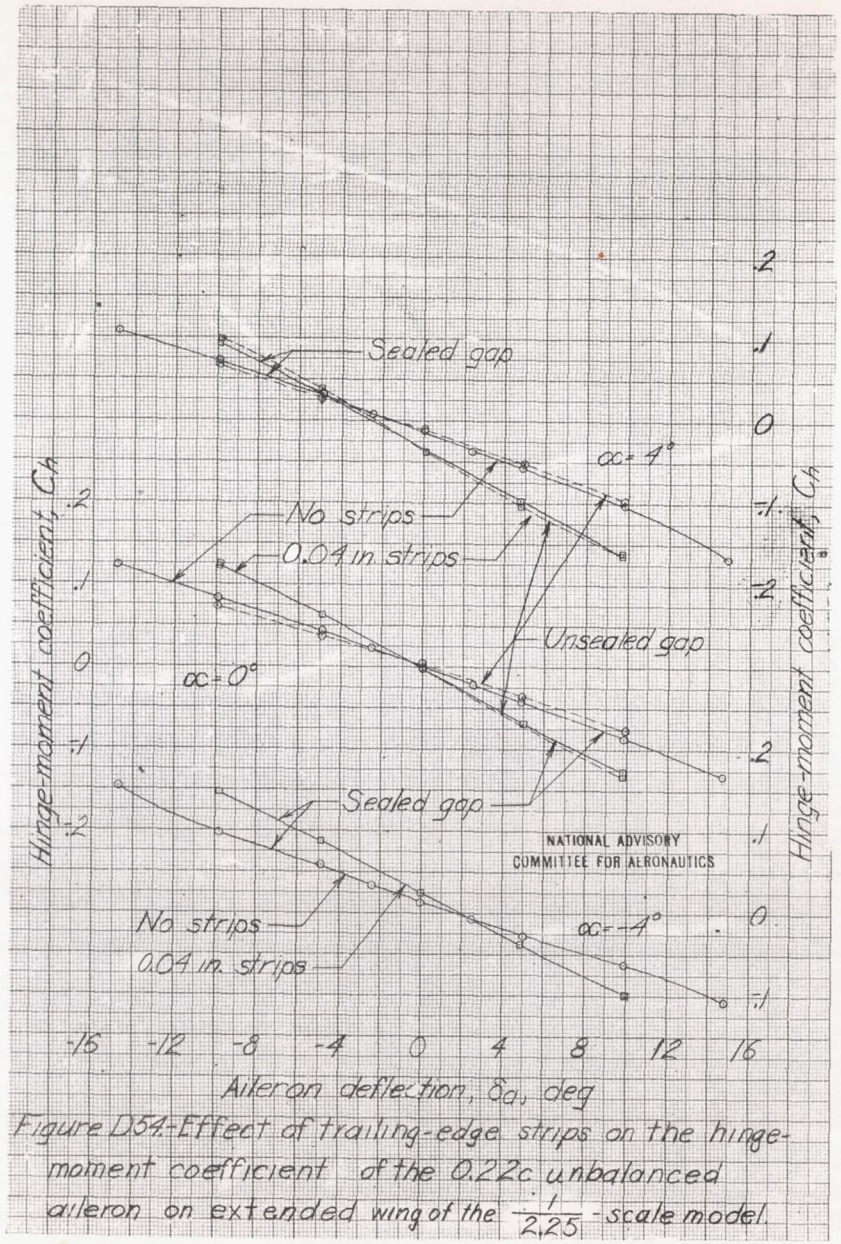

Figure D54-Effect of trailing-edge strips on the hinge-moment coefficient of the 0.22c unbalanced aileron on extended wing of the $\frac{1}{2.25}$ - scale model.

Model D-X

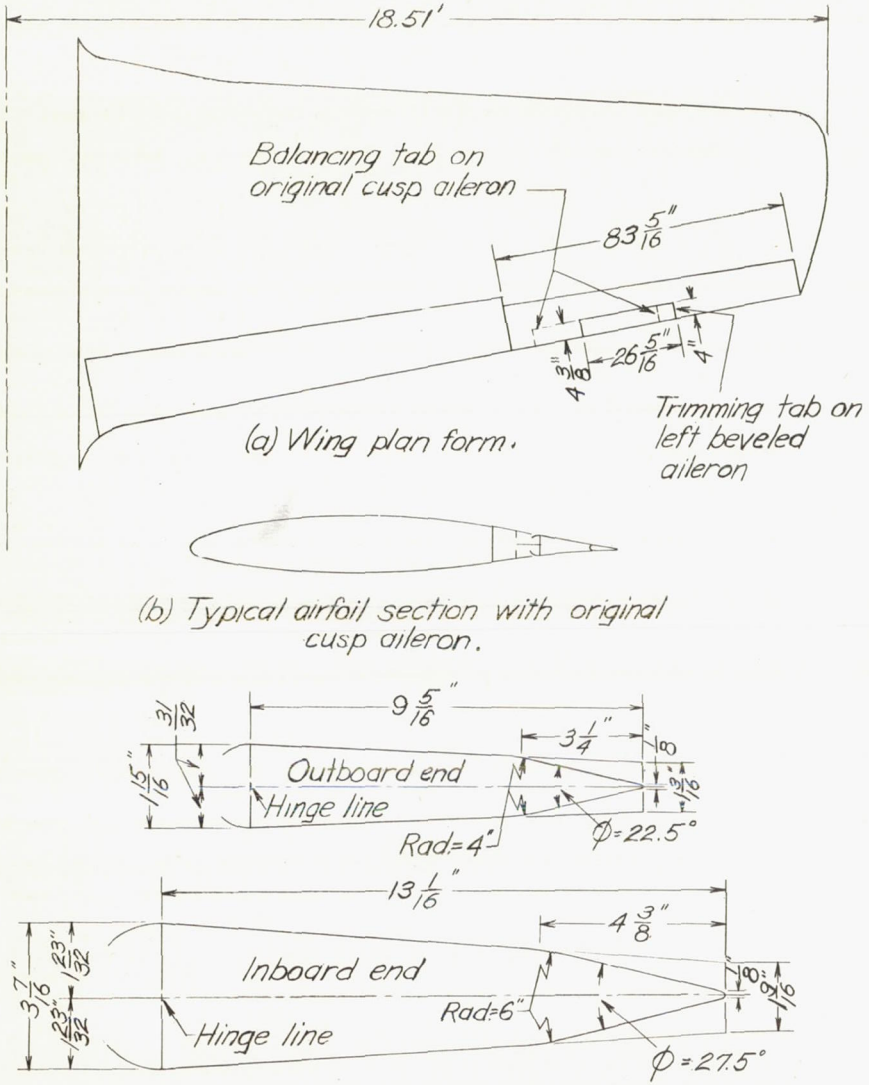

Figure D55.-Wing plan form and aileron sections of fighter airplane used in flight tests at LMAL.

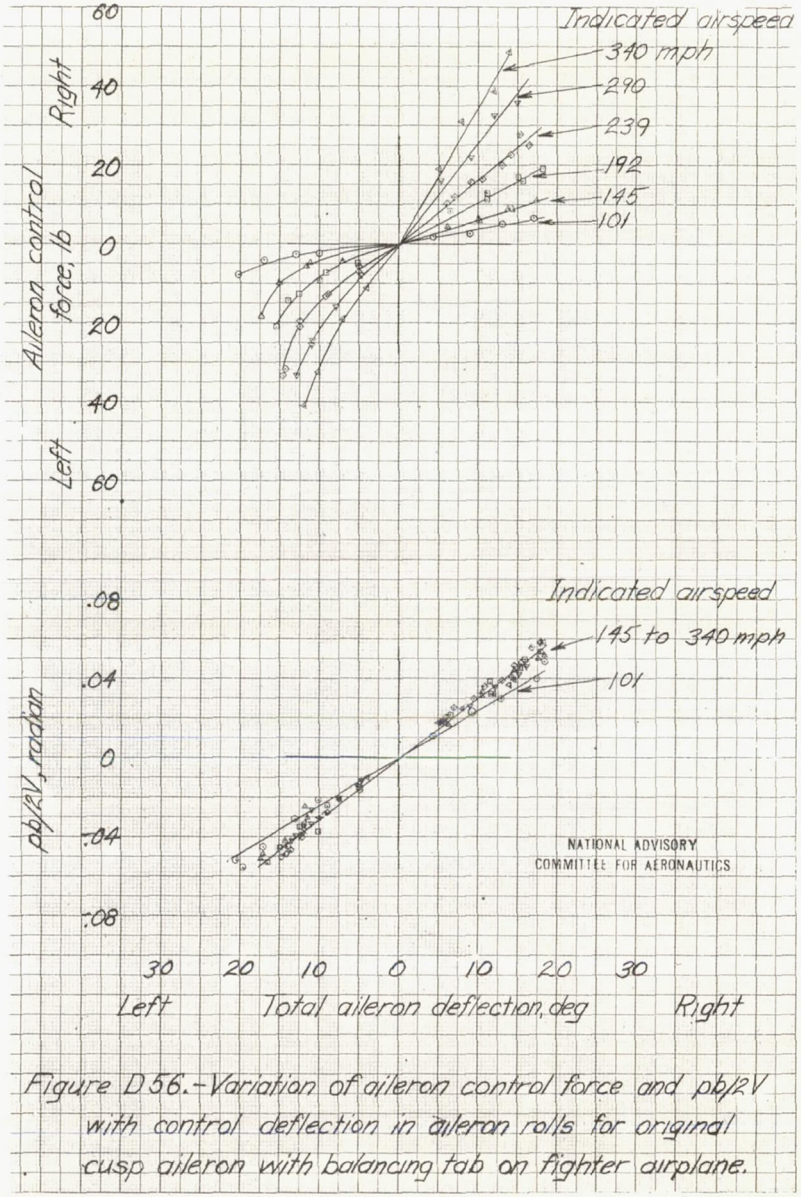

Figure D56.-Variation of aileron control force and pb/2V with control deflection in aileron rolls for original cusp aileron with balancing tab on fighter airplane.

Airplane D-XI

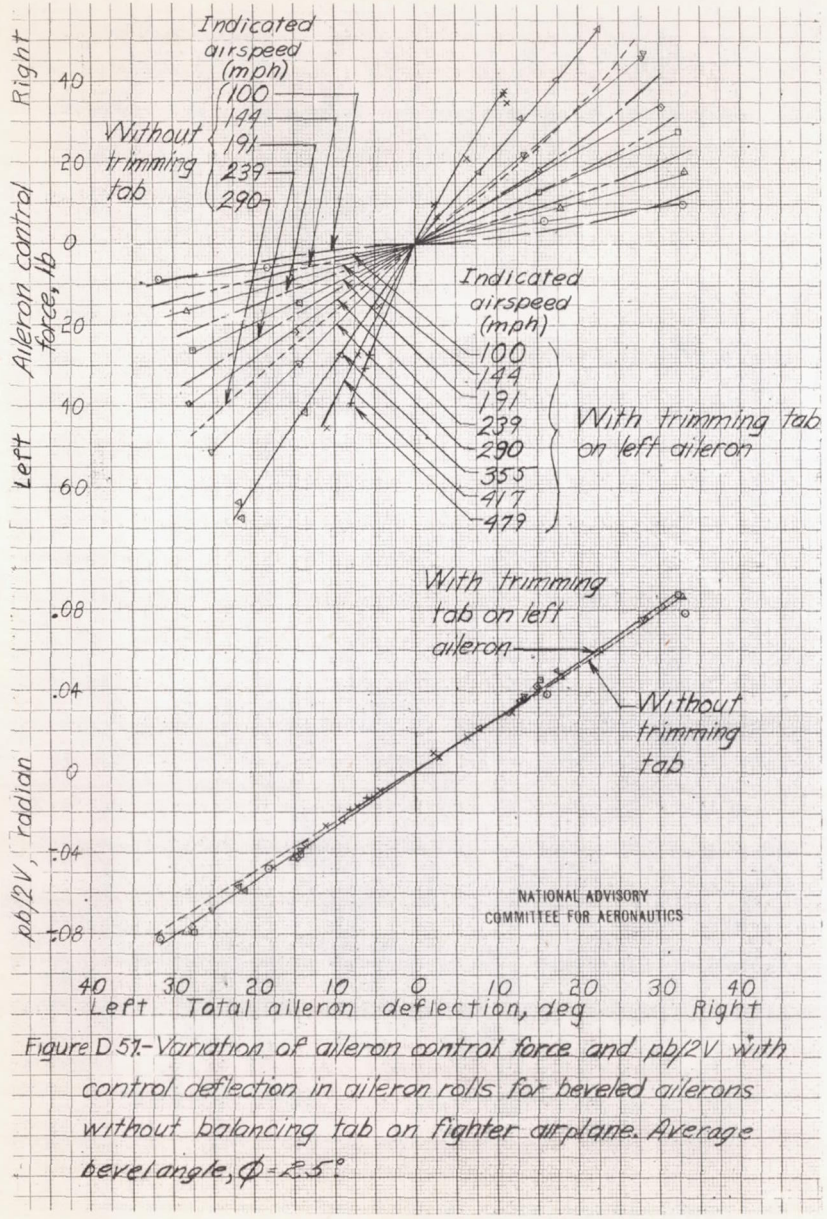

Figure D 57.- Variation of aileron control force and pb/2V with control deflection in aileron rolls for beveled ailerons without balancing tab on fighter airplane. Average bevel angle, $\phi = 2.5°$.

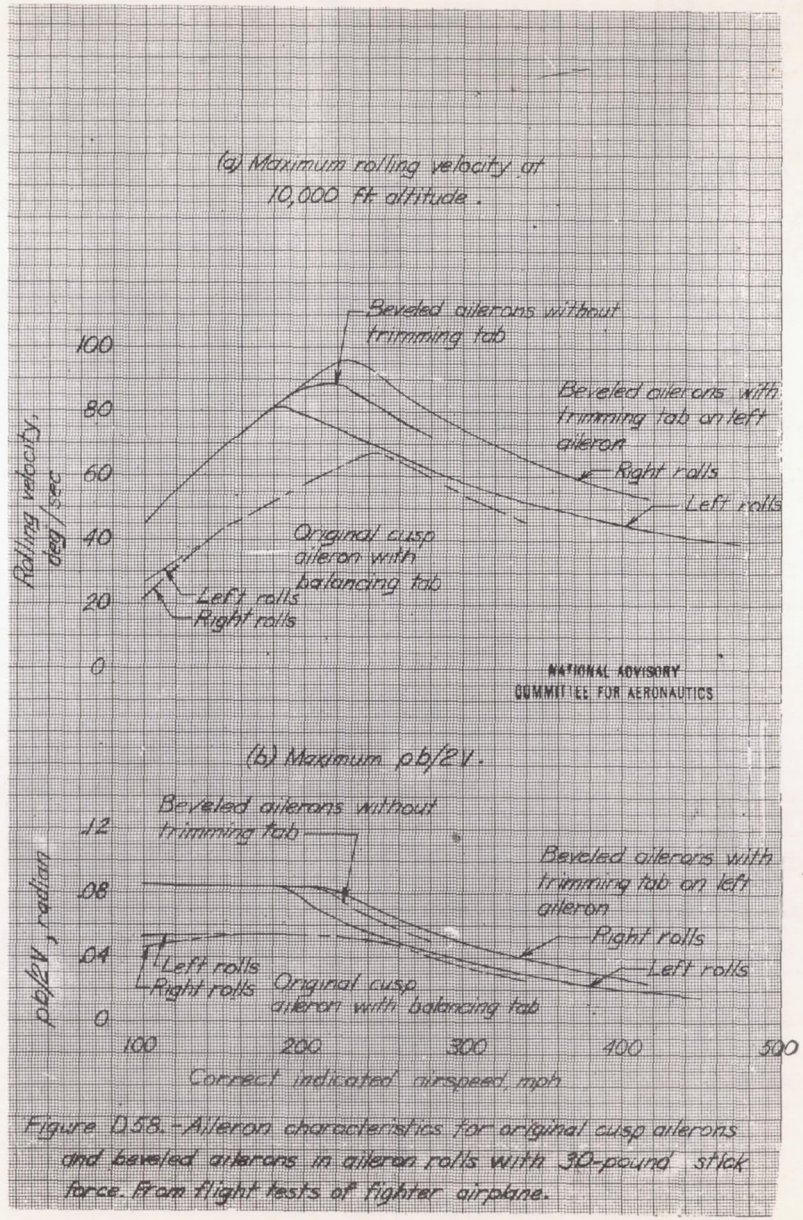

Figure D 58.- Aileron characteristics for original cusp ailerons and beveled ailerons in aileron rolls with 30-pound stick force. From flight tests of fighter airplane.

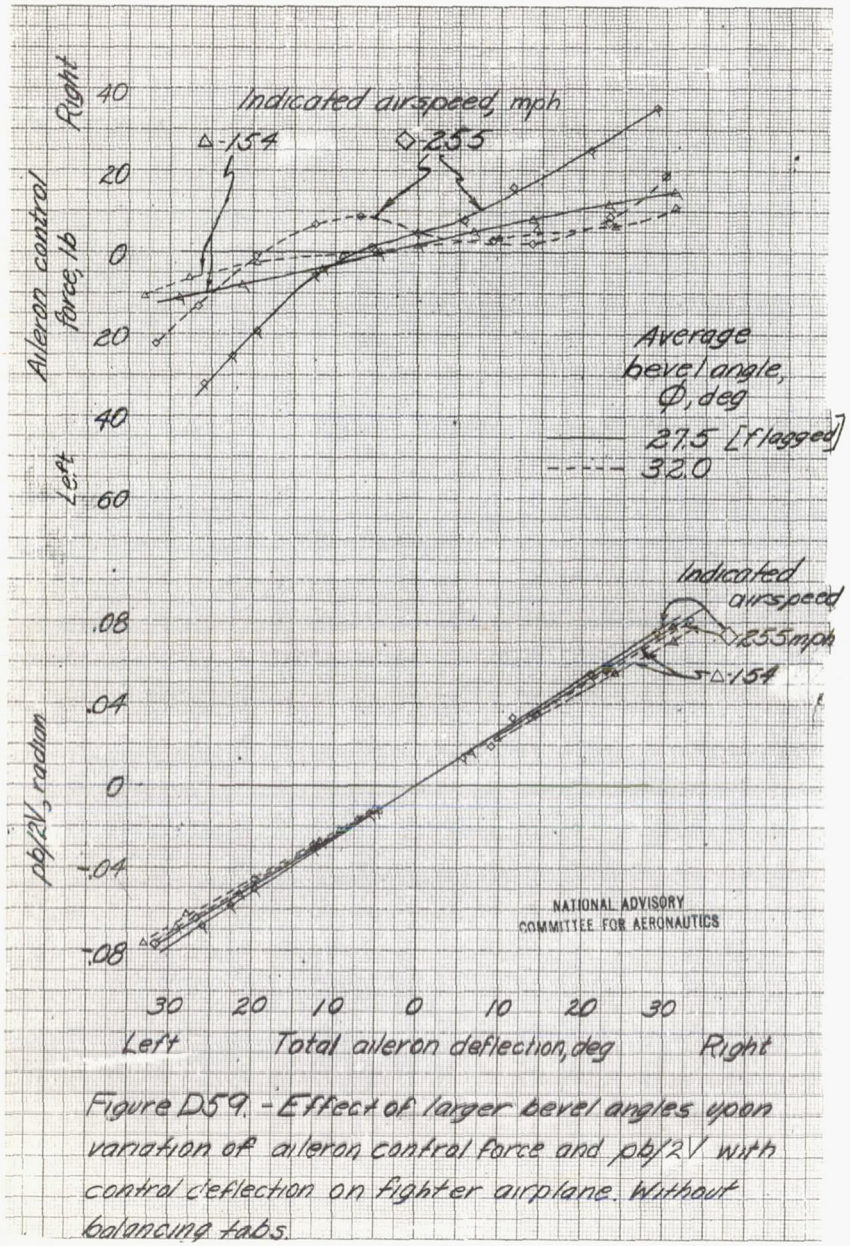

Figure D59.- Effect of larger bevel angles upon variation of aileron control force and pb/2V with control deflection on fighter airplane. Without balancing tabs.

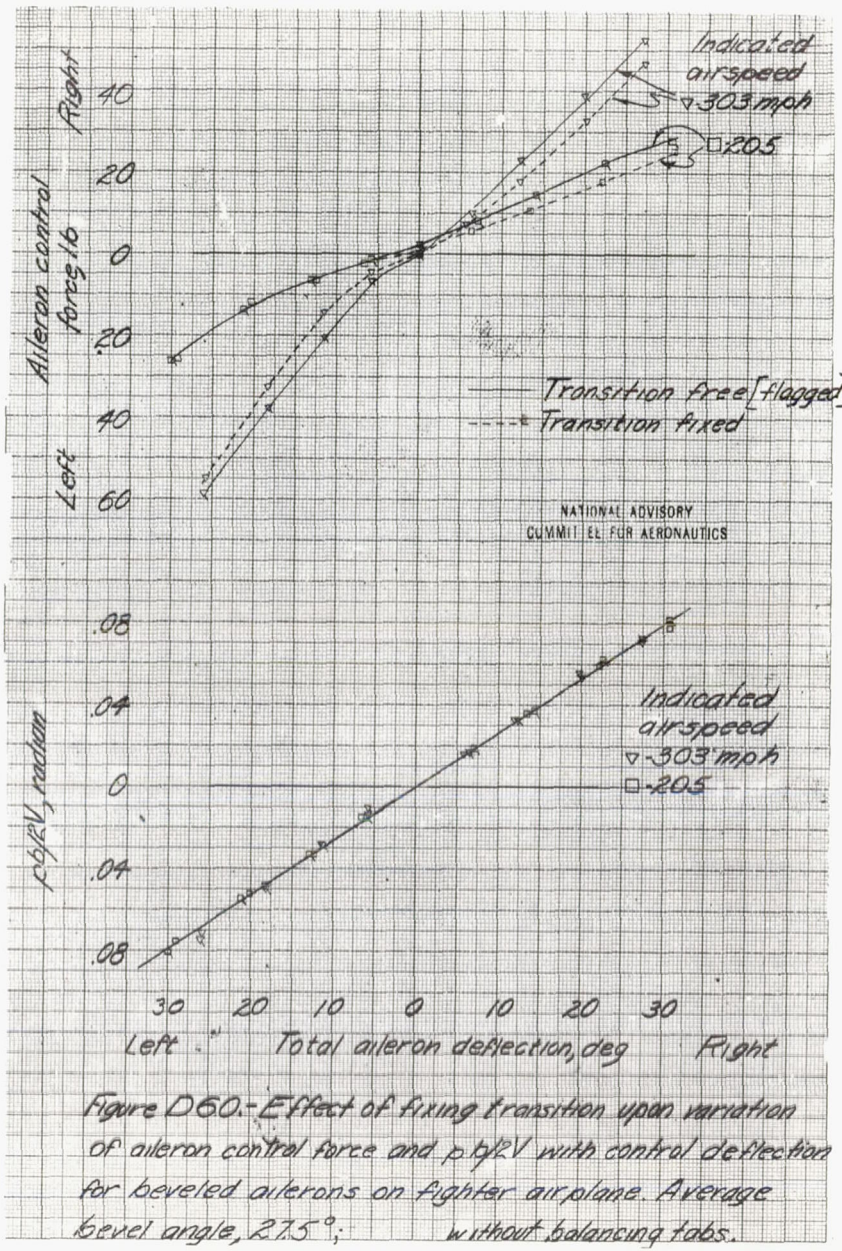

Figure D60.- Effect of fixing transition upon variation of aileron control force and pb/2V with control deflection for beveled ailerons on fighter airplane. Average bevel angle, 27.5°; without balancing tabs.

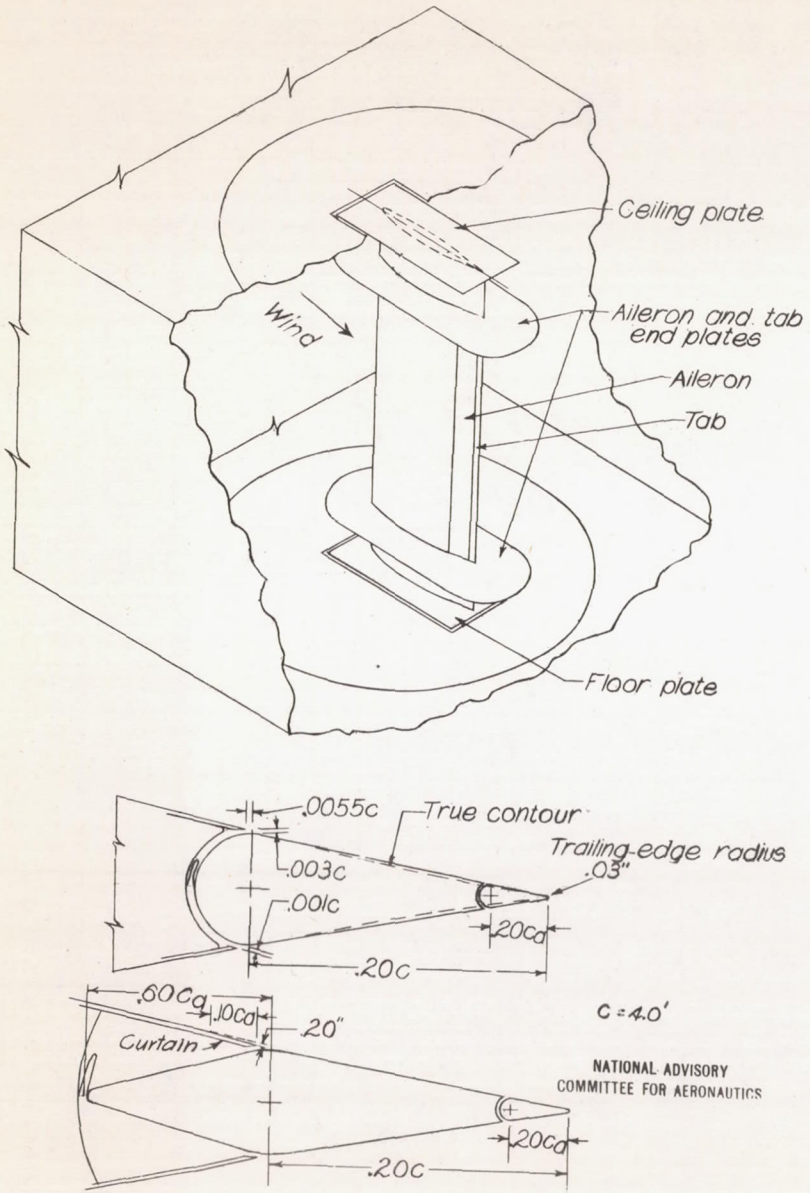

Figure E1.- Two-dimensional test installation and the 0.20c_a tab tested on a 0.20c straight-sided aileron with two balance arrangements. NACA 66(215)-216, a=.06 airfoil. AAL 7- by 10-foot tunnel.

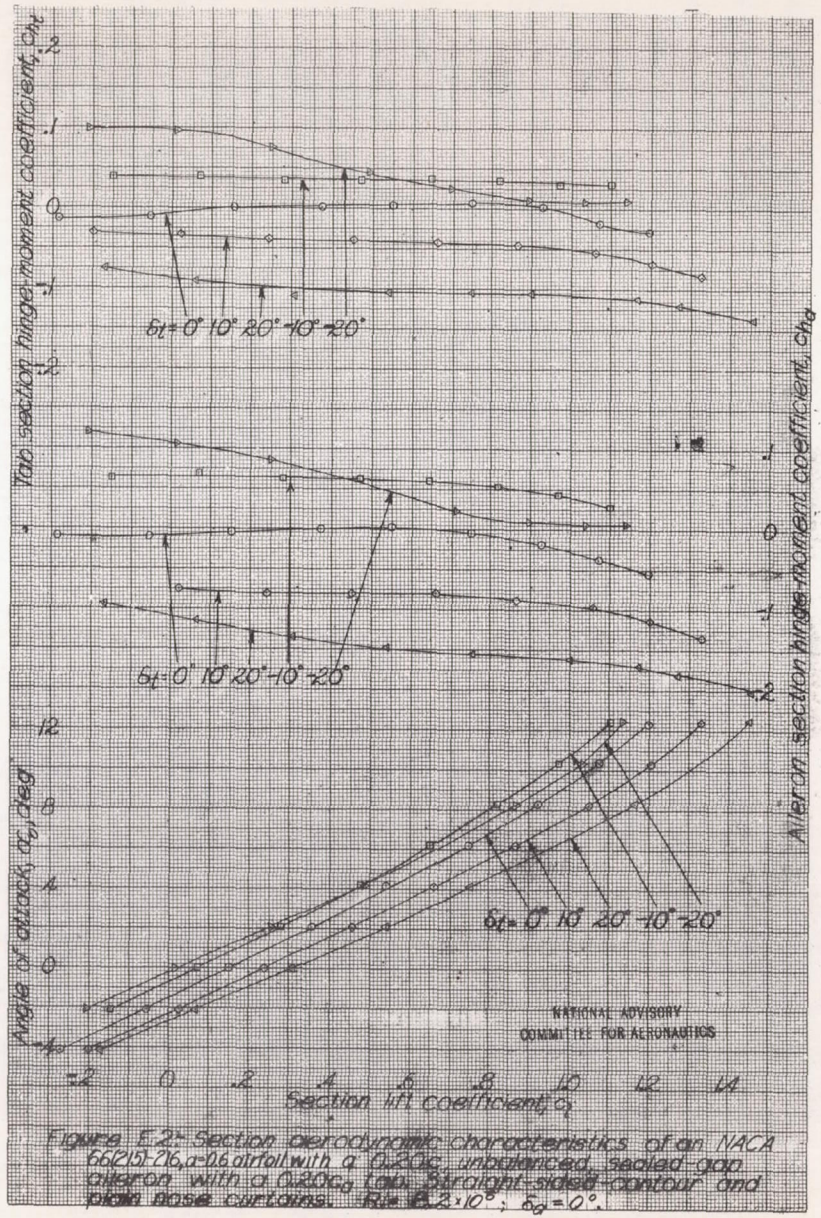

Figure E 2.- Section aerodynamic characteristics of an NACA 66(215)-216, a=.06 airfoil with a 0.20c unbalanced, sealed gap aileron with a 0.20c_a tab. Straight-sided contour and plain base curtains. $R = 6.2 \times 10^6$; $\delta_a = 0°$.

Model E-1

Model E-1

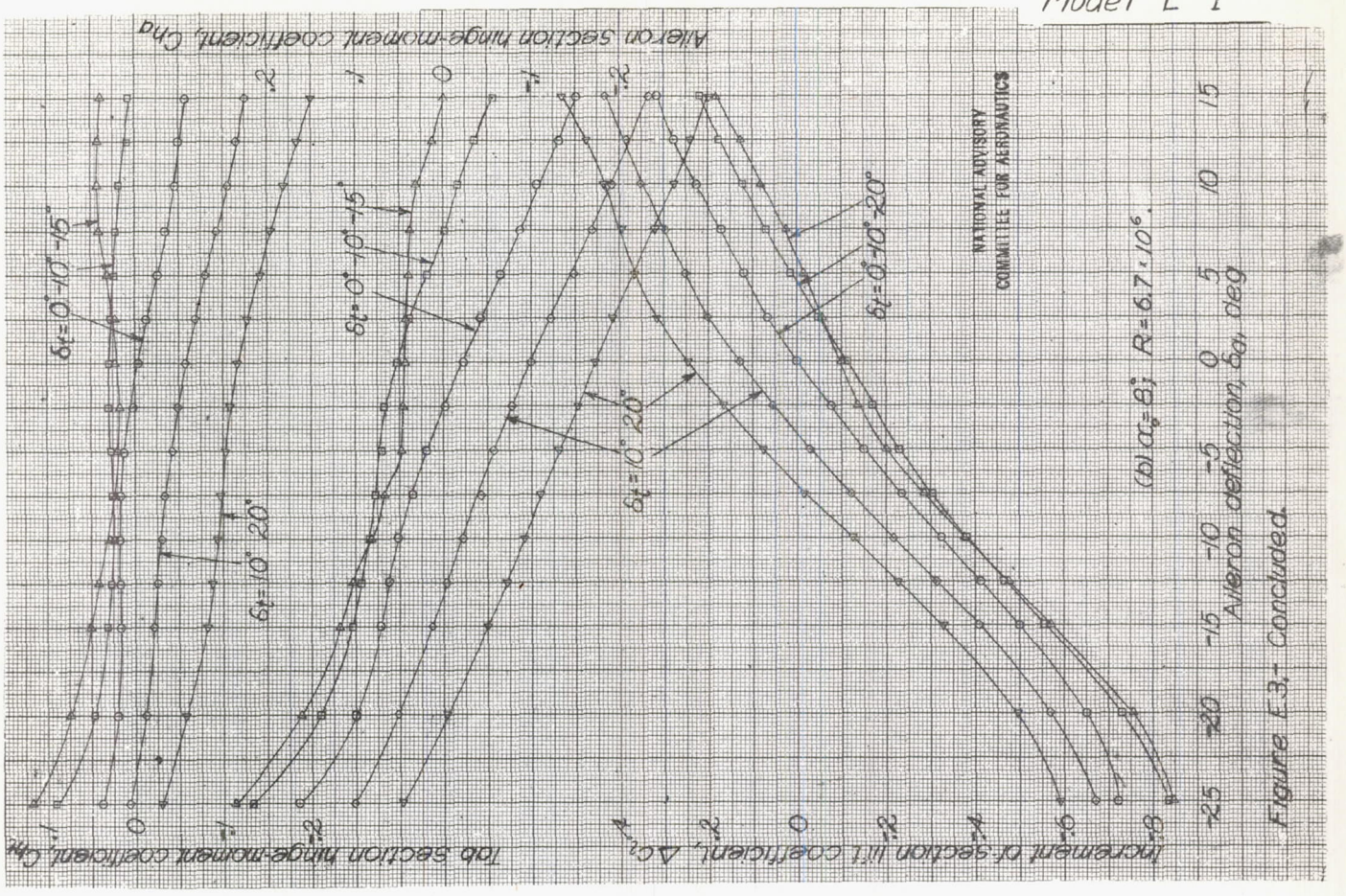

Figure E3.- Concluded.

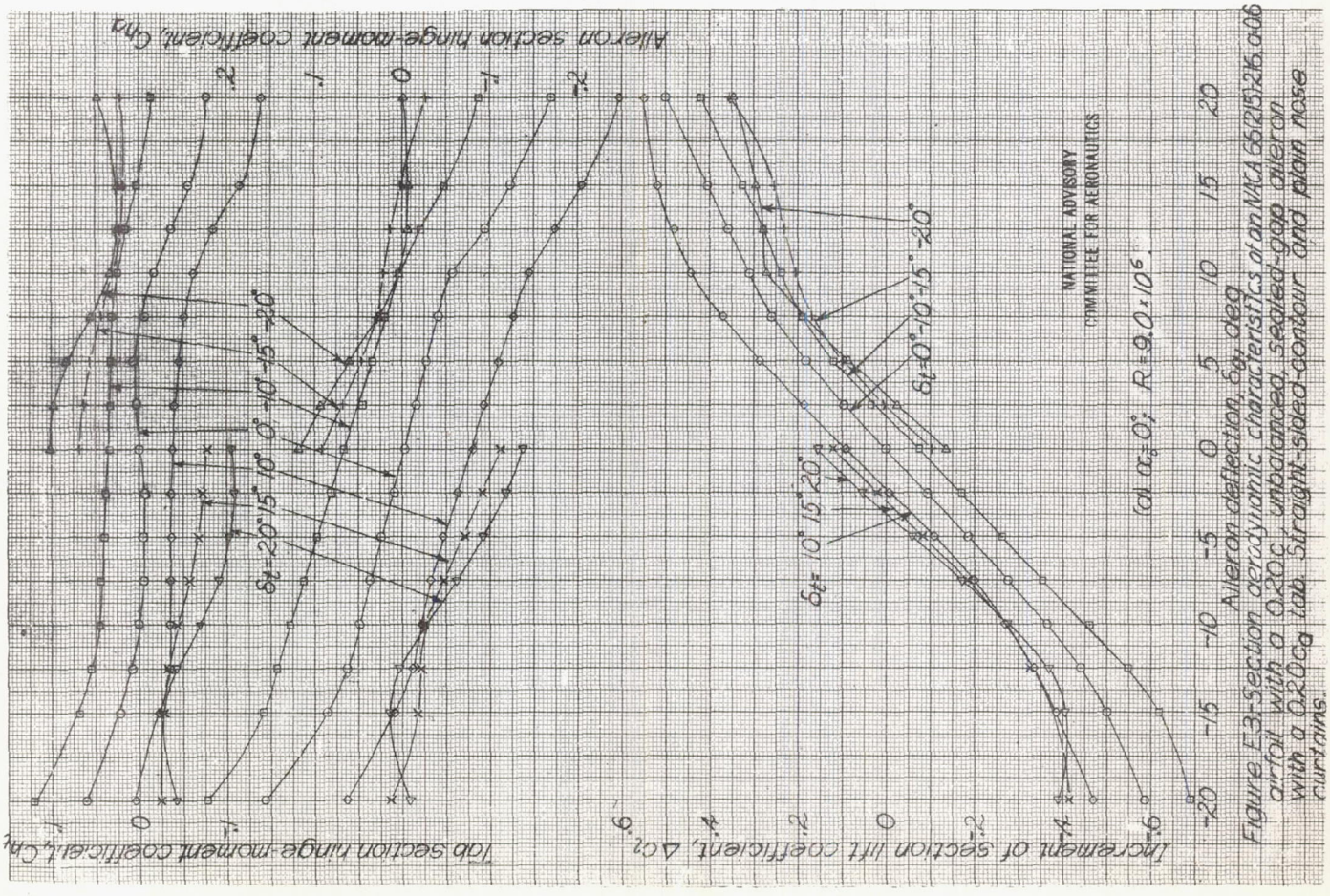

Figure E3.- Section aerodynamic characteristics of an NACA 66(215)216,a=0.6 airfoil with a 0.20c unbalanced, sealed-gap aileron with a 0.20c$_a$ tab. Straight-sided contour and plain nose curtains.

Model E-I

Figure E-5.- Section aerodynamic characteristics of an NACA 66(215)-216 airfoil with a 0.20c aileron with 0.60c sealed internal balance and a 0.20c unsealed tab. Straight-sided-contour and bent nose curtains. $R = 9.0 \times 10^6$; $\alpha_0 = 0°$.

Figure E-4.- Section aerodynamic characteristics of an NACA 66(215)-216 airfoil with a 0.20c aileron with 0.60c sealed internal balance and a 0.20c unsealed tab. Straight-sided-contour and bent nose curtains. $R = 8.2 \times 10^6$; $\alpha_0 = 0°$.

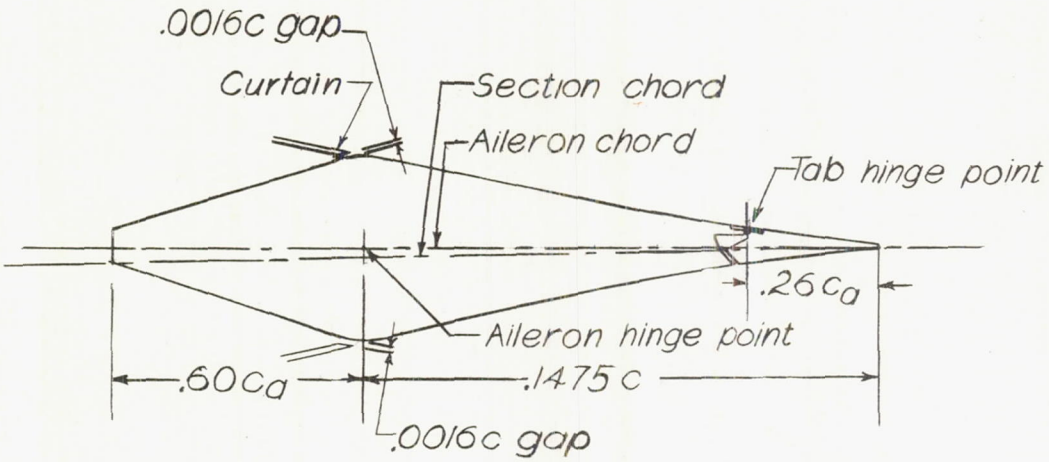

Figure E6.- 0.1475c, sealed, internally balanced aileron with a 0.26c_a tab tested on NACA 66,2-118.a = 1.0 (approx.) airfoil section. Effective aileron balance, 0.689c_a; NACA two-dimensional low-turbulence tunnel.

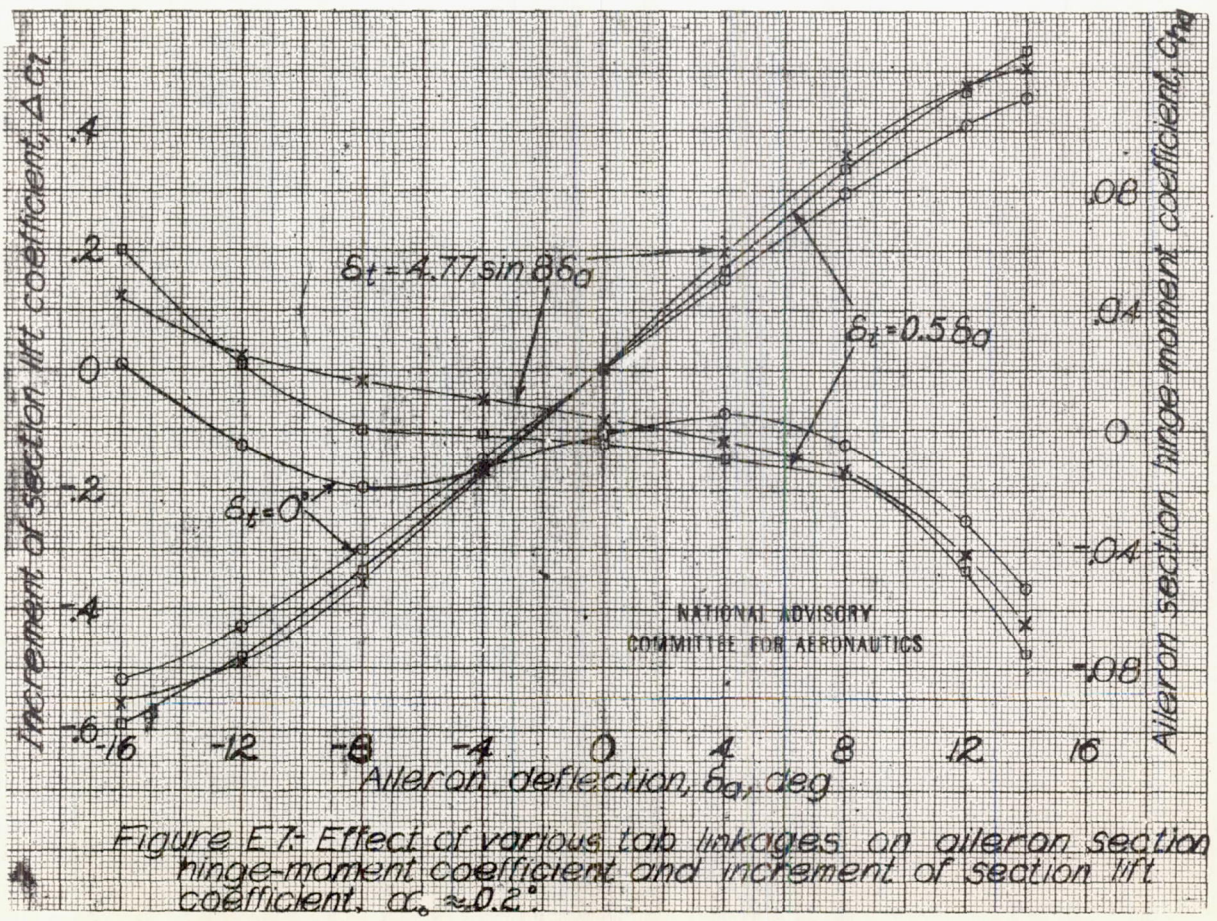

Figure E7.- Effect of various tab linkages on aileron section hinge-moment coefficient and increment of section lift coefficient, $\alpha_o \approx 0.2°$.

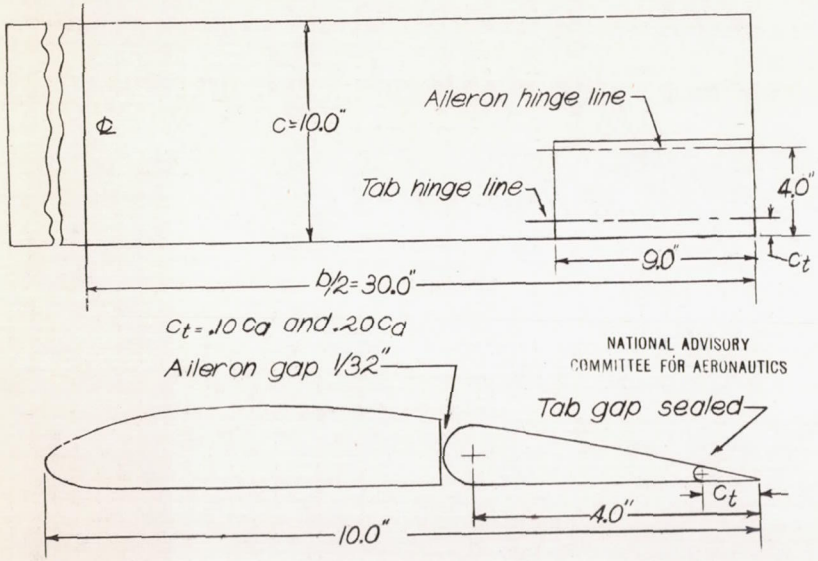

Figure E8.- 0.40c by 0.30 b/2 aileron with 0.10c_a and 0.20c_a full-span tabs on a 10" by 60" Clark Y wing. ∠MAL 7-by 10-foot tunnel.

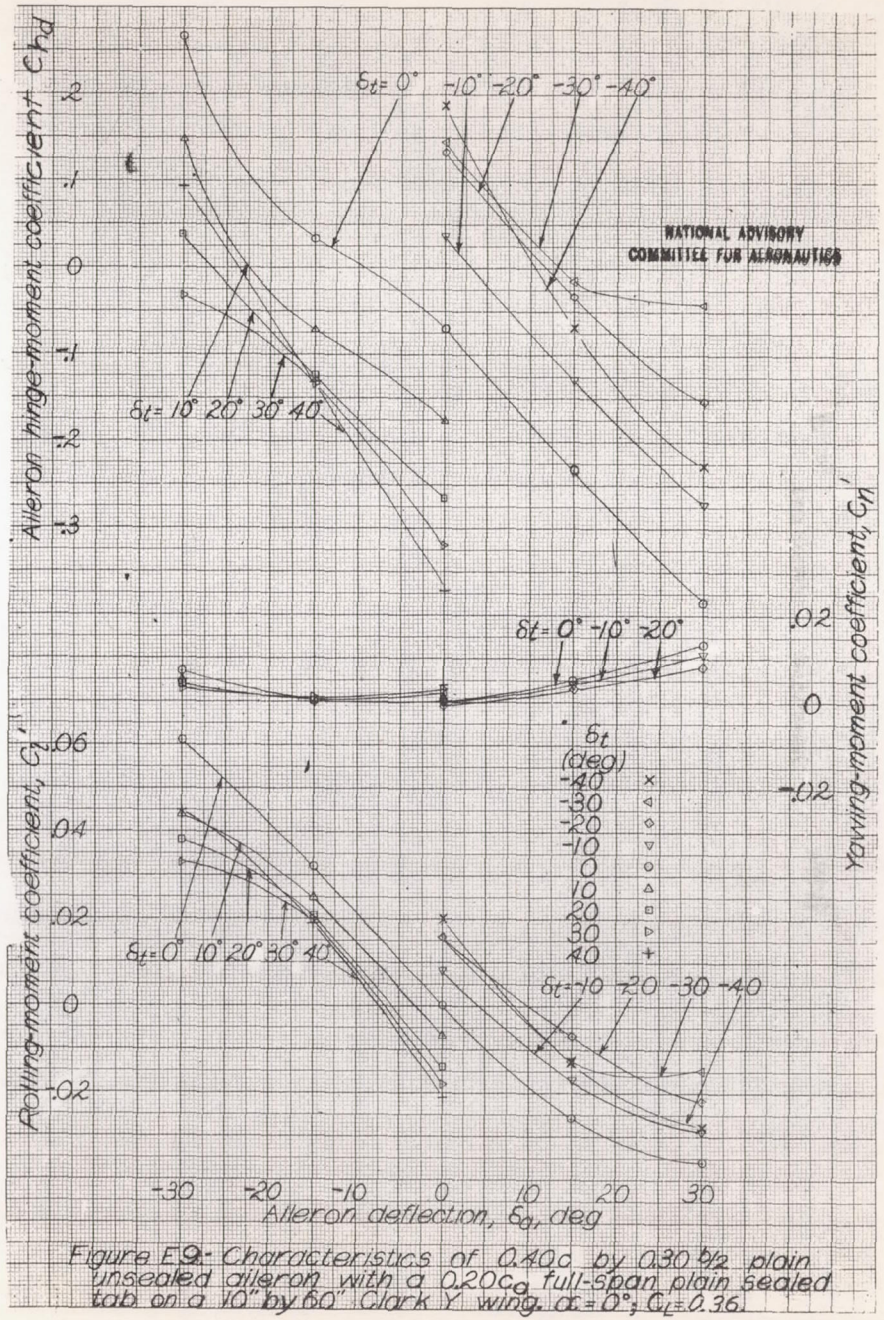

Figure E9.- Characteristics of 0.40c by 0.30 b/2 plain unsealed aileron with a 0.20c_a full-span plain sealed tab on a 10" by 60" Clark Y wing. α=0°; C_L=0.36.

Model E-III

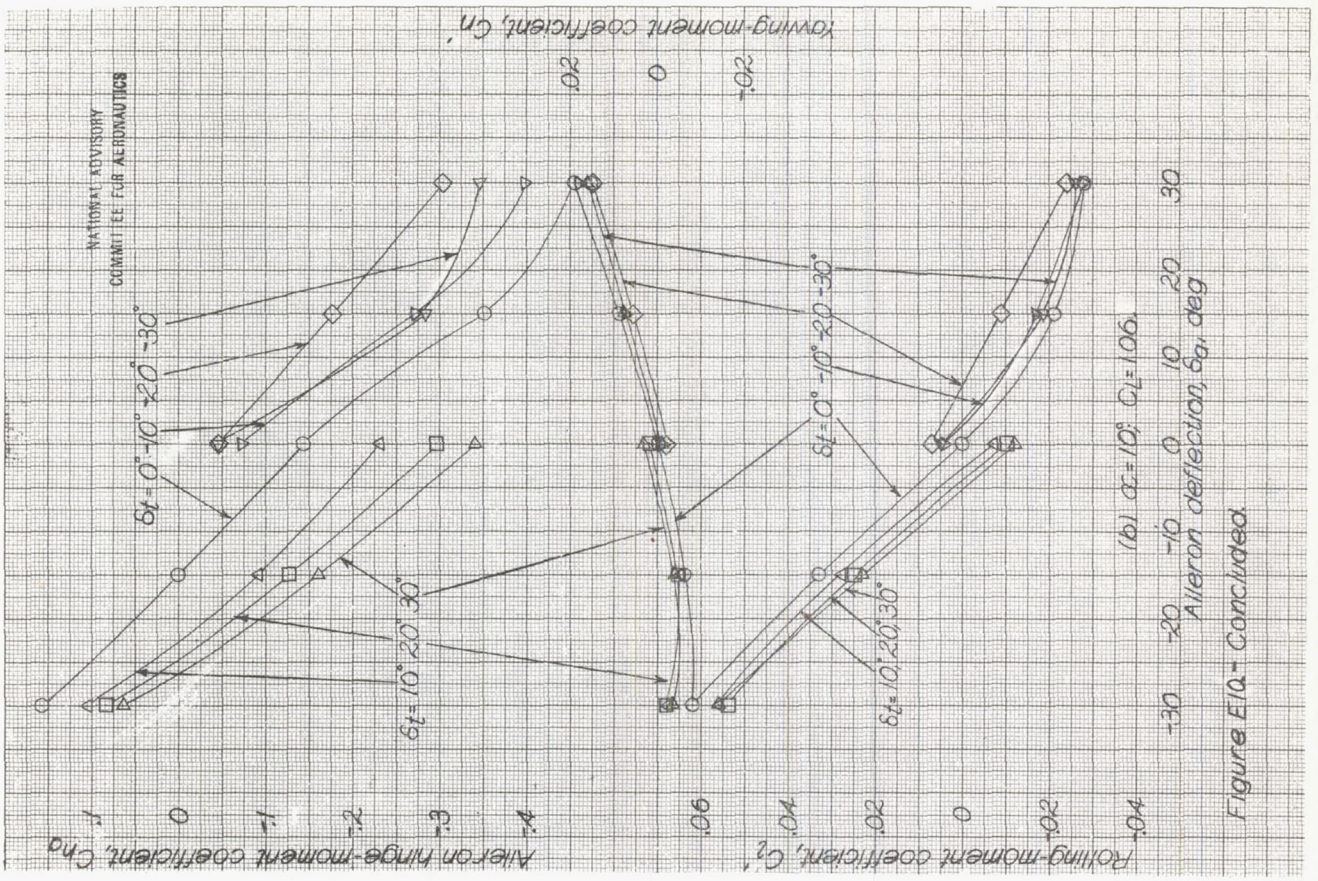

Figure E10.- Concluded.

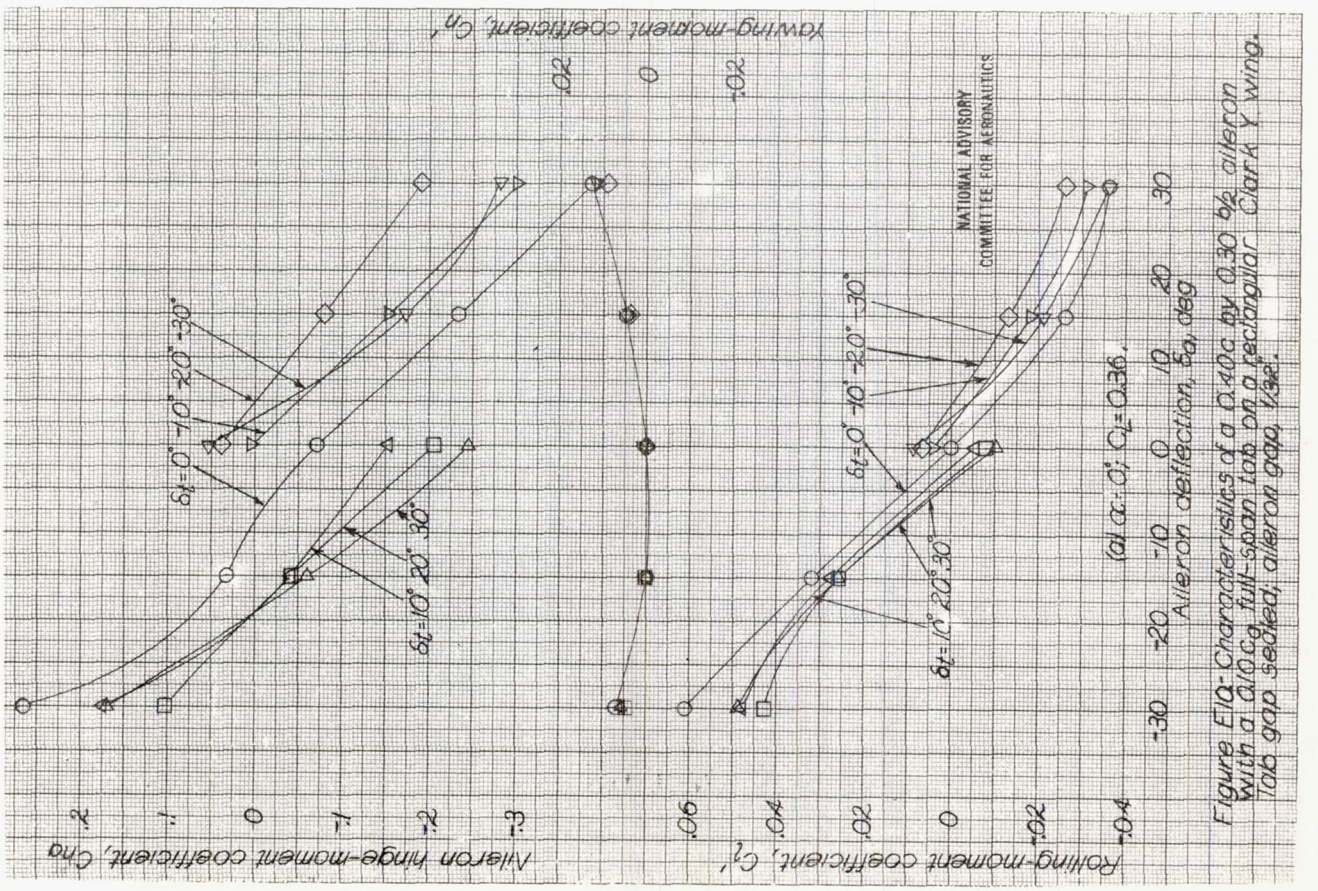

Figure E10.- Characteristics of a 0.40c by 0.30 b/2 aileron with a 0.10c, full-span tab on a rectangular Clark Y wing. Tab gap sealed; aileron gap open.

Model E-IV

L-419

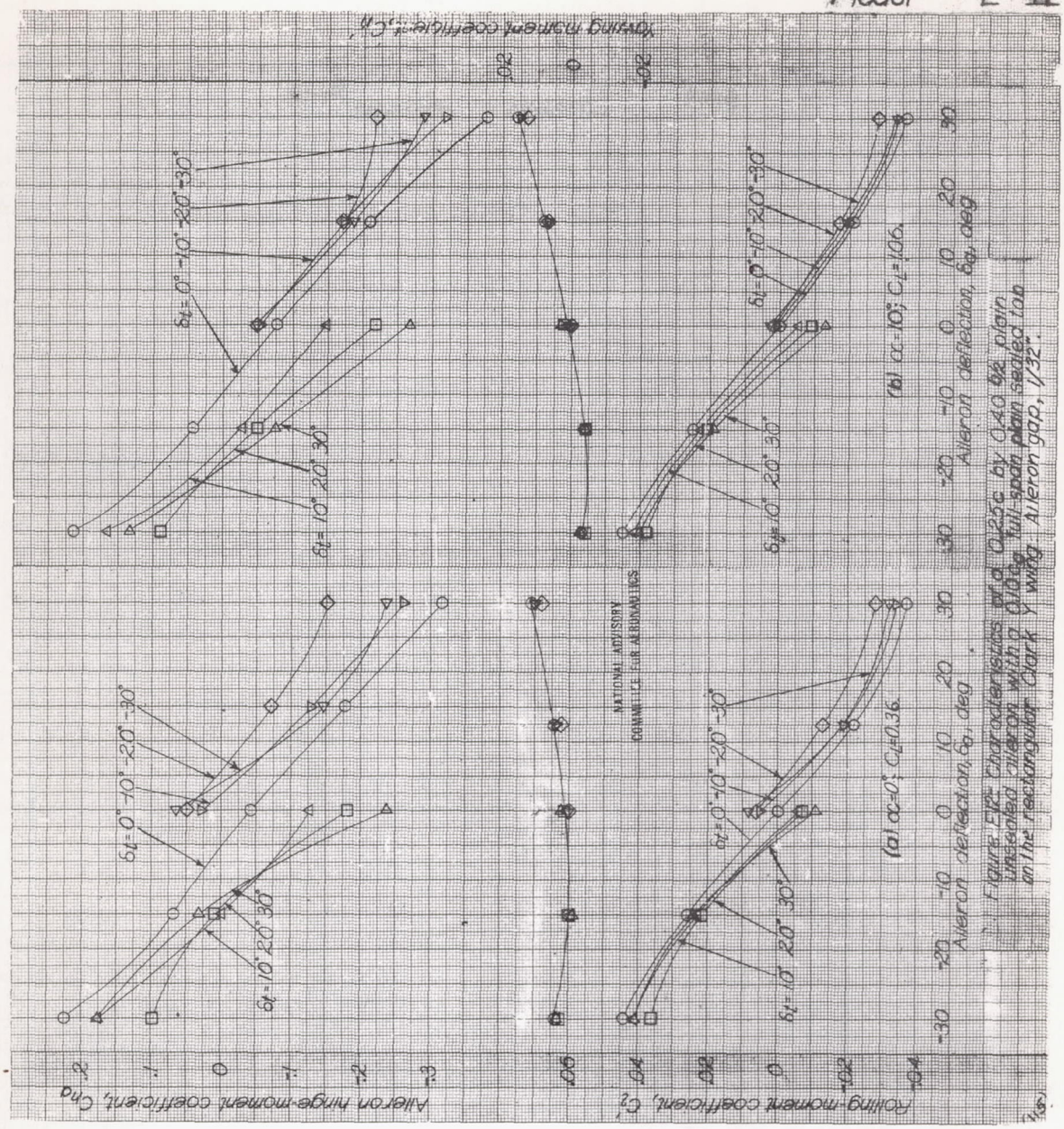

Figure E11.- Characteristics of 0.25c by 0.40 b/2 plain unsealed aileron with 0.10c$_a$ full-span plain sealed tab on the rectangular Clark Y wing. Aileron gap, 1/32".

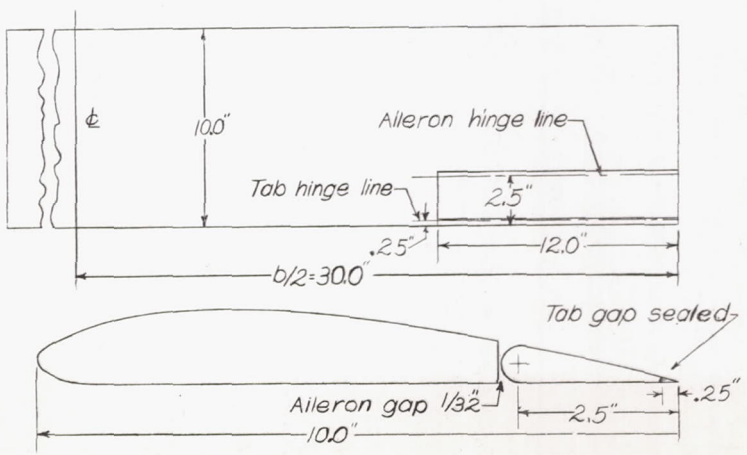

Figure E11.- 0.25c by 0.40 b/2 aileron with 0.10c$_a$ full-span tab on a 10" by 60" Clark Y wing. LMAL 7-by 10-foot tunnel.

NATIONAL ADVISORY
COMMITTEE FOR AERONAUTICS

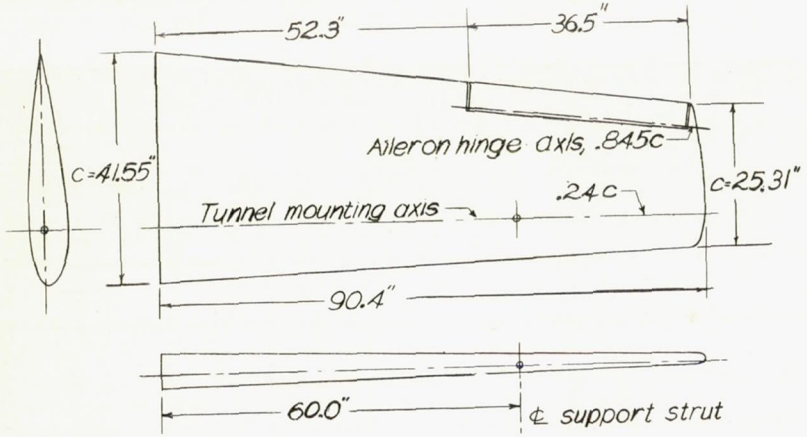

Figure E13.-Semispan model of tapered wing. LMAL 7-by 10-foot tunnel.

NATIONAL ADVISORY COMMITTEE FOR AERONAUTICS

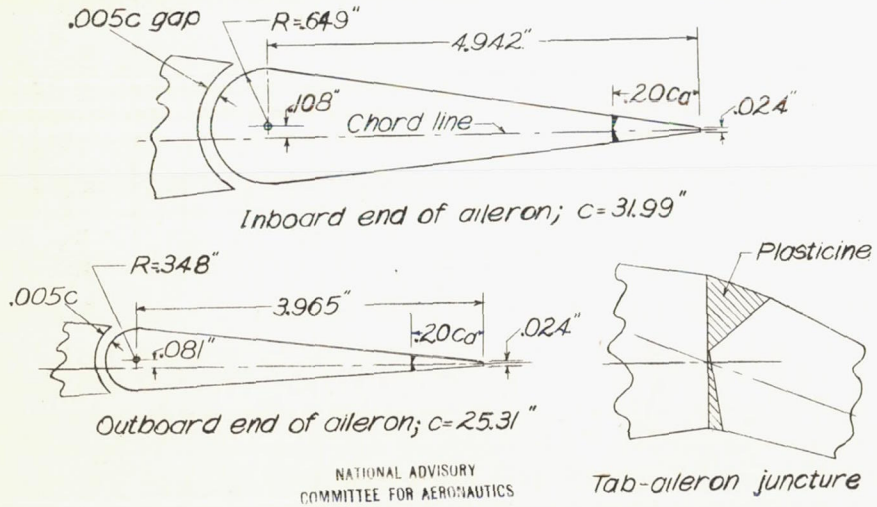

NATIONAL ADVISORY COMMITTEE FOR AERONAUTICS

Figure E14.- 0.155c by 0.405 $b/2$ plain aileron with a 0.20c_a by 1.0 b_a inset tab.

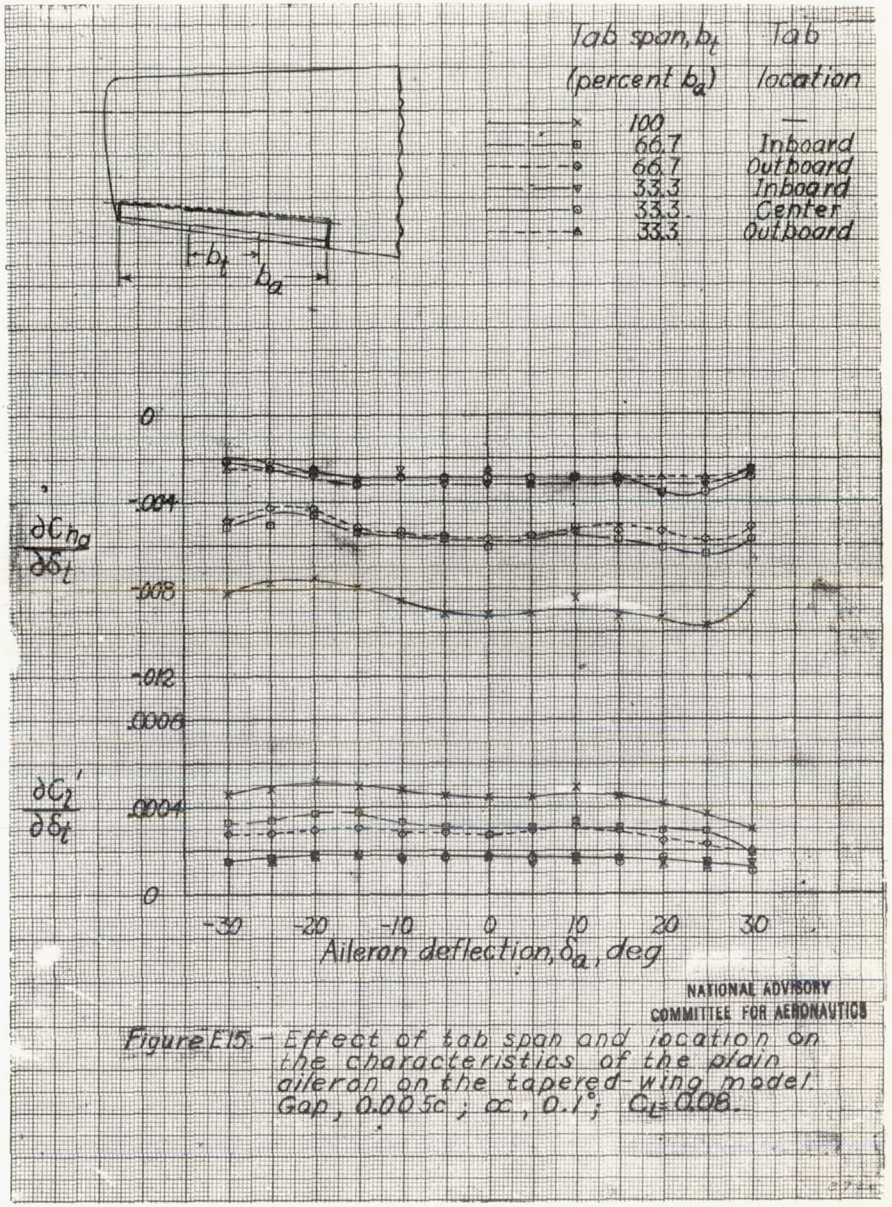

NATIONAL ADVISORY COMMITTEE FOR AERONAUTICS

Figure E15.- Effect of tab span and location on the characteristics of the plain aileron on the tapered-wing model. Gap, 0.005c; α, 0.1°; C_L=0.06.

Model E-V

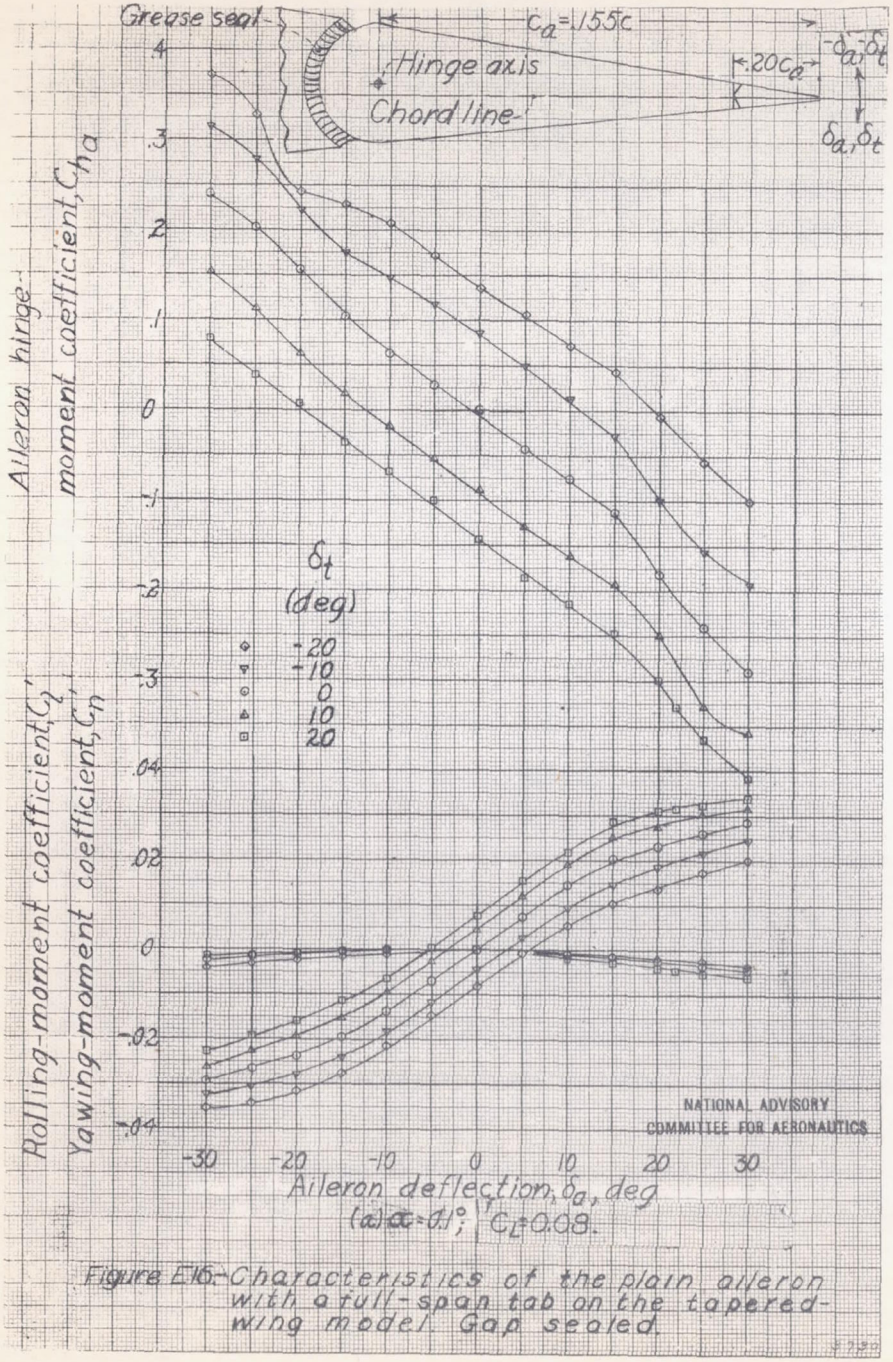

(a) α=0.1°; C_L=0.08.

Figure E16.- Characteristics of the plain aileron with a full-span tab on the tapered-wing model. Gap sealed.

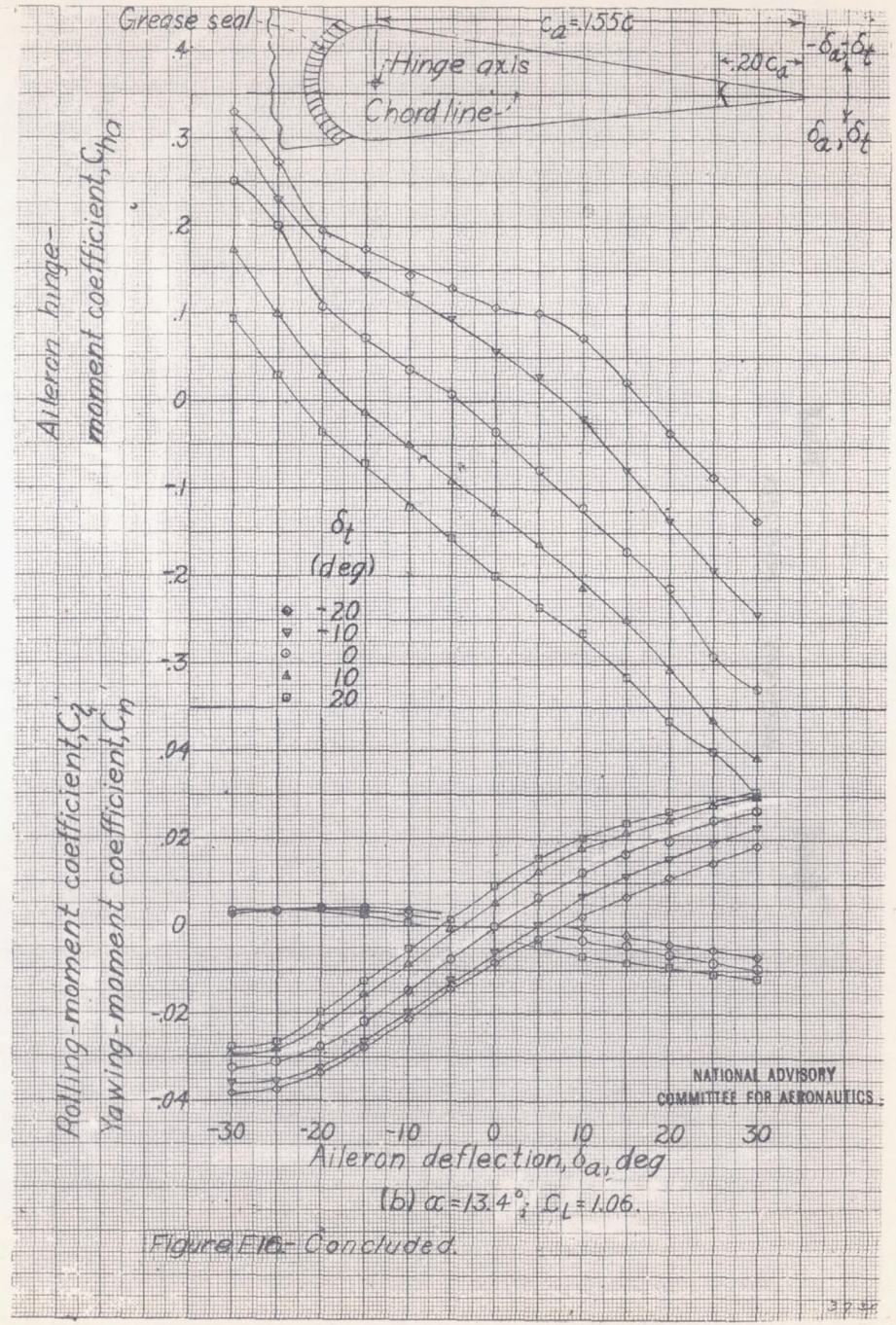

(b) α=13.4°; C_L=1.06.

Figure E16.- Concluded.

Model E-1

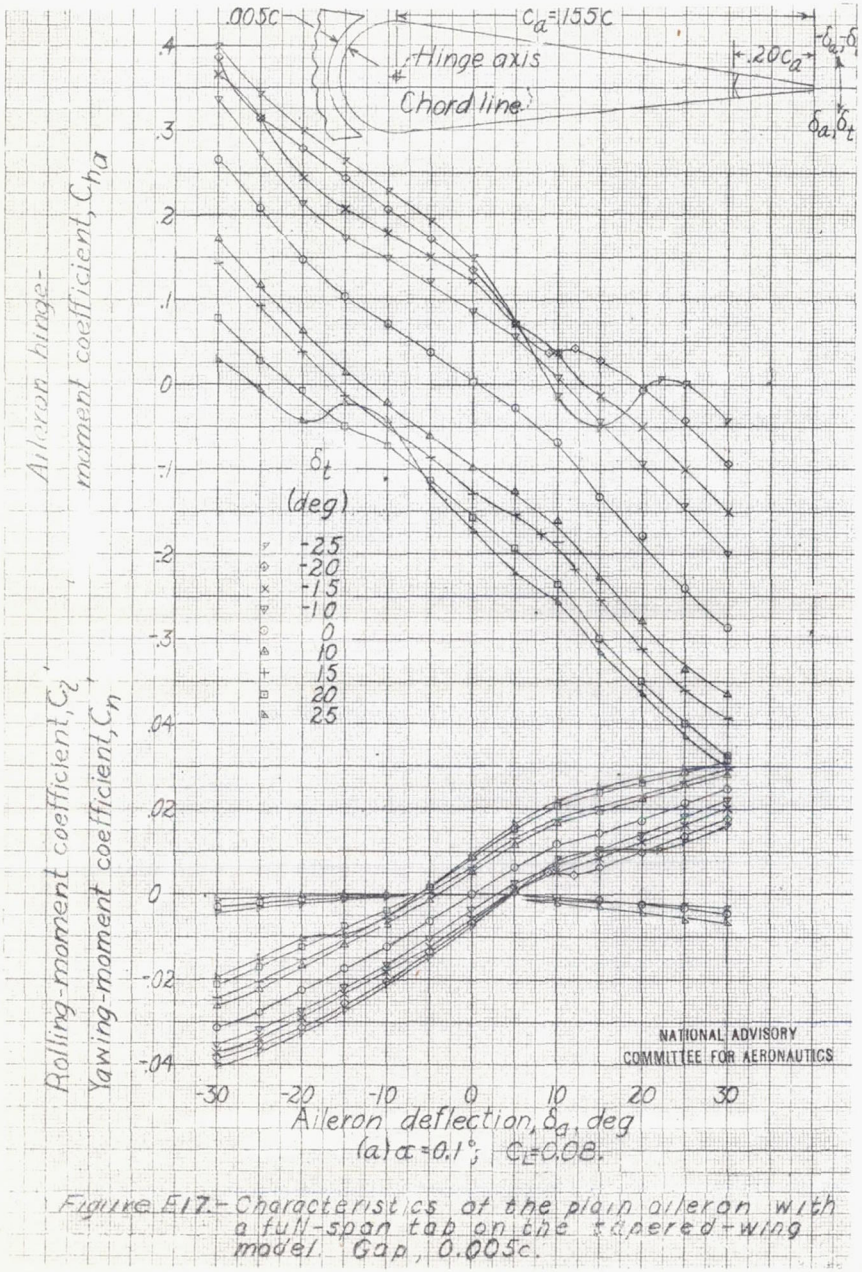

(a) α=0.1°; C_L=0.08.

Figure E17.- Characteristics of the plain aileron with a full-span tab on the tapered-wing model. Gap, 0.005c.

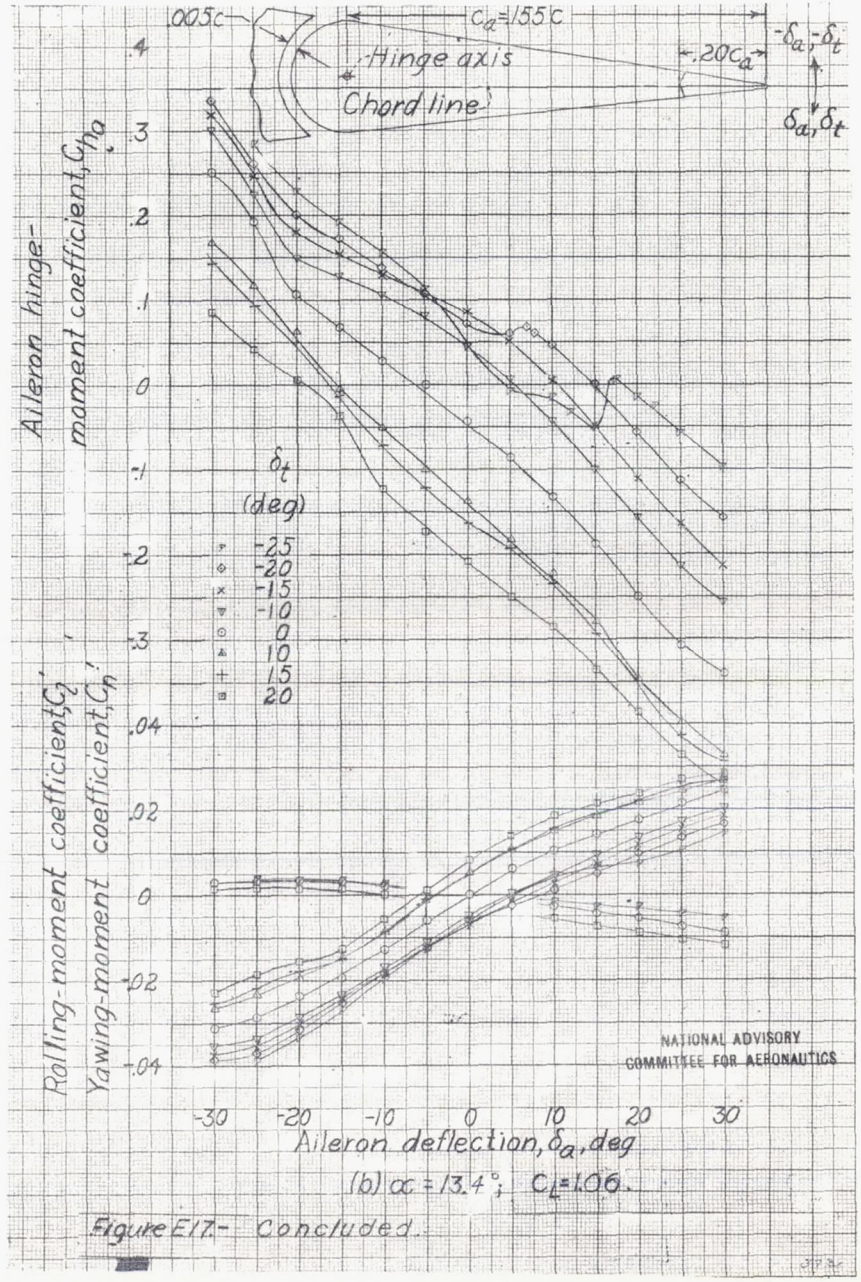

(b) α=13.4°; C_L=1.06.

Figure E17.- Concluded.

Model E-V

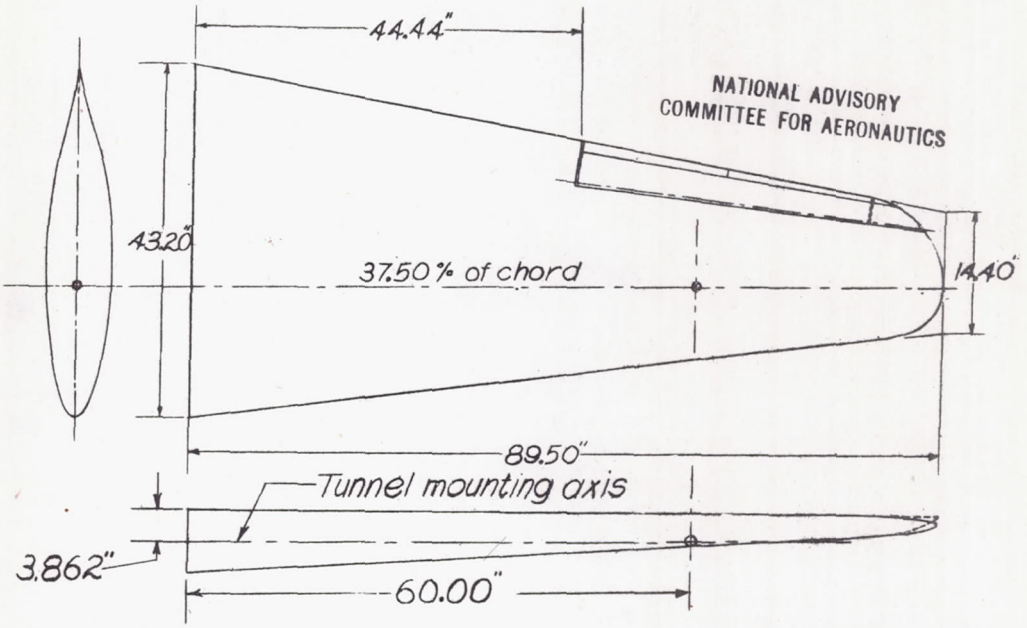

Figure E18.- 0.36-scale semispan model of a tapered low-drag wing. LMAL 7- by 10-foot tunnel.

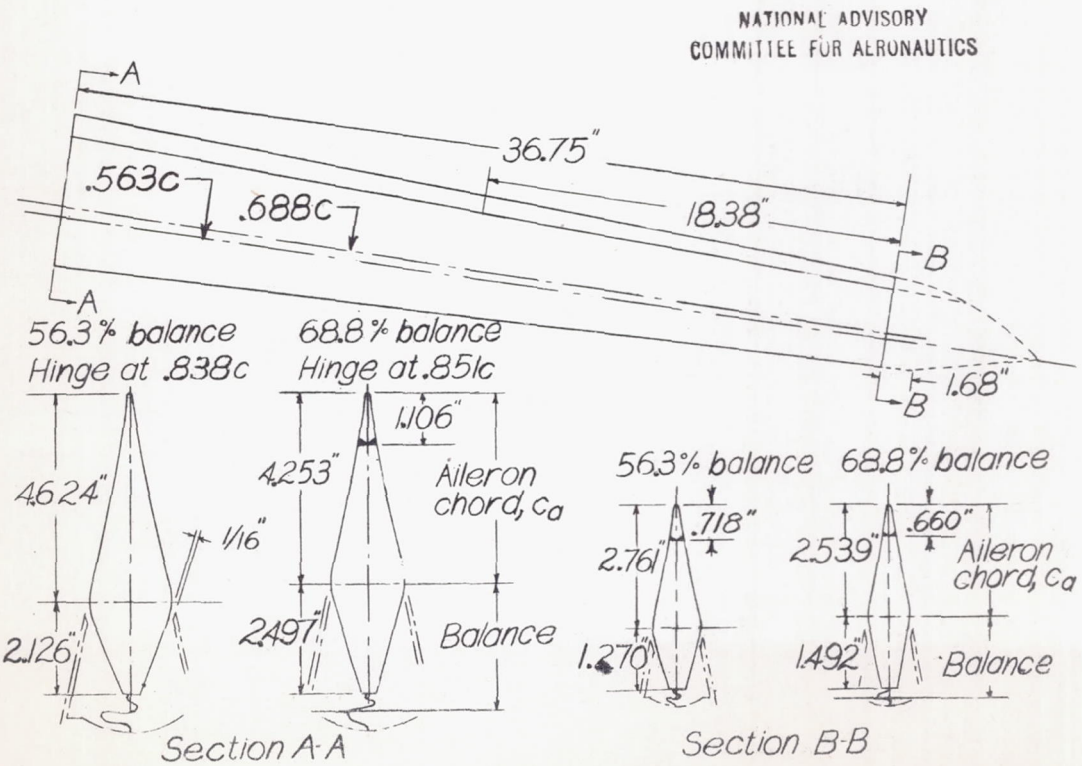

Figure E19.- Aileron-tab arrangements tested on a 0.36-scale semispan model of a low-drag wing.

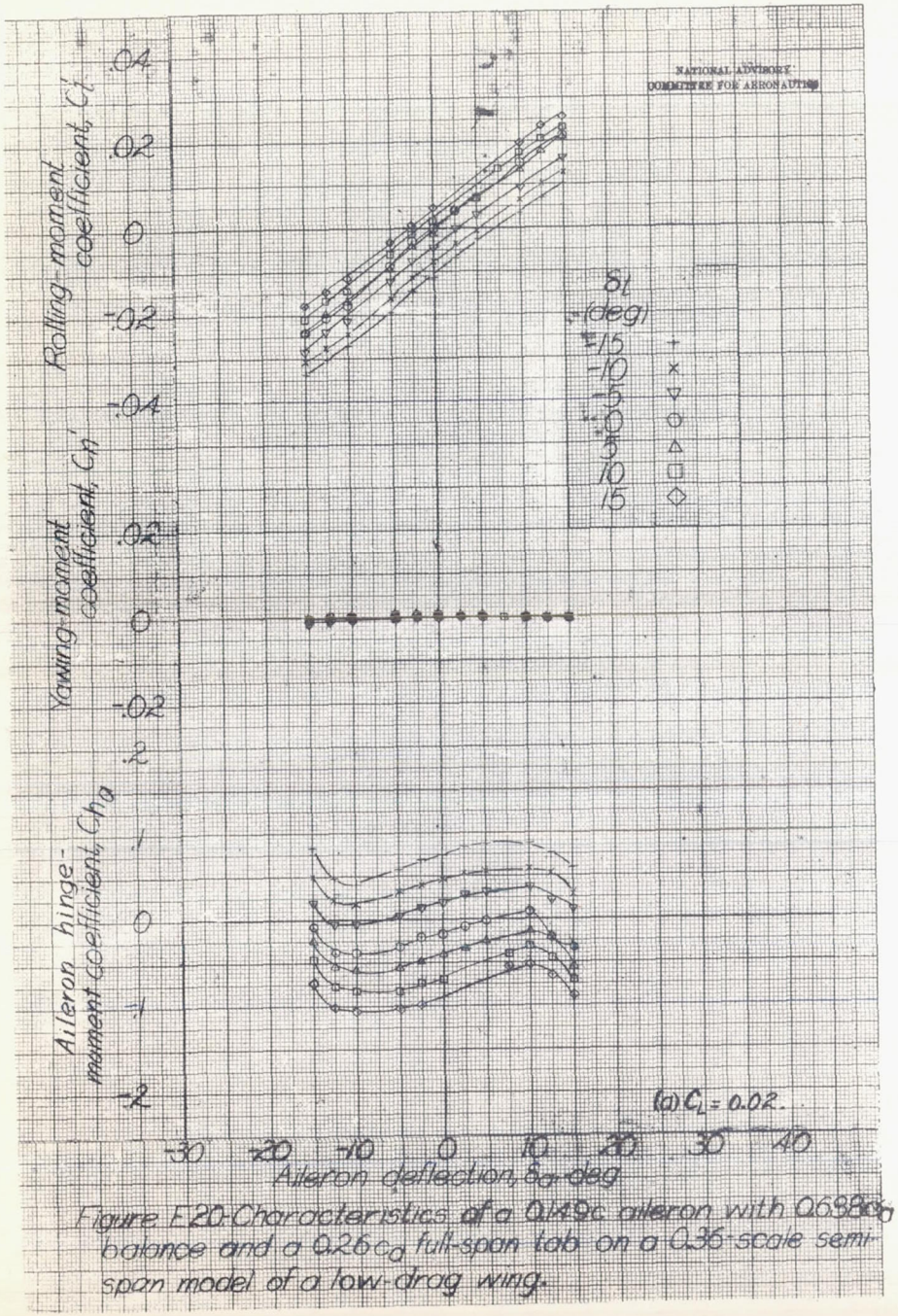

Figure E20.- Characteristics of a $0.42c$ aleron with $0.68c_a$ balance and a $0.26c_a$ full-span tab on a 0.35-scale semi-span model of a low-drag wing.

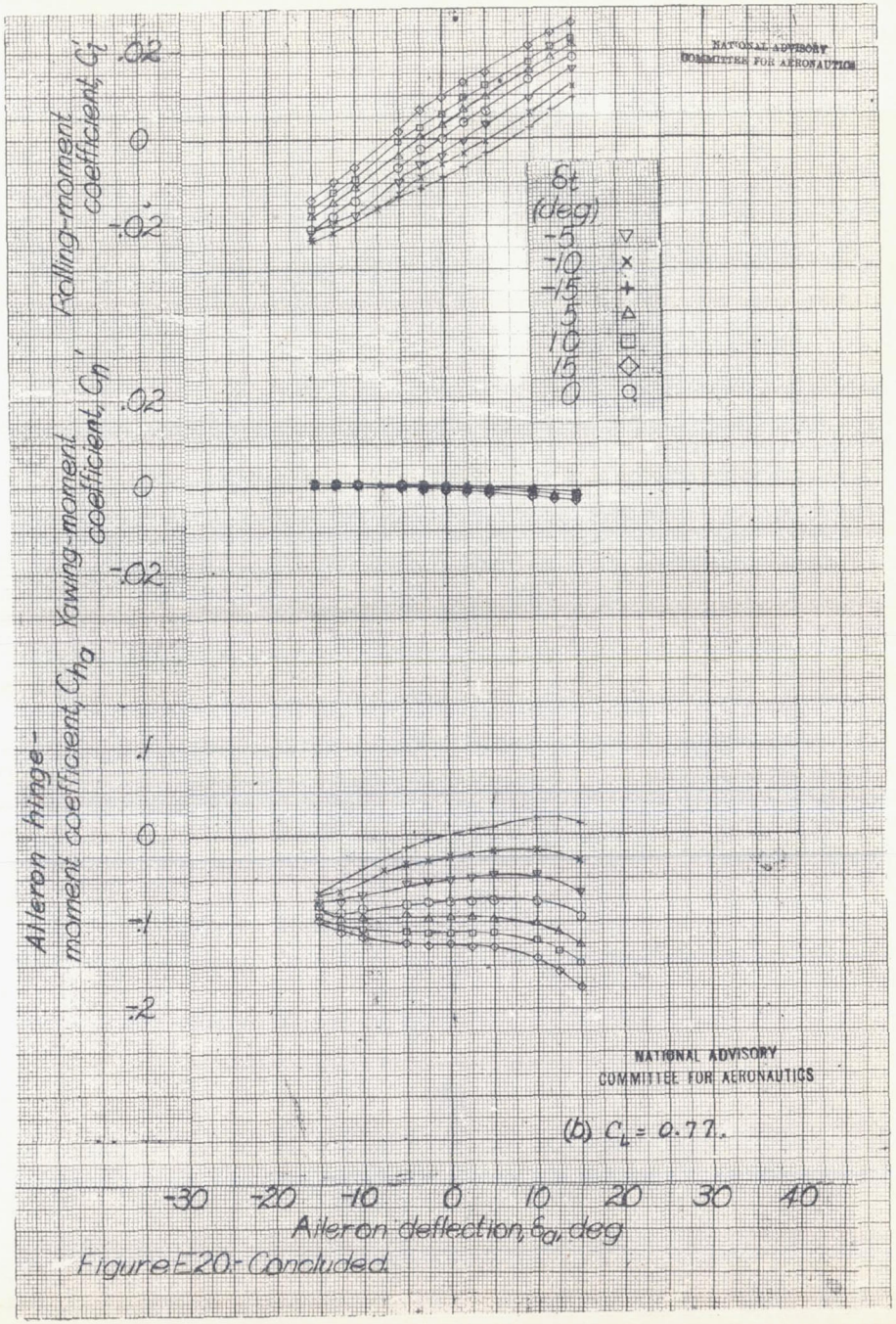

Figure E20.- Concluded.

Model E-VI

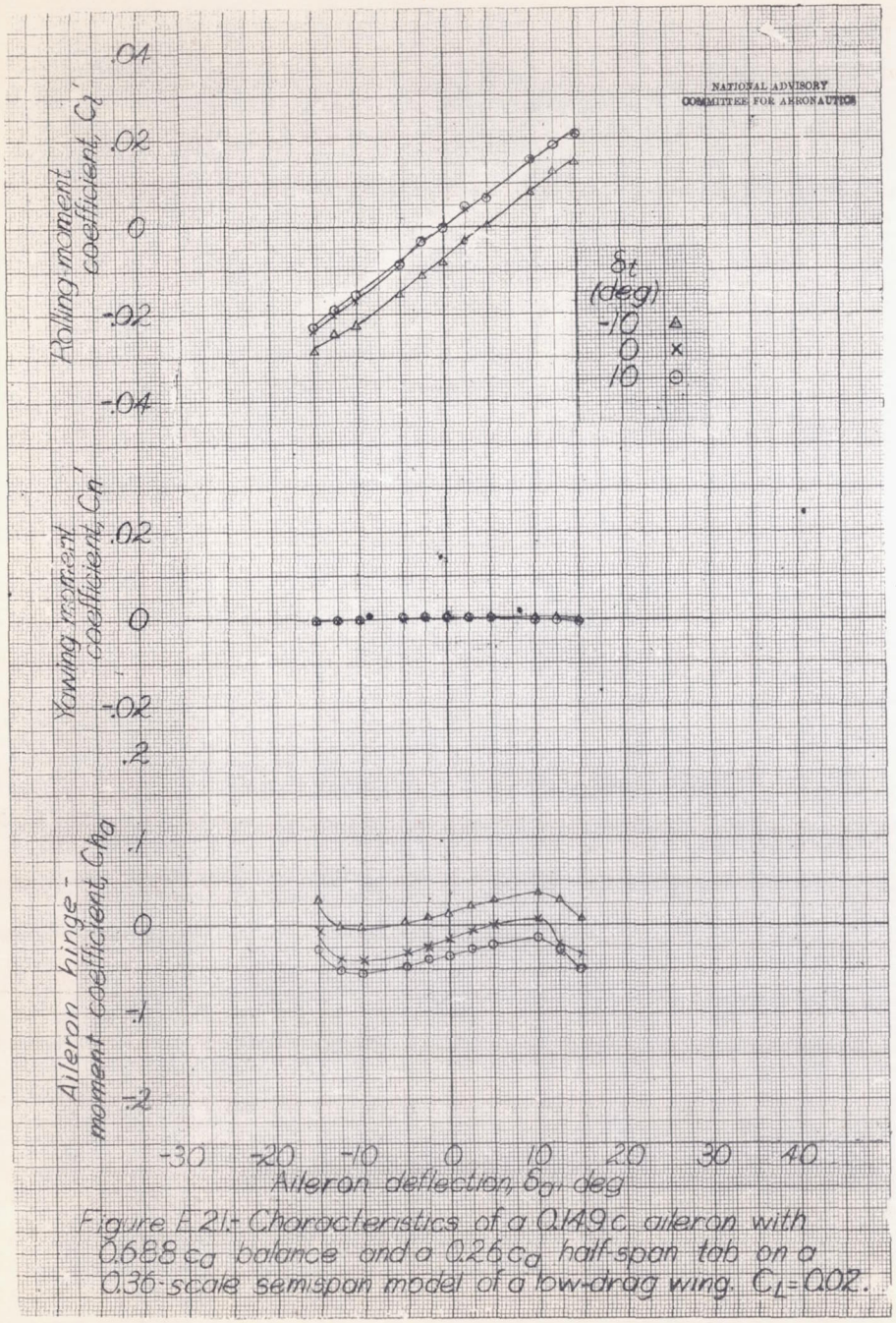

Figure E21.- Characteristics of a 0.149c aileron with 0.688 c_a balance and a 0.25 c_a half-span tab on a 0.36-scale semispan model of a low-drag wing. C_L=.002.

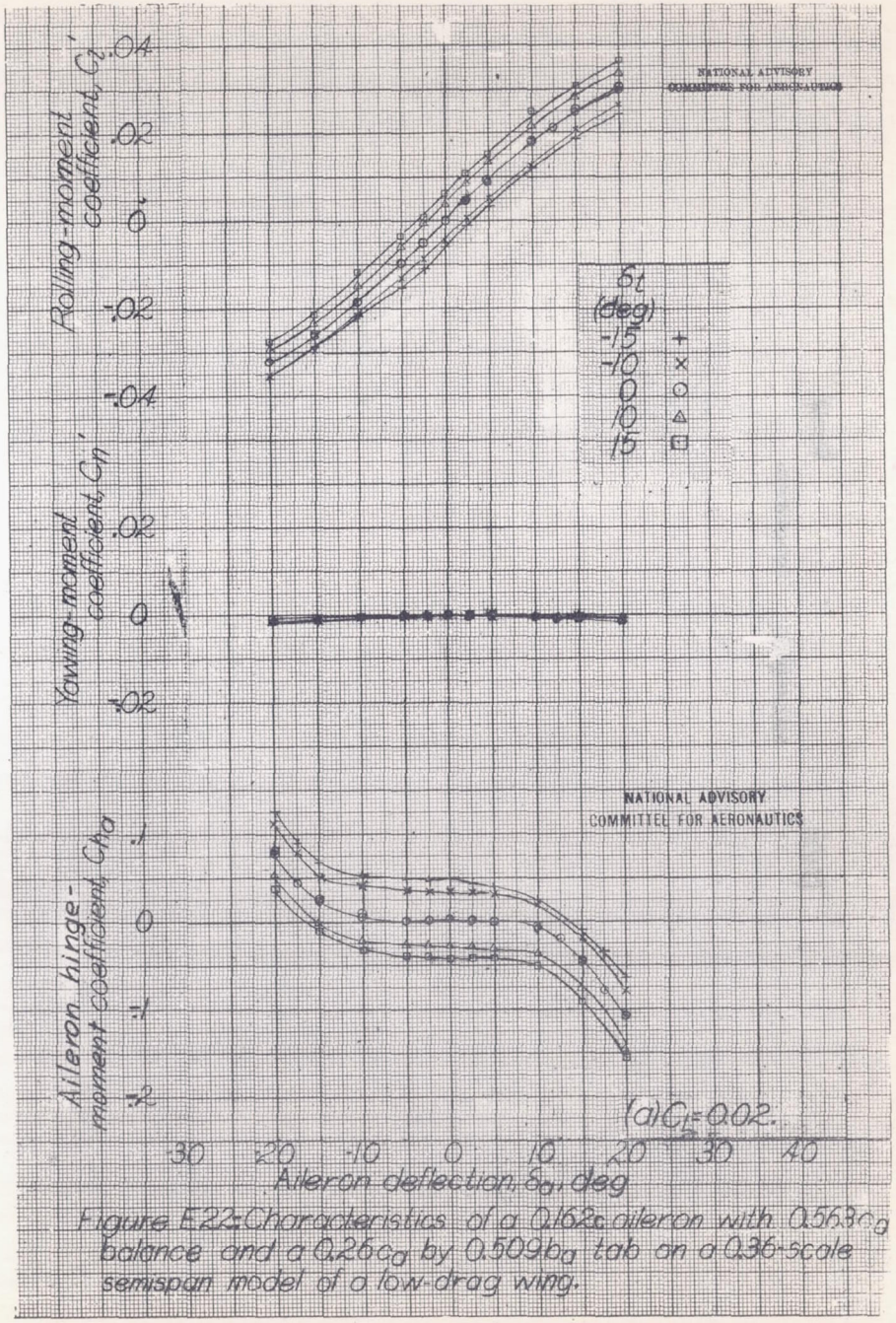

Figure E22.-Characteristics of a 0.162c aileron with 0.563 c_a balance and a 0.25 c_a by 0.509 b_a tab on a 0.36-scale semispan model of a low-drag wing.

Model E-VI

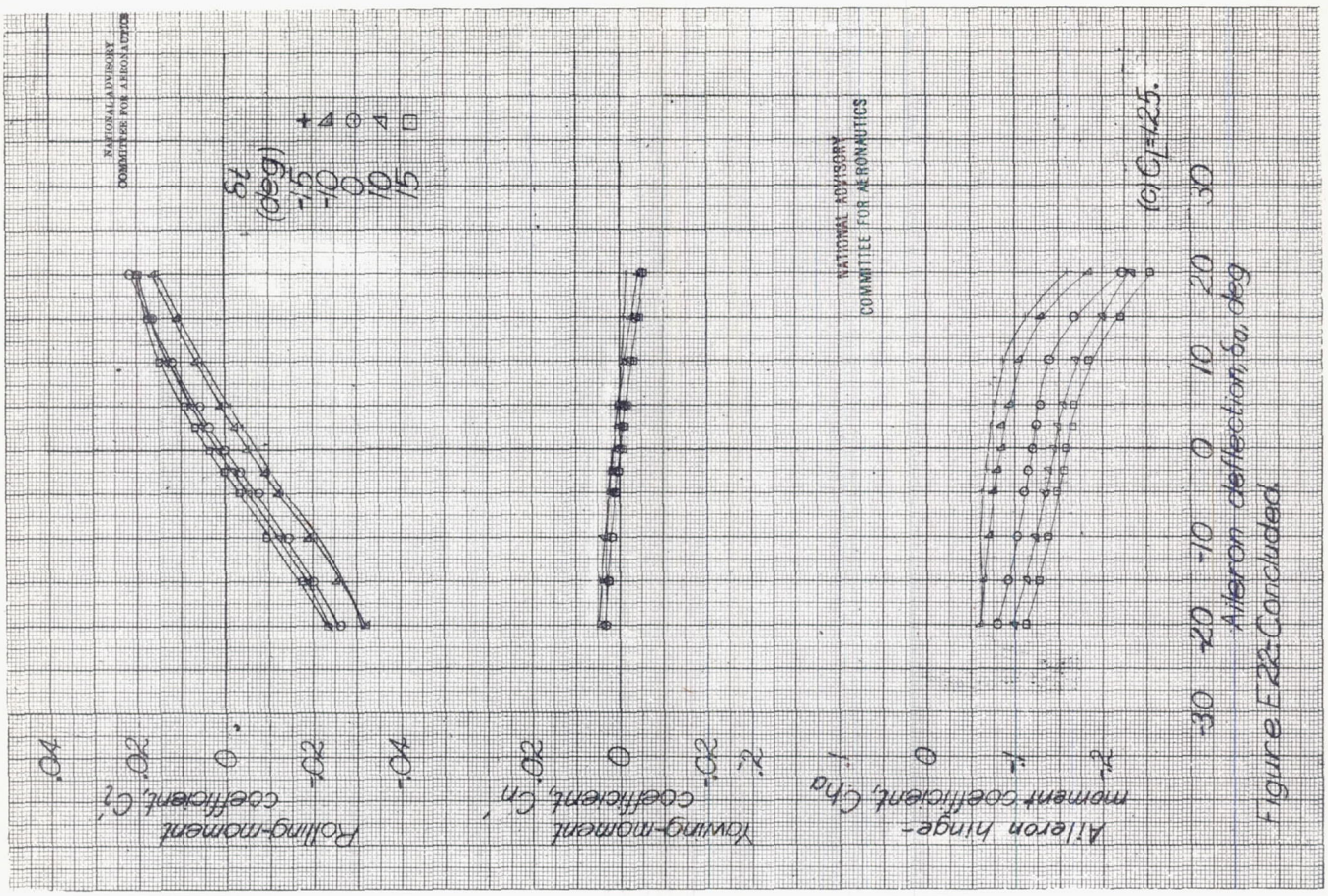

Figure E22.-Concluded.

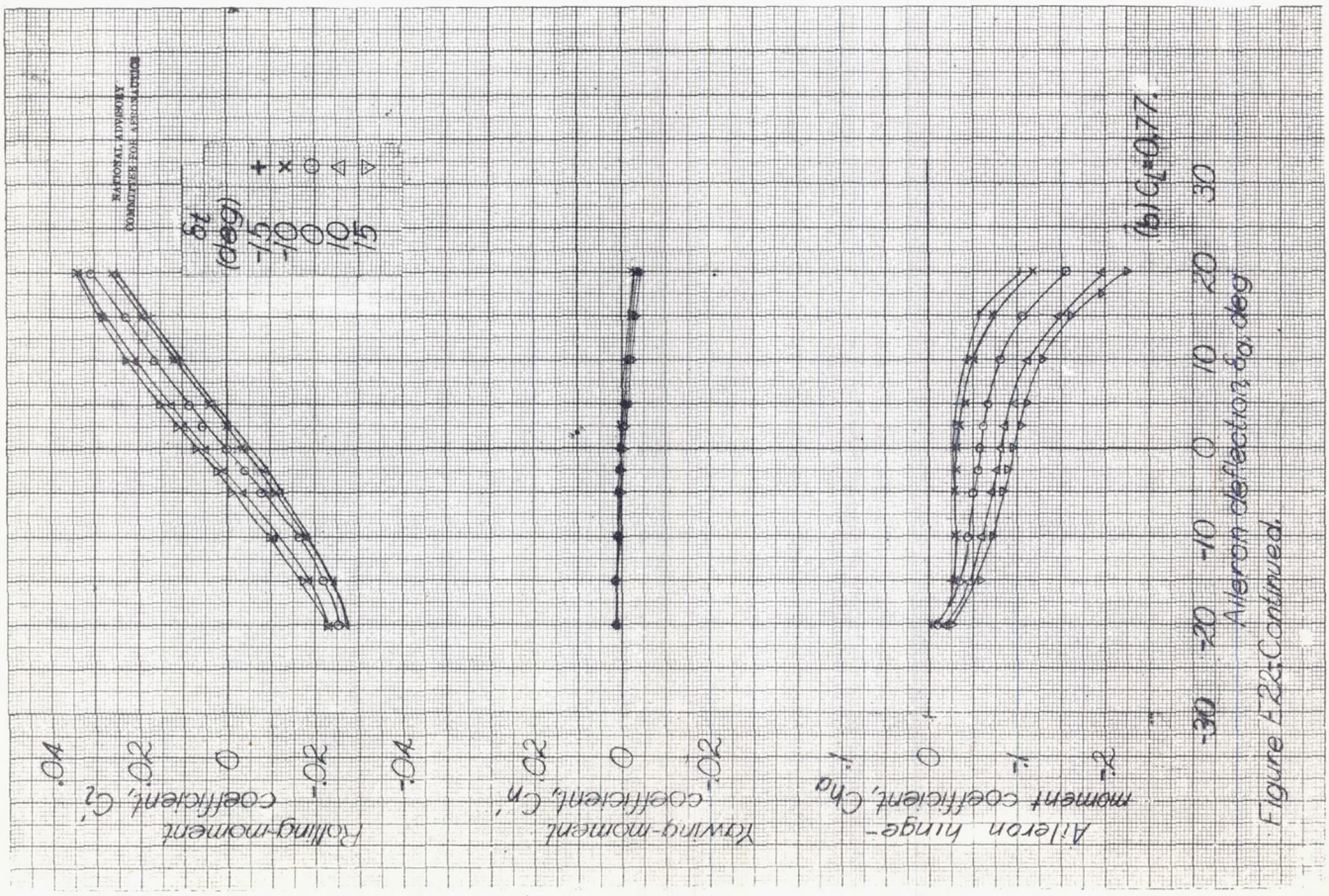

Figure E22.-Continued.

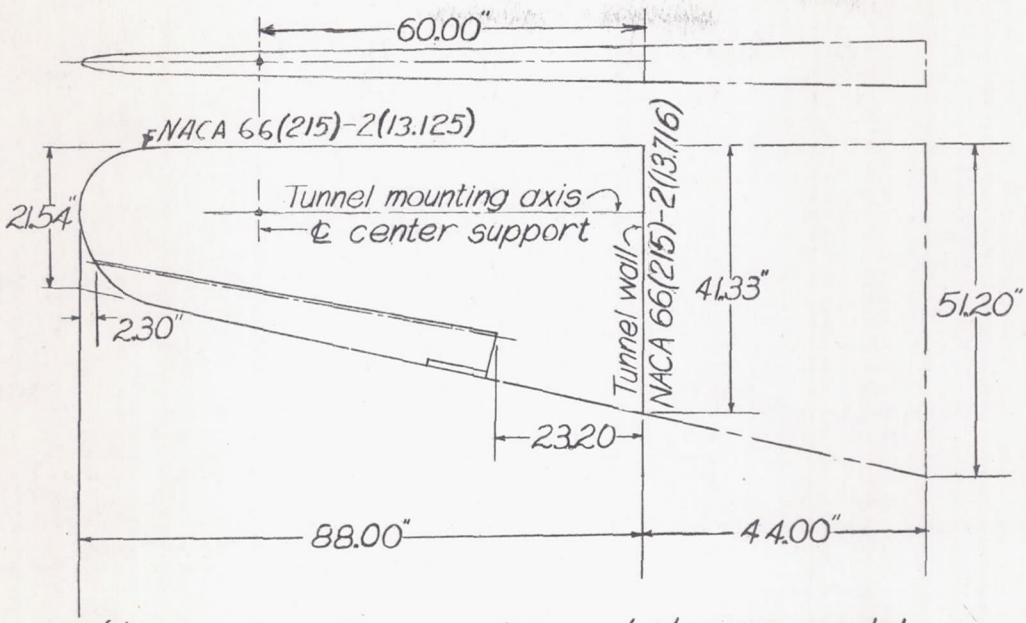

(a) Plan form of 0.40-scale partial-span model.

NATIONAL ADVISORY
COMMITTEE FOR AERONAUTICS

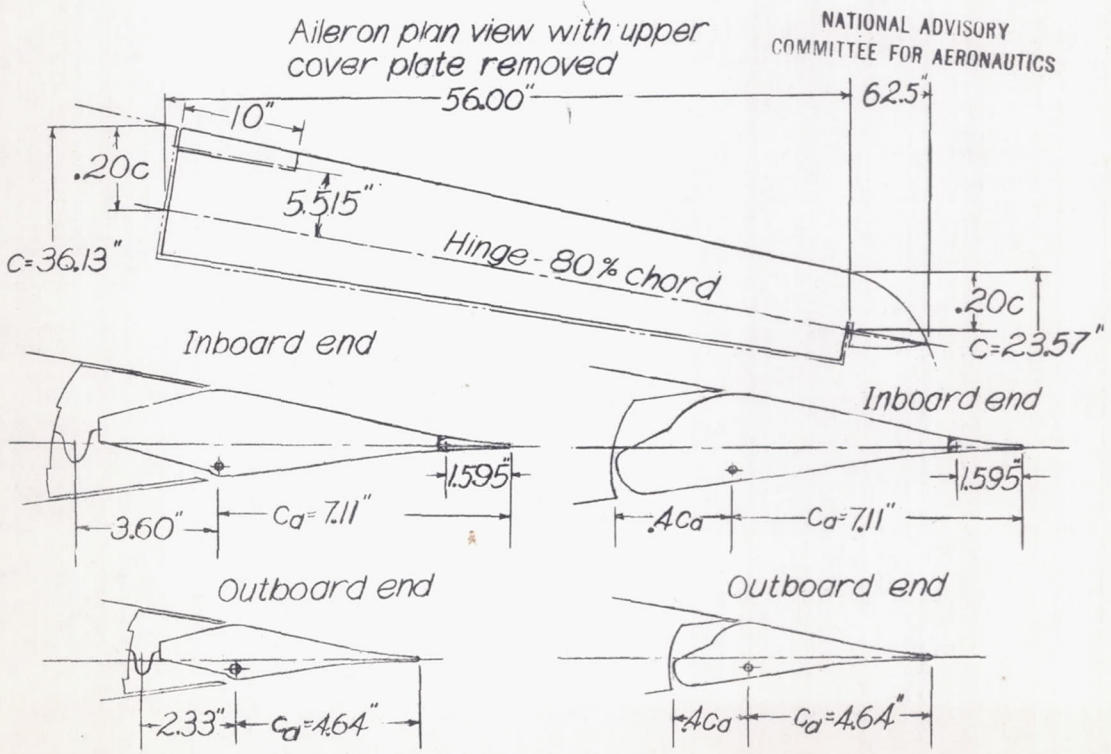

(b) 0.505c_a sealed balance (c) 0.4c_a Frise balance.

Figure E23: Partial-span model of a low-drag wing and tab arrangement on a sealed internal-balance aileron and a Frise aileron. LMAL 7 by 10-foot tunnel.

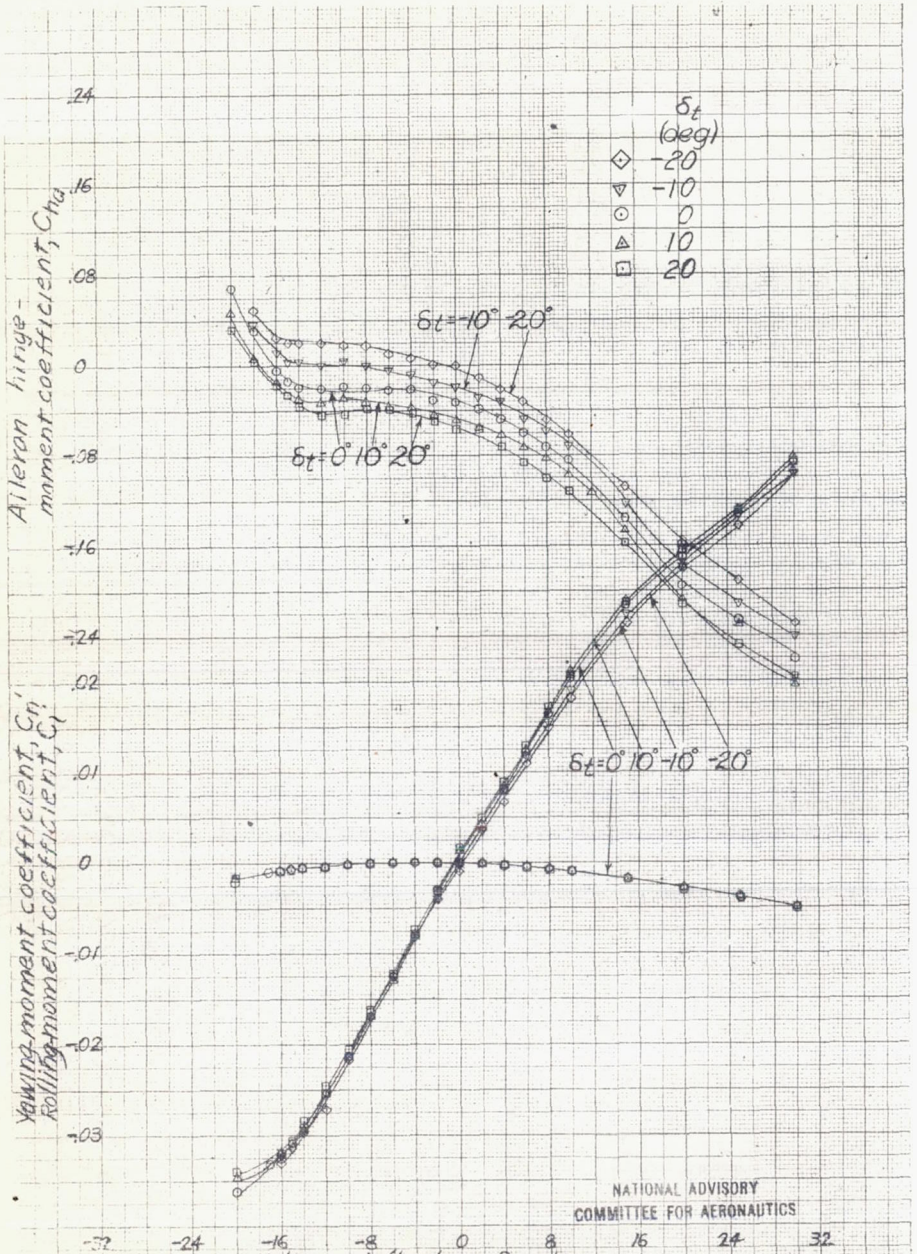

Figure E24.-Effect of tab deflection on the characteristics of the modified 0.4c_a-balance F-rise aileron on the 0.40-scale partial-span wing model of an airplane. α = 1°.

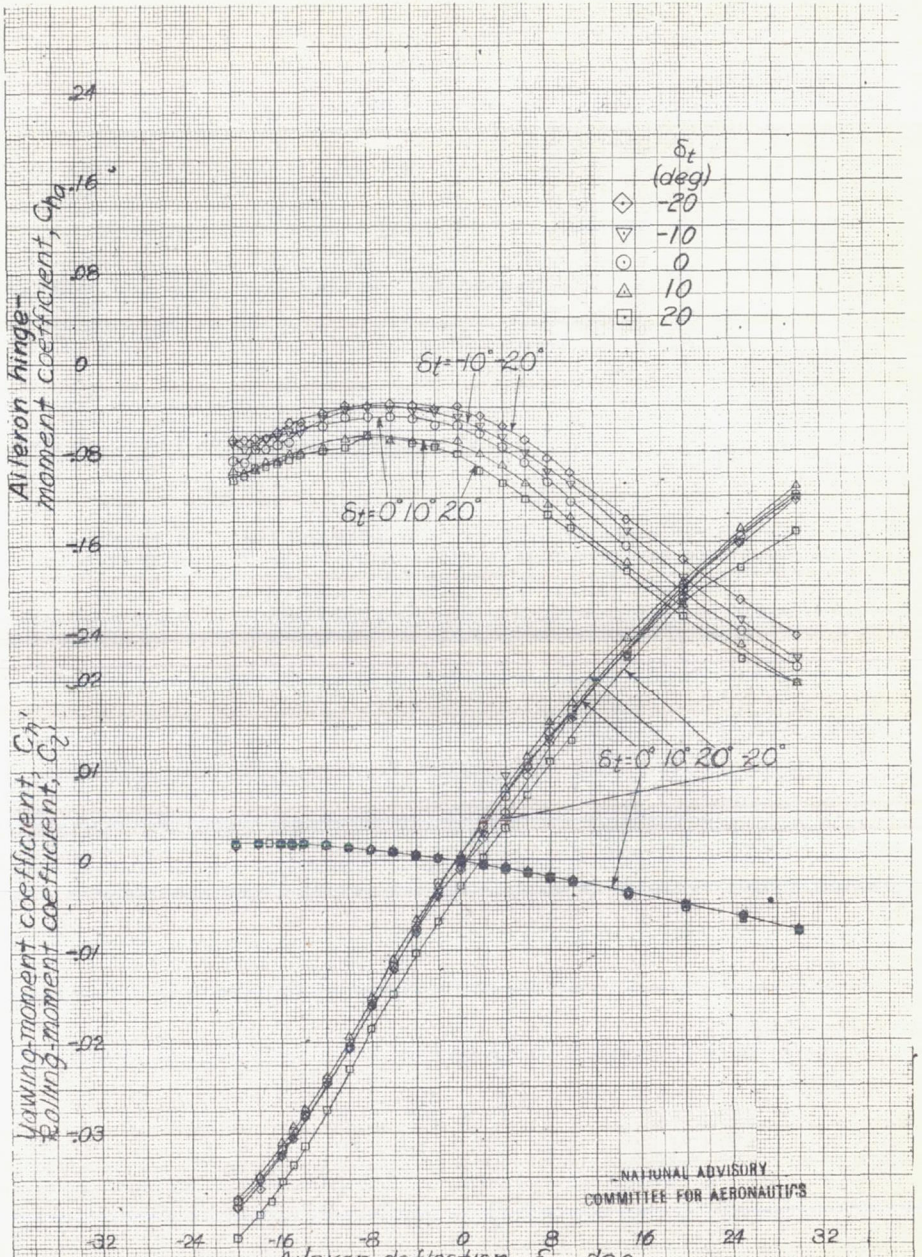

Figure E25.-Effect of tab deflection on the characteristics of the modified 0.4c_a-balance F-rise aileron on the 0.40-scale partial-span wing model of an airplane. α = 11.52°.

Model E-VII

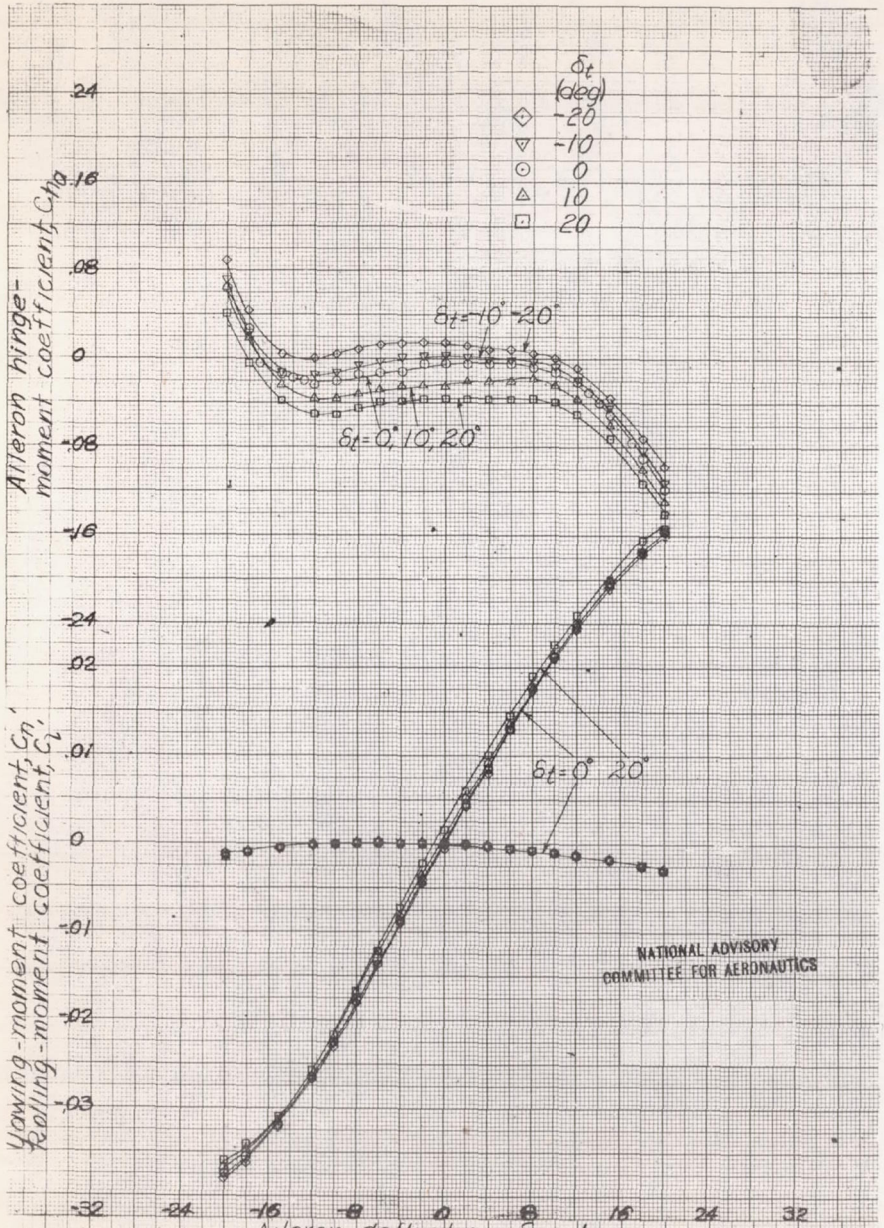

Figure E26.-Effect of tab deflection on the characteristics of the internally balanced aileron with 0.505c_a balance on the 0.40-scale partial-span wing model of an airplane. Balance completely sealed; α, 0.1°.

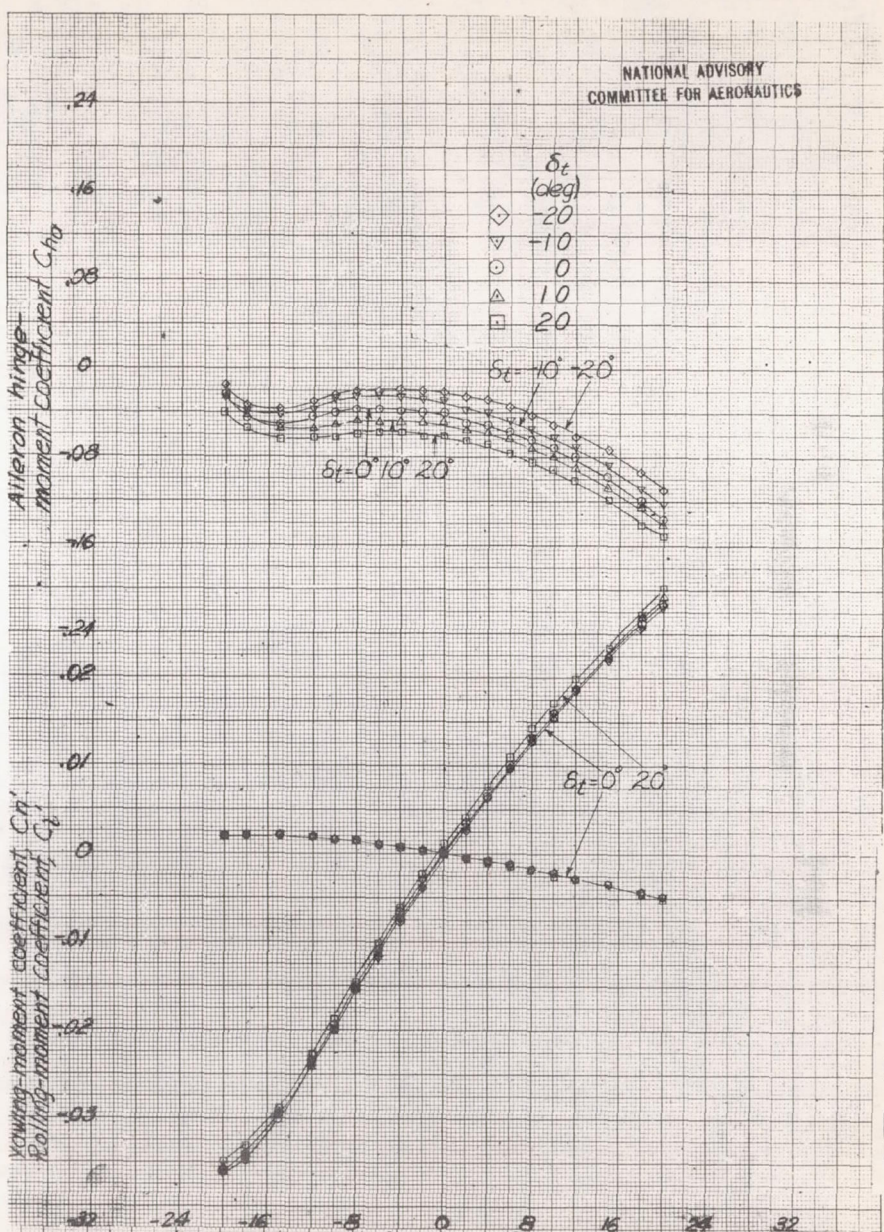

Figure E27-Effect of tab deflection on the characteristics of the internally balanced aileron on the 0.40-scale partial-span wing model of an airplane. Balance completely sealed; α, 11.52°.

Model E-VII

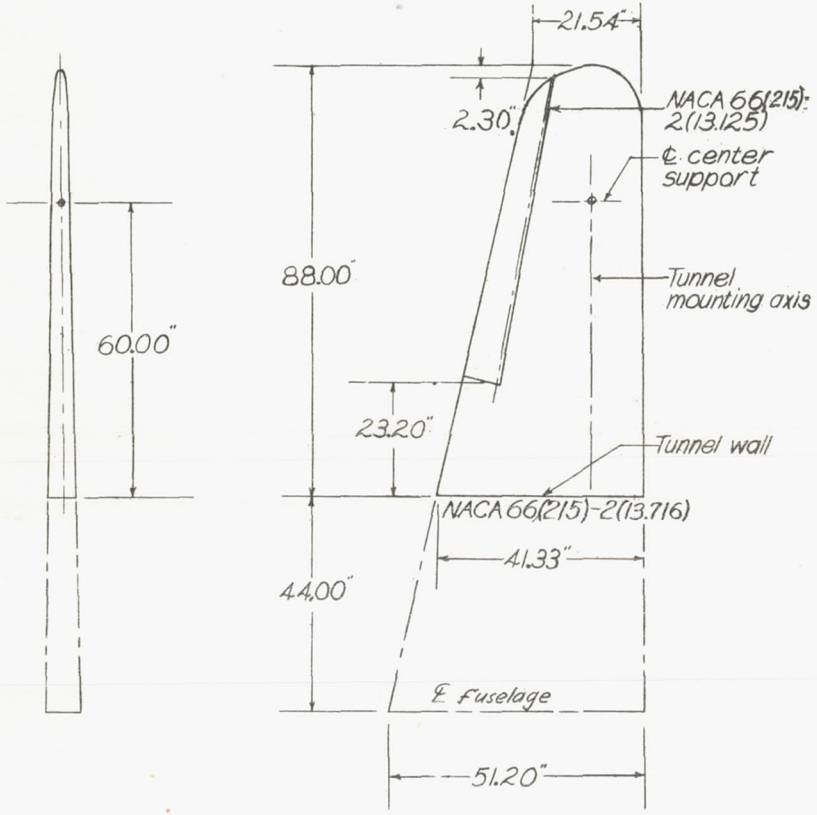

Figure E28.- Plan form of wing panel tested and semispan of complete wing for which characteristics are given. LMAL 7-by 10-foot tunnel.

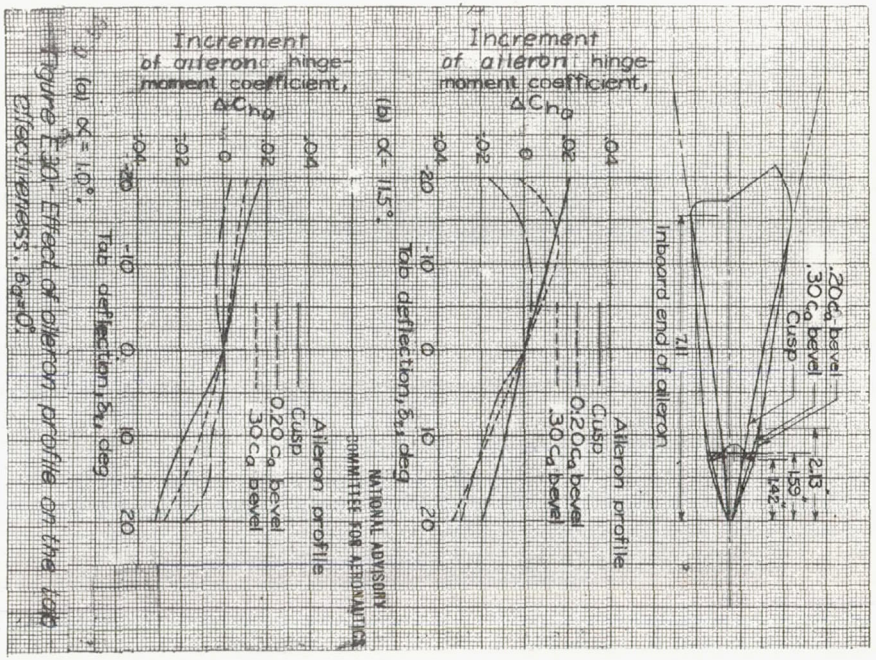

Figure E29.- Effect of aileron profile on the hinge effectiveness. $\delta_a = 0°$.

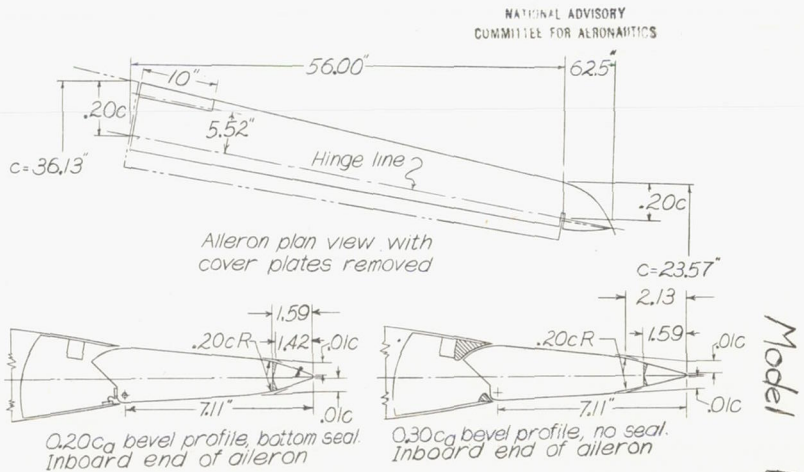

Figure E29.- Details of tab on aileron with 0.20c_a and 0.30c_a beveled trailing edges.

Model E-VIII

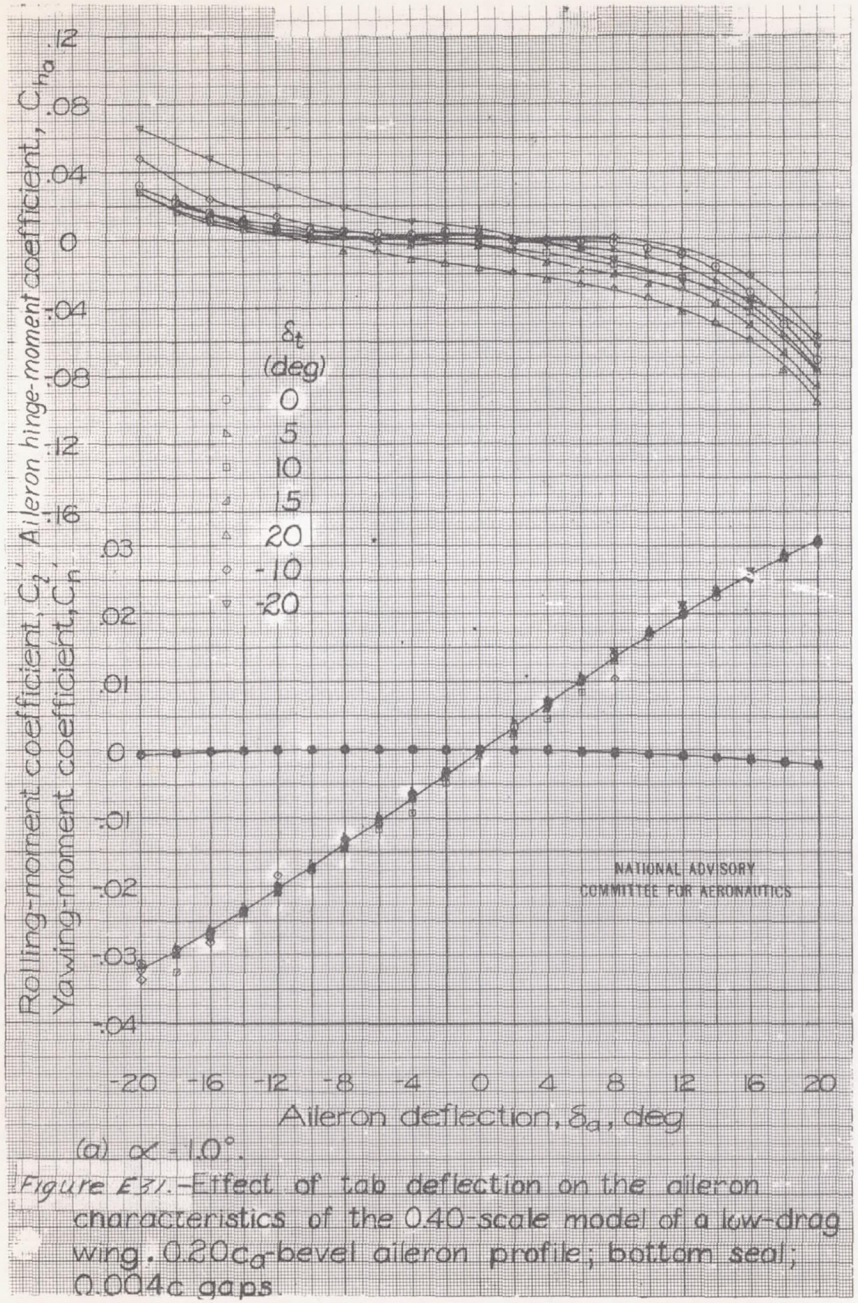

(a) α - 1.0°.

Figure E31.-Effect of tab deflection on the aileron characteristics of the 0.40-scale model of a low-drag wing. $0.20c_a$-bevel aileron profile; bottom seal; 0.004c gaps.

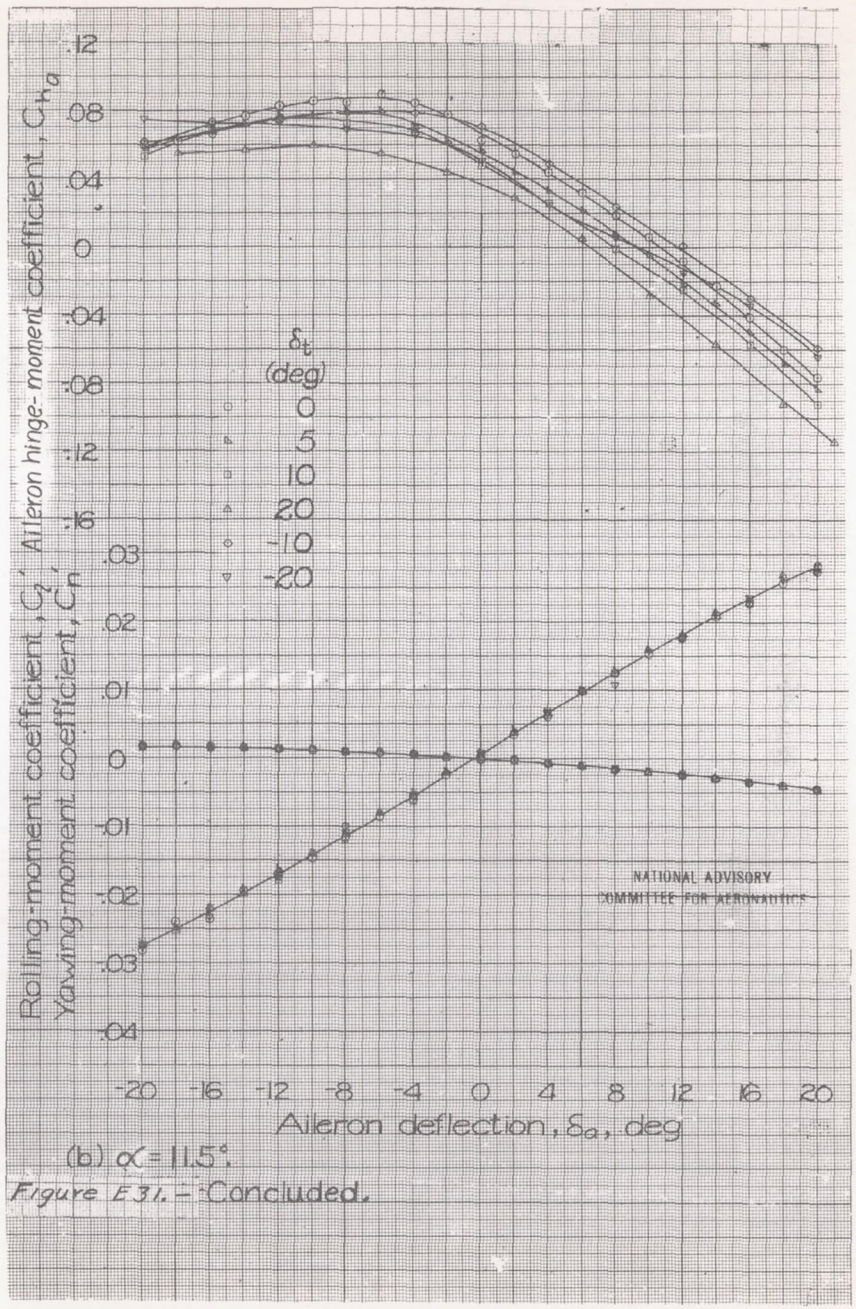

(b) α = 11.5°.

Figure E31.- Concluded.

Model E-VIII

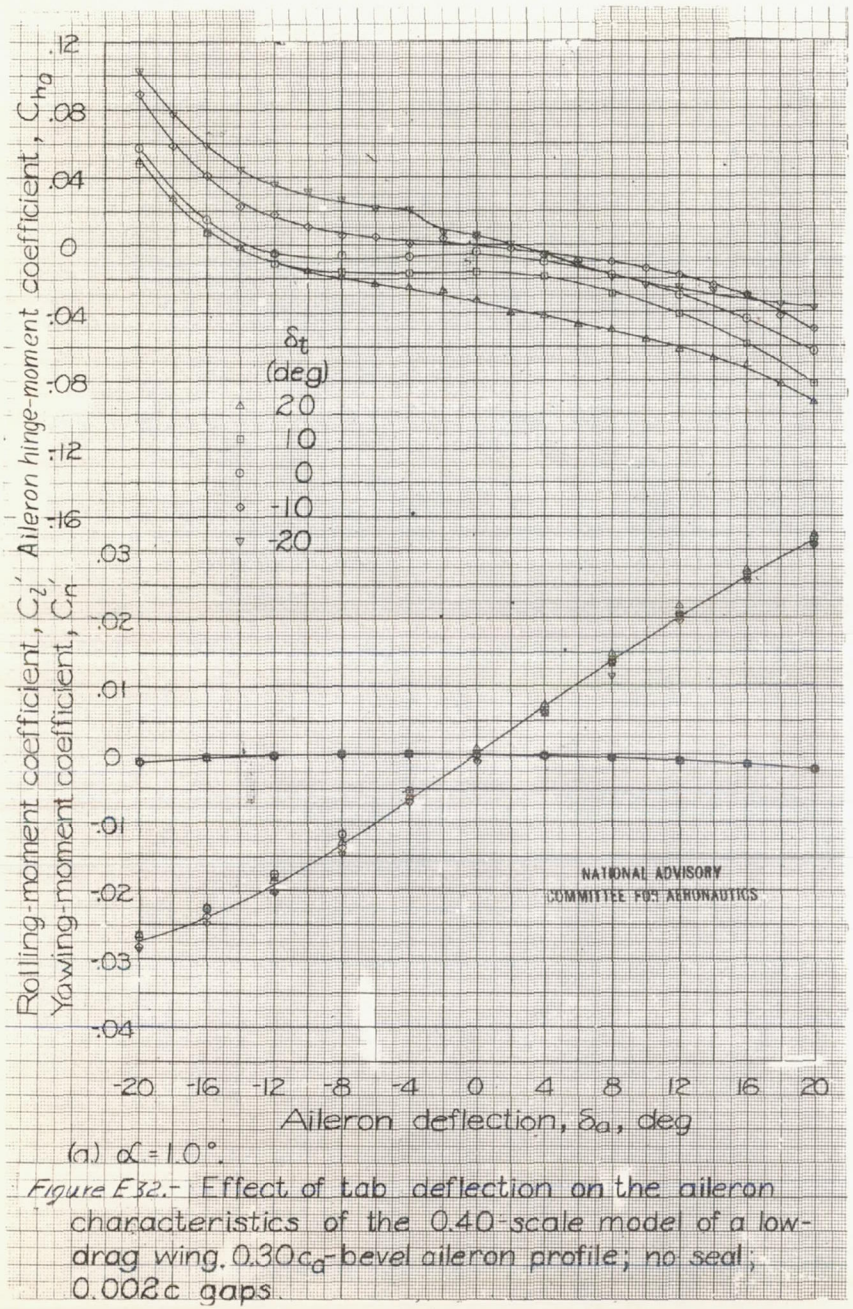

(a) $\alpha = 1.0°$.

Figure E32.- Effect of tab deflection on the aileron characteristics of the 0.40-scale model of a low-drag wing. $0.30c_a$-bevel aileron profile; no seal, 0.002c gaps.

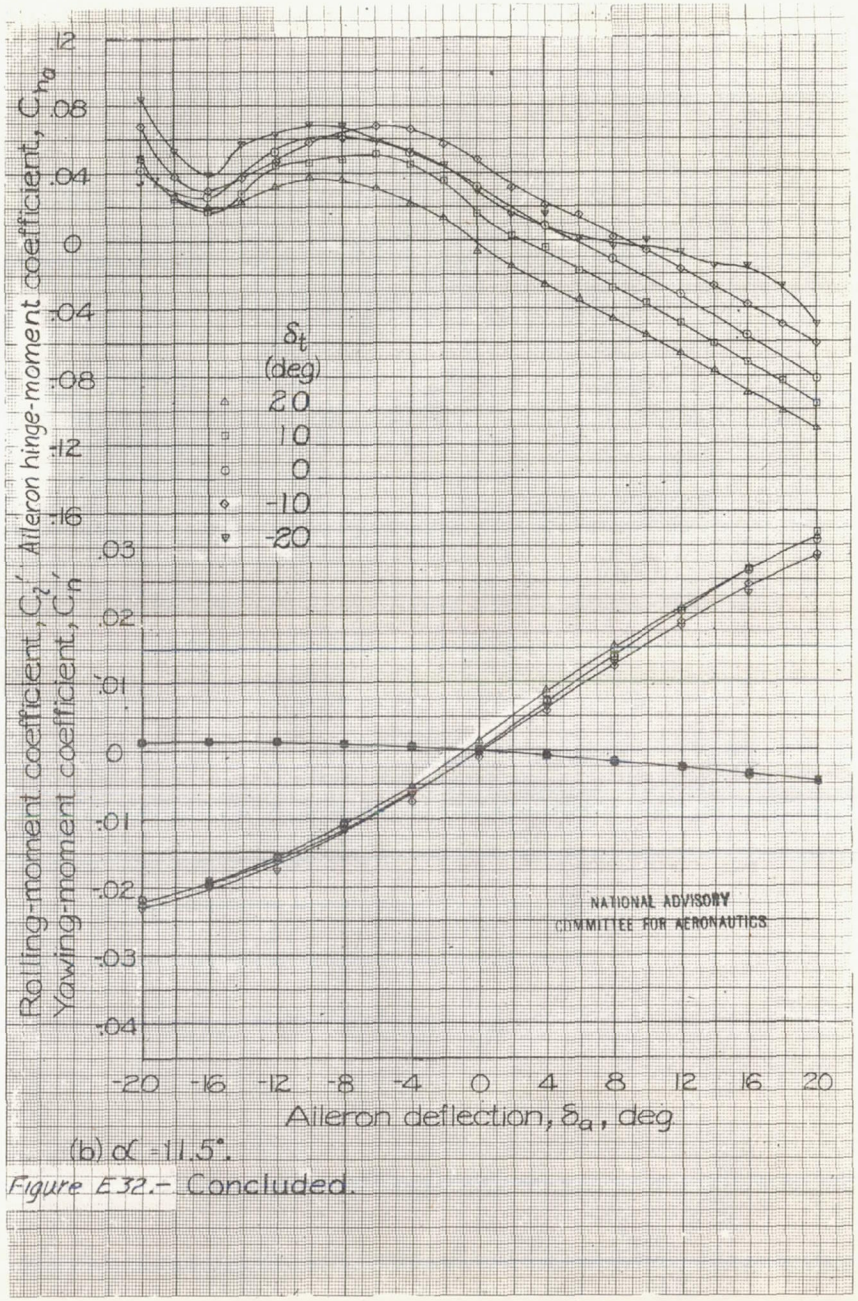

(b) α -11.5°.

Figure E32.- Concluded.

Model E-VIII

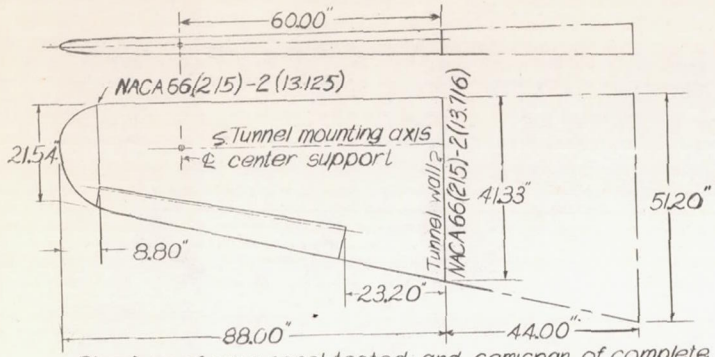

Plan form of wing panel tested and semispan of complete wing for which characteristics are given.

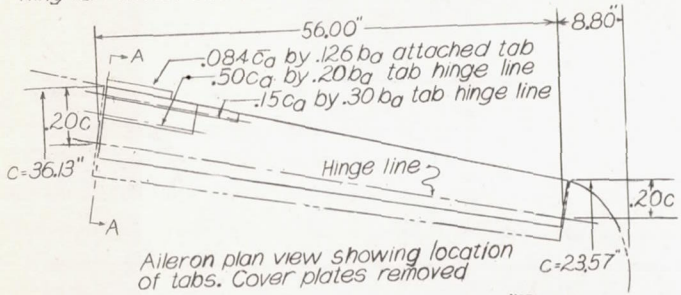

Aileron plan view showing location of tabs. Cover plates removed

NATIONAL ADVISORY COMMITTEE FOR AERONAUTICS

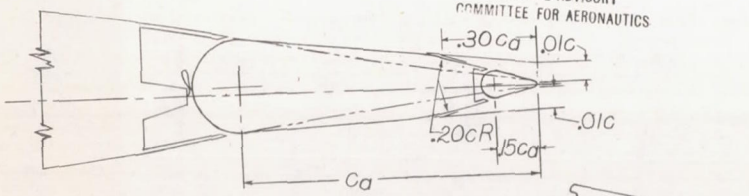

0.15 c_a by 0.30 b_a tab. Section A-A

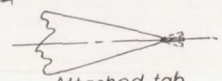

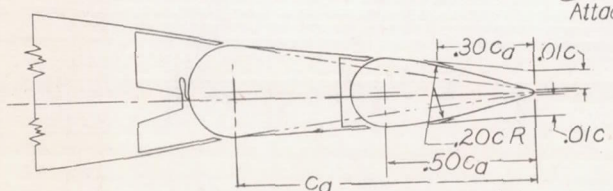

0.50 c_a by 0.20 b_a tab. Section A-A

Figure E33.- Various tab arrangements tested on a thickened-and beveled-trailing-edge aileron on a partial-span model of a tapered low-drag wing. LMAL 7-by10-foot tunnel.

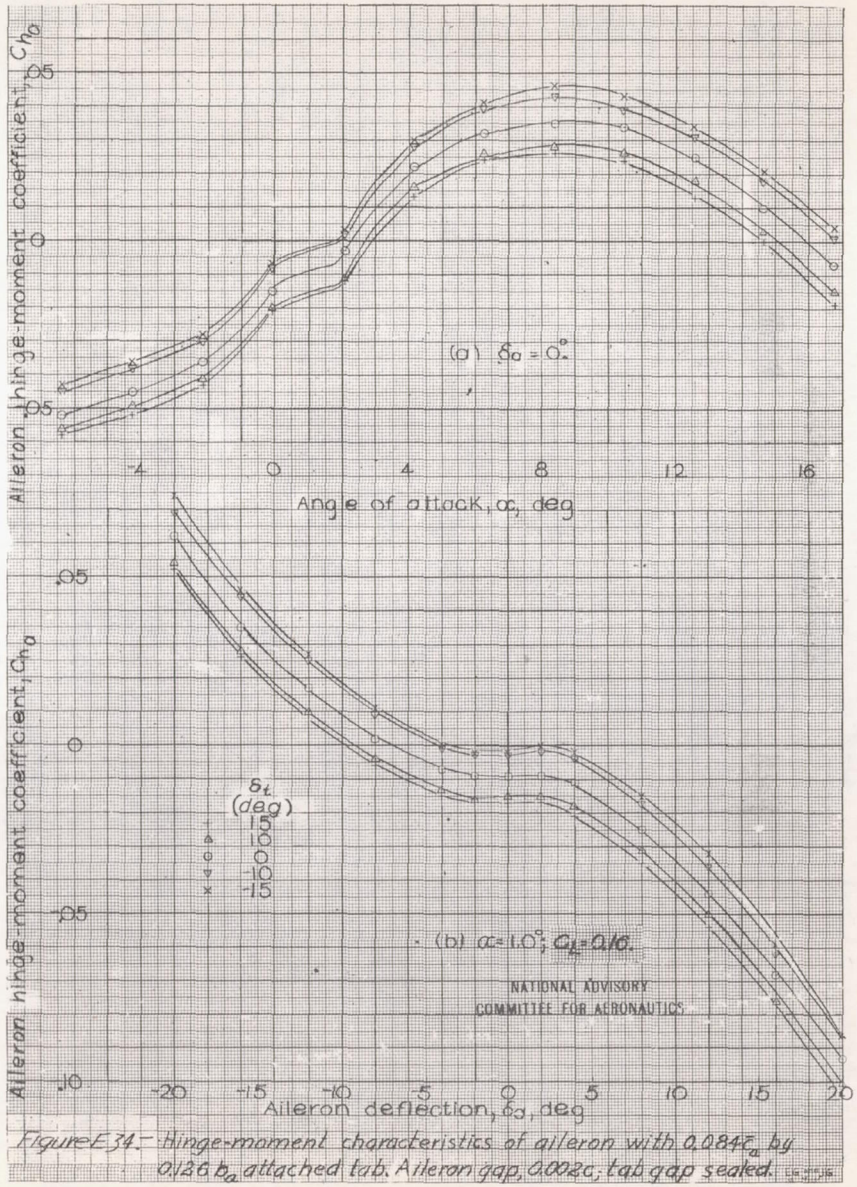

Figure E34.- Hinge-moment characteristics of aileron with 0.084 c_a by 0.126 b_a attached tab. Aileron gap, 0.002c; tab gap sealed.

Model E-IX

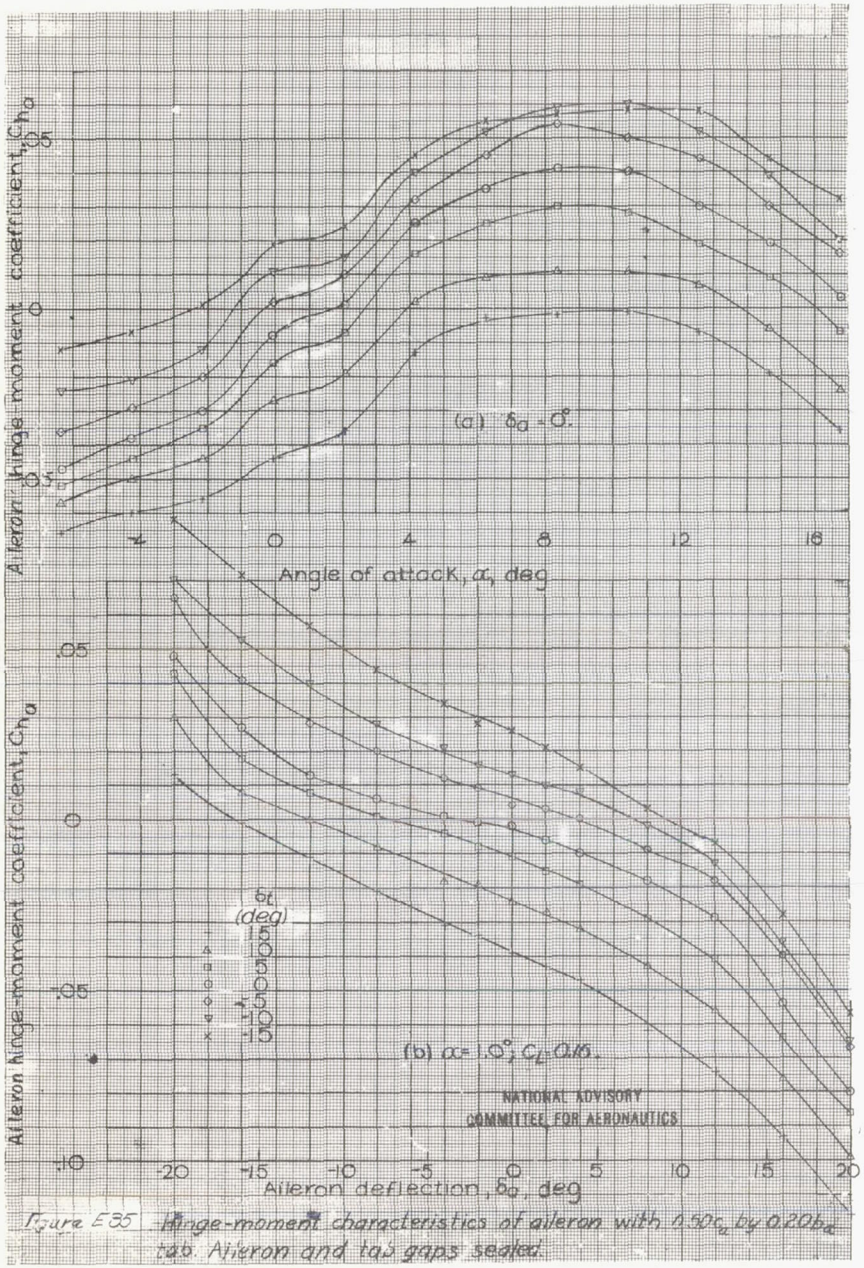

Figure E35 Hinge-moment characteristics of aileron with $0.50c_a$ by $0.20b_a$ tab. Aileron and tab gaps sealed.

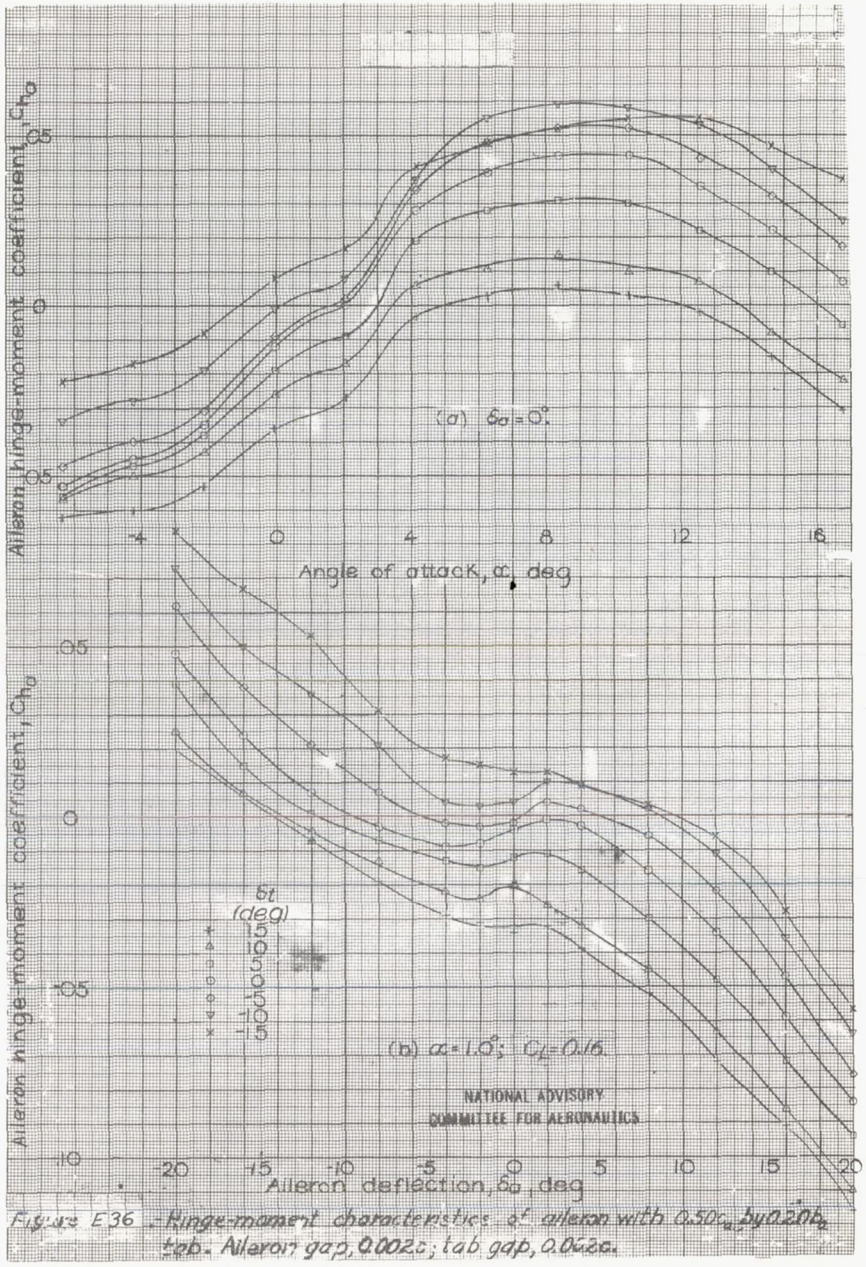

Figure E36 Hinge-moment characteristics of aileron with $0.50c_a$ by $0.20b_a$ tab. Aileron gap, 0.002c; tab gap, 0.002c.

Model F-IX

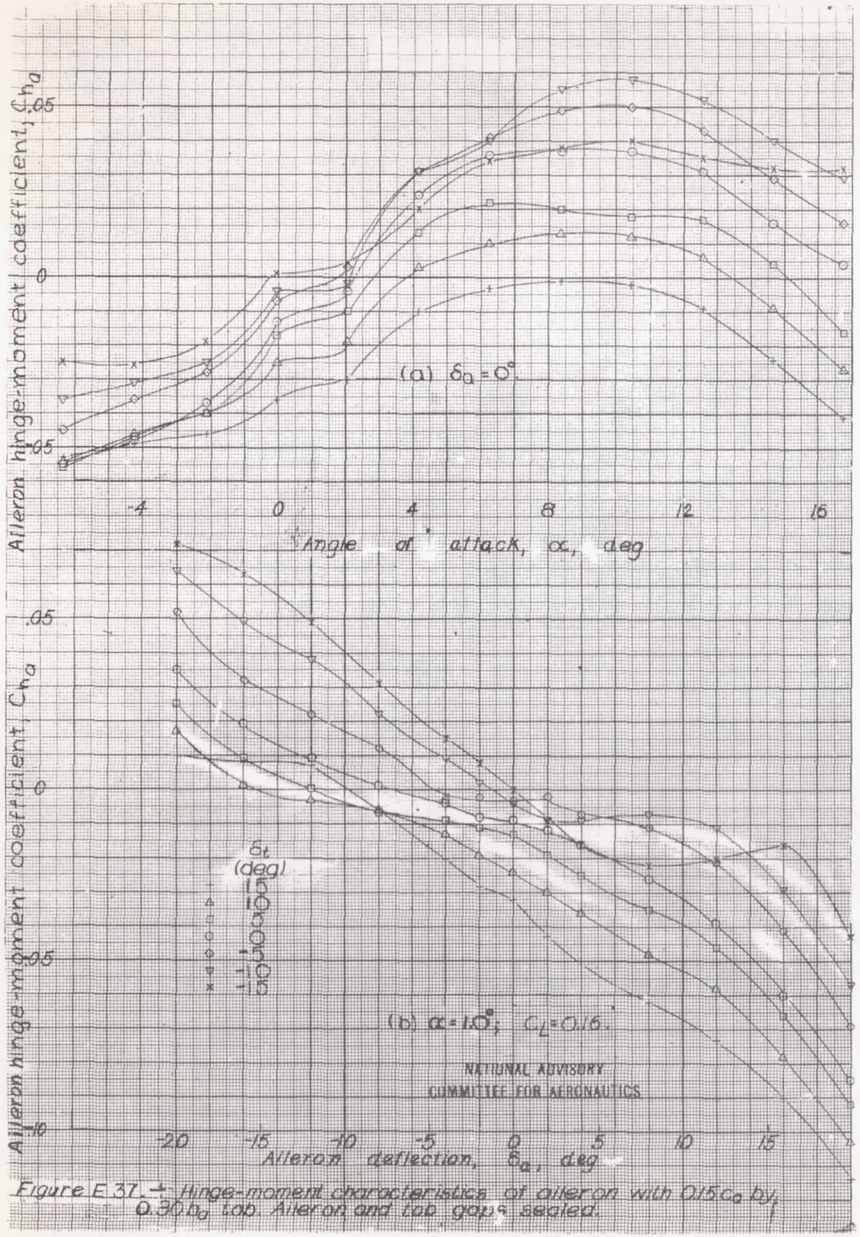

Figure E.37.- Hinge-moment characteristics of aileron with $0.15c_a$ by $0.30b_a$ tab. Aileron and tab gaps sealed.

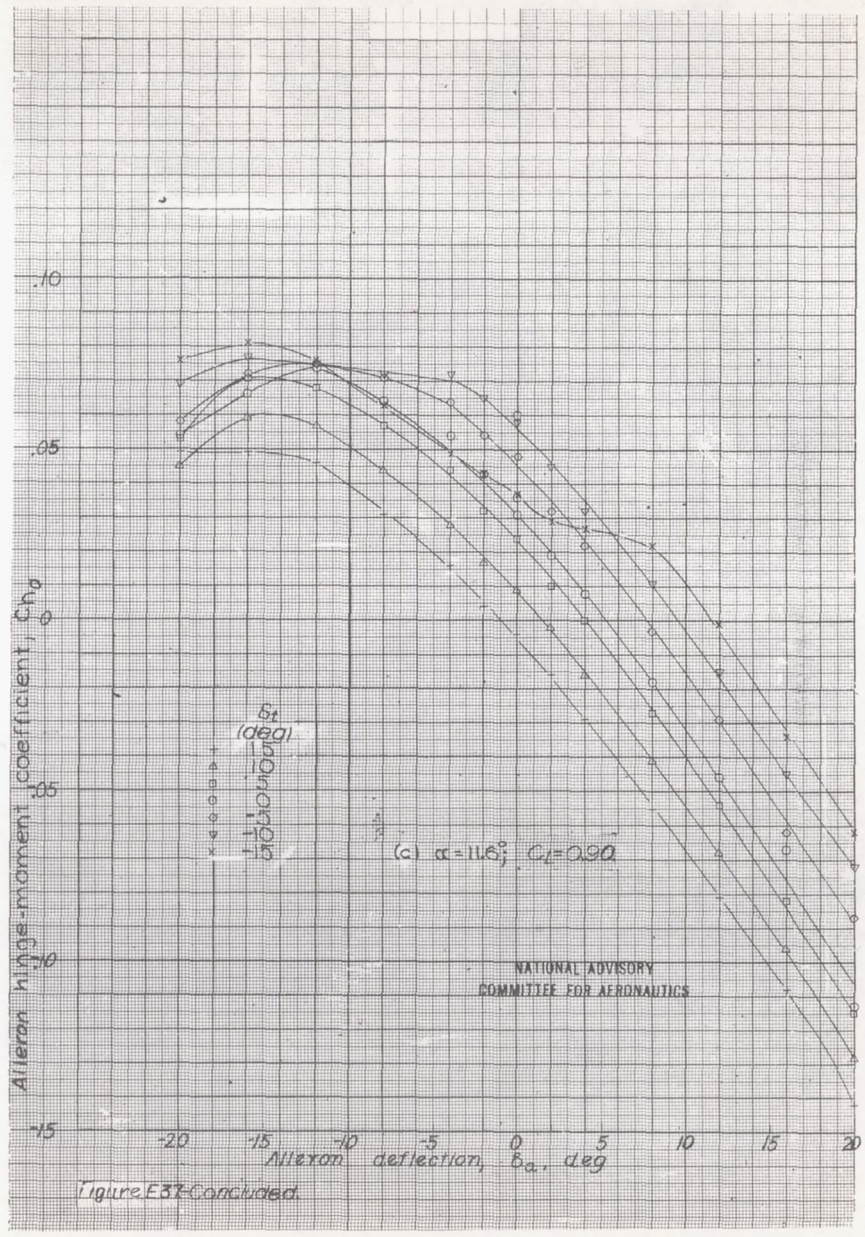

Figure E.37.-Concluded.

Model E-IX

Model E-X

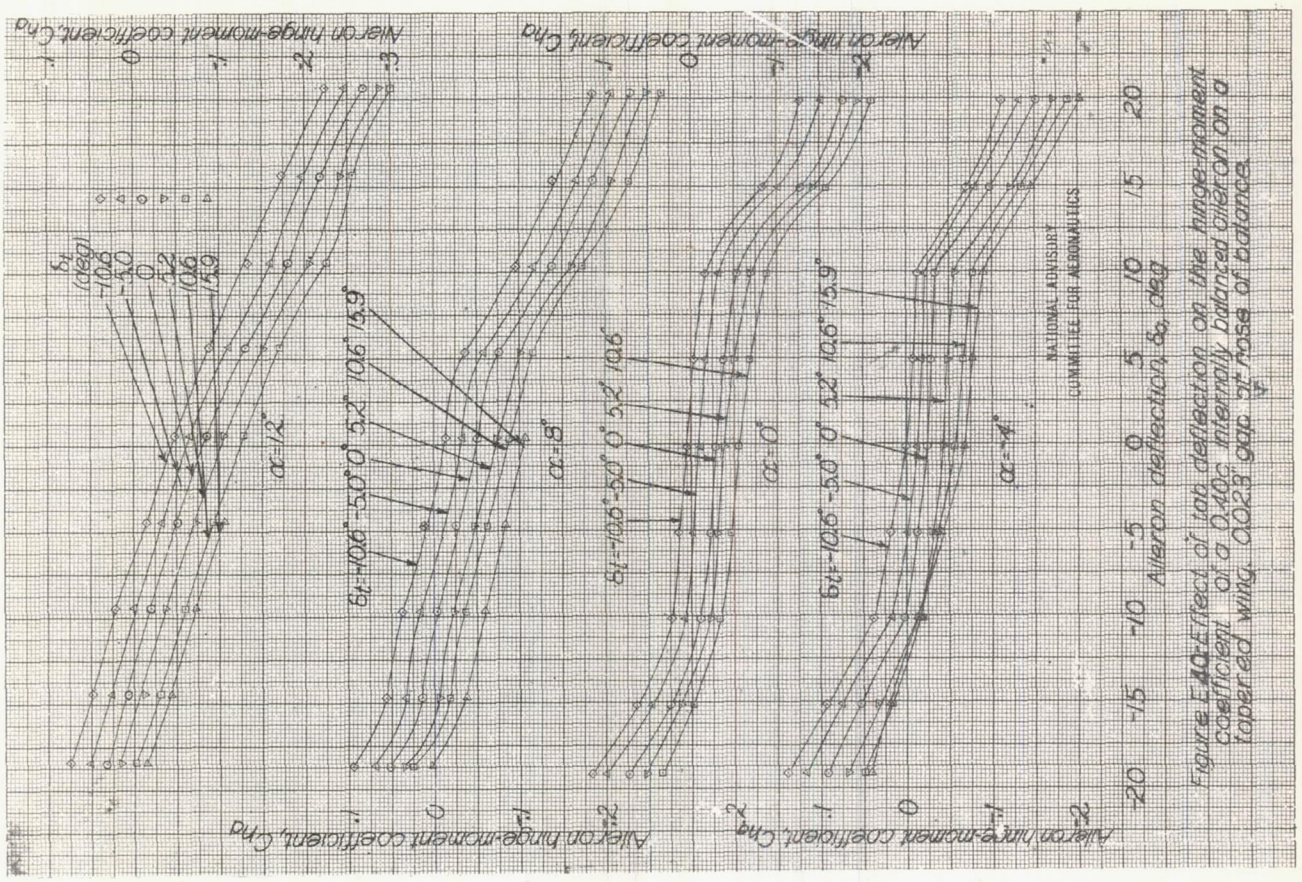

Figure E40.- Effect of tab deflection on the hinge-moment coefficient of a 0.40c internally balanced aileron on a tapered wing. 0.023" gap 2" nose of balance.

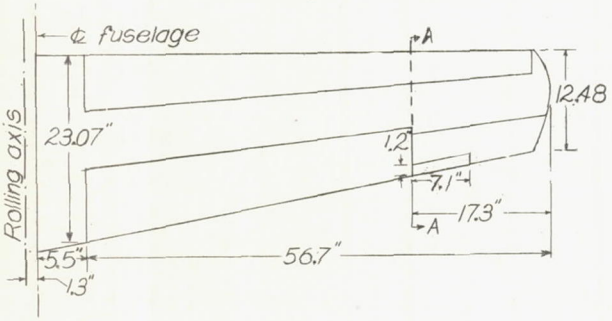

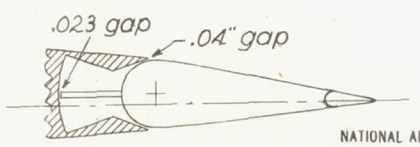

NATIONAL ADVISORY COMMITTEE FOR AERONAUTICS

Figure E38:- $\frac{1}{5.06}$-scale model of an airplane wing with internally balanced 0.40c aileron N.P.L. 7-foot No. 2 tunnel.

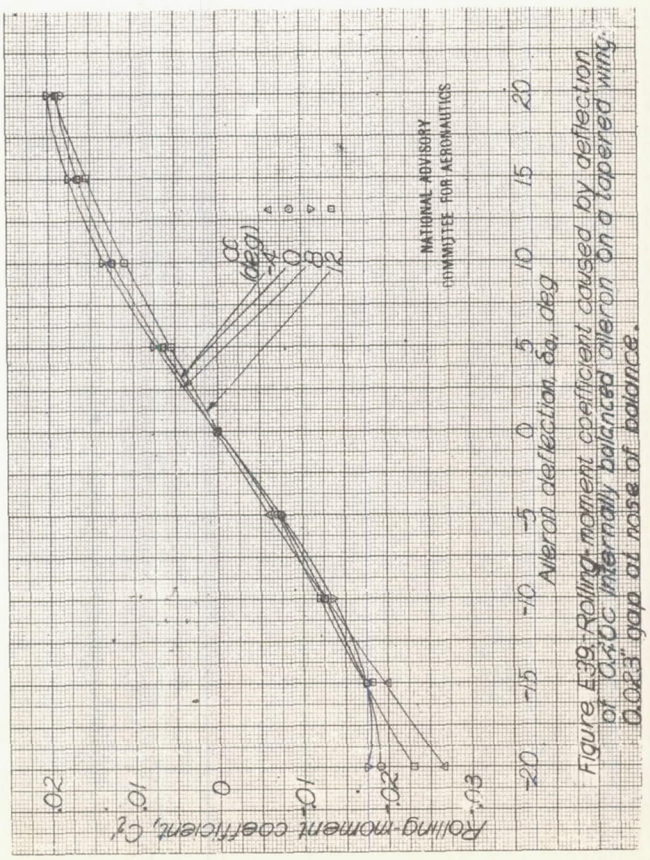

Figure E39.- Rolling-moment coefficient caused by deflection of 0.40c internally balanced aileron on a tapered wing. 0.023" gap at nose of balance.

Geometric characteristics of aileron and tabs

	Area aft of hinge line	Mean chord
Aileron	2.275 sq ft	0.663 ft
Small inner tab	.177 sq ft	.119 ft
Large inner tab	.367 sq ft	.246 ft
Small double tab	.363 sq ft	.123 ft
Large double tab	.663 sq ft	.225 ft

Wing thickness at aileron 9%
Span of semispan 0.50-scale model 111.00"

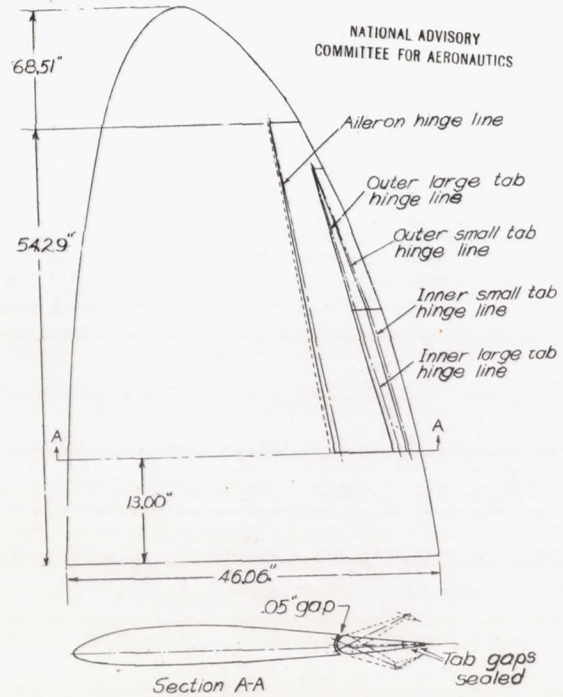

Figure E41:-Tab arrangement on a plain aileron on a 0.50-scale partial-span model of elliptical wing. N.P.L. 7-foot tunnel

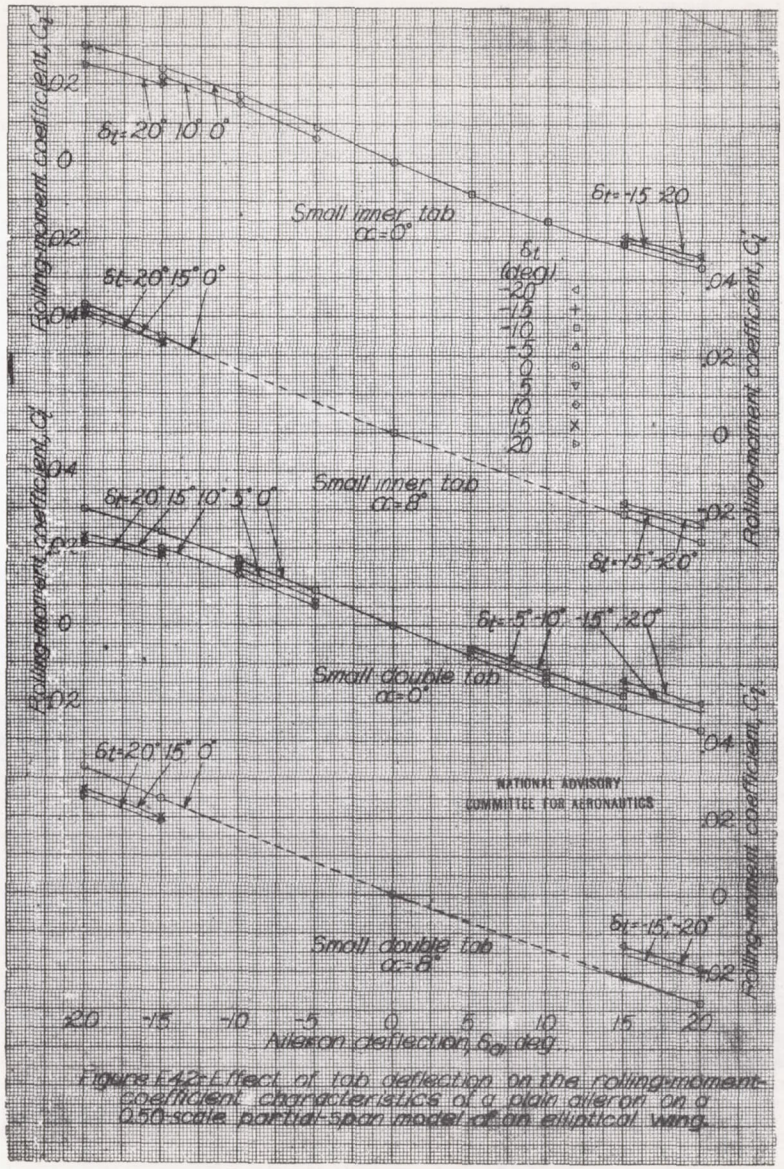

Figure E42:-Effect of tab deflection on the rolling-moment coefficient characteristics of a plain aileron on a 0.50-scale partial-span model of an elliptical wing.

Model E-XI

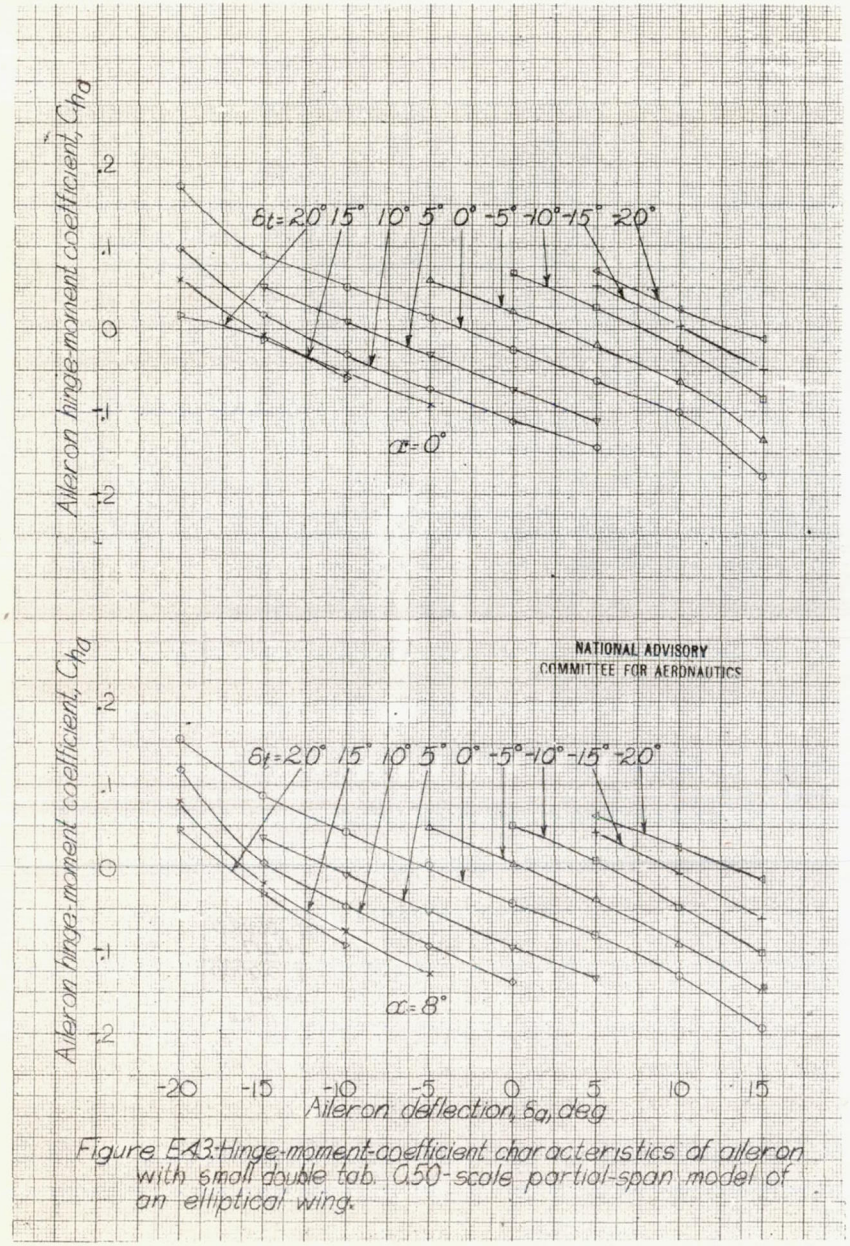

Figure E43.-Hinge-moment-coefficient characteristics of aileron with small double tab. 0.50-scale partial-span model of an elliptical wing.

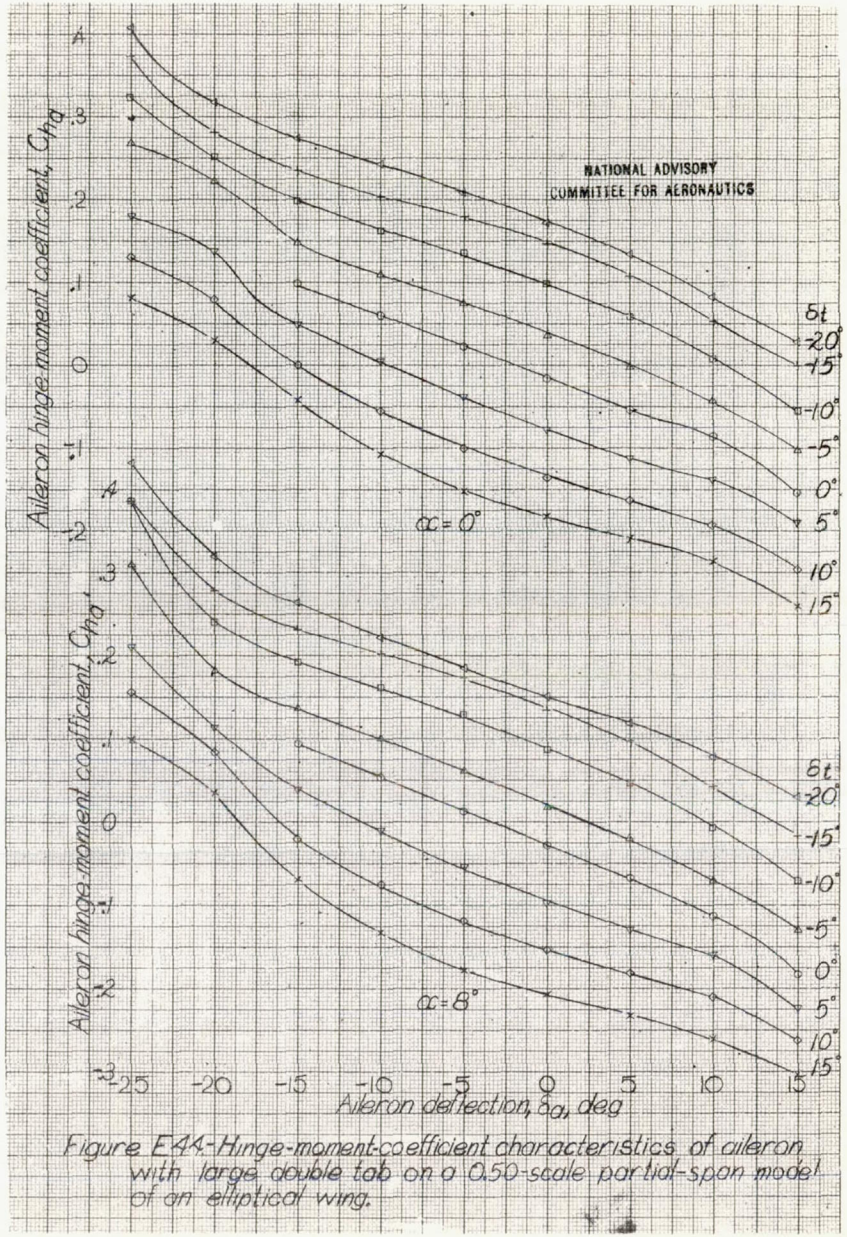

Figure E44.-Hinge-moment-coefficient characteristics of aileron with large double tab on a 0.50-scale partial-span model of an elliptical wing.

Model E-XI

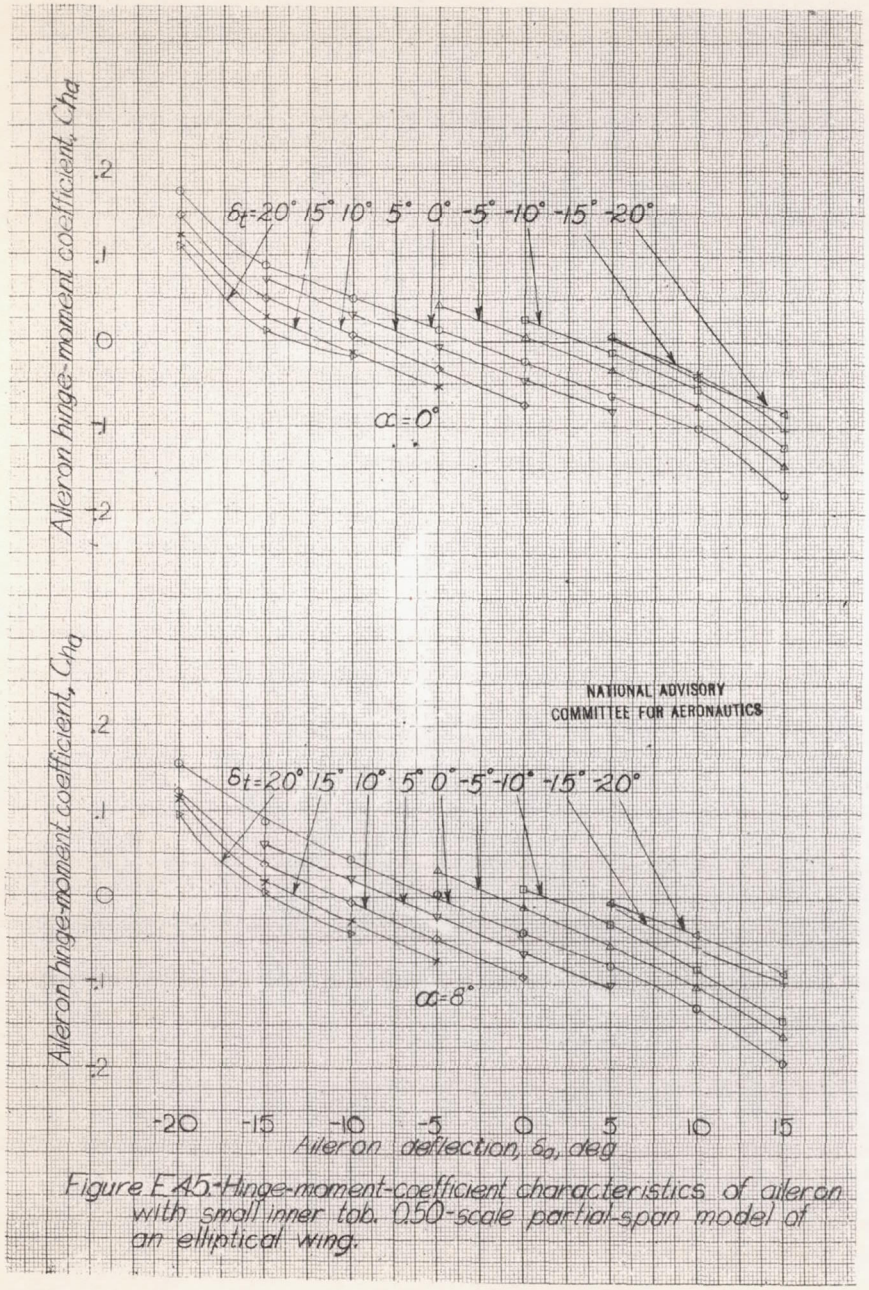

Figure E.45.-Hinge-moment-coefficient characteristics of aileron with small inner tab. 0.50-scale partial-span model of an elliptical wing.

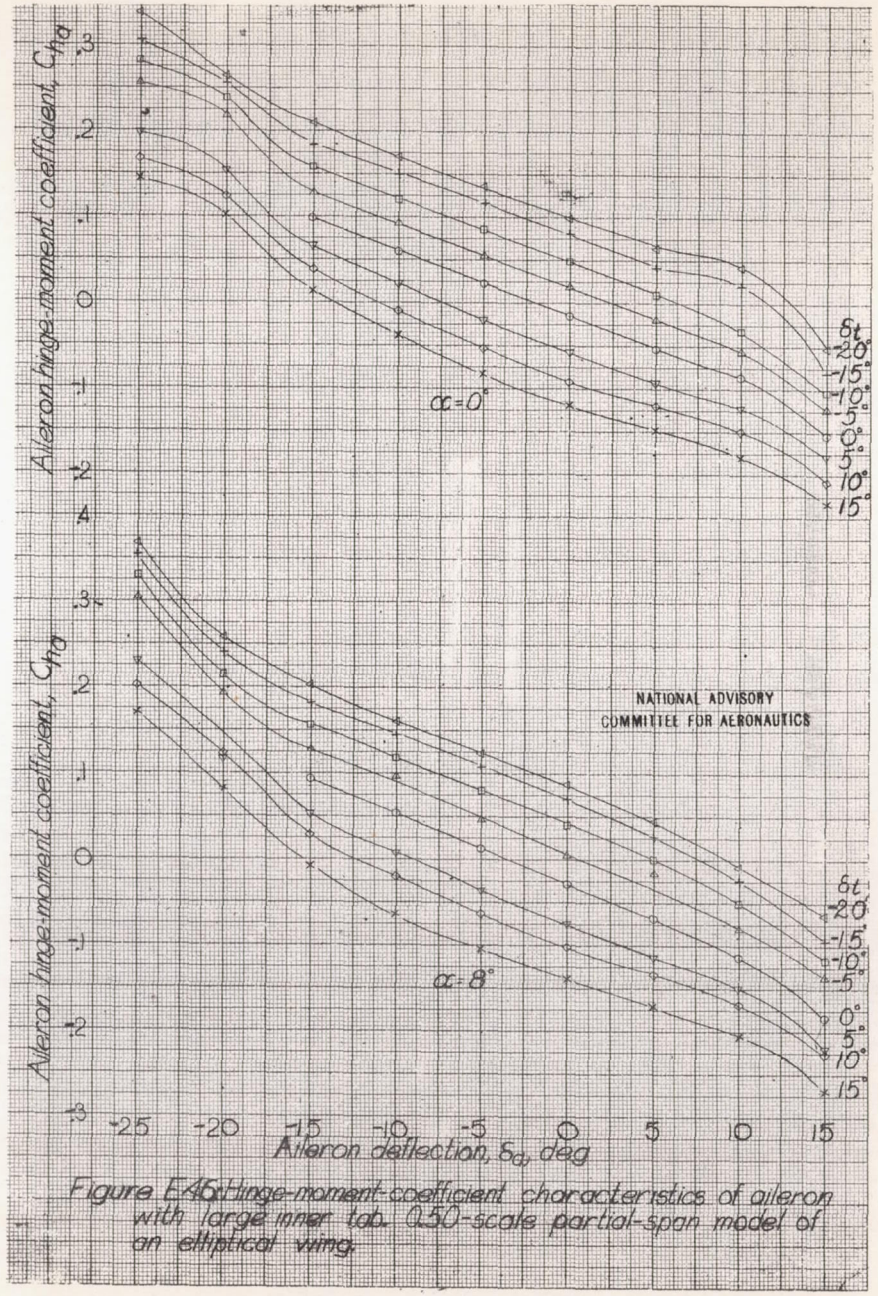

Figure E.46.-Hinge-moment-coefficient characteristics of aileron with large inner tab. 0.50-scale partial-span model of an elliptical wing.

Model E-XI

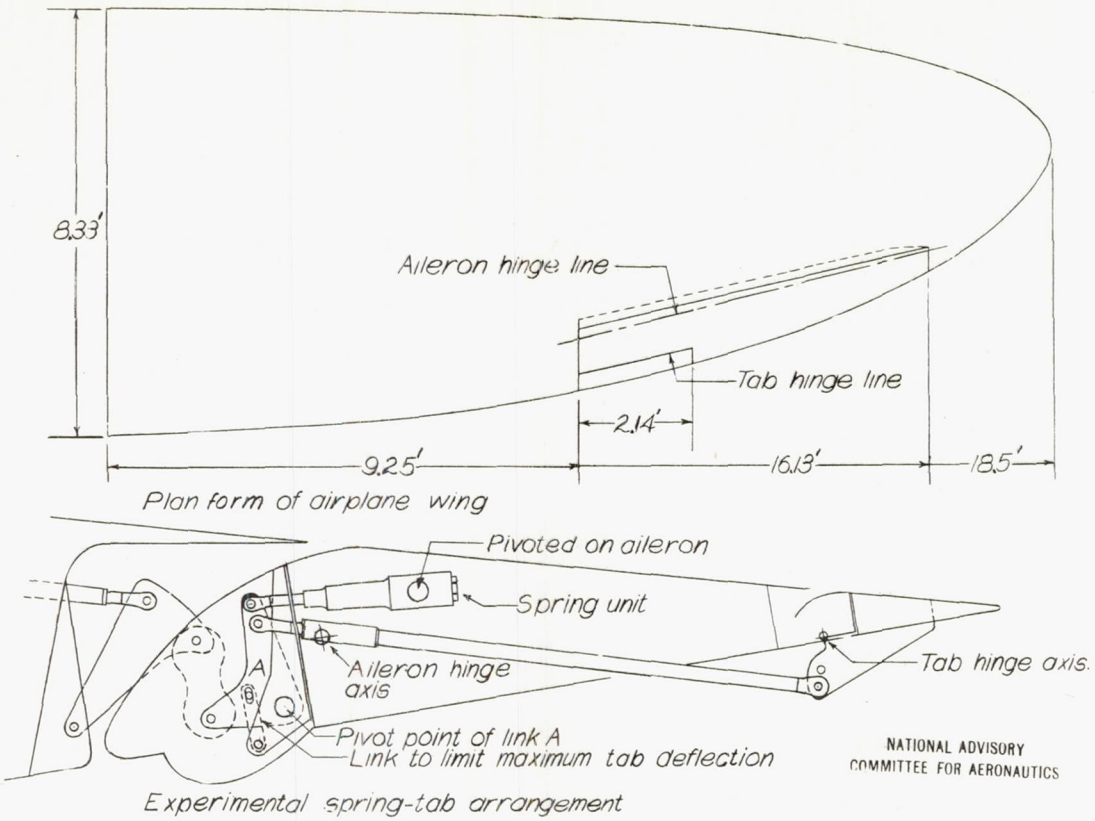

Figure E47: Plan form of elliptical wing of airplane and spring-tab arrangement used in flight tests in England.

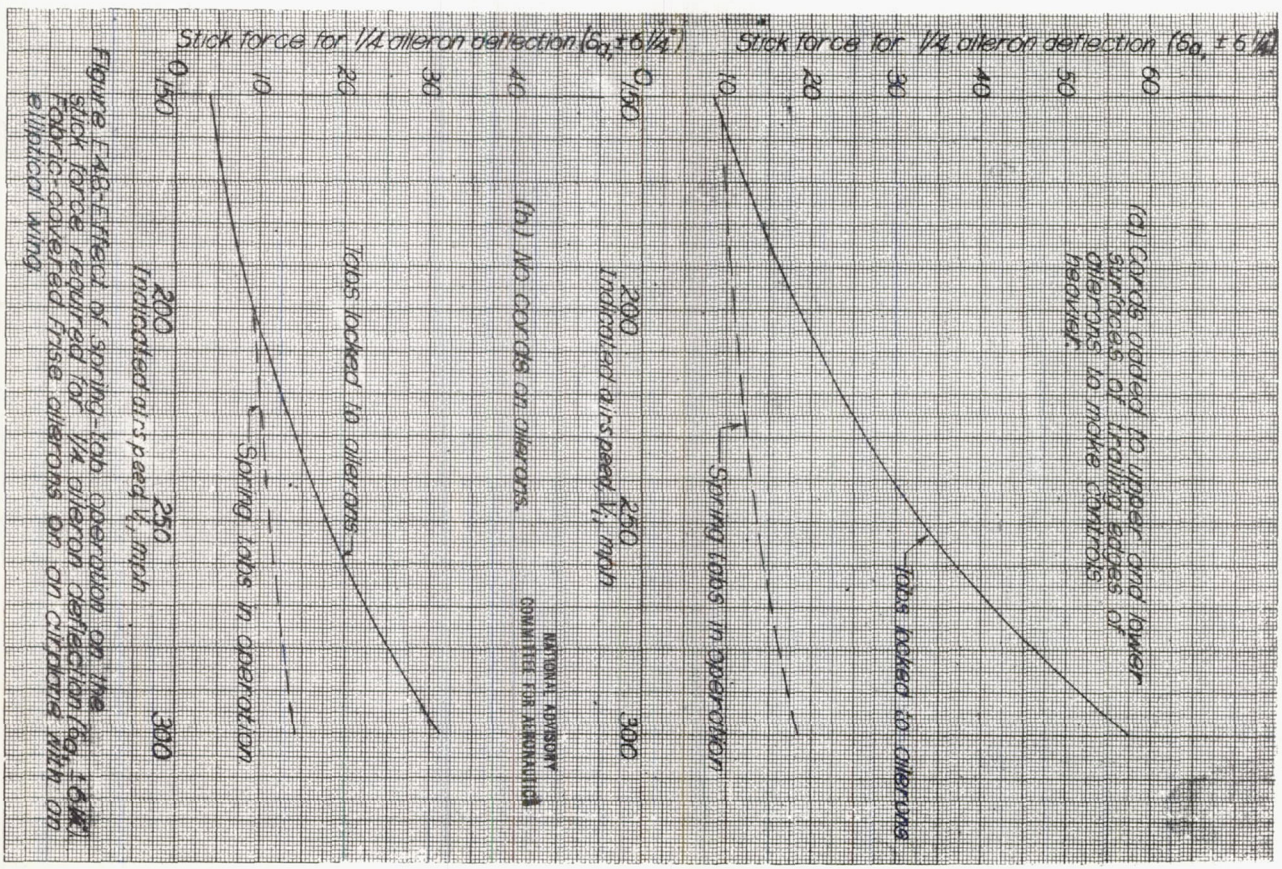

Figure E48: Effect of spring-tab operation on the stick force required for 1/4 aileron deflection ($\delta_a \pm 6\frac{1}{4}°$) at various indicated airspeeds on an airplane with fabric-covered rigid ailerons on an cantilever wing of elliptical plan form.

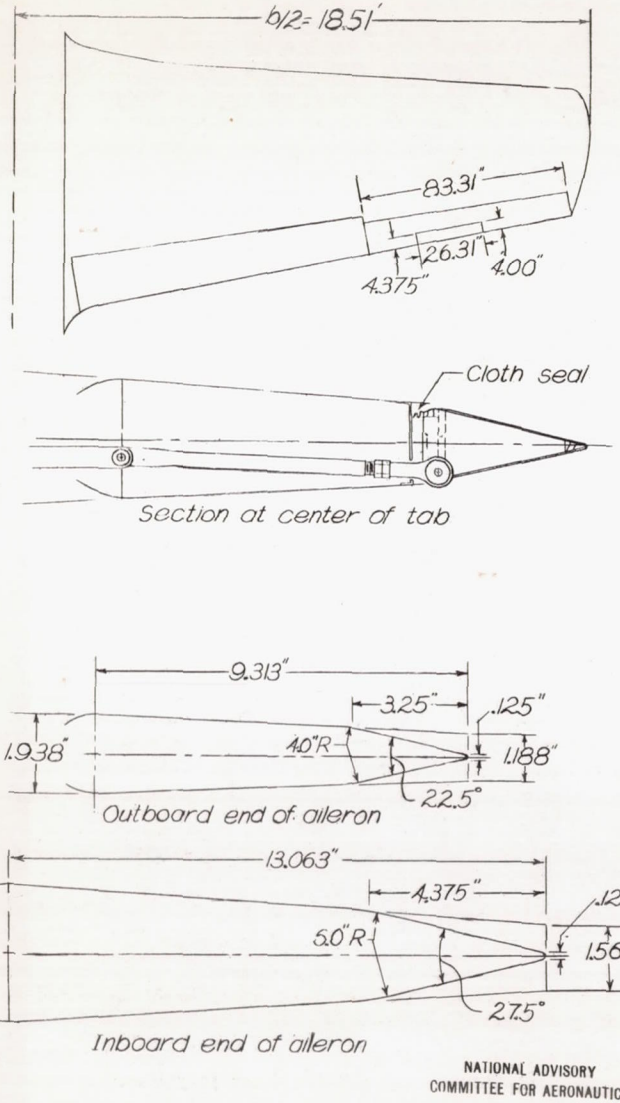

Figure E 49.- Details of beveled-trailing-edge ailerons with balancing tabs and plan form of wing on airplane used in flight tests at LMAL.

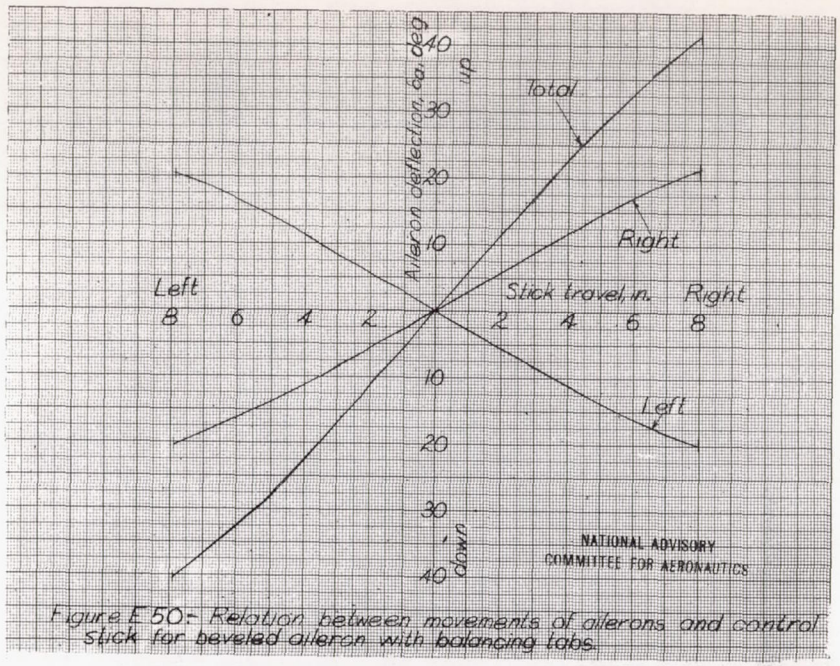

Figure E 50.- Relation between movements of ailerons and control stick for beveled aileron with balancing tabs.

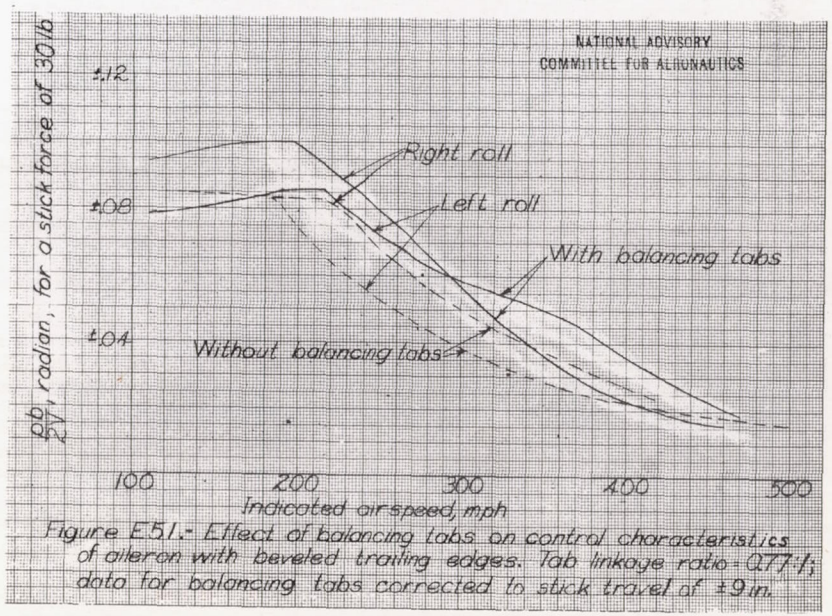

Figure E 51.- Effect of balancing tabs on control characteristics of aileron with beveled trailing edges. Tab linkage ratio - 0.77:1; data for balancing tabs corrected to stick travel of ±9 in.

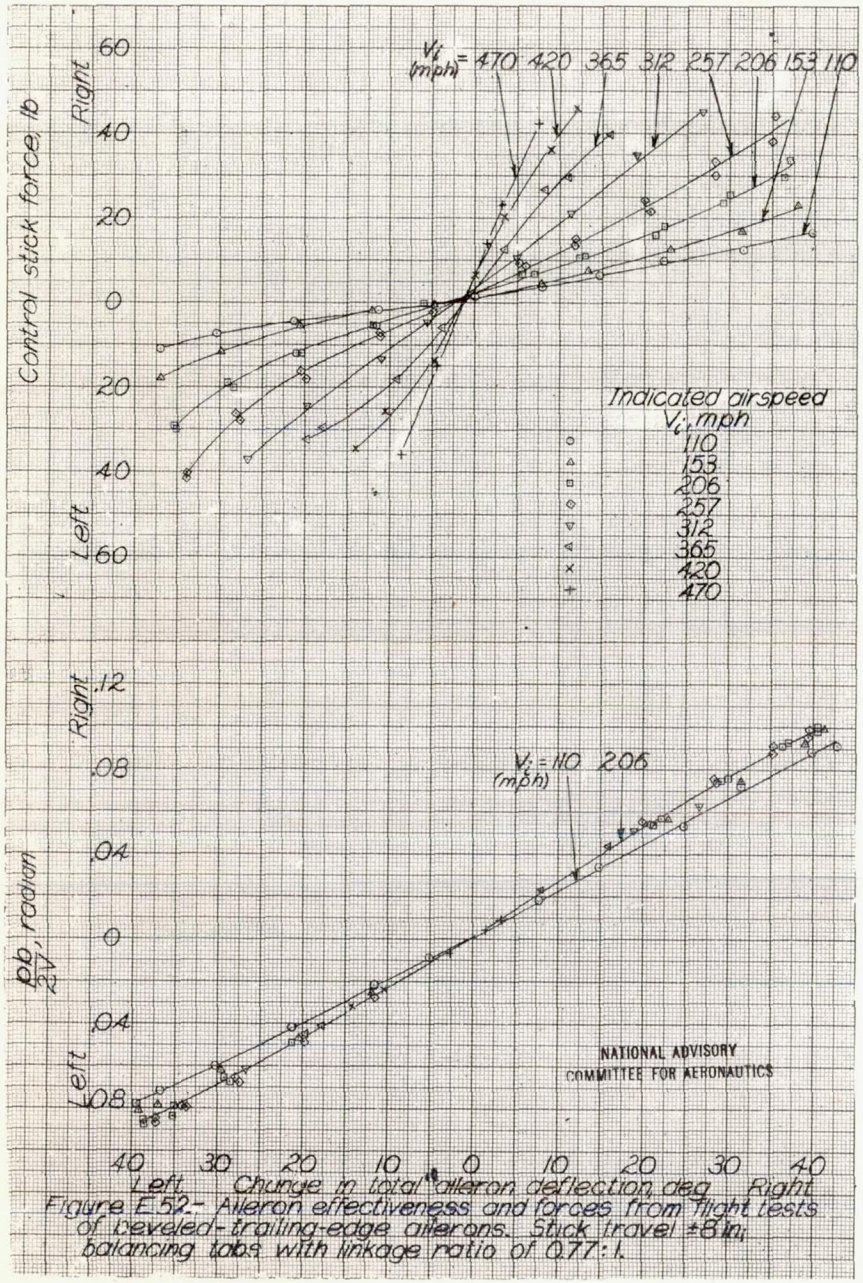

Figure E 52.- Aileron effectiveness and forces from flight tests of beveled-trailing-edge ailerons. Stick travel ±8 in.; balancing tabs with linkage ratio of 0.77:1.

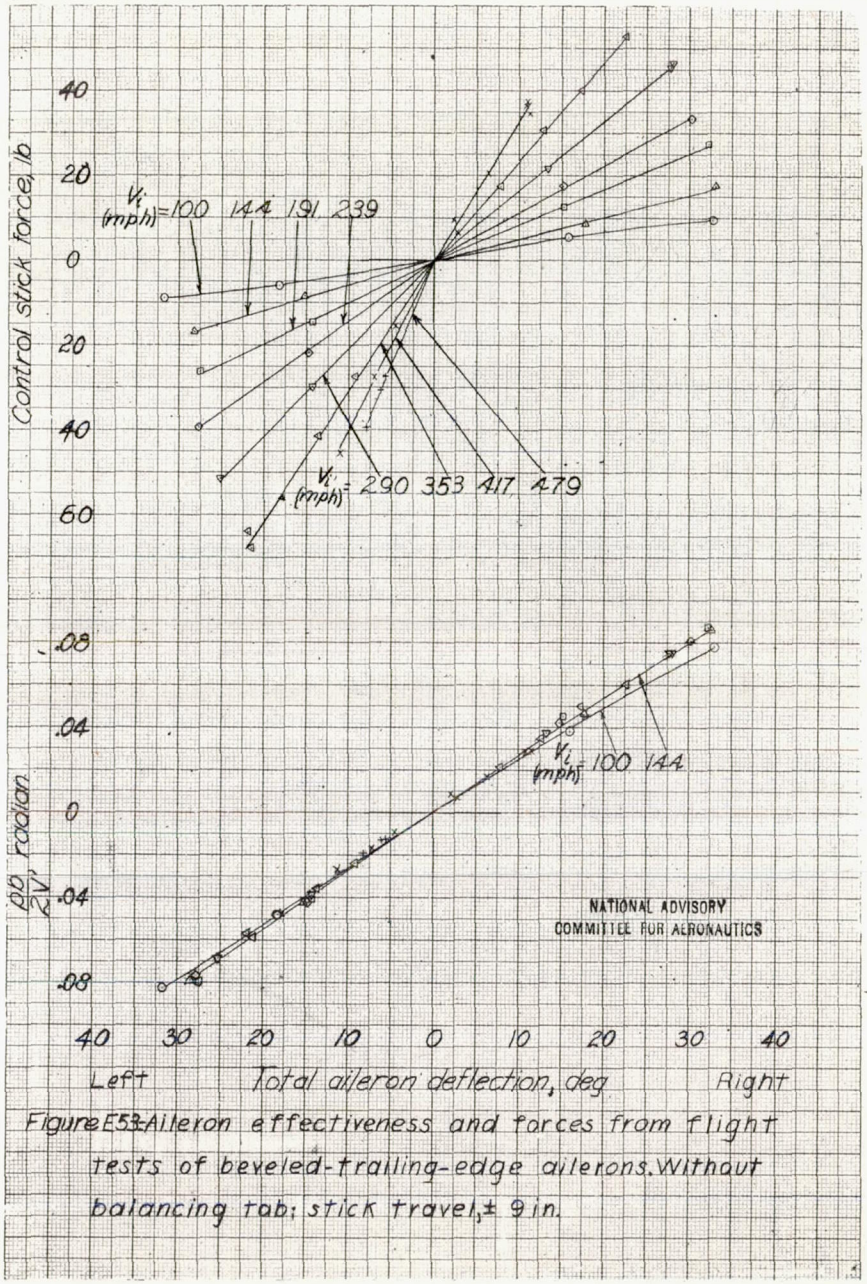

Figure E53.- Aileron effectiveness and forces from flight tests of beveled-trailing-edge ailerons. Without balancing tab; stick travel, ± 9 in.